The effects of elevated CO_2 and ocean acidification on the production of marine biogenic trace gases

A thesis submitted to the School of Environmental Science of the University of East Anglia in candidature for the degree of

Doctor of Philosophy

Alison Webb

March 2015

Abstract

The human-induced increases in atmospheric carbon dioxide since the beginning of the industrial revolution have led to increasing oceanic carbon uptake and changes in seawater carbonate chemistry, resulting in lowering of surface water pH. To date, surface ocean acidity has increased by 30% compared with pre-industrial times. The aim of this study was to investigate the relationship between increasing pCO_2, decreasing pH and changes in volatile dimethylsulphide (DMS) and halocarbon concentrations, through 70,000 litre, high pCO_2 mesocosm experiments and laboratory culture studies. DMS is a climatically important trace gas produced by marine algae: it transfers sulphur into the atmosphere and is a major influence on biogeochemical climate feedbacks. Halocarbons are also important biogenic trace gases which undergo atmospheric photochemical degradation, releasing halide radicals to participate in atmospheric ozone cycling, and transfer halogens from sea to land.

Evidence is presented from a Norwegian coastal study which showed a 60% DMS, 30% DMSP and 40% iodocarbon reduction in high pCO_2 mesocosms, and in the Baltic Sea, known for its low-salinity, cyanobacterial dominated community, where DMS concentrations showed an 80% reduction under high pCO_2 but halocarbon concentrations were unaffected. No decrease in DMS or DMSP concentrations were identified in high pCO_2 laboratory cultures of the DMS-producing species *Emiliania huxleyi* RCC1229, and halocarbons were undetectable. Changes in trace gas concentrations may arise due to pH effects on the interactions between microbial producers and consumers. Other effects may arise from cell biochemistry due to long-term adaptation to increased pCO_2 and reduced pH on the enzymatic activity production of the compounds. Further studies should determine the nature of the pCO_2 and pH effect on bacterial interactions with DMS, DMSP and halocarbon production and breakdown. There should also be attention given to the DMS source in the cyanobacterial-dominated community of the Baltic Sea.

Acknowledgements

This work was funded by a UK Natural Environment Research Council Directed Research Studentship (NE/H025588/1) through the UK Ocean Acidification Research Programme, with CASE funding from Plymouth Marine Laboratory. My supervisory team have been invaluable for their support, advice and time over the past four years, for Peter, Gill, Claire and Roland at UEA and Frankie at PML. My particular thanks to Frankie for all the reading I made her do for this thesis and the editing of a number of fairly awful drafts, and also for Peter for letting me follow him all over the department for his signature on a regular basis. Gill and Claire, your part as a sounding board for different parts of the project was always appreciated, and Roland, you always offered a different perspective to a number of problems.

There are a large number of other people in ENV I would like to mention, but I will probably forget, so I will just say: To the other hard workers in ENV 01.37 and MTGB old and new! I also would like to thank Rob Utting for his help in the lab, and Gareth Lee, Andy Macdonald and Steve Woodward for all their help with the fieldwork management and shipping, and particularly lifting of the GC-MS on more than one occasion.

I would like to acknowledge the team at GEOMAR Helmholtz Centre for Ocean Research in Kiel for the organisation and operation of both mesocosm field campaigns of which I was thankful to be a part: Ulf Riebesell, Kai Schulz, Jan Czerny, Lenny Bach and Michael Meyerhöfer, and Andrea Ludwig for her tireless organisational skills. I would also like to mention all the other participants of the mesocosm experiments which made them such a good time: Scarlett Sett, Luisa Galgani, Allanah Paul, Josie Goldstein, Rafi Bermudez and Tim Boxhammer to name just a few. Thanks for making me feel welcome in Kiel and abroad, and I look forward to the next time. The Bergen 2011 and Tvarminne 2012 mesocosm experiments were part of the SOPRAN (Surface Ocean Processes in the Anthropocene; 03F0611C) 2 Programme funded by the German Ministry for Education and Research (BMBF) and led by the GEOMAR Helmholtz Centre for Ocean Research Kiel, Germany.

I couldn't have made it through the past 4 years without some fairly incredible people: Nev, Clare, Emma, Amy, Laura, Henry, Pav, Holly, Sam, Phil, Dave, Elke, Jim and Steve. I also need to mention Mauricette and Martin for their generosity and support, putting up with many a crazy scheme, hospital visits, cake, tea, pigsitting and allowing me the privilege of knowing some of the most honest friends I have ever known. Oh, and for letting me clean up after them as well.

Love and thanks to my Family: Grandma, Grandpa, Katie and Mark, Abbie and Sophie, and Mum and Dad for supporting me all the way.

Table of Contents

Chapter 1. Background to the Investigation

Chapter 2. Methods of Trace Gas Analysis

Chapter 3. SOPRAN 2 Mesocosm Experiment, Bergen, 2011

Chapter 4. *Emiliania huxleyi* CO_2 Enrichment Experiments

Chapter 5. SOPRAN 2 Mesocosm Experiment, Tvärminne, Finland, 2012

List of Figures

Chapter 1: Background to the Investigation

Chapter 2. Methods

Chapter 3. SOPRAN 2 Mesocosm Experiment Bergen 2011

Chapter 4. *E. huxleyi* CO_2 Enrichment Experiments

Chapter 5. SOPRAN 2 Mesocosm Experiment Tvärminne 2012

Chapter 6. Discussion

List of Tables

Chapter 1. Background to the Investigation

Chapter 2. Methods

Chapter 3. SOPRAN 2 Mesocosm Experiment Bergen 2011

Chapter 4. *E. huxleyi* CO_2 Enrichment Experiments

Chapter 5. SOPRAN 2 Mesocosm Experiment Tvärminne 2012

Chapter 6. Discussion

Acronyms

3HP: 3-hydroxypropionate

A

ANOVA: Analysis of variance

B

C

CCAP: Culture Collection of Algae and Protozoa

CCM: Carbon concentrating mechanism

CCMP:Provasoli-Guillard National Culture Centre for Marine Phytoplankton

CCN: cloud condensation nuclei

CDOM: Chromophoric dissolved organic matter

CFC: Chlorofluorocarbon

CHEMTAX: a program for estimating class abundances from chemical markers

CLAW: (Charlson, Lovelock, Andreae and Warren) Authors

CTD: Conductivity, temperature and depth probe

D

DAPI: 4',6-diamidino-2-phenylindole stain

Ddd: DMSP-dependent-DMS (gene)

DIC: Dissolved inorganic carbon

Dmd: DMSP demethylation (gene)

DMS: Dimethyl sulphide

DMSO: dimethylsulphoxide

DMSP: dimethylsulphoniopropionate

DOM: dissolved organic matter

E

EhV: Emiliania huxleyi Virus

EPICA: European Project for Ice Coring in Antarctica

EPOCA: European Project on Ocean Acidification

ESAW: Enriched Seawater Artificial Water

ESNW: Enriched Seawater Natural Water

F

G

GC-FPD: Gas chromatography flame photometric detector

GC-MS: Gas chromatography mass spectrometry/ mass selective detector

GEOMAR: Helmholtz Centre for Ocean Research

GF/F: Glass fibre filter

GTC: Giga ton of Carbon

H

HELCOM: Helsinki Convention

HPLC: High performance liquid chromatography

I

IPCC: Intergovernmental Panel on Climate Change

IWS: integrated water sampler

J

K

Km: Michaelis-Menten constant

KOSMOS: Kiel Offshore Mesocosms for Future Ocean Scenarios

L

M

MBL: Marine boundary layer

MeSH: Methanethiol

MMPA: methylmercaptopropionate

MSA: methane sulphonate

N

NBS: National Bureau of Standards

NCDC: United States National Climatic Data Centre

NERC: Natural Environment Research Council

NIOZ: Royal Netherlands Institute for Sea Research

NOAA: United States National Oceanographic and Atmospheric Administration

NSS: non-sea-salt (aerosols)

O

OA: Ocean acidification

OFN: Oxygen free nitrogen

P

PAR: Photosynthetically Active Radiation

PeECE: Pelagic Ecosystem CO2 Enrichment

PHS: photosynthesis

PIC: Particulate inorganic carbon

PIC: Particulate inorganic carbon

PML: Plymouth Marine Laboratory

POC: Particulate organic carbon

PON: Particulate organic nitrogen

POP: particulate organic phosphate

PTFE: Polytetrafluoroethylene

Q

R

R: Revelle Factor

RCC: Roscoff Culture Collection

RCP: Intergovernmental Panel on Climate Change Representative Concentration Pathway Scenarios

ROS: Reactive oxygen species

RubisCO: Ribulose biphosphate carboxylase oxygenase

S

SAM: S-adenosyl L methionine

SAR: Intergovernmental Panel on Climate Change Second Assessment Report

SCFA-LWCC: Segmented continuous flow autoanalyser with liquid waveguide capillary cell

SD: standard deviation

SIM: single ion mode

SMBA: Scottish Marine Biological Association

SOPRAN: Surface Ocean Processes in the Anthropocene

SRES: Intergovernmental Panel on Climate Change Socio-economic-driven Special Report on Emissions Scenarios

SSM: Sea surface microlayer

SST : Sea surface temperatures

SSV: safe sampling volume

SW: seawater

SWS: seawater scale (of pH)

T

TA (also AT): Total alkalinity

TPU: Thermoplastic polyurethane

U

UEA: University of East Anglia

UKOARP: UK Ocean Acidification Research Programme

UV: ultraviolet (light)

V

VOCs: Volatile organic compounds

VSLS: Very short-lived (halogenated) substances

W,X,Y,Z

Chapter 1. Background to the Investigation

1. Overview of the Investigation

This thesis focusses on a range of halogen-containing carbon compounds, and a sulphur compound, dimethylsulphide (DMS), which are able to pass between the oceans and the atmosphere to transport elements from the sea to the air, and by atmospheric deposition, back to the land. These compounds are important in cycling various elements from the sea to the land, as well as participating in climate-relevant atmospheric processes and reactions.

These gases are produced in the surface oceans and both concentrations and production rates are influenced by a number of factors: physical, chemical and biological. The change in surface seawater chemistry as a result of anthropogenic CO_2 inputs to the atmosphere is affecting these processes.

These elemental cycles have important knock-on effects for atmospheric elemental cycling and climate regulation, and any change in the production rates or flux from the surface oceans can have serious ramifications for climate regulation and the management of climate change. This introduction serves to detail the background to this investigation, where the gaps lie in our knowledge, and what the aims of this investigation are.

2. The effect of increasing CO_2 and ocean acidification on marine organisms and ecosystems

2.1. Anthropogenic input of CO_2 to the atmosphere

Since the beginning of the industrial revolution, atmospheric pCO_2 levels have increased from 280 µatm to 400 µatm in direct relationship with human activities. Precise and accurate measurements of atmospheric pCO_2 started to be recorded by Keeling in the 1950s at the Mauna Loa Observatory, Hawaii, and during the period 1957 to 1972 showed a trend of increasing mean annual atmospheric pCO_2 from circa 315 to circa 325 µatm (Keeling *et al.*, 1976). These measurements have continued to the present day, and this past year (2013) the measured atmospheric pCO_2 at Mauna Loa exceeded 400 µatm for the first time (Figure 1). Although a seasonal cycle can be identified through photosynthesis and respiration of the terrestrial biosphere, the principle contributors to the increasing pCO_2 are fossil fuel combustion, change in land-use to intensive agriculture, cement production and industrial development (Davidovits, 1994). From 1980 to 2011, the average annual increase in globally averaged CO_2 was 1.7 µatm per year, which has risen to an average of 2.0 µatm per year since 2001 (Hartmann *et al.*, 2013).

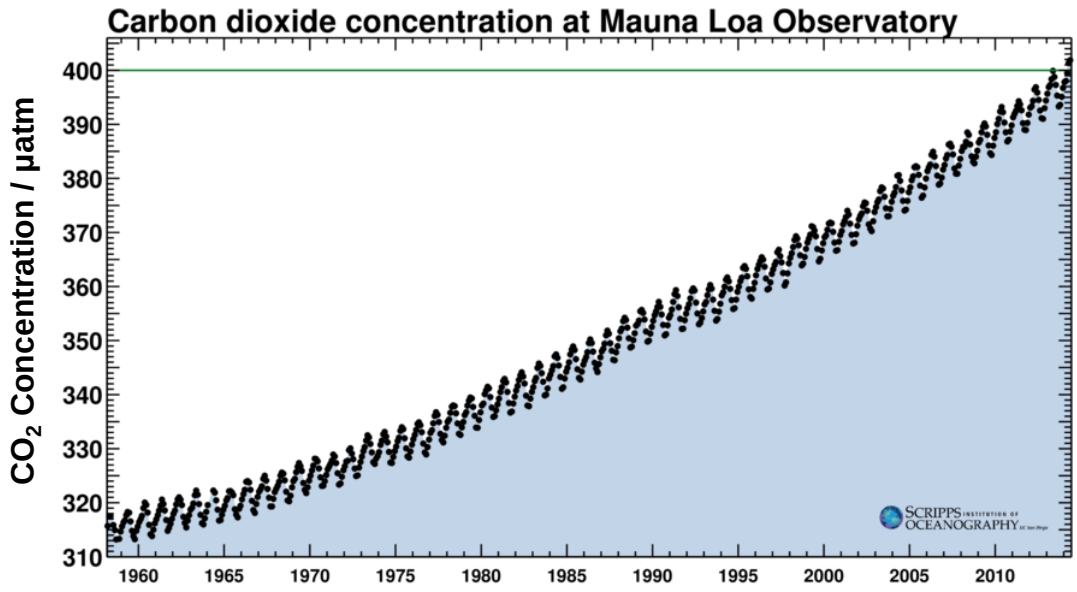

Figure 1. The Keeling Curve of atmospheric pCO_2 measured at Mauna Loa in Hawaii, up to 10th June 2014. From Scripps Institution of Oceanography at UC San Diego.

2.2. Variations in climate over geological timescales

Global climate has undergone a series of glacial and interglacial periods in the late Quaternary Period of the past 1 million years, and climate records of this period have been compiled from a number of different sources, including ice cores, ocean and lake sediments and tree rings (www.ncdc.noaa.gov). Much of this variability is a direct effect of variations in the Earth's orbit around the sun, known as Milankovich cycles that repeat every 100,000 years (Imbrie *et al.*, 1992). However, to understand the climate response to this initial forcing it is important to examine recent trends in atmospheric pCO_2.

Analysis of ice cores from Vostok and EPICA Dome C in Antarctica can provide data on temperatures, aerosol fluxes from a variety of sources including marine and anthropogenic, and precipitation and wind strength. Air bubbles within the ice provide a direct record of atmospheric gas concentrations at the time of ice formation, allowing compilation of a long-term atmospheric CO_2 dataset reaching back 800,000 years (Figure 2; Lüthi *et al.*, 2008; Petit *et al.*, 1999). Evidence from both cores shows almost regular fluctuations in concentration in the past 400,000 years from 180 µatm to 300 µatm in cycles approximately every 100,000 years (Barnola *et al.*, 2003), so providing evidence that atmospheric pCO_2 is linked to the orbital variations.

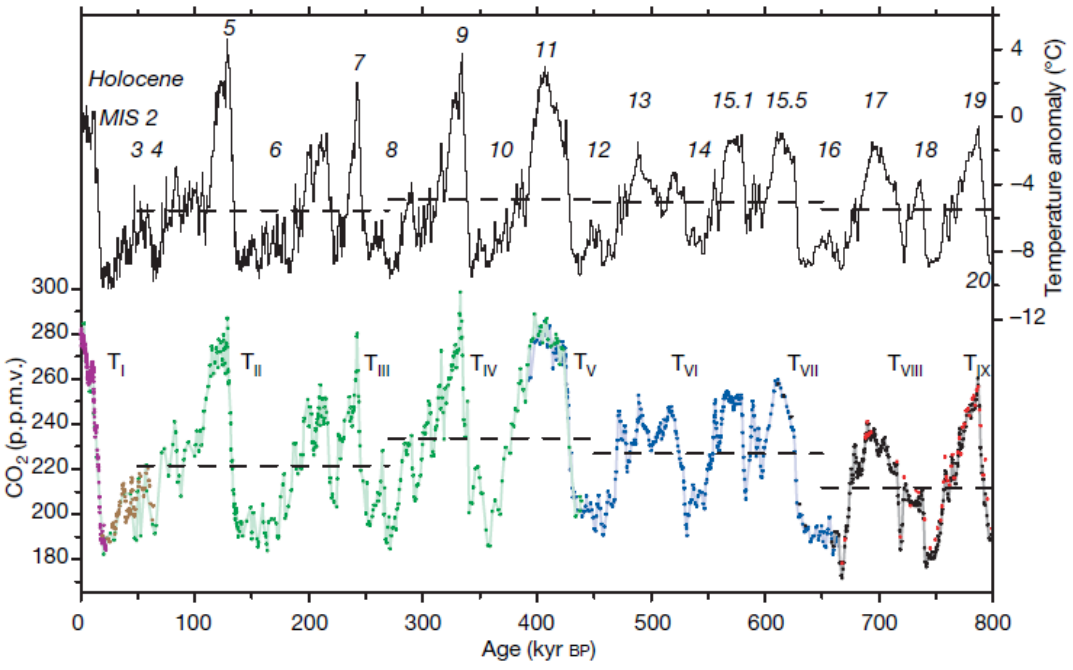

Figure 2. Comparison of CO_2 and temperature data from the EPICA C ice dome in Antarctica for the past 800,000 years. The black line gives the data for the Dome C temperature anomaly; Data from Dome C CO_2 anomaly are given in purple, blue, black and red solid circles, while green circles show

CO_2 data from Vostok. Horizontal lines are the mean values of temperature and CO_2. Diagram adapted from Lüthi *et al.* (2008).

Antarctic temperatures are strongly correlated with atmospheric pCO_2, with the implication that the greenhouse gases are amplifiers of the initial climate forcing from the orbital changes, and may have significantly contributed to the glacial-interglacial changes (Genthon *et al.*, 1987). During the interglacial periods, pCO_2 was significantly higher than during the glacial periods, likely as a result of absorption of excess carbon into the oceans in the cooler temperatures (Lüthi *et al.*, 2008). Present day concentrations of 400 µatm CO_2 are unprecedented in either the Vostok or EPICA Dome C ice cores, and the rate of increase is higher than in the past 400,000 years.

Although the precise role of CO_2 in climate variability as a cause or amplifier is uncertain, there is agreement that atmospheric pCO_2 is primarily regulated by oceanic processes and productivity (approximately 3.1 GTC dissolved into the ocean versus 1.5 GTC sequestered by land ecosystems; Ciais *et al.*, 1995; Broecker, 1982; Falkowski *et al.*, 1992; Imbrie *et al.*, 1992). In particular, Sigman *et al.* (2010) suggest that the current Southern Ocean release of sequestered CO_2 from deep ocean waters was stemmed during glacial periods, allowing additional uptake of CO_2 from the atmosphere. An understanding of the interactions between atmospheric and oceanic CO_2 during glacial and interglacial periods is required for model projections of future CO_2 scenarios.

Analysis of boron-isotope ratios to reconstruct atmospheric pCO_2 over even longer geological timescales have shown that pCO_2 was higher than current day, but has not exceeded 500 µatm over the past 24 million years (Pearson and Palmer, 2000). Any increase in atmospheric pCO_2 past this level is likely to have major consequences for biological and chemical processes.

2.3. Scenarios and projections of future climate change

Long-term projections for CO_2 and other greenhouse gases, and their associated changes in temperature and climate, are required to reflect the changes in human activities over decades and centuries (Collins *et al.*, 2013). These scenarios are used in the design of many experiments, including those presented in this thesis, to determine appropriate pCO_2 in purposeful system perturbations.

The Intergovernmental Panel on Climate Change (IPCC) Assessment Reports (1990 – 2013) have developed a number of scenarios for models to project future climate and pCO_2 based on different projections of human activities. The basic mid-range CO_2 emission scenario was

proposed in the Second Assessment Report (SAR) as an idealised concentration scenario of 1% yr^{-1} compound increase in CO_2, inducing a linear increase in the radiative forcing, and was known as IS92a. This projected the atmospheric pCO_2 in the year 2100 to be approximately 700 µatm CO_2, and was considered to be the 'best estimate' for climate sensitivity (IPCC, 1995). These different scenarios led to significant differences in atmospheric pCO_2 in the year 2100.

The year 2000 saw the development of further scenarios, termed the SRES (Socio-economic-driven Special Report on Emissions Scenarios), with projected pCO_2 ranging from 500 (Scenario B1) to 1300 (Scenario A1F1) µatm (Table 1; IPCC, 2001).

Table 1. Outline of the Marker SRES Scenarios A2, A1B A1F1 and B1, as defined in IPCC 2001, for which the appropriate CO_2 projections are shown in Figure 3.

Scenario Number	A2	A1B (Balanced)	A1F1 (Fossil Intensive)	B1
Atmospheric CO_2	840 µatm	700 µatm	1300 µatm	540 µatm
Scenario Characteristic	Consolidation into economic regions, with self-reliance on resources, and less emphasis on regional interactions	Rapid and successful economic development, abundant resources and value on environmental amenities	Very rapid economic growth, rapid introduction of new technology, pursuit of personal wealth rather than environmental quality.	High level of environmental and social consciousness, combined with sustainable development and resource use.
Population Growth	High	Low	Low	Low
Gross Community Production (GCP)	Medium	Very high	Very High	High
Energy Use	High	Very high	Very High	Low
Land-use Changes	Medium/high	Low	Low	High
Resource Availability	Low	Medium	Medium	Low
Pace and Direction of Technological Change favouring	Slow / regional	Rapid / balanced	Rapid	Medium efficiency / demineralisation

The Fifth Assessment Report of the IPCC (2013) redeveloped the model projections for the period up until year 2100 as Representative Concentration Pathway Scenarios (RCP). These

scenarios were developed to include more consistent short-lived gases and land use changes, and are developed along a different approach to the socio-economic storylines such as the scenarios shown in Table 1. The RCP produce projected CO_2 values from 400 µatm (RCP 2.6) to 1000 µatm (RCP 8.5) in 2100, with further projections to the year 2300 which could see CO_2 values either decrease from the current 400 µatm, or further increase to 2000 µatm (RCP 8.5; Figure 3; Cubasch *et al.*, 2013; Riahi *et al.*, 2007).

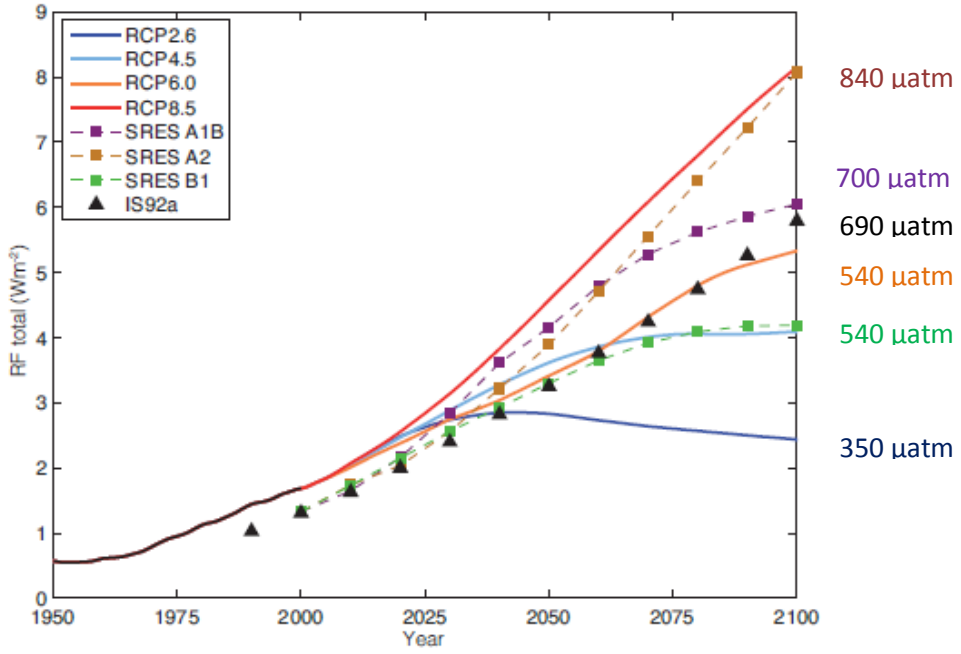

Figure 3 Historical and projected total anthropogenic radiative forcing relative to pre-industrial for scenarios up to the year 2100. Shown are the IPCC assessments IS92a from the IPCC Second Assessment Report (1995), and SRES scenarios from the Fourth Assessment Report (2007), compared to the RCP scenarios from the Fifth Assessment Report (2013), with the associated projected atmospheric pCO_2. Taken from Climate Change 2013: the Physical Science Basis (Cubasch *et al.*, 2013)

2.4. Dynamics of ocean carbonate chemistry and the effects of increasing pCO_2

The ocean is in constant exchange with the atmosphere in terms of pCO_2 over thousand-year timescales, and is a carbon reservoir which can drive atmospheric changes (Broecker, 1982). The variations seen in the glacial/ interglacial changes are driven by changes to the terrestrial and marine biospheres (Sigman and Boyle, 2000), which are reacting to the changes to the seawater and atmospheric chemistry: of the CO_2 already released by human activities into the atmosphere, between 30 - 50% has been absorbed into the surface waters of the oceans (Canadell *et al.*, 2007; IPCC, 2001), and subsequently stored in deeper waters . Chemical and biological interactions ensure the carbon is removed or transformed into different carbon

sinks, both physical and biological. The main constituent elements that determine the seawater carbonate chemistry are described here.

2.4.1. Variation in dissolved inorganic carbon

Dissolution of CO_2 in seawater forms carbonic acid, represented by the equations:

$$CO_{2(g)} \rightleftharpoons CO_{2(aq)} \quad (1)$$

$$CO_{2(aq)} + H_2O_{(l)} \longrightarrow H_2CO_{3(aq)} \quad (2)$$

However this equation is reversible, and is better thought of as a series of reversible reactions and equilibria, which are dependent upon the starting pCO_2, the temperature and the in-situ pH (Dickson, 2010):

$$CO_{2(aq)} + H_2O_{(l)} \rightleftharpoons H^+_{(aq)} + HCO_3^-{}_{(aq)} \quad (3)$$

$$HCO_3^-{}_{(aq)} + H^+_{(aq)} \rightleftharpoons 2H^+_{(aq)} + CO_3^{2-}{}_{(aq)} \quad (4)$$

The carbon-containing species (dissolved CO_2, bicarbonate and carbonate) which are formed in these equilibria are collectively described as dissolved inorganic carbon (DIC), and the proportions of each are dictated by the surface seawater pH and temperature. At the pH of seawater (currently approximately 8.2; Orr *et al.*, 2005), the ions occur in proportions according to the pH: approximately 90% bicarbonate, 8% carbonate and 2% CO_2 (Figure 4; Dickson, 2010).

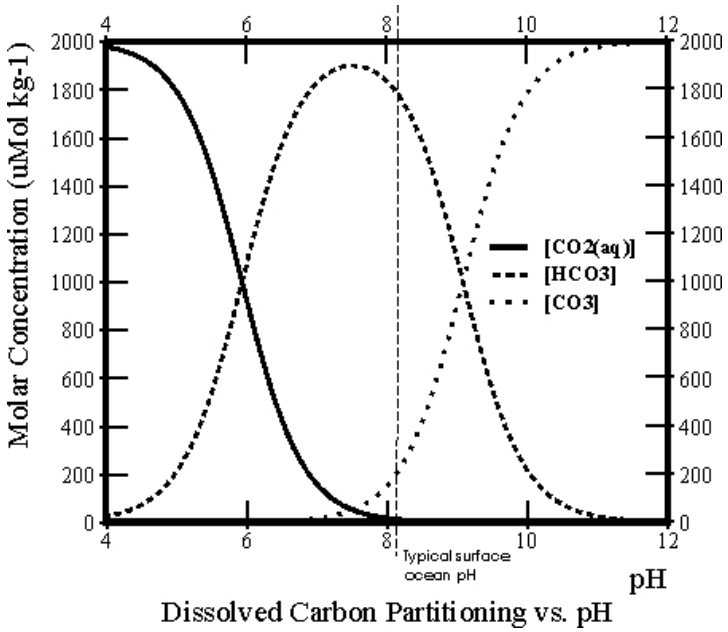

Figure 4. Partitioning of carbon between the three forms of DIC at different pH. The dotted line indicates current oceanic pH and carbon partitioning.

A simple way of encapsulating the equilibrium relationship between the concentrations of the various CO_2 species is:

$$CO_{2(aq)} + CO_3^{2-}{}_{(aq)} + H_2O_{(l)} \rightleftharpoons 2HCO_3^-{}_{(aq)} \qquad 5$$

According to this equation, as additional CO_2 is absorbed from the atmosphere, the additional CO_2 reacts with carbonate to form bicarbonate, the net effect of which is to increase concentrations of dissolved CO_2 and bicarbonate but decreasing the carbonate ion. Modern day carbonate concentrations vary across the global oceans, with concentrations in the Southern Ocean standing around 100 µmol kg^{-1} and tropical waters around 240 µmol kg^{-1}. Low carbonate in the Southern Ocean is a result of low surface temperatures and high pCO_2 in upwelled deep waters as a result of remineralised organic matter (Orr *et al.*, 2005). Two other important equilibria for determining the buffering capacity of seawater are the dissociation of boric acid and the dissociation of water.

$$B(OH)_{3\,(aq)} + H_2O_{\,(l)} \rightleftharpoons H^+_{(aq)} + B(OH)_4^-{}_{(aq)} \qquad 6$$

$$H_2O_{\,(l)} \rightleftharpoons H^+_{\,(aq)} + OH^-_{\,(aq)} \qquad 7$$

2.4.2. Variation in total alkalinity

A definition of total alkalinity is the number of moles of hydrogen ion equivalent to the excess of proton acceptors (bases formed from weak acids with dissociation constant $K<10^{-4.5}$ at 25°C and zero ionic strength) over proton donors (acids with $K>10^{-4.5}$) in 1kg of sample. (Dickson, 1981).

Total alkalinity is comprised of the sum of all the proton acceptors, including those of phosphate, silicate, ammonia and sulphide, but for open ocean seawater it can be approximated to:

$$A_T = [HCO_3^-] + 2[CO_3^{2-}] + [B(OH)_4^-] + [OH^-] - [H^+] \qquad 8$$

This is otherwise known as practical alkalinity, and is the term most frequently used when discussing alkalinity in seawater (Dickson, 2010). The availability of these proton acceptors allows seawater a high degree of pH buffering. Higher alkalinity causes more DIC to be in the carbonate form, and less of it to be dissolved CO_2; areas of higher alkalinity can be assumed to be sinks for atmospheric carbon entering the surface waters (Sigman *et al.*, 2010). In opposition to this, increasing the DIC under constant alkalinity raises the dissolved pCO_2, lowers the carbonate concentration, and causes the water to become more acidic.

Alkalinity in seawater is measured by acidimetric titration, and is expressed as moles per kilogram of solution (Dickson, 2010).

2.4.3. Variation in pH

As atmospheric pCO_2 increases, the surface seawaters will absorb greater amounts of CO_2, which has the result of lowering the pH and making the ocean less alkaline. It is this 'ocean acidification' which is termed 'The Other CO_2 Problem' (Brewer and Barry, 2008; Caldeira and Wickett, 2003; Doney *et al.*, 2009) and is the key reason for this investigation. pH is defined as the negative of the logarithm of the hydrogen ion concentration (Dickson, 1993):

$$pH = -\log_{10}[H^+] \qquad 9$$

where [H+] is indicative of the total concentration of H^+ (including those from reactions 3, 4, 6 and 7 above), together with the concentrations of all the H complexes formed with the components of the ionic medium (ie H_2O, Na^+, Mg^{2+}, K^+, Ca^{2+}, Cl^- and SO_4^{2-}; Dickson, 2010). Interactions of H^+ with the sulphate ion are important in formation of the anion HSO_4^-. Total hydrogen ion concentration can also be expressed as:

$$[H^+]_T = [H^+]_F + [HSO_4^-] \qquad 10$$

pH can be measured on different scales: the NBS scale, the total hydrogen ion concentration scale, the free hydrogen ion concentration scale, and the seawater scale (Dickson, 2010; Hansson, 1973). As pH involves a single ion activity, it is immeasurable (Covington *et al.*, 1985) but is defined operationally on the NBS scale using a series of standard buffer solutions with assigned pH values. As the buffer solutions have low ionic strength (0.1) compared to seawater (0.7), these buffers were not recommended for seawater use (Zeebe and Wolf-Gladrow, 2001) and a new set of buffers were developed in artificial seawater, known as the total scale (Hansson, 1973).

$$pH_T = -\log ([H^+]_F + [HSO_4^-]) = -\log_{10} [H^+]_T \qquad 11$$

This total scale can be converted to the free scale without the inclusion of the sulphate ion in the calculation, but this can introduce error into the determination of accurate pH.

A further scale is used known as the seawater scale, which takes into account both the influence of $[HSO_4^-]$ and $[F^-]$ (Zeebe and Wolf-Gladrow, 2001).

$$pH_{SWS} = -\log ([H^+]_F + [HSO_4^-] + [HF]) = -\log [H^+]_{SWS} \qquad 12$$

Measurement of pH is generally by one of two options: potentiometrically using a hydrogen-sensitive electrode versus a reference electrode, or via a spectrophotometric technique using an indicator dye where the acid and base forms have different colours (Dickson, 2010).

Changes to pH, surface water DIC and alkalinity vary on global and local scales, and are dependent on temperature, salinity, riverine inputs, geology and upwelling of low pCO_2 waters. A global mean decrease in surface water pH of 0.08 was calculated for the period 1765 to 1994 based on annually averaged historical radiative forcing and pCO_2, with variations in change from -0.05 in the subtropical South Pacific to -0.1 in the North Atlantic (Orr *et al.*, 2005; Sabine *et al.*, 2004). Time series measurements from the Hawaii Ocean Time-series Program over 19 years until 2009 showed that that surface water pH has decreased at an average rate of -0.0019 y^{-1}, from a mean of 8.12 (in 1988) to 8.08 (in 2007; Dore *et al.*, 2009). Projections of global average surface pH in the year 2100 are as low as 7.7 (Orr *et al.*, 2005; Turley and Findlay, 2009).

2.4.4. Variation in pCO_2

The partial pressure of CO_2 when the air is in equilibrium with seawater is the gas phase pressure of CO_2 in the atmosphere which would be in equilibrium with the dissolved CO_2, and is highly dependent upon the ambient temperature (Dickson, 2010).

2.4.5. Capacity of seawater to buffer changes in pCO_2

The pH of seawater is stabilised to some extent by the ability to buffer against changes in pH caused by addition of extra weak acid dissociation (or the addition of strong acid, but the system is far less effective in this case). Any addition of CO_2 to seawater, as shown in equation 3 will result in an excess of H^+, which will be absorbed by CO_3^{2-} reacting to produce HCO_3^-. This buffering ability ensures that seawater remains at constant alkalinity, as the addition of further CO_2 adds to the $[HCO_3^-]$ in equation 4, but is cancelled out by the equivalent increase in $[H^+]$ (the number of proton donors entering the system is the same as the number of proton acceptors).

2.5. The 'Carbonate Pump'

Chemical reactions are not the only processes taking place in the surface oceans: biological interactions have high importance as a mechanism for removing and producing CO_2 as well as altering the buffering capacity (either increasing or decreasing). Carbonate is fixed in surface ocean waters by marine organisms producing the mineral calcium carbonate ($CaCO_3$),

removing carbonate from the soluble form. This material, in the form of tests, skeletons and shells, sinks into deeper waters, transferring carbonate out of surface waters (approximately 100m). This process is known as the carbonate pump.

2.6. The 'Biological Carbon Pump'

Photosynthesis by marine phytoplankton takes up a significant proportion of the CO_2 absorbed from the atmosphere and converts it into carbohydrate, where it is used for a number of processes within the cell. The majority of phytoplankton growth is limited by nutrients such as phosphate and nitrate before carbon becomes a limiting factor. However, as CO_2 is the preferential form of inorganic carbon uptake by phytoplankton, dissolved CO_2 can become limiting during bloom events and in times of inorganic nutrient availability (Riebesell *et al.*, 1993). This depletion of surface water CO_2 encourages additional atmospheric draw-down of CO_2 into surface waters. Grazing and viral lysis releases significant amounts of the carbon fixed by photosynthesis back into the surface waters, resulting in a high degree of carbon recycling, up to 90%. The material which manages to sink into deeper waters is a mixture of detritus, faecal matter, live cells and dead organisms (particulate organic matter, POM). This transfer of carbonaceous material from surface to deep waters where it is stored for hundreds to millions of years is known as the biological pump (Elderfield, 2002).

2.7. The 'Solubility Pump'

The solubility pump is an additional mechanism whereby carbon is transferred to deeper waters. In lower temperatures, CO_2 solubility in seawater increases. Deep convection at higher latitudes as part of the overturning circulation draws CO_2-rich cold waters down into the deep waters. Due to the continual transfer of carbon-rich material from surface waters into ocean bottom waters and sediments through the biological and carbonate pumps, deep waters are supersaturated with CO_2 relative to the surface waters and atmosphere. Relatively 'young' North Atlantic Deep Waters (NADW) are high in carbonate and relatively low in CO_2, but the 'aged' Pacific Deep Waters (PDW) are low in carbonate and high in CO_2 accumulated during the thousand-year transport from the Atlantic (Elderfield, 2002).

2.8. Uptake and utilisation of carbon during photosynthesis

Carbon utilised during photosynthesis (PHS) is derived from the DIC within the water column. CO_2 is utilised within the chloroplast by the enzyme ribulose-1,5-bis-phosphate carboxylase/ oxygenase (RubisCO) as the initial point of assimilation for PHS during the Calvin Cycle (Wyman

et al., 1998). Due to the low concentrations of dissolved CO_2 within the surface waters (Figure 4), and the inability of RubisCO to function with diffusive entry of CO_2 alone (Raven, 1997; Riebesell, 2004), marine organisms have developed so-called carbon concentrating mechanisms (CCMs) to actively uptake CO_2 into the cell. Different phytoplankton have developed different CCMs depending on the required substrate for PHS: some species are able to utilise HCO_3^- instead of CO_2, and have HCO_3^- appropriate CCMs (Buitenhuis *et al.*, 1999; Raven, 1997). Utilisation of the much more readily available HCO_3^- through carbonic anhydrase catabolism into CO_2 is energy-intensive but will allow PHS when the CO_2 was otherwise not sufficiently concentrated (Riebesell, 2004).

2.9. Production of biogenic calcium carbonate in the ocean

Calcium carbonate is produced by a number of phytoplankton as an external layer of calcium carbonate ($CaCO_3$), with some of the most prominent species members of the coccolithophorids, who produce plates of $CaCO_3$ known as coccoliths. This group is widely diverse in size and coccolith formation, and the ubiquitous *E. huxleyi* is now the most numerically important coccolithophorid in the ocean (Paasche, 2001).

Calcifiers are by no means limited to the phytoplankton, and include molluscs, corals and coralline algae: combined with the coccolithophores, the latter two are responsible for over half of the global $CaCO_3$ production (Milliman and Droxler, 1996). Three polymorphs of $CaCO_3$ occur: coral reefs build their structures out of aragonite (Gattuso *et al.*, 1998), whereas coccoliths are formed from the more stable polymorph, calcite (Gattuso and Buddemeier, 2000), with a third polymorph as high Mg calcite. Some organisms have fully external calcium carbonate, others enclose the formation in a membrane, which may influence the exchange of the constituent ions of $CaCO_3$ with the surrounding waters (Rodolfo-Metalpa *et al.*, 2011).

Ions of the crystalline lattice structure of marine biogenic $CaCO_3$ are in exchange with the surrounding seawater, but surface waters are supersaturated with respect to $CaCO_3$, preventing the dissolution of the crystalline structures. The uptake of CO_3^{2-} during calcification results in a shift of equation 5 above to release CO_2, which is released into the water. Equation 5 can be rewritten to include calcium, to show that CO_2 is released:

$$Ca^{2+}_{(aq)} + 2HCO_3^-{}_{(aq)} \rightleftharpoons CaCO_{3(aq)} + CO_{2(aq)} + H_2O_{(l)} \qquad 13$$

Dissolution of polymorphs of calcium carbonate in seawater is controlled by the saturation state of the two polymorphs, Ω_{arag} and Ω_{calc}. The degree of saturation of seawater with respect to both polymorphs is the product of the concentrations of calcium and carbonate ions, at the

in-situ temperature, salinity and pressure, divided by the apparent stoichiometric solubility product (K_{sp}) for those conditions (Feely *et al.*, 2010).

$$\Omega_{arag} = [Ca^{2+}][CO_3^{2-}]/ K_{arag} \quad 14$$

$$\Omega_{calc} = [Ca^{2+}][CO_3^{2-}]/K_{calc} \quad 15$$

Ca^{2+} is essentially in constant proportion to the salinity and carbonate is calculated from two out of the four variables: DIC, total alkalinity, pH or pCO_2. In surface waters, all polymorphs of the mineral are in a supersaturated state ($\Omega > 1$; Feely *et al.*, 2009). When the saturation state drops below saturation ($\Omega = 1$), the mineral may start to dissolve: this may occur due to a lower carbonate concentration in surface waters due to CO_2 addition (by increasing atmospheric CO_2, or from respiration), or at depth due to lower carbonate concentrations in deep waters due to the biological pump (Section 2.5) and associated respiration by microbial production at depth. Of the polymorphs, aragonite has greater solubility than calcite (Zeebe and Wolf-Gladrow, 2001), yet high Mg calcite is more soluble still.

The $CaCO_3$ produced by the coccolithophores is subject to loss to the deep oceans as the cells die and sink, and is stored in deep ocean sediments. The depth at which the saturation state changes to $\Omega < 1$ is called the saturation horizon, below which $CaCO_3$ will start to dissolve (Zeebe and Wolf-Gladrow, 2001). In the carbonate rich Atlantic waters, the saturation horizon is deeper (>4000m for calcite, >2300m for aragonite; Li *et al.*, 1969) than in the carbonate-poor Pacific waters (>1500m for calcite, >300m for aragonite; Li *et al.*, 1969), and globally, the saturation depth will show local and large-scale variations in relation to temperature and carbonate concentration (Figure 5). Solubility of $CaCO_3$ increases at lower temperatures, however due to the similar distribution of temperature, salinity and pressure in the deep waters of both the Pacific and Atlantic, the difference in water depths at which water becomes undersaturated is mainly due to the difference in CO_2 (Li *et al.*, 1969).

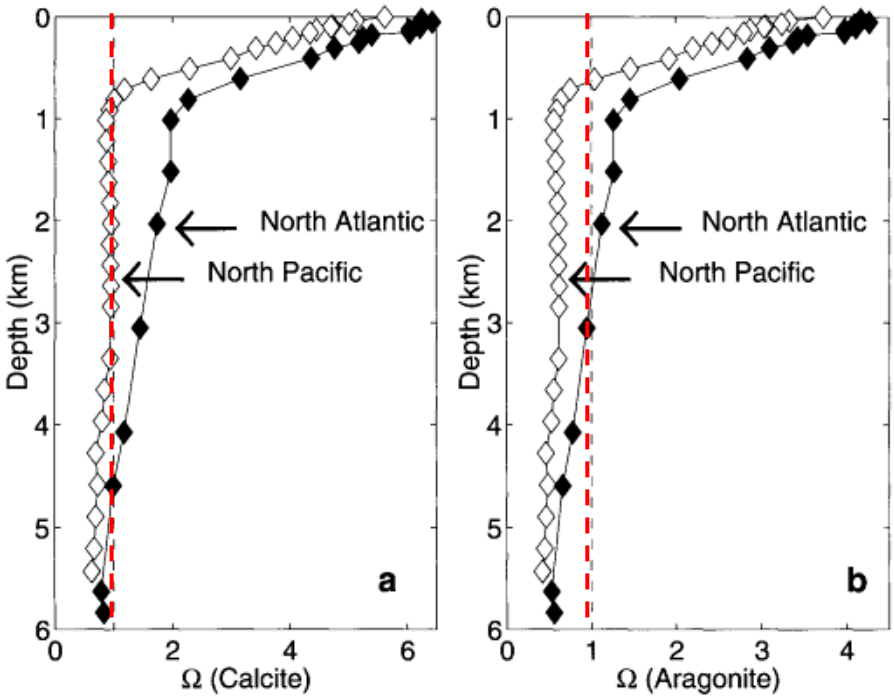

Figure 5. Saturation state of seawater Ω with respect to calcite and aragonite as a function of depth in the Atlantic and Pacific basins. The red line indicates Ω = 1, below which the calcium carbonate will dissolve. From Zeebe and Wolf-Gladrow (2001).

2.10. What are the effects of anthropogenic CO_2 on physical, chemical and biological carbonate chemistry?

Changes in pCO_2, carbonate chemistry and pH due to anthropogenic CO_2 production and ocean acidification (Figure 6) will have effects on both chemical and biological systems in all ecosystems across the globe, the overall results of which are difficult to project.

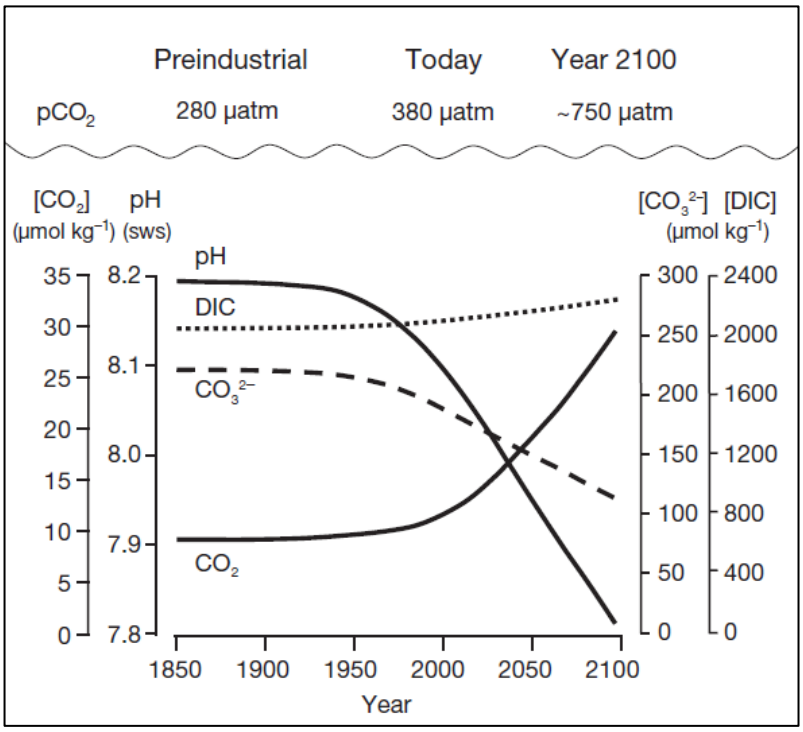

Figure 6. Projected changes in surface ocean carbonate chemistry in response to increasing atmospheric pCO_2. Modified from Wolf-Gladrow *et al.* (1999)

In 1957 it was determined by Revelle and Suess (1957) that the time a molecule of CO_2 spent in the atmosphere was 10 years before it dissolved in the ocean, and that the amount of CO_2 the ocean was able to assimilate (without large change in pH) was limited. The fractional change in pCO_2 over the fractional change in DIC is known as the Revelle Factor (R) (Broecker *et al.*, 1979; Egleston *et al.*, 2010). This is calculated as:

$$R = \delta \ln[pCO_2] / \delta \ln DIC \qquad 16$$

Current calculations of R show values of around 9 in low-latitude tropical waters and up to 15 in the Southern Ocean near Antarctica: these values are one unit higher than in the pre-industrial ocean due to the uptake of atmospheric pCO_2 (Egleston *et al.*, 2010). The R value is inversely proportional to the capacity for CO_2 uptake in ocean waters (Sabine *et al.*, 2004).

When pCO_2 in the atmosphere increase and additional CO_2 dissolves into the oceans, the oceanic pCO_2 changes are moderated by the buffering effect of the CO_3^{2-} forming bicarbonate. The additional H^+ within the system will lower the pH. However, the concentration of carbonate will decrease. As a direct result, oceanic absorption of CO_2 will result in a lowering of pH through the addition of CO_2 to the system, resulting in a pH change of up to 0.77 units (1900 µatm CO_2 in the year 2300), which is significantly larger than any previous change in the past 300 million years (Caldeira and Wickett, 2003).

2.10.1. What are the direct effects of carbonate chemistry changes on marine biota and community composition?

Marine organisms are very closely linked with the external water pH and DIC concentration within the body tissues, which will affect different physiological aspects such as growth, survival, settlement, competition and reproduction. An increase in surface water pCO_2 will be encouraging for autotrophic growth due to the increased availability of inorganic carbon and dissolved CO_2 and the lowered likelihood of RubisCO limitation (Hein & Sand-Jensen 1997; Riebesell *et al.*, 2007; Rost *et al.*, 2008). However, as most phytoplankton already utilise CCMs to ensure sufficient DIC for RubisCO requirements, the expected rise in productivity is not likely to occur, and more likely is a down-regulation of CCM activity within the phytoplankton in response to increasing CO_2 (Giordano *et al.*, 2005). However, the projected decrease in pH levels will also affect intracellular membrane potential and enzyme activity within the cell, which will have knock-on effects on the overall cell fitness and survival rate (Beardall and Raven, 2004). Experimental data on the direct effects of pH on the growth of phytoplankton does not show a clear trend as to the effects. Laboratory studies on monocultures of different *E. huxleyi* strains have shown increased (e.g. Dong *et al.*, 1993; Sciandra *et al.*, 2003), decreased (e.g. Barcelos e Ramos *et al.*, 2010; Iglesias-Rodriguez *et al.*, 2008) and unchanged (e.g. Spielmeyer and Pohnert, 2012) growth rates, with similar results for both calcification and carbon fixation (these experiments and their trends will be discussed in further detail in Chapter 4 of this thesis). Other experiments on *Trichodesmium* (Barcelos e Ramos *et al.*, 2007; Hutchins *et al.*, 2007) showed increased nitrogen and carbon fixation under elevated CO_2, while *Chlamydomonas* adapted over 1000 generations to elevated CO_2 with higher rates of photosynthesis and respiration than those grown at ambient CO_2 (Collins and Bell, 2004). Similar effects were identified in the diatom *Phaeodactylum tricornutum*, where growth and carbon fixation were elevated after acclimation to high CO_2 (Wu *et al.*, 2010), but with a corresponding photoinhibition of photosystem II. The interplay of multiple environmental parameters is investigated further in Section 3.

Additional changes within the phytoplankton cell can include changes to the nutrient stoichiometry, although changes in CO_2 availability may also adversely affect the production of dissolved organic matter, particularly in the increased production of transparent exopolymer particles (TEP; Engel, 2002; Galgani and Engel, 2013).

The associated changes in pH may have different effects on different phytoplankton species in terms of their growth rates and physiology. Berge *et al.*(2010) found few changes in the growth rates of 8 individual species of phytoplankton, including representatives of the

diatoms, dinoflagellates, cryptophytes and haptophytes. Natural variations in pH on several different scales will expose phytoplankton to lower (and higher) pH over the long and short-term. These variations include upwelling regions of high CO_2/ low pH waters (Berge *et al.*, 2010), and mixing with freshwaters in estuaries (Hinga, 2002)and inland seas such as the Baltic Sea (Omstedt *et al.*, 2010). Exposure to different natural pH variations will allow phytoplankton to adapt to changing conditions: many phytoplankton show a wide range of pH in which growth is successful, with several species showing the ability to continue to grow in pH far below that projected by climate models for surface oceans in 2100 (Berge *et al.*, 2010).

Although the effect of increased CO_2 on primary production is important, of equal importance is the effect of CO_2 on the transfer of energy through the trophic levels, from the heterotrophs and zooplankton that feed directly on the phytoplankton in the water column, up through the food web. Studies on zooplankton community in mesocosm studies have shown little effect of CO_2 on zooplankton community structure (Aberle *et al.*, 2013; Niehoff *et al.*, 2013; Suffrian *et al.*, 2008). The main effect on the zooplankton community structure was the food availability and phytoplankton composition, which showed clear trends with CO_2. However, despite these changes, Aberle *et al.* (2013) found relatively few differences between microzooplankton populations within a series of nine mesocosms at different pCO_2.

The majority of zooplankton within the water column are planktonic stages of benthic and pelagic macrofauna, including molluscs and other invertebrates, fish and corals. There is evidence that decreased pH can affect the fertilisation success and survival rates of planktonic larvae, and affect the contribution of the larval form to the adult population. Some examples include:

- Parker *et al.*(2010) studied two oyster species and determined that *Crassostrea gigas* may outcompete *Saccostrea glomerata* due to its greater success of embryo development during elevated CO_2, with fewer malformed embryos, and as a result shift the distribution of both species around the coast of Australia.
- Sea urchin *Tripneustes* showed an overall decrease in the size of settling larvae, which would have important impacts on the adult population (Sheppard Brennand *et al.*, 2010).
- Settlement and larval survival of *Acropora* corals were not affected by lowered pH in laboratory studies (Suwa *et al.*, 2010).
- Both corals (*Balanophyllia europaea* and *Cladocora caespitosa*) and molluscs (*Mytilus galloprovincialis* and *Patella caerulea*) transplanted to natural CO_2 vents grew better at low pH (Rodolfo-Metalpa *et al.*, 2011).

- Atlantic herring (*Clupea harengus*) showed no effect on embryo development or hatching rate, however there was an increase in RNA production, leading to decreased protein biosynthesis, and subsequently the metabolic processes within the larvae (Franke and Clemmesen, 2011).

It is clear in many of these laboratory studies that longer term experiments are required to study the effects of adaptation to the changed conditions. Some of the questions posed can be answered by the use of natural pCO_2 gradients, such as those found at hydrothermal vent sites or natural CO_2 seeps, as these can be associated with an equivalent doubling of atmospheric pCO_2 (Rost *et al.*, 2008). Studies on a natural site in Ischia, Italy, showed that subtidal communities shifted from abundant calcareous organisms to communities lacking scleractinian corals and lowered sea urchin and coralline algal abundance (Hall-Spencer *et al.*, 2008), and over the entire site the community structure was predominantly those organisms showing resilience to elevated CO_2. In addition, changes were noted in the settlement of benthic invertebrates (Cigliano *et al.*, 2010), cover and diversity of macroalgae (Porzio *et al.*, 2011) and the assemblages of foraminifera from calcified to agglutinated (Dias *et al.*, 2010). These types of natural experiment allow time for the development of direct chronic effects of acidification over long timescales, as well as the indirect effects on entire ecosystems (Barry *et al.*, 2010). A number of meta-analyses of available datasets indicate either mixed or overall negative responses, on factors such as survival, growth and reproduction (Harvey *et al.*, 2013; Kroeker *et al.*, 2010, Ross *et al.*, 2011). Unsurprisingly, the effects were larger in calcifying organisms, and varied between organisms using the two different forms of calcium carbonate (Kroeker *et al.*, 2010).

This exposure of more than a single species to the CO_2 perturbation can also be studied through the use of mesocosm experiments, although the timescale of these experiments is still limited in relation to the natural CO_2 sites. The existing literature on mesocosm experiments will be covered in Chapter 3 of this thesis, and includes shift in primary productivity and community structures with increasing pCO_2, as well as some effects on larval organisms and zooplankton.

2.10.2. What are the effects of carbonate chemistry changes on marine calcification?

As previously shown, an increase in pCO_2 will affect the carbonate saturation depth, bringing the depth at which $CaCO_3$ starts to dissolve to shallower waters across the globe for both aragonite and calcite. Models run by Orr *et al.*(2005) based the IS92A Scenario, show surface

ocean pH levels will be 0.3-0.4 units lower by 2100, translating to a 100-150% increase in H^+ concentration. Carbonate levels in the Southern Ocean in 2100 will drop below the aragonite saturation threshold throughout the water column, with the calcite saturation horizon rising closer to the surface. Tropical waters would reach a 45% reduction in carbonate relative to pre-industrial levels. This has severe consequence for marine calcifying organisms, which will find it increasingly energetically challenging to produce new $CaCO_3$ (Wood *et al.*, 2008), as well as suffering dissolution of the material already present (Gattuso and Buddemeier, 2000). This is especially true for cold-water corals which provide significant habitats for fish and other commercially important species (Orr *et al.*, 2005). However, a decrease in calcification could also result in lower calcification-based CO_2 production (equation 13) which could result in increased CO_2 storage capacity in the upper oceans (Gattuso & Buddemeier 2000).

Almost all organisms that have a saturation-state response to increasing CO_2 depend on photosynthesis (Gattuso and Buddemeier, 2000), either themselves or through photosynthetic symbiosis (i.e. corals). Surface-dwelling photosynthetic microalgae such as the calcite-forming coccolithophores are of less risk of dissolution near the calcite saturation horizon, and produce calcite in association with photosynthesis. Decreasing calcification has been reported in a number of studies using *E. huxleyi* and *Gephyrocapsa oceanica*, along with increasing numbers of deformed coccoliths and incomplete coccospheres (Nimer and Merrett, 1992; Riebesell *et al.*, 2000; Sciandra *et al.*, 2003). Bach *et al.*, (2013) reported further work to untangle the complex interplay of photosynthesis and calcification in *E. huxleyi*, and determined that *E. huxleyi* growth was sensitive to low CO_2 (for growth and PHS), and low bicarbonate (for calcification), but tolerated relatively low pH levels, along with elevated CO_2 and bicarbonate. It was determined that calcification in this example did not function as a CCM, but was inhibited at low DIC to allow redistribution of DIC from calcification to PHS. An associated study found that increasing coccolith malformations in *E. huxleyi* in CO_2 ranging from 20 to 6000 µatm suggest that the increase in H^+ is the main factor responsible for coccolith malformation, but variations in HCO_3^- might also be responsible for changes in coccolith size (Bach *et al.*, 2012).

In a mesocosm study, Engel *et al.* (2005) found physiological differences in growth of *E. huxleyi* at lower pH, with smaller coccoliths and coccosphere sizes and associated reduced calcification rate, although there was no change in population density. Despite the reduction in calcification, no associated reduction in net primary productivity was noted during the bloom (Delille *et al.*, 2005), however, a second mesocosm experiment performed under similar conditions found no change in net calcification in *E. huxleyi*. During this experiment it was noted that overall particulate inorganic carbon (PIC) was low.

As mentioned previously, coccolithophores are one of the most significant calcifiers in the ocean, and bloom decline of *E. huxleyi* can transfer high volumes of $CaCO_3$ and fixed carbon to the deep ocean. Grazing on *E. huxleyi* cells can also produce significant $CaCO_3$ waste, in both general detritus and zooplankton faecal pellets. Any change in calcification within the *E. huxleyi* population in the surface oceans will have significant impact on the flux of material to deeper waters, but also, the shallower depth of the calcite saturation horizon will dissolve this material before it reaches depth, allowing carbonate to be recycled into the surface water instead of being stored (Engel *et al.*, 2005).

E. huxleyi are not the only calcifiers that have strong links to photosynthesis: coralline macroalgae and coral reefs also depend on autotrophy, and are also subject to the same problems with calcification, with the added problem of being unable to avoid exposure through movement to different geographical areas. Coral reefs are considered to be one of the most diverse and complex marine environments, all built on a calcium carbonate skeleton, with production estimated at 1500 g m^{-2} per year for the entire reef complex (Smith, 1978). Studies by Gattuso *et al.* (1998) found that aragonite calcification in five colonies of the zooxanthellate coral *Stylophora pistillata* decreased as aragonite saturation decreased from 500 to 98%, and supposed that any change to the aragonite saturation as a result of anthropogenic CO_2 addition would decrease calcification further. Their studies showed that *Acropora* species followed the same trend. Projections of atmospheric pCO_2 exceeding 450 µatm will result in terminal decline of the global reef systems through coral bleaching and reduced calcification, and subsequent losses of biodiversity and economic value to the human populations dependant on the reefs (Veron *et al.*, 2009). A study investigating the coral calcification rates in a naturally occurring high CO_2 environment found that corals were unable to grow in pH of 7.8 (as projected for the year 2100) due to the increased metabolic costs associated with the lower pH (Rodolfo-Metalpa *et al.*, 2011), and that increased temperatures exacerbated the situation further.

Although the projections for future calcium carbonate production and dissolution based on the existing studies seem to have dire consequences, there is a great deal that is yet unknown about the calcification processes in different organisms. Some organisms may be able to better control pH near calcification sites and under differing conditions, and may be better equipped to cope with the effects of acidification (Berry *et al.*, 2002), while others may be able to increase calcification in response to rising pCO_2 (Gutowska *et al.*, 2008).

3. The effect of increasing multiple stress factors on marine organisms and ecosystems

Different ecosystems are likely to be affected by acidification to differing degrees, and acidification is not the only factor affecting these ecosystems; temperature, pollutants, hypoxia and stratification and changes to light penetration are also having an effect. Coastal seas are already impacted by additional nitrogen and sulphur depositions, nutrient inputs and the mixing of river water, all of which affect the alkalinity. Many coastal environments are habitats for invertebrate larval development, including echinoderms, brittlestars and bivalves, although variations in response are likely due to differences in calcification mechanisms and adaptation to low alkalinity waters (Hofmann *et al.*, 2010). The effects of these multiple stressors are often difficult to project from single factor experiments.

Increasing atmospheric pCO_2 does not just have an impact on the pCO_2 of surface waters: global annual average sea surface temperatures (SST) have increased by 0.89°C since the beginning of the 20th Century, with all ten of the warmest years on record occurring since 1997 (Hartmann *et al.*, 2013). This increasing temperature will affect the CO_2 uptake, but will also affect the geographical temperature ranges in which organisms are able to survive, and affect physiology, abundance and community composition (Hughes, 2000). Combined together, elevated temperature and pCO_2 are likely to impact organisms to a greater degree than individually. There is evidence from the laboratory that the effect of temperature has a positive effect on phytoplankton growth, and often combines with the positive effect of elevated CO_2 (Arnold *et al.*, 2013; Feng *et al.*, 2008). There have, as yet, been no community studies on the combined effects of CO_2 and temperature, but it is well documented that temperature stress can cause expulsion of the zooxanthellae in corals (coral bleaching; Gates *et al.*, 1992) and the CO_2 effect can cause decreased aragonite saturation in tropical waters and potential dissolution of the reef structure.

It is likely that increases in nutrient concentration are unlikely to affect overall primary productivity within different communities, but the addition of CO_2 into the system could influence the community structure into a shift to new dominant species. However, it is likely that nutrient depletion will still occur in the mid-oceans, and in this situation Sciandra *et al.*, (2003) identified that *E. huxleyi* would show lower calcification but also a decrease in gross community production.

4. Cycling of sulphur from and within the marine environment: the importance of Dimethylsulphide

4.1. Introduction to the marine sulphur cycle

Oceanic sulphur plays an important role in the biogeochemical cycling of the element, both dissolved and in sedimentary mineral form. Sulphur is available in a range of oxidation states: from sulphide and reduced organic sulphur (-2 valence state) to the most stable form, sulphate (+6 valence state; Sievert *et al.*, 2007). Cycling of sulphur through the atmosphere, oceans, land and sediments is by a range of processes, with volatile organic compounds such as dimethylsulphide (DMS) transporting sulphur from the oceans to the atmosphere, where breakdown in the atmosphere can affect climate variability through the formation of cloud condensation nuclei (CCN; Figure 7). In biological systems, sulphur is an important element in protein production, as well as lithotrophy (Ghosh and Dam, 2009).

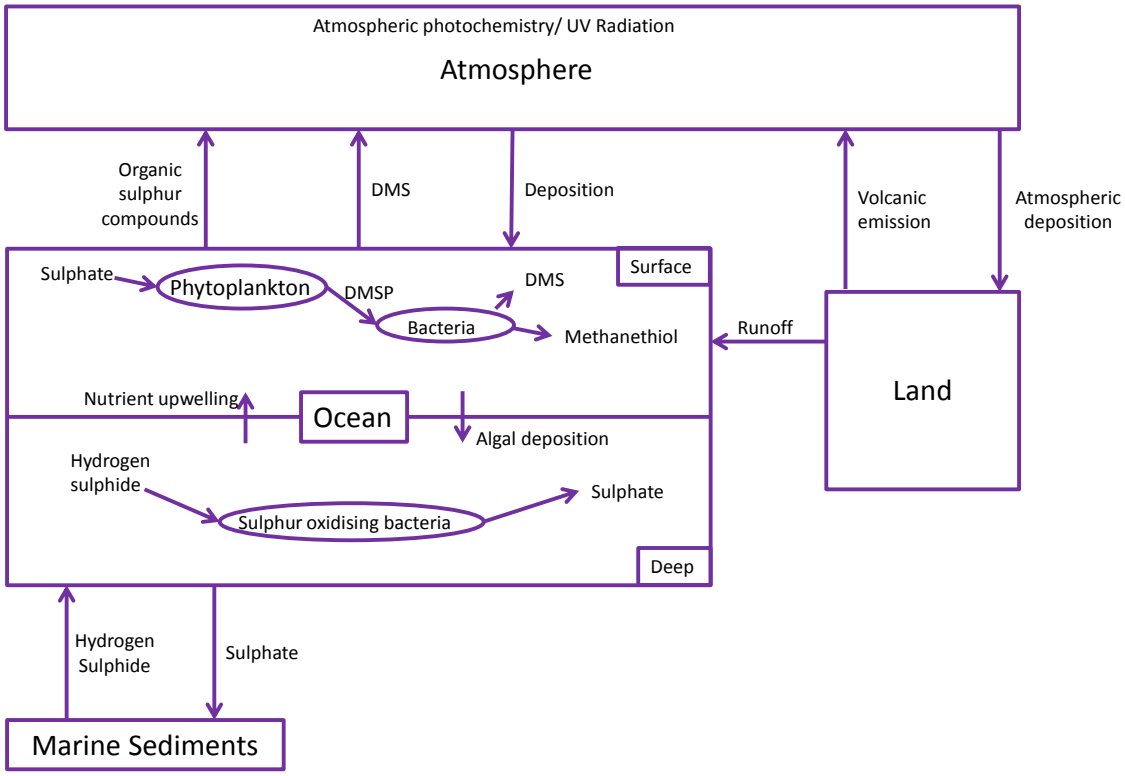

Figure 7. Simplified diagram of the global cycling of sulphur compounds, focussing on the oceanic processes. Adapted from Sievert *et al.* (2007).

DMS was identified by Lovelock *et al.* (1972) as a naturally produced sulphur compound which is the principle route by which sulphur transfers from the sea to the marine atmosphere, and which fills the role originally ascribed to H_2S. In 1987, a hypothesis was proposed in which DMS held an important role in climate regulation (Charlson *et al.*, 1987), in which production of

DMS on both local and global scales encouraged climate feedbacks which negatively affected further DMS production. Although this hypothesis has never been proven either way (Halloran *et al.*, 2010), it is of no argument that DMS related sulphur-flux is important: the most recent model estimates of sea-to-air sulphur flux through DMS were 28.1 Tg S yr^{-1} (Lana *et al.*, 2011).

DMS is produced globally, but production varies both spatially and temporally on timescales of minutes to months. On shorter timescales, DMS concentrations are seen to increase at night (Hewitt and Davison, 1997; Visscher *et al.*, 2003) or through short-term changes in physic-chemical environments in the surface ocean (Simó, 2004). In the longer term, distinct differences in DMS concentrations measured in winter and summer have been detected: mean summer concentrations around the British Isles were measured at 2200 ng S (DMS) L^{-1}, compared to 4 ng S (DMS) L^{-1} in winter (Turner *et al.* 1988), and these patterns are replicated in the Baltic Sea (Leck *et al.*, 1990) and the Arctic (Levasseur, 2013). Development of the Global Surface Seawater DMS Database allowed the calculation of mean monthly DMS concentrations on a global scale, which show consistently higher DMS concentrations in Summer, in particular in the North Atlantic, as well as around the Antarctic coastline and north Pacific Ocean (Kettle *et al.*, 1999; Lana *et al.*, 2011). This has led to the development of what is known as the DMS Summer Paradox: DMS is only weakly associated with standard measures of primary productivity, such as chlorophyll-*a* and has maximum concentrations in the Summer months when chlorophyll-*a* and related primary productivity is relatively low (Toole *et al.*, 2003).

DMS has a wide range of biological effects, including acting as a chemoattractant for both zooplankton as well as larger organisms such as penguins (*Spheniscus demersu*s; Wright *et al.* 2011), and has even been suggested as facilitating a tri-trophic interaction between Southern Ocean krill (*Euphasia superba*) and procellariiform seabirds (Savoca and Nevitt, 2014).

4.2. Sources of DMS

The majority of marine DMS originates from the degradation of dimethylsulphoniopropionate (DMSP), a compound produced by certain (but not all) marine phytoplankton (Caruana *et al.*, 2012; Franklin *et al.*, 2010), corals (Van Alstyne *et al.*, 2006) and macroalgae (Stefels, 2000). Additional sources of DMS include the reduction of dimethylsulphoxide (DMSO), an oxidation product of DMSP and DMS, but also produced by phytoplankton, and also direct phytoplanktonic release from the breakdown of DMSP and DMSO within the cell. The pathways of DMS production are shown in Figure 8.

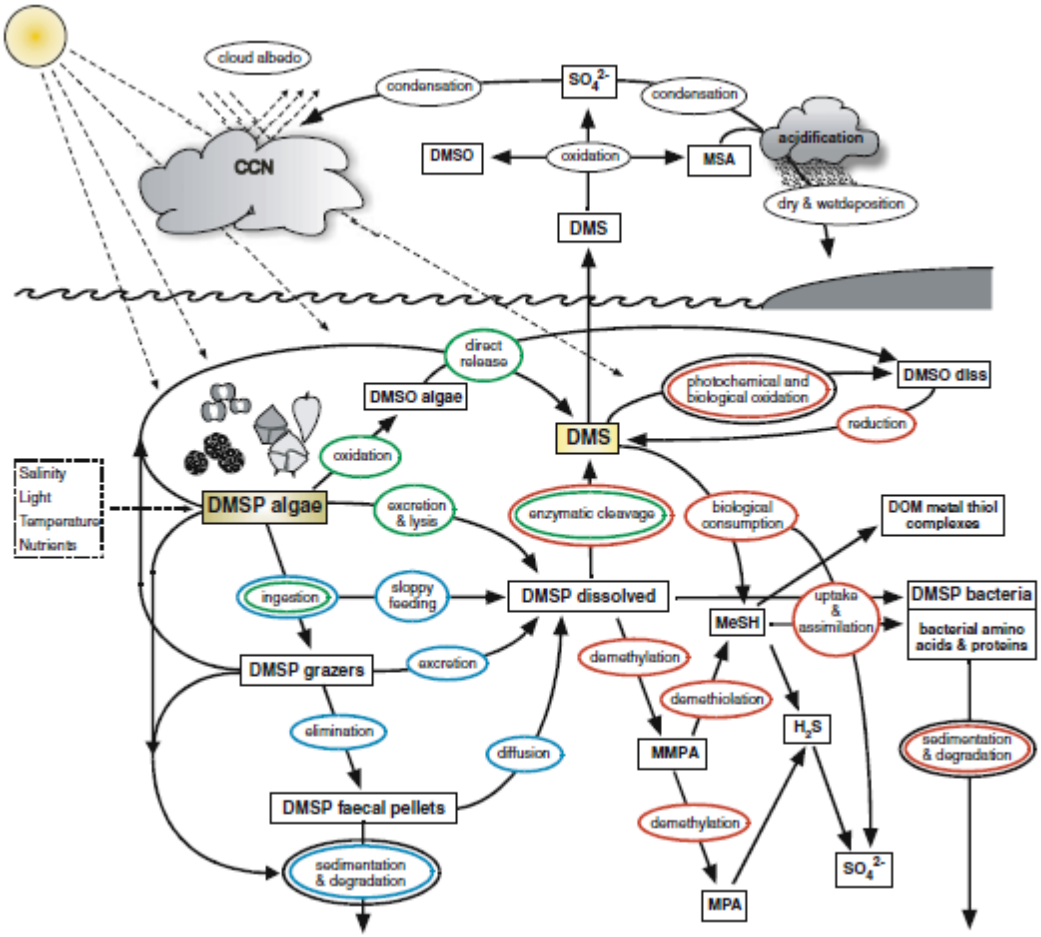

Figure 8. Simplified diagram of the marine sulphur cycle, as described by Stefels *et al.* (2007)

Of prime focus during this investigation was DMSP production from marine phytoplankton, of which the major producing groups are the dinophyceae and prymnesiophyceae (Keller, 1989). Intracellular DMSP can vary between zero and 1-2 mol L^{-1} in some dinoflagellates (Caruana *et al.*, 2012; Keller, 1989). More typical values are 50-500 mmol L^{-1}. A major DMSP producing group within the prymnesiophyceae are the coccolithophores, which are covered in Section 4.7.

Some members of Chrysophyceae and Bacillariophyceae (diatoms) can also produce significant amounts of DMSP (Stefels, 2000), as well as some cyanobacteria such as *Trichodesmium* spp. (Bucciarelli *et al.*, 2013). In general, diatoms are considered poor producers of DMSP, with low intra-cellular DMSP content (Vila-Costa *et al.*, 2006). Some DMSP has also been found in terrestrial plants, mainly those located near marine environments in salt-tolerant angiosperms such as *Spartina* spp. (Pakulski and Kiene, 1992), as well as in marine corals where DMSP is an indicator of zooxanthellae expulsion (Fischer and Jones, 2012). It is also an indicator of membrane damage in coralline algae (Burdett *et al.*, 2012).

The production of DMSP has been suggested for a range of purposes: As an osmoregulatory compound (Ackman *et al.*, 1966), a grazing defence (Wolfe *et al.*, 1997), a cryoprotectant (Kirst *et al.* 1991) as anti-oxidant protection (Sunda *et al.*, 2002) or mechanism of overflow of sulphur compounds (Stefels, 2000). A debate has arisen around the latter two roles of DMSP and the arguments for and against each view is described in Sections 4.2.4 and 4.2.5.

4.2.1. The role of DMSP as an osmoregulatory compound

During axenic culture experiments, variations in intracellular DMSP in the coccolithophore *Hymenomonas carterae* were detected within hours of transfer into a medium of different osmotic pressure (Vairavamurthy *et al.*, 1985). This, and noted changes in DMSP content in *Ulva lactuca* under changes in salinity (Dickson *et al.*, 1980) suggest an osmoregulatory function for DMSP. DMSP has a similar structure and chemical behaviour to other known osmolytes such as glycine betaine, but may be preferred to these in nutrient poor environments (Andreae, 1990).

4.2.2. The role of DMSP as defence against grazing

Grazers are an important method of release of DMSP into the dissolved phase, through the consumption of phytoplankton and 'messy feeding' (Johnston *et al.*, 2008). However, the production of DMSP may itself be triggered by grazing activity as a defence mechanism, causing grazers to actively avoid high DMSP-containing cells (Strom *et al.*, 2003; Wolfe *et al.*, 1997). Feeding rates of protists were also decreased upon addition of DMSP to a culture (Fredrickson and Strom, 2009).

4.2.3. The role of DMSP as a cryoprotectant

Sea-ice algal blooms underneath the ice cover are often accompanied by very high concentrations of DMSP (up to 12000 nmol L^{-1}; Levasseur *et al.*, 1994), and sea-ice brines contain concentrations of dissolved DMSP over 200 nmol L^{-1} (Asher *et al.*, 2011). DMSP content has been found to be higher in the Arctic than in temperate latitudes, indicating a vital role for this and related sulphur compounds at lower temperatures (Lee *et al.*, 2001).

4.2.4. The role of DMSP as an anti-oxidant

Oxidative stress is defined as the production and accumulation of Reactive Oxygen Species (ROS) beyond the organism's ability to quench them (Lesser, 2006). These species include

singlet oxygen $^1O_2$, superoxide radicals O_2^-, hydrogen peroxide H_2O_2, reactive nitrogen species such as $NO^\bullet$ and hydroxyl radicals $OH^\bullet$. ROS are produced in the cell 'machinery': chloroplasts, peroxisome, membrane and mitochondria during normal cell operations, and the majority are removed by Superoxide Dismutase and other enzymes, but these are often metal limited and do not remove the $OH^\bullet$ (Lesser, 2006). If left unchecked, ROS production will damage DNA, lipids and proteins within the cell, and eventually cause cell death.

The case for DMSP as an anti-oxidant is twofold: Sunda *et al.* (2002) demonstrated that DMSP and its breakdown products, including DMS, readily scavenge hydroxyl radicals, and concentrations of DMSP and DMSP-lyase can be seen to increase under periods of physiological stress, and implied oxidative stress. High DMSP content within cells at all times may prevent the development of oxidative stress.

Examples for this theory are:

- Oxidative stress is common in intertidal macroalgae regularly exposed to the air during low tide (Collen and Davison, 1999), but also in phytoplankton through exposure to less than ideal growth conditions
- Oxidative stress can lead to bleaching of corals by zooxanthellae exocytosis from the coral cell hosts (Lesser, 1997) or by aptosis (Lesser and Farrell, 2004).

This hypothesis does not exclude DMSP from functioning in other suggested roles. However, for the anti-oxidant function to be the primary purpose of DMSP production, it is expected that DMSP is synthesised close to the source of ROS, and extremely rapidly under periods of oxidative stress. As yet, it is unknown where in the cell the majority of DMSP is synthesised.

4.2.5. The role of DMSP as a sulphur overflow mechanism

However, in counter to this argument is that DMSP is not always produced immediately following periods of physiological (and therefore implied oxidative) stress. Stefels (2000) demonstrated that DMSP was more effective at acting as an overflow mechanism for cysteine and methionine production, due to DMSP concentrations being more closely linked to carbon fixation than stress responses. Further to this, an increased DMSP concentration may save on the cells nitrogen requirement (Stefels, 2000), which will infer advantages over competitors.

4.2.6. Biological synthesis of DMSP

In addition to being species- specific, algal DMSP cell concentration is influenced by environmental factors such as salinity (Vairavamurthy *et al.*, 1985) , temperature (Spielmeyer

and Pohnert, 2012), light (Miles *et al.*, 2012; Ruiz-gonza *et al.*, 2013) and nutrients (Gröne and Kirst, 1992; Sunda *et al.*, 2002). During the growth and decline of phytoplankton blooms, release of dissolved DMSP occurs mainly through cell autolysis during the senescent phase of growth (Nguyen *et al.*, 1988), but also through cell damage from zooplankton grazing (Dacey and Wakeham, 1986).

DMSP has been identified as having three distinct biosynthesis pathways, each involving either methylation or transamination of methionine (Stefels, 2000). Several factors influence DMSP production, including light stimulation (not dependency), salinity (which reinforces the theory of it being an osmolyte), temperature (reinforcing the theory of cryoprotection) and nitrogen limitation (as a potential replacement for Glycine Betaine due to the similar molecular structure) (Challenger, 1951).

4.2.7. DMS production from the breakdown of DMSP

Two separate pathways were identified for DMSP breakdown: the demethylation/ demethiolation pathway to produce methanethiol (MeSH) (Kiene *et al.*, 1999; Reisch *et al.*, 2011) and the cleavage pathway to produce DMS and acrylate. Further investigations using identification of gene functions has identified a third pathway during which DMS is produced alongside 3-hydroxypropionate (3HP) instead of acrylate (Curson *et al.*, 2011; Souza and Yoch, 1995; Todd *et al.*, 2010).

The first pathway is the demethylation of DMSP mediated by the dmdA (DMSP demethylation) protein to methylmercaptopropionate (MMPA) identified in the Roseobacter and SAR11 taxa (Howard *et al.*, 2006; Reisch *et al.*, 2008) and is estimated to be the route via which 80% of DMSP is removed from the marine environment and the major sulphur source for bacterioplankton (Kiene *et al.*, 2000). Through the operation of this pathway, it has been suggested that marine bacteria regulate the flux of DMS-based sulphur to the atmosphere by consumption of DMSP through the demethylation pathway, by converting the sulphur into alternate non-volatile sulphur-containing compounds (Howard *et al.*, 2006; Kiene *et al.*, 2000).

Of most importance to this work are the DMS-producing (Ddd: DMSP dependent DMS) cleavage pathways, brought about by two routes. The DddD enzymes generate 3HP and DMS (Todd *et al.*, 2007), and at least 5 identified enzymes (DddP, DddL, DddQ, DddW and DddY) that act in the role of 'DMSP-Lyase' and cleave DMSP into acrylate and DMS (Table 2; Johnston *et al.*, 2008; Todd *et al.*, 2007 Curson *et al.*, 2011).

Table 2. Projected functions of Ddd gene products in different bacterial groups. Adapted from Curson *et al.* (2011).

Protein	Reaction Catalysed	Distribution
DddD	DMSP cleavage to DMS and 3HP	Often found in bacteria that grow well on DMSP as sole carbon source.
DddP	DMSP cleavage to DMS and acrylate, plus a proton	Mainly in Roseobacters
DddL	DMSP cleavage to DMS and acrylate, plus a proton	Marine alphaproteobacteria, mainly Roseobacters
DddQ	DMSP cleavage to DMS and acrylate, plus a proton	Exclusive to Roseobacters
DddW	DMSP cleavage to DMS and acrylate, plus a proton	Exclusive to 2 strains of Roseobacters
DddY	DMSP cleavage to DMS and acrylate, plus a proton	Sporadic occurrence in beta- gamma- delta- and epsilonproteobacters

The 'DMSP-lyase' enzymes have been projected globally in both phytoplankton and marine bacteria. DMSP cleavage in the phytoplankton takes place both intra and extra-cellularly (Stefels and van Boekel, 1993; Wolfe and Steinke, 1996). Little is known about the location of the DMSP-lyase enzymes within the cell, and especially their location in relation to DMSP production (which is also unknown). This information is important in determining if the two can come into contact during normal cell operations, or if it is only during cell damage or lysis. DMSP can be identified in one of two forms: DMSP particulate is the DMSP considered within the cells themselves and DMSP dissolved is the free DMSP in the water column available for bacterial breakdown. It has been proven in cultures of the flagellate *Phaeocystis pouchetti* that exposure to strain-specific viruses can increase DMS levels four-fold after the cells lysed (Malin *et al.*, 1998).

4.2.8. DMS production from sources other than DMSP

In the terrestrial environment, half of DMS production (approximately 1.5 Tg a^{-1}) was derived from tropical forests (Watts, 2000). There are some additional anthropogenic sources of DMS as products of the wood pulping process in the paper industry. These sources tend to be of more concern to local environments and not global budgets (Schäfer *et al.*, 2010). An alternative DMS production pathway is through the reduction of dimethylsulphoxide (DMSO) by a wide variety of micro-organisms in the marine environment, most notably bacteria (Gonzalez *et al.*, 1999; Spiese *et al.*, 2009; Zinder and Brock, 1978), although direct

measurements in this area are sparse. DMSO reduction was recently identified as a major pathway of DMS production in Antarctic sea ice (Asher *et al.*, 2011).

4.3. DMS loss processes and sinks

DMS produced in the upper water column is broken down by two mechanisms: abiotic (Brimblecombe and Shooter, 1986) and microbial degradation (Kiene and Bates, 1990; Schäfer *et al.*, 2010). Very approximately 10% of DMS produced passes through the sea-surface microlayer into the atmosphere (dependant on wind speed and gas transfer velocity; Nightingale, 2009). The atmospheric component of DMS is discussed further in Section 4.4.

4.3.1. DMS loss by photochemical breakdown

Abiotic methods of DMS loss from the surface oceans include oxidation by metal ions, photochemical oxidation and adsorption onto suspended sediment (Brimblecombe and Shooter, 1986). This latter process will cause the removal of DMS out of the surface waters as particles sink into the deep oceans. Laboratory experiments showed that irradiation alone did not cause DMS breakdown, however oxidation to DMSO was rapid in the presence of photosensitisers such as chromophoric dissolved organic matter (CDOM; Toole *et al.*, 2003). Estimates by Taalba *et al.* (2013) in the Arctic showed that photooxidation was comparable to the DMS loss by ventilation to the atmosphere at approximately 21% of gross DMS loss, indicating that this is a significant sink for DMS.

4.3.2. DMS loss by microbial breakdown

Aerobic microbial degradation utilises DMS as a sulphur and carbon source (Kiene *et al.*, 2000; Visscher and Taylor, 1993), with the associated production of methanethiol and formaldehyde (de Bont *et al.*, 1981) in the major bacterial groups hyphomicrobia or thiobacilli. Further studies using radioisotopes showed that assimilation of DMS was equal to that respired as CO_2 (Wolfe and Kiene, 1993). Additional roles of DMS are as part of the anti-oxidant processes of the cell, which were discussed in section 4.2.1, and concerns the conversion of DMS to DMSO (Sunda *et al.*, 2002). DMS loss to microbial processes is responsible for the majority of DMS removal from surface waters (Schäfer *et al.*, 2010).

4.4. Atmospheric cycling and climate regulation by sulphur compounds

In 1974, Lovelock & Margulis put forward the Gaia Hypothesis, whereby the 'total ensemble of living organisms which constitute the biosphere can act as a single entity to regulate chemical composition, pH and possibly climate.' Under this theory, cycling of chemical compounds such as carbon, sulphur and nitrogen are responsible for climate regulation: in particular, sulphur-containing biogenic gases such as DMS react in the atmosphere to produce particles which interact with the solar radiation field and affect climate (Shaw, 1983).

DMS production from the oceans is released into the atmosphere where it undergoes breakdown into sulphate and methane sulphonate (MSA) aerosols, alternatively known as non-sea-salt (NSS) sulphate aerosols (Charlson *et al.*, 1987), which act as CCN in the marine atmosphere. This production of NSS is dependent upon primary productivity and the production of DMS, and therefore a feedback loop is created whereby the climate changes will affect the production of DMS and vice versa. This is known as the CLAW hypothesis (Figure 9). Through this theory, the stress on the biological system was regulated by physical processes which alleviate the stressing conditions. In remote oceanic regions, marine emissions of DMS are thought to play an important climatic role by increasing the backscattering of solar radiation and by providing additional CCN (Falkowski *et al.*, 1992; Malin *et al.*, 1992).

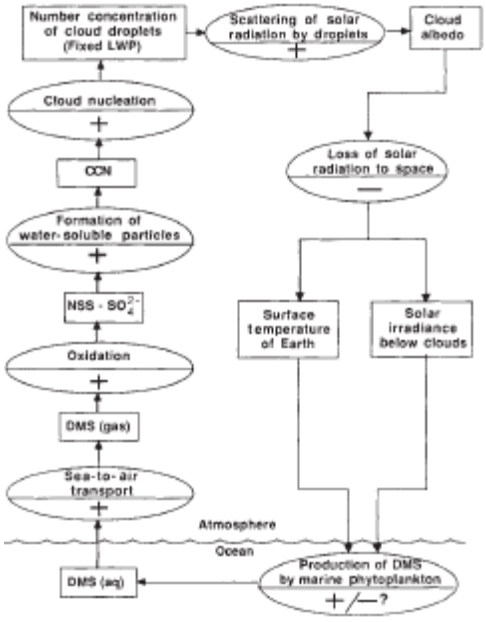

Figure 9. Diagram of the CLAW hypothesis. Taken from (Charlson *et al.*, 1987).

There has been much debate over the lack of evidence for the existence of the CLAW hypothesis, with Quinn & Bates (2011) declaring that DMS control over CCN 'probably does not exist', after reviewing the data from two decades of DMS analysis. However, a review by Halloran *et al.* (2010) discussed the need to incorporate realistic parameterisations of

phytoplankton production and microbial interactions with DMS into Earth System models, which requires increasing the observational evidence, in order to reject or confirm the hypothesis as it stands. DMS parameterisation in Earth System Models is discussed in Section 4.5.

4.5. Development of current DMS climatology

Suggested in 1992 during the first symposium focussed on dimethylsulphide (Commission of the European Communities, 1992), the Global Surface Seawater DMS Database has been developed which will allow comparison of new and existing DMS measurements, and allow development of models to better project DMS production, and likely changes under changing ocean conditions. In 1999, the first ~15000 measurements were used to develop a climatology to project DMS production alongside additional parameters such as DMSP, chlorophyll *a*, salinity and temperature (Kettle *et al.*, 1999). During this project, no significant correlation was found for DMS and any of these other parameters, but a map of sea-surface DMS was produced, limited by a paucity of DMS measurements. This climatology was updated in 2011, when the number of available DMS measurements had exceeded 47000, with new measurements in additionally severely under-sampled areas (e.g. Southern Indian Ocean; Lana *et al.*, 2011). Using the new climatology and the latest parameterisations for gas transfer velocity and wind fields, the global emissions were re-estimated at 17% higher than estimated in 1999, with production in the range 17.6 – 34.4 Tg of sulphur to the atmosphere annually.

4.6. *Emiliania huxleyi* as an important marine calcifier

There is a clear link between calcification and carbon fixation in *E. huxleyi*; experiments on strain Ch 24-90 isolated from the North Sea showed that bicarbonate is the major substrate for intracellular production of CO_2 for photosynthesis, with an additional bicarbonate splitting to donate a proton (Buitenhuis *et al.*, 1999). The remaining carbonate is used in calcite synthesis within the cell, and the subsequent production of coccoliths (Buitenhuis *et al.*, 1999; Nimer and Merrett, 1992). Support for HCO_3^- being the foundation for calcite synthesis was seen when high calcifying *E. huxleyi* cultures caused a decrease in DIC compared to a low calcifying culture (Dong *et al.*, 1993). Calcification has been suggested as a supplier of CO_2 for photosynthesis, allowing high calcifiers to survive in low CO_2 environments and allowing the cell to avoid the need for additional CCMs (Dong *et al.*, 1993; Nielsen, 1995; Paasche, 2001).

There is evidence that strongly suggests that calcification rates will decrease with increasing pCO_2 in surface waters, which will have an effect on the ratio of PIC: POC (Riebesell *et al.*,

2000; Sciandra *et al.* 2003). Lohbeck *et al.* (2012) found a 51% restoration in calcification with 500 generations adaption to CO_2, implying that adaptive evolution in the case of *E. huxleyi* is capable of keeping pace with climate change. However, there are also several examples of increases in calcification which have been identified (Iglesias-Rodriguez *et al.*, 2008; Shi *et al.*, 2009).

Coccolith formation is undertaken within the coccolith vesicle in the cell, and takes place in approximately an hour (Paasche, 1962). Calcifying cells produce many more coccoliths than required to cover the cell, resulting in the outermost coccoliths being shed into the water column (Paasche, 2001). In general it is the 10-20 detached coccoliths per *E. huxleyi* cell which cause significant lightening of the water column during a bloom scenario, and which are responsible for a significant proportion of the calcite transport to deep waters.

4.7. The coccolithophore *Emiliania huxleyi* as a key DMSP producer

As previously mentioned, DMSP is produced by certain groups of phytoplankton, one of which is the coccolithophores, a member of the prymnesiophyceae. This group is highly diverse in size and shape, each individual producing a calcite (calcium carbonate) skeleton comprised of multiple plates or 'coccoliths'. The purpose of the coccoliths is unclear, but they have been suggested as a form of grazing defence, an adaptation to light interception, and also to protect the integrity of the cell and surrounding micro-environment (Young, 1994). There is also evidence that production of calcium carbonate produces additional HCO_3^- for photosynthetic use (Feng *et al.*, 2008; Nimer and Merrett, 1992) or the idea that they are a cost-effective route of elevating the CO_2 concentration in the chloroplast (Anning *et al.*, 1996).

The globally distributed *E. huxleyi* (3-10 µm) species creates large-scale blooms visible from satellite imagery of temperate shelf seas (e.g. the North Sea shelf), and is found from the tropics to high latitude regions. Due to its role as the most productive calcifying organism on Earth, *E. huxleyi* has a huge impact on biogeochemical cycling, specifically cycling of carbon and transport of calcium carbonate to the deep oceans via the biological pump (Holligan *et al.*, 1993; Riebesell *et al.*, 2000).

E. huxleyi is known to have multiple cell-types in its life cycle: the coccolith-bearing C-cell, non-motile naked N-cells and flagellated motile S-cells (Klaveness, 1972; Lohmann, 1902). The C-cell is the most commonly observed, being the morphotype which causes the extensive blooms of *E. huxleyi*. Flow cytometry and fluorochrome staining of the different cell DNA showed that the S-cells were haploid in relation to the diploid state of the C-cells (Green *et al.*, 1996). The motile cells were capable of division, as were the naked, diploid N-cells and the calcified C-cells

(Klaveness, 1972). Non-motile N-cells exhibit the same morphological features as C-cells, including the coccolith apparatus, with a seeming inability to produce coccoliths, and are considered mutants to the calcified 'wild-type'. The S-cell is characterised by two flagella and organic scales on the cell surface (Paasche, 2001).

E. huxleyi is focussed on in this study as a significant producer of DMSP, as well as being a calcifier and therefore susceptible to the effects of ocean acidification. Much of the spatial variability in DMS production in coastal waters can be attributed to variations in *E.huxleyi* population density, as well as zooplankton grazing and bacterial or viral interactions with *E.huxleyi* cells (Avgoustidi, 2006), which release DMSP and allow bacterial interactions to form DMS.

5. Cycling of halocarbons from and within the marine environment

5.1. Introduction to halogen cycling

There are additional gases produced by marine organisms which are the main routes of halogen flux to the atmosphere. These include carbon compounds containing one or more atoms of iodine, bromine, chlorine or fluorine, and are known as halocarbons. Sources of halocarbons besides biogenic production include volcanic vents, geothermal processes and anthropogenic inputs. Halocarbons can be extremely volatile and highly reactive.

Halocarbons are important in biogeochemical cycles, and once in the atmosphere undergo a number of reactions including those important in ozone cycling. This investigation will focus on the concentrations of a number of halocarbons produced by phytoplankton, and the changes in production occurring as a result of elevated CO_2 and resulting ocean acidification. Table 3 gives an overview of the halocarbons studied in this investigation, with their chemical formulae and atmospheric lifetimes.

Table 3. Target Halocarbons and their atmospheric lifetimes. Taken from Montzka *et al.* (2011)

Compound	Chemical Formula	Atmospheric lifetime (days)
Iodocarbons		
Methyl iodide	CH_3I	7
Diiodomethane	CH_2I_2	0.003
Iodoethane	C_2H_5I	4
Iodopropane	$_{C3}H_7I$	0.5
Bromocarbons		
Bromoform	$CHBr_3$	123
Dibromomethane	CH_2Br_2	24
Mixed Halocarbons		
Dibromochloromethane	$CHBr_2Cl$	59
Bromoiodomethane	CH_2BrI	0.04
Chloroiodomethane	CH_2ClI	0.1

5.2. Synthesis of halocarbons

Seawater is rich in halide ions and provides ample source for biotic uptake into the cell: Saenko *et al.* (1978) presented percentages of bromine and iodine in seawater as 6.6 x 10^{-3} % and 5.1 x 10^{-6} %, respectively. Two biological production mechanisms exist for halocarbons: production of methyl halides by methyl transferases and production of polyhalogenated compounds by haloperoxidases (Manley, 2002; Theiler *et al.*, 1978; Wuosmaa and Hager, 1990).

Methyl halides are produced through the enzymatic methylation of Cl^-, Br^- or I^- by *S*-adenosyl-L-methionine (SAM) utilising methyl transferases (Wuosmaa and Hager, 1990). K_m (Michaelis – Menten constants) values for the methyltransferases and halides suggest that the latter are not the intended methyl acceptor and as a result, methyl halides may be a by-product of other metabolic processes, such as the production of polyketides, phenolics or steroids (Manley, 2002). It has also been suggested by Ni and Hager (1999) that methyl halide production is a method of excess halide excretion.

Polyhalomethanes are produced as an indirect result of haloperoxidase activity; in marine algae, bromoperoxidase and iodoperoxidase are found, with both able to oxidise I^- and the former able to oxidise Br^- also (Manley, 2002). In examination of the K_m for the halide reactions

with haloperoxidases shows them to be high, indicating low affinity of the active site for halides in comparison to H_2O_2. This suggests a major function of halocarbon production is to act as an antioxidant system (Butler and Carter-Franklin, 2004; Pedersen *et al.*, 1996). Antioxidant activity within marine phytoplankton has been described in Section 4.2.4 for DMS, and it is encountered in intertidal macroalgae on a regular basis when they are exposed during low tides (Collen and Davison, 1999; Leedham-Elvidge *et al.*, 2014), and on exposure to high light levels (Nightingale *et al.*, 1995). This is a likely explanation of the higher halocarbon production in macroalgae than phytoplankton. Additionally, it has been suggested that some halocarbons are produced as a chemical defence, either to prevent surface growth of diatoms on macroalgae (Ohsawa *et al.*, 2001) or as a grazing deterrent (Nightingale *et al.*, 1995). Both bromocarbons and iodocarbons have been shown to be produced by macroalgae and phytoplankton, in the Atlantic Ocean (Read *et al.* 2008; Hense & Quack 2009), European coastal zones (Archer *et al.* 2007; Jones *et al.* 2009), Western Pacific (Yokouchi *et al.*, 1997) and the Southern Ocean (Laturnus *et al.* 2000; Chuck *et al.* 2005; Hughes *et al.* 2009).

5.2.1. Halocarbon production by phytoplankton

Global phytoplankton production of halocarbons is of potentially high importance due to the large-scale coverage of productive waters on the planet. CH_3I was the first halocarbon to be suggested as a phytoplanktonic source of atmospheric iodine (Lovelock, 1975), a reactive and volatile compound, which has been found to be the most efficient compound for cycling I from the sea back to the land (Liss & Slater 1974). CH_3I has been found to be produced from coastal macroalgal zones, and also open oceans from phytoplankton activity (Lovelock 1975; Baker *et al.* 2000), but a direct link between chlorophyll-*a* concentrations and CH_3I has not been identified (Hopkins *et al.* 2010). Production of additional halogenated compounds from marine phytoplankton was proposed by Klick and Abrahamsson (1992) when C_3H_7I, CH_2ClI, C_4H_9I, CH_2I_2 and $CHBr_3$ were detected in open ocean waters.

Concentrations of CH_3I were detected in the Atlantic and Indian Oceans of up to 45 pmol L^{-1}, which correlated well with the ubiquitous cyanobacterium *Prochlorococcus* (Smythe-Wright *et al.*, 2006), and *Synechococcus* has also been identified as a CH_3I producer (Brownell *et al.*, 2010). The findings of Brownell *et al.* (2010) were contested in laboratory cultures of the two species performed by Hughes *et al.* (2011), who found no trace gas production from *Synechococcus* (Strain CCMP2370) , but did agree on CH_3I production from *Prochlorococcus marinus* (Strain CCMP2389), depending on cell physiology and health. Calculations of CH_3I production from *Prochlorococcus* in the central Atlantic Ocean indicate that this organism

makes a significant contribution to the flux of CH_3I to the atmosphere in this area, calculated at a total of 0.1 pmol L^{-1} day^{-1} (Hughes *et al.*, 2011).

The importance of halocarbon production in different geographical areas will vary spatially and temporally: production of chlorinated and brominated compounds in the Arabian Sea was higher during the summer monsoon high productivity, and was particularly linked to diatom and prymnesiophytes production (Roy, 2010). Further to this, a study in the western English Channel by Archer *et al.* (2007) studied iodocarbons for 20 months, and found distinct minima in winter and maxima in late summer/ autumn.

5.2.2. Halocarbon production by macroalgae

The first field measurements of marine halocarbons were around the British Isles by Lovelock in 1975. Of particular interest were the measurements over the *Laminaria digitata* beds in Ireland, where concentrations of CH_3I were measured at 1000 times higher than over the open oceans. These results were replicated with measurements of additional bromide-containing compounds ($CHBr_3$, CH_2Br_2, $CHBr_2Cl$, $CHBrCl_2$), by Nightingale *et al.* (1995), who further proved that halocarbon release was influenced by partial desiccation, light availability, tissue age and grazing. Rates of release varied both between species of macroalgae within the same group (ie *Fucus* species) but also between specimens of the same species (Chance *et al.*, 2009). Measurements of halocarbons within the water column by Moore and Tokarczyk (1993) identified that concentrations of the same halocarbons were higher in coastal waters, consistent with macroalgal production. Macroalgal halocarbon production has been recorded in the water column and also directly into the atmosphere during dessication (Leedham, 2013). Total global macroalgal production is considered to be significantly lower than microbial production, due to the relatively small distribution of coastal areas with macroalgal coverage in comparison to open ocean environments.

5.2.3. Halocarbon production by other sources

Additional marine sources of halocarbons are marine volcanoes and production from coastal mangroves (Leedham *et al.*, 2013) and seagrass meadows (Weinberg, 2013). The major terrestrial sources of halocarbons are volcanoes and wood-rotting fungi (Keppler *et al.*, 2000), with compounds including methyl halides (CH_3I, CH_3Br and CH_3Cl), chloroform ($CHCl_3$), carbon tetrafluoride (CCl_4) and CFCs (Frische *et al.*, 2006).

It has been suggested that marine bacterial turnover and production of iodocarbons, particularly CH_3I, is of greater importance than previously thought (Amachi, 2008), and

methylating capabilities have been identified in a wide range of marine bacteria (Amachi *et al.*, 2001). C_2H_5I and C_3H_7I production were enhanced in marine detrital aggregates by high bacterial heterotrophic activity, and due to the absence of dihalogenated compounds, haloperoxidase production was unlikely (Hughes *et al.*, 2008). No reports have been made of bromocarbon production from bacterial activity.

5.2.4. Halocarbon production by abiotic processes

CH_3I production in surface waters was also shown to be via a light-dependent production pathway that was not dependent on biological activity (Richter and Wallace, 2004), through a series of incubations treated to eliminate the in-flask biological activity, and agreed with an earlier study demonstrating CH_3I production in filtered seawater irradiated with natural light levels (Moore and Zafiriou, 1994). This route was projected to support at least 50% of the average sea-air flux for the tropical Atlantic.

5.3. Halocarbon loss processes and sinks

5.3.1. Halocarbon flux to the atmosphere

Air-sea flux of biogenic halocarbons represent the primary loss of these compounds from the surface ocean, and the major source to the atmosphere (Class and Ballschmiter, 1988; Moore and Groszko, 1999; Moore and Tokarczyk, 1993). Estimates on global fluxes of organic iodinated compounds from macro-algae are in the order of 10^7 g yr^{-1} (Giese *et al.* 1999), however this can vary according to the species of macroalgae and the biomass available at any one time. Estimates of microalgal Iodocarbon production range from 10^{11}-10^{12} g yr^{-1} from across the oceans (O'Dowd *et al.*, 2002), with CH_3I being the primary compound emitted into the atmosphere (Moore and Groszko, 1999).

Goodwin *et al.* (1997) calculated global combined $CHBr_3$, CH_2Br_2 and CH_3Br emissions at 10^{10} – 10^{11} g Br yr^{-1}, with 88% of this total originating from $CHBr_3$ (Quack and Wallace, 2003). Biogenic sources of bromoform were found to be greater than inputs from anthropogenic sources.

5.3.2. Halide ion substitution and halocarbon hydrolysis

Nucleophilic substitution of halocarbons is a temperature dependent abiotic loss process, symbolised for the methyl halides by the equation:

$$CH_3X + Y^- \longrightarrow CH_3Y + X^- \qquad 17$$

Where both X and Y are any combination of I, Cl or Br. Further substitution of bromocarbons was suggested by Class and Ballschmiter (1988) in the equations:

$$CHBr_3 + Cl^- \longrightarrow CHBr_2Cl + Br^- \quad 18$$

$$CHBr_2Cl + Cl^- \longrightarrow CHBrCl_2 + Br^- \quad 19$$

$$CHBrCl_2 + Cl^- \longrightarrow CHCl_3 + Br^- \quad 20$$

It has been suggested that these processes are more important in deeper waters away from the air-sea interface and potential sources of biotic production (Carpenter and Liss, 2000; Moore and Tokarczyk, 1993).

Hydrolysis of $CHBr_3$ was reported by Quack and Wallace (2003) as an extremely slow process with a half-life of 1000 years at 2-4°C. Even at higher temperatures, the half-life would still be 50 years. At mean oceanic temperatures of 3.5 °C in the deep oceans and 15°C for the mixed layer, the overall hydrolysis loss would be minimal at 5.5 mmol $CHBr_3$ yr^{-1}.

5.3.3. Halocarbon loss by photolysis

Breakdown of halocarbons occurs in the surface waters: photo-dissociation of CH_2I_2, CH_2BrI and CH_2ClI were reported by Martino *et al.* (2005) and Jones and Carpenter (2005), with breakdown products of iodide and CH_2ClX, where *X* can represent I, Br or Cl. This suggests this pathway is an important source of CH_2ClI. Photolytic loss will be most important in the top few metres, and will vary spatially and temporally depending on turbidity. The same breakdown processes have been reported for $CHBr_3$, and estimates have the loss to be approximately 2% of the air-sea flux (Carpenter and Liss, 2000; Quack and Wallace, 2003), but still the largest internal oceanic sink.

5.3.4. Halocarbon loss by dehalogenation and bacterial oxidation

Microbial activity is responsible for the dehalogenation of a range of halocarbons in the use of the compounds as a biological energy source. Goodwin *et al.* (1998) used radiolabelling to show how $^{14}CH_2Br_2$ was broken down to $^{14}CO_2$, but there was no evidence of $CHBr_3$ breakdown. Breakdown was identified for a wide range of halogenated compounds by Bouwer and McCarty (1983) under anaerobic conditions by methanogenic bacteria.

5.3.5. Halocarbon atmospheric chemistry

Atmospheric halocarbons are known as very short lived substances (VSLS) due to their atmospheric lifetimes being less than six months (Montzka *et al.*, 2011), and the majority are

from biogenic sources with small (3%), locally important anthropogenic sources such as water chlorination and desalination (Quack and Wallace, 2003). Both iodine and bromine-containing trace compounds have been identified as emissions from the marine boundary layer, and once transported across the air-sea interface, the halocarbons participate in a variety of atmospheric chemical reactions at relatively short timescales. Halocarbons breakdown in both the troposphere and stratosphere, forming the reactive radical species Cl, Br, I, ClO, IO, BrO, HOBr and OIO (O'Dowd *et al.*, 2002; Solomon *et al.*, 1994). Life-times of iodine compounds and breakdown products within the atmosphere are considered very short (Table 3), and generally iodine reactions occur almost immediately in the troposphere (Chameides and Davis, 1980; Chatfield and Crutzen, 1990), whereas bromine and chlorine products and radicals are longer-lived and can impact on stratospheric chemistry (Sturges *et al.*, 2000; Yung *et al.*, 1980). Due to the longer atmospheric lifetime than other iodocarbons, CH_3I could have potential impacts on the lower stratosphere (Solomon *et al.*, 1994), allowing iodine to participate in stratospheric ozone reactions.

The reactive halide species above are responsible for the initiation of ozone breakdown cycles in the stratosphere, and can also act as CCN (O'Dowd *et al.*, 2002). Ozone has a unique role in the stratosphere in absorbing certain wavelengths of incoming ultraviolet light, but in the troposphere it acts as a potent greenhouse gas and biological irritant. Ozone occurs in the troposphere through two main routes: downward transport from the stratosphere and in-situ photochemical production through a series of reactions with NO_x, CO and CH_4, and has a key role in smog formation (Chameides and Walker, 1973; Crutzen, 1973; Lin *et al.*, 2014). Tropospheric ozone loss occurs through photolysis or deposition (Tang *et al.*, 1998), the former of which is responsible for the formation of OH through photolysis near 300 nm:

$$O_3 + h\nu \longrightarrow O(^1D) + O_2 \qquad 18$$

$$O(^1D) + H_2O \longrightarrow 2OH \qquad 19$$

OH is responsible for the removal of a variety of atmospheric species, including halocarbons. In the absence of pollutants, ozone breakdown is higher than production, and leads to an increase in OH radicals in the atmosphere, providing greater oxidative capacity (Tang *et al.*, 1998). OH production is also important in determining the lifetime of DMS within the atmosphere.

In the troposphere, both bromo- and iodocarbons released in the marine boundary layer are oxidised (XO, where X represents Br or I) and can result in further loss of ozone through the following reactions (Read *et al.*, 2008):

$$X + O_3 \longrightarrow XO + O_2 \quad (20)$$

$$XO + XO \longrightarrow 2X + O_2 \quad (21)$$

During strong atmospheric convection, iodocarbons and iodine-containing radicals can be transported to the stratosphere, where they undertake further ozone depletion reactions alongside the more photolytically stable bromocarbons (Sturges *et al.*, 2000).

6. Changes to trace gas concentrations under ocean acidification

6.1. Changes to seawater DMS and DMSP concentrations under ocean acidification

DMS is an important link between oceanic primary productivity and global climate, and certainly has an important role in the global sulphur cycle. The effects of elevated pCO_2 on primary productivity have been discussed in Section 2.10.1 and are likely to have an effect on DMSP and subsequent DMS production. Previous studies investigating the changes in DMS under elevated pCO_2 have found significant changes in direct response to acidification: the majority of mesocosm studies showed consistently reduced DMS concentrations (Archer *et al.*, 2013; Hopkins *et al.*, 2010; Vogt *et al.*, 2008), however incubation experiments by Hopkins and Archer (2014) of natural community assemblages showed consistently increased DMS production. A similar picture emerges for DMSP: in some studies the DMS and DMSP concentrations have both been reduced by exposure to high CO_2 (Avgoustidi *et al.*, 2012; Hopkins *et al.*, 2010; Park *et al.*, 2014), others showed DMS (Kim *et al.*, 2010) or DMSP (Archer *et al.*, 2013; Vogt *et al.*, 2008) increasing in the high CO_2 treatments. Responses of laboratory investigations into DMS and DMSP production from monocultures of *E. huxleyi* are similarly varied: Spielmeyer and Pohnert (2012) found no significant difference in DMSP, Wuori (2012) and Arnold *et al.* (2013) saw an increase in DMSP. From looking at the combined results of these studies, it can be seen that there is no conclusive outcome on the effect of increasing atmospheric pCO_2 and subsequent ocean acidification on DMS production.

This lack prevents the development of sufficiently accurate projective models for DMS concentrations under future climate scenarios. Existing projections of changes in DMS production and flux show small (3%) increases in DMS flux, but also large spatial

heterogeneities (-15% - 30%; Bopp *et al.*, 2003, 2004), in adapted nitrogen-based community structure models (Gabric *et al.*, 1993). Further model development has shown that increasing model complexity starts to develop a pattern of reduced DMS production at the equator and higher production at high latitudes due to changes in sea ice cover, temperature, mixing and light regimes (Cameron-Smith *et al.*, 2011), however these models are based on the changes in community composition and productivity with global warming, but no mention is made of the parameterisation of ocean acidification alongside climate change. An attempt to include ocean acidification within DMS flux models was made by Six *et al.* (2013), based upon the data collected during the Svalbard EPOCA mesocosm experiment (Archer *et al.*, 2013), and showed a global reduction in DMS emissions by 18% in 2100 compared to pre-industrial times. This model was relatively unconstrained in terms of the parameterisations and did not take into account the changes with temperature or community compositions. As with all models, additional data on surface DMS concentrations and changes under high pCO_2 would only enhance the model output. Further modelling of DMS under ocean acidification showed that in the last 50 years, eutrophication and intense blooming of *Phaeocystis* led to an increase in DMS emissions which overruled any effect of Ocean acidification (Gypens and Borges, 2014).

6.2. Changes to halocarbon concentration under ocean acidification

Like DMS, halocarbons are biogenically produced and are likely to be affected by ocean acidification. As yet, very few detailed investigations have taken place to study halocarbon production in a high CO_2/ low pH environment, and the majority of these have been in mesocosm experiments (Hopkins *et al.*, 2010, 2013; Wingenter *et al.*, 2007). While Hopkins *et al.* (2010) determined no significant differences in bromocarbon concentrations under elevated pCO_2, iodocarbon concentrations were significantly reduced, which was in contrast to the findings of Wingenter *et al.* (2007) where CH_2ClI concentrations significantly increased under pCO_2 of 760 and 1150 µatm. A further mesocosm study in the Arctic showed no significant difference in production of any of the studied halocarbons despite changes to community development in pCO_2 up to 1085 µatm (Hopkins *et al.*, 2013). Seawater incubation experiments (Hopkins, 2010) of samples collected in the English Channel again showed decreases in iodocarbons but very little change in bromocarbon production. It is clear that the data available on the halocarbon production changes under ocean acidification are significantly lacking, which will prevent parameterisation of these changes in the development of future atmospheric chemistry models, in the same way that this has been experienced with DMS.

7. Purpose of this study

Any change in the carbonate chemistry in the oceans due to increasing atmospheric pCO_2 and the resulting acidification is going to have ramifications on the marine organisms living with those changes. In this introduction the importance of a range of biogenic marine trace gases has been discussed in terms of their production and transfer to the atmosphere, as well as the limited knowledge of the changes in production as ocean acidification progresses. Any change in the production is likely to have significant effects on both oceanic and atmospheric processes on both a local and global scale.

This investigation aims to further the sparse knowledge in this field through the following experimental designs:

7.1. SOPRAN 2 Mesocosm Experiment, Bergen, Norway, 2011

A large-scale mesocosm experiment was performed off the coast of Bergen, Norway, under a range of CO_2 treatments to simulate atmospheric pCO_2 from pre-industrial through to 3000 µatm.

- Are there differences in DMS or DMSP concentrations with increasing pCO_2, and is there any evidence of a linear trend with increasing pCO_2?
- Are there any differences in iodocarbon or bromocarbon production with increasing CO_2, and is there any evidence of linear trends with increasing pCO_2?
- What changes to the physical, chemical and biological parameters within the community development are responsible for the changes in gas concentrations?

7.2. *Emiliania huxleyi* monoculture experiments under elevated pCO_2.

As a globally important phytoplankton, changes in either *E. huxleyi* population density or DMSP production as a result of ocean acidification or elevated pCO_2 will have significant effects on the availability of DMS-related organic sulphur compounds within the microbial food web, as well as the flux of DMS into the atmosphere. These experiments aim to answer the following questions:

- Are there differences in DMSP and DMS production from *E. huxleyi* under acidification conditions caused by an increase in atmospheric pCO_2 to 860 µatm, under the IPCC A2 projections for 2100?
- Does medium-term exposure of *E. huxleyi* to acidified conditions result in changes to DMS and DMSP production or the dynamics between the two?

7.3. SOPRAN 2 Mesocosm Experiment, Tvärminne, Finland, 2012

A second large-scale mesocosm experiment was performed in the unique environment of the Baltic Sea, to study the effects of elevated pCO_2 on nitrogen cycling and fixation by diazotrophic cyanobacteria. This environment, although highly nutrient perturbed, had never been studied for the effects of elevated pCO_2, and some prior studies on production in the Baltic Sea indicated that the cyanobacteria were significant producers of halocarbons.

- Are there changes in iodocarbon or bromocarbon production with increasing pCO_2?
- Are there any changes in DMS or DMSP concentrations with increasing pCO_2?
- Did cyanobacterial growth significantly affect the production of the trace gases, and what were the significant physical, chemical and biological parameters linked to the changes in concentration?

BLANK

Chapter 2. Methods of Trace Gas Analysis

1. Overview of analytical techniques used in this thesis

In this work, dissolved DMS and DMSP at nanomolar (10^9) and halocarbons at picomolar (10^{12}) concentrations are investigated. These trace gases need to be first extracted from the bulk seawater and then pre-concentrated to levels that can be detected by the analytical systems. Methods of extraction and pre-concentration are presented in Section 2. All samples were separated using gas chromatography (GC), linked to either a mass selective detector (MSD; Section 3) or a flame photometric detector (FPD; Section 4).

Details of the design and operation of SOPRAN Bergen (Chapter 3) and SOPRAN Tvärminne (Chapter 5) mesocosm experiments, along with details of the preparation of trace gas samples for this study prior to analysis by the methods presented here, are given in the relevant chapters. The *E. huxleyi* CO_2 enrichment experiment design and operation is given in Chapter 4, also with details on the preparation of samples prior to analysis. The analysis techniques described in this Chapter are taken from the point where samples have been previously collected and prepared from the mesocosms or cultures. Table 1, Table 2 and Table 3 give an overview of which of the methods presented here were used during each Chapter.

In 2013, UEA was a participant in the first International Proficiency Study for DMS in Seawater (National Measurement Institute of Australia, 2013). The study was designed to allow for intercomparability of DMS measurements between laboratories, and to introduce quality control to the data presented to the global surface seawater DMS database (Bell *et al.*, 2012; Turner *et al.*, 1990), which is particularly important with the introduction of new, high speed DMS measurements. All samples analysed for this proficiency study used the GC-FPD techniques presented in this Chapter and which were used for this investigation, and allowed not only a good estimate of the precision of the techniques, but also the accuracy of the analysis technique compared to nine other laboratories. An overview of the results of this study and calculated sampling error is given in Section 4.5.

BLANK

Table 1. Summary of methods used to collect, pre-concentration and analyse samples of DMS, halocarbons and DMSP during each phase of the SOPRAN Bergen mesocosm experiment. Phases were determined by Chl-α development and were split into 'natural' bloom, 'artificial' bloom and post-bloom phases.

Target Compound	Phase of experiment	Sample collection and storage (Chapter 3)	Extraction and pre-concentration technique (Section 2)	Analysis method
DMS	Phase 1	Samples purged onto commercial Markes Sorbent tubes and stored at -20°C for 8-10 weeks prior to analysis	Commercial Markes Unity™ system with UltrA autosampler unit	Agilent 6890 GC with DB-VRX column Agilent 5975 MS in electron ionisation Single Ion Mode (SIM) (Section 3)
	Phase 2 and 3	Samples collected and stored at 4°C in the dark. Analysis was performed within 4 hours of collection	Nylon purge-and-cryotrap system	
DMSP	Phases 1, 2 and 3	Samples collected and stored under acidified conditions at ambient temperature for 8-10 weeks prior to analysis	PTFE purge-and-cryotrap system	Shimadzu GC2010 equipped with FPD (Section 4)
Halocarbons	Phase 1	Samples purged onto commercial Markes Sorbent tubes and stored at -20°C for 8-10 weeks prior to analysis	Commercial Markes Unity™ system with UltrA™ autosampler unit	Agilent 6890 GC with DB-VRX column Agilent 5975 MS in electron ionisation Single Ion Mode (SIM) (Section 3)
	Phase 2 and 3	Samples collected and stored at 4°C in the dark. Analysis was performed within 4 hours of collection	Nylon purge-and-cryotrap system	

BLANK

Table 2. Summary of methods used to collect, pre-concentration and analyse samples of DMS, halocarbons and DMSP during the CO_2 enrichment experiments on *E. huxleyi*.

Target compound	Sample collection and storage (Chapter 4)	Extraction and pre-concentration technique (Section 2)	Analysis method
DMS	Samples collected and stored at 4°C in the dark. Analysis was performed within 2 hours of collection	PTFE purge-and-cryotrap system	Shimadzu GC2010 equipped with FPD (Section 4)
DMSP	Samples collected and stored overnight at 30 °C in 4ml crimp-sealed vials with NaOH addition. Samples analysed within 24 hours	Headspace sampling by Gerstel Multi-Purpose Autosampler	Shimadzu GC2010 equipped with FPD (Section 4)
Halocarbons	Samples collected and stored at 4°C in the dark. Analysis was performed within 2 hours of collection	Nylon purge-and-cryotrap system	Agilent 6890 GC with DB-VRX column Agilent 5975 MS in electron ionisation Single Ion Mode (SIM) (Section 3)

BLANK

Table 3. Summary of methods used to collect, pre-concentration and analyse samples of DMS, halocarbons and DMSP during the SOPRAN Tvärminne mesocosm experiment.

Target compound	Sample collection and storage (Chapter 5)	Extraction and pre-concentration technique (Section 2)	Analysis method for DMS
DMS	Samples collected and stored at 4°C in the dark. Analysis was performed within 4 hours of collection	Nylon purge-and-cryotrap system	Agilent 6890 GC with DB-VRX column Agilent 5975 MS in electron ionisation Single Ion Mode (SIM) (Section 3)
DMSP	Samples collected and stored under acidified conditions at ambient temperature for 6-8 weeks	PTFE purge-and-cryotrap system	Shimadzu GC2010 equipped with FPD (Section 4)
Halocarbons	Samples collected and stored at 4°C in the dark. Analysis was performed within 4 hours of collection	Nylon purge-and-cryotrap system	Agilent 6890 GC with DB-VRX column Agilent 5975 MS in electron ionisation Single Ion Mode (SIM) (Section 3)

BLANK

2. Extraction and pre-concentration of DMS, DMSP and halocarbons from seawater

Purge-and-trap is an effective method for extracting volatile trace gases from seawater for separation by gas chromatography. During this investigation, the majority of gas samples were extracted by this method, on two separate designs of purge-and-cryotrap. A nylon system was used for analysis of DMS and halocarbons on GC-MSD (Section 2.1) and a PTFE system (Section 2.2) for the measurement of DMS and DMSP on GC-FPD. Samples analysed on the Markes Unity™ thermal desorption system (Section 2.3) also used the nylon purge system, but were diverted into the sorbent tube before the cryotrap (Figure 1). All the Markes tube samples were analysed by GC-MSD.

DMSP samples prepared during the *E. huxleyi* CO_2 enrichment experiments were analysed by headspace extraction (Section 4.2).

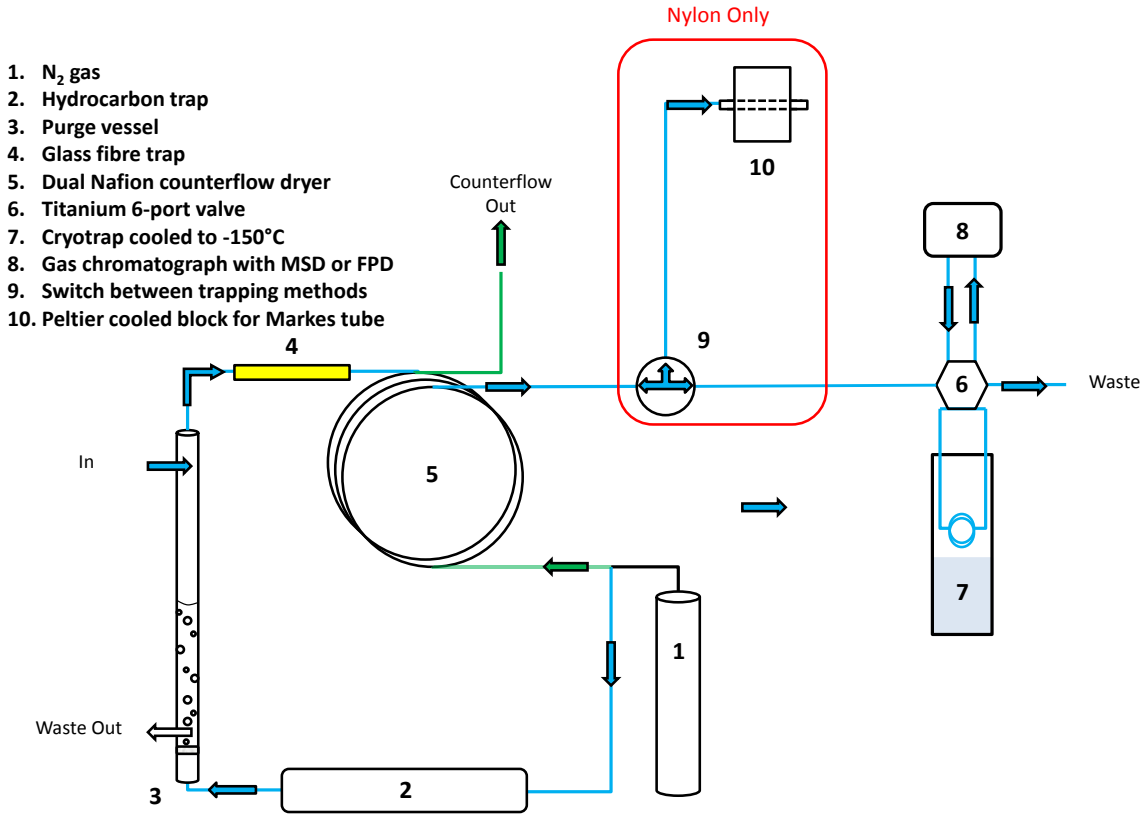

Figure 1. Diagram of the nylon and PTFE purge-and-trap systems used for the analysis of DMS and halocarbons. The area marked in red was present only on the nylon system and connected the purge system to the Markes tube, negating the need for the cryotrap.

2.1. Design and operation of the nylon purge-and-cryotrap system (GC-MSD)

It is commonly believed that DMS may react with stainless steel, making conventional purge-and-trap systems unsuitable for DMS analysis. However, no scientific evidence for this was found in the existing literature. To ameliorate any concerns we used a purge-and-trap system that was predominantly nylon, the exception being the 6-port valve which was made of inert titanium and the sample loop which had to remain of stainless steel due to the inability of nylon to cope with the temperature demands required of the loop (-150 to 100 °C). Repeated calibration showed this to be suitable for analysis of DMS, with no change in DMS signal during continuous use of the system (see calibrations presented in Section 3.3).

Samples of 40 mL of seawater requiring analysis were prepared in 100 mL glass syringes, where an internal standard of surrogate analytes was added (further details will be given in Section 3.4). Each sample was passed through a 25 mm, 0.7 µm Whatman (Whatman PLC) filter in a swinnex filter-holder to remove particulate matter and cells, and injected into a custom glass purge tube (Figure 1). The purge-and-trap system itself has been described in Hughes *et al.* (2006, 2008) for halocarbon analysis. Oxygen-free nitrogen (OFN, BOC, Ltd, UK) was passed through a hydrocarbon trap (Alltech Associates, UK) at a rate of 80 mL min^{-1} before bubbling through a sintered glass frit (16-40 µm pore size) into the seawater sample. Purging lasted for 10 minutes. Flow rates were checked with an ADM 2000 (Agilent) flowmeter daily prior to analysis of the first sample, and frequently between samples to ensure no leaks or blockages within the system. The system was regularly checked for leaks using SNOOP™ liquid leak detector (Swagelok, UK), and periodic replacements were made of the purge tube and hydrocarbon traps to ensure optimum performance and prevent build-up of salt crystals on the frit. A full calibration for all compounds was conducted after any maintenance of the purge system. Each calibration was performed using standards prepared in seawater of equivalent salinity to the samples (Section 3.3) and took into account the operation of the purge system and gas chromatograph as well as just the detector.

The efficiency at which compounds were purged from the seawater was inversely proportional to the molecular weight, but any variation was accounted for in the calibration of each compound using the same purge system. Chuck *et al.* (2005) determined the purge efficiencies for various halocarbons ranged from 75% for dichlorobromomethane ($CHBrCl_2$, not studied here) to 90% for CH_3I.

After purging, the gaseous sample passed through a glass wool trap to remove water droplets and aerosolised particulate matter, before passing through two nafion counterflow driers (PermaPure, USA) arranged in series with a counterflow of 150 mL min^{-1}. The sample was

directed through a Valco 6-port valve (VICI AG International) into a stainless steel sample loop held at -150°C in the headspace of a thermostatically controlled (UEA Electronics Workshop) liquid nitrogen-filled dewar. Alteration of the valve position isolated the valve from the purge system and into the path of the GC helium carrier gas. The sample was stable in the sample loop for several minutes after purging, and was re-volatilised into the carrier gas stream of the GC by immersion of the sample loop in boiling water (>90°C).

2.2. Design and operation of the PTFE purge-and-cryotrap system (GC-FPD)

Analysis of DMSP samples from the SOPRAN mesocosm experiments were analysed by GC-FPD equipped with purge-and-cryotrap. This method has been used at UEA for many years, and is well-established (see Turner and Liss, 1985; Turner *et al.*, 1990; Hopkins *et al.*, 2010). For this reason, it was decided to keep the established purge-and-cryotrap setup, very similar to that of the nylon system but with PTFE tubing and nylon fittings. For analysis of DMSP, cold alkaline hydrolysis is used to cleave DMSP to DMS and acrylate, and the DMS is purged from the sample and collected in the cryotrap for analysis.

Before each sample was added to the purge tube, 1 mL of 10 M sodium hydroxide (NaOH) was added to facilitate cold alkaline hydrolysis of the sample to DMS and acrylate, in a molar ratio of 1 of DMS to DMSP (Turner *et al.*, 1990). Two mL of the seawater sample to be analysed for DMSP was injected into the purge vessel using a 10 mL glass syringe, and the cleavage reaction and purging took place simultaneously for 5 minutes at an OFN flow rate of 80 mL min^{-1}. Tests on the efficiency of hydrolysing the DMSP and purging within the purge vessel proved that over 95% of the DMSP was released as DMS within 4 minutes of purging (Figure 2). Purged gases were swept along the OFN flow through a glass wool trap and nafion counterflow drier (Dry-Perm, International Science Consultants) before being caught in the PTFE sample loop held in the liquid nitrogen cryotrap at -150°C. Injection into the GC-FPD was by submerging the sample loop in boiling water (>90°C).

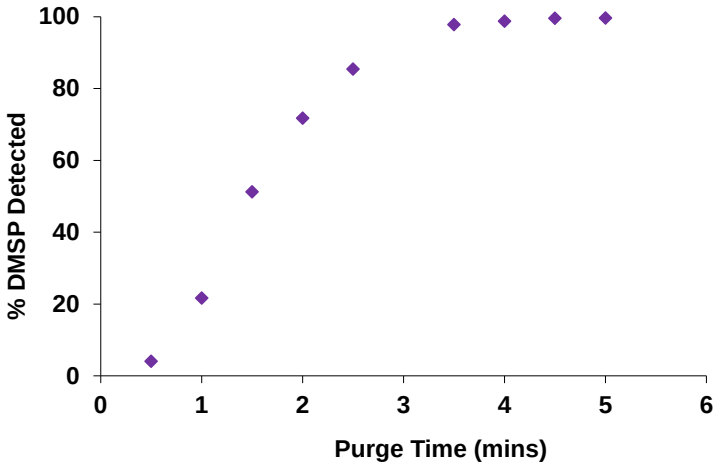

Figure 2. Efficiency of the DMSP purge-and-cryotrap showing the percentage DMSP detected from a sample of known concentration with increasing purge time.

DMS samples from the *E. huxleyi* CO_2 enrichment experiments were extracted by the PTFE purge-and-cryotrap system, but without the cleavage of DMSP with NaOH. Prior to analysis of DMS samples on the purge-and-cryotrap system, the purge tube was acid washed three times with 10% HCl and Milli-Q to remove any remaining NaOH from the purge vessel, and prevent hydrolysis of DMSP within the sample which could interfere with accurate measurements. Due to the cleavage process, the GC-FPD was analysing the concentration of DMS within the sample; DMS samples were analysed with the same calibration standards as DMSP samples. Details of the system calibration are given in Section 4.4.

2.3. Design and setup of headspace extraction samples

Full details of the preparation of samples for this method are given in Chapter 4 during the *E. huxleyi* CO_2 enrichment experiments. Cold alkaline hydrolysis of samples took place in a sealed screw-capped 4mL vial containing 3 mL of sample and 0.5 mL of 1 mol L^{-1} NaOH (Caruana *et al.*, 2012; Malin *et al.*, 1993). Samples were left in a heated block at 30°C overnight prior to analysis (Section 4.2).

2.4. Operation of the Markes Unity™ thermal desorption technique

2.4.1. Sample extraction and trapping on sorbent tubes

The use of the Unity™ thermal desorption system from Markes International Ltd was demonstrated as a successful method of halocarbon collection and storage by Hopkins *et al.* (2013) and Hughes *et al.* (2009) for the same compounds as under investigation here. The

Markes system required the halocarbons to be extracted from seawater by purging before being trapped onto a sorbent-filled tube (highlighted in red in Figure 1). Sorbent tubes were packed with three separate sorbents in order of increasing sorbency: Tenax TA, Carbograph 1TD and Carboxen 1000 (Markes International Technical Support, 2014b). The sorbent tube was held between 0-3°C in a custom-designed Peltier-cooled block (UEA Electronics Workshop), and the purged sample was passed through the sorbent tube at a rate of 80 mL min^{-1} for 10 minutes, trapping the target halocarbons but allowing the majority of the gases in the sample to pass through. Once the sample purging period had elapsed, the sorbent tube was removed from the Peltier-cooled block and again capped with ¼'' brass caps with PTFE ferrules before storage in a -20°C freezer until analysis. Previous investigations in our laboratory showed that sorbent tubes maintained stable concentrations of most halocarbons for up to 16 months when stored at -18°C (Hughes *et al.*, 2009).

Markes guidelines (Markes International Technical Support, 2014a) provided information on the safe sampling volumes (SSVs) of several of the compounds analysed for Tenax TA and Carbograph 1TD. The SSV was determined as approximately 2/3rds of the breakthrough volume for the sorbent, the volume of gas that can be sampled before analytes elute from the vent end of the sorbent tube. All SSVs available for compounds analysed were above the volume of gas passed through the tube during sampling (Leedham, 2013), except both DMS and CH_3I were found to experience breakthrough due to their low molecular weights and high volatility. No analysis was performed for these two compounds.

2.4.2. Operation of the Markes thermal desorption system

Samples were analysed using the Markes Unity™ thermal desorption system equipped with an UltrA™ autosampler, which provided the ability to analyse up to 100 tubes at one time. Prior to analysis, the tubes had the brass end-caps removed and replaced with Markes Difflok™ caps, which reduced diffusion of ambient air into and out of the tubes while they were in the autosampler. Each tube in turn was moved into the 'active' position, into the path of the helium carrier gas flow, where a leak test was performed, after which the tube was purged at ambient temperature for 1 minute to prevent oxidation of sorbents during the temperature increase. The tube was heated to 300°C for 5 minutes to desorb the analytes into the helium flow, which passed through a short heated transfer line into the Unity™ cold-trap. The cold-trap installed in the Unity™ system was a commercially available 'Water Management' trap, comprising glass wool, Tenax TA, Carbograph 1TD and Carboxen 1000, and was held at -10°C during tube desorption. After the tube had desorbed, the UltrA™ selected the next tube in the set ready for desorption once analysis of the previous sample was complete. To prevent the

tubes being held at ambient temperature for too long, only 10 tubes were loaded into the UltrA™ at any one time.

After the desorption stage where the gases were pre-concentrated onto the cold-trap, the cold-trap was heated to 300°C with a reverse flow of helium for 4 minutes, and the sample passed along a heated transfer line to the GC column. A diagram of the setup of the Unity™ and UltrA™ system is shown in Figure 3.

The Markes system was used to analyse the halocarbon data from SOPRAN Bergen (Chapter 3) during Phase 1 of the experiment, and analysis of all the tubes took place within a single week using the UltrA™ autosampler on return to UEA after the experiment. Calibrations were prepared on the purge system during SOPRAN Bergen directly onto the sorbent tubes and were treated in the same way as the sample tubes. In this way the calibration covered the entire sample analysis process and not just the detector. Calibrations were carried out before any of the samples were analysed, mid-way through the number of sample tubes, and after all sampling had been completed. Each sample and standard had the surrogate analytes added before purging, which were used to compare system drift (Section 3.4)

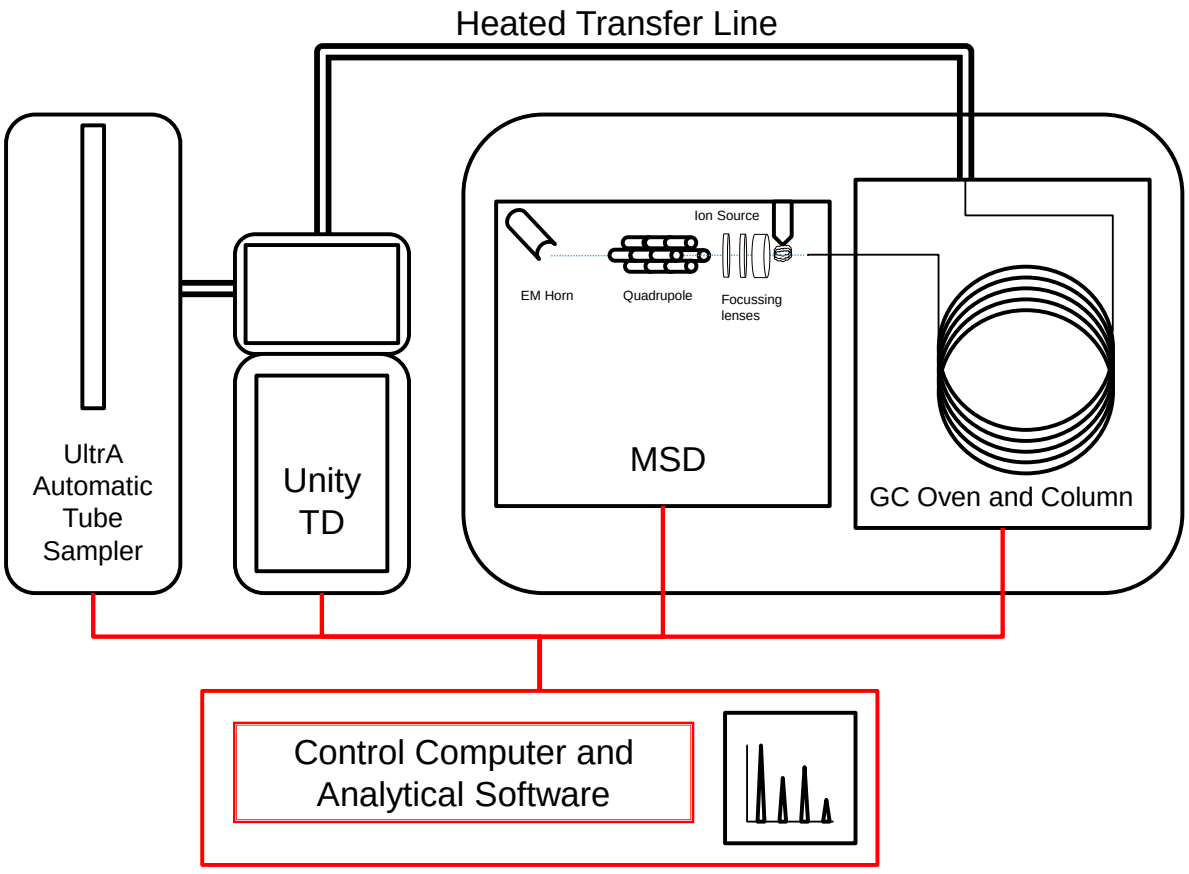

Figure 3. Schematic of the Markes Unity™ and UltrA™ systems connected to the GC-MSD.

2.4.3. Conditioning of Markes sorbent tubes

After analysis, tubes were conditioned in a Markes TC20™ tube conditioning oven, which passed a flow of clean OFN through 20 tubes in increasing temperatures (100°C, 200°C, 300°C and 320°C) for 20 minutes at each temperature, before cooling with the nitrogen flow. During analysis, one out of every 20 tubes analysed was a 'tube blank': this tube was analysed without exposure to the sample flow and would provide a background reading for any halocarbons which had not been removed by the conditioning process. Tubes were then capped and stored.

3. Sample Analysis by GC-MSD

3.1. Setup and operation of the GC

The sample from both the purge-and-cryotrap system and the Markes Unity^{TM} was transferred into the Agilent 6890 Gas Chromatograph by a transfer line heated to 100°C to ensure the volatile compounds remained in the gaseous phase. The sample passed directly into a 60 m DB-VRX column (0.32 mm diameter, 1.8 µm film thickness, J&W Ltd). Separation of the target analytes was by the following programme:

1. Hold at 40°C for 5 minutes
2. Temperature increase at rate of 20°C min^{-1} until 200°C
3. Hold at 200°C for 2 minutes
4. Temperature increase of 40°C min^{-1} until 240°C
5. Hold for 3 minutes
6. Vent and cool.

The total run time of the GC programme was 25 minutes to return to equilibrating temperature for another sample to be analysed.

3.2. Setup and operation of the MSD

Quantification of the target compounds was by Agilent 5973 quadrupole mass selective detector (MSD), operating in single ion mode (SIM) with electron ionisation. MSD allows compounds to be identified by the mass to charge ratio (m/z) of the ion fragments of each

compound, the fragmentation patterns of which are predictable. After eluting from the GC column, each compound was ionised by a stream of electrons, before passing through a series of lenses and through the quadrupole itself. The use of SIM allows the detector to focus on a limited number of ion masses, and therefore increases the sensitivity of the system by using the quadrupole to discard ions not of the required mass. A programme was developed in the control software to focus on two ions for each compound at the retention times which the compound was found to elute from the column (Table 4). The GC-MSD was controlled by the Agilent Chemstation software, and mass spectra were analysed using the Agilent Chemstation Data Analysis software. Quantitative analysis was determined by analysis of the peak areas of the target ions at the specific retention time.

Table 4. Retention times and target ions for compounds investigated during this study.

Compound	Formula	Retention time (mins)	Target ions
Target Compounds			
DMS	C_2H_6S	6.4	62, 46
Methyl iodide	CH_3I	6.1	142, 127
Diiodomethane	CH_2I_2	14.0	268, 141
Iodoethane	C_2H_5I	8.5	156, 127
Chloroiodomethane	CH_2ClI	10.7	176, 127
Bromoform	$CHBr_3$	13.5	173, 175
Dibromomethane	CH_2Br_2	10.2	174, 129
Dibromochloromethane	$CHBr_2Cl$	12.0	129, 127
Iodopropane	C_3H_7I	10.7	170, 127
Bromoiodomethane	CH_2BrI	12.2	222, 141
Surrogate Analytes			
Deuterated DMS	C_2D_6S	6.4	68, 48
Deuterated methyl iodide	CD_3I	6.2	145, 127
^{13}C Dibromoethane	$^{13}C_2H_4Br_2$	12.2	111, 188

3.3. Calibrating the GC-MSD for DMS and halocarbons

Calibrations were performed on the GC-MSD using commercially available standards (Sigma Aldrich) with purities ranging from 97-99%. Gravimetric dilution was used to produce a serial dilution series in high purity HPLC grade methanol to produce secondary and tertiary standards. All standards were produced in 4 mL amber glass vials: primary and secondary standards were sealed with PTFE caps and parafilm and stored in 50 mL Corning tubes; tertiary and quaternary standards were capped with Mininert valves (VICI AG International) to form a leak tight closure which could still be accessed via syringe. As samples took approximately 30 minutes to analyse, mixed working standards were produced from the secondary and tertiary standards to allow calibration of several compounds simultaneously. Three standard mixes were produced: iodocarbons (CH_3I, CH_2I_2, CH_2ClI, C_2H_5I and C_3H_7I), bromocarbons ($CHBr_3$, CH_2Br_2, $CHBr_2Cl$ and CH_2BrI) and DMS separately. The ranges for which these compounds were calibrated during the whole investigation are given in Table 5. New working standards were mixed prior to calibration during each field campaign and prior to each new experiment in the *E. huxleyi* CO_2 enrichment experiments.

Table 5. Range of compound concentrations for which calibrations were carried out on the GC-MSD using liquid standards in methanol.

Compound	Formula	Calibration range (pmol L^{-1})
DMS	C_2H_6S	40 - 29300
Methyl iodide	CH_3I	0.1 – 64.8
Diiodomethane	CH_2I_2	0.08 – 820
Iodoethane	C_2H_5I	0.01 – 9.81
Chloroiodomethane	CH_2ClI	1.98 – 198
Bromoform	$CHBr_3$	0.21 – 408
Dibromomethane	CH_2Br_2	0.21 – 98.3
Dibromochloromethane	$CHBr_2Cl$	0.26 – 51.5
Iodopropane	C_3H_7I	0.3 – 11.98
Bromoiodomethane	CH_2BrI	0.03 – 0.69

Any changes to the sample analysis system and a new series of standards would be analysed to recalibrate the system. This allows the calibration to include the purge efficiency of the system, as well as any losses which may take place through trapping or drying. New standard dilution series were developed before each field campaign and fresh tertiary standard mixtures were made weekly.

For consistency, standards were treated in as similar a manner as possible to samples. A tower of prepurged seawater was prepared by filtering through a 0.7 µm Whatman GF/F and purged with hydrocarbon-clean compressed air for over 24 hours prior to calibrations. Using the same glass syringes as for samples (Section 2.1) 40 mL water were taken up from the pre-purged seawater tower and injected microliter additions of standard through the Luer fitting with a Hamilton syringe to prevent ingress of air. This allows injection of the sample into the purge vessel through a 25 mm GF/F in same method as the experimental samples, using same volume of seawater. This will calibrate not just detector but entire purge-and-cryotrap, transfer line and analytical system.

A blank standard was run by analysis of the pre-purged seawater, and the standards were corrected to the values given by this sample. Regression was used to determine the relationship between the calculated concentration of standard and the peak area calculated from the chromatogram of the GC-MSD; calibrations comprised at least 4 points, and were only accepted if the r^2 of the line was above 0.9. An example calibration for DMS from SOPRAN Tvärminne is given in Figure 4.

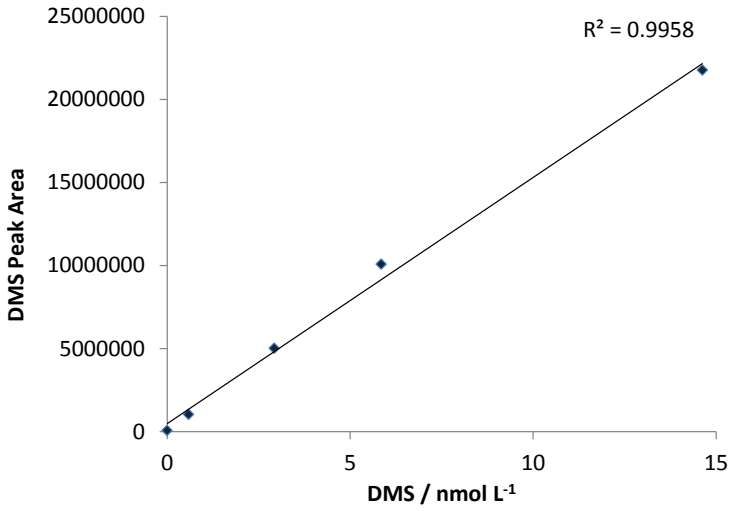

Figure 4. Example calibration for DMS on GC-MSD.

3.4. Use of surrogate analytes to correct for MSD system sensitivity drift.

Any drift in GC-MSD sensitivity could result in significant error or bias being introduced to the sampling regime, and poor repeatability of results. Sensitivity drift in GC-MSD is highly pronounced, and changes over timescales of days through months, depending on the intensity of instrument use and the time since the instrument was last tuned. The sensitivity drift of GC-MSD has previously been discussed by Hughes (2004).

On initial start-up of the instrument, a procedure known as 'autotuning' was performed: this autotune relied on the use of perfluorotributylamine (PFTBA), an internal standard provided by Agilent to allow for optimisation of the MSD itself. In general, there is a decrease in ion peak areas over the time period the instrument is in operation, and this can be attributed to the build-up of deposition products on the ion source walls, repeller and focus lenses. The source underwent rigorous cleaning on a six-monthly basis, and this combined with autotune and regular 'quicktuning' can keep sensitivity high.

It is very difficult to determine the scale of this drift in instrument sensitivity, without analysing multiple replicates of standards on a daily basis. The addition of three synthetic 'surrogate analytes' allowed the constant monitoring of sensitivity in relation to recent calibrations, quicktuning and autotuning. This allows for consistent quality of data (as demonstrated in Figure 5). Three different surrogate analytes were used throughout these experiments: deuterated DMS (D_6-DMS) was used as a direct comparison to DMS, deuterated methyl iodide (CD_3I) as a comparison to CH_3I and ^{13}C dibromoethane ($^{13}C_2H_4Br_2$) as a comparison to the other halocarbons as less volatile compounds. A working standard comprised of all three compounds was developed at the start of both field campaigns and was used throughout: 2 µL additions of this working standard were added to each sample and calibration immediately prior to analysis, and a blank was performed during each calibration by adding the working standard to 40 mL of the pre-purged seawater and ensuring no contamination of the surrogate analyte with non-deuterated standard compounds by comparison with the seawater blank.

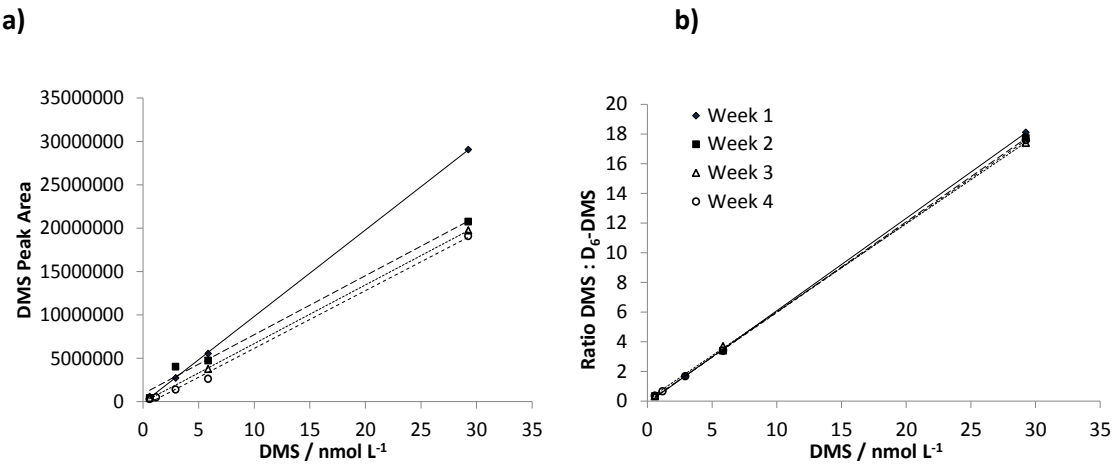

Figure 5. Calibrations for the GC-MSD for DMS, showing a) individual calibrations plotted with peak area against DMS concentration and b) the same calibrations plotted with peak area against the DMS/ D_6DMS ratio for four weekly calibrations during SOPRAN Tvärminne.

All three surrogate analytes responded differently to the loss of sensitivity (Figure 6), but all showed a decrease in sensitivity after initial setup, followed by stabilisation of peak areas as time progresses. The GC-MSD was quicktuned twice during the experiment (Figure 6 dashed lines), and showed an increase in sensitivity after tuning. The steep reduction in sensitivity at initial setup was attributed to immediate accumulation of decomposition products within the MS and degradation or deformation of the filament (G. Mills, Pers Comm). Fluctuations occur not only between tunes, but also on a daily basis during analysis of samples, and it is this fluctuation which is corrected by the use of the surrogate analytes. Hughes (2004) has previously discussed the change in sensitivity over the course of a day, and has attributed this to a build-up of humidity and non-target compounds in the MSD chamber when running repeated samples. On comparison of the percentage changes the D_6-DMS showed the greatest percentage change at 79% reduction in mean daily peak area, followed by $^{13}C_2H_4Br_2$ at 60% and CD_3I at 59%.

a) Deuterated DMS (C_2D_6S)

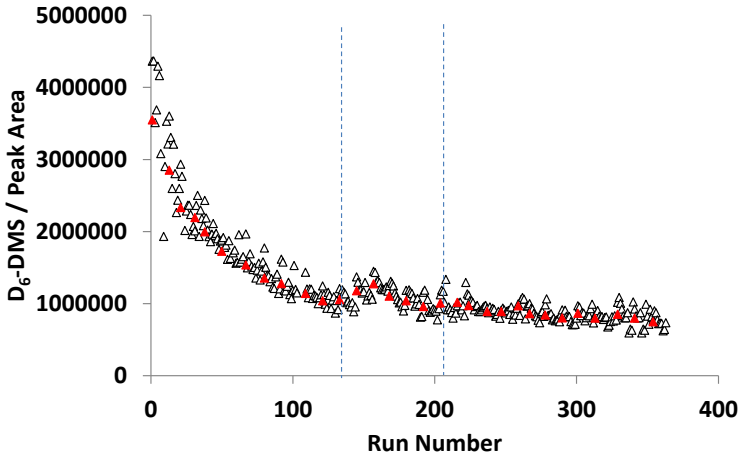

b) ^{13}C dibromomethane ($^{13}C_2H_4Br_2$)

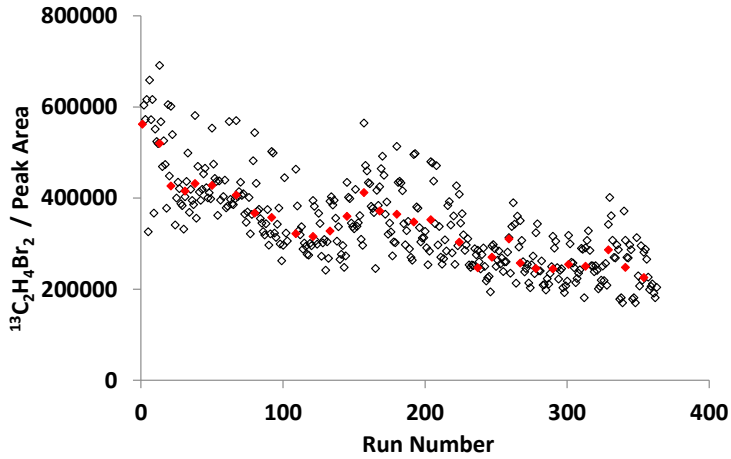

c) Deuterated methyl iodide (CD_3I)

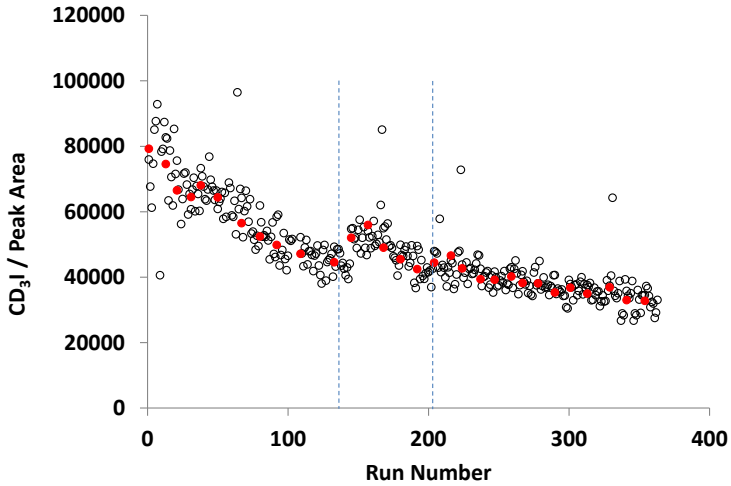

Figure 6. Fluctuations in measured peak areas for the three surrogate analytes a) deuterated DMS, b) ^{13}C dibromomethane and c) deuterated methyl iodide) during the SOPRAN Tvärminne mesocosm experiment, plotted by run number. Open symbols show the peak area from individual runs, while red points show the mean peak areas for each sampling day. Dashed lines show the days when the GC-MSD was quicktuned.

4. Sample Analysis by GC-FPD

Two types of DMSP sample were analysed by GC-FPD: those analysed by purge-and-cryotrap and those analysed by headspace analysis. Two separate GCs were in operation, one for either method, and each GC was calibrated separately.

4.1. Analysis of DMS and DMSP by PTFE purge-and-cryotrap and GC-FPD

DMS from the *E. huxleyi* CO_2 enrichment experiments and the acidified SOPRAN Bergen DMSP samples were analysed by PTFE purge-and-cryotrap. After the sample was trapped in DMS form in the PTFE sample loop, the 6-port valve was turned to expose the sample to the carrier gas of the GC and the trap was transferred into boiling water. The sample passed directly through a non-heated transfer line into a Shimadzu GC2010 gas chromatograph fitted with a Varian Chrompack CP-Sil-5CB column (30 m, 0.53 mm ID) with a carrier gas rate of 60 mL min^{-1}. The oven was operated isothermally at 60°C, and DMS eluted at 2.1 minutes into the flame photometric detector. The total time for analysis of a sample was under 10 minutes, and samples were analysed individually.

4.2. Analysis of DMSP by headspace sampling and GC-FPD

DMSP samples were prepared as outlined in Section 2.3 and remained overnight at 30°C to ensure total hydrolysis and equilibration. Sample vials were arranged in the heated block of a Gerstel Twister™ multi-purpose autosampler, fitted with a 250 µL Hamilton syringe. The control software programme was set up to sample and analyse up to 50 samples in a single run on the GC: 100 µL of a sample was taken from the headspace gas in each vial and injected into the injection port (held at 200°C) of the Shimadzu GC2010 at 2 minute intervals. The column was a Varian Chrompack CP-Sil-5CB column (30 m, 0.53 mm ID) operated isothermally at 120°C, and DMS eluted after 2 minutes into the FPD.

4.3. Setup and operation of the FPD

The Chrompack CP-Sil-5CB column was specifically designed to separate sulphur compounds, and allowed them to pass individually into the flame photometric detector. The detector flame was fuelled by an air/hydrogen mix (BOC), set to a flow rate of 50 and 60 mL min^{-1} respectively. This instrument operates on the premise of quantifying the chemiluminescence of sulphur in the flame of the detector. Once a sample enters the combustion chamber, the emissions by sulphur-containing compounds pass through a thermal and sulphur selective filter before

detection by the photomultiplier tube. The temperature of the detector was set at 175°C on both instruments.

Software for GC-FPD operations was the GCSolution Realtime Analysis Software, and data analysis was carried out using the GC Postrun Analysis software.

4.4. Calibrating the FPD for DMS and DMSP

4.4.1. Calibration of the PTFE purge-and-cryotrap FPD

The purge-and-cryotrap GC-FPD was calibrated for both DMS and DMSP using cold alkaline hydrolysis of liquid DMSP standards with 10M NaOH within the purge vessel. Primary stock standards of DMSP at 812.46ngS mL^{-1} were pre-prepared and stored in the -80°C freezer for use during purge-and-cryotrap calibration. Working standards in the range 1.01 – 253.9 µmol L^{-1} DMSP were prepared on a weekly basis using dilution of differing volumes of the stock standard in 50mL of Milli-Q water, and were stored in the dark at 4°C. Tests showed that the salinity of the standards did not affect the calibration results. Two mL of standard were added to the purge tube in an identical method to each DMSP sample, as given in Section 2.2. The error in the system was 7% calculated by multiple analyses of different standards. Five-point calibrations were performed weekly with fresh working standards, and a check was performed daily using one standard to ensure the instrument had not drifted. GC-FPD operation was very stable and showed little drift. Blanks were performed using Milli-Q water, and never showed any signal.

4.4.2. Calibration of the headspace sampling FPD

Stock solutions for the headspace calibrations were pre-prepared and stored in the -80°C freezer in 0.5 mL aliquots at concentrations of 0.75, 7.5 and 30 nmol L^{-1}. Three millilitres of the sterile culture media were added to a glass vial with 1mL of 1M NaOH, and volumes between 1 and 10 µL of the standard solutions were carefully pipetted onto the septa of the screw-cap. Media was used instead of Milli-Q, as tests showed that the salinity of the standards affected the equilibrium with the gas phase and therefore the percentage of DMS in the headspace of the standards compared to the samples. The cap was inverted and screwed onto the vial, and then each vial was shaken to mix the standard into the media/ NaOH mix. Each vial was kept at 30°C in the dark overnight to hydrolyse and equilibrate before analysis by the headspace sampler. Calibrations were carried out in triplicate. Error of the system was 5%, based upon the triplicate measurements of the standards.

4.5. DMSP Proficiency Test 2013

In Spring 2013, the Australian National Measurement Institute undertook a proficiency test for global DMSP measurements, as a pilot study to enable laboratories to assess their ability to measure trace DMS in seawater. The results of the study would confirm if DMS measurements from different institutes around the globe were comparable, with a plan for this study to become a regular part of the NMI proficiency testing program. The study was conducted in accordance with ISO 17043.

Each laboratory participant received two 100 mL samples of an undetermined DMSP solution of between 1 and 10 µmol L^{-1} in acidified 3.5% sodium chloride (NaCl). A summary of the method used was returned with the reported concentration of DMSP. No individual performance evaluations were made for each laboratory.

Both FPD-based DMSP analysis techniques at UEA were entered into this study (headspace and purge-and-cryotrap). The systems were calibrated with 10 point calibrations in triplicate for each system, before the samples were analysed according to the methods outlined above. Ten sub-samples were analysed on each system for each of the two unknown samples. Samples were analysed on the headspace analyser without prior preparation, but required dilution before analysis in the purge-and-cryotrap. This proficiency study provided opportunity to cross-calibrate the two GC-FPD instruments used for the investigation. The GC-MSD analysis method was not included within the study as it was not designed to accommodate DMSP samples. The calibrations used within the proficiency study are shown in Figure 7.

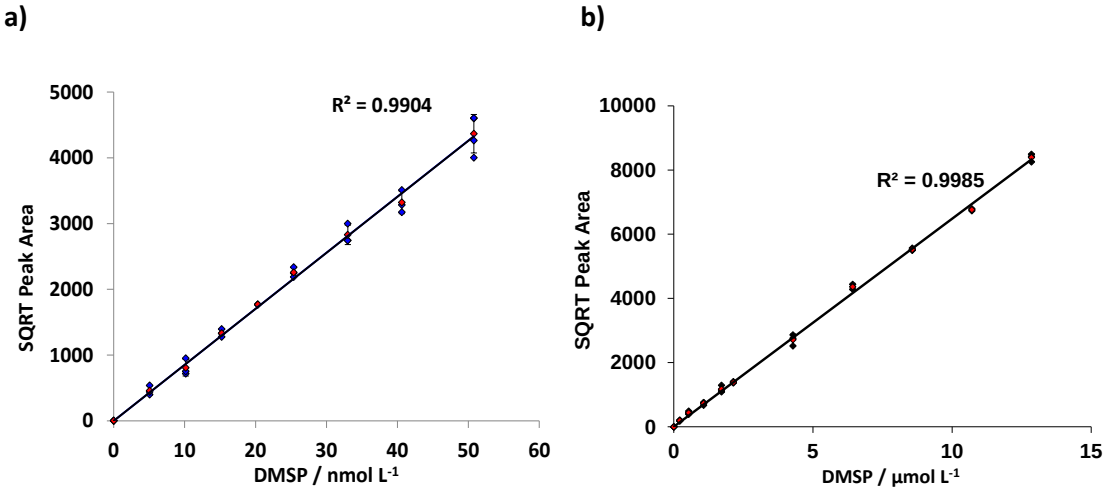

Figure 7. Calibration used in the DMSP proficiency test for a) purge-and-cryotrap and b) headspace analysis. Blue points show the individual calibration samples; red points are the averages of the triplicate analyses with standard deviation as error bars.

The final report into the pilot study (National Measurement Institute of Australia, 2013) gave the concentration of both DMSP solutions as 2.52 µmol L^{-1}; the measured mean and standard deviation for the two analytical methods used during this study for both samples are shown in Table 6. The headspace analysis was the most precise, with a maximum % error of 3.83, and the purge-and-cryotrap had a maximum error of 6.10%.

Table 6. Results of the two analysis methods for the pilot DMS proficiency study, showing the mean, standard deviation and % error from the known concentrations of the two solutions.

Analysis method		Mean (µmol L^{-1})	Standard deviation	Formulated Concentration (µmol L^{-1})	% error in method
Purge-and-cryotrap	Sample 1	2.605	0.095	2.52	3.37
	Sample 2	2.674	0.105	2.52	6.10
Headspace	Sample 1	2.424	0.119	2.52	3.83
	Sample 2	2.459	0.139	2.52	2.44

Eleven other laboratories (13 in total including the two analysis methods included here) took part in the exercise, and the report into the findings of the pilot study showed the statistics of the group (National Measurement Institute of Australia, 2013; Table 7). The highest recorded percentage error was 36.9% in sample 2 and 16.3% in sample 1. No reference was made as to which laboratories recorded these errors. Compared to the range of measured values from the group, both the analysis methods at UEA performed well in the proficiency study with relatively low percentage errors.

Table 7. Group statistics from the DMS pilot proficiency study for both samples, showing the median, mean, minimum and maximum calculated values from the group of 13 laboratories. Reproduced from National Measurement Institute of Australia (2013).

	Sample 1		Sample 2	
	Group Statistics	% error	Group Statistics	% error
Median	2.49	-	2.42	-
Mean	2.43	3.57	2.34	7.14
Min	2.11	16.3	1.59	36.9
Max	2.72	7.9	2.75	9.13

This intercomparison study is planned to be performed as a larger investigation into the accuracy of DMSP measurements by different analysis methods and to improve quality control for the global DMSP database (Bell *et al.*, 2012), and this study was only a preliminary

investigation. The one important note was the concentration of DMSP was formulated in µmol L^{-1} concentrations, when the usual concentration of DMSP in seawater was an order of magnitude lower. This will be taken into account in the next study; although higher concentrations can be diluted, the dilution of the sample is likely to increase the % error. In the purge-and-cryotrap analysis, samples were diluted by a factor of 125 to allow measurement and this may have increased the percentage error seen in this method.

Chapter 3. SOPRAN 2 Mesocosm Experiment, Bergen, Norway: Evaluating the effects of elevated pCO_2 on community production of trace gases in a coastal environment

1. Overview of the SOPRAN Bergen mesocosm experiment

This large-scale experiment was undertaken to investigate the effects of elevated pCO_2 on the coastal microbial community of the Norwegian North Sea using a series of large-scale mesocosm enclosures, and to compare the results to several smaller-scale experiments undertaken at the same location and under similar conditions of elevated pCO_2. Of particular focus during this experiment were the community responses associated with a bloom of the haptophyte *Emiliania huxleyi*. To further investigate linear relationships identified during a mesocosm experiment in the Arctic (EPOCA Svalbard) between increasing seawater pCO_2 and a several different community parameters (e.g. Brussaard *et al.*, 2013; de Kluijver *et al.*, 2013; Piontek *et al.*, 2013), this experiment included two CO_2 treatments higher than any previous experiment had investigated in this context (2000 and 3000 µatm), in addition to a range of CO_2 treatments identified in the IPCC climate change scenarios (Chapter1, Section 2.3).

E. huxleyi, as a known producer of DMSP, has been previously studied under elevated pCO_2 in a number of laboratory and field experiments (e.g. Archer *et al.*, 2013; Arnold *et al.*, 2013; Lee *et al.*, 2009), with varying responses of growth and calcification, and on the interactions of DMS, DMSP and the microbial community. The response of DMS, DMSP and a range of halocarbons to elevated pCO_2 had never been measured in the Norwegian coastal community in a mesocosm experiment of this scale, and to this end, the following research questions were asked:

- What were the changes in DMS and DMSP in relation to changes in microbial community structure in a mesocosm experiment focussed on the growth of the coccolithophore *E. huxleyi* under the effects of elevated pCO_2?
- Was there a linear relationship between increasing seawater pCO_2 and mean concentrations of DMS and DMSP during the experiment, as in previous mesocosm experiments (Archer *et al.*, 2013; Park *et al.*, 2014)?

- What were the changes to iodocarbon and bromocarbon concentrations in the microbial community under elevated pCO_2, and were any linear responses identified, as in previous experiments (e.g. Hopkins *et al.*, 2013)?

1.1. What is a mesocosm?

Mesocosms are a tool for examining complex ecosystems in a controlled environment, allowing manipulation of single or combined parameters in close to natural conditions. They offer a more flexible study environment than unconfined open water studies, yet allow much greater natural variation in environmental factors than a laboratory study. Mesocosms fill a unique niche in the range of experimental designs available for studying perturbations of a system. Laboratory studies are relatively small scale and focus predominately on a single species or culture, whereas field-based studies are limited in their ability to accurately isolate the effects of a single perturbation on the system, and furthermore, to extend such individual responses to ocean-scale projections. Mesocosm experiments have the advantages of being able to study the population dynamics of a system over an extended period of time, and the ability to realistically manipulate the environment of the entire water column for a single treatment (Parsons, 1981). The disadvantage of these systems is that they are not subject to the full environmental impacts that the '*in-situ*' water column is subject to (e.g. turbulence, weather, light), although the community response can be affected by a secondary variable (i.e. changes to nutrient concentration; Le B. Williams and Egge, 1998).

Mesocosm enclosures used in previous experiments have ranged in volume from a 20L carboy (Zubkov *et al.*, 2004) to >50,000 L (Riebesell *et al*., 2013a). Through the experimental design, external parameters influencing the mesocosms such as light, temperature and nutrients can be either tightly controlled (i.e. by the use of indoor mesocosms; Pinhassi *et al.*, 2005), or allowed to follow the variation in natural environments in an open-water system (Kim *et al*., 2010; Osingal *et al*., 1996; Riebesell *et al*., 2013a). Both methods can allow the controlled perturbation of either single or multiple parameters such as temperature, nutrients, CO_2 and light.

The effectiveness of mesocosms as an experimental method has led to the establishment of facilities dedicated solely to mesocosm perturbation experiments around the world, including Espegrend Station (Bergen, Norway; this study), CRETACOSMOS (Heraklion, Greece), the Aquatron Laboratory (Halifax, Canada) and MEDIMEER (Montpellier-Sete, France). Facilities such as these allow for detailed and regular sampling from the mesocosm enclosures, alongside dedicated laboratory facilities for immediate sample processing and analysis which would be otherwise difficult on-board ship.

1.2. Demonstrated use of mesocosms as an investigative tool for CO_2 studies

Mesocosm experiments are a key tool for undertaking studies investigating the effect of elevated pCO_2 on community composition and interactions, and a number of such studies have been carried out in the past decade. These include three experiments for the PeECE (Pelagic Ecosystem CO_2 Enrichment) Programme and so far three experiments for the SOPRAN (Surface Ocean Processes in the Anthropocene) Programme: EPOCA Svalbard, SOPRAN Bergen (this investigation) and SOPRAN Tvärminne (Chapter 5). Two further CO_2 perturbation experiments has been recently undertaken in Korea to investigate the dual effect of elevated pCO_2 and temperature on the phytoplankton community (Kim *et al.*, 2010; Park *et al.*, 2014).

Three PeECE experiments were carried out at the Bergen Espegrend Marine Biological station: PeECE I in 2001 (Benthien *et al.* 2007; Delille, 2005; Engel *et al.* 2005) PeECE II in 2003 (Engel *et al.* 2008; Joassin *et al.* 2011) and PeECE III in 2005 (Larsen *et al.* 2008). All three experiments used 9 mesocosm enclosures 11,000-27,000 L in volume, moored in the centre of Espegrend Bay, and exposed to 3 different pCO_2. A similar experiment was also carried out in 2006 as part of the NERC Microbial Metagenomics Experiment (Hopkins *et al.* 2010) under similar conditions to the PeECE experiments.

1.2.1. Pelagic Ecosystem CO_2 Enrichment (PeECE) I

The mesocosm enclosures used during PeECE I held approximately 11,000 L of seawater, with a depth of 4.5m. Three pCO_2 in triplicate enclosures were used: 750 µatm (IPCC A1B scenario), 350 µatm ('present day' pCO_2) and 190 µatm ('glacial' pCO_2). The headspace of the enclosures was made gas-tight using ethylene tetrafluoroethylene foil (Foiltec, Bremen, Germany).

This experiment ran for 20 days, and covered the pre-bloom, exponential and post-bloom phases of an *E. huxleyi* bloom. Elevated CO_2 had no effect on the overall community productivity during any of the phases (Engel *et al.*, 2005), however, there was a delay in the onset of *E. huxleyi* calcification, and concurrent decrease in calcification in the whole community (Delille *et al.*, 2005). Nutrient uptake was unaffected by CO_2 (Engel *et al.*, 2005).

1.2.2. Pelagic Ecosystem CO_2 Enrichment (PeECE) II

PeECE II was carried out using the same seawater pCO_2 (190, 350 and 750 µatm) and focussed on the pre-exponential and post bloom phases of a nutrient induced phytoplankton bloom. CO_2 had no identifiable effect on Chlorophyll-*a* (Chl-*a*) concentrations, or nutrient drawdown (Engel *et al.*, 2008). Noticeable variations in abundance and dominance of phytoplankton were associated with different pCO_2, with *E. huxleyi* showing the highest abundance at present-day

CO_2, and *Micromonas* spp. more abundant in the highest pCO_2. Further differences were noted by increased bacterial abundance and protein production under high pCO_2, as well as extracellular enzyme activity (Grossart *et al.*, 2006).

1.2.3. Pelagic Ecosystem CO_2 Enrichment (PeECE) III

PeECE III increased pCO_2 to 350 µatm, 700 µatm and 1050 µatm, but CO_2 still did not affect Chl-*a* concentrations, community composition or the bloom development (Paulino *et al.*, 2008), nor on the inorganic nutrient utilisation (Schulz *et al.*, 2008) or calcification (Bellerby *et al.*, 2008). In contrast to PeECE II, there was no difference in bacterial abundance or production according to ^{14}C leucine addition (Allgaier *et al.*, 2008), nor on zooplankton grazing rates (Suffrian *et al.*, 2008). Measured parameters in which high pCO_2 had an effect were: decreased viral abundance and diversity (Larsen *et al.*, 2008) and increased carbon consumption (Riebesell *et al.*, 2007). It was acknowledged, with all the PeECE experiments, that the addition of nutrients to the mesocosms may mask possible effects of CO_2 addition, which may account for the high number of studies which found no difference with increasing CO_2.

1.2.4. NERC Microbial Metagenomics Experiment

In a similar design to the PeECE experiments, the NERC Microbial Metagenomics Experiment was also performed at the National Mesocosm Centre in Bergen, and involved six mesocosms of 11,000 L seawater at pCO_2 of 300 and 750 µatm. No significant difference was identified in bacterial abundance or community composition as a result of CO_2 elevation, but picoeukaryotes were able to better exploit the higher CO_2 and the picometre community composition changed as a result (Meakin and Wyman, 2011; Newbold *et al.*, 2012).

1.2.5. Jangmok Korean Mesocosm Experiment 1, 2008

Nine mesocosms were prepared with 2400 L seawater: three at ambient CO_2 and temperature, three at ambient temperature and 900 µatm CO_2 and three 3°C higher at 900 µatm CO_2 (greenhouse; Kim *et al.*, 2010) and were sampled over 20 days. Heterotrophic dinoflagellates increased under both high pCO_2 and the greenhouse treatment, whereas *Skeletonema* and *Chaetoceros* diatoms only increased under high pCO_2: the greenhouse treatment was of similar abundance to the ambient conditions. Picoeukaryotes showed higher abundance in the greenhouse and high pCO_2 conditions.

1.2.6. EPOCA Arctic Pelagic Ecosystem Experiment, Svalbard 2010

It was clear from the previous experiments that large-scale mesocosm experiments were successful for the study of community changes under elevated pCO_2, leading to the requirement for larger, more independent enclosures (Riebesell *et al* 2010). In the mid- to late-2000s, a new generation of mesocosms were developed by GEOMAR, Kiel, Germany (KOSMOS: Kiel Off-shore Mesocosms for Future Ocean Simulations). Using different bag sizes, the enclosures were capable of containing over 70,000 L of seawater and could be tethered or float free in the open ocean, increasing the potential geographical coverage of such experiments which were no longer limited to specific mesocosm research centres.

The first major deployment of the new mesocosms took place for the EPOCA (European Project on Ocean Acidification) Arctic Pelagic Ecosystem Experiment in Svalbard in 2010 with nine mesocosms of 50,000 L volume (Schulz *et al.*, 2013), with a range of CO_2 treatments from 170 to 1420 µatm. During this experiment, run over 30 days, three distinct phases of community development (Phases I, II and III) were identified based on the addition of inorganic nutrients and the dynamics of Chl-*a* (Schulz *et al.*, 2013). Each phase was characterised by differing responses of the community to the CO_2 treatments. During Phase I, immediately after CO_2 addition, no effects of CO_2 were observed. Following the addition of inorganic nutrients (Phase II), a positive effect of CO_2 on the Chl-*a* was identified, which reversed in the post-bloom Phase III (Schulz *et al.*, 2013) . Net community production was higher during the first two phases at high pCO_2, but lower during Phase III, indicating an effect of CO_2 on community succession (Silyakova *et al.*, 2013). A clear shift towards smaller phytoplankton species was identified as CO_2 increased, having a subsequent effect on carbon distribution between the particulate and dissolved pools (Brussaard *et al.*, 2013) due to the greater efficiency of picophytoplankton to take up nutrients. No effect of increased CO_2 was identified on the microzooplankton community (Aberle *et al.*, 2013), and no significant effect on the overall community structure (Niehoff *et al.*, 2013).

1.2.7. Jangmok Korean Mesocosm Experiment 2, 2012

The second Korean mesocosm experiment used six mesocosms of 2500 L with a range of pCO_2 from 160 to 830 µatm, and three additional mesocosms at 280, 690 and 790 µatm pCO_2 elevated by 2°C. Neither pCO_2 or temperature had an effect on Chl-*a* (Park *et al.*, 2014).

1.3. Previous studies of DMS and DMSP in mesocosms under elevated pCO_2

Avgoustidi *et al.* (2012), during PeECE II, found reduced concentrations of both DMS and DMSP in the 750 µatm CO_2 mesocosms. In PeECE III, DMS was measured in two separate investigations: Vogt *et al.* (2008) did not observe differences in DMS or DMSP concentrations between ambient and 1150 µatm CO_2, but the temporal production of DMS was delayed in the high pCO_2 treatments. Wingenter *et al.* (2007) identified significantly lower DMS production in the high pCO_2 mesocosms, but these differences were attributed to different statistical analysis. During the NERC Microbial Metagenomics Experiment, Hopkins *et al.* (2010) measured DMS and DMSP, and found a significant reduction in both DMS and DMSP concentrations under 750 µatm CO_2. Archer *et al.* (2013) measured DMS and DMSP during EPOCA Svalbard, and again found that CO_2 (up to 1400 µatm) had a negative effect on DMS and DMSP concentrations. The first Korean mesocosm experiment showed increased DMS concentrations under 900 µatm CO_2, and in the greenhouse treatment attributed to increased grazing pressure (Kim *et al.*, 2010), but the second experiment showed decreased DMS and DMSP in the greenhouse conditions, attributed to a decrease in DMSP-producing dinoflagellates (Park *et al.*, 2014).

1.4. Previous studies of halocarbons in mesocosms under elevated pCO_2

Wingenter *et al*. (2007) reported concentrations of CH_2ClI and found significantly higher concentrations in the elevated pCO_2 mesocosms, with the peak in concentrations nearly 10 days later than the maximum in Chl-*a*. During the NERC experiment in 2006, iodocarbons showed a reduction of around 30% in the 750 µatm CO_2 treatment, whereas bromocarbons showed a slight increase (Hopkins *et al.* 2010). In contrast, elevated pCO_2 had no effect on concentrations of any of the halocarbons in EPOCA Svalbard, except for CH_2I_2 which increased significantly as CO_2 increased (Hopkins *et al.*, 2013).

1.5. Focus of the Surface Ocean Processes in the Anthropocene (SOPRAN) Program

This mesocosm experiment was performed as part of the SOPRAN (Surface Ocean Processes in the Anthropocene) project, funded by the BMBF and the international SOLAS programme. The SOPRAN programme studies three aspects of ocean-atmosphere biogeochemical interaction:

1. How changing atmospheric composition affects the surface ocean
2. How changing surface processes can alter oceanic emissions to the atmosphere
3. The mechanisms and rates of ocean-atmosphere material exchanges.

The SOPRAN programme encouraged the development of the KOSMOS and would allow further investigations into the impacts of ocean acidification on pelagic ecosystems in multidisciplinary experiments.

2. Design, setup and operation of SOPRAN Bergen 2011

2.1. Geographic location

The experiment was performed at the Espegrend Marine Biological Station, host to the Norwegian National Mesocosm Centre near Bergen, Norway. Nine mesocosms were deployed 1 mile offshore in RaunesFjord (N 60° 16.000', E5° 12.500'; Figure 1) from the 30th April 2011, Mesocosms were moored in lines of three, approximately 30-40m apart, with a small degree of lateral movement for each bag.

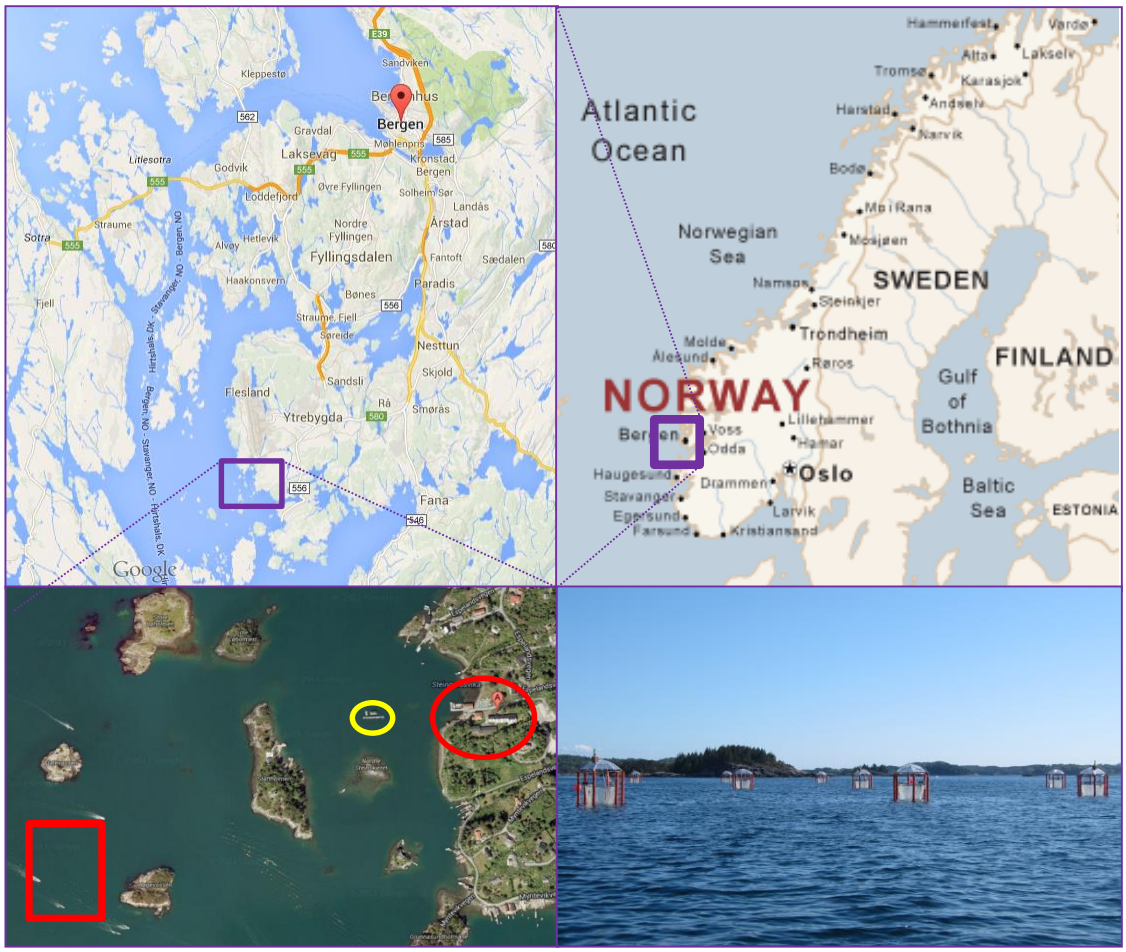

Figure 1. Map of the RaunesFjord, showing the location of the Espegrend marine station (red circle) and the area in which the nine mesocosms were moored (red square). The yellow circle defines the location of previous elevated pCO_2 mesocosm experiments at Bergen.

2.2. SOPRAN Bergen mesocosm design and deployment

Figure 2. Design of the mesocosms during SOPRAN Bergen

Each mesocosm (Figure 2) was comprised of a circular bag of thermoplastic polyurethane, 2m wide by 25m deep, a circular sediment trap affixed to the base of the bag itself, and a floating support apparatus for the mesocosm bag comprising 6 floatation pillars (Riebesell et al., 2013a). Circular retaining rings were located every 2m down the length of the bag to prevent collapse. The floatation structure was capped with a polyvinyl chloride cover to prevent excessive rainwater ingress but allowed free exchange with the atmosphere. Prior tests on the mesocosm material ensured similar depth profiles of photosynthetically active radiation (PAR) in the mesocosms with near 100% absorbance of UV light (Riebesell *et al.*, 2013).

The mesocosms were initially deployed by lowering the bags through the water with the bottom covered with 3 mm mesh to allow free exchange of phytoplankton but exclude larger organisms. Full closure by removal of the mesh and attachment of the sediment traps occurred five days after deployment, with the first CO_2 manipulation taking place nine days after deployment. Mesocosm volumes (Mean 76778 ± 2414. Kg SW) were determined by the use of salinity as a tracer (Czerny *et al.* 2013).

2.3. Addition and incorporation of CO_2 into mesocosm waters

Carbon dioxide concentrations for this experiment were based upon proposed pCO_2 from the IPCC projections for 2100 (Chapter 1, Section 2.3), with the highest CO_2 mesocosms (2000 and 3000 µatm) selected as potential atmospheric pCO_2 for beyond 2100 (Cubasch *et al.*, 2013; Houghton *et al.*, 2001).

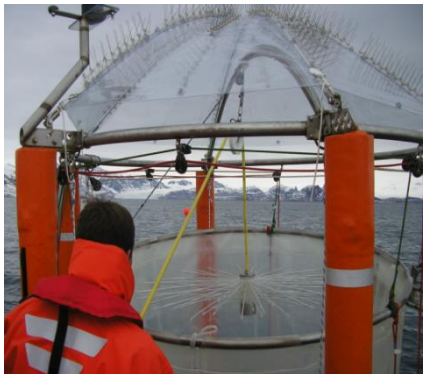

Figure 3. Deployment of the 'Spider' to distribute CO_2 enriched water to the mesocosms. Water is pumped in the pipe and trickles through multiple 'arms' as the pipe is raised and lowered through the mesocosm

The seawater within the mesocosms was mixed using an airlift to homogenise physical and chemical parameters, including nutrients, prior to the addition of CO_2. Manipulations to the carbonate chemistry of the seawater within the mesocosms was undertaken by the addition of CO_2 enriched waters (Riebesell et al., 2013a) prepared on-site using Fjord water. This method combines a technically simple way of altering the carbonate chemistry in a manner representative of elevated atmospheric CO_2, while keeping total alkalinity constant (Gattuso *et al.*, 2010), without adversely affecting trace gas concentrations or community structure. Approximately 1.5 m^3 of Fjord water was filtered and saturated with high purity CO_2, before addition of varying quantities to each mesocosm using a bespoke device ('Spider': Figure 3) to disperse the additions along all depths.

M1 **840 µatm**	**M4** **280 µatm**	**M7** **2000 µatm**
M2 **280 µatm**	**M5** **1400 µatm**	**M8** **560 µatm**
M3 **1120 µatm**	**M6** **390 µatm**	**M9** **3000 µatm**

Table 1. pCO_2 and distribution in mesocosms during SOPRAN Bergen.

Additions of CO_2-enriched seawater were made over the course of five days (T0 to T4), to achieve pCO_2 in the range 280 – 3000 µatm (Table 1). Control mesocosms (280 µatm) received no addition of CO_2 enriched water, but the 390 µatm mesocosm received a small amount to bring the pCO_2 of post-bloom waters up to atmospheric equivalent after removal of CO_2 by photosynthesis. The full details of the method used to alter the carbonate chemistry has been presented before for EPOCA Svalbard (Schulz *et al.*, 2013).

2.4. Measurement of core experiment parameters

Measurement and analysis of experimental parameters during the experiment were by standard methods unless stated otherwise (Table 2). Samples for most parameters were taken daily using a depth-integrated water sampler (IWS; Hydrobios, Kiel, Germany) deployed from a small boat. On average, 6 samplers were taken from each mesocosm daily, with the first samples from each mesocosm provided for trace gas analysis and carbonate chemistry evaluation. Each sampler was programmed to collect a sample integrated from the full 25m depth of the mesocosm. CTD casts were taken daily after the main sampling.

Table 2. Experimental parameters measured during the SOPRAN Bergen mesocosm experiment for which the data has been used during this investigation. Also given are the methods and the relevant data authors.

Parameter	Method	Author
Light	CTD mounted LI-193 quantum sensor (LICOR)	Kai Schulz (GEOMAR)
Temperature	CTD (Sun and Sea Technology PT100 temperature sensor)	
Salinity	CTD (ADM 7-pole conductivity cell)	
pH (total scale)	CTD (AMT pH sensor)	Gisle Nondal (University of Bergen)
DIC	Coulometric analysis	
Total Alkalinity	Potentiometric titration	
Chlorophyll-*a*	1. CTD (Turner Design CYCLOPS-7) 2. Fluorometry (Turner Designs)	Kai Schulz (GEOMAR)
Nutrients	Autoanalyser (AA II)	Allanah Paul (GEOMAR)
POC and PON	EuroVector Elemental Analyser (EuroEA 3000)	Kai Schulz, GEOMAR
POP	Photometric Analysis	
Pigment Analysis	HPLC (reverse-phase high performance liquid chromatography)	Yves Trense (GEOMAR)
Phytoplankton Cell Counts	Flow Cytometry (Becton Dickinson FACSCalibur)	Aud Larsen (University of Bergen)
Bacterial Abundance	Flow Cytometry and Epifluorescence microscopy	Angelika Rieck and Claudia Dziallas (Liebniz institute of Freshwater Ecology and Inland Fisheries)
Bacterial Production	^{14}C Leucine incorporation	
DMS	GC-MS	This Study
Halocarbons	GC-MS	
DMSP	GC-FPD	
DMS/ DMSP	GC-FPD	Hannah Lutterbeck AND Cathleen Zindler (GEOMAR)

2.4.1. Evaluation of pH and carbonate chemistry parameters

Samples for carbonate chemistry were taken from the first IWS deployed in each mesocosm prior to disturbance of the gas equilibria by sampling. A sub-sample of 500 mL was taken in a borosilicate bottle with a solid stopper to prevent air bubbles, before analysis for total alkalinity (Gran potentiometric titration) and total dissolved inorganic carbon (coulometric titration) (Bellerby *et al.*, 2012; Johnson *et al.*, 1985). Samples were collected from the 0-25m IWS and were analysed at 25°C. pH measurements were taken daily using the CTD equipped with AMT pH sensor with a 1 second response time; these results were corrected using the TA, DIC, temperature and salinity data to calculate pH on the total scale and using linear regression to convert the CTD measurements to the total scale. Integrated pH during the experiment was calculated from DIC and total alkalinity using the CO_2SYS software (Lewis and Wallace, 1988). Total alkalinity in the field campaigns was measured using the Gran potentiometric titration method (Bellerby *et al.*, 2012; Gran, 1952).

2.4.2. Determination and addition of inorganic nutrients

No inorganic nutrient addition took place in the mesocosms at the beginning of the experiment to allow natural progression of the community structure. Concentrations of nitrate, phosphate, silicate and ammonium were determined on a daily basis by autoanalyser, (Czerny *et al.*, 2013a; Schulz *et al.*, 2013). When nutrient concentrations approached the limits of detection, inorganic nitrate and phosphate were added to the mesocosms to stimulate a second phytoplankton bloom ('artificial bloom') on T14. Nutrient addition was by preparation of a stock solution of nitrate and phosphate using filtered Fjord water, using the sodium salts $NaNO_3$ and $NaH_2PO_4.2H_2O$, and dispersed using the CO_2 dispersal 'spider'.

2.4.3. Determination of Chlorophyll-*a* concentration

Daily Chl-*a* samples were prepared by filtering 250-500 mL of seawater onto GF/F, followed by freezing for 24 hours followed by homogenisation in acetone. Chl-*a* was determined fluorometrically using a Turner AU-10 Fluorometer (Czerny *et al.*, 2013a; Welschmeyer, 1994).

2.4.4. Determination of photo-sensitive phytoplankton pigment concentrations by HPLC

Phytoplankton pigment samples were prepared by filtering 250-500 mL of seawater onto GF/F before homogenisation in 100% acetone (HPLC grade) and centrifuging. Analysis of samples was by high performance liquid chromatography (WATERS HPLC; Barlow *et al.*, 1997).

Phytoplankton community composition was calculated according to the CHEMTAX algorithm (Mackey *et al.*, 1996; Schulz *et al.*, 2013) to determine the individual pigment concentrations, which were presented as equivalent Chl-*a* concentration for each phytoplankton grouping.

2.4.5. Determination of phytoplankton abundance

A Becton Dickinson FACSCalibur flow cytometer was used to analyse daily samples from the IWS for abundance of different phytoplankton cell groupings. This data is used in conjunction with the HPLC data and manual microscopy to determine the development and identity of the community structure during the experiment.

2.4.6. Determination of bacterial abundance and protein production

Determination of bacterial abundance for both free-living and particle associated bacteria were obtained using flow cytometry and epifluorescence microscopy, from daily samples taken from the IWS. Bacterial protein production was determined by the ^{14}C leucine addition method (Fischer and Pusch, 1999; Kirchman *et al.*, 1985).

2.5. Measurement of marine biogenic trace gas concentrations

Trace gas samples were transferred from the IWS into a 250 mL amber glass bottle in a laminar flow through a section of Tygon tubing. The bottles were rinsed twice with the sample water, before placing the tubing to the bottom of the bottle, filling from the bottom and allowing the water to overflow the volume of the bottle approximately three times before the glass stopper was inserted to prevent bubbles. Bottles were stored in a dark closed cool box for return to the laboratory.

2.5.1. Preparation and analysis of water samples for DMS and halocarbons

Analysis of trace gas samples was carried out using GC-MS for DMS, iodocarbons (CH_3I, CH_2I_2, C_2H_5I and CH_2ClI) and bromocarbons ($CHBr_3$, CH_2Br_2 and $CHBr_2Cl$; Chapter 2, Section 3). Two additional compounds (C_3H_7I and CH_2BrI) included in the analyses were below detection limit in all samples. One sample was analysed from each mesocosm daily.

On return to the laboratory, 40 mL of each mesocosm sample was drawn into a pre-rinsed 100 mL glass syringe through ¼'' nylon tubing. A 2 µL volume of a pre-prepared solution containing three surrogate analytes (Chapter 2, Section 3.4) was injected into each sample using a Hamilton syringe. Samples were injected into the purge tower through a 0.7 µm filter

(Whatman GF/F) to remove particulate matter, before purging with oxygen free nitrogen for 10 minutes at a flow rate of 90 mL min^{-1}.

During Phase 1 of the experiment (T-1 – T12), samples were trapped onto a Markes sorbent tube for analysis by the Markes Unity Thermal Desorption System (Chapter 2, Section 2.4). Technical difficulties made analysis in the field unfeasible, so the tubes were capped with Swagelok brass end caps, stored at -20°C and transferred to UEA for later analysis. During Phases 2 and 3, samples were purged and cryogenically trapped prior to injection into the GC-MS, where analysis was immediate (Chapter 2, Section 2.1).

On return to UEA, it was found that the Markes tubes had been stored at the incorrect temperature after the experiment had ended, and the samples were considered lost.

2.5.2. GC-MS Calibration

Calibrations for DMS, iodocarbons and bromocarbons were performed every 4 days (Chapter 2, Section 3.3), and used the surrogate analytes to correct for instrument drift of the GC-MS instrument. All standards were stored at -20°C in a sealed freezer away from the natural seawater samples

2.5.3. Evaluation of trace gas concentration sampling error

On each sampling day, an additional two samples were taken from a single mesocosm, resulting in three samples taken from that mesocosm. A different mesocosm was replicated each day. These triplicate samples allowed calculation of the percentage mean relative standard error for each compound analysed, but were not used in the analysis of trace gas concentrations as only one mesocosm was replicated daily. The triplicate data from each day were used to calculate the relative standard error for the entire experiment for each compound, and these were presented as a percentage of the mean concentration for each compound. These are presented in Table 3.

Table 3. Calculated percentage mean relative standard error for nine compounds analysed during SOPRAN Bergen

Compound	% Mean Relative Standard Error
DMS	10.85
CH_3I	15.05
CH_2I_2	8.53
C_2H_5I	19.23
CH_2ClI	23.26
$CHBr_3$	9.73
CH_2Br_2	10.68
$CHBr_2Cl$	6.75

2.5.4. GC-FPD analysis of DMS and DMSP

Separate water samples were analysed by Hannah Lutterbeck of GEOMAR for DMS using a separate GC-FPD system with samples injected using purge and cryotrap. This system will be used to compare the DMS samples analysed by GC-MS and the DMSP samples by GC-FPD.

2.6. Preparation and analysis of water samples for DMSP concentrations

Immediately after the gas samples had been collected into the glass syringes for the GC-MS samples, further sub-samples were taken from each glass bottle for analysis of DMSP total and particulate. The samples were prepared for analysis using the acid addition method of Curran *et al.* (1998)), and were stored in the dark at ambient temperature until the completion of the experiment and analysis at UEA.

2.6.1. Preparation of $DMSP_T$ samples

Using a pipette, 7 mL of each mesocosm sample was removed from the glass bottles and transferred to an 8 mL glass sample vial (Labhut Ltd, UK), to which 0.35 µL of 50% H_2SO_4 was added. The bottles were sealed with PTFE septum and screw caps.

2.6.2. Preparation of $DMSP_p$ samples

Using a pipette, 7 mL of sample was gravity filtered through a 25 mm GF/F. Once completed, the filter was removed and carefully folded into an 8 mL glass sample bottle containing 7 mL of high purity water (Millipore) and 0.35 µL of 50% H_2SO_4.

2.6.3. Analysis of DMSP samples

DMSP analysis was carried out at UEA using purge and cryotrap to inject samples into the GC-FPD (Chapter 2, Section 4). The system was calibrated using pre-prepared liquid DMSP standards on a weekly basis, and comparison of the calibrations showed no instrument drift.

2.7. Statistics

Minitab Version 16 software was used for statistical analysis. Tests for normality were performed on the data and if the data were found to be non-normal, they were logarithmically transformed. One-way ANOVAs were performed on the data to identify if there was significant difference between CO_2 treatments, followed by Tukey's tests to identify where the differences occurred. Each phase of the experiment underwent separate ANOVAs. The ANOVAs were performed on the three different parts of the experiment. Correlations between the datasets were identified using Spearman's Rank Correlations.

3. Results of core experimental parameters

Core parameters (salinity, turbidity, temperature, pH, nutrients, chlorophyll-*a* were measured daily. An overview of these parameters is given here.

3.1. Light penetration within the mesocosms

The results of the PAR exposure of the mesocosms showed measurements of up to 2500 µmol m^{-2} s^{-1} on some days, and below 500 µmol m^{-2} s^{-1} on T29 (Data not shown). Measurements at night were close to 0 µmol m^{-2} s^{-1}. A typical vertical profile of light measured in the mesocosms (Figure 4) shows the 10% level of incident light at 10m compared to that in the Fjord. Turbidity was higher in the mesocosms.

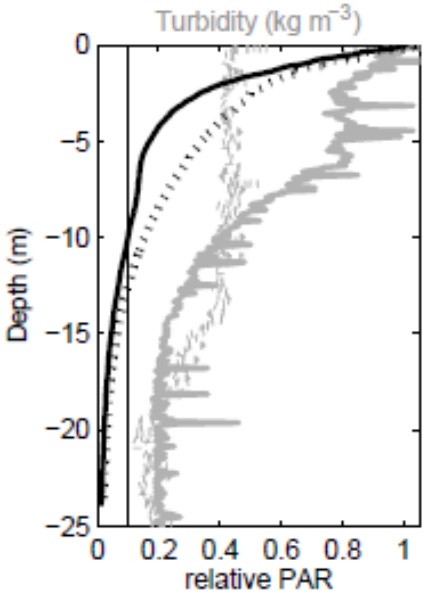

Figure 4. A typical vertical light (black) and turbidity (grey) profile of relative photosynthetic active radiation (PAR) in a mesocosm (solid) and the Fjord (dotted). The solid line marks the 10% level of incident light. Data courtesy of Kai Schulz, GEOMAR.

3.2. Temporal variations in temperature

At the beginning of the experiment the integrated seawater temperature within the mesocosm was 6.6°C and increased to 10.0°C on T15 (Figure 5). The integrated temperature range was 6.9 – 10.1 °C with a mean of 9.2°C ± 0.7.

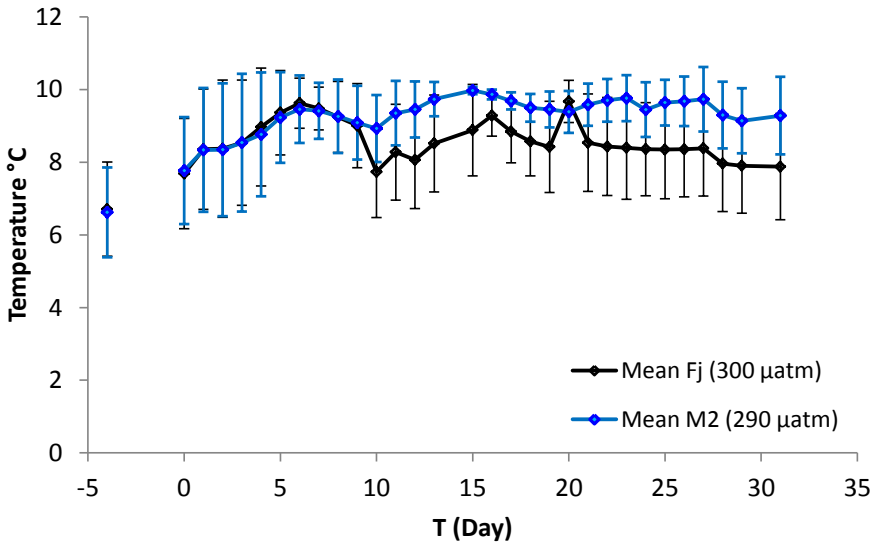

Figure 5. Depth integrated changes in temperature across the course of SOPRAN Bergen from M2 and the Fjord (Fj), based on the CTD measurements. Data courtesy of Kai Schulz, GEOMAR

Contour plots of the CTD data show that temperatures within the mesocosms followed those in the surrounding Fjord waters closely (Figure 6). The waters below 15m on T0 to T4 were below 7°C and contributed to the low temperatures seen in the integrated measurements in Figure 5; a clear thermocline had developed between 10 m and 15 m. After T4, the waters showed an increase in temperature in the deeper waters, indicative of better mixing within the Fjord water column. Surface water (0-5m) temperatures exceeded 10°C in the period T1-T7 and T26-T27, and on T15 there was no evidence of any stratification as the temperature was very similar at all depths. The temperature range was 5 – 12°C.

a) Fjord (300 µatm)

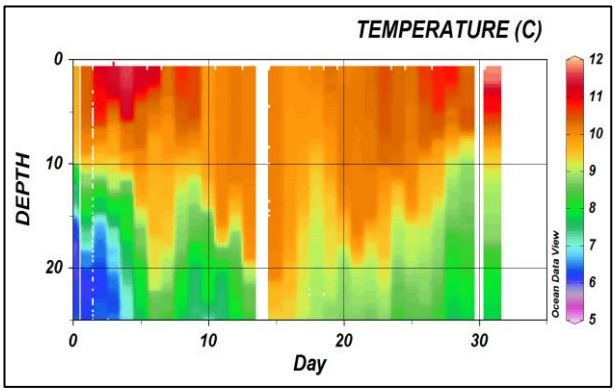

b) M2 (280 µatm)

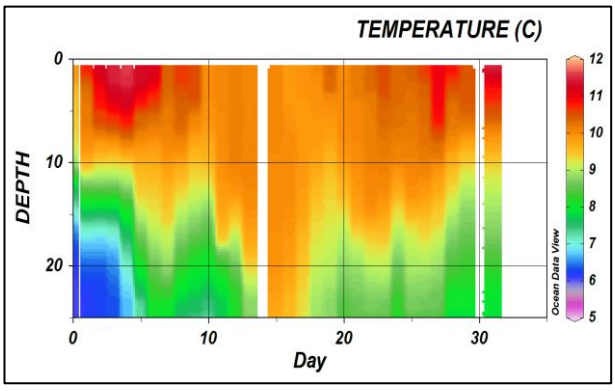

Figure 6. Measured changes to vertical distribution of temperature within the a) Fjord (Fj) and b) M2 (280 µatm) as an example mesocosm. All mesocosms showed virtually identical temperature profiles. Data courtesy of Kai Schulz, GEOMAR

3.3. Temporal variations in salinity

Practical salinity was calculated from the conductivity and temperature data from the CTD. Salinity within the Fjord varied between 29 and 33, with clear stratification (Figure 7). The

mixing of the mesocosms between T-4 and T0 resulted in an even salinity across the entire depth of the mesocosms (e.g. M2 in Figure 7). Addition of salt to determine mesocosm volume increased salinity by approximately 0.4 in all mesocosms. After T15 the effect of freshwater input from rainfall was evident in the surface 5 m of M2, and also in the Fjord waters.

a) Fjord (300 µatm)

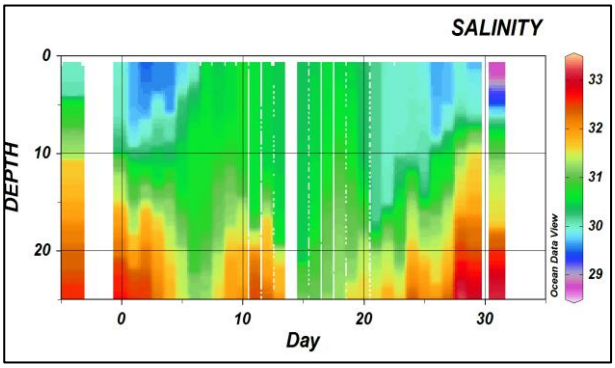

b) M2 (280 µatm)

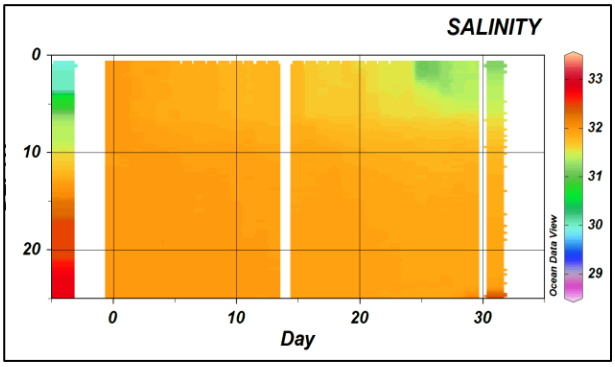

Figure 7. Measured changes to vertical distribution of salinity with time within a) the Fjord (Fj) and b) M2 (280 µatm) as an example mesocosm. All mesocosms showed virtually identical profiles. Data courtesy of Kai Schulz, GEOMAR

3.4. Changes to pH and carbonate chemistry

Carbonate chemistry parameters were calculated from pH and total alkalinity, in the methods detailed by (Schulz and Riebesell, 2013): Figure 8a shows the variation in calculated pCO_2 and Figure 8b shows the pH., with an overview of the measured CO_2 and pH changes in the whole experiment and the three separate phases is given in Table 4 for each mesocosm and the Fjord. Initial pCO_2 in all mesocosms was below the previously stated atmospheric pCO_2 of 400 µatm due to utilisation of DIC during the spring phytoplankton bloom. M6 had addition of CO_2-enriched waters to bring the pCO_2 to the atmospheric equivalent.

Table 4. Summary of mean pCO_2 and pH (total scale) during SOPRAN Bergen for the whole experiment and the individual Phases.

		Whole Experiment (T0 to T29)		Phase 1 (T0 to T9)		Phase 2 (T9 – T23)		Phase 3 (T23 – T29)	
Mesocosm	Target pCO_2 (µatm)	Mean pCO_2 (µatm)	Mean pH (pH_T)	Mean pCO_2 (µatm)	Mean pH (pH_T)	Mean pCO_2 (µatm)	Mean pH (pH_T)	Mean pCO_2 (µatm)	Mean pH (pH_T)
M2	Control	304	7.90	306	7.89	305	7.90	297	7.91
M4	Control	309	7.89	312	7.88	311	7.89	295	7.91
M6	390	372	7.83	370	7.82	379	7.82	352	7.85
M8	560	522	7.70	539	7.69	528	7.70	470	7.74
M1	840	706	7.59	742	7.58	715	7.59	603	7.65
M3	1120	850	7.53	878	7.53	870	7.51	733	7.58
M5	1400	977	7.48	1033	7.47	1006	7.46	783	7.55
M7	2000	1308	7.38	1405	7.39	1359	7.35	1006	7.46
M9	3000	1782	7.28	1963	7.28	1833	7.24	1355	7.35
Fjord	~300	297	7.91	284	7.92	302	7.91	309	7.89

BLANK

The differences between treatments are clear from T1, with the increasing additions of CO_2 enriched water giving the lowest pH at 7.03 and maximum pCO_2 (3044.9 µatm) in M9 on T5. CO_2 release through sea-air exchange and biogenic uptake for carbon fixation can be seen with the gradual decrease in CO_2 across the experiment. Although the target pCO_2 were obtained in all mesocosms, loss of CO_2 through sea-air exchange resulted in lower mean pCO_2 during the later phases.

a) CO_2

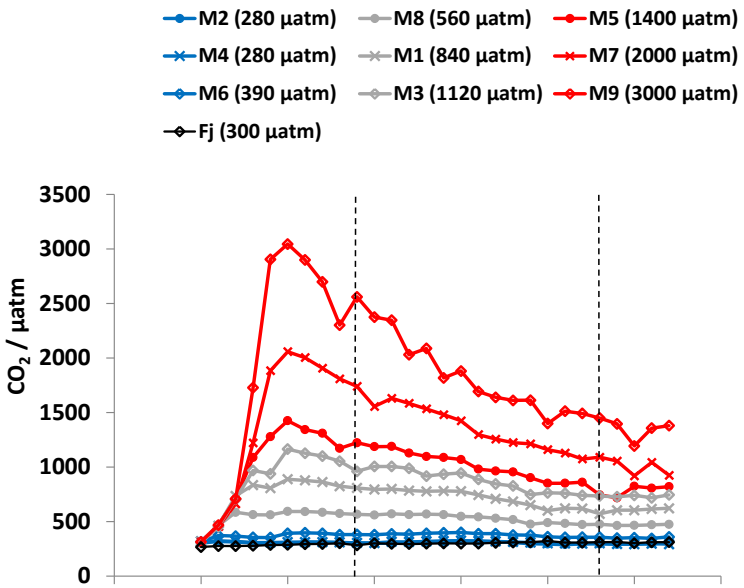

b) pH (total scale)

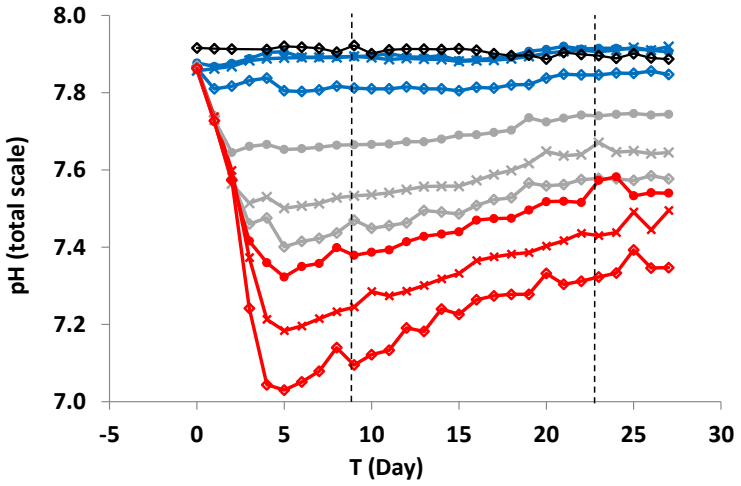

Figure 8. Daily measurements of a) pH (total scale) and b) pCO_2 (µatm) as calculated daily throughout the SOPRAN Bergen mesocosm experiment. Dashed lines indicate the sectioning into three Phases of the experiment. Data courtesy of Gisle Nondal, University of Bergen.

3.5. Microbial community development and succession

3.5.1. Temporal development of Chlorophyll-*a* concentration

Chl-*a* exhibited two distinct peaks during the experiment in all mesocosms (Figure 9). The experiment was split into three separate phases, based upon these Chl-*a* measurements and the addition of inorganic nutrients. These Phases are defined as:

- Phase 1, T-1 to T9 (11 days): the 'natural' bloom from homogenised *in-situ* nutrients;
- Phase 2, T9 to T23 (15 days): the 'artificial' bloom as a result of artificial nutrient input;
- Phase 3: T23 to 29 (7 days): the post-bloom phase.

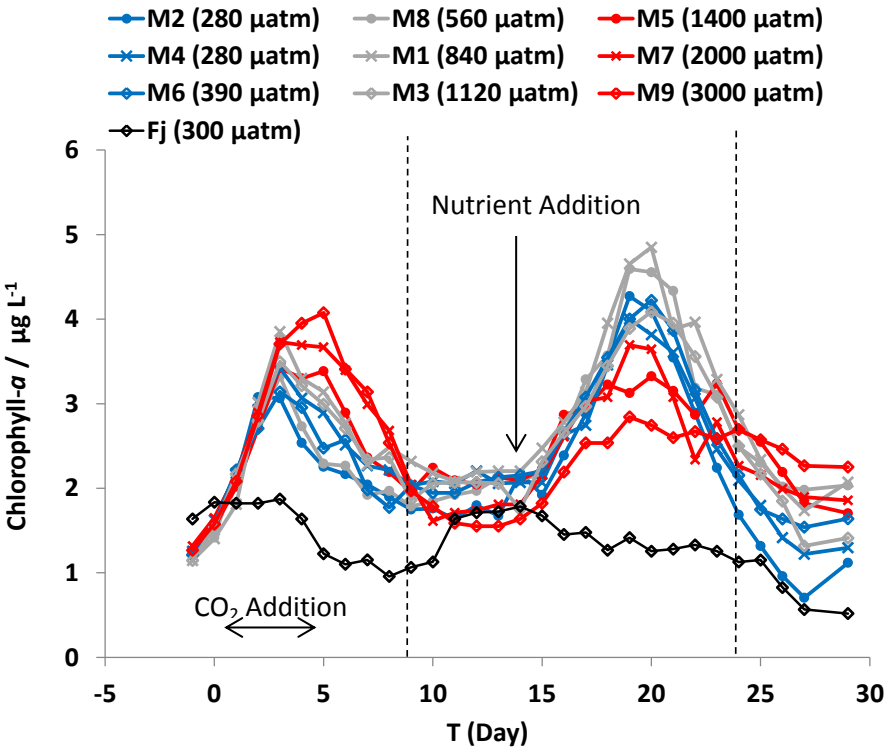

Figure 9. Concentrations of Chl-*a* (µg L^{-1}) in the nine mesocosms and the Fjord, measured by fluorometry. Dotted lines indicate the different phases of the experiment based upon this Chl-*a* data: Phase 1 as the first bloom, Phase 2 the artificial bloom and Phase 3 the post-bloom. Data courtesy of Kai Schulz, GEOMAR.

Mixing of the mesocosms at the start of the experiment brought nutrients into the upper productive water layer. This triggered the first bloom of the experiment, the 'natural' bloom. As the mesocosms were closed on T-4 and sampling began on T-1, the beginning of the bloom was missed. The Chl-*a* concentrations from the first natural bloom reach their peak at 4.07 µg L^{-1} in M9 on T5. The initial growth of phytoplankton in the period T-1 to T3 was very similar between mesocosms. However after T3, Chl-*a* concentrations start to diverge; concentrations

in the high pCO_2 mesocosms started to decline after T5 but those in the control mesocosms (280 µatm) CO_2 start to decrease on T3.

No significant differences between mesocosms were observed for the period T-1 to T3 (F=0.78, p=0.610, DF=87). There is very little difference in Chl-*a* for the first 5 days measured (up to T3), and subsequently a clear trend began to develop in relation to pCO_2 (Figure 9). A significantly higher Chl-α concentration was identified between M9 (3000 µatm) and the control M2 (280 µatm; F=2.34, p<0.05, DF=55) in the period T3 – T9.

Addition of inorganic phosphate and nitrate on T14 promoted nutrient growth in the mesocosm yet again, triggering the artificial bloom. Chl-*a* concentrations were highest in the mid-range mesocosms peaking at 4.85 µg L^{-1} in M1 (840 µatm). The lowest Chl-*a* concentrations during Phase 2 were measured in M7 at 2.34 µg L^{-1} on T22 When data for the whole of Phase 2 was analysed, no significant difference between the mesocosms were seen (F=1.83, p=0.09, DF=111). However for the period T15-T23, a significant difference between M9 and M1 was observed (F=2.52, p<0.05, DF=71).

During the final phase of the experiment (T23 – T29) Chl-*a* concentrations in the mid and low pCO_2 mesocosms fell below those of the high pCO_2 mesocosms, accompanied by significant differences in response between mesocosms. (F=8.86, p<0.05, DF=71 and see Matrix 1). In general Chl-*a* concentrations in the Fjord were lower than those observed in the mesocosms.

Matrix 1. Significant differences in Chlorophyll-*a* concentration between mesocosms during Phase 3.

	M2 (280 µatm)	M4 (280 µatm)	M6 (390 µatm)	M8 (560 µatm)	M1 (840 µatm)	M3 (1120 µatm)	M5 (1400 µatm)	M7 (2000 µatm)	M9 (3000 µatm)	FJ (300 µatm)
M2			X	X	X		X	X	X	
M4					X		X		X	
M6									X	
M8										
M1										
M3									X	
M5										
M7										
M9										
FJ										

Depth profiles of Chl-*a* fluorescence from the CTD show more detail of the growth and decline of the bloom in the mesocosms. Examples of these depth profiles are given in Figure 10. The highest detected Chl-*a* from the CTD measurements was directly corresponding to the peaks detected in the integrated samples.

a) M2: 280 µatm

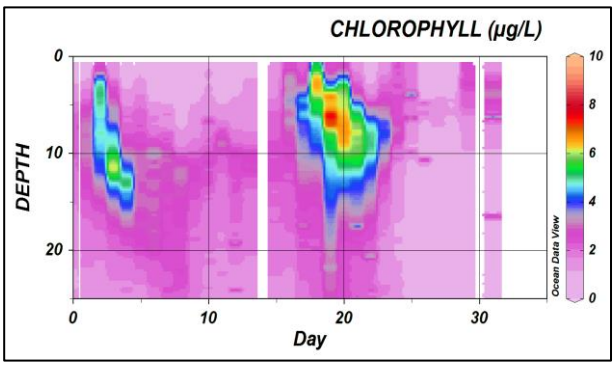

b) M9: 3000 µatm

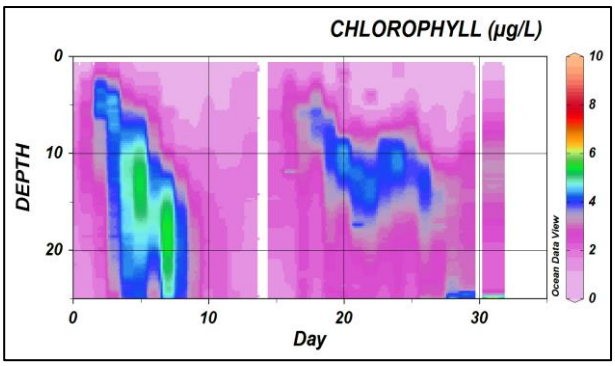

c) Fjord: 300 µatm

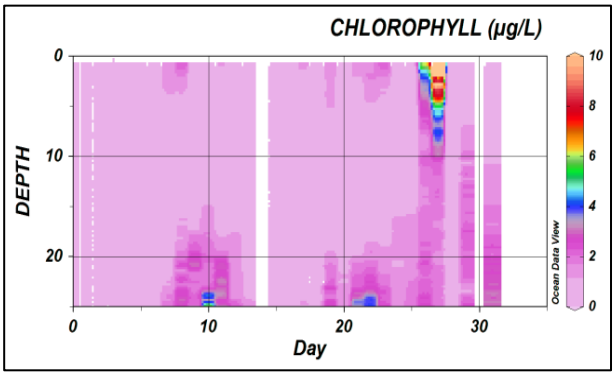

Figure 10. Measured changes to vertical distribution of Chl-*a* fluorescence with time within a) M2, b) M9 and c) Fjord. Data courtesy of Kai Schulz, GEOMAR.

3.5.2. Changes to inorganic nutrient concentrations

All nutrient concentrations decreased from the first day of measurement, and addition of nitrate and phosphate occurred to stimulate a second phytoplankton bloom after the first bloom had utilised the majority of the available nutrients (see Figure 11 and Table 5). Nitrate concentrations at the end of the experiment were at a similar concentration to the beginning, but phosphate was much lower.

Silicate showed steady decline throughout the experimental period; ammonium showed initial decreases during the first phase, and then started to increase again during the second (data not shown). In order to discourage the growth of diatoms and allow an *E. huxleyi* bloom to develop, silicate was not added to the mesocosms. Ammonium concentrations were similar between the mesocosms and the Fjord and followed the same trend as silicate, however silicate in the Fjord showed a gradual increase throughout the experiment from 0.59 µmol L^{-1} on T-1 to 1.56 µmol L^{-1} on T29 The nutrient uptake rate was approximately 20% per day, which suggested nutrient recycling was taking place. Concentrations of all nutrients in the Fjord fluctuated throughout the experiment, as tidal action transported different water masses into and out of the Fjord.

Table 5. Mean nutrient concentrations in the mesocosms at the start, end and after nutrient addition, showing the standard deviation in brackets.

Nutrient	Mean concentration T-1 (µmol L^{-1})	Mean concentration T14 prior addition (µmol L^{-1})	Mean concentration T14 after addition (µmol L^{-1})	Mean Concentration T29 (µmol L^{-1})
Nitrate	1.54 (± 0.17)	0.11 (± 0.03)	5.40 (± 0.20)	1.49 (± 0.28)
Phosphate	0.21 (± 0.01)	0.05 (± 0.01)	0.18 (± 0.02)	0.06 (± 0.02)
Ammonium	0.47 (± 0.06)	0.09 (± 0.04)	0.08 (± 0.03)	0.29 (± 0.13)
Silicate	1.21 (± 0.03)	0.46 (± 0.08)	0.46 (± 0.09)	0.11 (± 0.06)

a) Nitrate **b) Phosphate**

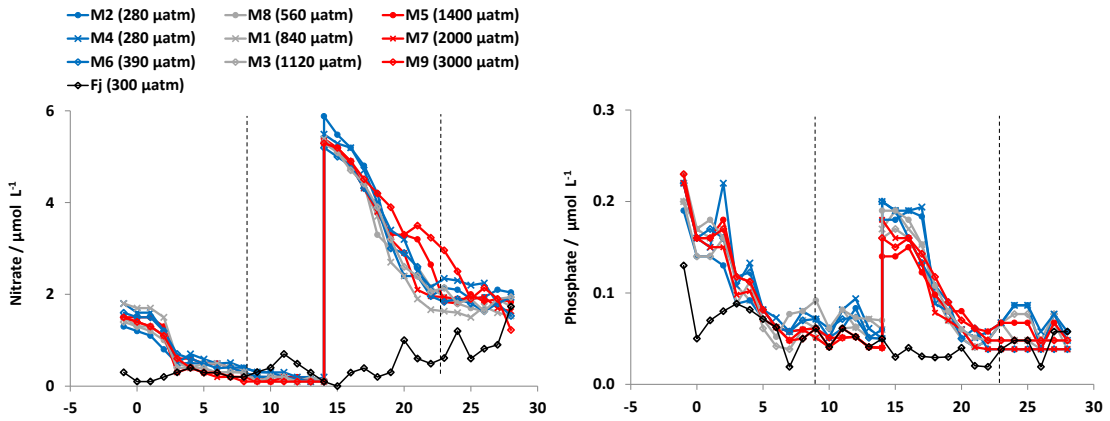

Figure 11. Depth integrated a) nitrate and b) phosphate concentrations measured in all mesocosms and the Fjord. The addition of inorganic nitrate and phosphate can be identified on T14. Dashed lines indicate the sectioning into three Phases of the experiment. Data courtesy of Allanah Paul, GEOMAR.

3.5.3. Temporal development of phytoplankton groups as identified by photo-sensitive pigments.

Phytoplankton HPLC pigment analysis showed that diatoms were the most abundant group, particularly *Skeletonema* spp. and *Nitzchia* spp. (identified from light microscopy), as well as Cryptophytes and Haptophytes which include *E. huxleyi* (Figure 12). All-together, dinoflagellates, chrysophytes and cyanobacteria contributed <4% of the total Chl-*a* during the entire experiment.

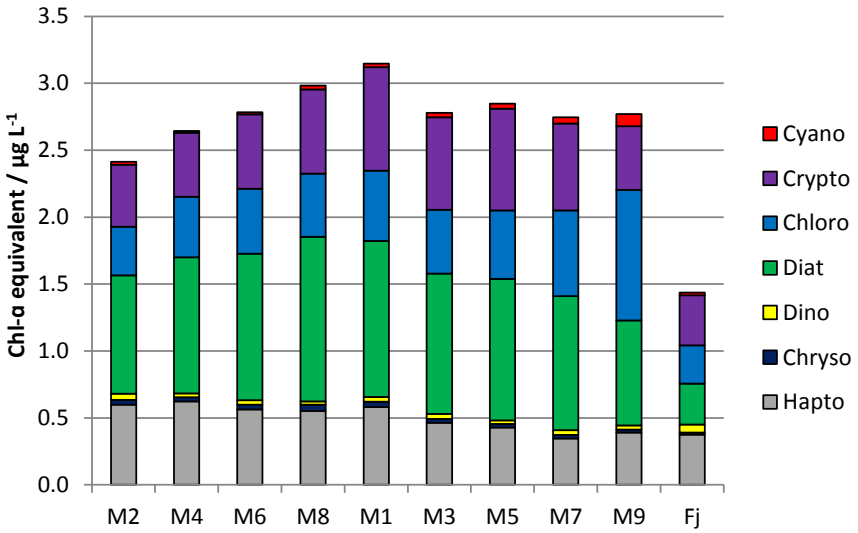

Figure 12. Mean total Chl-*a* for SOPRAN Bergen showing the breakdown per taxa for each mesocosm and the Fjord for the entire experiment. Data courtesy of Yves Trense, GEOMAR.

3.5.3.1. Community development during Phase 1

Total Chl-*a* measured by HPLC showed similar trends to fluorescence Chl-*a* measurements (Figure 9), although concentrations in the latter on average corresponded to 85.6% of the former. Total chlorophyll concentrations (Figure 13a), in Phase 1 increased from about 1.52 µg L^{-1} on T-1 to a maximum of 4.76 µg L^{-1} in M9 (3000 µatm) on T5, which was 2 days after the maximum peak in the other mesocosms. Diatoms and Haptophytes (Figure 13 e and b) corresponded with the peak in Chl-*a* in Phase 1 on T3 with concentrations of around 1.6 µg L^{-1} and 0.80 µg L^{-1} respectively. Also peaking at the same time in the low and mid-range CO_2 were the chlorophytes (*Chlamydomonas* spp., Figure 13f), which continued to grow in the high pCO_2 mesocosms past T3 and peaked on T5 at 2.16 µg L^{-1}. During Phase 1, only the chlorophytes showed notable increase in growth under elevated pCO_2 out of all the taxa ($F= 7.29$, $p<0.01$, $DF=95$).

Chrysophytes (Figure 13c) showed growth during Phase 1, but peaked much later than the total Chl-*a* peak, on T9, with highest concentrations in M1 (840 µatm) and lowest in M9 (3000 µatm) at 0.03 µg L^{-1} on the same day.

3.5.3.2. Community development during Phase 2 and Phase 3

Chrysophytes declined in concentration during Phases 2 and 3 and displayed significantly higher equivalent Chl-*a* concentrations in the mid-range and low mesocosms ($F= 5.02$, $p<0.01$, $DF=274$).

Cryptophytes grew exponentially during Phase 2, where, alongside diatom growth, this group was a key contributor to the peak in total Chl-*a*. Highest cryptophyte equivalent Chl-*a* was recorded in M5 (1400 µatm) at 1.89 µg L^{-1} on T 23, and the lowest in M9 (3000 µatm) where concentrations did not exceed 0.71 µg L^{-1}. Growth of cryptophytes was higher in the mid-range CO_2 mesocosms over the low pCO_2 mesocosms, and this indicates additional CO_2 is beneficial to cryptophyte growth but higher concentrations can be detrimental.

Haptophytes showed growth during Phases 2 and 3, when *E. huxleyi* was identified as growing exponentially. Haptophyte derived equivalent Chl-*a* continued to increase during Phase 3 when all other groups were in decline, and concentrations in the high pCO_2 mesocosms (M5, M7 and M9) was significantly lower than the control mesocosms (280 µatm) throughout the experiment ($F=8.88$, $p<0.01$, $DF=299$), in particular during Phases 2 and 3.

The dinoflagellates showed a steady decline throughout the experiment in all mesocosms with no noticeable CO_2 effect (Figure 13d), and cyanobacteria (primarily *Synechococcus* spp.)

showed slow growth through all phases, with higher equivalent Chl-*a* in the high pCO_2 mesocosms. This was especially noticeable during Phase 3, when the cyanobacterial Chl-*a* concentrations peaked in M9 (3000 µatm) at 0.4 µg L^{-1} on T28.

a) Total Chl-*a*

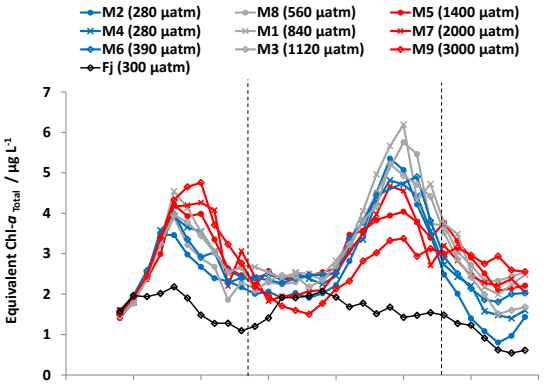

b) Haptophytes

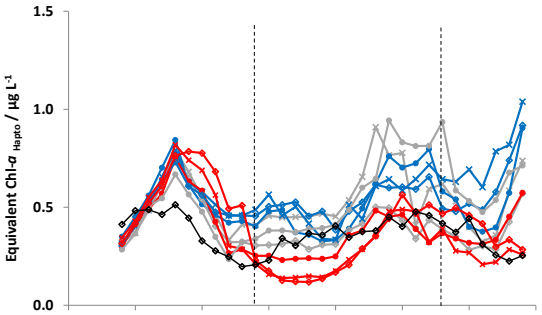

c) Chrysophytes

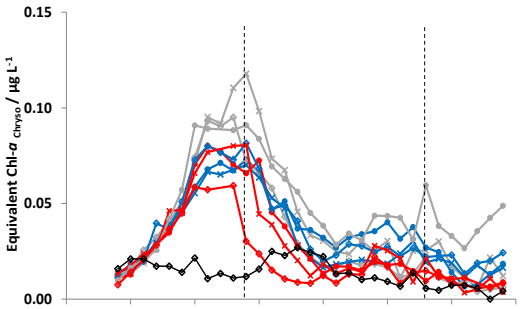

d) Dinoflagellates

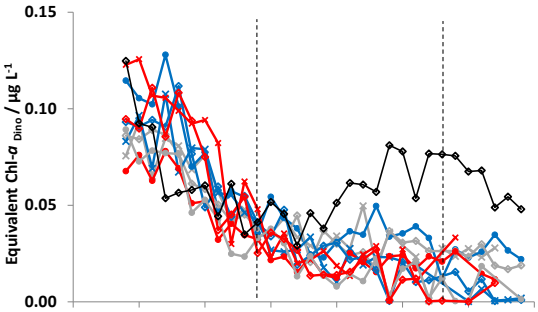

c

e) Diatoms

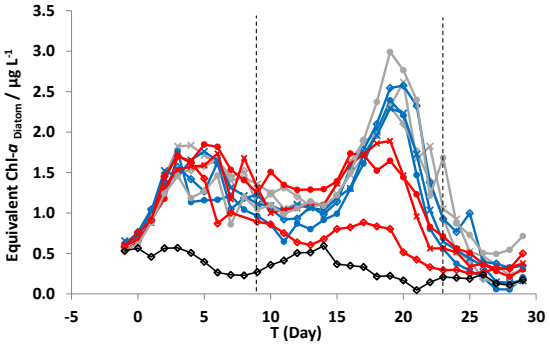

f) Chlorophytes

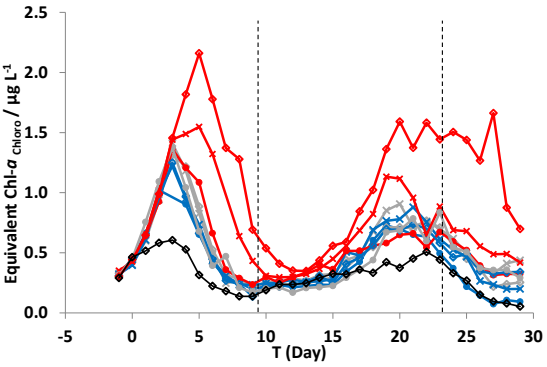

g) Cryptophytes **h) Cyanobacteria**

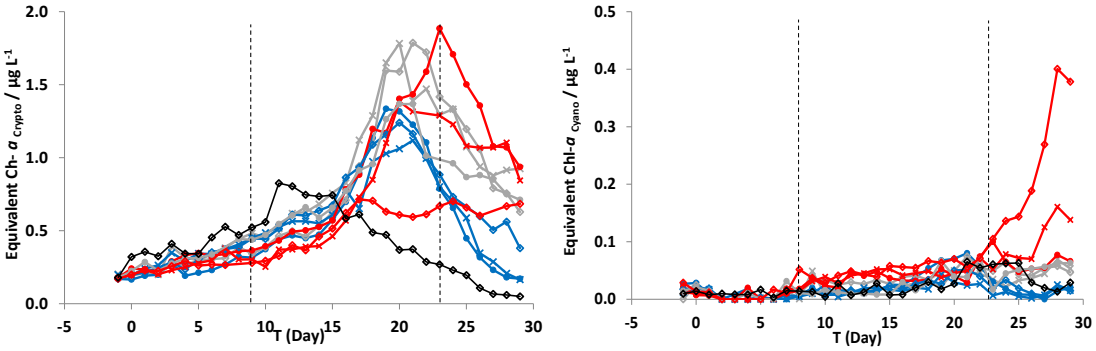

Figure 13. Temporal development of depth-averaged Chl-*a* equivalent concentrations (µg L^{-1}) of a) total equivalent Chl-*a*, within the mesocosms total depth, measured by HPLC and showing individual Chl-*a* contributions by b) haptophytes c) chrysophytes d) dinoflagellates e) diatoms f) chlorophytes g) cryptophytes and h) cyanobacteria calculated using the CHEMTAX algorithm. Dashed lines indicate the sectioning into three Phases of the experiment. Data courtesy of Yves Trense of GEOMAR, Kiel, Germany.

3.5.4. Temporal development of phytoplankton abundance as measured by Flow Cytometry

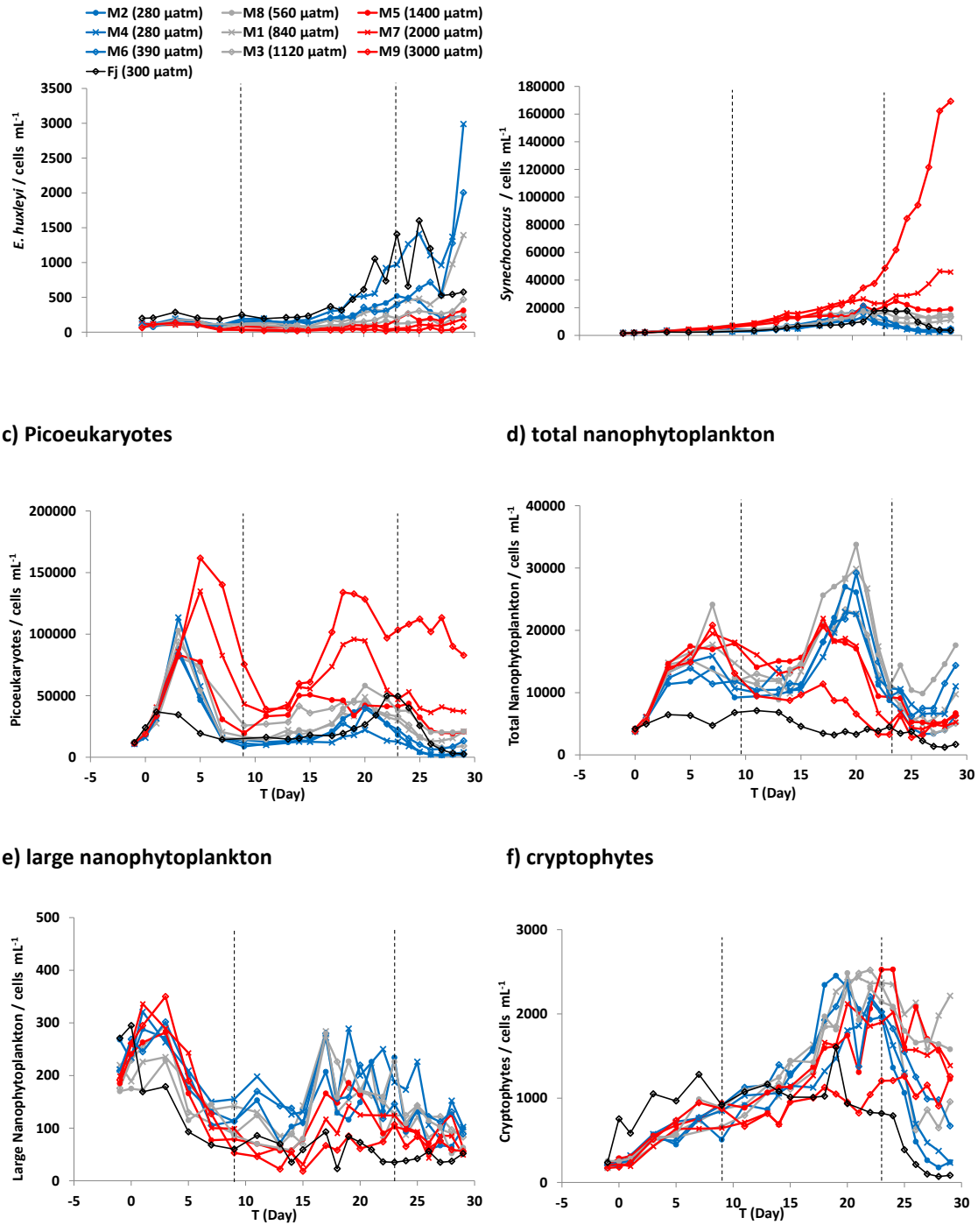

Figure 14. Flow cytometry results (cells mL^{-1}) for a) *Emiliania huxleyi*, b) *Synechococcus* c) picoeukaryotes d) total nanophytoplankton, e) large nanophytoplankton and f) cryptophytes. Dashed lines indicate the sectioning into three Phases of the experiment. Data courtesy of Aud Larsen, University of Bergen.

3.5.4.1. Community development during Phase 1

During Phase 1, an increase in abundance was observed for picoeukaryotes, the large nanophytoplankton and total nanophytoplankton. *E. huxleyi* showed little growth during Phase 1, with stable abundance of around 100 cells mL^{-1}, but cryptophytes and *Synechococcus* showed steady increases. A strong response to CO_2 was observed for the picoeukaryotes in all high pCO_2 mesocosms relative to medium and low pCO_2; M2 (280 µatm) showing 42% lower cell counts than M9 (3000 µatm), but statistically this was found to be insignificant for the period of Phase 1. No response to CO_2 was observed for all other groups (See Table 6).

3.5.4.2. Community development during Phase 2

The positive effect of CO_2 on the picoeukaryotes continued through Phase 2, where small increases were seen in the low and mid-range CO_2 peaking on T20 at 58,000 cells mL^{-1} in M8 (540 µatm), but far higher in M9 (3000 µatm) at 134,000 cells mL^{-1} on T18. This trend continued into Phase 3. Total nanophytoplankton, large nanophytoplankton and cryptophytes showed growth during Phase 2 which corresponded to the artificial bloom in Chl-*a* and which peaked on T20. Notable during this during this period was the steady growth of *E. huxleyi* which carried on into Phase 3, during which a clear trend of lower cell abundance under elevated pCO_2 was developing.

3.5.4.3. Community development during Phase 3

During this phase, *Synechococcus* in M9 (3000 µatm) grew exponentially: maximum cell count was recorded as 169,000 cells mL^{-1} in M9 but only 2500 cells mL^{-1} in M2 (280 µatm) on T29; growth was significantly higher in the elevated pCO_2 mesocosms over the control ($F=11.45$, $p<0.01$, $DF=158$). The growth of calcified *E. huxleyi* continued during Phase 3, with maximum cell counts in M4 (280 µatm) of 3000 cells mL^{-1} on T29. Overall, *E. huxleyi* cell counts in the high pCO_2 mesocosms were significantly lower than the low and mid-range CO_2 treatments (See Table 6). Non-calcified *E. huxleyi* are indistinguishable from other nanophytoplankton in the flow cytometry groupings.

Community data were analysed by one-way ANOVA to identify differences in cell abundance and chlorophyll between mesocosms and CO_2 treatments (Table 6). For dinoflagellates and cryptophytes, significant differences were identified between mesocosms, but the differences were not driven by CO_2 treatment, and were likely a result of differences in nutrient concentration or community interactions as there was no significant difference between the control and highest pCO_2.

Table 6. Summary of the statistical analysis of the phytoplankton groupings (HPLC Pigment analysis) and cell abundance (flow cytometry) for Phase 1, and Phases 2 and 3 combined. Values shown are the F-values ($p<0.01$) after one-way ANOVA on the datasets, and the effect of CO_2 is noted as either a positive or negative effect of increasing CO_2 on growth. (*) identified differences between mesocosms not due to CO_2. SD: significant difference.

	Phase 1			Phases 2 and 3		
	F-value	Degrees of Freedom	Effect of CO_2	F-value	Degrees of Freedom	Effect of CO_2
Phytoplankton grouping						
Diatoms	No SD	96		2.75	188	Negative
Haptophytes	No SD	97		16.74	188	Negative
Chrysophytes	No SD	95		5.87	187	Negative
Dinoflagellates	2.23*	98		6.96*	163	
Chlorophytes	2.80	95	Positive	12.21	188	Positive
Cryptophytes	No SD	95		4.46*	184	
Cyanobacteria	No SD	97		10.32	187	Positive
Total Chlorophyll	No SD	97		8.48	188	Positive Phase 3.
Cell abundance						
E. huxleyi	No SD	61		13.45	111	Negative
Synechococcus	No SD	61		11.45	158	Positive
Picoeukaryotes	No SD	61		46.07	153	Positive
Total nanophytoplankton	No SD	61		2.74	154	Only M9 Sig lower
Large nanophytoplankton	No SD	61		7.35	154	Negative
Cryptophytes	No SD	61		3.88	160	Only M9 Sig lower

3.5.5. Changes in bacterial abundance and protein production

The bacterial abundance increased from around 500,000 cells mL^{-1} on T-1 through Phase 1 (Figure 15a). A peak in bacterial numbers was seen on T15 in the high pCO_2 treatments, but not until T21 in the control mesocosms (280 µatm), at which point the high pCO_2 mesocosm abundance had started to increase once more. The bacterial abundance in the low and medium pCO_2 mesocosms decreased through the post-bloom Phase. CO_2 had a strong positive effect on bacterial abundance (F-4.90, p<0.01, DF=203), with maximum bacterial abundances of 4.5 million cells mL^{-1} in M9 (3000 µatm) on T25. Numbers in the Fjord were lower than in the mesocosms in Phases 2 and 3.

a) Total bacterial abundance **b) Total bacterial protein production**

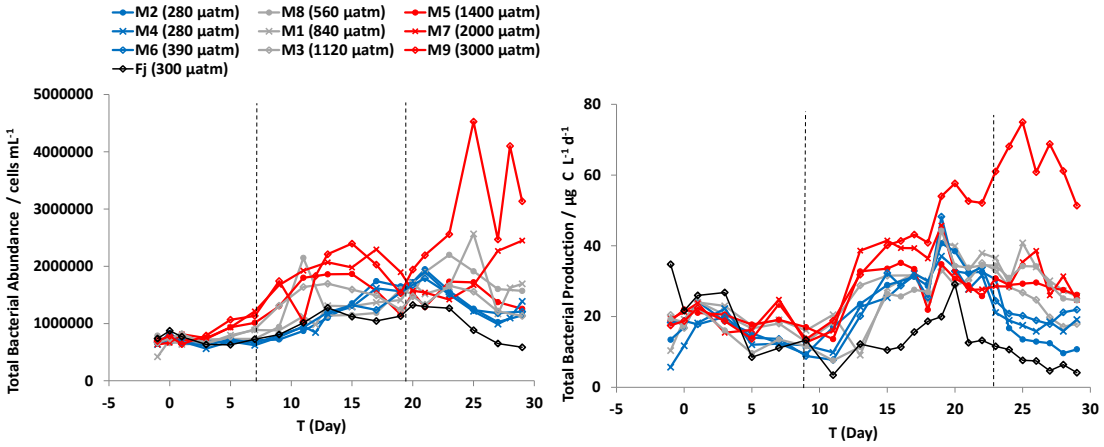

Figure 15.a) Total bacterial abundance (cells mL^{-1}) and b) total bacterial protein production (µg C L^{-1} d^{-1}) in the mesocosms. Dashed lines indicate the sectioning into three Phases of the experiment. Data courtesy of Angelika Reisch, IGB-Berlin.

All mesocosms showed similar bacterial protein production during Phase 1 (a mean of 15.0 µg C L^{-1} d^{-1} on T-1) before increasing during Phase 2 and 3 to a maximum of 75.0 µg C L^{-1} d^{-1} in M9 (3000 µatm) on T25 (Figure 15b). Bacterial protein production was significantly elevated in M9 (3000 µatm; F=8.61, p<0.01, DF=209) compared to the other mesocosms, but no other significant differences were observed. The Fjord showed significantly lower production than the mesocosms during Phases 2 and 3 (F=18.16, p<0.01, DF=172).

4. Trace gas concentrations

4.1. Dynamics of DMS and DMSP

4.1.1. Measured DMS and DMSP concentrations

DMS measurements began on T12 and were recorded daily throughout Phases 2 and 3 up until T29 (Figure 16). The results of the precursor DMSP measured as total ($DMSP_T$) and particulate ($DMSP_P$) are given in Figure 17a and b, with dissolved DMSP calculated from the total and particulate measurements (Figure 17c).

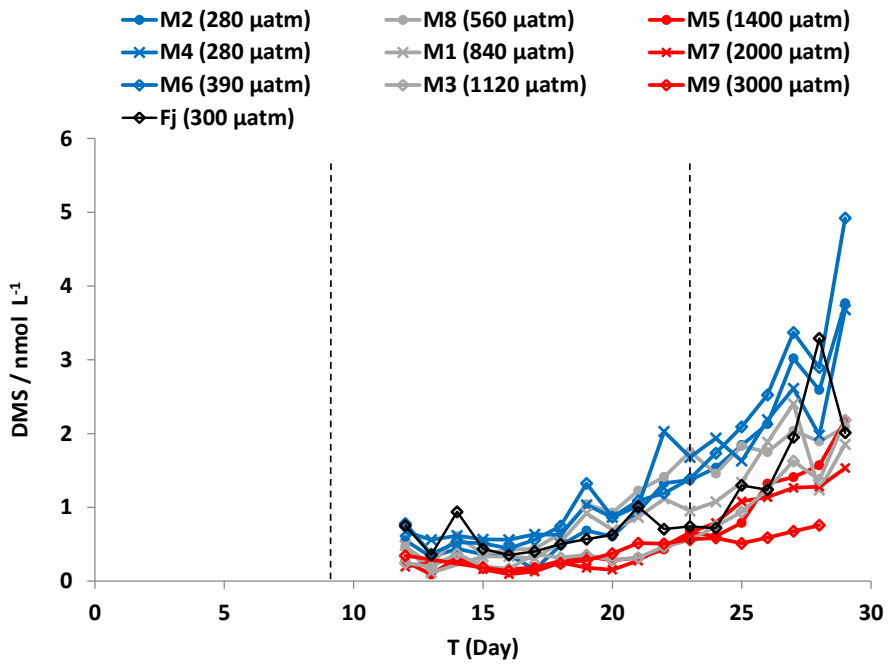

Figure 16. Temporal changes in DMS concentrations (nmol L^{-1}) from all mesocosm and the Fjord during the SOPRAN Bergen mesocosm experiment. Dashed lines indicate the sectioning into three Phases of the experiment.

a) $DMSP_T$

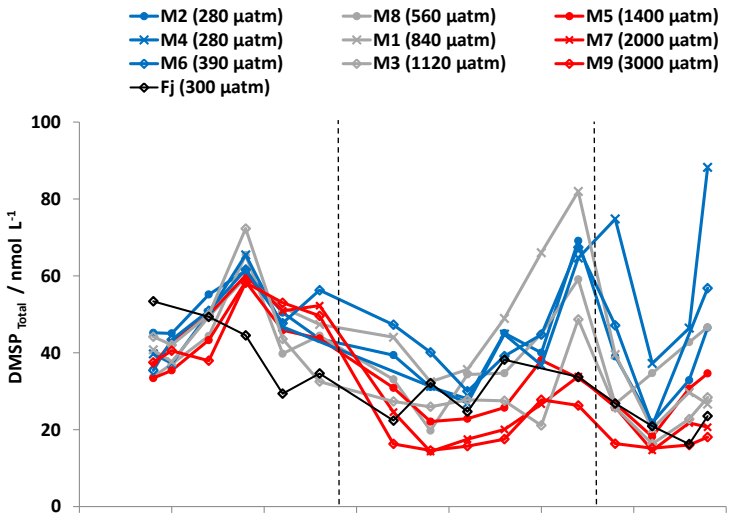

b) $DMSP_P$

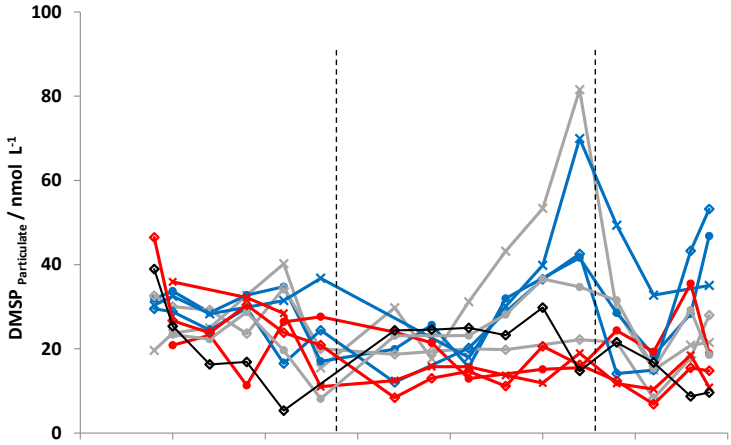

c) $DMSP_D$

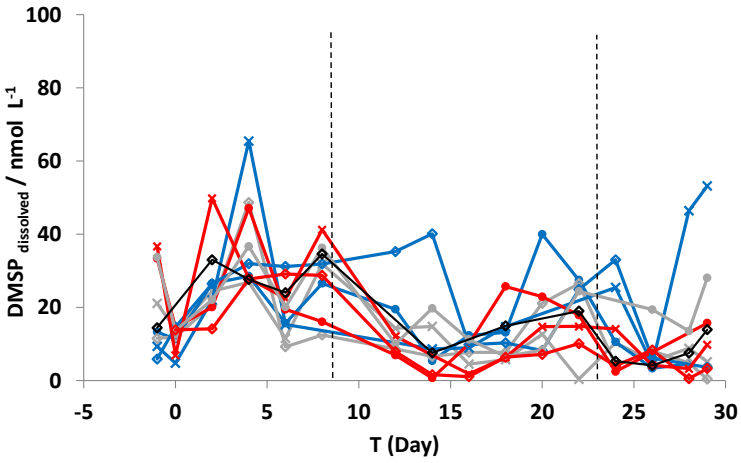

Figure 17. Temporal changes in a) $DMSP_T$ b) $DMSP_P$ and C) $DMSP_D$ concentrations (nmol L^{-1}) during SOPRAN Bergen. Dashed lines indicate the sectioning into three Phases of the experiment.

Concentrations of DMS were found to be low (<0.5 nmol L^{-1}) in all mesocosms prior to the addition of nutrients on T14, but started to increase on T18, with CO_2 adversely affecting DMS concentrations. Maximum DMS concentrations in the mesocosms were seen in the control M4 (280 µatm) at 4.9 nmol L^{-1} on T29; in comparison, the lowest DMS measurement at the end of the experiment was in M9 (3000 µatm) at 0.76 nmol L^{-1} on T28. DMS concentrations showed only steady increases in all mesocosms towards T29. The high pCO_2 mesocosms (>1120 µatm) showed significantly lower DMS concentrations compared to the control mesocosms (<560 µatm; F=9.54, p<0.05, DF=115). Significant differences identified during both Phases are highlighted in Matrix 2.

Matrix 2. Significant differences highlighted by the Tukey's Test between mesocosms for DMS concentration during the second (upper portion) and third (lower portion) phases of the experiment.

	M2 280 µatm	M4 280 µatm	M6 390 µatm	M8 560 µatm	M1 840 µatm	M3 1120 µatm	M5 1400 µatm	M7 2000 µatm	M9 3000 µatm	FJ 300 µatm	
M2							X	X			
M4						X	X	X	X		
M6						X	X	X	X		
M8						X	X	X	X		Phase 2
M1								X			
M3	X		X								
M5	X	X	X	X	X	X				X	
M7	X	X	X	X	X	X				X	
M9	X	X	X	X	X	X	X	X			
FJ											
Phase 3											

$DMSP_T$ increased from the first day of analysis (T-1) until T4, a day after the Chl-*a* peak for the natural bloom (Figure 9), after which concentrations decreased (once more) in all mesocosms. The highest $DMSP_T$ concentration during Phase 1 was measured in M8 (560 µatm) at 72.3 nmol L^{-1}. During Phase 1, there was no significant effect of CO_2 on $DMSP_T$ concentrations (F= 0.42, p =0.916, DF=57). The results from the Fjord do not follow the same trends as the mesocosms,

where $DMSP_T$ and $DMSP_P$ decrease through Phase 1. $DMSP_P$ did not show evidence of the increases in $DMSP_T$ during Phase 1 (Figure 17b): no peaks were determined in any of the mesocosms, and no overall change in concentration was noted from T-1 to T9. Although some variation can be seen both between and within mesocosms, the mean $DMSP_P$ for the period T0-T6 was 28.5 (± 7.9) nmol L^{-1}.

Concentrations of $DMSP_T$ and $DMSP_P$ in the high pCO_2 mesocosms during Phase 2 were significantly lower than the control mesocosms ($F=4.41$ $p<0.05$, $DF=58$). A second peak in $DMSP_T$ occurred on T20 in the high pCO_2 mesocosms (M9, M7 and M5) and on T22 in all other treatments. This peak corresponded with the peak in Chl-*a* on T19. No increase was seen in $DMSP_P$ concentrations during Phase 2 in the high pCO_2 mesocosms (M9, M7 and M5) or in M3 (1120 µatm), where concentrations stayed around 20 nmol L^{-1}, but a peak was identifiable in the low and medium pCO_2 mesocosms (M1 and M8) on T22. The maximum $DMSP_P$ of the whole experiment was measured in M1 on T22 at 81.54 nmol L^{-1}.

Unlike DMS, where concentrations during Phase 3 continued to increase, $DMSP_T$ decreased in all mesocosms after Phase 2, to minima on T26, before concentrations again increased up until T29. This same trend was identified in $DMSP_P$, and was similar to the trends showed by Chl-*a*.

Table 7. Summary of statistical analyses on DMS and DMSP data to determine the presence of significant effects of high pCO_2. As Phase 3 contained limited data points, Phases 2 and 3 were analysed together.

	Statistical Details		
	Phase 1	Phases 2 and 3	Degrees of Freedom
DMS	No Data	$F = 5.52$, $p<0.01$	174
$DMSP_T$	No SD	$F = 5.63$ $p<0.01$	78
$DMSP_P$	No SD	$F = 7.15$, $p<0.01$	56

Mean DMS and $DMSP_T$ concentrations from each mesocosm show a linear decrease as CO_2 increased (Figure 18) up to 3000 µatm (Mean pCO_2 of 1782 µatm). Mean DMS in the medium pCO_2 mesocosms were 33% lower than the low (280 and 390 µatm), with high pCO_2 mesocosms 60% lower. Mean $DMSP_T$ was 13.9% and 31.6% lower respectively.

a) DMS **b) $DMSP_T$**

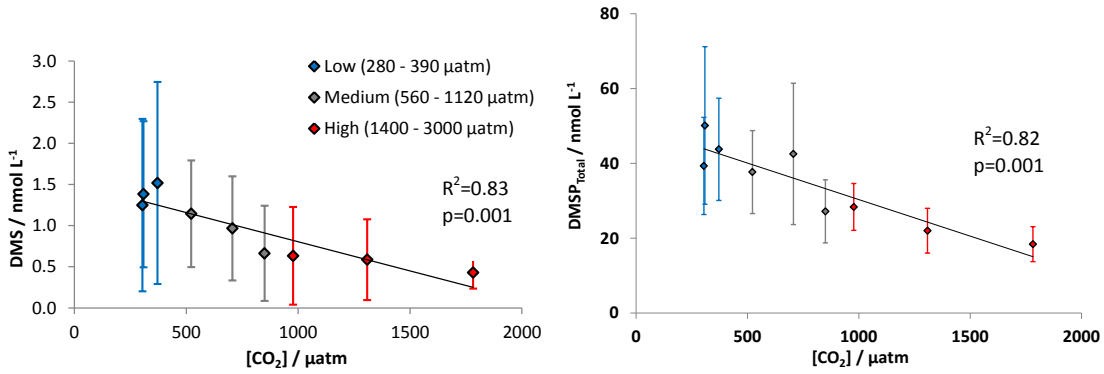

Figure 18. Mean a) DMS and b) $DMSP_T$ concentrations (nmol L^{-1}) in each mesocosm plotted against mean pCO_2 for Phases 2 and 3. Error bars show the standard deviation of measurements.

4.1.2. Ratios of DMS: $DMSP_T$ and $DMSP_P$

The ratio of DMS to $DMSP_T$ (Figure 19a) showed little difference between treatments during Phase 2. During Phase 3 the ratio started to increase due to increasing DMS concentrations, with 14% mean reduction between the high pCO_2 and the control (280 and 390 µatm) treatments. In contrast, the ratio of $DMSP_T$: $DMSP_P$ showed no significant differences between CO_2 treatments at any Phase of the experiment (Figure 19b).

a) DMS: $DMSP_T$ **b) $DMSP_T$: $DMSP_P$**

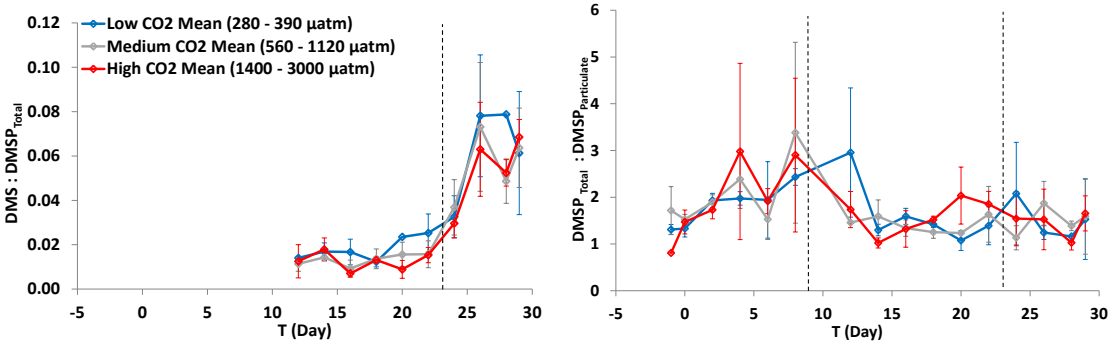

Figure 19. Ratio of a) DMS to $DMSP_T$ and b) $DMSP_T$: $DMSP_P$ showing the mean for three different CO_2 conditions: low pCO_2 (280 – 390 µatm), medium pCO_2 (560 – 1120 µatm) and high pCO_2 (1400 – 3000 µatm). Error bars show standard deviation within the CO_2 ranges. Dashed lines indicate the sectioning into three Phases of the experiment.

4.1.3. DMS and DMSP correlations with microbial community development

To identify the correlations between the different measurements carried out during the experiment, Spearman's Rank Correlation Analysis was used to identify relationships between

DMS and DMSP and other parameters. Results from the test range from strong negative correlation (-1), no correlation (0) or strong positive correlation (1). As DMS data was only available during Phases 2 and 3, the correlations for DMS do not include Phase 1 data. Correlations for $DMSP_T$ and $DMSP_P$ include all three Phases.

Table 8. Spearman's Rank correlation coefficients for DMS (Phases 2 and 3) and DMSP (All Phases) data compared to Chl-*a*, the phytoplankton taxonomy (from HPLC pigment data) and abundance of small phytoplankton (<10µm) (from flow cytometry). Coefficients are significant at 99% confidence limits, except those highlighted (*) at only being significant at 95%. NS: Non-significant. A dash corresponds to datasets without sufficient available data to perform a Spearman's Rank correlation.

	All CO_2			
	DMS	$DMSP_T$	$DMSP_P$	Chl-*a*
DMS (nmol L^{-1})				
$DMSP_T$ (nmol L^{-1})	0.339			
$DMSP_P$ (nmol L^{-1})	0.277	0.650		
Chl-*a* (µg L^{-1})	-0.406	0.400	0.198*	
Phytoplankton Taxonomy (Equivalent Chlorophyll µg L^{-1})				
Total Equivalent Chlorophyll-*a*	-0.302	0.291	-	-
Diatoms	-0.487	0.301	-	-
Haptophytes	0.508	0.635	-	-
Chrysophytes	NS	0.579	-	-
Dinoflagellates	-0.222*	0.383	-	-
Chlorophytes	-0.213*	0.296	-	-
Cryptophytes	NS	0.323	-	-
Cyanobacteria	NS	-0.488	-	-
Small Phytoplankton (<10µm) abundance (cells mL^{-1})				
Synechococcus	-0.209*	-0.491	-0.391	0.365
E. huxleyi	0.615	NS	0.241	NS
Picoeukaryotes	-0.477	NS	NS	0.466
Total nanophytoplankton	-0.279	0.283	NS	0.698
Large nanophytoplankton	NS	0.435	0.489	0.239
Cryptophytes	-0.255	NS	NS	0.457
Bacterial Abundance and Rates				
Bacterial Abundance (cells mL^{-1})	-0.216*	-	-	-
Bacterial Protein Production (µg C L^{-1} d^{-1})	-0.375	-0.288	-	-

4.1.4. DMS and DMSP and the relationships with Chl-*a*

The ratio of DMS to Chl-*a* was calculated for each mesocosm daily and was then averaged for the low, medium and high pCO_2 mesocosms (Figure 20a); during Phase 2, the ratio was below 1, before increasing in all mesocosms throughout Phase 3.

a) DMS: Chl-*a*

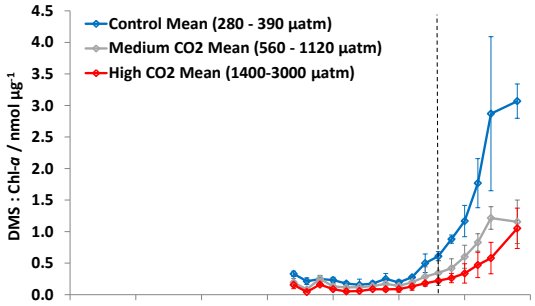

b) $DMSP_T$: Chl-*a*

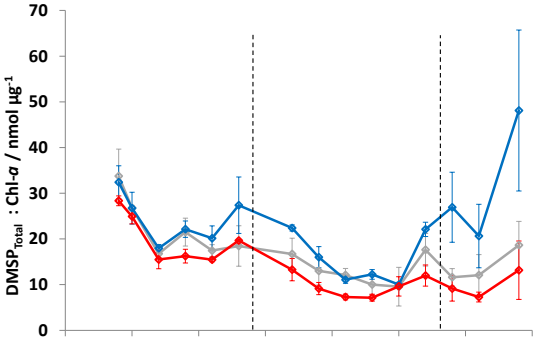

c) $DMSP_P$: Chl-*a*

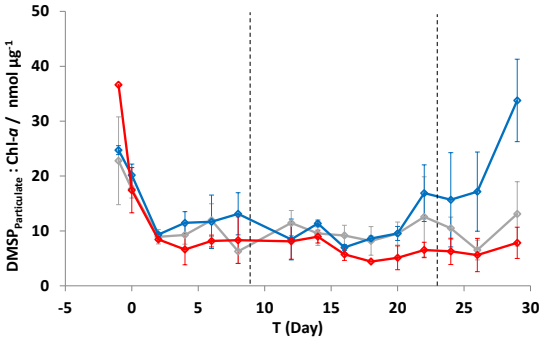

Figure 20. Temporal changes in the ratio between Chl-*a* and a) DMS, b) $DMSP_T$ and c) $DMSP_P$ (nmol μg^{-1}) for three different CO_2 conditions: low pCO_2 (280 – 390 µatm), medium pCO_2 (560 – 1120 µatm) and high pCO_2 (1400 – 3000 µatm). Error bars show standard deviation within the CO_2 ranges. Dashed lines indicate the sectioning into three Phases of the experiment.

DMS was negatively correlated with Chl-*a* (ρ=0.406, p<0.01), but total DMSP was positively correlated (All data given in Table 8). However this was not reflected in the correlation with Chl-α and particulate DMSP (ρ=0.198, p<0.05), despite the strong correlation with $DMSP_T$ (ρ=0.650, p<0.01).

4.1.5. DMS and DMSP and the relationships with community composition

Increasing CO_2 had a positive effect on the ratios between DMS, DMSP and *E. huxleyi* abundance. This suggests that higher DMS and DMSP production per cell occurred as CO_2 increased, particularly during Phase 3 (Figure 21 a and b). DMS production normalised per calcified *E. huxleyi* cell remained stable below 5 fmol $cell^{-1}$ in all mesocosms until T21, when mean production from the high pCO_2 mesocosms increased to below 20 fmol $cell^{-1}$. In the low and mid-range treatments, the ratio remained stable until T26 when it increased. Limited data are available for DMSP per cell due to alternating sampling days between the flow cytometry and the $DMSP_T$ measurements, however $DMSP_T$ concentration normalised per calcified cell showed a clear CO_2 effect and was higher in the highest CO_2 mesocosms, peaking on T23 at 0.99 (± 0.71) pmol $cell^{-1}$.

These trends are not observed in the ratios of DMS and DMSP to Haptophyte Chl-*a* (Figure 21c and d). DMS per unit of Haptophyte Chl-*a* showed steady increases in all mesocosms from T12 up until T27, with the high pCO_2 treatment mesocosms showing significantly lower DMS per unit haptophyte Chl-*a* than the low and mid-range treatments. $DMSP_T$ per unit haptophyte Chl-*a* showed variation across the experiment, but an effect of high pCO_2 on only T8 – T13, where the ratio was higher in the high pCO_2 mesocosms.

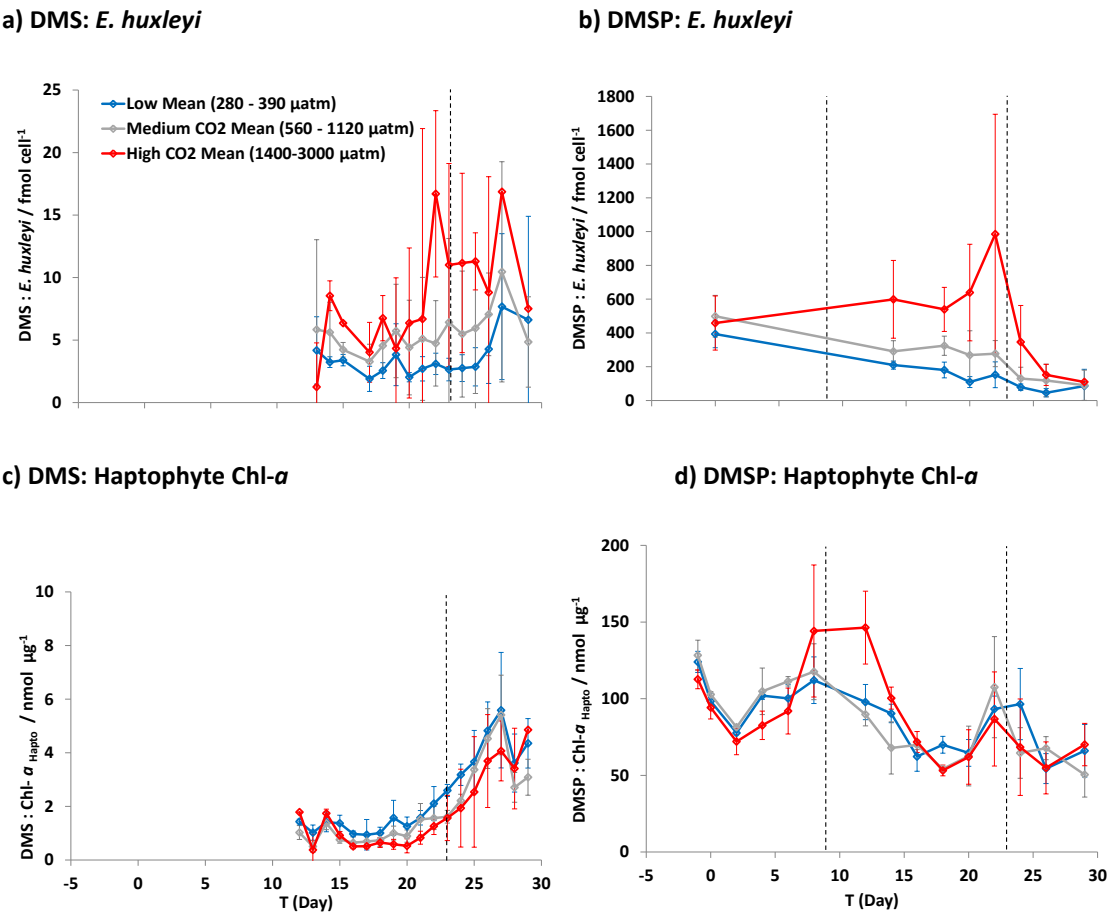

Figure 21. Temporal changes in the ratio between a) DMS and *E. huxleyi* (fmol cell^{-1}) b) DMSP$_T$ and *E. huxleyi* (fmol cell^{-1}) c) DMS and Haptophyte Chl-*a* (nmol µg^{-1}) and d) DMSP$_T$ and Haptophyte Chl-*a* (nmol µg^{-1}) for three different CO_2 conditions: low pCO_2 (280 – 390 µatm), medium pCO_2 (560 – 1120 µatm) and high pCO_2 (1400 – 3000 µatm). Error bars show standard deviation within the CO_2 ranges and dashed lines indicate the sectioning into three Phases of the experiment. *E. huxleyi* data were obtained from the flow cytometry data analysed by Aud Larsen (University of Bergen) and Haptophyte Chl-*a* data were obtained from the HPLC CHEMTAX analysis by Yves Trense (Geomar).

Both DMS and DMSP show strong positive correlations with the Haptophyte Chl-*a* concentration (ρ=0.508 and 0.635 respectively, p<0.01; Table 8) but only DMS had a significant correlation with *E. huxleyi* cell count (ρ=0.615, p<0.01). DMSP$_T$ was non-significantly correlated with *E. huxleyi*, but showed significant correlation with total and large nanophytoplankton (which DMS did not correlate with), (ρ=0.283 and 0.435 respectively, p<0.01). There was also significant negative correlation with *Synechococcus* (ρ=-0.491, p<0.01).

Almost all the major phytoplankton groupings identified using HPLC showed positive correlations with DMSP$_T$ (Table 8), except for the cyanobacteria. The same correlations were not seen with DMS concentrations, where diatoms (ρ=-0.487, p<0.01), dinoflagellates (ρ=-

0.222, p<0.05) and Chlorophytes (ρ=-0.213<0.05) all showed significant negative correlations, and cryptophytes, cyanobacteria and chrysophytes showed no correlation with DMS.

4.1.6. DMS, DMSP and the relationship with bacterial abundance and protein production

DMS was negatively correlated with both bacterial abundance (ρ=-0.216, p<0.05) and bacterial protein production (ρ=-0.375, p<0.01; Table 8). Negative correlation was also identified between $DMSP_T$ and bacterial protein production (ρ=-0.288, p<0.01), but no comparison could be made between $DMSP_T$ and bacterial abundance due to a mismatch between days of data analysis.

In the high pCO_2 mesocosms the ratio of DMS to bacterial activity (µmol µg C^{-1} $L^{-1}d^{-1}$) was lower than in the medium and low pCO_2 mesocosms, particularly during Phase 3 (Figure 22a). Figure 22b shows the mean bacterial production in the low, medium and high pCO_2 mesocosms, plotted with the DMS: DMSP ratio for the same mesocosm groups. Bacterial activity peaked on T20 in all three CO_2 treatments, the same day that the DMS: DMSP ratio started to increase.

a) DMS: bacterial abundance

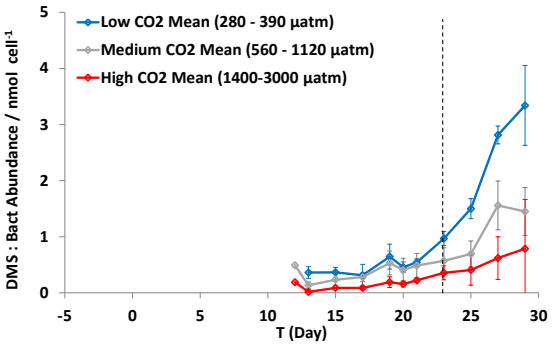

b) DMS: bacterial protein production

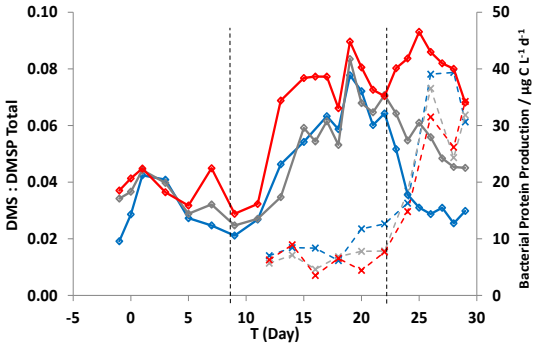

Figure 22. a) DMS per unit of bacterial activity (nmol $cell^{-1}$); b) Comparison of the mean bacterial protein production (µg C L^{-1} d^{-1}) for the three treatment levels (diamonds) against the mean DMS: $DMSP_T$ ratio (crosses) in the CO_2 treatments, for three different CO_2 conditions: low pCO_2 (280 – 390 µatm), medium pCO_2 (560 – 1120 µatm) and high pCO_2 (1400 – 3000 µatm). Error bars show standard deviation within the CO_2 ranges and dashed lines indicate the sectioning into three Phases of the experiment. Bacterial data courtesy of Angelika Reisch, IGB-Berlin.

There were too few data available to perform Spearman's Rank Correlation Analysis for each mesocosm, so the data from the low, medium and high mesocosms were combined, and the DMS: $DMSP_T$ ratio compared to the bacterial productivity (See Table 9). As CO_2 increased, the

correlation between DMS: DMSP and bacterial productivity decreased, from a significant – ρ=0.804 (p<0.01) in the control mesocosms (280 µatm) to a non-significant correlation of ρ=-0.203 (p>0.05) in the high pCO_2 mesocosm.

Table 9. Spearman's rank correlation coefficients and p-values for the analysis of the correlation between DMS: DMSP ratio and bacterial productivity for the three averaged CO_2 treatments.

CO_2 treatment	ρ value (Spearman's Correlation Coefficient)	P-value (Significance level)
Low pCO_2 (280 – 390 µatm)	-0.804	0.002
Medium pCO_2 (560 – 1120 µatm)	-0.500	0.007
High pCO_2 (1400 – 3000 µatm)	-0.203	0.366

4.1.7. Intercomparison of DMS and DMSP analysis techniques

The results of the GC-FPD analysis using purge and cryotrap techniques by Hannah Lutterbeck of GEOMAR are shown below (Figure 23) to allow a comparison with the GC-MS analysis of DMS and the GC-FPD analysis of DMSP at UEA.

a) DMS

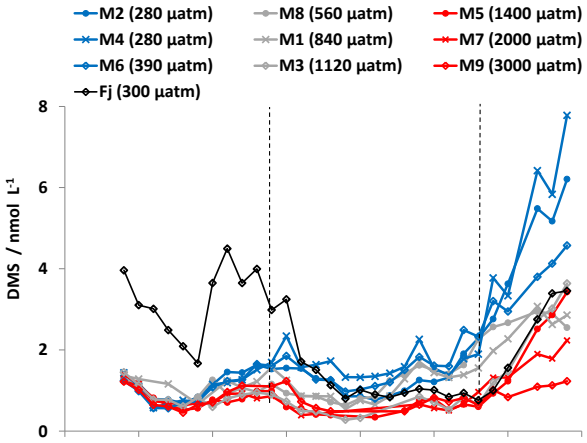

b) $DMSP_T$

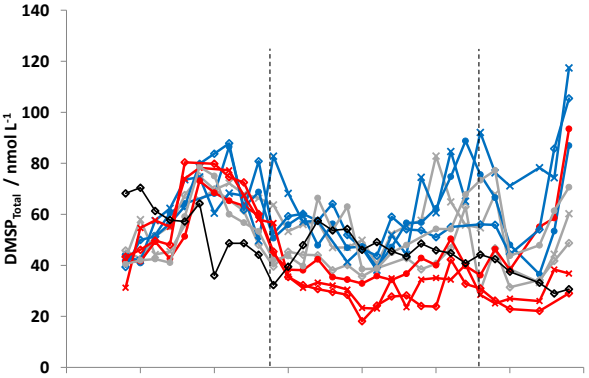

c) $DMSP_P$

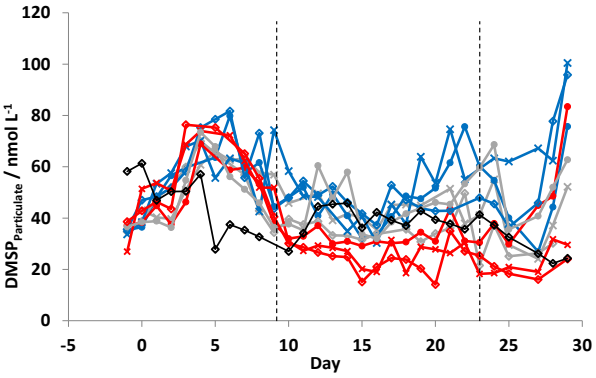

Figure 23. Temporal changes in a) DMS, b) $DMSP_T$ and c) $DMSP_P$ concentrations (nmol L^{-1}) measured daily by Hannah Lutterbeck (GEOMAR) on GC-FPD during SOPRAN Bergen. Dashed lines indicate the sectioning into three Phases of the experiment.

The data range for both datasets from this study is given in Table 10, with an experimental mean of 0.97 nmol L^{-1} DMS from the UEA GC-MS and 1.47 nmol L^{-1} DMS from the GEOMAR GC-FPD (Figure 24). The GC-MS data measure 42.3% lower on average than the measurements by GEOMAR.

Table 10. Comparison of DMS and DMSP results measured during this investigation and by GEOMAR during the SOPRAN Bergen mesocosm experiment. Shown are the total range, mean and standard deviation of all data and the mean (±SD) for each mesocosm and the Fjord.

	DMS (nmol L^{-1})		$DMSP_T$ (nmol L^{-1})	
Analysis Method	GC-MS (UEA)	GC-FPD (GEOMAR)	GC-FPD (UEA)	GC-FPD (GEOMAR)
Analysis Period	T12 – T29	T-1 – T29	T-1 – T29	T-1 – T29
Total Range	0.09 – 4.92	0.28 – 7.78	14.33 – 88.24	18.07 – 117.37
Experiment Mean All Mesocosms (±SD)	0.97 (± 0.82)	1.47 (± 1.11)	38.39 (± 14.78)	51.78 (± 16.32)
M2 280 µatm	1.25 (±1.05)	1.82 (±1.46)	43.4 (±12.1)	58.8 (±14.1)
M4 280 µatm	1.38 (±0.89)	2.08 (±1.72)	49.3 (±17.7)	64.9 (±17.5)
M6 390 µatm	1.52 (±1.23)	1.74 (±1.06)	45.9 (±12.1)	60.8 (±15.3)
M8 540 µatm	1.14 (±0.65)	1.37 (±0.72)	40.1 (±11.2)	54.4 (±12.8)
M1 860 µatm	0.97 (±0.63)	1.40 (±0.66)	44.5 (±15.6)	55.7 (±11.2)
M3 1120 µatm	0.66 (±0.58)	1.07 (±0.82)	34.8 (±14.3)	46.7 (±11.5)
M5 1400 µatm	0.63(±0.59)	0.97 (±0.76)	34.0 (±10.3)	47.6 (±14.1)
M7 2000 µatm	0.59 (±0.49)	0.98 (±0.48)	32.0 (±14.9)	41.5 (±17.0)
M9 3000 µatm	0.43 (±0.20)	0.84 (±0.25)	28.8 (±15.2)	39.6 (±18.4)
Fjord 300 µatm	0.99 (±0.76)	2.13 (±1.22)	32.1 (±11.0)	47.4 (±10.7)

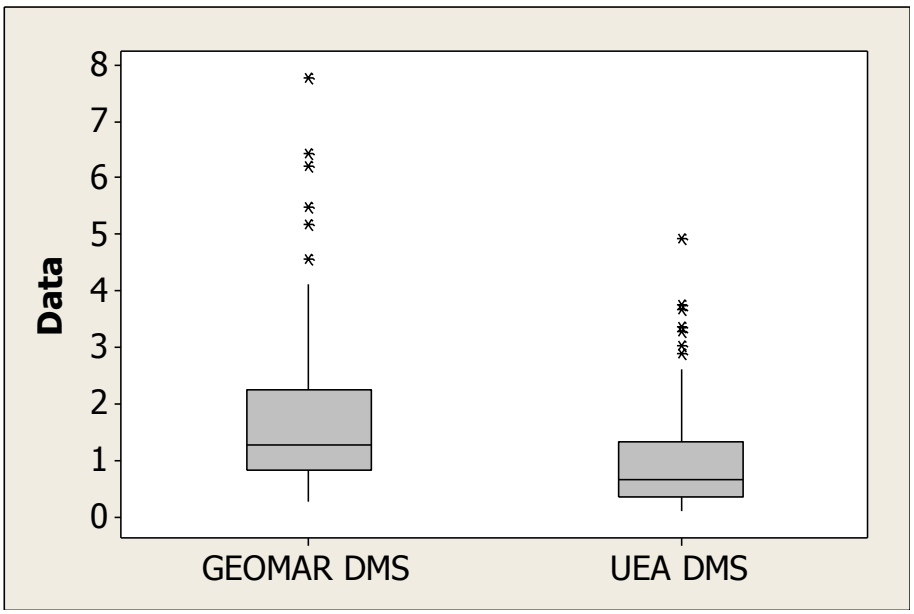

Figure 24. Boxplot of concentrations (nmol L^{-1}) for DMS, as measured by GEOMAR on GC-FPD and UEA on GC-MS (this study).

Figure 25 is a scatterplot between the DMS measured on GC-MS and GC-FPD datasets. Outliers identified from boxplots (Figure 24) are plotted in red diamonds, and all correspond to data-points from the three lowest CO_2 mesocosms control mesocosms (280 – 390 µatm). A regression analysis of the data gave an R^2 value of 83% (F=672 p<0.01, DF=138).

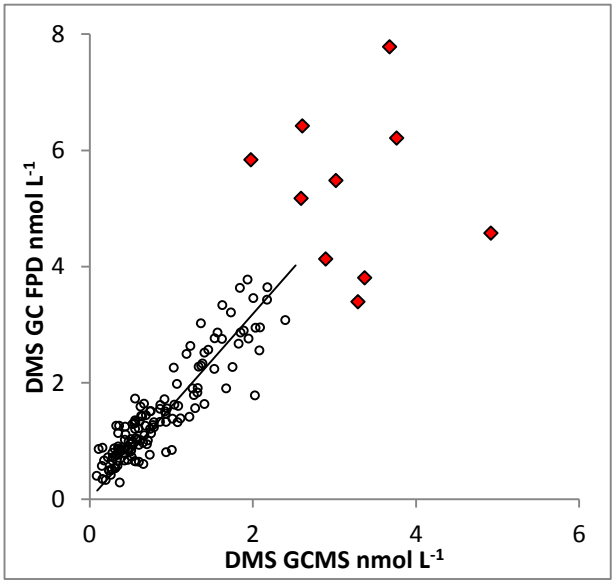

Figure 25. Comparison of DMS concentrations (nmol L^{-1}) measured on GC-MS (UEA) and GC-FPD (GEOMAR) (p<0.01). Outliers identified during the comparison in either dataset are highlighted in red.

The concentrations of $DMSP_T$ from this study were 26% lower than those from GEOMAR, while $DMSP_P$ was 58% lower (Figure 26). The mean $DMSP_T$ of this study was 38.4 (± 14.8) nmol L^{-1} and the mean $DMSP_P$ was 24.8 (±11.5) nmol L^{-1}, compared to GEOMAR values of 51.8 (± 16.3) nmol L^{-1} and 44.50 (±15.38) nmol L^{-1} respectively. Maximum $DMSP_T$ concentrations were 88.24 nmol L^{-1} in this study and 117.37 nmol L^{-1} from GEOMAR. Figure 27 shows the two datasets in a scatterplot.

a) $DMSP_T$ **b) $DMSP_P$**

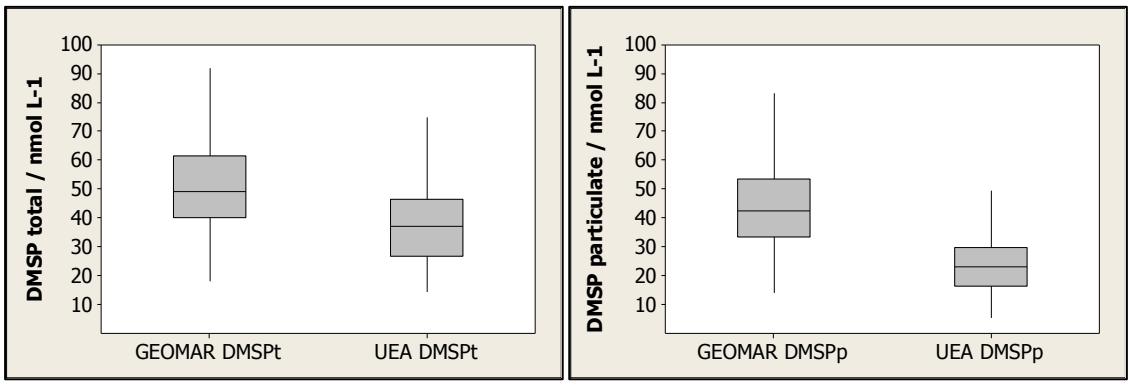

Figure 26. Boxplot of data for a) total DMSP and b) particulate DMSP concentrations (nmol L^{-1}), as measured by GEOMAR on GC-FPD during the experiment and this study on GC-FPD at UEA.

a) $DMSP_T$ **b) $DMSP_P$**

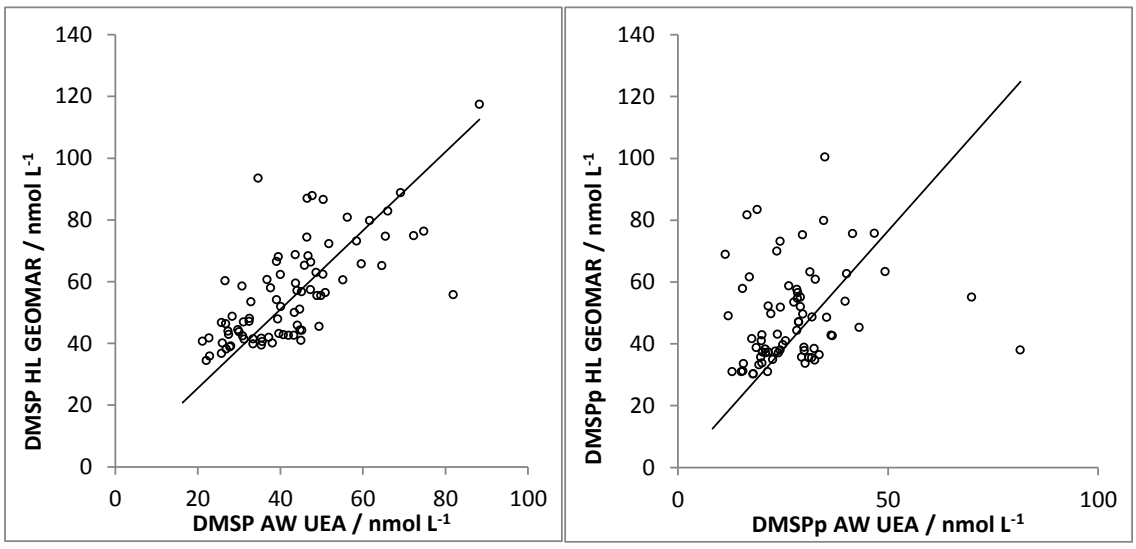

Figure 27. Scatterplot of the a) total DMSP and b) particulate DMSP concentrations (nmol L^{-1}) from SOPRAN Bergen, with the UEA data on the x-axis and the GEOMAR data on the y-axis ($p<0.01$). Outliers identified from either dataset are highlighted in red.

4.2. Dynamics of iodocarbon concentrations

4.2.1. Iodocarbon concentrations

Four Iodocarbons (CH_3I, CH_2I_2, C_2H_5I, and CH_2ClI) were measured on the GC-MS for the same period as DMS: T12 – T29 inclusive, and all four measured compounds generally showed the same trends. Concentrations of all compounds generally decreased in all mesocosms over the course of the experiment (Figure 28). Analysis of the data did not differentiate between Phases 2 and 3 due to the small number of data points in Phase 3.

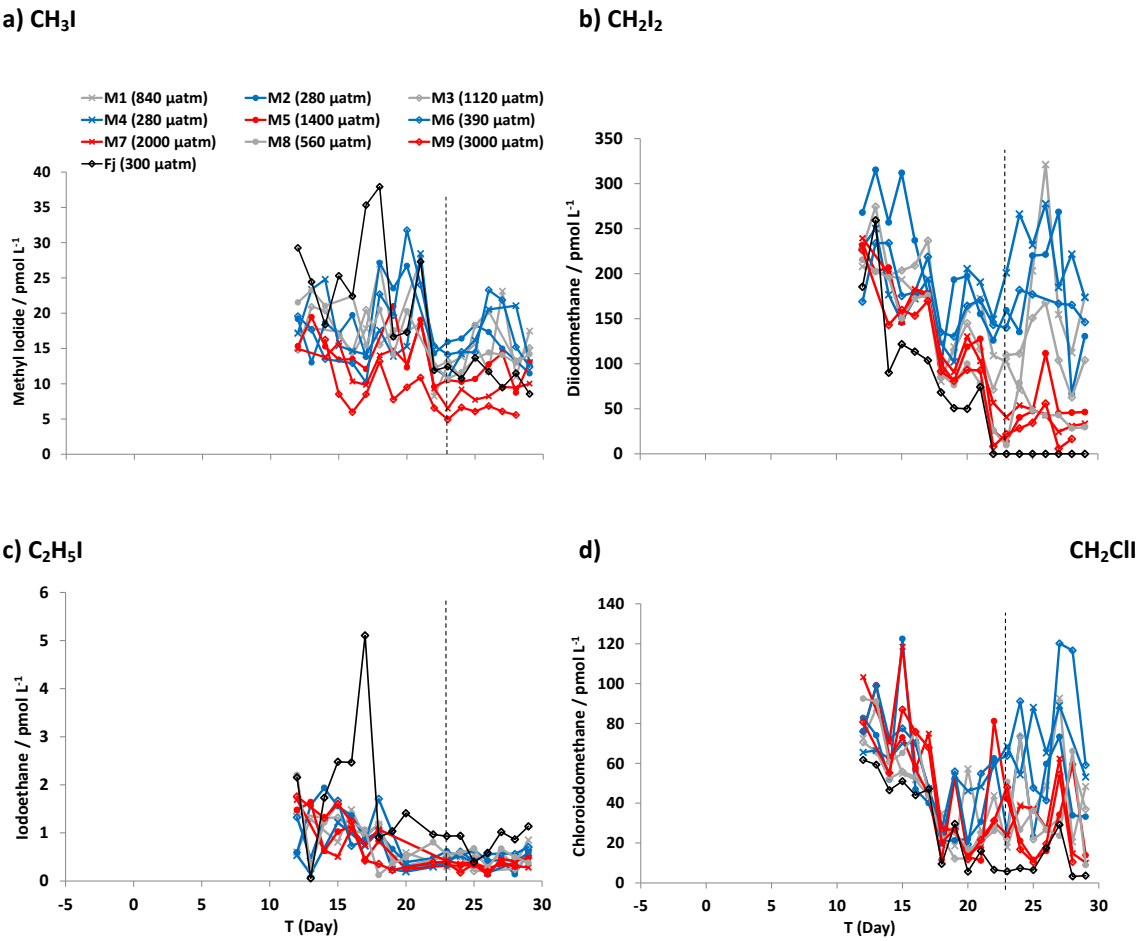

Figure 28. Temporal changes in iodocarbons: a) CH_3I, b) CH_2I_2, c) C_2H_5I, d) CH_2ClI concentrations (pmol L^{-1}) during SOPRAN Bergen. Dashed lines indicate the sectioning into three Phases of the experiment.

Table 11. Summary of F-values and p-values for iodocarbon analysis of CO_2 treatments As Phase 3 contained limited data points, Phases 2 and 3 were analysed together.

Compound	Statistical Details		
	Phases 2 and 3	Significant	Degrees of Freedom
CH_3I	F=11.61, p<0.01	Yes	149
CH_2I_2	F=8.62, p<0.01	Yes	155
C_2H_5I	F=0.88, p=0.534	No	134
CH_5ClI	F=2.93, p<0.01	Yes	154

CH_3I and CH_2I_2 show lower concentrations in high pCO_2 mesocosms (Figure 28a and b). Concentrations of C_2H_5I were very close to detection limit, and showed no significant difference between mesocosms. All iodocarbons show fluctuations in concentration during the experiment: the percentage standard deviation relative to the mean for all four iodocarbons is between 37.3 % (CH_3I) and 79.1 % (C_2H_5I), and shows the variation is high. Table 12 shows the mean and standard deviation for each mesocosm.

Table 12. Range and mean (±SD) concentrations of iodocarbons within the mesocosms.

	CH_3I (pmol L^{-1})	CH_2I_2 (pmol L^{-1})	C_2H_5I (pmol L^{-1})	CH_2ClI (pmol L^{-1})
Range	4.92 – 37.93	5.78 – 321.27	0.06 – 5.11	3.25 – 122.48
M2 (280 µatm)	17.69 (± 4.56)	196.82 (± 71.41)	0.81 (± 0.50)	49.86 (± 27.71)
M4 (280 µatm)	17.22 (± 4.84)	194.35 (± 47.30)	0.52 (± 0.33)	60.44 (± 16.91)
M6 (390 µatm)	17.84 (± 5.53)	172.46 (± 31.45)	0.81 (± 0.46)	66.68 (± 27.40)
M8 (560 µatm)	16.42 (± 4.27)	97.95 (± 69.09)	0.76 (± 0.54)	43.25 (± 26.05)
M1 (840 µatm)	16.81 (± 5.37)	158.28 (± 61.31)	0.70 (± 0.38)	46.59 (± 22.09)
M3 (1120 µatm)	16.47 (± 3.13)	149.73 (± 62.26)	0.73 (± 0.45)	39.96 (± 19.99)
M5 (1400 µatm)	13.60 (± 3.53)	108.12 (± 69.47)	0.66 (± 0.46)	43.35 (± 28.25)
M7 (2000 µatm)	11.48 (± 3.37)	101.19 (± 68.33)	0.62 (± 0.43)	44.49 (± 31.89)
M9 (3000 µatm)	8.22 (± 3.13)	86.40 (± 67.53)	0.65 (± 0.56)	39.88 (± 26.95)
Fj (300 µatm)	19.12 (± 9.04)	62.09 (± 74.44)	1.42 (± 1.16)	25.00 (± 21.13)
Mean % Standard Deviation	37.3	57.8	79.1	58.7
Effect of CO_2	Yes	Yes	No	Yes

CH_3I concentrations showed experiment mean concentrations of 14.4 pmol L^{-1} in the high pCO_2, and 20.3 pmol L^{-1} in the control treatments. Concentrations increased in all mesocosms on T23, coincident with the peak in Chl-*a* during Phase 2. CH_3I concentrations were significantly lower at high pCO_2: M9 (3000 µatm) and M7 (2000 µatm), were significantly lower than control mesocosms (F=11.61, p<0.05, DF=149). CH_3I (Figure 29a) showed a 36.9% reduction in the high pCO_2 treatments compared to the control (280 µatm), in a linear relationship.

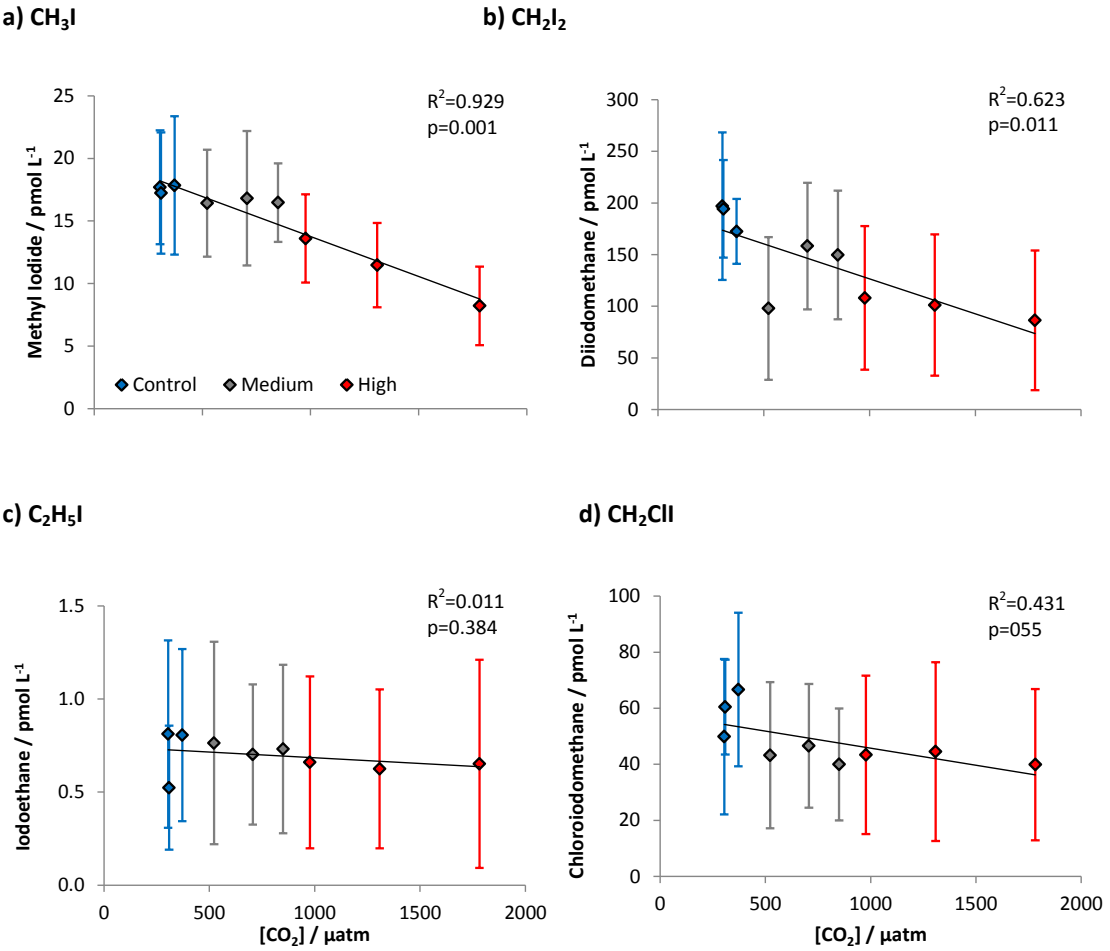

Figure 29. Changes in mean concentration (pmol L^{-1}) of a) CH_3I, b) CH_2I_2, c) C_2H_5I and d) CH_2ClI in each mesocosm plotted versus mean pCO_2 (µatm). Error bars denote the standard deviation for each mesocosm, and the r^2 values for each line of best fit.

CH_2I_2 concentrations in the high pCO_2 mesocosms showed a steady decrease during Phases 2 and 3, a trend not replicated in the control mesocosms (Figure 28b). CH_2I_2 concentrations (Figure 29b) were 48% lower in M9 (3000 µatm) compared to control (280 µatm; F=8.62, p<0.01, DF=155). The highest concentration recorded in the mesocosms was 321.3 pmol L^{-1} in M1 (840 µatm) and the lowest 5.78 pmol L^{-1} in M9 on T27 (Table 12). A peak in CH_2I_2 was seen in many of the mesocosms on T27, a peak which was mirrored in CH_2ClI, and in some

mesocosms in CH_3I. Concentrations of CH_2I_2 in the Fjord became undetectable after T22, and remained at these low levels until the end of the experiment.

Concentrations of CH_2ClI showed no difference between CO_2 treatments during Phase 2 (Figure 28d), but during Phase 3, control mesocosms concentrations were significantly higher. ($F=2.93$, $p<0.015$, $DF=154$). CH_2ClI concentrations were 28% lower in the high pCO_2 mesocosms during Phase 3.

4.2.2. Iodocarbon correlations with microbial community development

Spearman's Rank Correlation analysis was carried out to identify relationships between concentrations of iodocarbons and other parameters (Table 13).

Table 13. Spearman's Rank correlation coefficients for iodocarbon data compared to Chl-*a*, the phytoplankton taxonomy (from HPLC pigment analysis) and abundance of small phytoplankton (<10µm; from flow cytometry). Coefficients are significant at 99% confidence limits, except those highlighted at only being significant at 95%. NS: non-significant.

Compound	CH_3I	CH_2I_2	C_2H_5I	CH_2ClI
Chl-*a* (µg L^{-1})	NS	-0.285	NS	-0.452
Phytoplankton Taxonomy (Equivalent Chlorophyll µg L^{-1})				
Total Equivalent Chlorophyll-*a*	NS	-0.338	NS	-0.495
Diatoms	0.295	NS	0.365	NS
Haptophytes	NS	-0.276	NS	-0.375
Chrysophytes	0.381	0.231*	-0.172	NS
Dinoflagellates	0.302	0.296	NS	NS
Chlorophytes	-0.320	-0.539	NS	-0.477
Cryptophytes	NS	-0.483	0.273	-0.594
Cyanobacteria	-0.423	-0.592	-0.223*	0.372
Small Phytoplankton (<10µm) abundance (cells mL^{-1})				
Synechococcus	-0.540	-0.678	-0.323	-0.460
E huxleyi	0.297	0.285	NS	NS
Picoeukaryotes	-0.355	-0.451	NS	-0.339
Total nanophytoplankton	0.458	0.257	0.382	NS
Large nanophytoplankton	0.329	0.210*	NS	NS
Cryptophytes	NS	-0.227*	NS	-0.405
Bacterial Abundance and Protein Production Rates				
Bacterial Abundance (cells mL^{-1})	-0.470	-0.429	NS	NS
Bacterial Protein Production (µg C L^{-1} d^{-1})	-0.295*	-0.327	NS	NS

4.2.3. Iodocarbons and the relationships with Chl-*a*

Chl-*a* was negatively correlated with CH_2I_2 and CH_2ClI (ρ=-0.285 and -0.452 respectively), but no correlations were identified with CH_3I or C_2H_5I. The same trend was noted for the total equivalent Chl-*a* (from HPLC). CH_3I production per unit Chl-*a* was reduced under elevated pCO_2 in Phases 2 and 3 (Figure 30), and the other iodocarbons showed similar trends in Phase 3 only (Figure 30b, c and d).

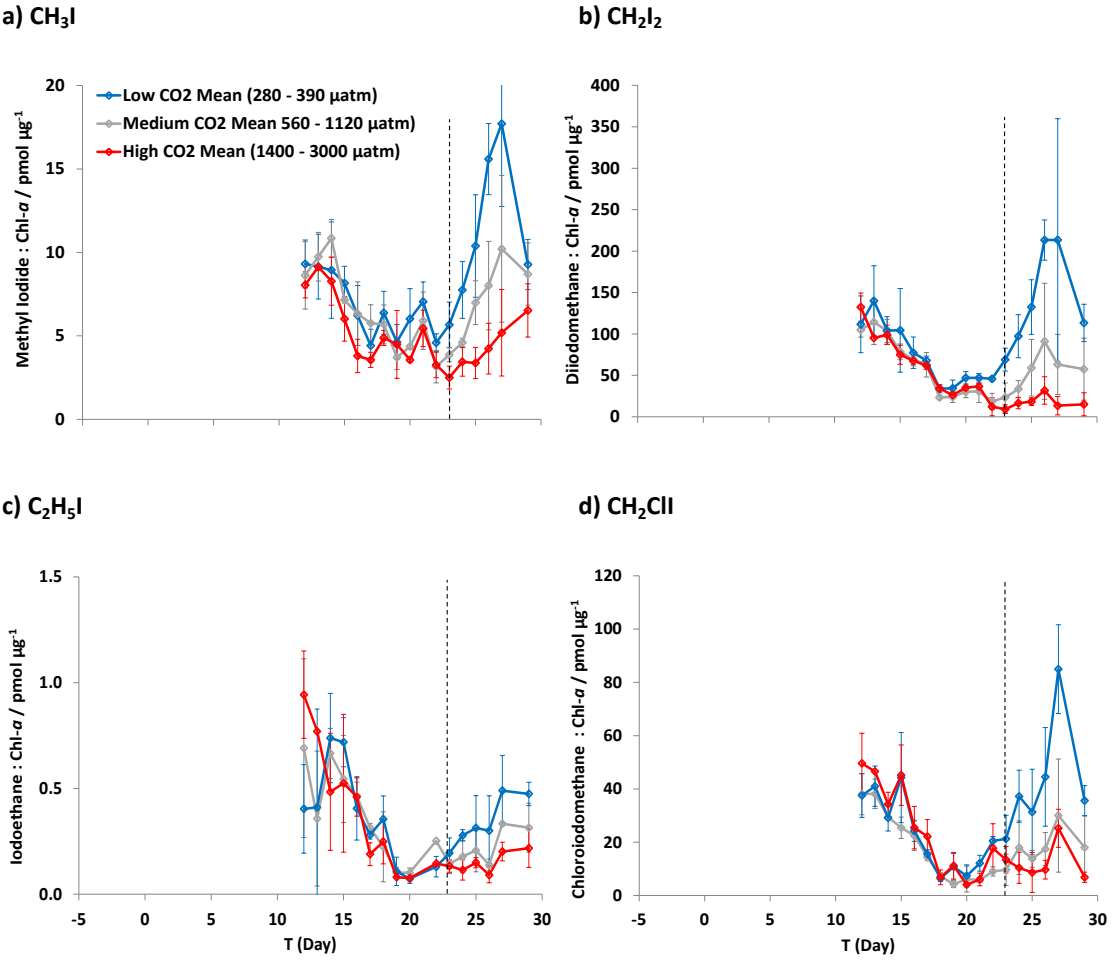

Figure 30. Temporal changes in the ratio between Chl-*a* and a) CH_3I, b) CH_2I_2, c) C_2H_5I and d) CH_2ClI (pmol μg^{-1}) for three different CO_2 conditions: low pCO_2 (280 – 390 µatm), medium pCO_2 (560 – 1120 µatm) and high pCO_2 (1400 – 3000 µatm). Error bars show standard deviation within the CO_2 ranges. Dashed lines indicate the sectioning into three Phases of the experiment.

4.2.4. Iodocarbons and the relationships with community composition

Iodocarbons showed varying responses to community composition identified by HPLC. None of the groups showed consistently positive or negative correlations with all four iodocarbons (Table 13); only the cyanobacteria equivalent Chl-*a* correlated to all four compounds yet only CH_2ClI showed a positive response to cyanobacterial cell abundance (ρ=0.372, $p<0.01$).

However, all four compounds were significantly negatively correlated with the growth of *Synechococcus*.

Both CH_3I and CH_2I_2 were negatively correlated with bacterial abundance and protein production (Table 13); in contrast to C_2H_5I and CH_2ClI.

4.3. Dynamics of bromocarbon concentrations

4.3.1. Measured bromocarbon concentrations

Concentrations of $CHBr_3$, CH_2Br_2 and $CHBr_2Cl$ are shown in Figure 31 and summarised in Table 14. Variation between Bromocarbon concentrations was lower than the Iodocarbons: the percentage standard deviation relative to the mean was lower than 30% for all three compounds. No significant difference was seen between CO_2 treatments for any of the three bromocarbons (Table 15, Figure 32a – c).

Fjord concentrations were higher than the mesocosms, and all three compounds showed a peak in Fjord concentrations on T21 at 550 pmol L^{-1} for $CHBr_3$, 38 pmol L^{-1} for CH_2Br_2 and 11 pmol L^{-1} for CH_2Br_2Cl.

a) $CHBr_3$

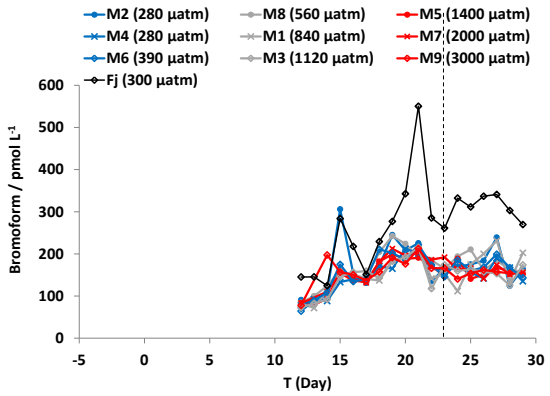

b) CH_2Br_2

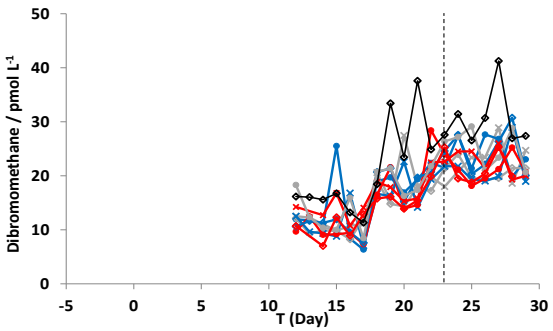

c) $CHBr_2Cl$

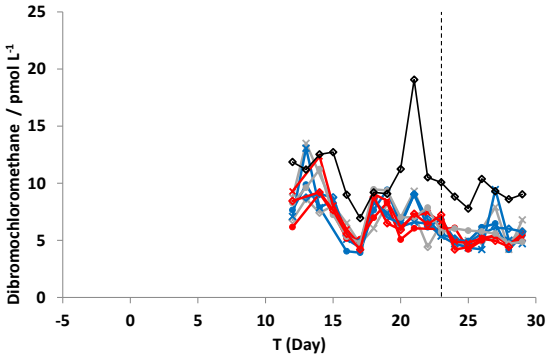

Figure 31. Temporal changes in bromocarbons: a) CH_3Br, b) CH_2Br_2 and c) $CHBr_2Cl$ (pmol L^{-1}) during SOPRAN Bergen. Dashed lines indicate the sectioning into three Phases of the experiment.

Table 14. Range and mean (±SD) of bromocarbons (pmol L^{-1}) within the mesocosms.

	$CHBr_3$ (pmol L^{-1})	CH_2Br_2 (pmol L^{-1})	$CHBr_2Cl$ (pmol L^{-1})
Range	64.18 – 306.02	6.33 – 41.24	3.92 – 19.08
M2 (280 µatm)	170.78 (±58.00)	18.86 (±6.59)	6.53 (±1.85)
M4 (280 µatm)	150.55 (±36.66)	16.82 (±5.71)	6.60 (±2.28)
M6 (390 µatm)	159.68 (±41.88)	18.44 (±6.79)	6.70 (±1.56)
M8 (560 µatm)	168.85 (40.88)	19.40 (±6.37)	6.99 (1.94)
M1 (840 µatm)	157.66 (±44.28)	18.56 (±5.92)	6.97 (±2.26)
M3 (1120 µatm)	148.11 (±37.77)	16.18 (±4.96)	6.19 (±1.40)
M5 (1400 µatm)	150.91 (±36.09)	16.78 (±6.35)	6.02 (±1.34)
M7 (2000 µatm)	161.36 (±33.86)	18.67 (±4.50)	6.78 (±2.13)
M9 (3000 µatm)	159.73 (±29.79)	16.38 (±5.34)	6.28 (±1.69)
Fj (~300 µatm)	272.66 (±100.41)	24.37 (±8.63)	10.41 (±2.67)
Mean % Standard deviation	27.0	33.1	27.5
Effect of CO_2	No	No	No

Table 15. Summary of ANOVA F-values and p-values for bromocarbon analysis between CO_2 treatments. As Phase 3 contained limited data points, Phases 2 and 3 were analysed together.

Compound	Statistical Details		
	Phases 2 and 3	Significant?	Degrees of Freedom
$CHBr_3$	F=0.73, p=0.661	No	156
CH_2Br_2	F=0.76, p=0.637	No	157
$CHBr_2Cl$	F=0.53, p=0.831	No	153

$CHBr_3$ concentration mean was 158.6 (± 40.4) pmol L^{-1} within the mesocosms, with highest concentration of 306.0pmol L^{-1} in M2 on T15. During Phase 2, concentrations increased and remained relatively stable through Phase 3, with no significant effect of CO_2 during either Phase (Table 15 and Figure 32). Concentrations in the Fjord were significantly higher (F=9.69, $p<0.01$, DF=174). CH_2Br_2 concentrations increased in all mesocosms from the start of measurement to the end of the experiment, but CO_2 did not affect concentrations. The mean ratio of $CHBr_3$: CH_2Br_2 for the entire experiment was 9.88 (See Section 5.6.2). The mean concentration in the mesocosms at the start of measurements (T12) was 12.5 pmol L^{-1}, and at the end on T29 21.2 pmol L^{-1}. $CHBr_2Cl$ concentrations, in contrast to CH_2Br_2, showed slight decrease through Phase 2, but remained stable in Phase 3 (5.2 ± 0.9 pmol L^{-1}).

a) $CHBr_3$

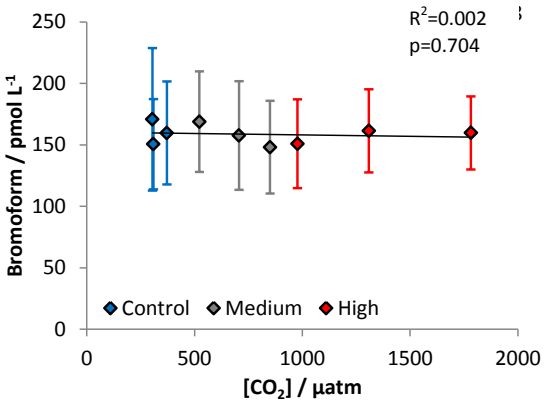

b) CH_2Br_2

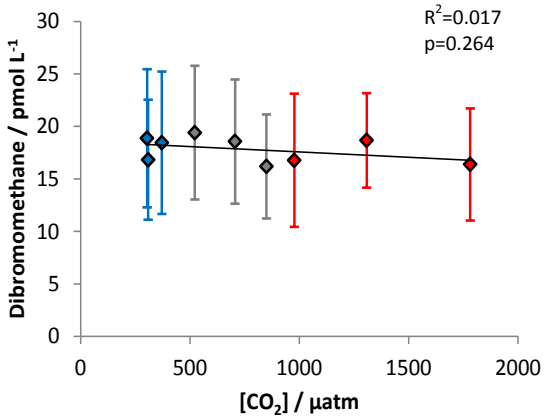

c) $CHBr_2Cl$

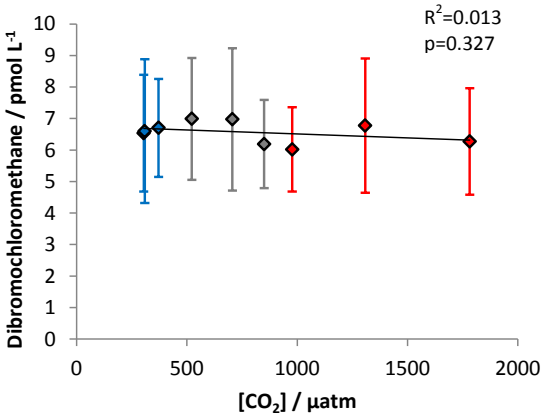

Figure 32. Changes in mean concentration (pmol L^{-1}) of a) $CHBr_3$, b) CH_2Br_2 and c) $CHBr_2Cl$ in each mesocosm plotted versus target pCO_2 (µatm). Error bars denote the experiment standard deviation for each mesocosm, and the r^2 values for each line of best fit.

4.3.2. Bromocarbon correlations with microbial community development

Spearman's Rank Correlation analysis was carried out to identify relationships between bromocarbons and the other parameters (Table 16).

Table 16. Spearman's Rank correlation coefficients for bromocarbon data compared to Chl-*a*, phytoplankton taxonomy (HPLC pigment analysis) and abundance of small phytoplankton (<10µm) from flow cytometry. Coefficients are significant at 99% confidence limits, except those highlighted at only being significant at 95%. NS: non-significant.

Parameter	$CHBr_3$	CH_2Br_2	CH_2BrCl
Chl-*a* (µg L^{-1})	0.210*	NS	NS
Phytoplankton Taxonomy (Equivalent Chlorophyll µg L^{-1})			
Total Equivalent Chlorophyll-*a*	0.229*	NS	NS
Diatoms	NS	-0.534	0.269
Haptophytes	0.258*	0.310	NS
Chrysophytes	-0.284	-0.227	0.300
Dinoflagellates	NS	NS	NS
Chlorophytes	0.419	NS	NS
Cryptophytes	0.410	0.210*	NS
Cyanobacteria	0.338	0.215*	NS
Small Phytoplankton (<10µm) abundance (cells mL^{-1})			
Synechococcus	NS	NS	NS
E huxleyi	NS	0.371	-0.262
Picoeukaryotes	NS	-0.225*	NS
Total nanophytoplankton	NS	-0.437*	0.344
Large nanophytoplankton	0.212*	NS	NS
Cryptophytes	0.370	0.227*	NS
Bacterial Abundance and Protein Production Rates			
Bacterial Abundance (cells mL^{-1})	NS	NS	NS
Bacterial Protein Production (µg C L^{-1} d^{-1})	NS	NS	NS

4.3.3. Bromocarbons and the relationships with Chl-*a*

During Phase 2, there was little change in the bromocarbon to Chl-*a* ratio for $CHBr_3$ or CH_2Br_2 and no effect of CO_2. After T22, the ratios for these two compounds were significantly higher

in the control mesocosms (280 µatm) than the high pCO_2 (Figure 33 a and b). $CHBr_2Cl$ showed a different trend, with higher ratios in the high pCO_2 mesocosms during Phase 2, but which reversed to match the $CHBr_3$ and CH_2Br_2 trends in Phase 3 (Figure 33c). Only $CHBr_3$ showed a correlation with Chl-*a* (ρ=0.210, p<0.05) for both the measured total Chl-*a* and the HPLC total equivalent Chl-*a* (Table 16).

a) $CHBr_3$

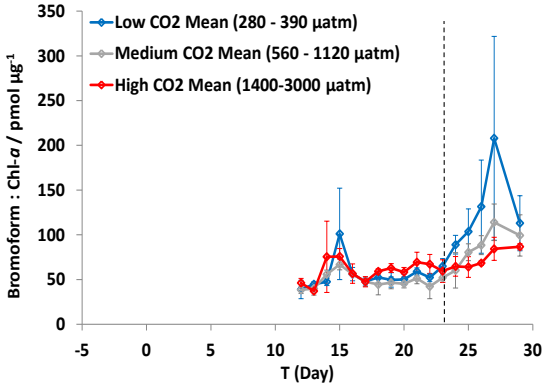

b) CH_2Br_2

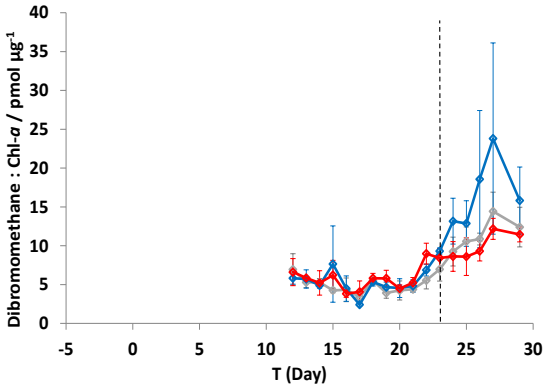

c) $CHBr_2Cl$

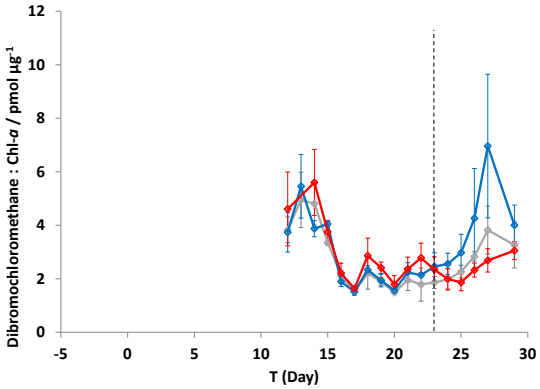

Figure 33. Temporal changes in the ratio between Chl-*a* and a) $CHBr_3$, b) CH_2Br_2 and c) $CHBr_2Cl$ (pmol μg^{-1}) for three different CO_2 conditions: low pCO_2 (280 – 390 µatm), medium pCO_2 (560 – 1120 µatm) and high pCO_2 (1400 – 3000 µatm). Error bars show standard deviation within the CO_2 ranges and dashed lines indicate the sectioning into three Phases of the experiment.

4.3.4. Bromocarbons and the relationship with community composition

No consistent relationships were observed between concentrations of bromocarbons and community composition (Table 16). $CHBr_3$ showed significant positive correlations with Chlorophytes (ρ=0.419, p<0.01) and cryptophytes (ρ=0.410, p<0.01), but no correlation with dinoflagellates or diatoms. $CHBr_2Cl$ showed the weakest relationships with any of the community groupings: correlations were only seen for diatoms (ρ=0.269, p<0.01) and

chrysophytes (ρ=0.300, p<0.01). No correlations between bromocarbons and *Synechococcus* were identified.

No significant correlations were observed between the bromocarbons and bacterial abundance or protein production (Table 16).

4.4. Summary of trace gas concentrations

All trace gas data underwent correlation analysis to identify inter-relationships (Table 17). Of all halocarbons, only CH_3I was correlated correlation with DMSP, but CH_2Br_2 and $CHBr_3$ was correlated with DMS (ρ=0.411 and 0.761 respectively). Strong correlations were noted between CH_3I and CH_2I_2 (ρ=0.520, p<0.01) and $CHBr_3$ and CH_2Br_2 (ρ=0.558, p<0.01).

Table 17. Spearman's Rank correlation coefficients for all trace gas data. Coefficients are significant at 99% confidence limits, except those highlighted (*) as being significant at 95%. NS – non-significant.

Compound	CH_3I	CH_2I_2	C_2H_5I	CH_2ClI	$CHBr_3$	CH_2Br_2	CH_2BrCl
DMS	NS	-0.251	-0.384	NS	0.411	0.761	-0.278
DMSP	0.370	NS	NS	NS	NS	NS	NS
CH_3I							
CH_2I_2	0.520						
C_2H_5I	0.273	0.426					
CH_2ClI	NS	0.549	0.404				
$CHBr_3$	NS	-0.320	-0.231*	-0.387			
CH_2Br_2	-0.201*	-0.468	-0.399	NS	0.558		
$CHBr_2Cl$	0.394	0.201*	0.325	0.189*	NS	NS	

4.4.1. DMS and DMSP

- DMS concentrations were inversely related to increasing pCO_2 up to 3000 µatm (mean pCO_2 1782 µatm).
- DMS concentrations were lower under elevated pCO_2 compared to the control from the start of measurement at the beginning of Phase 2, and remained lower until the end of the experiment.
- $DMSP_T$ and $DMSP_P$ concentrations were not significantly different between pCO_2 treatments until Phase 2, when concentrations were lower at high pCO_2 compared to the control.
- The ratio of DMS: DMSP was higher in Phase 3 than Phase 2.
- DMS was non-correlated with total Chl-*a*, but was strongly correlated with Haptophyte equivalent Chl-α and calcified *E. huxleyi* abundance.
- DMSP was significantly correlated with total Chl-α and equivalent Haptophyte Chl-*a* but not calcified *E. huxleyi* abundance.

4.4.2. Halocarbons

- CH_3I, CH_2I_2 AND CH_2ClI concentrations were inversely related to increasing pCO_2 up to 3000 µatm (mean pCO_2 1782 µatm).
- None of the iodocarbons were positively correlated with total Chl-*a*.
- Iodocarbons showed no overarching trend of correlation with the different indicators of primary production.
- Bromocarbon concentrations were unaffected by pCO_2 increase to 3000 µatm (mean pCO_2 1782 µatm)..
- Only $CHBr_3$ was correlated with total Chl-*a*, and there was no overarching trend of correlations of bromocarbons with different indicators of primary production.
- Bromocarbon concentrations were significantly higher in the Fjord waters than the mesocosms.

5. Discussion

5.1. Mesocosm behaviour and physical changes during SOPRAN Bergen

The KOSMOS open-water mesocosms were first used during EPOCA Svalbard in 2010 (Riebesell *et al.*, 2013b; Schulz *et al.*, 2013), and this experiment followed on directly by deploying the mesocosms in Espegrend, Norway, where a number of previous high pCO_2 mesocosm experiments had taken place (Hopkins *et al.*, 2010; Riebesell *et al.*, 2008). The experiment was situated in a water depth of 70m and close to the main channel of the Fjord.

Temperatures within the mesocosms ranged from 6.9 – 10.1, similar to those encountered during the PeECE experiments at 9-13°C (Engel *et al.*, 2005; Schulz *et al.*, 2008). Similarly, variations in salinity were of the same range (29-33) as during PeECE III (Schulz *et al.*, 2008). Comparative temperatures during EPOCA Svalbard were 2-6°C, with salinity at 29-34 (Schulz *et al.*, 2013). Temperature in the Fjord was important in determining the mesocosm temperature (Figure 6); temperature stratification within the mesocosms re-established within a day of mixing, but salinity remained well-mixed throughout (Figure 7). Tidal range at Espegrend was 1m (Kersen *et al.*, 2011).

Addition of nutrients to the mesocosm mid-way through the experiment was important to stimulate the growth of further community development and encourage response of the community to elevated pCO_2, as well as to encourage the growth of *E. huxleyi*. CO_2 did not affect the nutrient uptake rates which were significantly higher in Phases 2 and 3 (mean 23.2 ± 1.4 mmol d^{-1}) than Phase 1 (mean 8.5 ± 0.9 mmol d^{-1}). The changes in phytoplankton community composition in mesocosms at Bergen have been discussed for previous experiments perturbed by CO_2 (Engel *et al.*, 2005, 2008; Hopkins *et al.*, 2010) and nutrient additions (Levasseur *et al.*, 1996; Martinez-Martinez *et al.*, 2006). The community can be altered through the addition or depletion of nutrients: addition of silicate for diatom growth (Le B. Williams and Egge, 1998), or phosphate limitation for promotion of cyanobacteria (Wilson *et al.*, 1998). It was clear that in the stratified, unmixed Fjord that Chl-*a* showed very little development due to limitation of nutrients in the surface waters: mixing of the mesocosms redistributed the nutrients trapped below the salinity and temperature stratification into surface waters encouraging the bloom (Figure 10).

A comparison of nutrient concentrations from this and previous mesocosm experiments is shown in Table 18. Nutrient additions were equivalent to EPOCA Svalbard, but both these experiments had lower inorganic nitrate addition than any other mesocosm experiment (Schulz *et al.*, 2013); inorganic phosphate concentrations from SOPRAN Bergen were

equivalent to the other experiments (Engel *et al.*, 2005, 2008; Kim *et al.*, 2010; Schulz *et al.*, 2008).

Table 18. Comparison of nutrient concentrations measured in this study and past mesocosms.

	Max Nitrate ($\mu mol\ L^{-1}$)	Max Phosphate ($\mu mol\ L^{-1}$)	Max Ammonium ($\mu mol\ L^{-1}$)	Max Silicate ($\mu mol\ L^{-1}$)	Study
Bergen Phase 1	1.54 ± 0.17	0.21 ± 0.01	0.47 ± 0.06	1.24 ± 0.03	This Study
Bergen Phase 2 and 3	5.40 ± 0.20	0.22 ± 0.02	0.31 ± 0.09	0.46 ± 0.09	
PeECE I 2001	15.3 ± 0.2	0.48 ± 0.02	Undetectable	No data	Engel *et al.* (2005)
PeECE II 2003	8.6	0.38	No Data	12	Engel *et al.* (2008)
PeECE III 2005	15	0.7	1.0	3.5	Schulz *et al.* (2008)
NERC Microbial Metagenomics Experiment 2006	17	1.0	No Data	No Data	Hopkins *et al.* (2010)
Korean Mesocosm Experiment 2008	41	2.5	No Data	40	
EPOCA Svalbard 2010 Phase 1 and 2	0.1	0.7	0.09	No Data	Schulz *et al.* (2013)
EPOCA Svalbard 2010 Phase 3 and 4	5.5	0.4	0.04	No Data	

5.2. Impact of high pCO_2 on community structure and composition

5.2.1. The impact of high pCO_2 on community structure and composition

Maximum Chl-*a* concentrations in this experiment were comparable to previous mesocosm experiments both in the control and high pCO_2 mesocosms (Table 19). During this experiment, CO_2 had a positive effect during Phase 1 and the reverse during Phase 2. During the PeECE experiments CO_2 had no significant effect on Chl-*a*, but during the NERC Microbial Metagenomics Experiment, Chl-*a* concentrations were lower under high pCO_2 (Hopkins *et al.*, 2010).

Table 19. Comparison of maximum chlorophyll concentrations under different CO_2 treatments measured in this study and in other mesocosm experiments.

	Max Chlorophyll (µg L^{-1}) CO_2 Control	Max Chlorophyll (µg L^{-1}) CO_2 <1400 µatm	Max Chlorophyll (µg L^{-1}) CO_2 >1400 µatm	Significant CO_2 effect?	Study
SOPRAN Bergen Phase 1	3.4	3.9	4.1	Positive	This Study
SOPRAN Bergen Phase 2 and 3	4.6	4.9	3.7	Negative	
PeECE I 2001	12.5	6.5	-	No	Engel *et al.* (2005)
PeECE II 2003	4.0	3.0	-	No	Engel *et al.* (2008)
PeECE III 2005	11.0	13.5	13.0	No	Schulz *et al.* (2008)
NERC Microbial Metagenomics Experiment 2006	10	6	-	Negative	Hopkins *et al.* (2010)
Korean Mesocosm Experiment 2008	No Data	No Data	-	No Data	Kim *et al.* (2010)
EPOCA Svalbard 2010 Phase 1	1.4	1.4	1.4	None	Schulz *et al.* (2013)
EPOCA Svalbard 2010 Phase 2	1.0	1.5	2.0	Positive	
EPOCA Svalbard 2010 Phase 3	3.0	4.0	2.0	Negative	
Korean Mesocosm Experiment 2012	17	17	-	None	Park *et al.* (2014)

During the spring, a phytoplankton bloom occurs across the North Atlantic, from open seas into coastal waters. This bloom generally follows a succession of initial diatom dominance, followed by nanophytoplankton such as coccolithophores (Jacobsen *et al.*, 1995; Lochte *et al.*, 1993). This changeover in species dominance to the coccolithophores has been shown to be a result of one or more factors: silicate depletion following the diatom-dominated bloom (Sieracki *et al.*, 1993), high light conditions (Tyrrell and Taylor, 1996) or low dissolved CO_2 and high carbonate saturation state (Tyrrell and Merico, 2004). During SOPRAN Bergen, both the haptophytes and diatoms showed high abundance during both natural and artificial blooms, but both taxa showed decreased abundance during Phase 2 as a direct result of CO_2 increase. Diatoms were the most dominant phytoplankton throughout the experiment, with haptophytes and cryptophytes second in abundance. Engel *et al.* (2008) identified no difference in diatom growth between low and high pCO_2 treatments, but the maximum pCO_2 during SOPRAN Bergen was 3000 µatm (mean pCO_2 1782 µatm), compared to the maximum 700 µatm in PeECE II. Diatom growth was highest during the second bloom in mid-range CO_2, suggesting that a doubling of current atmospheric CO_2 might support higher diatom abundance, but further increases in pCO_2 might start to restrict diatom growth.

This idea of an optimum pCO_2 for Chl-α production is further supported by Figure 12: total equivalent Chl-*a* increased up to 840 µatm pCO_2 (M1), but total Chl-α was lower in higher pCO_2 mesocosms. During PeECE III, the existence of a critical pCO_2 for optimum phytoplankton growth was recognised, but it was proposed that concentration had not been reached at 1050 µatm (Schulz *et al.*, 2008). The increase in CO_2 to 3000 µatm however might have brought some phytoplankton species close to their maximum tolerable pCO_2. No experiment has been carried out at these high pCO_2 levels to determine the pCO_2 tolerance of many species.

The two control mesocosms in general showed similar trends, but were not identical in their community development; abundance of *E. huxleyi* and cryptophytes showed notable differences in maximum abundance. The mesocosms showed near identical changes to the equivalent Chl-*a* up until T3, after which the effects of the differences in CO_2 were identifiable. Community development within the mesocosms is very dependent on the initial community composition, and spatially uneven phytoplankton distributions can result in different starting conditions in the mesocosms, as previously identified by Kwint and Kramer (1995). In a mesocosm experiment in the Azores, Eggers *et al.* (2014) identified the initial community composition to be of greater importance in determining the phytoplankton biomass than the pCO_2. The initial ratios of diatoms, cyanobacteria, and dinoflagellates were highly important in determining the competitive advantage for each group. Although the mesocosms are submerged for several days prior to closure, limited mixing in the mesocosm bag will likely not

overcome irregular spatial distribution of phytoplankton (Martinez-Martinez *et al.*, 2006). Although most species showed very similar abundance on the first sampling days, the nanophytoplankton and *E. huxleyi* abundances showed differences between mesocosms, but overall the mesocosms contained very similar microbial communities and developed in the same ways.

Removal and exclusion of large grazers and predators can cause high zooplankton abundance due to lowered predation and high availability of food, however removal of the higher levels of the trophic web allows for greater development of community changes in the perturbed system. In the mesocosms, the main mesozooplankton species were *Calanus finmarchicus* and *Pseudocalanus elongates*, comprising up to 93% of the zooplankton in the water column (Hildebrandt *et al.*, 2014). The abundance of neither of these species was affected by CO_2, but that of bivalve and gastropod larvae were significantly reduced. Reductions in abundance of larval forms due to elevated pCO_2 could lead to lower grazing rates and reduced nutrient recycling within the water column. In a previous mesocosm experiment, Suffrian *et al.* (2008) found increased CO_2 did not affect grazing rates by microzooplankton, however Park *et al.* (2014) found that heterotrophic dinoflagellate grazing was reduced under 800 µatm CO_2.

5.2.2. Growth of *Emiliania huxleyi*

E. huxleyi has been studied extensively during elevated anthropogenic CO_2 experiments, both in the laboratory and the field (See Chapter 1 and 4). During SOPRAN Bergen, *E. huxleyi* growth identified by flow cytometry and light microscopy (data not shown), started mid-way through Phase 2, with lower abundance in high pCO_2 mesocosms. Haptophyte- equivalent Chl-α showed different distributions than *E. huxleyi* cell abundance from flow cytometry, but only one other haptophyte was identified by light microscopy: *Calciopappus caudatus* at very low cell abundances (maximum 19 cells mL^{-1}). Haptophyte equivalent Chl-*a* could also have included contributions from *Phaeocystis* spp. (Jacobsen *et al.*, 1995) but this species was not identified within the mesocosms. Haptophyte Chl-α also likely had contributions from other haptophytes in the water column, which were not identified by light microscopy but which had been identified as being present by Leadbeater (1972) Engel *et al.* (2005) found sensitivity of net specific growth rate and calcification in *E. huxleyi* to elevated pCO_2 during PeECE I and PeECE II (Engel *et al.*, 2008). Cell abundance measurements by flow cytometry have previously found it difficult to distinguish non-calcified *E. huxleyi* cell abundance from calcified cells (Jacquet *et al.*, 2002), but mesocosm studies on a bloom in 2008 identified significant abundance of non-calcified cells within the water column (Frada *et al.*, 2012) using COD-FISH techniques.

Calcified *E. huxleyi* cell counts were extremely low: a maximum of 3000 cells mL^{-1} were identified; this count is compared to 50,000 cells mL^{-1} in PeECE I (June 2001: Delille *et al.*, 2005); 70,000 cells mL^{-1} in June 2003 (Steinke *et al.*, 2007), 6 x 10^6 cells mL^{-1} in PeECE III (June 2005; Vogt *et al.*, 2008; Paulino *et al.*, 2008). As haptophytes were the second highest contributor to the total equivalent Chl-α, *E. huxleyi* cell density would be expected to be higher, unless additional contributors were present. Although calcification rates were not measured during SOPRAN Bergen, previous experiments have found lower calcification in *E. huxleyi* under elevated pCO_2 (Delille *et al.*, 2005; Feng *et al.*, 2009), but also no change (Bellerby *et al.*, 2008). It is suggested that the additional contributor to haptophyte Chl-*a* were non-calcified *E. huxleyi* cells and other haptophyte species, indistinguishable from the nanophytoplankton, but which still showed restrictions in growth at the highest pCO_2.

The abundance of naked cells does not automatically presume a reduction in calcification rate at higher CO_2, as coccolithophores growing under nutrient replete conditions in the laboratory are often non-calcified. Further details on these laboratory cultures is given in Chapter 4.

In situ and satellite measurements of coccolithophore blooms in the North Atlantic indicate the highest abundance during late spring to early summer, peaking in June (Raitsos *et al.*, 2006). Previous studies have indicated that *E. huxleyi* bloom when the mixed layer depth was shallow (above 20m; Balch *et al.*, 1992; Raitsos *et al.*, 2006), which would have been the case in the mesocosms of this investigation, and that high light intensity and positive temperature anomalies would stimulate the growth (Feng *et al.*, 2009; Nanninga and Tyrrell, 1996; Smyth *et al.*, 2004). Temperature profiles (Figure 6) showed constant temperature at all depths on T15, at around the same time as the *E. huxleyi* started to show increases in abundance.

Addition of inorganic nitrate and phosphate to the mesocosms was designed to encourage the growth of *E. huxleyi*: where depleted inorganic phosphate concentrations were originally found to be essential to the development of the *E. huxleyi* bloom, more recent investigations have identified *E. huxleyi* blooms in areas of phosphate repletion (Lessard *et al.*, 2005; Smyth *et al.*, 2004), hence the addition of significant inorganic phosphate amounts to the mesocosms.

5.3. Production of DMS and DMSP

The concentration range of DMS within the mesocosms and the Fjord (0.09 – 4.92 nmol L^{-1}) fall within the range of concentrations measured in previous experiments (Table 20) but the maximum concentration was lower than during PeECE II (30 nmol L^{-1}; Avgoustidi *et al.*, 2012), PeECE III (35 nmol L^{-1}; Vogt *et al.*, 2008) and the NERC Metagenomics experiment (50 nmol L^{-1}; Hopkins *et al.*, 2010). $DMSP_T$ concentration range (14.33 – 88.24 nmol L^{-1}) was also within the

ranges of previous experiments, although lower than the maximum concentration of 500 nmol L^{-1} measured in PeECE II and III and the NERC Metagenomics experiment.

DMS and DMSP production processes will be discussed, followed by evaluation of the community responses and bacterial activity on the DMS and DMSP concentrations.

Table 20. Summary of DMS and DMSP measurements from mesocosm experiments conducted under elevated pCO_2.

	Location	CO_2 Range (µatm)	Range DMS (nmol L^{-1})	% change DMS	Range DMSP (nmol L^{-1})	% change DMSP	Author
SOPRAN Bergen 2011	RaunesFjorden Norway	Control (280 µatm)	0.16 – 4.92	-60.3	21.1 – 88.2	-31.6	This Study
SOPRAN Bergen 2011		High CO_2 (1400 – 3000 µatm)	0.09 – 2.18		14.3 – 60.13		
Korean Mesocosm Experiment 2 2012	Jangmok Korea	160 - 830	1.0 - 100	-82	10-350	-71	Park *et al.* (2014)
EPOCA Svalbard 2010	KongsFjorden Svalbard	180 - 1420	ND - 14	-60	ND-80	+50	Archer *et al.* (2013)
NERC Microbial Metagenomics Experiment 2006	RaunesFjorden Norway	300-750	ND - 50	-57	30 - 500	-24	Hopkins (2010); Hopkins *et al.* (2010)
Korean Mesocosm Experiment 2008	Jangmok Korea	400 - 900	1 - 12	+80	-	-	Kim *et al.* (2010)
PeECE III	RaunesFjorden Norway	300 - 750	ND - 35	None	10 - 500	None	Vogt *et al.* (2008)
PeECE II	RaunesFjorden Norway	300 - 750	3 - 30	-40	ND - 300	-40	Avgoustidi *et al.* (2012)

BLANK

5.3.1. DMS and DMSP production in the mesocosms

Both DMS and $DMSP_T$ showed lower concentrations under high pCO_2 during Phase 2 and 3, with a 60% reduction in DMS concentrations in the high pCO_2 mesocosms compared to the control (280 µatm) and a 31% reduction in $DMSP_T$. These decreases were found to follow a linear relationship with increasing DMS as CO_2 increased to 3000 µatm. Hopkins *et al.* (2010) found a 57% reduction in DMS (range 5.7 – 42.0 nmol L^{-1}) concentrations and 24% reduction in $DMSP_T$ under high pCO_2 conditions, compared to present day CO_2 during the NERC Microbial Metagenomics experiment in 2006. The same trend was identified during PeECE II in 2003 at 40% reductions in both DMS and $DMSP_T$ (Avgoustidi *et al.*, 2012). PeECE III in 2005 identified no significant difference terms of maximum DMS or $DMSP_P$ concentrations, however a significant difference was identified in the temporal development of the production: high pCO_2 peaks of DMS and $DMSP_P$ were found to develop several days later than in ambient conditions (Wingenter *et al.* 2007; Vogt *et al.* 2008). In contrast, during the first Korea high pCO_2 mesocosm experiment, DMS in the acidified scenario was 80% higher than the present day scenario, and 60% higher in the 'greenhouse' scenario with elevated pCO_2 and temperature (Kim *et al.*, 2010).

Concentrations of DMS, $DMSP_T$ and $DMSP_P$ did not respond immediately following CO_2 addition during Phase 1. This would have been expected if DMSP was produced to combat oxidative stress under perturbed growth conditions (Sunda *et al.*, 2002). Although the highest CO_2 treatments were adjusted over a period of 5 days, there was still limited time for phytoplankton populations to adjust to the changing CO_2.

5.3.2. DMS production processes

DMSP is degraded in marine waters through three separate pathways, which regulate the concentration of DMS in seawater, and the subsequent atmospheric flux of sulphur. DMSP breakdown can be intracellular, releasing DMS directly from the cell, or extra-cellular by marine bacteria in the surrounding seawaters (Howard *et al.*, 2011; Zubkov *et al.*, 2004). The roles of marine bacteria in the regulation of DMS and DMSP concentrations are given in Section 5.3.4.

The demethylation pathway removes a methane group from DMSP, producing a number of degradation products such as methanethiol (MeSH) and methylmercaptopropionate (MMPA) but not DMS (Howard *et al.*, 2006). This process is regulated by the activities of the DMSP demethylation gene (DmdA) in marine phytoplankton and bacteria and is responsible for the

loss of an estimated 50-90% of DMSP (Kiene *et al.*, 2000). The second and third pathways were previously known only as the DMSP-Lyase (cleavage) pathway, but are now known to be regulated by a number of different DMSP dependent DMS (Ddd) enzymes (See Chapter 1, Section 4.2.7). DMS is produced from all the Ddd pathways, with the two separate reactions forming either acrylate or 3-hydroxypropionate (Curson *et al.*, 2011; Todd *et al.*, 2007). Lower $DMSP_P$, as identified in SOPRAN Bergen, implies that higher CO_2 affects the production of DMSP, which will lower the concentration of $DMSP_D$ exuded into surrounding waters. The direct release of DMS from the phytoplankton cells would also be negatively affected. However, if lower DMSP production was the only factor at work, it would not explain why DMS concentrations were 60% lower in the highest CO_2 mesocosms, compared to a 30% reduction in $DMSP_T$.

DMS concentrations during Phase 2 comprised approximately 1-2% of the $DMSP_T$ concentrations, before rising to 6-8% during Phase 3. This is lower than the 10-50% DMSP broken down to DMS calculated by Kiene *et al.* (2000). This increased ratio implies changes to the DMSP breakdown pathway, reducing demethylation and increasing cleavage. However, Zubkov *et al.*, (2004) showed that during a bloom cycle, DMS production from DMSP can become uncoupled from DMS-removal pathways, resulting in higher proportions of DMS to DMSP. Although the proportion of DMS to DMSP increased during Phase 3, CO_2 did not affect the ratio: the factors which affected the conversion of DMSP to DMS were not affected by increased CO_2 or lowered pH. This was also identified during the NERC Microbial Metagenomics experiment (Hopkins, 2010; Hopkins *et al.*, 2010). The ratio of $DMSP_T$: $DMSP_P$ was also unaffected by CO_2 and did not change as the experiment progressed; $DMSP_D$ concentrations were low, indicating rapid extra-cellular $DMSP_D$ turnover, and that the majority of $DMSP_T$ was in the particulate phase.

5.3.3. DMS responses to microbial community development

DMS showed very poor correlation with Chl-*a*, as has been reported previously (Lana *et al.*, 2012; Leck *et al.*, 1990; Scarratt *et al.*, 2007) and is attributed to the differential ability of different phytoplankton groups to manufacture DMSP and Chl-*a* (Liss *et al.*, 1997). In contrast, DMSP showed strong correlation with Chl-*a* in the experiment as a whole (ρ=0.400), however the change in the ratios of DMS and DMSP to Chl-*a* during Phase 3 in the control indicated that the production of both compounds was decoupled from Chl-*a* during the *E. huxleyi* bloom. DMSP: Chl-*a* ratios of 10-60 nmol μg^{-1} were strongly in agreement with those identified by Vogt *et al.* (2008) of 20 nmol μg^{-1} during the bloom, and 50 nmol μg^{-1} post-bloom, also with a negative effect of increased CO_2. The same were true of the DMS: Chl-*a* ratios of 0-2 nmol μg^{-1}.

During EPOCA Svalbard with a different community structure, the DMSP: Chl-*a* was well correlated and remained stable at around 50 nmol μg^{-1}, showing no effect of CO_2.

E. huxleyi is a known producer of DMSP, and during blooms, significantly elevated concentrations of both DMS and DMSP have been detected which correspond well to *E. huxleyi* cell density (Steinke *et al.*, 2007; Vogt *et al.*, 2008). During SOPRAN Bergen, both DMS and DMSP showed strong correlations with haptophyte derived Chl-*a*, but only DMS was correlated with *E. huxleyi* cell numbers. This mismatch between the cell abundance and the haptophyte pigment analysis for DMSP implies there was a DMSP production source other than calcified *E. huxleyi* cells, and likely from non-calcified cells discussed in Section 5.2.2. In a previous mesocosm a bloom of *E. huxleyi* produced DMSP concentrations only one order of magnitude higher than this experiment (Vogt *et al.*, 2008), despite cell densities being higher by three orders of magnitude.

Calcified *E. huxleyi* showed an increase after the second nutrient induced bloom, when the nitrate concentration was half the post-addition concentration and phosphate concentrations had dropped near to the values before the nutrient addition. Sunda *et al* (2007) studied the effects of nitrogen limitation on DMSP and DMS, and found that low nitrogen increased DMSP-lyase activity, but not DMSP. This fits the findings of Franklin *et al.* (2010) who found that lowered nutrient concentrations had no effect on DMSP concentration. Inorganic nitrate at the beginning of Phase 1 was higher than at the start of the experiment, therefore it is unlikely that nitrate limitation triggered DMSP-Lyase activity and therefore an increase in DMS. The lower nitrate and phosphate concentrations might however have stimulated the growth of a calcified sub-population of *E. huxleyi*.

DMSP concentrations in *E. huxleyi* have not been studied in all previous mesocosm experiments: PeECE II was focussed on a diatom bloom (Avgoustidi *et al.*, 2012), Hopkins *et al.* (2010) showed very low *E. huxleyi* abundance at 6% of total community abundance (although cell density comparable to this experiment), and no *E. huxleyi* were identified during the EPOCA Svalbard campaign (Archer *et al.*, 2013). In these experiments, although *E. huxleyi* was not found to be the primary producer of DMSP, reductions in DMSP and DMS concentrations were still identified under high pCO_2. Archer *et al.* (2013) found it difficult to determine how the changes in community composition were related to CO_2 and DMSP production, and the subsequent release of DMS. It is clear that the effect of elevated pCO_2 on the production of DMSP and the consistent reduction in DMS concentrations is not as simple as production by a single species.

Due to significant numbers of diatoms such as *Thalassiosira* and *Skeletonema* spp. within the mesocosms, diatom production of DMSP cannot be ruled out (Bucciarelli *et al.*, 2013; Yang *et al.*, 2011). Diatoms are relatively minor producers of DMSP. In laboratory cultures of *Thalassiosira pseudonana*, total DMSP declined during cell death, which occurred shortly after nutrient depletion, and DMS showed rapid increases (Franklin *et al.*, 2012). In contrast, *E. huxleyi* showed only increases in DMS and DMSP, and relatively long periods of stationary phase. Given that DMSP did not continue to increase in Phases 2 and 3 when *E. huxleyi* was growing, but DMS continued to increase, these patterns of production could have originated from the decline of diatoms, rather than growth of *E. huxleyi*. $DMSP_T$ showed reasonable positive correlation with diatom equivalent Chl-*a* and DMS significant negative correlation: as diatom equivalent Chl-*a* decreased, DMS increased. This same high DMS concentration on the demise of the diatom bloom was identified by Wilson *et al.* (1998).

Although only a small proportion of the overall biomass at 6%, *Synechococcus* has been identified in producing DMSP in a mesocosm previously (Wilson *et al.*, 1998) although cellular concentrations were low at a mean of 0.04 fmol $cell^{-1}$ (Corn *et al.*, 1996). *Synechococcus* likely has greater importance in its assimilation of DMSP for sulphur (Vila-Costa *et al.*, 2006), which will be discussed in Section 5.3.4. Other DMSP producers identified in the mesocosms included the dinoflagellates, of which *Gymnodinium* spp. was identified by light microscopy as having the highest biomass. These phototrophic dinoflagellates have been identified as having high DMSP-lyase activity (Steinke *et al.*, 2002) and relatively high intercellular concentrations of DMSP (Dacey and Wakeham, 1986). However as dinoflagellate numbers showed a steady decrease from the start to the end of the experiment, with 1.5% of the total equivalent Chl-*a* production, DMSP production from dinoflagellates was likely extremely low.

5.3.4. Effects of bacterial abundance and protein production

Both DMSP and DMS are important substrates for marine bacteria, as carbon and energy sources, as well as transfer of sulphur into bacterial amino acids and thus into the microbial food web (Kiene *et al.*, 1999, 2000). Consumption of DMSP by marine bacteria for sulphur will prevent the formation of DMS: the bacterial uptake of DMSP for this purpose in the mesocosms will dictate if DMS is formed. In a previous mesocosm experiment, increased CO_2 had no effect on bacterial community abundance, structure or composition (Oliver *et al.*, 2014), however no analysis was made of bacterial community composition during SOPRAN Bergen, so it was impossible to determine if the community structure shifted during the experiment to alter the pathways of DMSP breakdown.

As the *E. huxleyi* bloom progressed during Phase 2, the bacterial abundance increased in all mesocosms, but showed 28% higher abundance in the high pCO_2 treatments, along with a positive linear relationship between CO_2 and bacterial abundance (Figure 15 and Endres *et al.*, 2014). Although DMSP concentration and bacterial abundance could not be directly correlated, it can be seen from examination of Figures 15 and 17 that bacterial abundance increased before DMSP concentrations started to increase. This was in opposition to the findings of Pinhassi *et al.* (2005) where DMSP enrichment stimulated bacterial growth in the Gulf of Mexico. This higher bacterial abundance is likely going to increase DMS and DMSP consumption at higher levels of CO_2, as indicated by the negative correlation (ρ=-0.216) between bacterial abundance and DMS concentration.

Alongside the bacterial abundance, higher CO_2 gave three times higher leucine aminopeptidase activity compared to the control, as an indicator of enzymatic hydrolysis of organic compounds, including DMSP and DMS. Increased bacterial enzymatic consumption at high *p*CO2 can be a significant contributor to lower DMS concentrations in surface waters. Archer *et al.* (2013) identified that positive correlation between DMS: $DMSP_T$ ratio and bacterial productivity became more significant with increasing CO_2 (plotted as $[H^+]$). This is a similar trend as identified in this experiment; however the data was not available to perform the analysis on each mesocosm individually. Performing a Spearman's Rank Correlation analysis on the combined data from the control, medium and high pCO_2 mesocosms separately for DMS: $DMSP_T$ and bacterial productivity, the control mesocosms showed strong negative correlation (DMS: DMSP decreased with increasing bacterial productivity showing limited breakdown of DMSP) but no correlation at all in the high pCO_2 mesocosms (compared to the control mesocosms, the DMS: $DMSP_T$ ratio has increased).

5.3.5. Other external parameters affecting DMS concentrations

Grazing can have a significant effect on the release of DMSP into the dissolved phase, and allows the interaction of DMSP with the DMSP-lyase stored within the cells (Wolfe *et al.*, 1994). A direct link between grazing activity of heterotrophic dinoflagellates and DMS was identified by Park *et al.* (2014), who identified lowered DMS concentrations under elevated pCO_2 as a direct result of a reduction in grazing activity. It is not possible to determine if this is the case during SOPRAN Bergen due to the absence of data on heterotrophic dinoflagellate abundance or grazing rates. However, high abundance of *Calanus* and *Pseudocalanus* copepods within the mesocosms unaffected by CO_2 (Hildebrandt *et al.*, 2014) would have controlled the abundance of herbivorous micro-zooplankton (Levasseur *et al.*, 1996) which would otherwise consume nanophytoplankton such as *E. huxleyi*. This would have had a

positive effect on DMSP production and would not explain therefore the decrease in DMS with increasing CO_2.

Another factor which could facilitate the release of DMSP to the water column and therefore DMS concentration is the presence of marine viruses affecting *E. huxleyi* (EhV; Hill *et al.*, 1998). An increase in virus numbers was observed by Delille *et al.* (2005) during PeECE I as being influential to cell abundance several days after the peak of the *E. huxleyi* bloom, however *E. huxleyi* had not reached maximum cell density before the conclusion of SOPRAN Bergen. Martinez-Martinez *et al.* (2012) determined that the movement of water masses bringing new EhV into an area was important in determining structure and intraspecific succession during a bloom. In the mesocosm, the viral influence on *E. huxleyi* would be dependent on the viral composition when the mesocosms were closed. It was assumed than viral lysis of *E. huxleyi* and subsequent release of DMSP would not occur until after the experiment had ended, and was therefore of minimal importance to DMSP and DMS concentrations. This could not be proven as no determination was made of EhV activity.

5.4. DMS and DMSP comparison with other analysis

5.4.1. DMSP Measurements: GC-FPD vs GC-FPD

The DMSP GC-FPD results measured by UEA were on average 26% lower than those measured by GEOMAR but the regression analysis showed the overall trends shown from both datasets were the same with an R^2 of 0.594 for $DMSP_T$ (Figure 27a). As the samples from UEA were analysed after the campaign, no intercalibration between GC-FPD systems or standards was performed, but the UEA system performed extremely well during the international intercalibration exercise (full details in Chapter 2, Section 4.5), measuring concentrations very close to the mean of all the participating laboratories. GEOMAR DMSP concentrations were measured using a liquid DMS standard made up in Milli-Q water: the lower DMS solubility in water compared to the solubility of DMSP used in the UEA standards will give a higher peak area for a given concentration of standard. The main difference between the two analysis techniques was that the samples analysed at UEA were stored for up to 6 weeks prior to analysis, rather than analysed immediately.

The correlation between $DMSP_P$ measurements was far lower at $R^2 = 0.215$ and still 58% lower than GEOMAR, but this may be explained by the method for filtering the sample: this study used a gravity filtration setup to filter 7 mL of sample through a GF/F, over a period of up to 60 minutes per sample, depending on cell density. The 25 mL samples from GEOMAR were

syringe filtered through the same type of GF/F (Zindler *et al.*, 2012), however this method has shown potential to release DMSP from the particulate phase into the dissolved phase (Kiene and Slezak, 2006). This does not explain why the GEOMAR samples were higher in mean concentration to the UEA samples, but may explain the higher variation between the $DMSP_P$ and the $DMSP_T$ analyses.

5.4.2. DMS Measurements: GC-MS vs GC-FPD

The DMS GC-MS results correspond within the same range as those from the GC-FPD, with the same trends being identified: lower DMS production with increasing CO_2 exposure, and DMS increasing in all mesocosms towards the end of Phase 2 and through Phase 3. The regression analysis also confirms that both methods are producing data which show the same trends in the data, with an R^2 of 0.829 there is close relationship between the two datasets. However, the measurement difference of 58.8% is more of a concern. It is proposed that this difference was mainly a result of the solubility of the liquid DMS standards made up in methanol (this study) versus Milli-Q water (GEOMAR). No intercalibration was made between the two systems due to a lack of time during the experiment, and as a DMS standard was used in the UEA GC-MS, the system was not included in the international DMSP intercalibration exercise outlined in Chapter 2. No intercalibration has been performed between the GC-MS and GC-FPD systems at UEA, as it was impossible to calibrate a DMSP standard on the GC-MS purge and cryotrap system. DMS samples on GC-MS and GC-FPD were analysed within 6 hours of collection, so differences were unlikely to be a result of sample storage.

It should be noted that the GEOMAR GC-FPD was operated at ambient temperature without the oven between the 13th and 26th May, with the oven repaired on the 27th May. During this time, DMS concentrations were below detection limits in samples from M9 (3000 µatm), M7 (2000 µatm), M5 (1400 µatm) and M3 (1120 µatm), the four mesocosms with the highest CO_2 treatments.

The differences identified between identical samples using different equipment and standards during this experiment reinforce the idea of the development of an international standard for DMSP (National Measurement Institute of Australia, 2013). If identical standards were used for all DMSP analysis, it would highlight problems with technique or equipment when comparing samples such as these.

5.5. Iodocarbons

Concentrations of iodocarbons (CH_3I, CH_2I_2, C_2H_5I and CH_2ClI) were within the range of previous mesocosm experiments; however the mean of CH_3I was higher than previously identified (Table 21). Mean CH_3I concentration was calculated as 17.5 pmol L^{-1} in the low pCO_2 mesocosms, compared to 9.2 pmol L^{-1} measured by Hopkins *et al.* (2010) and 2.6 pmol L^{-1} by (Hopkins *et al.*, 2013) in EPOCA Svalbard. These values are similar to coastal surface water concentrations of 6.1 pmol L^{-1} in the English Channel (Archer *et al.*, 2007) and 5.3 pmol L^{-1} in Spring in the Kiel Fjord (Shi *et al.*, 2014). Concentrations of C_2H_5I were low and near detection limit of the analysis technique, similar to the situation in the NERC Metagenomics experiment in 2006. Mean concentrations of 0.7 pmol L^{-1} were the same as measured in previous mesocosm experiments (Hopkins *et al.*, 2010, 2013).

CH_2I_2 and CH_2ClI were the significant contributors to total iodocarbons of the four measured; in the case of CH_2I_2 concentrations were an order of magnitude higher than CH_3I. Concentrations of both compounds were the same as have been measured at Bergen previously (Hopkins *et al.*, 2010) but were higher than concentrations measured in coastal waters (Archer *et al.*, 2007), open waters (Kurihara *et al.*, 2010) and in the EPOCA Svalbard campaign.

Table 21. Mean and range of iodocarbon concentrations from SOPRAN Bergen compared to previous mesocosm experiments. Experiments where a significant difference was identified between control and high pCO_2 treatment have been split into two rows. All concentrations are in pmol L^{-1}, except those highlighted (*) which are fmol L^{-1}. ND – not detected.

Experiment	CH_3I		CH_2I_2		C_2H_5I		CH_2ClI		Author
	Mean (pmol L^{-1})	Range (pmol L^{-1})	Mean (pmol L^{-1})	Range (pmol L^{-1})	Mean (pmol L^{-1})	Range (pmol L^{-1})	Mean (pmol L^{-1})	Range (pmol L^{-1})	
SOPRAN Bergen 2011 Control (280 µatm)	17.5	10.9 – 28.5	195.6	66.9 – 315.4	0.7	0.1 – 1.9	54.8	19.2 – 122.5	This Study
SOPRAN Bergen 2011 High CO_2 (1400 – 3000 µatm)	11.2	4.9 – 21.0	99.0	5.8 – 239.4	0.7	0.1 – 1.8	42.6	10.1 – 118.5	
EPOCA Svalbard 2010	2.6	0.04 – 10.3	0.2	0.01 – 2.5	0.9	0.1 – 3.3	0.8	0.3 – 1.6	Hopkins *et al.* (2013)
NERC Microbial Metagenomics Experiment 2006 Control (300 µatm)	9.2	1.0 – 25.0	200.8	ND – 750.0	0.7	ND – 2.0	191.0	ND – 650.0	Hopkins (2010); Hopkins *et al.* (2010)
NERC Microbial Metagenomics Experiment 2006 High CO_2 (750 µatm)	5.4	1.0 – 15.0	134.6	ND – 500.0	0.5	ND – 2.0	136.9	ND – 600.0	
PeECE II Control								3.0 – 12.0*	Wingenter *et al.* (2007)
PeECE II High CO_2 (1150 µatm)								3.0 – 37.0*	

BLANK

5.5.1. Iodocarbon concentrations in the mesocosms

All the measured iodocarbons showed a decrease in concentration as CO_2 increased, with the linear decrease most apparent for CH_3I and CH_2I_2. Very few studies exist on the changes to iodocarbon concentrations under the effects of elevated pCO_2. The mesocosm studies of the NERC Metagenomics experiment (Hopkins *et al.*, 2010) showed a similar reduction in iodocarbons in the high pCO_2 treatment of 750 µatm, but CO_2 did not affect concentration during EPOCA Svalbard (Hopkins *et al.*, 2013). The only iodocarbon measured during PeECE II was CH_2ClI, which showed concentrations higher by 131% under CO_2 treatments of 1150 µatm by Wingenter *et al.* (2007) compared to the control.

5.5.2. Monoiodinated compounds (CH_3I and C_2H_5I)

Monohalides such as CH_3I and C_2H_5I are produced by enzymatic methylation of halide ions (I^-, Br^- or Cl^-) by *S*-adenosyl-L-methionine utilising methyl transferases (Manley, 2002). Additional production processes are through the breakdown of larger molecular weight iodocarbon compounds and photochemical production (Richter and Wallace, 2004). Loss of CH_3I in seawater results from chemical reactions such as nucleophilic substitution (Moore, 2006), hydrolysis (Elliott and Rowland, 1995), photolysis (Zika *et al.*, 1984) and air-sea flux to the marine boundary layer. Hopkins *et al.* (2013) determined that air-sea flux was only a minor loss (<4%) process during the EPOCA Svalbard (2010) mesocosm experiment. In the mesocosms, there are also likely to be microbial interactions taking place around the formation and breakdown of iodocarbons, however, relatively little is known about these interactions.

Photochemical production of CH_3I , either through reactions with DOM or radical recombination of CH_3 and I (Moore and Zafiriou, 1994) within the mesocosms may have been limited to the surface waters, as the thermoplastic polyurethane (TPU) mesocosm film is known to absorb nearly 100% of UV light (Riebesell *et al.*, 2013a). Photodegradation (Zika *et al.*, 1984) of halocarbons is also unlikely for the same reason. As samples were integrated over 0 –25m, it was impossible to determine if photochemistry was affecting iodocarbon concentrations near the surface.

It has been suggested that CH_3I is produced by both macroalgae and phytoplankton (Lovelock 1975; Baker *et al.* 2000). CH_3I showed strong negative correlations with *Synechococcus*, which corresponds to laboratory experiments where no CH_3I was detected from *Synechococcus* cultures (Hughes *et al.*, 2011; Manley and De La Cuesta, 1997), although Wang *et al.* (2009) reported *Synechococcus* as having strong positive correlations with CH_3I. Positive correlations

were identified between CH_3I and diatoms; Manley and De La Cuesta (1997) found CH_3I production in *Nitzschia* spp. and *Thalassiosira* spp., both of which were identified by light microscopy in the mesocosms. *Skeletonema* spp. were also identified, but these species were found to produce no detectable CH_3I (Manley and De La Cuesta, 1997). The two nanophytoplankton groups identified by flow cytometry also correlated with CH_3I, but there was no identification for these groupings.

Despite the similar production processes for C_2H_5I, this compound had different correlations to the indicators of primary productivity than CH_3I, although the strongest correlations were with diatoms and nanophytoplankton. Marine aggregates were found to produce monoiodinated compounds by Hughes *et al.* (2008), and it was suggested this was from the alkylation of inorganic iodine (Urhahn and Ballschmiter, 1998) or the breakdown of higher mass halogenated compounds (Fenical, 1982). Aggregation has been previously studied within mesocosms at the termination of bloom phases, however the iodocarbon concentrations during SOPRAN Bergen decreased during the later part of Phase 2, when the Chl-*a* peak was decreasing and the bloom was collapsing, indicating that aggregate production of these compounds may not have been a major source.

5.5.2.1. Polyhalogenated iodocarbons (CH_2ClI and CH_2I_2)

Polyhalogenated compounds such as CH_2I_2 can be produced by the activity of bromo- or iodoperoxidase enzymes, the former of which is known to produce polybrominated as well as polyiodinated compounds (Manley, 2002). Loss processes for these compounds are similar to the monoiodinated compounds: air-sea flux, microbial degradation or chemical reactions.

CH_2I_2 undergoes photolysis in natural sunlight under 300-350 nm wavelength, leading to the formation of CH_2ClI (Jones and Carpenter, 2005; Martino *et al.*, 2006; Moore and Tokarczyk, 1993). Strong correlation of CH_2I_2 and CH_2ClI in the mesocosms supports this production route, although as previously stated, any photoreactions of halocarbons within the mesocosms cannot be quantified. In line with their different production pathways, the polyiodinated compounds showed mostly negative correlations with the phytoplankton groups. DMS concentrations have been correlated with high grazing rates in mesocosms (Park *et al.*, 2014), and it is likely the concentrations of halocarbons would be similarly affected: unless extreme selective grazing was in operation, release of halocarbons during grazing would be from a range of species, both high and low producers, and would therefore have weak correlations of these compounds with both phytoplankton grouping and grazing activity. Grazing pressure

within the mesocosms was relatively high due to high numbers of copepods and no top-down control due to removal of predators.

5.6. Bromocarbons

Mean concentrations of bromocarbons ($CHBr_3$, CH_2Br_2 and $CHBr_2Cl$) were higher than those measured during previous mesocosm experiments, but were within the same order of magnitude (Table 22). Concentrations of all compounds measured in the Fjord were consistently higher than in the mesocosms. Mean bromoform concentrations of 160 pmol L^{-1} in the control mesocosms compared to 35 pmol L^{-1} in the NERC Metagenomics experiment in 2006, and 84 pmol L^{-1} in the EPOCA Arctic experiment. The differences in concentration suggest differences in phytoplankton assemblages between the mesocosm experiments. These concentrations were similar to those measured in global locations: in the Antarctic summer phytoplankton bloom (276 pmol L^{-1}; Hughes *et al.*, 2009), in the Gulf of Mexico in summer (66 pmol L^{-1}; Liu *et al.*, 2011), in a coastal bay in Japan (33.8 pmol L^{-1}; Kurihara *et al.*, 2012) and in the North Atlantic (115 pmol L^{-1}; Carpenter *et al.*, 2009). The concentrations were also well within the range documented by Quack and Wallace (2003) where maximum concentration presented was 4590 pmol L^{-1}.

CH_2Br_2 and $CHBr_2Cl$ were within the same range as measured during the EPOCA Arctic experiment (6.3 – 33.3 pmol L^{-1} and 1.6 – 4.7 pmol L^{-1} respectively) and higher than the NERC Metagenomics experiment (ND – 5.5 pmol L^{-1} and 0.2 – 1.1 pmol L^{-1} respectively; Hopkins *et al.*, 2010). These two compounds were measured at 10.6 and 1.0 pmol L^{-1} in the Gulf of Mexico (Liu *et al.*, 2011).

BLANK

Table 22. Mean and range of bromocarbon concentrations (pmol L^{-1}) from SOPRAN Bergen compared to previous mesocosm experiments.

Experiment	$CHBr_3$		CH_2Br_2		$CHBr_2Cl$		Author
	Mean (pmol L^{-1})[1]	Range (pmol L^{-1})	Mean (pmol L^{-1})[1]	Range (pmol L^{-1})	Mean (pmol L^{-1})[1]	Range (pmol L^{-1})	
SOPRAN Bergen 2011	158.6	64 - 306	17.8	6.3 – 30.8	6.6	3.9 – 13.5	This Study
EPOCA Svalbard 2010	84.0	35.3 – 151.5	12.7	6.3 – 33.3	2.9	1.6 – 4.7	Hopkins *et al.* (2013)
NERC Microbial Metagenomics Experiment 2006	37.3	5.0 – 80	2.3	1.0 – 5.5	0.6	0.2 – 1.1	Hopkins *et al.* (2010)

BLANK

5.6.1. Bromocarbon concentrations in the mesocosms

$CHBr_3$ or CH_2Br_2 concentrations showed no effect of elevated pCO_2 even up to 3000 µatm, nor did the ratio of $CHBr_3$: CH_2Br_2, which is a finding mirrored by Hopkins *et al.* (2010) during the NERC Metagenomics experiment and Hopkins *et al.* (2013) in the EPOCA Svalbard experiment. During SOPRAN Bergen, $CHBr_2Cl$ was also unaffected by increased CO_2, but in 2006 there were significantly higher concentrations at a pCO_2 of 750 µatm (Hopkins *et al.*, 2010).

Bromocarbons show greater positive correlations with the different community parameters, including $CHBr_3$ showing a weak positive correlation with Chl-*a*. Changes to the bromocarbon ratios with Chl-*a* are driven by the Chl-*a* concentration, especially in Phase 3 of the experiment. No correlation was given between any of the bromocarbons and the measurements of bacterial activity.

The overall relationship between $CHBr_3$ and Chl-*a* in surface oceans is complex: $CHBr_3$ has been found to be elevated in regions of high Chl-*a* (Carpenter *et al.*, 2009; Quack *et al.*, 2007; Schall *et al.*, 1997) but other studies found no significant relationship between the two (Hughes *et al.*, 2009; Liu *et al.*, 2011; Mattson *et al.*, 2012). A stronger correlation was identified between Chl-*a* and CH_2Br_2, a situation identified by Liu *et al.* (2013) in a number of open ocean cruises. However CH_2Br_2 showed only a steady decrease during the experiment and did not show the variations seen in the Chl-*a* particularly during Phase 1. Variations in sea-air fluxes of bromocarbons, differential production rates by phytoplankton, and differential degradation rates in seawater alter the correlations between bromocarbons and Chl-*a*. $CHBr_3$ has also been identified as a by-product of chlorine-based water disinfection processes, and significant discharge of treated waters from urbanised areas could be a major source of $CHBr_3$ in the Baltic Sea (Liu *et al.*, 2011; Nieuwenhuijsen *et al.*, 2000; Quack and Wallace, 2003)

$CHBr_3$ and CH_2Br_2 are produced predominantly by biogenic sources in the marine environment, but not necessarily produced directly. Liu *et al.* (2013) suggested that $CHBr_3$ and CH_2Br_2 concentrations in the open oceans were qualitatively related to ocean photosynthetic biomass or the biogeochemical processes associated with biomass activity. Biological production is likely to be attributed to bromoperoxidase enzyme activity: either by bromination of ketones followed by breakdown of intermediates to $CHBr_3$ and CH_2Br_2 (Theiler *et al.*, 1978) or production of hypobromous acid (HOBr) which reacts with organic matter and humic acids to produce volatile brominated compounds (Carter *et al.*, 2002; Hill and Manley, 2009; Wever *et al.*, 1991). Several species of diatom have been identified as producers of these precursors (Hill and Manley, 2009; Moore *et al.*, 1996), as well as the cyanobacteria *Synechococcus* (Johnson *et al.*, 2011; Liu *et al.*, 2013). However in coastal waters, production of bromocarbon precursors is

predominantly from macroalgae (Leedham Elvidge *et al.*, 2014; Theiler *et al.*, 1978; Wever *et al.*, 1991)

$CHBr_3$ showed a number of correlations with biological parameters, including chlorophytes, cryptophytes and nanophytoplankton. It was also the only halocarbon which showed correlation with Chl-*a*, which has been reported in previous studies (Hopkins *et al.*, 2010; Moore and Tokarczyk, 1993). Although macroalgal production of $CHBr_3$ is one of the major biogenic sources for seawater concentrations and atmospheric flux, the production by marine phytoplankton is obviously an important secondary source. Concentrations of $CHBr_3$ in the Fjord outside the mesocosms were similar to the mesocosms for the majority of Phase 2, and 55% of the measured concentrations for Phase 3, indicating that phytoplankton are responsible for half of the $CHBr_3$ in the coastal region.

$CHBr_3$ showed strong correlation with CH_2Br_2 in contrast to the findings of Chuck *et al.* (2005) and Hopkins *et al.* (2010) who found little or no correlation between these compounds. Production of CH_2Br_2 is possible through the reductive dehalogenation of $CHBr_3$ or other larger brominated compounds (Quack and Wallace, 2003). CH_2Br_2 was correlated with haptophytes, particularly *E. huxleyi*, which was not found in the NERC Metagenomics experiment by Hopkins *et al.* (2010). No other studies exist to show the production of bromocarbons from *E. huxleyi*.

Although the production pathways through the haloperoxidase enzymes were supposed to be similar, neither $CHBr_3$ nor CH_2Br_2 show positive correlations with CH_2I_2 or CH_2ClI. The lack of correlations between different halocarbon gases is likely a result of differences in breakdown processes, as well as multiple production pathways including the abiotic routes.

5.6.2. Ratio of CH_2Br_2: $CHBr_3$

The ratio of CH_2Br_2 to $CHBr_3$ was unaffected by CO_2 and stayed within the range 0.05 – 0.2 (Figure 34). Ratios are at their highest at the beginning of Phase 2 and during the whole of Phase 3, where they remained stable until the end of the experiment. The steady increase of both these compounds indicated a common source, however comparisons of CH_2Br_2 and $CHBr_3$ in the Mauritanian upwelling revealed different vertical and horizontal distributions of concentrations, implying that these two compounds originated from different sources (Quack *et al.*, 2007). Evidence of a similar source is in the correlations with different parameters and the other gases: both $CHBr_3$ and CH_2Br_2 correlate strongly with DMS, and with haptophytes and cryptophytes, and neither positively correlate with diatoms or chrysophytes.

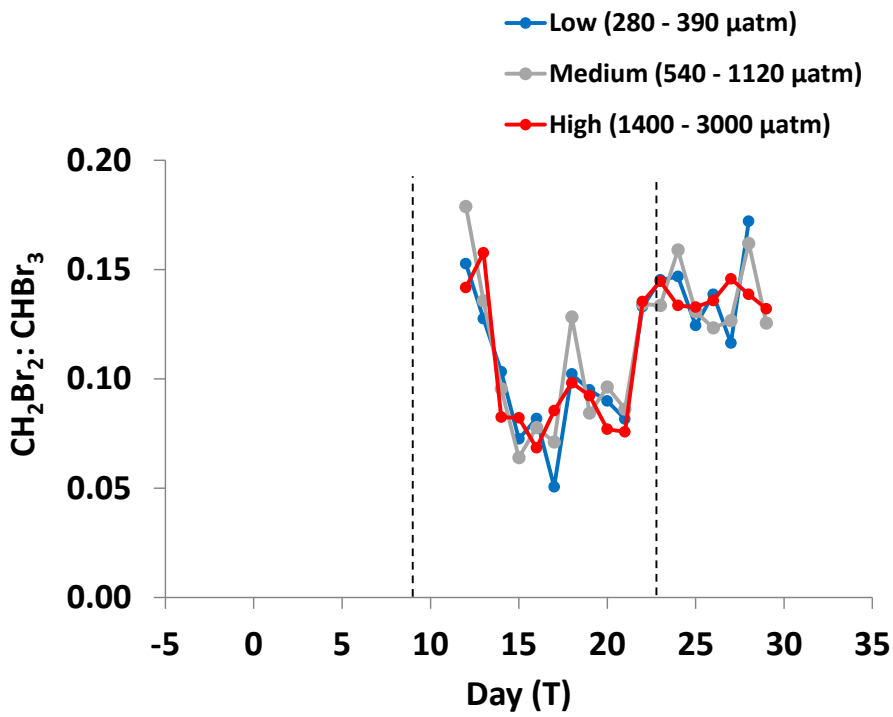

Figure 34. Ratio of CH_2Br_2 to $CHBr_3$ during SOPRAN Bergen in the three different CO_2 treatments: low (control at 280-390 µatm), medium (540 – 11200 µatm) and high (1400 – 3000 µatm). Dashed lines indicate the sectioning into three Phases of the experiment.

5.7. Summary

The purpose of SOPRAN Bergen was to investigate the changes in DMS, DMSP and halocarbons alongside community variation in a mesocosm experiment, with seawater pCO_2 up to 3000 µatm.

Elevated CO_2 had different effects on the microbial community of the Norwegian Fjords: Chl-α was strongly affected by CO_2 in all three Phases of the experiment, both showing both the highest and lowest production during the peak of a phytoplankton bloom in the 3000 µatm mesocosm. Haptophytes and chlorophytes grew better at ambient CO_2, whereas cyanobacteria and chlorophytes showed significantly better growth as CO2 increased.

DMS, DMSP and the iodocarbons showed significantly lower concentrations under high pCO_2, as a result of lowered production within cells and due to changes in bacterial abundance and degradation activities in the water column. DMS and DMSP cycling and dynamics are hard to determine in the current mesocosm setup and are reliant upon independent measurements of primary productivity within the mesocosm. As a result, parameters such as calcification rates useful to the analysis of the dataset here have not been measured. Bromocarbons were unaffected by increased CO_2 up to 3000 µatm, although given that the majority of bromocarbon production in coastal waters is from macroalgal sources not the microbial

population, without knowledge of the effect of acidification on macroalgae, it is too soon to determine of sea-air flux of bromocarbons is likely to change in the future oceans.

The trace gas concentrations were compared with different biological parameters to evaluate the interactions of these parameters with the production of these compounds. The answer to the questions posed at the beginning of this chapter are that the concentrations of DMS, DMSP and some iodocarbons decreased as CO_2 increased, but that increasing CO_2 had no significant effect on bromocarbon concentrations.

Chapter 4. Evaluating the effect of CO_2 enrichment on the growth, DMSP content and trace gas production of trace gases by the coccolithophore *Emiliania huxleyi* RCC1229

1. Overview of the *E. huxleyi* CO_2 enrichment experiments

The SOPRAN Bergen mesocosm experiment (Chapter 3) showed that DMS and DMSP production decreased with increasing CO_2 during a bloom of wild-type *E. huxleyi* within the confines of mesocosms. This finding was in line with similar mesocosm experiments conducted in several locations around the world: Korea in 2012 (Park *et al.*, 2014), Svalbard in 2010 (Archer *et al.*, 2013) and in Bergen in 2006 (Hopkins *et al.*, 2010), 2005 (Vogt *et al.*, 2008) and earlier years. However, laboratory experiments with clonal *E. huxleyi* cultures have given variable results in response to high CO_2 in terms of DMS and DMSP production (Arnold *et al.*, 2013; Avgoustidi, 2006).

This series of experiments was designed to test the following research questions, which were deemed to have been answered after experiment S2:

- Do increasingly acidified conditions caused by an increase in atmospheric pCO_2 to 860 µatm, under the IPCC A2 Scenario projections for 2100 cause a change in DMS and DMSP production from *E. huxleyi* compared to current conditions?
- Does mid-term exposure of *E. huxleyi* to acidified conditions result in changes to DMS and DMSP production or the dynamics between the two?

The experiments detailed here were designed to expand on the Avgoustidi study, and used RCC1229 which had not previously been quantified in terms of DMS and DMSP production. This strain is known to be a good calcifier (Heinle, Pers Comm), but it's response to elevated pCO_2 was unknown.

1.1. Growth of *E. huxleyi* under laboratory conditions

E. huxleyi is a model organism for representing the coccolithophores, although given its wide geographical range and genetic and morphological variations, it is potentially flawed to consider *E. huxleyi* as a single species (Fabry, 2008). *E. huxleyi* acclimatises rapidly to the growth conditions: in studies this was proven to be sufficiently rapid that a short term pCO_2 experiment can provide the same information as one for 1000 generations (Müller *et al.*, 2010), and yet it is relatively simple to maintain in the laboratory under a variety of conditions, which allows greater scope for experimentation. Although easy to grow, different strains of *E. huxleyi* calcify at different rates, and a number of strains lose the ability to calcify in laboratory culture (G. Malin, Pers. Comm).

Many of the mesocosm experiments performed at the Bergen Mesocosm Facility have targeted an *E. huxleyi* bloom, and the effects observed during these studies have encouraged further studies in the laboratory. There have been a reasonable number of experiments investigating the behaviour of different strains of *E. huxleyi* grown under elevated pCO_2 (e.g. Riebesell *et al.* 2000; Langer *et al.* 2009; Moheimani & Borowitzka 2011), and a limited number of experiments evaluating the behaviour of *E. huxleyi* strains under the additional influence of light (Leonardos and Geider, 2005) or temperature (Feng *et al.*, 2008; Spielmeyer and Pohnert, 2012).

Table 1 shows the findings from a number of key laboratory studies on the effect of CO_2 on *E. huxleyi* cell physiology. There are very few experiments evaluating the changes in DMS and DMSP production from *E. huxleyi* under the influence of CO_2.

It is possible that there is no simple pattern in the published results on the effect of seawater pCO_2 on carbon fixation, calcification or growth rate. The different results may be due to different experimental conditions, such as nutrient concentrations, light levels and temperatures. Even if conditions remain constant differences may be observed due to strain differences: Langer *et al.*, (2009) studied four strains from the Roscoff Culture Collection (RCC 1212, 1216, 1238 and 1256) which were isolated from different geographical locations under identical conditions and identified varying responses of carbon fixation and growth rate between strains as a result of elevated pCO_2. Many of the laboratory experiments listed in Table 1 used different strains of *E. huxleyi*, isolated from different parts of the world kept in culture for differing periods of time. It is reasonable to assume that different strains will show different responses to changing environmental conditions (such as elevated pCO_2) depending on the genetic variability within each population. Another explanation could that the methods used to alter the carbonate chemistry and cell growth conditions have a direct effect on the

cell response, although this has been disproved by Shi *et al.* (2009) on studying *E. huxleyi* strain PLYM219 and on *Thalassiosira weissflogii* strain CCMP1336. An overview by Ridgwell *et al.* (2009) identified that it was highly unlikely the method used to manipulate the carbonate chemistry causes differences in response patterns.

In general, increased CO_2 has a positive effect on the carbon fixation (Table 1) often within short timescales of <24 hours (Barcelos e Ramos *et al.*, 2010). One of the strain differences mentioned in Langer *et al.* (2009) above was that the strains from both the Southern Pacific (RCC1216) and the South Atlantic (RCC1212) showed a decrease in carbon fixation under high CO_2. Shi *et al.* (2009) identified an increase in growth rate alongside the increase in carbon fixation, but, in contrast, Iglesias-Rodriguez *et al.* (2008) found the opposite effect with a decrease in growth rate. There have been some concerns voiced about the experimental design in the latter's investigation and how they were run over relatively short timescales of 2-3 days (Riebesell *et al.*, 2008). Further discussion about the timescales of experiments will take place in Chapter 6.

Both light and nutrient levels have an additional effect on carbon fixation in *E. huxleyi*: Leonardos & Geider (2005) identified that increased pCO_2 enhances fixation under high light and nutrient limitation, which is in agreement with the work by Zondervan *et al.* (2002), which showed that carbon fixation increases under all the conditions tested, including four different light levels and two different light: dark cycles.

Table 1. Summary of previously reported *E. huxleyi* culture experiments, showing the findings of enhanced CO_2 exposure for POC production, the effect on calcification, and the effect on growth rate. Arrows show if the parameters were increasing (↑), decreasing (↓) or no significant change (↔)

Author	*E. huxleyi* strain and key experimental notes	Effect of CO_2			Acidification method
		carbon fixation	calcification	growth rate	
High calcifying strains					
Dong *et al.* (1993)	Bigelow 88E (CCMP 378; Gulf of Maine)		↔	↔	Bubbling CO_2-rich air
Kottmeier *et al.* (2014)	RCC1216 (Tasman Sea)	↑	↓	↔	Bubbling CO_2-rich air
Low calcifying strains					
Dong *et al.* (1993)	SMBA 279 (Scotland)			↑	Bubbling CO_2-rich air
Non-calcifying strains					
Arnold *et al.* (2013)	CCMP 373 (Sargasso Sea)			↔	pH stat: Bubbling CO_2-rich air
Spielmeyer & Pohnert (2012)	RCC1242	↑		↔	Bubbling CO_2-rich air
Wuori (2012)	CCMP 374 (Gulf of Maine)	↔		↔	
Non-specified					
Nimer & Merrett (1993)	Bigelow 88e (CCMP 378; Gulf of Maine)	↑	↓		pH buffers
Riebesell *et al.* (2000)	PML B92/11A (North Sea)	↑	↓		Addition of acid/ base
Zondervan *et al.* (2002)	PML B92/11A (North Sea)	↑			Addition of acid/ base
Sciandra *et al.* (2003)	TW1 (W. Mediterranean)		↓	↑	pH stat: Bubbling CO_2-rich air
Leonardos & Geider (2005)	PML 92A	↑			Bubbling CO_2-rich air
Feng *et al.* (2008)	CCMP 371 (Sargasso Sea)	↑			Bubbling CO_2-rich air
Iglesias-Rodriguez *et al.* (2008)	NZEH CAWPO6 (South Pacific)	↑	↑	↓	Bubbling CO_2-rich air
Langer *et al.* (2009)	RCC 1212 (South Atlantic)	↓		↓	Addition of acid/ base
	RCC 1216 (Tasman Sea)	↓		↓	
	RCC1238 (North Pacific, Japan)	↔		↑	
	RCC1256 (North Atlantic)	↑			
Shi *et al.* (2009)	NZEH PLY M219 (South Pacific)	↑	↑	↑	Bubbling CO_2-rich air and acid/ base addition
Barcelos e Ramos *et al.* (2010)	Bergen Mesocosm 2005 isolate	↑		↓	Addition of acid/ base
Moheimani & Borowitzka (2011)	CCMP 371 (Sargasso Sea)		↓		Bubbling CO_2-rich air
Spielmeyer & Pohnert (2012)	RCC 1731 (Peruvian upwelling)	↑		↔	Bubbling CO_2-rich air
Wuori (2012)	CCMP 2668 (Gulf of Maine)	↔	↓	↔	Bubbling CO_2-rich air
Lohbeck *et al.*, (2012a)	Freshly isolated genotype, Bergen, Norway.	↑	↓	↑	Bubbling CO_2-rich air prior to inoculation

Culture collection abbreviations: Roscoff Culture Collection (RCC); Scottish Marine Biological Association (SMBA); Provasoli-Guillard National Culture Centre for Marine Phytoplankton (CCMP); Plymouth Marine Laboratory (PML); Culture Collection of Algae and Protozoa (CCAP).

There is no simple overarching effect that increased CO_2 has on the calcification of *E. huxleyi*, as both positive and negative results will be observed depending upon the physical experimental parameters (temperature, nutrients, media type, light level) and the biological parameters of the organism (calcifying or naked strain, haploid or diploid). Calcification relies on the availability of HCO_3^-; a decrease in pH under ocean acidification will result in an increase in the CO_2: HCO_3^- ratio and will make calcification energetically more difficult for the organism. No studies have so far been performed on the haploid phase of *E. huxleyi*. The majority of non-calcified *E. huxleyi* strains likely originated as calcified isolates and reduced calcification over long term culture; identification and isolation of non-calcified *E. huxleyi* from the wild is very difficult.

Lohbeck *et al.* (2012) showed that *E. huxleyi* cultures were able to adapt to changed conditions within 500 generations, on timescales able to cope with the changes imposed through climate change. Further, *E. huxleyi* was able to adapt to higher pCO_2 after 750-1000 generations, and that phenotypic convergence occurred in replicate cultures (Lohbeck *et al.*, 2012a). The strain used was isolated from Bergen, Norway, during the 2005 mesocosm experiment; in comparison to the majority of the other strains tested, this strain was not previously maintained, and therefore genetically selected, for growth under culture conditions.

There is increasing evidence that an increase in temperature has a greater impact on *E. huxleyi* growth rates than CO_2. Evidence suggests that a combination of the two conditions, as is likely in future climate change scenarios, will have an influence on the growth of *E. huxleyi*, and subsequently the calcification rate (Feng *et al.*, 2008).

1.2. DMS and DMSP production measured in *E. huxleyi* grown under elevated pCO_2 in the laboratory

Laboratory studies on differenrt clones of *E. huxleyi* have shown DMSP concentrations within the cell of 8.21 fmol $cell^{-1}$ (CCMP376; Keller, 1989), 5.97 fmol $cell^{-1}$ (RCC1216; Franklin *et al.*, 2010), 3.58 fmol $cell^{-1}$ (CCMP 370) and 7.59 fmol $cell^{-1}$ (CCMP 373; Wolfe and Steinke, 1996). Despite these relatively high intracellular DMSP concentrations, there have been few studies on the production of DMSP and DMS from this species under lowered pH/ elevated pCO_2. Initially, a series of batch culture experiment were carried out by Avgoustidi (2007) on the strain CCMP1516 under CO_2 of 760 µatm, during which measurements were taken of growth characteristics alongside DMS(P) concentrations. Of the three experiments, there was no consistent trend in the growth characteristics of the cells in response to increased CO_2, nor the production of DMS, dissolved or particulate DMSP:

- Experiment 1: decrease in DMS per cell relative to the control, but no change in particulate or dissolved DMSP and no change in growth rate.
- Experiment 2: decreased $DMSP_D$ throughout, lower $DMSP_P$ in stationary phase and lowered DMS during exponential growth. Cells grew larger in elevated pCO_2, lower growth rate in CO_2 treatment.
- Experiment 3: No change in cell volume, a decrease in DMS throughout, higher $DMSP_P$ in stationary phase and no change to $DMSP_D$, increased growth rate in CO_2 treatment.

In contrast to the batch experiments of Avgoustidi (2006), Arnold *et al.* (2013) developed a custom designed pH stat system to study the strain CCMP373 and found that DMS production was 50% lower in the CO_2 treatment at 1000 µatm, but that intracellular DMSP was higher.

Semi-continuous methods can be as effective as continuous chemo-or pH-stat systems in showing the medium (weeks to months) term effects of a particular treatment. Semi-continuous studies using *E. huxleyi* and DMSP under high CO_2 have also found differences in DMSP concentrations in calcifying strains, either where there has been no significant change (Spielmeyer and Pohnert, 2012) or where DMSP increased (Wuori, 2012). Of the non-batch culture experiments, only those mentioned above have investigated changes in DMSP under medium-term exposure to elevated pCO_2, and of these, only one investigated the changes in DMS production, and then only on a limited basis (4 DMS measurements over an 18 day growth period; Arnold *et al.* 2013).

The experiments performed during this investigation were designed to build on the batch experiments of Avgoustidi (2006) and then to measure DMSP and DMS on a daily basis during longer semi-continuous experiments. The aim was to build on the existing database of *E. huxleyi* experiments, working with a different strain, RCC1229 as a known non-motile calcifier (Roscoff Culture Collection). It was chosen for these experiments as a strain which had never been parameterised in terms of its DMSP producing capability, nor its growth behaviour under acidification and elevated pCO_2. It was also chosen due to its nature as a reliable calcifier under laboratory conditions: cells were examined and confirmed to be calcifying using light microscopy from multiple replicates of multiple cultures of the strain.

2. Design, setup and operation of the *E. huxleyi* CO_2 enrichment experiments

The experiments in this series started with batch experiments run over a standard growth curve for *E. huxleyi*, allowing for daily measurements of cell count, cell volume, pH, DMS and halocarbons. The experimental design developed with each further experiment, progressing to

a longer term semi-continuous culture method reinoculated into fresh media every 4 days. The semi-continuous system minimised the risk that changes in DMS and halocarbon emissions could be attributed to sudden changes in the environmental conditions, and allowed measurement of DMS and DMSP over medium-term exposure to elevated pCO_2.

2.1. Preparation of culture medium and nutrient concentrations

All media were prepared without the addition of silicate using aseptic techniques and the recipes in Andersen *et al.* (2005). There were adaptations to the seawater medium as the experiments progressed: the first experiment was carried out in K/5 medium, the second in ESAW (Enriched Seawater, Artificial Water) and the three other experiments in ESNW (Enriched Seawater, Natural Water). K/5 was the medium in which culture was maintained in the laboratory stocks and was known to support healthy cell growth, but the medium was changed to ESAW (without silicate addition) to test cell growth under a more constrained buffering system than natural seawater. Due to difficulties encountered in maintaining healthy culture growth in ESAW, the medium was once again modified to use the same nutrient and vitamin concentrations as ESAW (Andersen *et al.*, 2005) but with filtered seawater as a base instead of artificial water. Details of the media used in each experiment are given in Table 4.

The seawater used for media was collected from the Great Yarmouth Sealife Centre seawater inlet, which passed through a sand filter before filling a 20 L polycarbonate carboy. This was kept in the dark at 4 °C for a year prior to the experiments, and was filtered to 0.2 µm through a cellulose acetate filter prior to media preparation to remove any remaining organisms or biological material.

All glassware was autoclaved before any media was prepared. All media which was autoclaved had nutrients and vitamins added aseptically after cooling.

Table 2. Nutrient concentrations in the stock and final ESAW media. Taken from Andersen *et al.* (2005)

Nutrient	Stock Solution ($g\ L^{-1}$)	Volume added (L)	Concentration in final media ($mol\ L^{-1}$)
Nitrate	46.67	0.0017	0.000186
Phosphate	3.094	0.00341	7.62×10^{-6}

2.2. Maintenance and management of *E. huxleyi* RCC1229 cultures

Stock cultures of *E. huxleyi* RCC1229 were grown at 15°C with a light/ dark cycle of 16:8 hours and a light intensity of 178 µmol photon m^{-2} s^{-1}. This stock was reinoculated into fresh medium every 14 days at the end of exponential growth and a period of stationary phase.

Ten days before the start of each experiment, a sub-culture of the stock was treated with a mixture of five antibiotics (Table 3) and was grown on fresh media for 2-3 days before inoculation into further fresh media. DAPI staining was used to evaluate the culture before and after each experiment, and while bacterial levels were found to be very low, the cultures were not considered axenic.

Table 3. Antibiotic treatment concentrations and volumes added to the medium. Taken from Jaeckisch *et al.* (2011).

Antibiotic	Volume (µL per 100 mL medium)	Concentration (mg mL^{-1})	Concentration in final Medium (mg L^{-1})
Ampicillin	333	15	50
Gentamycin	333	1	3.33
Streptomycin	100	25	25
Chloramphenicol	3	34	1.02
Ciprofloxacin	1000	1	10

2.3. Design of *E. huxleyi* RCC1229 CO_2 enriched experiments

CO_2-controlled acidification, and the associated changes to the carbonate chemistry, will be most closely mimicked by the exposure of cultures to CO_2 enriched air, rather than by addition of acid (Gattuso *et al.*, 2010). This method will replicate the carbonate chemistry changes from the SOPRAN Bergen Mesocosm experiment (Chapter 3).

All experiments were grown in modified 1L Erlenmeyer flasks, custom designed with a liquid sampling outlet at the base of the flask closed with a luer-lock fitting, and a Quickfit ground glass gas-tight stopper with glass gas inlet and outlet tubes. Silica tubing was fitted to inlets and outlets and attached to 0.2 µm sterile minisart filters (Figure 1). Each experiment was performed with three flasks for the CO_2 treatment and three for the control, with 650 mL of media.

During the growth phase, the headspace of each flask was flushed daily for 10 minutes with the relevant treatment gas at a rate of 30 mL min^{-1}. Flasks were flushed individually, with the flow rate measured on an Agilent gas flowmeter from the outlet line, and the flushing and sampling was performed in a sterilised safety cabinet in case of flask breakage. Samples of the culture were taken daily through the outlet at the base of the flasks during headspace flushing.

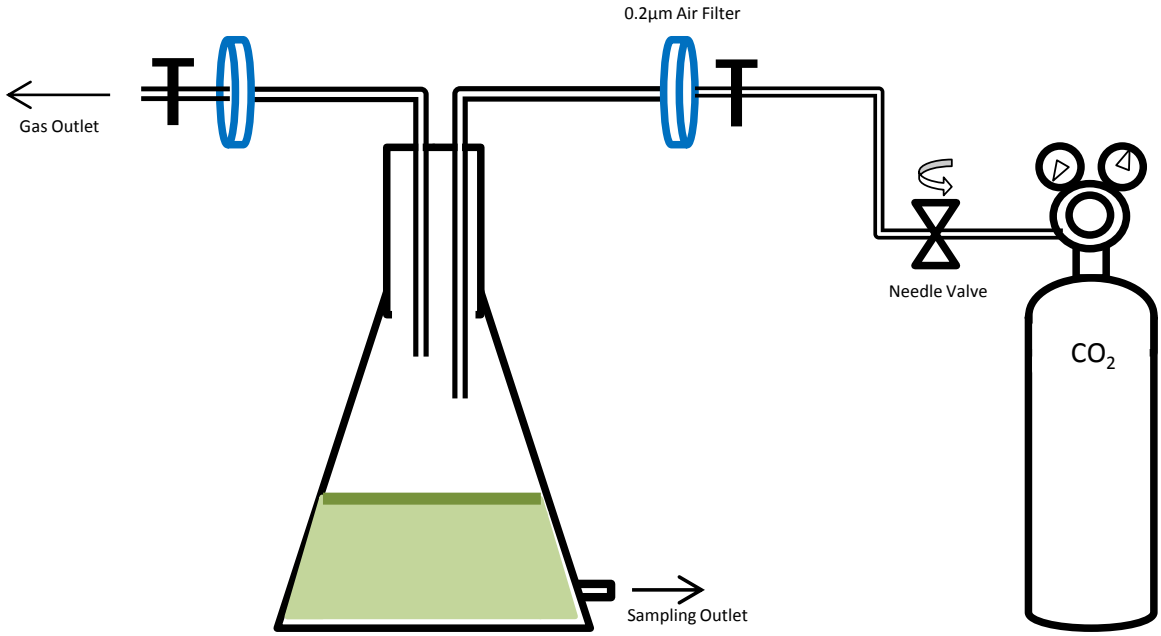

Figure 1. Flask design used throughout the experiments, shown as set up during the headspace flushing process. A second setup was used simultaneously for the air control flasks using compressed air

During each experiment, a sample of the cells was taken from each flask at the end of exponential growth and examined under the light microscope. Very few non-calcified cells were seen.

2.3.1. Design of *E. huxleyi* RCC1229 batch culture experiments

Flasks were autoclaved in advance and prepared with 650 mL of media, before inoculation with the prepared culture stock to make a starting cell count as shown in Table 4. After inoculation, no further alterations were made to the culture, save for gentle swirling to re-suspend cells before each daily sampling.

2.3.2. Design of *E. huxleyi* RCC1229 semi-continuous culture experiments

On analysis of the pH data from the batch experiments (e.g. Section 3.1.1) it was clear that the cultures were only under lowered pH (<8) for the first 2-3 days. To gain a better understanding

of the changes in DMS and DMSP produced from *E. huxleyi* under medium-term exposure to CO_2, the batch experimental setup was used in a semi-continuous culturing mode. Development of a semi-continuous system would allow cells to be continually reintroduced to the elevated pCO_2/ lowered pH media and acclimate to the changed conditions, but would also prevent the cells from undergoing stress from exposure to suddenly altered conditions (so-called shock-treatment). The experimental duration was set to last as long as the SOPRAN Bergen experiment (30 days), and which only showed changes in DMS concentration after Day 16.

The setup was identical to the batch experiments, except that freshly sterilised flasks were reinoculated every 4 days, with the inoculate taken from the previous experimental culture. The preparation method for the medium in these inoculations is given in Section 2.3.3.

2.3.3. Treatment of medium prior to addition of stock culture

The carbonate chemistry within the high pCO_2 treatment media was altered through sparging with a premixed CO_2-enriched air mix in a sterilised custom-designed 3 L sparge vessel prior to the addition of the cell culture. The gas mix was pre-prepared by BOC (Guildford, UK) at a certified concentration of 865 µatm (±5%) and was independently tested at UEA for pCO_2 and measured at 897.4 µatm. This pCO_2 was selected to correspond to that of the IPCC Scenario A2 of 860 µatm, and could be directly comparable to one of the mesocosm pCO_2 from SOPRAN Bergen. Control media were treated with air (BOC), which was independently measured for pCO_2 at a concentration of 395.4 µatm. Both gases were passed through hydrocarbon traps and a sterile minisart filter before contact with the media. Sparging took place for 4 days at a rate of 30 mL min^{-1} for both the control and CO_2 treatment media, and took place during each growth period of the cultures ready for the new inoculations.

During the batch experiments and the first semi-continuous culture, the media were autoclaved to sterilise, but during the second semi-continuous experiment, the media was filter sterilised to avoid changes to the carbonate chemistry through the autoclaving process.

Table 4. Summary of the CO_2 enrichment experiments performed with *E. huxleyi* RCC1229. (*) No data were obtained for DMSP samples due to equipment failure

Experiment Number	Media Type	Media preparation	Duration (Days)	Starting cell density (cells mL^{-1})	Measurements from each flask
Batch Experiments					
B1	K/5	• Medium autoclaved • Pre-bubbling with air-stones within the flasks	9	60,000	• 1x pH • 3x cell count • 1x DMS (Cryotrap GC-FPD)*
B2	ESAW	• Medium autoclaved • Sparging in two non-identical volume sparge towers but with identical frit size	10	40,000	• 1x pH • 3x cell count • 1x DMS (Cryotrap GC-FPD) • 1x DMSP ($_T$ and $_P$) (Headspace GC-FPD) • 1x Halocarbon (GC-MS)
B3	ESNW	• Medium autoclaved • Sparging in two identical sparge towers.	10	40,000	• 1x pH • 3x cell count • 1x DMS (Cryotrap GC-FPD) • 1x DMSP ($_T$ and $_P$)
Semi-Continuous Experiments					
S1	ESNW	• Medium autoclaved • Sparging in two identical sparge towers.	26	300,000	• 1x pH • 3x cell count • 1x DMS (Cryotrap GC-FPD) • 1x DMSP ($_T$ and $_P$) (Headspace GC-FPD)
S2	ESNW	• Medium filter sterilised • Sparging in two identical sparge towers.	23	120,000	• 1x pH • 3x total alkalinity • 3x cell count • 1x DMS (Cryotrap GC-FPD) • 3 x $DMSP_T$ (Headspace GC-FPD) • 1x $DMSP_P$ (Headspace GC-FPD)

BLANK

2.4. Determination of pH and total alkalinity in the medium during the *E. huxleyi* RCC1229 culture experiments

2.4.1. Determination of pH in culture medium

The majority of pH measurements during the growth experiments required analysis of the change in pH with addition of CO_2. A potentiometric probe (Mettler Toledo Seven Easy S20) was used for all measurements, and buffers were made up using NBS calibration buffer standards. The use of these buffers was not ideal for accurate measurements of pH in seawater media due to differences in salinity, however during these experiments only the relative change in pH with the addition of CO_2 was assessed.

Buffer solutions were made fresh weekly in 100 mL Milli-Q water in volumetric flasks. The pH probe was calibrated on a three point scale of 4.00, 7.00 and 10.01 on a daily basis before any samples were analysed. Buffers were stored at 15°C. Samples of the cultures were collected in a 20 mL cuvette and immediately analysed on the pH probe to prevent significant changes in temperature from the 15°C growth conditions. Due to time constraints, only one sample was analysed for pH from each culture flask. No probe was inserted into the culture vessels to prevent introduction of bacteria to the culture.

2.4.2. Determination of total alkalinity in culture medium

Total alkalinity (TA) was measured by the Gran method during the initial laboratory experiments, but several problems were encountered during the analyses, and no data were obtained. During the semi-continuous experiments, a spectrophotometric approach to total alkalinity measurements was adopted, based on the methods of Sarazin *et al.* (1999). This method will be outlined here.

2.4.3. Preparation of calibration standards for TA analysis

Three solutions were prepared and stored in the dark at ambient temperatures prior to any analysis: an artificial seawater, a colourimetric solution and a hydrogen carbonate stock solution. The artificial seawater was prepared using the following salts in 1 L of Milli-Q water:

- 28.411 g NaCl
- 3.5241 g $MgSO_4$
- 5.1801 g $MgCl_2$

- 1.5789 g $CaCl_2$
- 0.7887 g KCl

The hydrogen carbonate working standard stock was prepared by dilution of a 0.1 mol L^{-1} HCO_3 solution (Sigma Aldrich) to a concentration of 10 mmol L^{-1}. The colourimetric reagent was prepared in a 250 mL volumetric flask to the following formula:

- 25 mL 0.1 mol L^{-1} formic acid
- 25 mL bromophenol blue reagent
- 200 mL 0.7 mol L^{-1} NaCl

2.4.4. Calibration of the spectrophotometer for TA analysis

A standard curve for colourimetric determination was prepared in 10 mL aliquots, using differing volumes of the artificial seawater and HCO_3^- stock solution to prepare a standard curve from 0.3 – 6 mmol L^{-1} HCO_3^-. Two mL of the standards were sub-sampled into a 4 mL glass cuvette, with the addition of 2 mL of the colourimetric solution. The standards were measured on a spectrophotometer measuring the absorbance at 590 nm, and the resulting calibration curve was a second order polynomial equation. Tests on the method showed that the temperature of the solution did not have an effect on the calibrations, and all samples were measured at ambient temperatures.

2.4.5. Analysis of TA samples by spectrophotometry

Samples for TA were analysed immediately, and a new calibration was prepared daily. Each sample was analysed in the same cuvette as the standard curve, with 2 mL of the sample added to 2 mL of the colourimetric solution.

2.5. *E. huxleyi* RCC1229 culture maintenance and growth evaluation techniques

This section describes the sample preparation and operation of the Coulter Multisizer and the Turner Fluorometer for evaluating the exponential growth of the culture. The Multisizer was used to quantify the growth during the CO_2 enrichment experiments, and the fluorometer as a quick and simple method to determine growth and photosynthetic health within the stock culture (Tunzi *et al.,* 1974).

2.5.1. Operation of the Coulter Multisizer

Both the cell count and total cell volume were measured by use of a Coulter Multisizer (Beckman Coulter Ltd, UK). The multisizer works by inserting an aperture into the sample, separating two electrodes. The voltage applied between the two electrodes creates a 'sensing zone', and particles pass through the aperture and displace electrolyte, creating a signal proportional to the volume of the particle. The signals were analysed by the Coulter Software and gave distributions of cell number, volume, diameter and calculated individual cell volumes.

Individual samples of culture for analysis were prepared in 20 mL cuvettes, with 0.5 mL of culture diluted with 20 mL of sterile media. Samples were blank-corrected by the analysis of a 20 mL sample of the media with no culture addition prior to any of the samples being run. All cuvettes were capped and inverted before positioning in the Coulter counter to ensure suspension of all cells.

The Coulter Counter was used to determine the total volume of cells within the sample, as well as the total number of cells. Determination of individual cell volume was as an average calculated from these two values.

2.5.2. Operation of the Turner AU-10 Fluorometer

Growth of the cultures was monitored regularly by the measurement of in-vivo fluorescence in a Turner AU-10 fluorometer, both in the experimental cultures and the stock culture. This method was fast but provided no details on the number of cells within a culture and required the confirmation of the Coulter Multisizer. Fluorometry of a culture is related directly with Chlorophyll-*a* concentration, and hence cell number (Tunzi *et al.*, 1974). It is noted that this method does not take into account the variation in chlorophyll-*a* between species under different growth conditions (Slovacek and Hannann, 1977), but this investigation was focussed on a single strain of *E. huxleyi* under near-identical growth conditions, and the technique was used as a relative reference of the growth of the stock against existing values.

2.6. Determination of DMS, DMSP and halocarbons from the *E. huxleyi* RCC1229 CO_2 enrichment experiments

2.6.1. Determination of DMS and halocarbon concentrations by GC-MS

DMS analysis during experiment B1 was performed on GC-MS, using the purge and cryotrap technique (Chapter 2, Section 2.1) and standards developed in the concentration range 0.1 - 500 0.8 – 80 nmol L^{-1}. Culture samples were analysed for halocarbons during experiment B2. Non-CO_2-treated batch cultures of *E. huxleyi* RCC1229 prior to these experiments had shown extremely low halocarbon production; the cultures were analysed for halocarbons during B2 to determine if further analysis would be worthwhile in later experiments. The halocarbon analysis technique was by purge and cryotrap into GC-MS and using fresh prepared standards to the concentration range given in Table 5.

Table 5. Calibration concentration ranges for the halocarbons measured during Experiment B2 in pmol L^{-1}.

Compound	Concentration Range (pmol L^{-1})
CH_3I	1.1 – 45
CH_2I_2	7.0 - 280
C_2H_5I	0.05 – 2.0
CH_2ClI	0.2 – 80
$CHBr_3$	0.8 - 820
CH_2Br_2	0.02 - 21
$CHBr_2Cl$	0.04 – 40

2.6.2. Determination of DMS concentrations by purge-and-cryotrap GC-FPD

All DMS analysis after this experiment used the GC-FPD equipped with purge and cryotrap (Chapter 2, Section 2.2). This method was considerably quicker than analysing the samples on the GC-MS, and required 2 mL of sample compared to the 40 mL required for accurate analysis using the GC-MS. This was essential in conserving culture volume. Media samples (approximately 5ml) were drawn up in a 10 mL glass syringe, and prepared prior to purge and cryotrap by slow filtering through a Whatman GF/F (0.7 µm pore size) into a second 10 mL glass syringe. The volume in the second syringe was then reduced to the 2 mL analysis volume.

This method removed any cells from the sample, and prevented the loss of sample by direct injection of 2 mL sample through a GF/F.

During experiment B2, the vortexing technique suggested by del Valle *et al.* (2011) was tested as a quick and convenient method of analysing DMS using the headspace GC-FPD alongside the DMSP samples (Chapter 2, Section 2.3). The procedure required a 2 mL sample of culture to be vortexed for 1-3 minutes to speed up the equilibration of DMS with the headspace, followed by immediate analysis on GC-FPD.

On analysis of the samples, this technique was found to have extremely low sensitivity. The first day that DMS was detected by this method was on T7, when DMS measured on the purge-and-cryotrap was higher than 500 nmol L^{-1}. This technique was therefore abandoned and the DMS samples analysed on purge and cryotrap in future experiments.

2.6.3. Determination of DMSP concentrations by headspace GC-FPD

All analyses for DMSP (total and particulate) were analysed via headspace sampling and GC-FPD (Chapter 2, Section 2.3). All experiments had one sample per culture flask for $DMSP_T$ and one for $DMSP_P$, except for Experiment S2 where the $DMSP_T$ samples were taken in triplicate. These samples underwent overnight cold alkaline hydrolysis: 3 mL of sample was added to 0.5 mL of 1M NaOH in a 4 mL glass vial sealed with PTFE screw caps and silicone septa. Vials were stored in the dark at 30 °C for a minimum of 12 hours, prior to analysis by headspace GC-FPD.

2.7. Statistics

Statistical analysis was carried out on Minitab V16 software. All data was tested for normality using an Anderson-Darling Test, and if necessary, the data was transformed logarithmically and retested to ensure normality. Two-tailed T-tests were performed on all experimental data as a comparison between the two treatments undertaken. No further statistics were required in these experiments. All statistical significant was calculated at 99%, unless specifically stated as 95%.

3. Results from *E. huxleyi* RCC1229 CO2-enriched batch culture experiments (B1, B2 and B3)

Data for the batch experiments are presented as individual experiments, split into details about the pH, *E. huxleyi* growth and trace gas data. The values for these parameters are summarised in Table 7 at the end of this section. Three batch culture experiments were undertaken, and are labelled B1, B2 and B3. Experiment B1 used K/5 medium, B2 in ESAW medium and B3 in ESNW medium (Section 2.1), and all three used the same pCO_2 values of 390 µatm for the control and 890 µatm for the CO_2 treatment. Summaries of all DMS and DMSP data are given in Table 10 and Table 11 (Page 217).

3.1. *E. huxleyi* RCC1229 batch culture 1 (Experiment B1)

3.1.1. Changes in pH during Experiment B1

pH started low in both treatments, then increased in all flasks throughout the experiment (Figure 2). pH values are given later in summary Table 7: mean pH in the CO_2 treatment (890 µatm) stayed continuously below the control (390 µatm) with the exception of the final day.

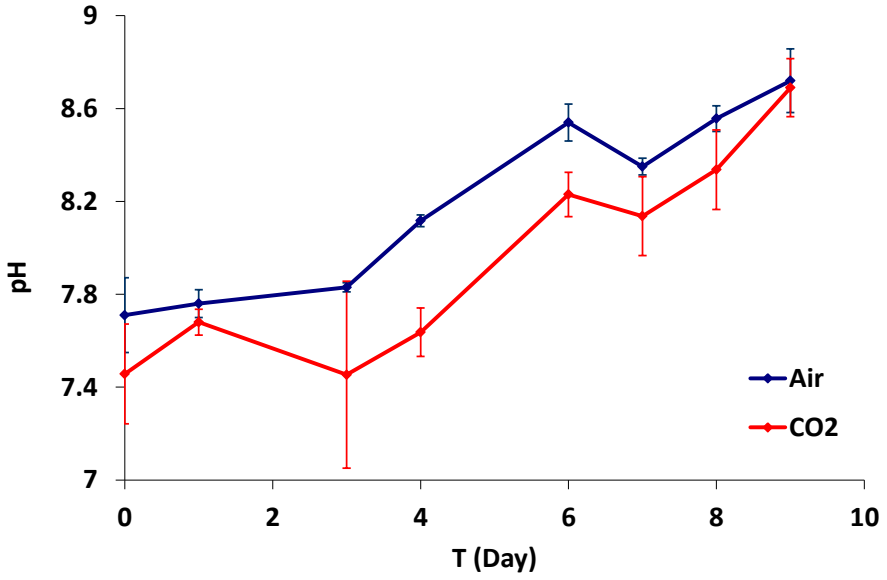

Figure 2. pH changes during Experiment B1. Red lines show the high CO_2 treatment and blue lines the air control, with error bars showing standard deviation of three flasks.

3.1.2. Changes in cell growth during Experiment B1

Growth curves for the two treatments were established from the daily measurements of cell count and cell volume established on the Coulter Multisizer (Figure 3). The culture showed immediate growth, and the exponential phase was determined to have lasted until T4, when all cultures entered stationary phase.

The cell counts in the treatment flasks were lower than those in the control throughout up to T9 when the experiment was halted due to the culture having been in stationary phase for 5 days. The mean specific growth rates were calculated as 0.48 in the CO_2 treatment (890 µatm) and 0.54 in the air control (Table 7). Elevated pCO_2 had no significant effect on the cell count or the growth rates between the two treatments for the whole experiment or for the exponential phase (T and p-values are shown in Table 6).

Table 6. T-values, P values and degrees of freedom for the t-tests performed on the multisizer cell counts.

Time period	Parameter	T-value	p-value	Degrees of Freedom
Whole Experiment	Cell count	0.72	0.477	42
T 0-4	Cell count	0.63	0.536	15
T 0-4	Growth rate	0.96	0.353	15

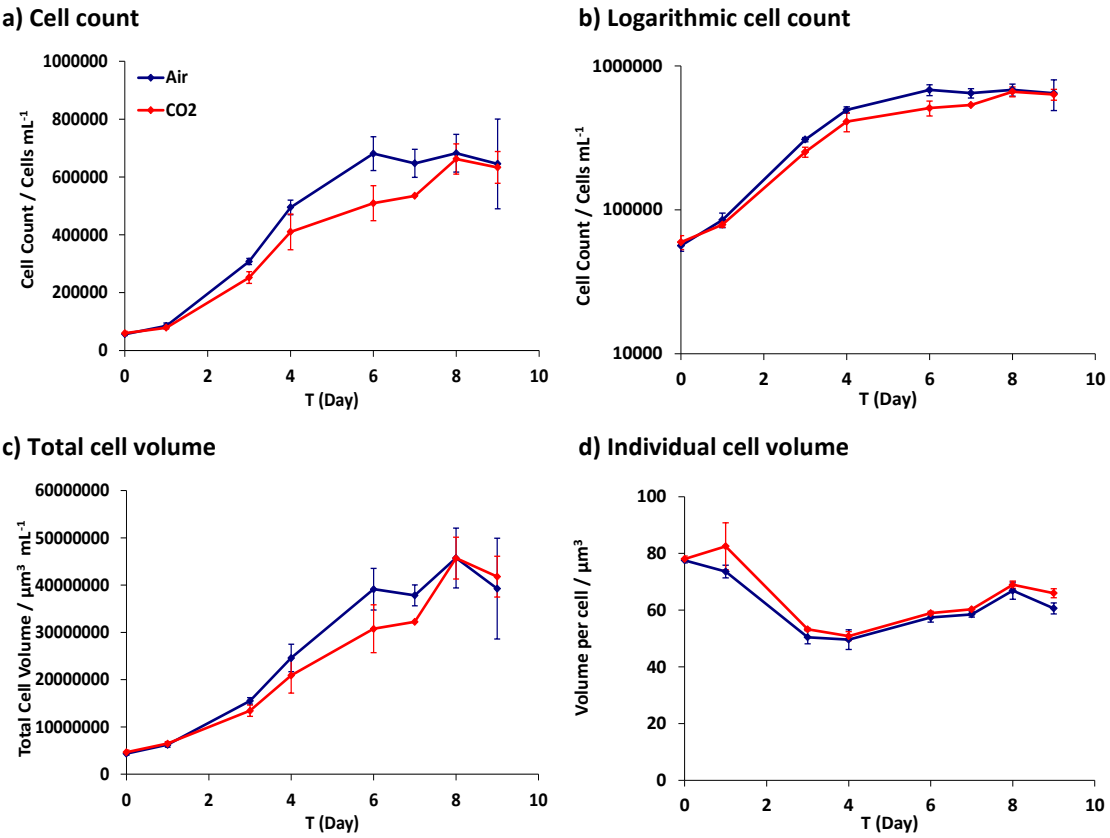

Figure 3. Growth dynamics of the air and CO_2 cultures during Experiment B1, showing the mean and standard deviation a) cell counts (cells mL^{-1}), b) cell counts on a logarithmic scale (cells mL^{-1}), c) total cell volume (μm^3 mL^{-1}) and d) volume per cell (μm^3). Red lines indicate the high CO_2 treatment and the blue the air control, with bars showing the standard deviation of three flasks.

The total volume of all cells in the culture (total cell volume) predictably increased along with cell numbers (Table 7 and Figure 3c), but the data was used to calculate the individual cell volume (Table 7 and Figure 3d). This was higher immediately after inoculation than at the end of exponential phase in both treatments, and CO_2 had no significant effect on the individual cell volume (T=-1.05, p=0.301) during either the exponential growth or stationary phases.

3.1.3. Changes in DMS during Experiment B1

The daily DMS concentrations (Figure 4a and Table 10) follow the trends of the cell growth data, increasing from T0 immediately after inoculation and increasing until T9.

No significant difference in DMS concentration was identified between the CO_2 treatment and control during exponential phase (T1-4; T=0.8, p=0.432), but during stationary phase (T6- 9 inclusive), DMS concentrations in the treatment flasks were lower on all days except T7. On analysis, the difference between treatments was not significant (T=1.93, p=0.064).

DMS calculated per cell (Figure 4b) followed similar trends to the measured DMS concentrations, with concentrations in the range 0.064 – 0.374 fmol cell^{-1} (Table 11). CO_2 (890 µatm) had no significant effect on DMS production per cell during exponential growth (T=1.21, p=0.24) but during stationary phase, DMS per cell was significantly lower in the CO_2 treatment (890 µatm) flasks (T=2.47, p<0.01).

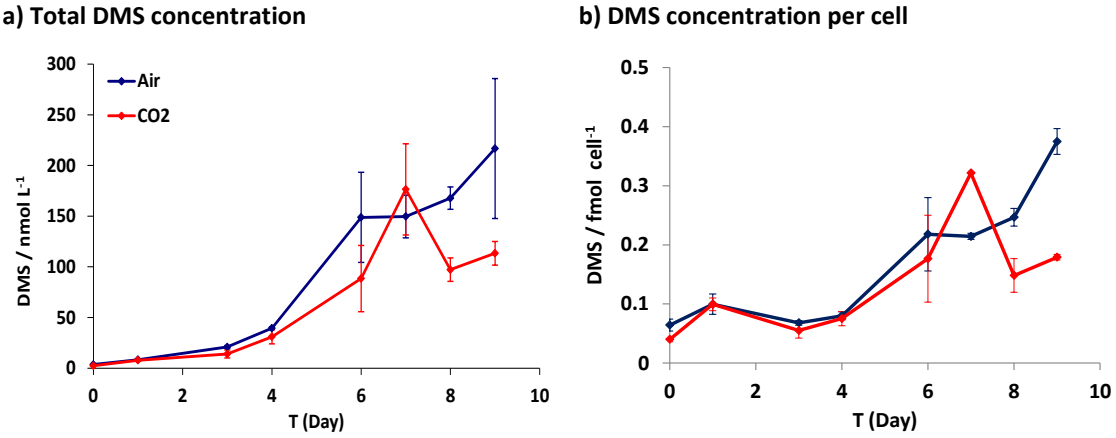

Figure 4. DMS concentrations (nmol L^{-1}) and calculated DMS produced per cell (fmol cell^{-1}) for Experiment B1. Red lines indicate the results from the CO_2 treatment and blue lines the air control, with error bars showing standard deviation of three flasks.

3.2. *E. huxleyi* RCC1229 batch culture 2 (Experiment B2)

The daily mean pH of the three flasks for each treatment is shown in Figure 5 with the standard deviation as error bars and the pH range in Table 7. The CO_2 treatment (890 µatm) pH was significantly lower than the control (390 µatm) from T0 until T4 (T=5.07, p<0.01) but during stationary phase, no significant difference was identified between the treatments (Day 4-10; T=0.71, p=0.481).

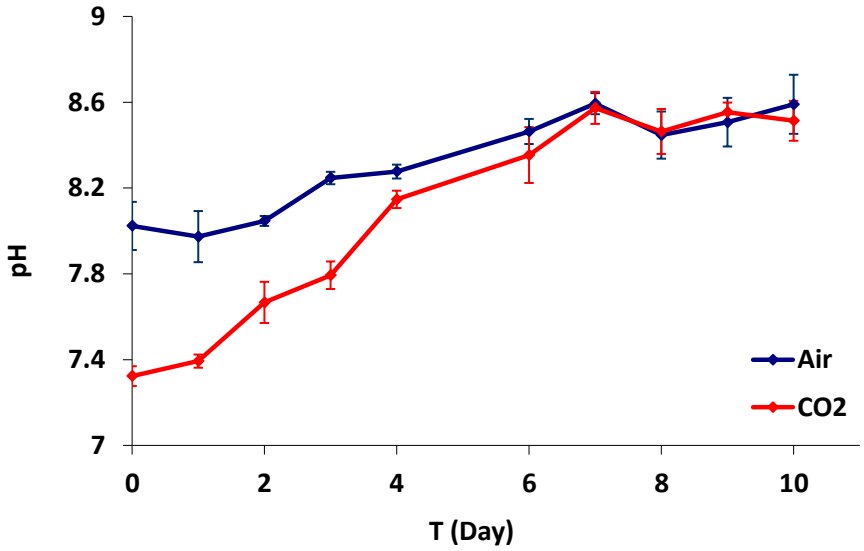

Figure 5. pH changes during Experiment B2. Red lines show the high CO_2 treatment and blue lines the air control, with error bars showing standard deviation of three flasks.

3.2.1. Changes in cell growth during Experiment B2

Figure 6 presents the growth curves and cell volume data for Experiment B2, and the data is summarised in Table 7. The culture showed immediate growth, and exponential phase was determined to last from T0 until T4. Counter to Experiment B1, growth was higher in the CO_2 treatment (890 µatm) than the control (390 µatm) flasks for the entire experiment. The experiment was halted on Day 10. The mean specific growth rates were calculated as 0.71 in the CO_2 treatment and 0.64 in the control (Table 7). There was no significant difference in the growth rates (T=-0.58, p=0.563, DF=50) between the treatments in either exponential phase or stationary phase. However there were significantly higher cell counts in the CO_2 treatment during T4-10 (T=-3.67, p<0.01, DF=24), implying that the CO_2 treatment flasks continued to grow after the air culture had slowed.

Total cell volumes (Figure 6c) were obtained from the Coulter Multisizer and were used to calculate individual cell volumes (Figure 6d and Table 7). Total cell volume showed no

significant difference between treatments. The peak mean cell volumes were measured at 43.1 µm^3 in the air control on T1 and 45.2 µm^3 in the CO_2 treatment on T2 before decreasing during stationary phase to a mean of 19.4 µm^3 (air) and 18.9 µm^3 (CO_2). CO_2 had no significant effect on the individual cell volumes (T=-0.37, p=0.711, DF=56).

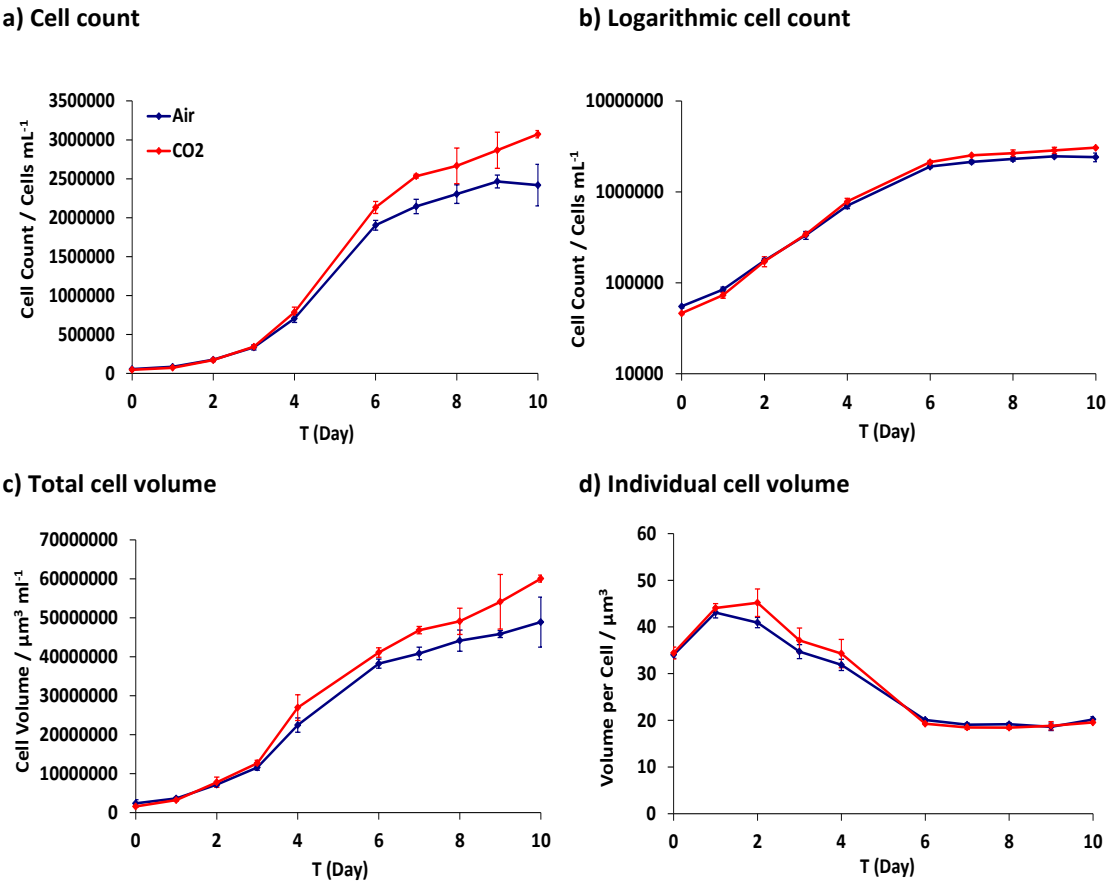

Figure 6. Growth dynamics of the air and CO_2 cultures during Experiment B2, showing the mean and standard deviation a) cell counts (cells mL^{-1}), b) cell counts on a logarithmic scale (cells mL^{-1}), c) total cell volume (µm^3 mL^{-1}) and d) volume per cell (µm^3). Red lines indicate the high CO_2 treatment and blue the air control, with error bars showing the standard deviation of three flasks.

3.2.2. Changes in DMS during Experiment B2

All DMS measurements in this and the following experiments were made on the GC-FPD. The total DMS concentrations (Figure 7a and Table 10) follow the trends of the growth curve, increasing from T0 until T9 to a maximum of 490.2 nmol L^{-1} in the CO_2 treatment (890 µatm). In the stationary phase after T6, DMS showed higher concentrations in the CO_2 treatment flasks than the control (390 µatm), but a T-test showed this difference was not significant (T=-1.25, p=0.221, DF=25).

The range of DMS per cell is presented in. DMS per cell (Figure 7 and Table 11) ranged from 0.04-0.214 fmol cell^{-1}, with CO_2 (890 µatm) showing no significant difference from the control (390 µatm; T=0.42, p=0.676, DF=51). DMS concentrations per cell increased during exponential growth and early stationary phase, before reaching a peak on T8 and remaining higher than the beginning of the experiment afterwards.

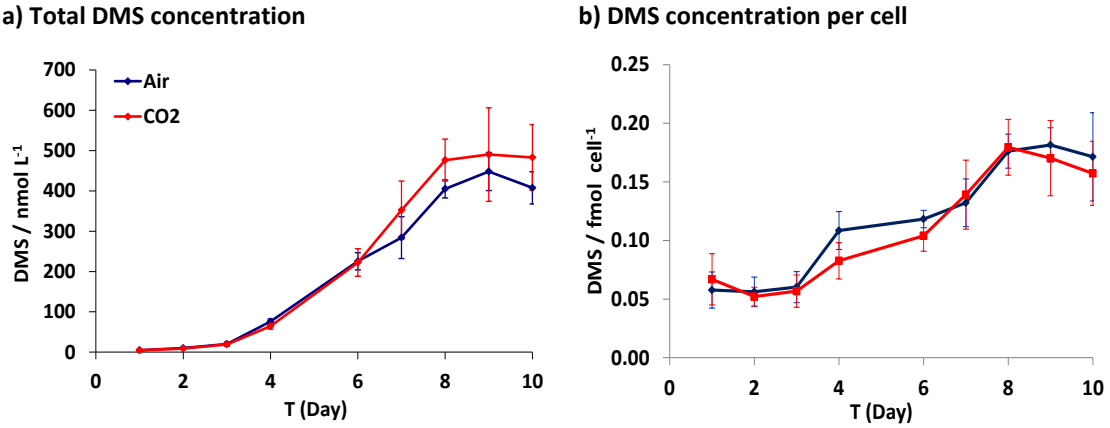

Figure 7. DMS concentrations (nmol L^{-1}), and calculated DMS produced per cell (fmol cell^{-1}) for Experiment B2. Red lines indicate the results from the CO_2 treatment and blue lines the air control, with error bars showing standard deviation of three flasks.

3.2.3. Changes in total DMSP during Experiment B2

Growth of the total DMSP increased in accordance with the changes in cell numbers as the culture progressed through exponential growth and into stationary phase (Figure 8a and Table 10). Total DMSP concentrations show significantly higher concentrations in the CO_2 treatments during stationary phase (T6-T10; T=-4.37, p<0.01, DF=27), but no difference during exponential phase.

$DMSP_T$ per cell (Figure 8b and Table 11) started high in exponential growth then decreased in stationary phase, in contrast to DMS per cell which stayed low for the first three days and then increased. CO_2 treatment had no significant effect on $DMSP_T$ calculated per cell (T=-0.80, p=0.469, DF=40).

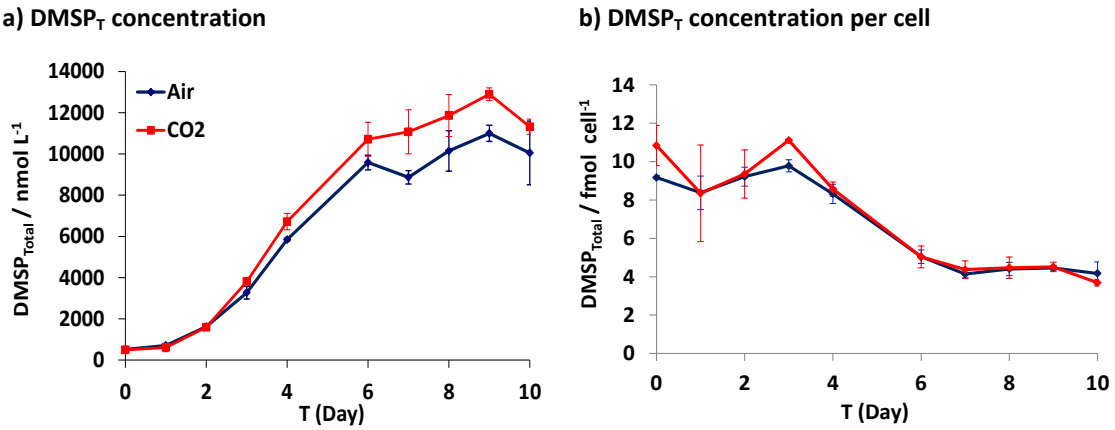

Figure 8. Total DMSP concentrations (nmol L^{-1}), and calculated total DMSP per cell (fmol $cell^{-1}$) for Experiment B2. Red lines indicate the results from the CO_2 treatment and blue lines the air control, with error bars showing standard deviation of three flasks.

3.2.4. Changes in particulate DMSP during Experiment B2

DMSP particulate showed very similar trends to those of the $DMSP_T$, starting low and increasing through exponential growth (Table 10 and Figure 9a). Measured $DMSP_P$ concentrations were higher in the CO_2 treatment flasks (890 µatm) after T3 and remained higher for the duration of the experiment; CO_2 had a significantly positive effect on $DMSP_P$ in the post-exponential days ($T=-3.9$, $p<0.01$, $DF=12$).

CO_2 had no significant difference on $DMSP_P$ concentration per cell (Table 11, Figure 9b, $T=-0.78$, $p=0.443$, $DF=40$). The changes across the duration of the experiment were similar as those for $DMSP_T$: higher during exponential phase and dropping off during stationary phase.

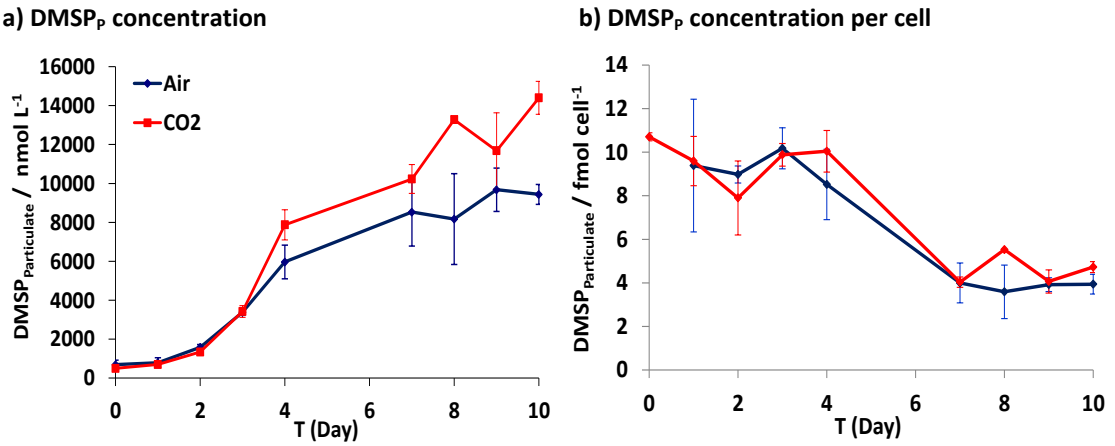

Figure 9. a) Particulate DMSP concentrations (nmol L^{-1}), and b) calculated particulate DMSP per cell (fmol $cell^{-1}$) during Experiment B2. Red lines indicate the results from the CO_2 treatment and blue lines the air control, with error bars showing standard deviation of three flasks.

3.2.5. Changes in dissolved DMSP during Experiment B2

Dissolved DMSP concentrations were calculated from the total and particulate DMSP measurements, and the results are shown in Figure 10 and Table 10. Several of the calculated values for $DMSP_D$ were negative, showing a mismatch between the $DMSP_T$ and $DMSP_P$ data, likely due to the filtering system for $DMSP_P$ samples. Previous experiments have also found it difficult to mesh the values for DMSP total, particulate and dissolved (Hopkins, pers comm; Caruana, pers comm).

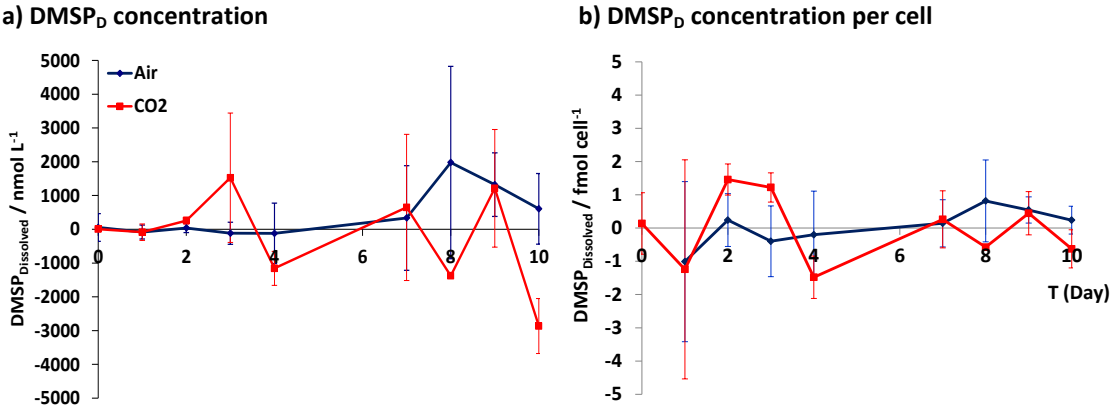

Figure 10. Calculated total dissolved DMSP concentrations (nmol L^{-1}), and calculated dissolved DMSP per cell (fmol $cell^{-1}$) during Experiment B2. Red lines indicate the results from the CO_2 treatment and blue lines the air control, with error bars showing standard deviation of three flasks.

3.2.6. Changes in halocarbon concentrations during Experiment B2

Halocarbons were measured on T0 and T7 of Experiment B2 to establish if any were produced during exponential growth. Batch cultures testing the growth rates of *E. huxleyi* RCC1229 (data not shown) showed halocarbon production to be negligible. The results from Experiment B2 showed a reduction in all halocarbon concentrations in the two treatment means between T0 and T7, with the exception of CH_2ClI. In this case, the mean concentrations on T7 were still within the standard deviation of T0 concentrations. No significant difference was identified between the concentrations of CH_2ClI on the two time points (Figure 11d).

All of the halocarbons were at low concentrations in the initial Day 0 samples. CH_3I and C_2H_5I were at concentrations similar to those found during the SOPRAN Bergen mesocosm experiment, whereas CH_2I_2 and CH_2ClI were 20 and 100 times lower than coastal concentrations respectively (Figure 11b and c). CH_2I_2 was below detection limits for the calibration of the GC-MS.

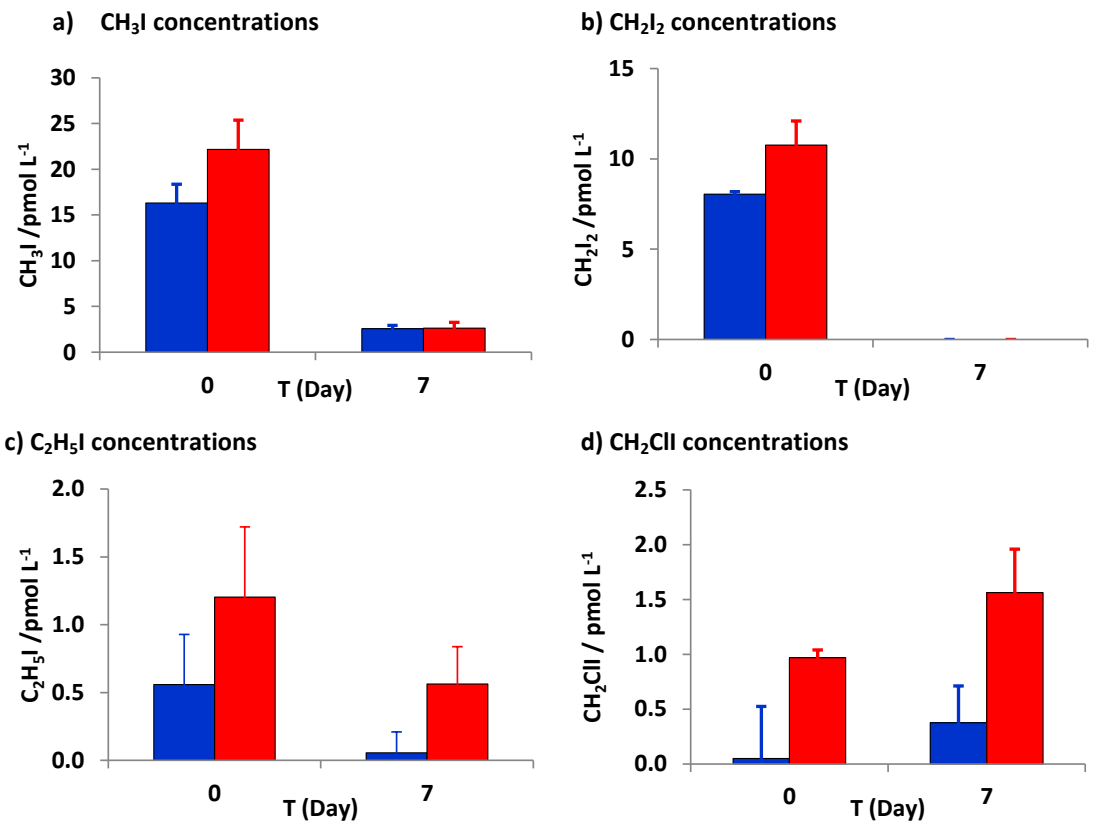

Figure 11. Iodocarbon concentrations (pmol L^{-1}) measured on T0 and T7 before and after exponential growth of Experiment B2, showing a) CH_3I, b) CH_2I_2, c) C_2H_5I and d) CH_2ClI. Red bars are the CO_2 treatment and blue the air control, with error bars showing the standard deviation of the three flasks of three flasks.

Bromocarbon concentrations within the first sampling day were within the concentrations for a coastal environment (SOPRAN Bergen), with the exception of CH_2Br_2 which was approximately 10 times lower (Figure 12b). Both this and $CHBr_3$ were significantly lower in both treatments after exponential growth, indicating loss through off-gassing. $CHBr_2Cl$ also showed no significant difference in concentration between the two time points (Figure 12c).

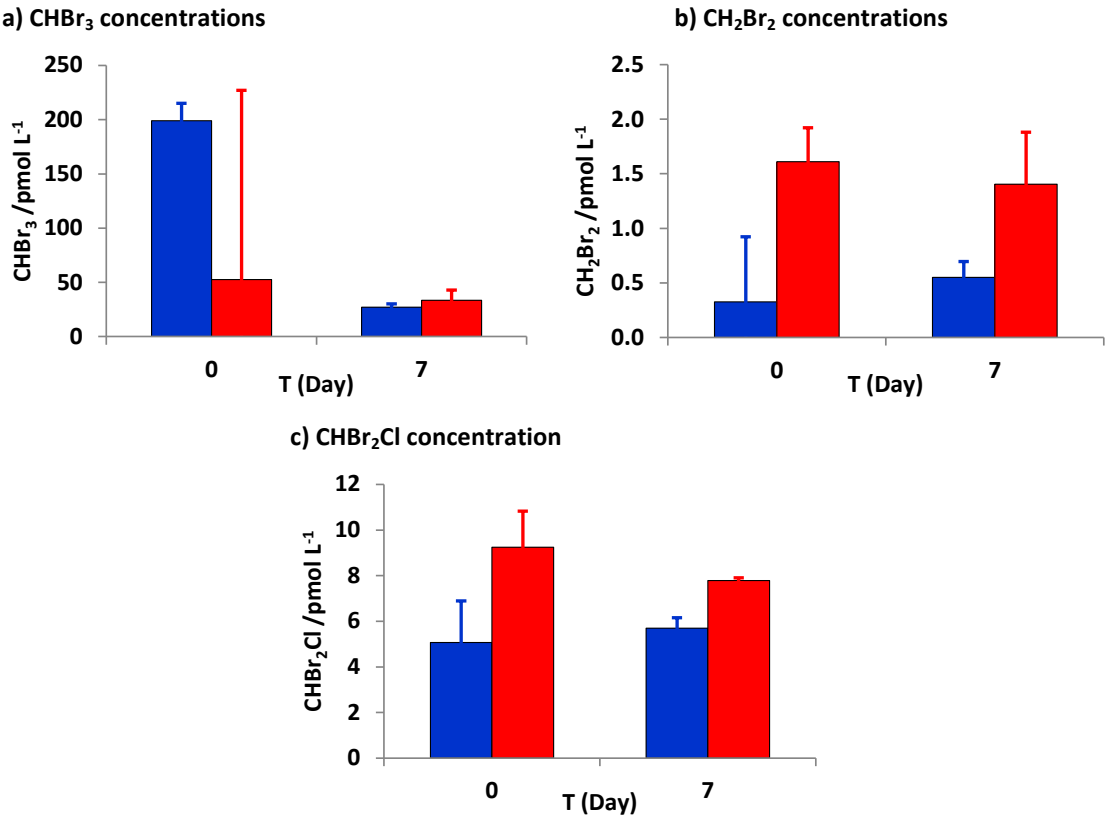

Figure 12. Bromocarbon concentrations (pmol L^{-1}) measured on T0 and T7 before and after exponential growth of Experiment B2, showing a) $CHBr_3$, b) CH_2Br_2, and c) $CHBr_2Cl$. Red bars are the CO_2 treatment and blue the air control, with error bars showing the standard deviation of the three flasks of three flasks.

3.3. *E. huxleyi* RCC1229 batch culture 3 (Experiment B3)

3.3.1. Changes in pH during Experiment B3

The pH followed a similar trend to the previous two batch experiments, steadily increasing in both treatments until Day 8 (Table 7, Figure 13). T-tests on the data show there was significant differences between the pH for the high CO_2 (890 µatm) and control (390 µatm) only during T0-T4 ($T=4.62$, $p<0.01$, $DF=26$), and during stationary phase the two cultures show little influence of increased CO_2 ($T=1.33$, $p=0.196$, $DF=21$).

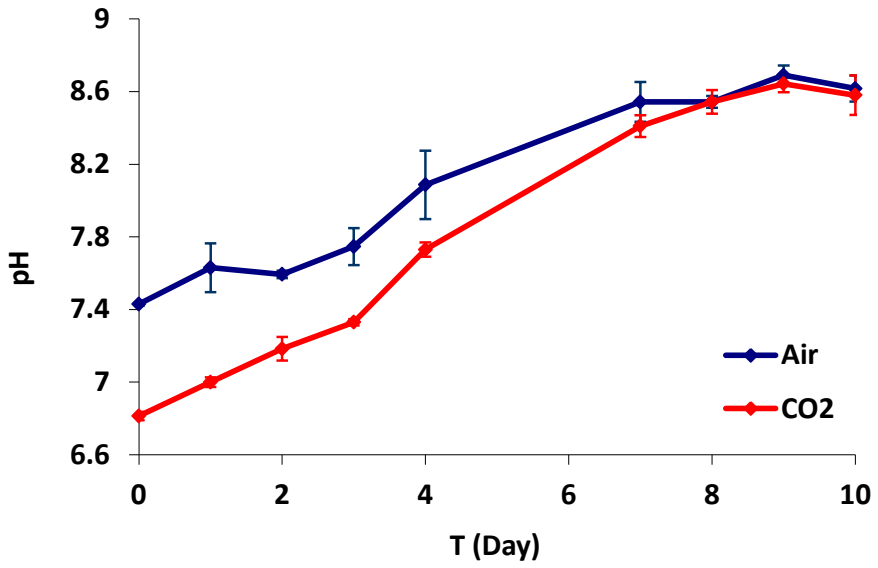

Figure 13. pH changes during Experiment B3. Red lines show the high CO_2 treatment and blue lines the air control, with error bars showing standard deviation of three flasks.

3.3.2. Changes in cell growth during Experiment B3

The growth curves from Experiment B3 are shown in Figure 14, with a summary of cell counts, volumes and growth rates in Table 7. Exponential phase lasted T0 until T3. As with Experiment B2, the cell counts in the control flasks were lower than those in the CO_2 treatment (890 µatm) for the entire experiment and the experiment was halted on Day 10. The mean specific growth rates were calculated at 0.72 in the CO_2 treatment and 0.79 in the control (390 µatm; Table 7). CO_2 had no significant effect on growth rates in either exponential phase or stationary phase (T=0.28, p=0.777, DF=51).

Total (Figure 14c) were used to calculate individual cell volumes (Figure 14d and Table 7). The peak individual cell volumes on T1 were measured as 66.74 μm^3 in the air control and 63.41 μm^3 in the CO_2 treatment; individual cell volumes from both treatments decreased and stabilised during stationary phase, to a mean of 24.73 μm^3 (air) and 24.22 μm^3 (CO_2) for T7-T0. There was no significant difference between calculated cell volumes (T=-0.03, p=0.975, DF=50).

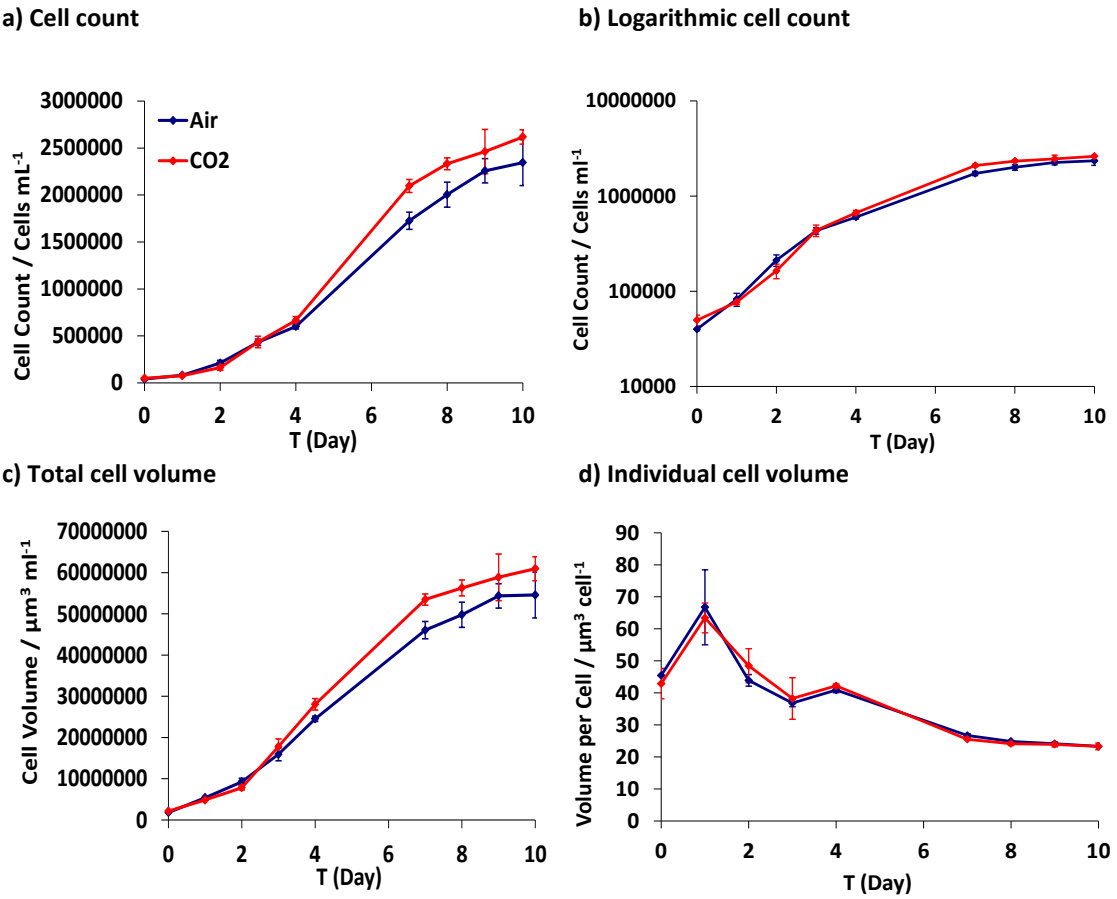

Figure 14. Growth dynamics of the air and CO_2 cultures during Experiment B3, showing the mean and standard deviation a) cell counts (cells mL^{-1}), b) cell counts on a logarithmic scale (cells mL^{-1}), c) total cell volume (μm^3 mL^{-1}) and d) volume per cell (μm^3). Red lines indicate the high CO_2 treatment and blue the air control, with error bars showing the standard deviation of three flasks.

3.3.3. Changes in DMS during Experiment B3

DMS concentrations in Experiment B3 showed marked differences to Experiments B1 and B2 (Figure 15 and Table 10). Unlike previous experiments, DMS concentrations do not closely follow the trend of the cell count data, increasing slowly to T7 then increasing sharply on T9. CO_2 (890 µatm) had no effect on total DMS concentration (T=-0.98, p=0.334, DF=40) or DMS per cell (Table 11; T=-0.66, P=0.515, DF=42).

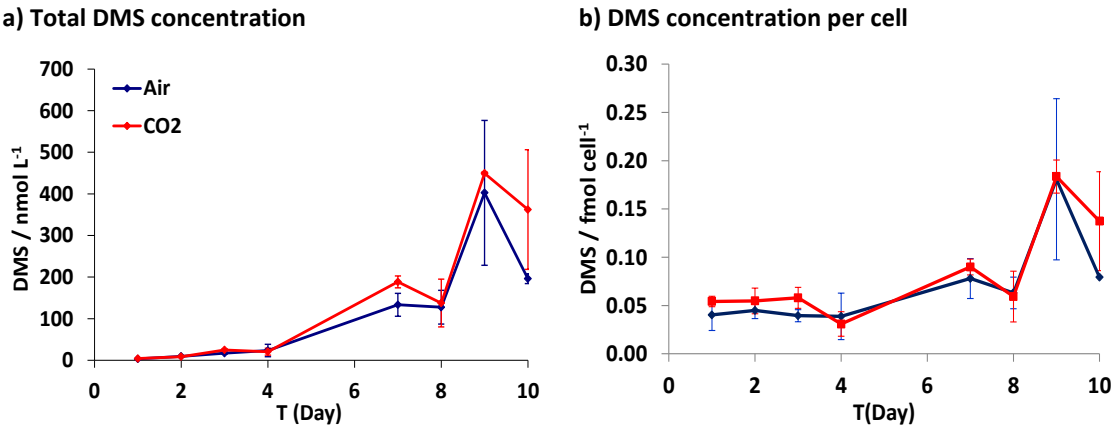

Figure 15. DMS concentrations (nmol L^{-1}), and calculated DMS produced per cell (fmol $cell^{-1}$) for Experiment B3. Red lines indicate the results from the CO_2 treatment and blue lines the air control, with error bars showing standard deviation of three flasks.

3.3.4. Changes in total DMSP during Experiment B3

Unlike DMS concentrations, $DMSP_T$ increased with increasing cell numbers (Figure 16). $DMSP_T$ concentrations were significantly higher in the CO_2 treatment (890 µatm) in the stationary phase (T=-3.97, p<0.01, DF=18), but not during exponential phase. In contrast to DMS per cell, $DMSP_T$ per cell started higher in exponential growth then decreased during stationary phase. There were no differences between the $DMSP_T$ calculated per cell in the two treatments (T=-1.04, p=0.305, DF=41).

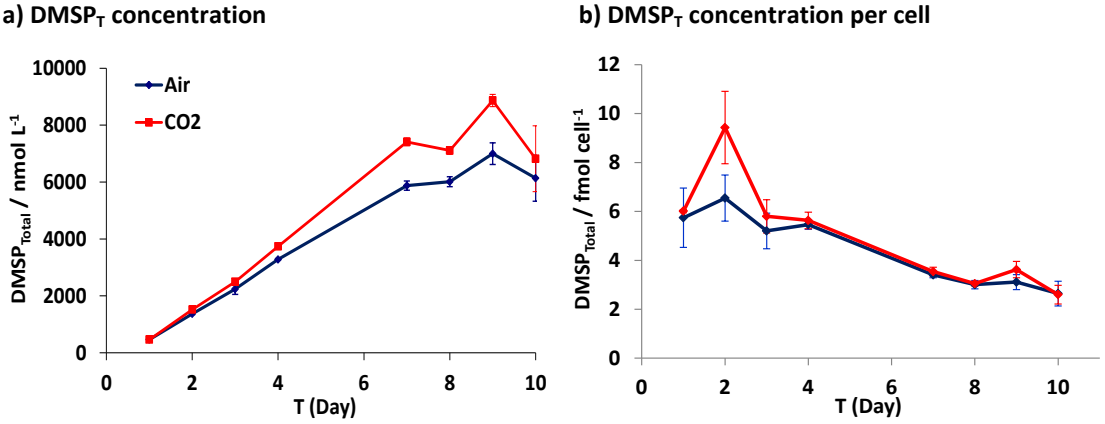

Figure 16. Total DMSP concentrations (nmol L^{-1}), and calculated total DMSP per cell (fmol $cell^{-1}$) for Experiment B2. Red lines indicate the results from the CO_2 treatment and blue lines the air control, with error bars showing standard deviation of three flasks.

3.3.5. Changes in particulate DMSP during Experiment B3

Similar to the previous experiment, measured $DMSP_P$ concentrations were higher in the CO_2 treatment (890 µatm) flasks than the control after T3 and remained higher for the duration of the experiment; $DMSP_P$ was higher in the post-exponential days, but this difference was not significant (T=-1.49, p=0.153, DF=20). In contrast to Experiment B2, the $DMSP_P$ shows a decline during stationary phase.

CO_2 had no significant effect on $DMSP_P$ per cell (Table 11, Figure 17b, T=-0.95, p=0.350, DF=33).

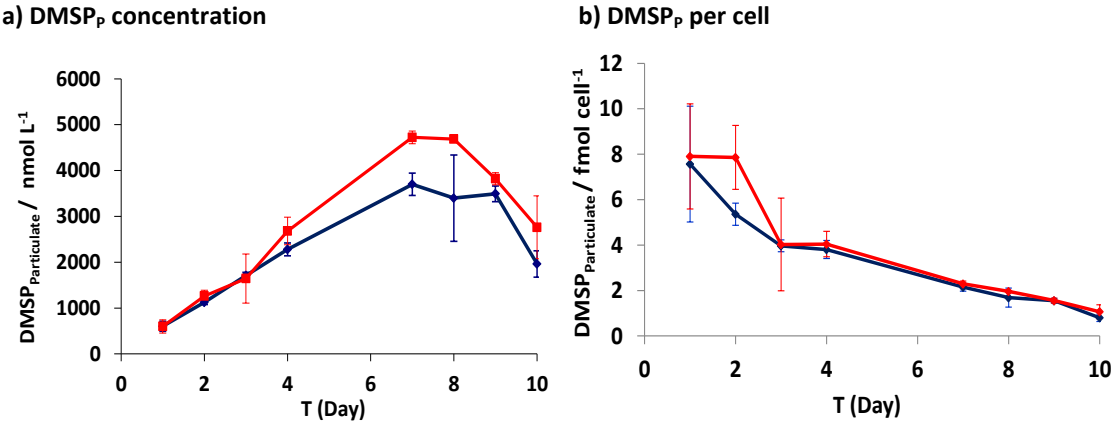

Figure 17. Particulate DMSP concentrations (nmol L^{-1}), and calculated particulate DMSP per cell (fmol $cell^{-1}$) during Experiment B3. Red lines indicate the results from the CO_2 treatment and blue lines the air control, with error bars showing standard deviation of three flasks.

3.3.6. Changes in dissolved DMSP during Experiment B3

Unlike Experiment B2, the $DMSP_D$ concentrations during Experiment B3 increased steadily in both treatments as the experiment progressed (Figure 18), but CO_2 did not significantly affect $DMSP_D$ concentrations. (T=-0.44, p=0.663, DF=33). $DMSP_D$ calculated per cell showed no change over 10 days (1.39±0.38 fmol $cell^{-1}$ and 1.61±0.63 fmol $cell^{-1}$ air and CO_2 respectively over Days 2-10), except for showing negative values on Day 1 in both treatments. No significant difference was identified in $DMSP_D$ production between treatments (T=-0.20, p=0.845, DF=33).

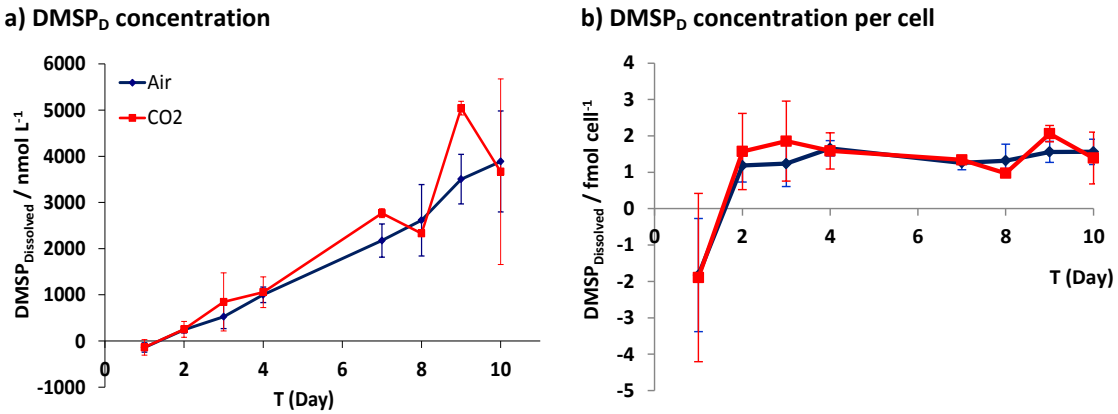

Figure 18. Calculated total dissolved DMSP concentrations (nmol L^{-1}), and calculated dissolved DMSP per cell (fmol $cell^{-1}$) during Experiment B3. Red lines indicate the results from the CO_2 treatment and blue lines the air control, with error bars showing standard deviation of three flasks.

BLANK

Table 7. Growth characteristics of experiments B1, B2 and B3 from this study, compared to Avgoustidi (2006) and Heinle (2013). Values in brackets show the standard deviation between the three replicate flasks. (*) These cells were measured after being decalcified.

Experiment No	pH range		Max cell count (Cells mL^{-1})				Mean Growth rate (d^{-1})		Mean Volume per cell (μm^3)	
	Air	CO_2	Air		CO_2		Air	CO_2	Air	CO_2
			Min	Max	Min	Max				
B1	7.71-8.72	7.45-8.69	5.63×10^4 ($\pm 4.75 \times 10^3$)	6.45×10^5 ($\pm 1.55 \times 10^5$)	5.96×10^4 ($\pm 6.55 \times 10^3$)	6.33×10^5 ($\pm 5.51 \times 10^4$)	0.54 (±0.03)	0.48 (±0.06)	62.03 (±10.31)	65.56 (±11.71)
B2	8.02-8.59	7.32-8.57	6.98×10^4 ($\pm 2.54 \times 10^4$)	2.42×10^6 ($\pm 2.67 \times 10^5$)	4.63×10^4 ($\pm 1.70 \times 10^3$)	3.07×10^6 ($\pm 4.66 \times 10^4$)	0.64 (±0.15)	0.71 (±0.20)	27.98 (±9.57)	28.97 (±10.86)
B3	7.43-8.62	6.81-8.58	3.99×10^4 ($\pm 1.56 \times 10^3$)	2.35×10^6 ($\pm 2.44 \times 10^5$)	4.96×10^4 ($\pm 6.49 \times 10^3$)	2.62×10^6 ($\pm 7.65 \times 10^4$)	0.79 (±0.03)	0.72 (±0.03)	36.96 (±14.11)	36.84 (±13.83)
Avgoustidi (2006) (CCMP 1516)										
Experiment 1	8.2-8.5	7.8-8.4	-	2.1×10^6	-	2.6×10^6	0.51	0.54	63.0	74.8
Experiment 2	8.2-8.5	7.8-8.5	-	4.2×10^6	-	2.3×10^6	0.52	0.45	20.2	23.0
Experiment 3	8.2-8.4	7.7-8.4	-	1.6×10^6	-	2.6×10^6	0.48	0.52	31.1	34.7
Heinle (2013)										
RCC1229	-	-	-	-	-	-	0.67	-	26.0*	-
RCC963	-	-	-	-	-	-	0.72	-	28.0*	-

BLANK

4. Results of *E. huxleyi* RCC1229 CO_2-enriched semi-continuous culture experiments (S1 and S2)

Data from the semi-continuous culture experiments (Section 2.3.2) is presented here. Two experiments were undertaken, labelled Experiment S1 and S2. Both experiment used ESNW medium treated with 890 µatm CO2-enriched air or a control air at 390 µatm, and data are summarised in Table 10 and Table 11.

4.1. *E. huxleyi* RCC1229 semi-continuous culture 1 (Experiment S1)

4.1.1. Changes in pH during Experiment S1

The mean pH from the three flasks of each treatment measured daily is given in Figure 19. On the inoculation days, measurements were taken from both the inoculum and the newly inoculated culture. In total, seven inoculations were performed. The mean CO_2 treatment (890 µatm) pH on the first day of all seven inoculations was 6.98 (±0.17). This compares to 7.44 (±0.16) in the air control (390 µatm). During the batch experiments, culture growth resulted in pH in the treatment exceeding the starting pH of the control within 3-4 days, so the growth periods would not exceed 4 days. This ensured the treatment cultures remained under lower pH influence than the control. The mean pH of the treatment flasks never exceeded that of the air control (dashed line, Figure 19). Mean CO_2 treatment pH on the final days of growth before reinoculation was 7.82 (±0.23) and 8.11 (±0.18) in the air control.

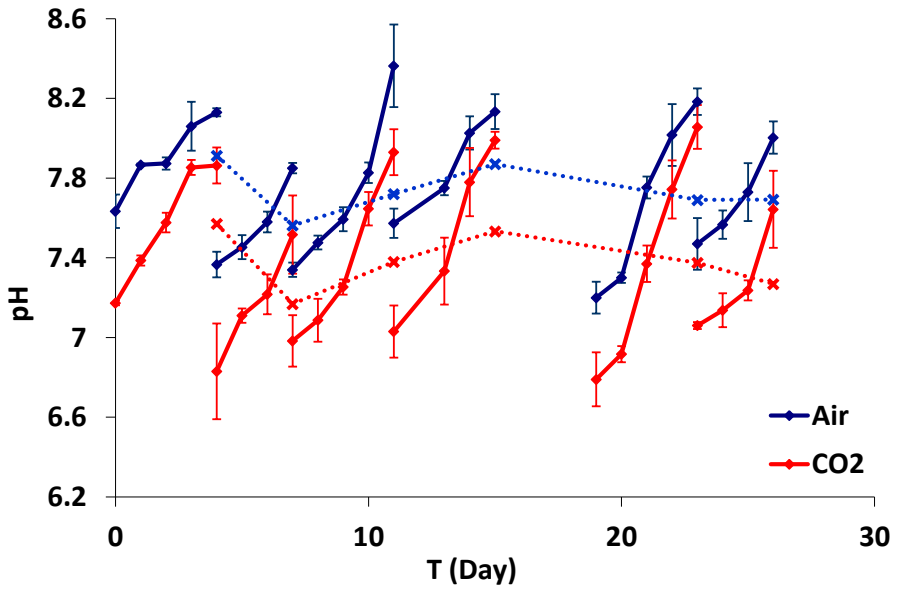

Figure 19. pH changes during Experiment S1. Red lines indicate the CO_2 treatment, blue lines the air control; solid symbols represent the daily mean pH between all three replicates each treatment and the error bars the standard deviation. Dashed lines and crosses show the mean pH during each 4-day inoculation period and in combination show the mean pH for the entire semi-continuous experiment.

As in Experiments B1-B3, the air culture started with a lower pH than expected, significantly below the mean pH of 8.01 measured in the filtered seawater prior to its preparation as media and sparging with the air or CO_2 treatment gas. A short experiment (Experiment M) was performed to determine if this was due to the autoclaving process unduly influencing the medium, and this provided a solution whereby the air control pH would not decrease. The details of Experiment M are given in Section 4.2.

4.1.2. Changes in cell growth during Experiment S1

The initial starting cell count was aimed at 300000 cells mL^{-1} to ensure immediate exponential growth within the culture. To avoid cell changes taking place when the cultures entered stationary phase due to nutrient limitation, every effort was made to keep them in exponential growth by reculturing ahead of the onset of stationary phase. The growth curves for this experiment can be seen in Figure 20 a and b.

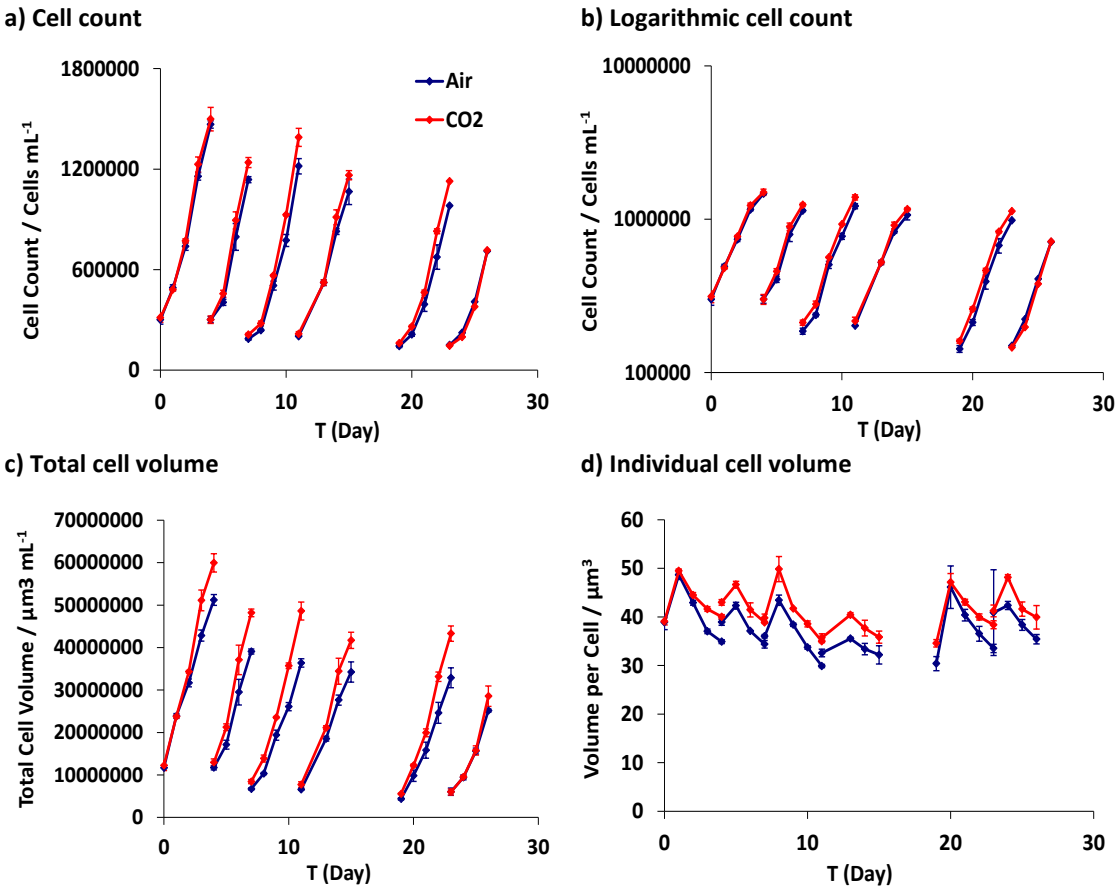

Figure 20. Growth dynamics of the air and CO_2 cultures during Experiment S1, showing the mean and standard deviation a) cell counts (cells mL^{-1}), b) cell counts on a logarithmic scale (cells mL^{-1}), c) total cell volume (μm^3 mL^{-1}) and d) volume per cell (μm^3). Red lines indicate the high CO_2 treatment and the blue the air control, with bars showing the standard deviation of three flasks.

The initial starting cell counts on Day 0 were 300300 cells mL^{-1} (air) and 312566 cells mL^{-1} (CO_2). The growth periods (GP) lasted 3-4 days. The initial and final cell counts for each growth period are shown in Table 8.

Table 8. Mean cell counts for the two treatments at the beginning and end of each growth period, with the mean growth rate for each.

Inoculation	Air			CO_2		
	Starting cell count (Cells mL^{-1})	Final cell count (Cells mL^{-1})	Growth Rate (d^{-1})	Starting cell count (Cells mL^{-1})	Final cell count (Cells mL^{-1})	Growth Rate (d^{-1})
1	300300	1466666	0.37	312566	1498333	0.38
2	301133	1137000	0.44	300500	1239667	0.47
3	186200	1217000	0.47	211500	1389667	0.47
4	201966	1064833	0.42	216100	1163333	0.42
5	325066	-	-	313500	-	-
6	142500	981033	0.48	160133	1127667	0.52
7	149066	710666	0.51	145433	714200	0.52

At each new inoculation, the initial starting cell count was decreased, until inoculation 7 when the mean starting cell count was 149006 cells mL^{-1} in the air control and 145433 cells mL^{-1} in the CO_2 treatment. All growth periods showed some evidence of starting stationary phase (Figure 20b). CO_2 (890 µatm) had a positive effect on the cell count in all the inoculation periods, but this was not statistically significant (T=-0.74, p=0.462, DF=92). Over the entire experiment, CO_2 had no effect on the growth rates of the cells over the 26-day experiment: overall mean growth rates were 0.46 for the CO_2 treatment and 0.45 for the air control (T=-0.84, p=0.406, DF=33).

Individual cell volume fluctuated throughout the experimental period (Figure 20d), with a mean cell volume on the first day of each inoculation at 35.9 μm^3 mL^{-1} (air) and 38.9 μm^3 mL^{-1} (CO_2). Exposure to CO_2 for longer periods than the batch experiments caused an increase in mean cell volume (T=-5.21, p=0.01, DF=160), despite variation in volume seen through each growth period. The second day of each inoculation showed a peak in the mean cell volume, most likely as the cells were actively expanding prior to dividing and so were larger. The number of these larger, dividing cells decreased as the culture approached stationary phase; the mean for the day after inoculation was 43.1 μm^3 mL^{-1} (air) and 46.9 μm^3 mL^{-1} (CO_2). The mean cell volume on the final day of each growth period was almost identical to that on T1 at 33.4 μm^3 mL^{-1} (air) and 38.0 μm^3 mL^{-1} (CO_2).

4.1.3. Changes in DMS during Experiment S1

The purpose of this semi-continuous culture experiment was to test the longer term effects of CO_2 exposure on the DMS and DMSP production of cultured *E. huxleyi,* under the same timescale as SOPRAN Bergen, during which an effect was seen after 16 days of elevated pCO_2 exposure (see Chapter 3). As with the batch experiments, measured DMS in the treatment flasks increased in accordance with cell count (Figure 21 and Table 10). CO_2 (890 µatm) caused a significant increase in DMS concentrations (T=-2.21, p<0.05, DF=89), however, this was not apparent when DMS was calculated per cell (T=-1.71, p=0.09, DF=93). The highest difference between the mean air and CO_2 treatments was during the third inoculation at 193.5 nmol L^{-1}.

DMS per cell (Figure 21b and Table 11) was calculated to compare to the batch and second semi-continuous experiment. The highest DMS concentrations per cell were measured on T24 in both treatments at 0.49 fmol $cell^{-1}$ (air) and 0.58 fmol $cell^{-1}$ (CO_2), before concentrations decreased during that growth period.

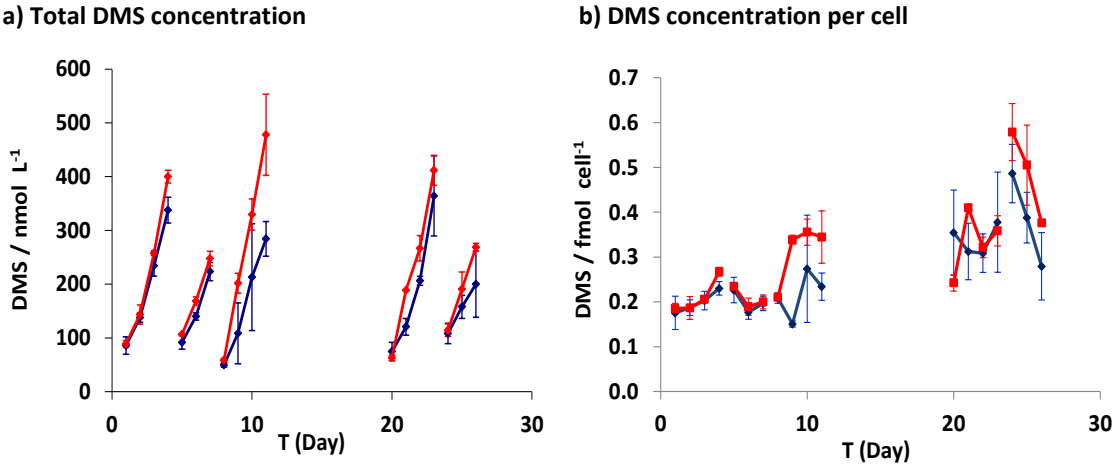

Figure 21. DMS concentrations (nmol L^{-1}) and calculated DMS concentration per cell (fmol $cell^{-1}$) for Experiment S1. Red lines indicate the results from the CO_2 treatment (890 µatm) and blue lines the air control (390 µatm), with error bars showing standard deviation of three flasks.

4.1.4. Changes in total DMSP during Experiment S1

The total DMSP increased from T1 for both treatments, but showed greater variability than for DMS (Figure 22a and Table 10). CO_2 did not have an effect on DMSP concentration (T=-1.55, p=0.123, DF=117) as in B2 and B3, however DMSP produced per cell was significantly higher in the CO_2 treatment than in the control (T=-1.99, p=0.049, DF=129, Figure 22b). On initial examination of the data, this difference is not immediately obvious because of the overall variation in concentrations with high standard deviation between replicate flasks. This was addressed in the Experiment S2 by the use of triplicate measurements for total DMSP from

each flask. Overall, there was no change in the concentrations of total DMSP in either treatment from the start of the experiment to the end, showing that there was no medium-term change in production with increased CO_2.

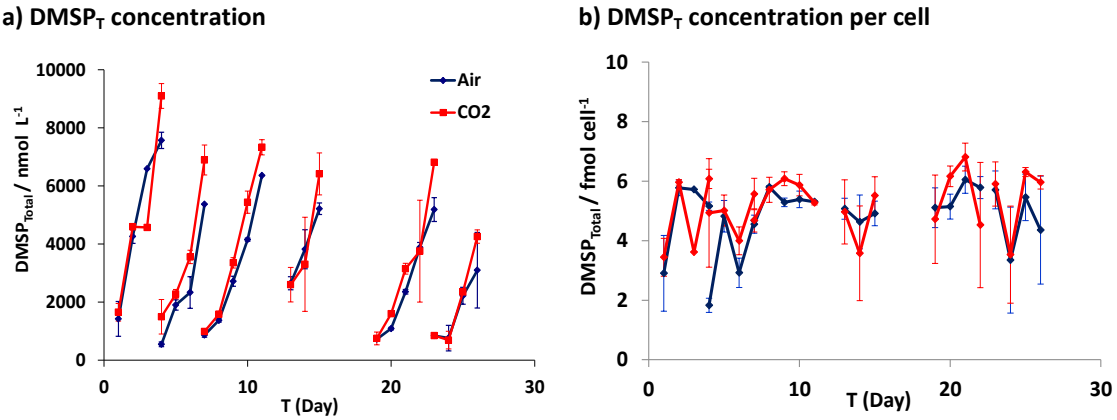

Figure 22. a) Total DMSP concentrations (nmol L^{-1}), and b) calculated total DMSP per cell (fmol $cell^{-1}$) for Experiment S1. Red lines indicate the results from the CO_2 treatment and blue lines the air control, with error bars showing standard deviation of three flasks.

4.1.5. Changes in particulate DMSP during Experiment S1

DMSP particulate concentrations accounted for the majority of the $DMSP_T$, and also increased in line with the cell counts, but CO_2 had no significant effect on DMSPP concentration (T=-1.36, p=0.175, DF=137). The mean $DMSP_P$ concentrations on the first day each growth period were 962.5 nmol L^{-1} (air) and 966.1 nmol L^{-1} (CO_2), but showed greater variation by the final day: 4633.4 (±1158.6) nmol L^{-1} in the air control flasks and 5485.6 (±1577.5) nmol L^{-1} in the CO_2 treatment flasks.

CO_2 had a positive effect on $DMSP_P$ concentrations per cell (T=-2.02, $p<0.05$, DF=128; Figure 23b). As with the $DMSP_T$ data, this is not readily apparent on initial examination of the data, except during the final two growth phases.

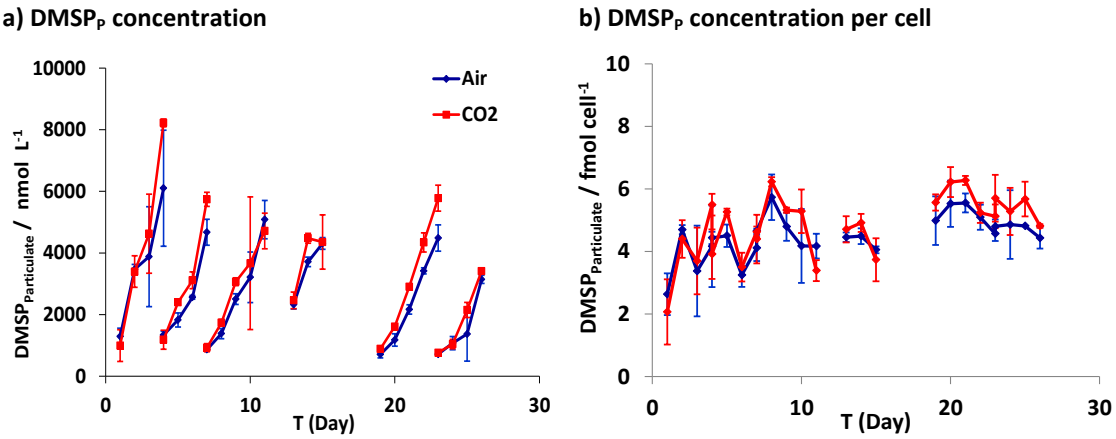

Figure 23. a) Particulate DMSP concentrations (nmol L^{-1}), and b) calculated particulate DMSP per cell (fmol $cell^{-1}$) during Experiment S1. Red lines indicate the results from the CO_2 treatment and blue lines the air control, with error bars showing standard deviation of three flasks.

4.1.6. Changes in dissolved DMSP during Experiment S1

As the cultures were kept in exponential growth medium-term, $DMSP_D$ concentrations were low in relation to $DMSP_P$; the ratio of $DMSP_D$: $DMSP_P$ was 0.18 in both treatments but was often calculated as a negative value (Figure 24). There was no significant difference between the calculated total $DMSP_D$ concentrations (T=-1.09, p=0.276, DF=115) or the calculated $DMSP_D$ produced per cell (T=0.37, p=0.710, DF=120).

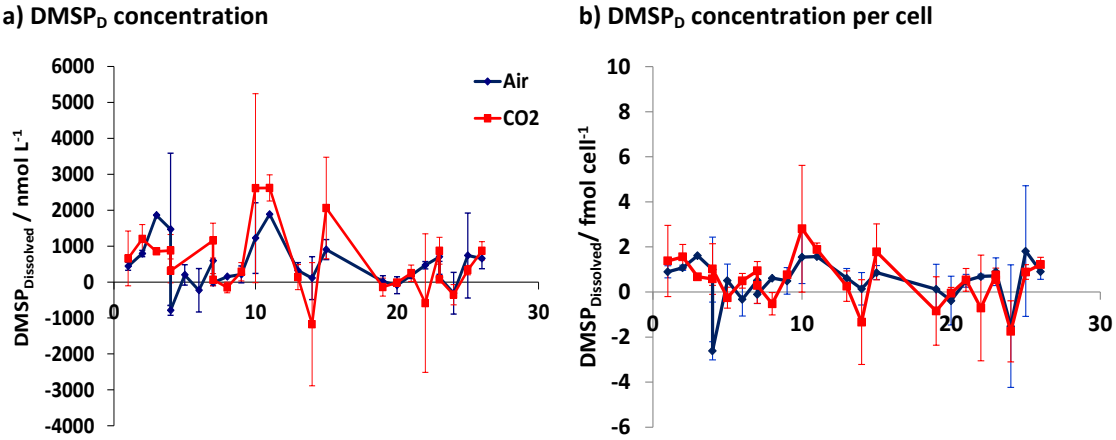

Figure 24. Calculated total dissolved DMSP concentrations (nmol L^{-1}), and calculated dissolved DMSP per cell (fmol $cell^{-1}$) during Experiment S1. Red lines indicate the results from the CO_2 treatment and blue lines the air control, with error bars showing standard deviation of three flasks.

4.2. Experiment M: Assessment of pH change during media preparation

4.2.1. Introduction

This series of tests was performed to measure the pH in the media and identify a method whereby no differences would be apparent in control media pH before and after the air sparging process. This section compares the results in pH from samples taken daily from the sparge towers of air and CO_2 if the medium was autoclaved and if it was filter sterilised.

4.2.2. Methods

The two 3L sparge towers were acid-washed and autoclaved before being filled with freshly made medium in the same setup as for the experimental media preparation. Media were prepared by the same method as for the experiments: 0.2 µm filtered seawater was autoclaved, and nutrients and vitamins were added aseptically. The medium was transferred to the sparge towers in the sterile safety cabinet, band then they were transferred to a culture cabinet held at 15 °C. The gas flow into the towers was set at 20ml min^{-1}. The towers were left for 5 days. Triplicate samples of the media were removed from both towers (air or CO_2) and measured for pH immediately upon setup and daily thereafter. The pH probe was calibrated before each sampling session.

Once the autoclaving test was complete, a second batch of medium was prepared by filtering 5 L of seawater through a pre-sterilised 0.2 µm cellulose acetate filter, before nutrients and trace metals were added aseptically. The medium was filtered a second time through a second pre-sterilised 0.2 µm cellulose acetate filter before it was transferred into the two acid-washed and autoclaved glass sparge towers. The towers were held at 15°C in the culture cabinet for 3 days, with the gas flows set to 20 mL min^{-1}. Samples were taken for immediate pH analysis in triplicate when the systems were set up, then on a daily basis for the following 3 days.

4.2.3. Results

During the autoclave experiment, pH in both sparge towers decreased between T0 and T2 with a greater decrease seen in the CO_2 treatment. Minimum mean pH measured in the CO_2 medium was 6.6 on T2 and 7.1 in the air medium. During the following 3 days, the pH in all towers remained relatively stable (Figure 25). This is the same trend in pH as seen on the first day of the experiments: that the pH in both air and CO_2 treatments in the sterile media is

lower than expected. This decrease was attributed to the autoclaving process stripping the ambient CO_2 from solution.

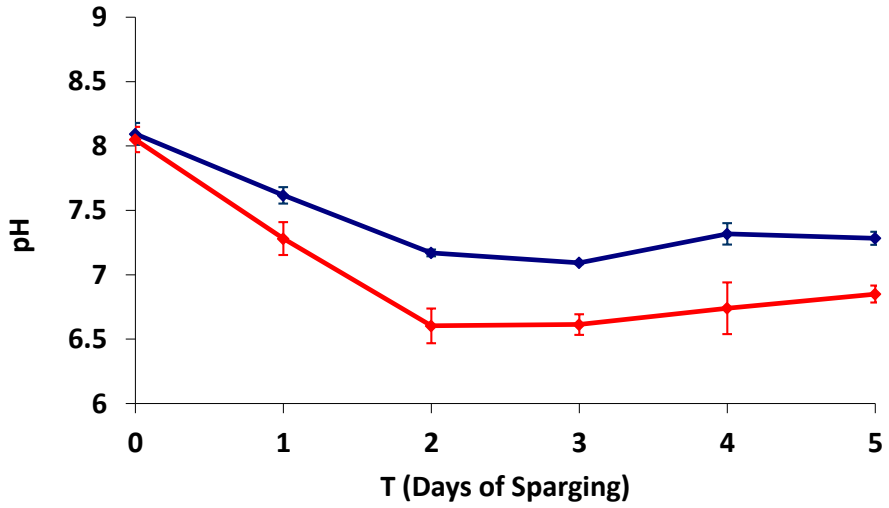

Figure 25. pH in the two 3L sparge towers filled with autoclaved medium, showing the sparging time and the recorded pH, measured in triplicate and shown as a mean with the error bars as standard deviation. Red points show the CO_2 enriched gas, blue the air control.

The following filter sterilisation test showed that the medium pH in the air sparge tower did not decrease in the first 2 days, but that of the CO_2 medium did (Figure 26). The pH in both treatments immediately after transfer to the sparge towers was 7.90. Further samples were taken at 16 hours, then daily for 3 days. The test was discontinued after Day 3, as there was no sign of the pH decrease seen in the previous test: air medium pH remained stable over 3 days at 7.93, whereas the CO_2 treatment pH 7.65. These results made it clear that the decrease in pH was resolved by the use of filter sterilisation, and this approach was used for all subsequent experiments.

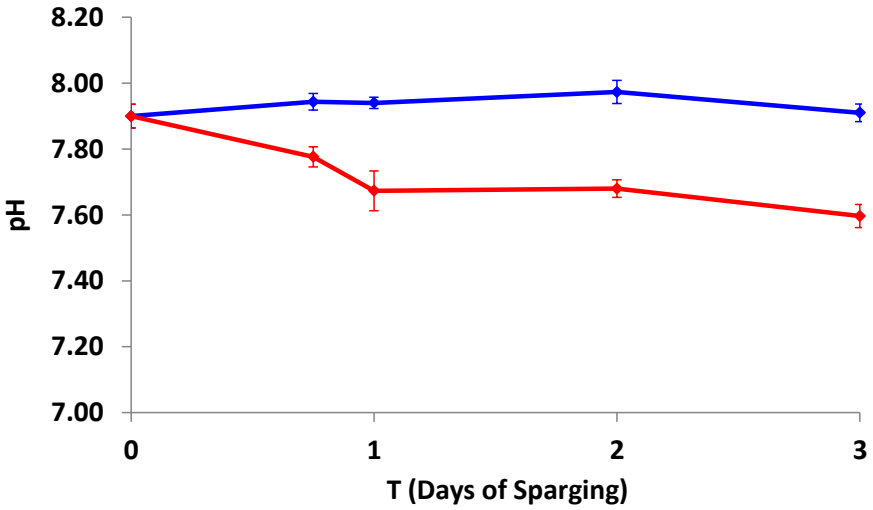

Figure 26. pH in two identical 3L sparge towers containing filter sterilised medium over three days. Measurements were taken twice in the first 24 hours, then on a daily basis, in triplicate and shown as a mean with the error bars as standard deviation. Red points show the CO_2 enriched gas, blue the air control.

4.3. *E. huxleyi* RCC1229 semi-continuous culture 2 (Experiment S2)

4.3.1. Changes in pH during Experiment S2

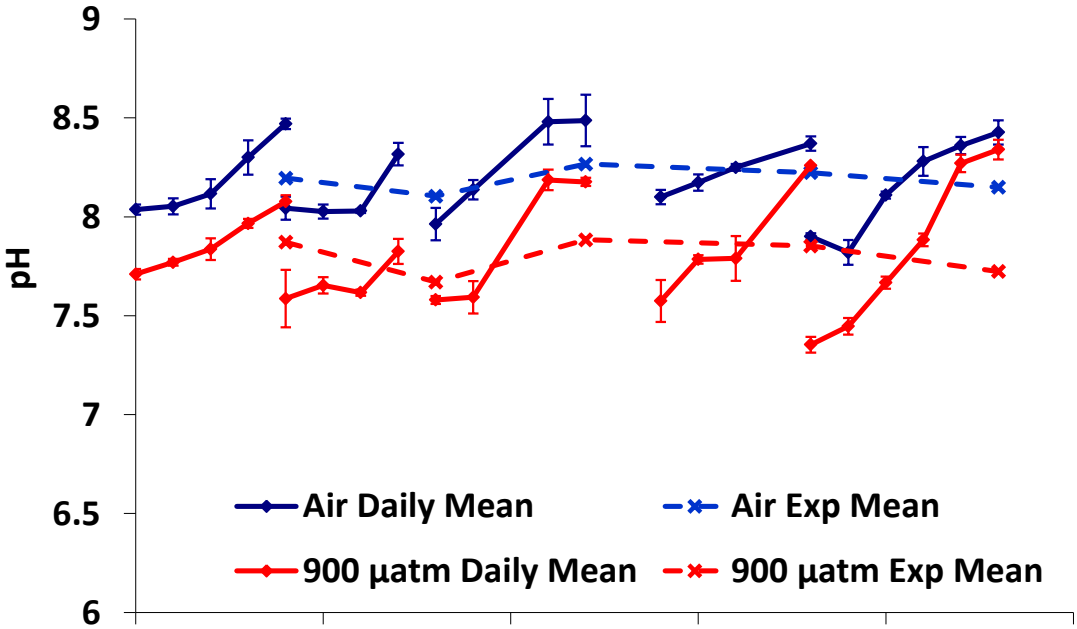

Figure 27. pH changes during Experiment S2. Red lines indicate the CO_2 treatment, blue lines the air control; solid lines represent the daily mean pH between all three replicates of either control or CO_2 treatment and the error bars the standard deviation. Dashed lines and crosses show the mean pH during each 4-day inoculation period and in combination show the mean pH for the entire semi-continuous experiment.

The medium was prepared according to the tests performed in section 4.2, and the pH measurements reflected this change in preparation (Figure 27) in total, five culture inoculations were performed. Mean pH for the entire experiment within the control media (390 µatm) was 8.13 and for the CO_2 cultures (890 µatm) was 7.72 ($T=7.68$, $p<0.01$, $DF=129$). This is shown in Figure 27 by the dashed lines. The mean CO_2 treatment pH immediately after inoculation was 7.43, calculated from the measurements on the first day of all five inoculations. This compares to 7.90 in the air control. The experiment was run at control and treatment pH values close to those of the SOPRAN Bergen experiment. Mean CO_2 treatment pH on the final day of all growth periods was 8.06, compared to 8.41 in the air control.

4.3.2. Changes in cell growth during Experiment S2

The target starting cell count was set to be lower at 100,000 cells mL^{-1} to reduce the risk that the culture would enter stationary phase and become nutrient limited. During this experiment

the inoculations were planned to grow for four days each, with seven inoculation periods. However, the growth rate noticeably changed during inoculations 4 and 5, and one of the flasks failed to show any growth during inoculation 4 (shown by the high standard deviation error bars). The experiment was abandoned during inoculation 6 as growth was not identified in any of the three CO_2 treatment (890 µatm) flasks. This was established as most likely due to contamination of the medium from a repaired sparge tower, and no replacement medium was available.

The initial starting cell counts on T0 were 133167 cells mL^{-1} (air) and 113511 cells mL^{-1} (CO_2), and growth was immediate (Figure 28). The first growth period lasted 4 days, and was still in exponential growth when it was recultured (Figure 28b). The initial and ending cell counts for each growth period are shown in Table 9.

Table 9. Mean cell counts for the two treatments at the beginning and end of each growth period, with the mean growth rate.

Inoculation	Air			CO_2		
	Starting cell count (Cells mL^{-1})	Final cell count (Cells mL^{-1})	Growth Rate (d^{-1})	Starting cell count (Cells mL^{-1})	Final cell count (Cells mL^{-1})	Growth Rate (d^{-1})
1	133167	812000	0.45	113511	849767	0.51
2	93583	977333	0.59	100849	981700	0.57
3	120800	1342333	0.60	114284	1225000	0.60
4	104575	796533	0.34	123067	633950	0.26
5	107158	752000	0.38	78091	729567	0.42
6	126567			152200		

Despite the use of a lower starting cell concentration, the final day of growth periods 2-5 still showed some evidence of growth slowing (Figure 28b). The change in growth rate can be seen on the fourth and fifth inoculations. CO_2 had no significant effect on cell growth at any time (T=0.79, p=0.432, DF=159), and no effect on the growth rates: overall mean growth rates all five inoculations were 0.48 for the CO_2 treatment (890 µatm) and 0.47 for the air (390 µatm) control (T=-0.16, p=0.871, DF=24).

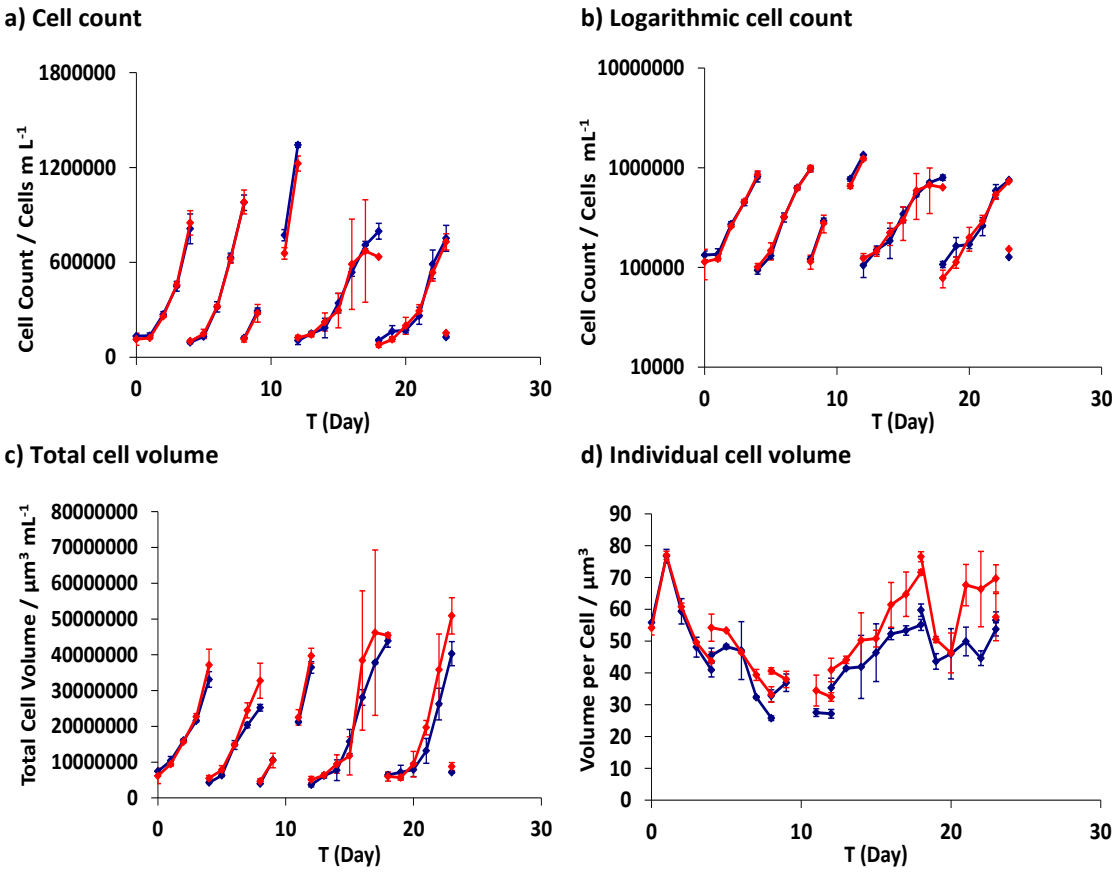

Figure 28. Growth dynamics of the air and CO_2 cultures during Experiment S2, showing the mean and standard deviation a) cell counts (cells mL^{-1}), b) cell counts on a logarithmic scale (cells mL^{-1}), c) total cell volume (μm^3 mL^{-1}) and d) volume per cell (μm^3). Red lines indicate the high CO_2 treatment and the blue the air control, with bars showing the standard deviation of three flasks.

After the first growth period, CO_2 had a significant effect on individual cell volume: cells in the CO_2 treatment flasks were significantly larger than the air control ($T=-3.65$, $p<0.01$, $DF=151$). Individual cell volume fluctuated throughout the experimental period (Figure 28d), with a mean cell volume on the first day of each inoculation at 55.8 μm^3 mL^{-1} (390 µatm) and 54.2 μm^3 mL^{-1} (890 µatm). The second day of each inoculation did not show the same peak in volume as in Experiment S1: the general trend was of decreasing cell size for the first three inoculations. When the cells were stressed during poor growth in the fourth and fifth growth periods the individual cell size increased.

4.3.3. Changes in DMS during Experiment S2

CO_2 did not have an effect on the DMS concentrations in the flasks ($T=0.03$, $p=0.975$, $DF=120$) or on the concentration per cell ($T=-0.64$, $p=0.525$, $DF=103$). Measured DMS concentrations did not follow the patterns of the cell counts: DMS within the first two inoculations did increase but in a linear pattern, then exponential increases were seen in growth periods 3-5

(Figure 29a). Mean DMS concentration from the first measurement of growth periods 1-4 was 15.2 nmol L^{-1} (air) and 20.8 nmol L^{-1} (CO_2), but DMS on the first day of growth period 5 was measured as 68.9 nmol L^{-1} (air) and 63.2 nmol L^{-1} (CO_2). These concentrations are notably higher than the previous growth periods, and yet are still lower than the initial DMS measurements from the previous semi-continuous experiment (Table 10).

DMS concentration per cell started at 0.14 fmol $cell^{-1}$ in the CO_2 treatment and 0.13 fmol $cell^{-1}$ in the air control. Concentrations decreased over the first two growth periods, but started to increase in the third and carried on increasing until period 5 (Figure 29b). The highest concentrations per cell were measured on T19 in both treatments at 0.56 fmol $cell^{-1}$ in the CO_2 treatment and 0.42 fmol $cell^{-1}$ in the air control; despite the variation observed, it is still within the same range as in the previous experiment (Table 11).

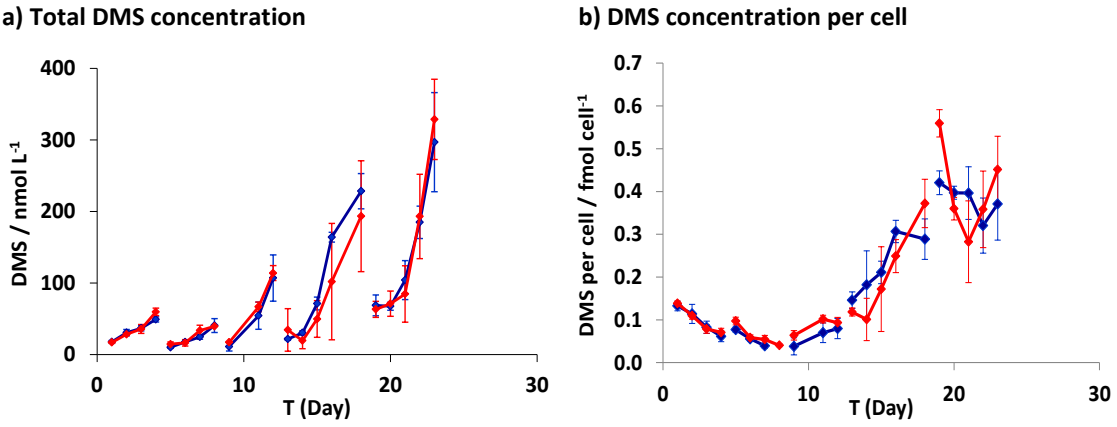

Figure 29. DMS concentrations (nmol L^{-1}) and calculated DMS concentration per cell (fmol $cell^{-1}$) for Experiment S2. Red lines indicate the results from the CO_2 treatment and blue lines the air control, with error bars showing standard deviation of three flasks.

4.3.4. Changes in total DMSP during Experiment S2

Total DMSP followed the pattern of the cell count data closely, with concentrations increasing exponentially during the first three growth periods, then reflecting the poorer growth of periods 4 and 5 (Figure 30a). The DMSP results do not follow the pattern seen in DMS (low concentrations during the first growth periods followed by rapid increase in concentrations during the final two growth periods); although it was clear the cells were growing while stressed, the DMSP concentration was not affected.

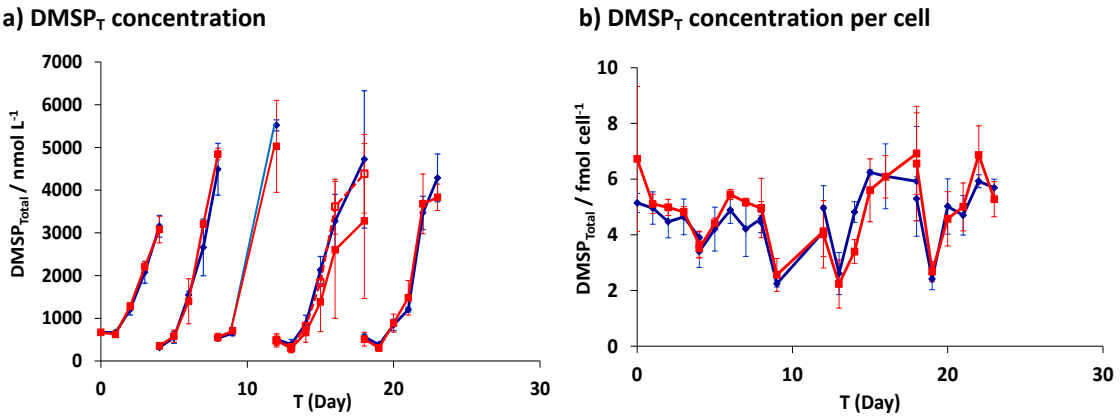

Figure 30. a) Total DMSP concentrations (nmol L^{-1}), and b) calculated total DMSP per cell (fmol $cell^{-1}$) for Experiment S1. Red lines indicate the results from the CO_2 treatment and blue lines the air control, with error bars showing standard deviation of three flasks. The dashed red line shows the results excluding the flasks that did not grow.

CO_2 did not significantly affect the $DMSP_T$ concentration in the cultures (T=1.17, p=0.244, DF=430). The mean total DMSP concentrations for the first day of inoculation were found to be 505.3 nmol L^{-1} in the control and 503.9 nmol L^{-1} in the CO_2 treatment flasks. During the fourth growth period, only two out of the three CO_2 flasks showed growth, although the DMSP concentrations were still measured daily. The results displayed in Figure 30a show the mean concentrations from all three flasks (red line), and also the total DMSP results from the two flasks that did show growth (dashed red line), which are very close to the concentrations observed in the air control.

No significant effect of CO_2 was identified between the two treatments (T=-1.36, p=0.174, DF=382). The mean total DMSP per cell production was calculated as 4.4 fmol $cell^{-1}$ in the control, and 4.5 fmol $cell^{-1}$ in the CO_2 treatment flasks, and showed no overall trends of increasing or decreasing concentration (Figure 30b). The range of total DMSP per cell is shown in Table 11.

4.3.5. Changes in particulate DMSP during Experiment S2

DMSP particulate measured concentrations are very similar to those of the total DMSP (Figure 31a). The mean $DMSP_P$ concentrations on the inoculation days were 500.34 ± 152.34 nmol L^{-1} (air) and 547.53 ± 139.34 nmol L^{-1} (CO_2). The mean concentrations on the final day of the growth periods showed much greater variation: 3999.07 ± 831.27 nmol L^{-1} in the air control flasks and 3896.22 ± 1180.11 nmol L^{-1} in the CO_2 treatment flasks; a two-tailed t-test showed no significant difference between the $DMSP_P$ concentrations (T=0.84, p=0.404, DF=143).

a) $DMSP_P$ concentration **b) $DMSP_P$ concentration per cell**

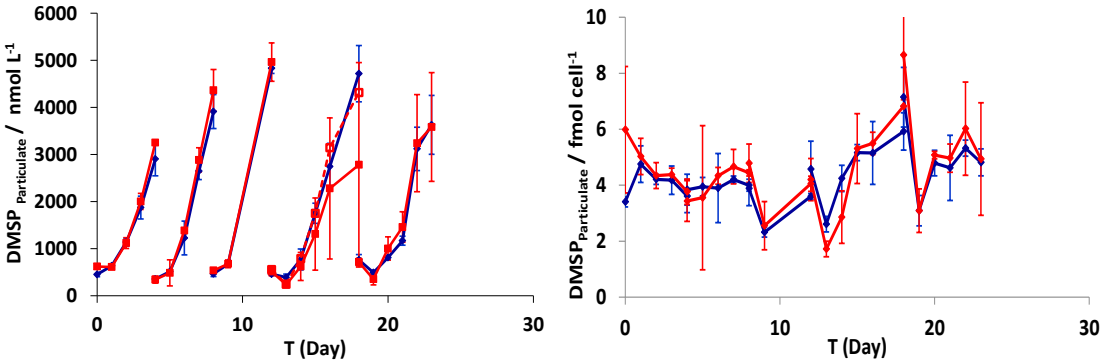

Figure 31. a) Particulate DMSP concentrations (nmol L^{-1}), and b) calculated particulate DMSP per cell (fmol $cell^{-1}$) during Experiment S1. Red lines indicate the results from the CO_2 treatment and blue lines the air control, with error bars showing standard deviation of three flasks.

$DMSP_P$ concentrations per cell showed no significant difference between the CO_2 treatment and the air control (Figure 31; T=-1.02, p=0.310). $DMSP_P$ per cell was measured at a mean of 4.3 fmol $cell^{-1}$ in the control and 4.5 fmol $cell^{-1}$ in the CO_2 treatment across the entire experiment, with very little overall change in calculated concentrations from T0 to T23. The highest concentrations per cell were calculated on T18, the day before the maximum DMS concentrations.

4.3.6. Changes in dissolved DMSP during Experiment B2

$DMSP_D$ increases towards the end of each inoculation period, but there was no significant difference between the control and the CO_2 treatment, either for the total $DMSP_D$ (T=1.59, p=0.114, DF=145) or the $DMSP_D$ produced per cell (Figure 32b; T=1.21, p=0.230, DF=129). Mean values of $DMSP_D$ for the air control were 163.1 nmol L^{-1} (0.29 fmol $cell^{-1}$) and the CO_2 treatment 81.7 nmol L^{-1} (0.11 fmol $cell^{-1}$).

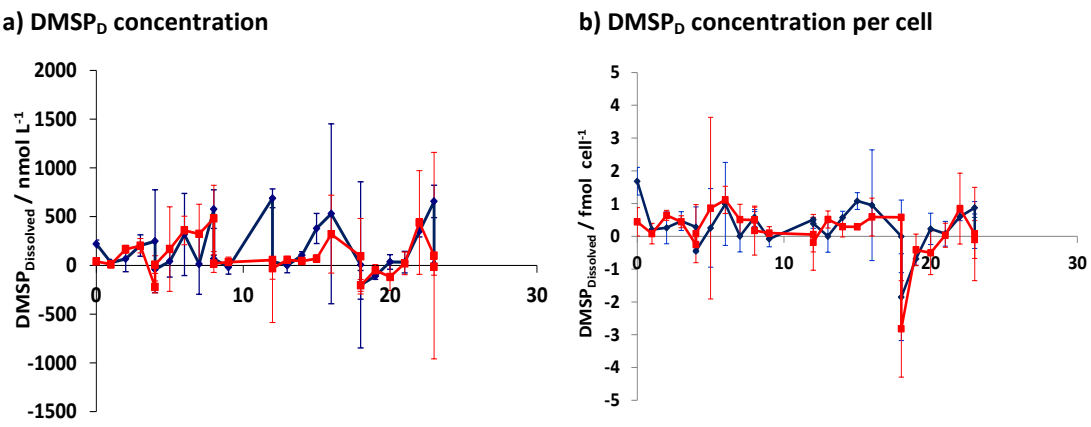

Figure 32. Calculated dissolved total and per cell DMSP production during Experiment S2. Red lines indicate the results from the CO_2 treatment and blue lines from the air control, with error bars showing standard deviation.

4.4. Comparison of Experimental Results

Table 10 and Table 11 allow a comparison to be made of the five experiments in terms of the range of data for the measured concentrations (Table 10) and the calculated concentrations per cell of DMS and DMSP (Table 11). The data from Avgoustidi (2006) who performed very similar batch experiments are given for comparison.

All five experiments show similar ranges for measured DMS and DMSP, with the exception of S1 where the lower limit of DMS concentration was an order of magnitude higher than the other experiments. That the lower limits of measured DMS were similar is interesting as the batch experiments started with much lower cell densities than the semi-continuous experiments. The difference in DMS concentration was not seen in the calculated DMS per cell for S1: these were similar for both S1 and S2, but were higher than the batch experiments.

BLANK

Table 10. DMS and $DMSP_T$ concentration ranges from all 5 experiments.

Experiment No	DMS (nmol L^{-1})		Total DMSP (nmol L^{-1})		Particulate DMSP (nmol L^{-1})		Dissolved DMSP* (nmol L^{-1})	
	Air	CO_2	Air	CO_2	Air	CO_2	Air	CO_2
B1	3.64 – 216.71	2.37 – 113.43	No Data					
B2	4.83 – 448.07	4.87 – 490.21	512.09 – 10998.73	500.71 – 12894.59	518.58 – 10916.01	480.55 – 14996.14	0 - 3897.37	0 – 3735.61
B3	3.17 – 402.41	4.05 – 449.41	462.11 – 6996.92	461.87 – 8864.65	602.27 - 3698.96	600.91 -4723.30	0 - 4662.04	0 - 5198.68
S1	44.98 – 416.89	55.00 – 559.24	294.61 - 7817.03	447.62 – 9588.71	587.04 – 7347.09	632.22 – 8348.00	0 – 3881.24	0 – 4473.54
S2	6.47 – 345.78	11.52 – 366.55	109.82 – 6233.60	144.11 – 6062.31	321.32 – 5158.60	217.0 – 5432.08	0 – 1285.25	0 – 1009.90

*Dissolved DMSP concentrations are presented from zero values rather than the calculated negative values.

BLANK

Table 11. DMS and DMSP mean (±standard deviation) per cell during all 5 experiments, compared to the range (DMS) and mean (DMSP) values obtained by Avgoustidi (2006).

Experiment No	DMS (fmol cell^{-1})		Total DMSP (fmol cell^{-1})		Particulate DMSP (fmol cell^{-1})		Dissolved DMSP (fmol cell^{-1})	
	Air	CO_2	Air	CO_2	Air	CO_2	Air	CO_2
B1	0.159 (±0.103)	0.120 (±0.074)	-	-	-	-	-	-
B2	0.118 (±0.052)	0.112 (±0.052)	6.62 (±2.37)	7.03 (±2.92)	6.56 (±3.03)	7.24 (2.80)	0 (±1.62)	0 (±1.51)
B3	0.072 (0.055)	0.086 (0.054)	4.39 (±1.54)	4.96 (±2.21)	3.47 (±2.30)	4.25 (±2.92)	0.97 (±1.25)	1.06 (±1.63)
S1	0.265 (±0.099)	0.302 (±0.118)	4.78 (±1.25)	5.20 (±1.21)	4.49 (±0.84)	4.83 (±1.11)	0.36 (±1.28)	0.41 (±1.36)
S2	0.179 (±0.137)	0.197 (±0.158)	4.59 (±1.27)	4.72 (±1.53)	4.25 (±1.13)	4.52 (±1.54)	0.294 (±0.844)	0.089 (±0.983)
Avgoustidi (2006) CCMP 1516								
Experiment 1	0 – 0.003	0 – 0.003	-	-	19.0	14.8	0.5	0.6
Experiment 2	0 – 0.004	0 – 0.005	-	-	2.0	3.0	0.8	0.3
Experiment 3	0 – 0.006	0 – 0.005	-	-	4.4	3.7	0.1	0.1

BLANK

5. Discussion

5.1. Overview of experimental findings and research focus

This series of experiments was designed to test the following research questions, which were deemed to have been answered after experiment S2:

- Do increasingly acidified conditions caused by an increase in atmospheric pCO_2 to 860 µatm, under the IPCC A2 Scenario projections for 2100 cause a change in DMS and DMSP production from *E. huxleyi* compared to current conditions?
- Does mid-term exposure of *E. huxleyi* to acidified conditions result in changes to DMS and DMSP production or the dynamics between the two?

The answer to both these research questions, for strain RCC1229 at least, was that growth at a pCO_2 of 860 µatm resulted in no change to the DMS and DMSP output of the cells, compared to a control at ambient current atmospheric pCO_2 of 396 µatm. The results obtained here will be discussed in terms of the available data in the literature on other experiments performed under similar experimental conditions, and compared with the existing data on DMS and DMSP from the mesocosm experiments.

5.2. General observations of *E. huxleyi* RCC1229 CO_2 enrichment experiments

5.2.1. General observations on batch Experiments B1, B2 and B3

Growth parameters for the batch experiments B1, B2 and B3 are given in Table 7, and are in accordance with data from the similar batch experiments of Avgoustidi (2006) and the growth rates recorded by Heinle (2013) at 14.5°C. The statistical p-values are shown in Table 12 for all five of the experiments performed here.

Cell counts in the batch experiments were comparable, and the growth curves for all three experiments proceeded along the same timescales. The only notable exception within these experiments was that the cell count in B1 was significantly higher in the control than the CO_2 treatment, and the cell volumes from this experiment were double that in experiments B2 and B3 Table 7). As there was no attempt to determine calcification rates during the experiments, changes in cell size could be determined by changes to the coccosphere thickness instead of cell size.

Table 12. Comparison of p-values for each experimental variable, with highlighted values showing significance and effect (in brackets) of high pCO_2.

Experiment No	B1	B2	B3	S1	S2
Max cell count (Cells mL^{-1})	0.477	0.001 (Higher)	0.465	0.462	0.432
Mean Growth rate (d^{-1})	0.353	0.563	0.777	0.406	0.871
Mean cell volume (μm^3)	0.301	0.711	0.975	0.00 (Larger)	0.00 (Larger)

5.2.2. General observations on semi-continuous Experiments S1 and S2

Batch experiments were limited in representing authentic growth under elevated pCO_2 due to the rapid change in pCO_2 and pH due to *E. huxleyi* exponential growth. It was determined that a continuous system would make it difficult to monitor trace gas concentrations on a daily basis, and a compromise was reached in the use of a semi-continuous setup. Experiments S1 and S2 showed similar growth curves for the reinoculations, although the growth rates were lower than those calculated in the batch experiments, at 0.46 d^{-1} (S1) and 0.48 d^{-1} (S2) for the CO_2 treatments, compared to a mean of 0.64 d^{-1} for all of the batch experiments. The only notable difference in the cell growth under the longer term exposure to CO_2 was that of the cell volumes increasing in the CO_2 treatment, which occurred in both S1 and S2 prior to the second inoculation. This increase was not identified in the batch experiments, perhaps because the cells were not exposed to the elevated pCO_2 for sufficient time.

The use of semi-continuous cultures in acidification experiments with reinoculations daily (Wuori 2012; Feng *et al.* 2008) or after several days (Barcelos e Ramos *et al.*, 2010) is an alternative to the often costly and complicated setup of continuous pH-stats. During this study, it was determined that the reinoculations would take place after 3-4 days of growth, for comparability with the previous batch experiments and to allow time for daily DMS and DMSP sampling. It was also a system which was easily comparable to the previous batch experiments, using much of the same equipment, and although costly in terms of time and manpower, provided much more detailed assessments of the changes in DMS and DMSP over time than other semi-continuous experiments which sacrificed DMS(P) sampling for daily reinoculation.

5.3. Effectiveness of medium enrichment with CO_2

Sparging the medium with a pre-mixed CO_2 enriched air was used during this study for two reasons. It was a method comparable with that used during the SOPRAN Bergen experiment to alter the mesocosm carbonate chemistry (though through the addition of CO_2-enriched waters to the mesocosms rather than bubbling), and It gives the most realistic alteration to carbonate chemistry in comparison to the increase in atmospheric pCO_2 expected in future climate scenarios (Gattuso and Lavigne, 2009). Addition of CO_2 is an efficient and simple method of altering the carbonate chemistry, by changing DIC and keeping Total Alkalinity (A_T) constant (Fabry, 2008; Gattuso *et al.*, 2010); however during culture growth, changes in the rate of calcification will affect the A_T. The addition of CO_2 enriched water has very similar effects on the carbonate chemistry parameters than bubbling with CO_2 enriched air.

Studying the effects of acidification on the growth and physiology of marine phytoplankton is difficult due to the interdependence of the key parameters and the effects of cell growth on them. Of the three main methods of carbonate acidification (acid or base addition, use of buffers or bubbling with CO_2 enriched air), Shi *et al.* (2009) found that bubbling induced greater variability into the phytoplankton physiological parameters than the other two methods. This is likely a stress reaction to the bubbling itself instead of to the changes in the medium chemistry, and the change in carbonate chemistry through the use of pre-sparged medium is unlikely to cause any negative effects on phytoplankton growth.

One of the major problems observed with growing phytoplankton under acidification conditions is the difficulty in keeping the pH artificially lowered while the culture was in exponential growth. *E. huxleyi* carbon concentrating mechanisms were discussed in Chapter 1, where the use of HCO_3^- for calcification can release CO_2 for PHS: calcification itself acts as a CCM (Buitenhuis *et al.*, 1999). It is likely that an increase in pCO_2 within the medium allows the cell to down-regulate CCM operation, and requires less calcification to provide the CO_2 required. Certainly in all the experiments save B1, the cell concentrations in the high pCO_2 cultures were higher than the controls at the end of exponential growth, indicating that the additional CO_2 has not been detrimental to the cell.

5.4. Evaluating the effects of CO_2 on cell growth and volume

All the batch experiments grew as expected, and none of the flasks failed to show growth. In comparing all three experiments, B2 and B3 had similar growth rates, phases and final cell

counts. Experiments S1 and S2 grew at growth rates slightly lower than the batch experiments, with no change when influenced by elevated pCO_2.

5.4.1. Effect of CO_2 on growth rates

Growth rates at 15°C were between 0.48-0.79 d^{-1}. These compare well to existing values from the literature. For example, growth rates of 0.67 were observed by Heinle (2013) for strain RCC1229 in semi-continuous culture at 14.5°C Similar results were also seen in continuous culture experiments conducted on CCMP373 by Arnold *et al.* (2013) and Wolfe & Steinke (1996) who reported growth rates of 0.62 (17°C, pH stat system) and 0.47 (15°C, sealed batch cultures) respectively. The rates calculated for strain CCMP1516 by Avgoustidi (2006) were at the lower end of the range identified in this investigation, at 0.45-0.54.

Additional studies have showed variation in growth rate after the addition of CO_2: Leonardos & Geider (2005) found no difference in growth rates between ambient and 2000 µatm pCO_2 in strain PML 92A but Moheimani & Borowitzka (2011) found that CCMP371 did not grow at a pH of lower than 7.5 in a pCO_2-regulated pH stat. In a study of four different *E. huxleyi* strains from different parts of the global ocean, Langer *et al.*, (2009) found that three different strains decreased in their growth rate while only one out of four increased under a pCO_2 of 1200 µatm. Fiorini *et al.* (2011) identified growth rates consistently higher under elevated pCO_2 treatments. As strain RCC1229 (this study) showed no variation in growth rate with increased CO_2, further investigations are needed into strain specific differences.

Other species have been shown to have no difference in growth rates under increasing pCO_2, despite the greater availability of DIC for photosynthesis. Berge *et al.* (2010) found no difference in *Prymnesium parvum*, under ecologically relevant pH ranges, but under pH 6.5, growth was affected. Further experiments on *Chlamydomonas* also showed no difference in growth rates or specific adaptation to CO_2 even after 1000 generations (Collins and Bell, 2004).

5.4.2. Effect of CO_2 on cell size and volumes

All three batch experiments showed there was no significant difference in average cell volume when the cultures were growing under high pCO_2, although the individual volumes showed large variations between experiment B1 and experiments B2 and B3. Cell volumes from the latter two batch experiments are similar to those determined by Heinle (2013), who decalcified the cells before calculating the cell volume.

The increase in cell size identified during the CO_2 treatment of S1 and only became apparent after the second inoculation. The mean cell volume in S1 in the air control for the duration of the experiment was 37.42 μm^3, compared to 41.14 μm^3 ($T=-5.21$, $p<0.01$, $DF=160$) in the control. During S2, the air treatment mean was 45.98 μm^3 compared to 53.26 μm^3 in the CO_2 treatment ($T=-3.65$, $p<0.01$, $DF=151$).

Additional variations were detected in cell volume during each inoculation as the cells grew: the cell volumes were often larger the day after inoculation (Figure 20 and Figure 28). In the second semi continuous experiment, the cell volume in both cultures showed a steady decrease over the first 10 days when the cells were growing well, but during the third inoculation when they started to show stress, the cell volumes increased again to the same volume seen at the beginning of the experiment. It is therefore clear that cells respond to stress by changing their volume, but that exposure to elevated pCO_2 does not cause this same stress reaction of increasing cell size. Arnold *et al.* (2013) found similar variation in cell volume over the time course of their experiments, although there was no evidence of volume increase after inoculation.

Lohbeck *et al.* (2012) reported no significant difference in cell size up to 1100 µatm pCO_2 in a culture grown for 500 generations, but strain AC472 showed significantly smaller cell volumes from 61 μm^3 down to 40 μm^3 in 760 µatm pCO_2 (Fiorini *et al.*, 2011). However, of these two experiments the latter is a batch culture, compared to a continuous culture grown much longer term.

5.5. Evaluating the effects of elevated pCO_2 on DMS and DMSP concentrations

5.5.1. Effect of elevated pCO_2 on DMS and DMSP during B1, B2 and B3

In general, DMS and DMSP increased with cell number in all three batch experiments. Statistical analysis was performed on the entire dataset, as well as the data for exponential growth and during stationary phase, although it is worth remembering in the batch experiments that the cells are only growing under the influence of elevated pCO_2 during exponential phase and not stationary phase. The p-values found during the analyses are presented in Table 13, with highlighted values showing significance, to identify any trends.

DMS per cell at the beginning of all three batch experiments was around 0.5 fmol $cell^{-1}$; DMS per cell was low in exponential phase but increased during stationary phase. DMSP total and particulate showed the opposite trend: concentrations per cell started between 6-12 fmol $cell^{-1}$

in experiments B2 and B3, stayed relatively stable during exponential growth and decreased to around 4 fmol cell^{-} when the cultures entered stationary phase. During stationary phase in B2 and B3, total measured DMSP was statistically higher, however this was not reflected in the production per cell. No difference was identified between dissolved DMSP values relative to pCO_2.

Table 13. Comparison of statistical p-values for DMS and DMSP, with highlighted values indicating significance of elevated pCO_2.

Experiment	B1	B2	B3	S1	S2
DMS (nmol L^{-1})	0.064 Lower	0.221	0.334	0.03 Higher	0.817
DMS (fmol $cell^{-1}$)	0.02 Lower	0.676	0.515	0.09	0.525
Total DMSP (nmol L^{-1})	-	0.001 Higher	0.001 Higher	0.123	0.244
Total DMSP (fmol $cell^{-1}$)	-	0.689	0.305	0.049 Higher, no clear trend	0.174
Particulate DMSP (nmol L^{-1})	-	0.002 Higher	0.153	0.175	0.404
Particulate DMSP (fmol $cell^{-1}$)	-	0.443	0.35	0.046 Higher, No clear Trend	0.31
Dissolved DMSP (nmol L^{-1})	-	-	0.663	0.276	0.114
Dissolved DMSP (fmol $cell^{-1}$)	-	-	0.845	0.71	0.23

5.5.2. Effect of elevated pCO_2 on DMS and DMSP during S1 and S2

During experiment S1, total DMS production was found to be statistically higher in the elevated pCO_2 treatment than the control, but this is not reflected in the DMS production per cell, nor in experiment S2. Figure 21 shows that inoculation 3 produced 1.7 times as much DMS in the CO_2 treatment than the air control, and this is reflected in the DMS per cell for that period.

In contrast to the batch experiments, measured DMSP (total or particulate) did not show any significant effect of elevated pCO_2 in either S1 or S2. DMSP per cell was statistically higher in S1 at 95% confidence, though there was a high degree of variation (Figure 22 and Figure 23) and this result was not replicated in S2. During the second semi-continuous experiment, DMSP total samples were taken in triplicate for each flask on each day to try and remove some of the variation seen in Figure 22b. While the standard deviation between samples and replicates within this experiment was reduced by the additional sampling, there was still a high level of variation within the DMSP total and particulate concentrations. These differences identified by statistics in the DMSP total and particulate were not apparent in the DMS or dissolved DMSP datasets.

Concentrations for DMS and DMSP during S1 and S2 remained within the same ranges (0 – 0.6 fmol $cell^{-1}$ DMS and 2-8 fmol $cell^{-1}$ DMSP total), and these concentrations compare with those identified in the batch experiments and in other investigations in the literature.

5.5.3. DMS and DMSP in other *E.huxleyi* cultures under elevated pCO_2

Despite the number of laboratory experiments on *E. huxleyi* and the effects of increased CO_2 on its growth rates (e.g. Bach *et al.* 2013; Barcelos e Ramos *et al.* 2010; Iglesias-Rodriguez *et al.* 2008; Langer *et al.* 2009), very few have included the measurement of DMS(P). Of those that have, only two studied the effect of elevated pCO_2 on DMSP (Avgoustidi, 2006; Wuori, 2012) and only Avgoustidi (2006) studied DMS production at the same time. There are also two studies investigating the combined effect of temperature and pCO_2 on DMSP production (Arnold *et al.*, 2013; Spielmeyer and Pohnert, 2012), and only one of those measured DMS during the investigation, and then only on a limited basis (Arnold *et al.*, 2013).

The batch experiments performed by Avgoustidi (2006) showed varying results for DMS and DMSP when comparing a pCO_2 of 760 µatm and an air control, with cultures continuously bubbled with pre-prepared gas mixtures at a rate of 5 mL min^{-1}. Of those three batch experiments which were only under elevated pCO_2 for the first 3 days, one showed no overall change in DMS or DMSP production, the second showed lowered DMS but no change in DMSP, and the third no change in DMSP but decreased DMS per cell in stationary phase. These three batch experiments showed very similar results and with much less variation between experiments. This same replicability of data was shown in the semi-continuous experiments, and the overall result was one of no change in DMS or DMSP production. A major factor in the variation in the Avgoustidi (2006) results was likely due to the bubbling of the cultures to maintain CO_2, albeit at a low flow rate, which may have had an effect on culture growth (Shi *et*

al., 2009) and DMS loss to the air. For this reason, the experiments in the current series used pre-prepared media and were not subject to bubbling.

Marine bacteria are responsible for a large proportion of DMSP breakdown, for example Howard *et al.* (2011) suggest that over half the bacterial cells in ocean surface waters were capable of demethylation of DMSP. The cultures used here were treated with antibiotics before the experiments began which substantially reduced bacterial numbers, DAPI testing of samples did show the presence of bacteria within the cultures at the end of the experiments. It is difficult to obtain and maintain a truly axenic culture, especially in a system that is opened daily for sampling.

Zimmer-Faust *et al.* (1996) found that bacterial cells with DMSP lyase are able to use chemotaxis to move towards sources of DMSP, but genetically similar bacteria without DMSP-lyase are not attracted to DMSP. This implies that DMS production is enhanced by DMSP release into the dissolved phase. As previously discussed, $DMSP_D$ concentrations were very low within the cultures.

Wolfe & Steinke (1996) proposed that DMSP and DMSP lyase are segregated within the cells and only come into contact upon cell death or damage. As there is no grazing within the laboratory cultures, the main method of DMSP coming into contact with DMSP lyase is through cell senescence, and this is reflected in DMS concentrations starting low and increasing throughout the growth periods. This might also explain why dissolved DMSP concentrations are very low, as the semi-continuous culture was designed to lower the likelihood of cell lysis. *E. huxleyi* often has a very long stationary phase prior to cell lysis, which reduces the release of significant concentrations of DMSP into the culture medium. If elevated pCO_2 had an effect on DMSP-Lyase activity, it would have shown up as differential production of DMS between the two treatments, and this was not the case.

5.5.4. DMS and DMSP in *E. huxleyi* RCC1229 CO_2 enrichment experiments in comparison to the SOPRAN Bergen experiment.

The semi-continuous experiments were designed to run for similar lengths of time as the SOPRAN Bergen mesocosm experiment (Chapter 3). During that 5 week experiment, there was an *E. huxleyi* bloom during the last two weeks, and abundance of *E. huxleyi* cells increased in all mesocosms. Elevated CO_2 had a significant negative effect on *E. huxleyi* cell abundance in the mesocosms, with the highest pCO_2 mesocosms (up to 3000 µatm) showing 90% reduction in cells. DMS increased in association with *E. huxleyi* numbers, with lower concentrations

detected in the higher pCO_2 mesocosms. DMSP also showed lower concentrations under elevated pCO_2, but not following the same pattern of production as *E. huxleyi*. In calculations of DMS and DMSP concentration per *calcified E. huxleyi* cell, as measured by flow cytometry (see Chapter 3 for full discussion), concentrations of both DMS and DMSP per cell were higher in the highest CO_2 mesocosms than the controls. The measured DMS and DMSP trends followed those of previous mesocosm experiments (ie Archer *et al.* 2013; Hopkins *et al.* 2010), and the trends of the halocarbons were within similar ranges (Hopkins, 2010). Further discussion of other mesocosm experiments and the measure trace gas concentrations is given in Chapter 6.

The DMS concentrations detected within all the laboratory experiments in this study were high in comparison to the mesocosm experiment, which is to be expected given that one is natural community production and the other is a concentrated laboratory culture. Table 14 shows the ranges of cell counts, DMSP and DMSP detected in the unialgal experiments and the mesocosm. It should be noted that the flow cytometry for the SOPRAN Bergen experiment would only differentiate calcified *E. huxleyi* cells, so the total *E. huxleyi* cell count might be higher if naked cells could have been distinguished. For this reason, no comparison was made of the DMS/P per cell production from SOPRAN Bergen.

BLANK

Table 14. *E. huxleyi* cell counts, DMS and DMSP concentrations comparing the laboratory experiments and the SOPRAN Bergen mesocosm experiment.

Experiment No	390 µatm CO_2				860 µatm CO_2			
	E. huxleyi cell range (cells mL^{-1})	DMS range (nmol L^{-1})	$DMSP_T$ range (nmol L^{-1})	$DMSP_P$ range (nmol L^{-1})	*E. huxleyi* cell range (cells mL^{-1})	DMS range (nmol L^{-1})	$DMSP_T$ range (nmol L^{-1})	$DMSP_P$ range (nmol L^{-1})
B3	38066 - 2578000	2.74 – 586.78	427.36 – 7413.30	529.02 – 4009.15	42924 - 2722000	3.93 – 496.46	428.35 – 8998.16	439.46 – 4624.43
S1	134000 - 1486000	44.8 – 416.9	294.6 – 7817.0	587.0 – 7347.1	124000 - 1554000	55.0 – 559.2	447.6 – 9588.7	632.2 – 8348.0
S2	87439 - 1355000	6.5 – 345.8	109.8 – 6233.6	321.3 – 5158.6	60598 - 1254000	11.5 – 366.6	144.1 – 6062.3	217.0 – 5432.1
SOPRAN Bergen* M6 (390 µatm) M1 (840 µatm)	81 - 2004	0.4 – 4.9	21.1 - 67.4	12.0 - 53.2	58 - 1393	0.1 – 2.4	20.3 - 81.9	15.0 - 81.5

*** Data from SOPRAN Bergen taken from two mesocosms at the relevant pCO_2 to this experiment.**

BLANK

During the SOPRAN Bergen experiment, no difference was seen between CO_2 treatments in terms of the DMS and DMSP concentrations until after the initial natural bloom when nutrients were depleted (after T12). In contrast, Experiments S1 and S2 where nutrient limitation did not occur, no noticeable change in DMS or DMSP production was identified after 12 days, and the extended period of exposure to elevated pCO_2 did not cause any form of gradual change in DMS/P production.

5.6. Effects of elevated pCO_2 on halocarbon production from *E. huxleyi* RCC1229

Halocarbon samples were analysed during B2. The results showed no evidence of halocarbon production from *E. huxleyi* RCC1229 as all halocarbons concentrations apart from CH_2ClI remained close to the detection limit of the analytical system (GC-MS, Chapter 2 Section 3). Halocarbon analyses were conducted twice, before and after the exponential growth phase, and CH_2ClI showed a slight but non-significant increase in concentration during this period, indicating no overall production.

Differences in the measured halocarbon concentrations were observed between the air and CO_2 treatments on T0. These differences are likely as a result of differences in the purge efficiency of the two different sparge towers used to prepare the media for the experiment. Different halocarbon compounds have varying purge efficiencies, and at the relatively low flow rate of sparging for CO_2 addition to the medium, any inherent differences between the two frits could show up as differences in halocarbon concentration, especially at these very low concentrations. As the main purpose of the experiment was to establish the differences in concentration and production between air and CO_2 treatments, no tests were performed on the halocarbon concentrations in the media prior to culture inoculation.

Decreasing halocarbon concentrations in the media were observed over the course of the experiment. This is attributed to the off-gassing of these compounds into the headspace of the flasks, followed by their removal from the headspace during the daily headspace flushings. Taking this effect of the media preparation into account, it is clear there is no effect of increased CO_2 on the production of these compounds.

The results are consistent with those of Manley & De La Cuesta (1997), who detected zero production of CH_3I from a culture of *E. huxleyi* CCMP370 through exponential growth and into the stationary phase. *E. huxleyi* CCMP373 was found to produce both CH_3Br and CH_3Cl, mainly during stationary phase, and this was unaffected by the presence of marine bacteria (Scarratt and Moore, 1998). Wong *et al.* (2002) also found that *E. huxleyi* CCMP373 was the least

efficient of six phytoplankton species in converting iodate to iodide, which may explain the low concentrations of methyl iodide detected.

No further laboratory experiments were identified in the literature which had tested the production of CH_2ClI, CH_2I_2, C_2H_5I, CH_2Br_2 or $CHBr_2Cl$. *E. huxleyi* CCMP371 was found to emit bromoform (0.0020 pmol L^{-1} μg^{-1} Chl-*a*) and other brominated and chlorinated compounds (Colomb *et al.*, 2008), however methyl iodide production was undetectable.

Chapter 5. SOPRAN 2 Mesocosm Experiment, Tvärminne, Finland: Evaluating the effects of elevated pCO_2 on trace gas production in a cyanobacteria-dominated low nitrate community

1. Overview of the SOPRAN Tvärminne mesocosm experiment

The Baltic Sea is a unique environment: the largest body of brackish water in the world experiences extreme temperature differences in surface waters between winter and summer (0-20°C), and makes a challenging environment for organisms to survive. A permanent halocline at 50-80m separates CO_2–rich saline bottom waters and fresher surface waters, and in summertime a thermocline at 20m separates warmer surface waters from those below 4°C (Janssen *et al.*, 1999). Upwelling of these bottom waters is a common summer occurrence, replenishing the surface nutrients while simultaneously lowering surface temperature and pH to a minimum of 7.4 (Brutemark *et al.*, 2011). Due to this, it has been suggested that the Baltic Sea can act as a natural analogue for ocean acidification, and that species will be adapted to lowered pH. This aspect of the investigation will also be considered.

This large-scale mesocosm experiment was undertaken at Tvärminne Zoological Station, Finland, to investigate the effects of elevated pCO_2 and associated lowered pH on the microbial community, particularly on a number of heterocystous, colony-forming cyanobacterial species known to flourish in the Baltic Sea in summer. Studies on the global diazotrophic cyanobacterium *Trichodesmium* spp. have shown increased nitrogen fixation under elevated pCO_2 in the laboratory (Barcelos e Ramos *et al.*, 2007; Hutchins *et al.*, 2007), but the Baltic Sea cyanobacterium *Nodularia spumigena* reduced nitrogen fixation as pCO_2 increased (Czerny *et al.*, 2009). Nitrogen fixation from cyanobacteria in the Baltic Sea was responsible for 20-40% of the nitrogen loading of the region (Larsson *et al.*, 2001), and changes in N_2-fixation could significantly affect atmospheric nitrogen chemistry across Northern Europe (Grennfelt, 1992).

Studies on DMS and halocarbons within the Baltic Sea are limited, and there is no available literature on DMSP concentrations. Halocarbon production has been shown from cyanobacteria (Karlsson *et al.*, 2008) and macroalgae (Abrahamsson *et al.*, 2003), but no

previous studies have evaluated trace gas concentrations under ocean acidification. To this end, the following research questions were posed:

- What were the changes in DMS and DMSP in relation to changes to microbial community structure in a mesocosm experiment focussed on the growth of nitrogen fixing cyanobacteria under the effects of elevated pCO_2?
- Did DMS and DMSP concentrations show inverse relationship with increasing pCO_2 as in previous high pCO_2 experiments (SOPRAN Bergen; Archer *et al.*, 2013)?
- What were the changes in iodocarbon and bromocarbon concentrations in a heterocystous cyanobacteria-dominated microbial community, and were concentrations affected by changes to pCO_2 as in previous experiments (Hopkins et al., 2013)?
- Is the Baltic Sea a suitable location for a new natural laboratory for ocean acidification studies, and how is the community within the Baltic Sea likely to change as global acidification progresses?

This experimental setup was similar to SOPRAN Bergen, but the community composition was expected to be significantly different. Methods of analysis of trace gases were intended to be as close as possible to allow for direct comparison of SOPRAN Tvärminne and SOPRAN Bergen, and to highlight the similarities and differences in gas concentration previously unrecorded between the Baltic Sea and the North Sea.

1.1. Physical oceanography in the Baltic Sea

The Baltic Sea is a semi-enclosed brackish body of water (ca 422,000 km^2, mean depth 55 m) characterised by pronounced temperature and salinity stratification. In the Baltic Sea, a high influx of riverine freshwater from Russia and the Baltic States is countered by limited inflow and mixing of seawater through the Kattegat from the North Sea. Surface waters show a salinity gradient of 1 in the innermost Gulf of Finland through to 15 in the Belt Sea leading to the Kattegat (Baltic Sea Portal, 2014). Deep waters underneath the permanent halocline at 60-80 m are between 14-18 in the Arkona Basin near Kiel, and 7-9 in the Gulf of Finland. The basin is non-tidal with a maximum depth of 450 m. The entire Baltic Sea shows strong seasonal temperature variation with a summer thermocline at 15-20 m and temperatures below the halocline stable at 4-6°C year-round (Janssen *et al.*, 1999).

Nutrient loading in the Baltic Sea from the large catchment area and associated human activities has caused significant nuisance phytoplankton blooms, and is now regulated by both

the EU Water Framework Directive and the Convention on the Protection of the Marine Environment of the Baltic Sea Area (Helsinki Convention; HELCOM, 2014). Significant changes to catchment management within the past 20 years have reduced nutrient input to the Baltic Sea, and to the further growth of nuisance species, which include cyanobacteria.

The major pathways of nutrient input into the sea are from river waters, atmospheric deposition, waterborne discharges from coastal point or diffuse sources, and discharges from shipping. St Petersburg has been identified as a major point source of nutrient loading via the River Neva. In general terms, N concentrations originate from riverine and atmospheric sources, and P from riverine sources and anoxic sediments (Sandén and Rahm, 1993). Overall, nutrient inputs to the Baltic Sea have decreased since the late 1980s after the agreements reached in the Helsinki Convention (1974). However, an assessment report in 2013 established that the entire Baltic Sea is still affected by eutrophication, despite the measures taken to reduce external inputs of nitrogen and phosphorus (HELCOM, 2014).

1.2. Microbial community composition and development

Typically, a large phytoplankton bloom occurs in spring throughout the Baltic Sea, comprised mainly of diatoms and dinoflagellates, with the principle species being *Achnanthes taeniata*, *Skeletonema costatum* and *Chaetoceros* spp. (Kivi *et al.*, 1993). Post-spring-bloom, the low DIN:DIP ratio, higher temperatures and higher light intensities encourage the growth of nitrogen-fixing cyanobacteria (Niemisto *et al.*, 1989; Raateoja *et al.*, 2011), primarily *Aphanizomenon flos-aquae*, *Nodularia spumigena* and *Anabaena* spp., particularly during July and August in preference to nitrate-dependent species (Finni *et al.*, 2001; Kononen *et al.*, 1996). Nitrogen fixation rates of up to up to 5.9 mmol N m^{-2} d^{-1} were averaged over the entire Baltic Sea (Larsson *et al.*, 2001; Wasmund *et al.*, 2001), with estimated annual fixation at up to 430 Gg N yr^{-1} and contributing 20-40 % of the nitrogen loading to the Baltic Sea (Larsson *et al.*, 2001). Also present in the blooms are non-nitrogen-fixing picocyanobacteria (*Synechococcus* spp.*;* Stal *et al.*, 2003 and *Coelospaerium* spp. Suikkanen *et al*., 2007).

Heterocystous diazotrophic cyanobacteria are filamentous, colony-forming organisms, possessing buoyant gas vesicles and can float up to 22 m per day (Walsby *et al.*, 1995, 1997). During calm conditions, large-scale surface accumulations of *A. flos-aquae* and *N. spumigena* occur throughout the Baltic Sea in a spatially patchy distribution (Niemisto *et al.*, 1989; Stal *et al.*, 2003), but disperse into surface waters above the halocline during mixing events. These surface aggregations occur in the Baltic Sea due to relatively calm, sheltered conditions and no tidal forcing. Accumulations of *N. spumigena* have been linked to the production of the

hepatotoxin nodularin, harming higher ecosystem levels as well as humans and domestic animals (Sivonen *et al.*, 1989). Although *A. flos-aquae* was identified as having low toxicity (Sivonen *et al.*, 1990) extensive aggregations are a nuisance in and around coastal areas, producing odours and high volumes of decomposing biomass, and thus decrease the recreational value of the environment (Plinski and Codd, 1998).

In addition to the filamentous and colonial cyanobacteria, the late summer community also typically contains several species of cryptophytes, dinoflagellates, chrysophytes, euglenophytes and chlorophytes (Kononen, 1988). In a review of seasonal monitoring data in the Northern Baltic Sea Proper (Suikkanen *et al.*, 2013), surface water temperature increased by 3 - 5°C from 1979 to 2011, and was the primary environmental driver of long-term changes to phytoplankton communities, with salinity decrease and inorganic nutrient loading of secondary importance. During this 30-year period, changes in the community structure included increases in Cyanophyceae, Prymnesiophyceae and Chrysophyceae, alongside decreases in Cryptophyceae and total zooplankton (Suikkanen *et al.*, 2013).

1.3. Concentrations of DMS and DMSP in the Baltic Sea

Leck *et al.* (1990) measured DMS concentrations in the range 0.03 – 3.23 nmol L^{-1} within 200 km of Tvärminne Station from January 1987 until July 1988. Clear maxima in DMS concentrations were identified in summer (July-August), with minimum DMS recorded in winter (December-January). During the summertime, *A. flos-aquae* significantly increased in abundance, up to 27% of the total biomass, alongside several dinoflagellate species. Further measurements in July 1988 by Leck and Rodhe (1991) found DMS within the range 0.4 – 3.63 nmol L^{-1}, with an estimated sulphur flux of up to 2.74 µmol S m^{-2} d^{-1}. During that study, the only measured parameter showing a correlation with DMS was the Prymnesiophyte *Chrysochromulina* spp. In samples taken throughout 2008 in the southern Baltic Sea Proper, DMS was measured in the range 0.3 to over 100 nmol L^{-1}, with maximum peaks during the spring bloom and July and August (Orlikowska and Schulz-Bull, 2009). Monthly measurements of DMSP in the southern Baltic Sea have been measured since 2008 by GEOMAR in Kiel, yet the data have not been published. The measurements of DMS and DMSP in Baltic Sea waters outside the mesocosms will add to the global database of DMS measurements.

1.4. Concentrations of halocarbons in the Baltic Sea

Concentrations of a large number of halocarbons were made during a cyanobacterial bloom in 2004 (Karlsson *et al.*, 2008), and in a mid-term time-series in the Southern Baltic Sea Proper

(Orlikowska and Schulz-Bull, 2009). In addition, a number of measurements of iodocarbons were made within the Skagerrak in 1990 (Klick and Abrahamsson, 1992). These studies have been summarised in Table 1, and represent the extent of available data on halocarbon production in the Baltic Sea.

Table 1. Mean concentrations of halocarbons measured within the Baltic Sea from the literature.

Compound	Baltic Proper Cruise 2004 (Karlsson *et al.*, 2008)	Skagerrak Coastal sites 1990 (Klick and Abrahamsson, 1992)	Southern Baltic Proper 2008 (Orlikowska and Schulz-Bull, 2009)
	Mean (pmol L^{-1})	Range (Jan – Nov; pmol L^{-1})	
CH_3I	4.7	-	1 – 16
CH_2I_2	-	48	0 – 85
C_2H_5I	1.1	-	0.4 – 1.2
CH_2ClI	29	7.1	5 - 50
$CHBr_3$	45	46	5 – 40
CH_2Br_2	8.0	-	2 – 10
$CHBr_2Cl$	3.2	-	0.8 – 2.5

The cyanophyceae *Pseudanabaena limnetica* was found to have the highest biomass in the bloom during a Baltic Sea cruise in 2004 (Karlsson *et al.*, 2008), and was identified as the major halocarbon source. Studies in the Skagerrak (Klick, 1992; Klick and Abrahamsson, 1992) showed that CH_2I_2 and CH_2ClI dominated the iodocarbon pool, with $CHBr_3$ concentrations corresponding to those found by Karlsson *et al.* (2008) (40-60 pmol L^{-1}). Further measurements of bromocarbons at the coastal site in the Skagerrak gave maximal values of $CHBr_3$ at nearly 3000 pmol L^{-1} and CH_2Br_2 at 86 pmol L^{-1} (annual mean 18 pmol L^{-1} and 2 pmol L^{-1} respectively) with clear seasonal variation in CH_2Br_2 concentrations with maxima in August (Klick, 1992). Measurements of halocarbons in the Southern Baltic Proper by Orlikowska and Schulz-Bull (2009) (Table 1) showed higher concentrations of C_2H_5I and CH_3I also occurred in late Summer. Significant concentrations of CH_2Br_2 and $CHBr_3$ were also identified from *Trichodesmium* spp. in the Arabian Sea (Roy *et al.*, 2011), and it is suggested that high concentrations of halocarbons will be detected in the Baltic Sea during a cyanobacterial bloom.

2. Design, setup and operation of SOPRAN Tvärminne 2012

2.1. Geographic location

SOPRAN Tvärminne was based at the Tvärminne Zoological Station (University of Helsinki), near Hanko, Finland, in the northern Baltic Sea Proper and close to the entrances to the Gulf of Finland and the Gulf of Bothnia. No previous mesocosm experiments designed to study elevated pCO_2 have been performed at this station. The mesocosms were deployed approximately 1 mile offshore in Tvärminne Storfjärden (N 59° 51.100', E23° 15.200'), and all sample handling and analyses were performed at the land-based laboratory facilities (Figure 1).

2.1. SOPRAN Tvärminne mesocosm design and deployment

Nine mesocosms were deployed on 10th June 2012, moored in lines of three. The design and framework of the mesocosms was identical to that deployed for SOPRAN Bergen; with the only difference the bag length at 17 m depth compared to the previously deeper 25m. For further information on the mesocosm design and setup, see Chapter 3, Section 2.2.

Prior to closure of the mesocosms, the water column both inside and outside the enclosures showed salinity and temperature stratification, with temperature ranging from 6°C at depth to 12°C at the surface. The mesocosms remained open at top and bottom for 7 days after deployment, and upon closure the bags were immediately mixed by use of an airlift to homogenise the waters and distribute nutrients evenly with depth. After mixing, the CTD showed a non-stratified water column in relation to salinity, temperature and pH. No further mixing took place during the experiment. The mean mesocosm volume, as determined by the addition of saline water as a tracer, was 53949.57 ± 771.77 Kg SW (Czerny *et al.*, 2013).

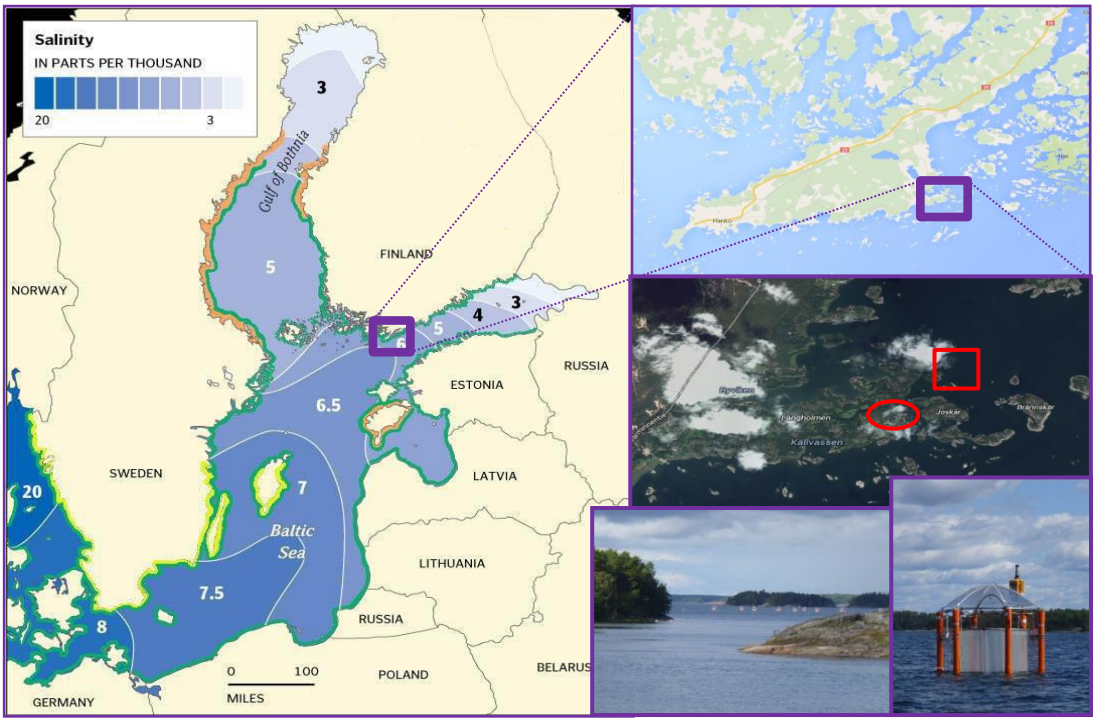

Figure 1. Surface salinity map of the Baltic Sea. Purple squares show the location of the Tvärminne marine station at the entrance to the Gulf of Finland, and the positions of the mesocosms within the Tvärminne archipelago (red square) in Tvärminne Storfjärden, Finland. The red oval is the location of the on-shore laboratory facilities. Inset are photos showing the mesocosm arrangement as seen from the shore, and a single mesocosm after deployment.

2.2. Addition and incorporation of CO_2 into mesocosm waters

CO_2 additions for this experiment were based upon IPCC projections for 2100 (Chapter 1, Section 2.3; Cubasch *et al.*, 2013; Houghton *et al.*, 2001), but did not exceed concentrations of 1400 µatm. Additions of CO_2 enriched waters (see Chapter 3 Section 2.3 and Riebesell *et al.*, 2013) took place after mixing of the mesocosms, over the course of 4 days (T0 to T3) to achieve pCO_2 in the range 390 – 1400 µatm (Table 2).

M1	**M4**	**M7**
340 µatm	X	390 µatm
M2	**M5**	**M8**
X	340 µatm	1400 µatm
M3	**M6**	**M9**
1120 µatm	840 µatm	X

Table 2. pCO_2 and mesocosm arrangement during SOPRAN Tvärminne. X denotes a mesocosm failure.

Control mesocosms (M1 and M5) received no addition of CO_2-enriched water and values shown are the experiment mean. Further enrichment of the surface layers of the mesocosms was performed on T15 to counteract the effect of CO_2 loss to the atmosphere. Equipment failure resulted in the loss of three mesocosms during the experiment (see Section 2.3).

2.3. Summary of mesocosm failures

CTD analysis of M4 and M9 after closure and CO_2 addition showed serious leaks around the flanges of the sediment traps, evidenced by salinity changes detected in the CTD profiles in the bottom of the mesocosms. An attempt was made to reseal these mesocosms, but this was unsuccessful, and these two mesocosms were abandoned for the entire experiment.

Analysis of the data after the completion of the experiment revealed that M2 had a serious leak only identified on T25 but likely present for several days prior to this. Several datasets (including DMS) gave unusual values for this mesocosm after T25, and it was decided to remove M2 from all datasets.

2.4. Measurement of core experiment parameters

Sampling and analysis of core parameters, including those of carbonate chemistry parameters, phytoplankton abundance and determination of pigment concentrations, were identical to the methods performed during the SOPRAN Bergen experiment (Chapter 3, Section 2.4), and all followed standard methods unless stated otherwise (Table 3). Samples for most parameters were taken daily using a depth-integrated water sampler (IWS, Hydrobios, Kiel, Germany) deployed from a small boat. On average, 8 samplers were taken from each mesocosm daily: 4 samplers from the full 0 – 17 m depth of the mesocosms, and 4 from the surface 0 – 10 m. The first samples from each mesocosm were dedicated to trace gas analysis and carbonate chemistry evaluation.

Table 3. Experimental parameters measured during the SOPRAN Tvärminne mesocosm experiment for which the data has been used during this investigation. Given are the methods and the relevant data authors.

Parameter	Method	Water Depth	Author
Light	CTD mounted LI-193 quantum sensor (LI-COR) on	0-17m	Kai Schulz (GEOMAR)
Temperature	CTD (Sun and Sea Technology PT100 temperature sensor)	0-17 m	
Salinity	CTD (ADM 7-pole conductivity cell)	0-17 m	
pH (total scale)	CTD (AMT pH sensor)	0-17 m	
pH (total scale)	Spectrophotometer	0-17 m	
DIC	Coulometric Analysis	0-17 m	
Total Alkalinity	Potentiometric titration	0-17 m	
Chl-*a*	1. CTD (Turner Design CYCLOPS-7) 2. Fluorometry (Turner Designs)	0-10 m 0-17 m	Lennart Bach (GEOMAR)
Nutrients	Liquid waveguide capillary cell linked to segmented flow autoanalyser	0-10 m 0-17 m	Jehane Ouriqua (Southampton Oceanography Centre)
POC and PON	EuroVector Elemental Analyser (EuroEA 3000)	0-10 m 0-17 m	Michael Sswat GEOMAR
POP	Photometric Analysis	0-10 m 0-17 m	
N2 Fixation Rates	(EA/GC) IRMS/ NanoSIMS	0-17 m	Allanah Paul (GEOMAR)
Pigment Analysis	HPLC (reverse-phase high performance liquid chromatography)	0-17 m	Yves Trense (GEOMAR)
Phytoplankton Cell Counts	Flow Cytometry (Becton Dickinson FACSCalibur)	0-10 m	Kate Crawfurd (NIOZ)
Bacterial Production	^{14}C Leucine incorporation	0-17 m	Thomas Hornick (IGB)
DMS	GC-MS	0-10 m	This Study
Halocarbons	GC-MS	0-10 m	
DMSP	GC-FPD	0-10 m	

2.4.1. Evaluation of pH and carbonate chemistry parameters

Samples of water from each mesocosm and the Baltic Sea were subsampled from the Integrated water sampler into 500 mL borosilicate glass bottles with a solid stopper to prevent air bubbles. Sub-samples were analysed using a spectrophotometric method for pH analysis (Clayton and Byrne, 1993) and DIC by Coulometric analysis (Johnson *et al.,* 1985). Additional samples were analysed for total alkalinity by the Gran potentiometric titration, but these were found to be consistently higher than calculated values from the pH and DIC measurements. The difference of 20-25 µmol kg^{-1} was attributed to the presence of coloured dissolved organic material (cDOM) in the mesocosms. This material was found to influence the pH with a proton accepting component and required correction to the pH measurements, but pCO_2 values were unaffected.

Non-integrated pH measurements used the same technique as SOPRAN Bergen, using daily CTD casts equipped with AMT pH sensor with a 1 second response time. These results were corrected using the TA, DIC, temperature and salinity data to calculate pH on the total scale and using linear regression to convert the CTD measurements to the total scale.

2.4.2. Determination of inorganic nutrient concentrations

Homogenisation of water column within the mesocosms prior to the start of the experiment resulted in the remixing of nutrients previously trapped below the stratified layers. Addition of inorganic nutrients would encourage the growth of nitrate-dependent species likely to out-compete the targeted diazotrophic cyanobacteria. The concentrations of inorganic phosphate were monitored daily but did not drop below detection limits and so addition of inorganic phosphate was not required.

As inorganic nutrient concentrations were in the nanomolar range for both nitrate and phosphate, the segmented continuous flow autoanalyser with a 2m liquid waveguide capillary cell (SCFA-LWCC) was used, as developed by Patey *et al.* (2008). Limits of detection for this system were 0.8 nmol L^{-1} PO_4^{3-} and 1.5 nmol L^{-1} NO_2^-/ NO_3^{2-} combined (Patey *et al.*, 2008).

2.4.3. Determination of community structure and composition

Samples for Chl-*a* analysis were taken from an integrated 0 - 10 m sample and were analysed on a Turner AU-10 fluorometer (Welschmeyer, 1994). Photosensitive pigment samples for analysis by HPLC (Barlow *et al.*, 1997) were taken from only the 0 - 17 m integrated water samples and were analysed using CHEMTAX algorithms. Cell abundance was performed using a

Becton Dickinson FACSCalibur flow cytometer from the 0-10 m IWS. These methods were the same as used during SOPRAN Bergen, and further details can be found in Chapter 3 Section 2.4. Microscopic enumeration of phytoplankton, including identification of heterocystous cyanobacterial filaments was performed, but only very preliminary data was available when this report was compiled.

2.5. Measurement of marine biogenic trace gas concentrations

All trace gas samples were taken from an integrated 0 - 10 m sample using the same method as described in Chapter 3 section 2.5. All samples were analysed on GC-MS within 6 hours of collection, using purge and cryotrap techniques. DMSP samples were fixed by the method of Curran *et al.* (1998) modified by Kiene and Slezak (2006; full method described in Chapter 3 Section 2.6) and were returned to UEA for analysis on GC-FPD.

2.6. Evaluation of trace gas concentration sampling error

Three replicate 0 – 10 m integrated samples were taken from two different mesocosms each day for trace gas analysis; these samples enabled the calculation of the standard error for each compound. Over the entire experiment, these analyses were converted into the percentage mean relative standard error (Table 4). These analyses were used only to calculate the standard error, and gave no further differences between mesocosms. The replicated mesocosms were changed daily to prevent any bias through repeated replication of a single mesocosm.

Table 4. Calculated percentage mean relative standard error for all nine compounds for the entire experiment.

Compound	% Mean Relative Standard Error
DMS	6.33
CH_3I	4.62
CH_2I_2	4.98
C_2H_5I	5.61
CH_2ClI	3.64
$CHBr_3$	4.03
CH_2Br_2	5.30
$CHBr_2Cl$	7.20

2.7. Statistics

Minitab Version 16 software was used for statistical analysis. Tests for normality were performed on the data and if the data were found to be non-normal, they were logarithmically transformed. One-way ANOVAs were performed on the data to identify if there were significant differences between pCO_2 treatments, followed by Tukey's tests to identify where the differences occurred. Each phase of the experiment underwent separate ANOVAs. The ANOVAs were performed on each phase of the experiment. Significant relationships between parameters were identified using Spearman's Rank Correlations.

3. Core experimental parameters

Core parameters (temperature, salinity, pH, nutrients, Chl-*a*) were measured daily. An overview of these parameters is given here.

3.1. Temporal variations in temperature

Temperatures in the mesocosms followed the external temperature in the Baltic Sea very closely (Figure 2). The integrated temperature range of the entire experiment was 7.8 - 15.9°C, with a mean of 11.5 (± 2.1) °C. Initial mean integrated temperatures were 9.0°C and increased over Phase 1 to a maximum of 15.9°C on T16 before decreasing to 8.2°C on T31.

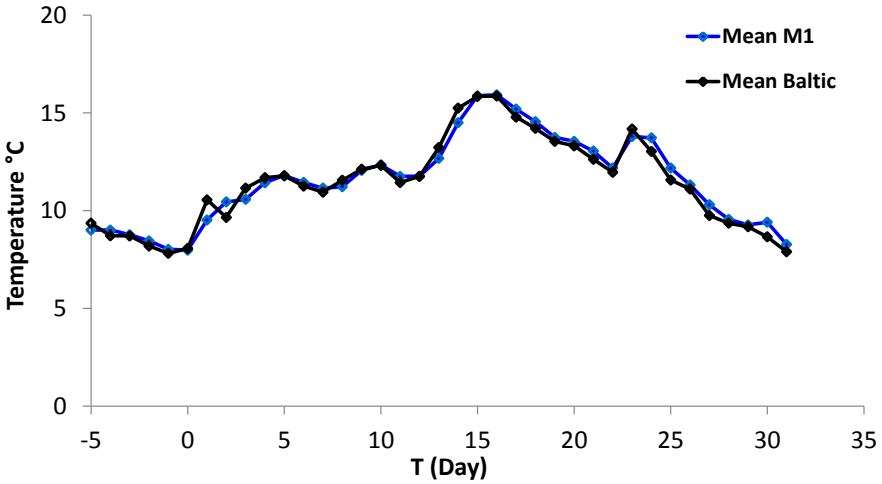

Figure 2. Depth integrated changes in temperature across the course of the SOPRAN Tvärminne mesocosm experiment from M1 (control) and the Baltic Sea, based on the CTD measurements.

a) Baltic Sea

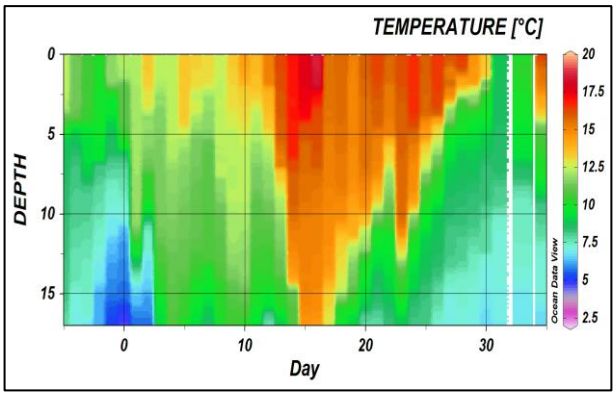

b) M1 (340 µatm)

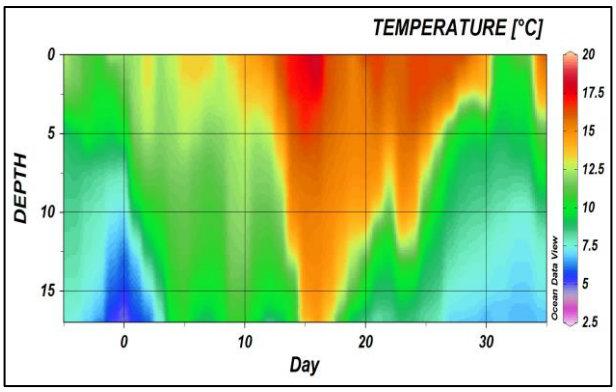

Figure 3. Measured changes to vertical distribution of temperature (°C) with time within a) the Baltic Sea and b) M1 (340 µatm). Profiles from all mesocosms showed strong similarity. Data courtesy of Kai Schulz, Geomar.

Temperatures in the mesocosms followed the Baltic Sea temperatures closely (Figure 3 a and b). Temperature stratification of waters broke down on T15, with temperatures over the full depth of the water column of around 15°C. After T18, the upwelling of colder waters lowered the temperatures to 10°C at the surface and below 7°C at 17 m, a situation which lasted until the end of the experiment. The variation in temperature ranged from 2.5 – 20°C.

3.2. Temporal variations in salinity

Practical salinity (calculated from temperature and conductivity data from the CTD) within the mesocosms showed very little variation at 5.70 (± 0.004) and no changes through depth at any time during the experiment (Figure 4). Salinity within the Baltic Sea ranged from 5.5 to 6.1, but very little stratification was shown in the surface 17 m. Addition of salt to establish mesocosm volume did not take place until after T45 so did not affect salinity. No sign of freshwater input from rainwater was identified in the mesocosms, but 'pulses' of freshwater in the surface waters were detected in the Baltic Sea on T1, T4 and T15.

a) Baltic Sea

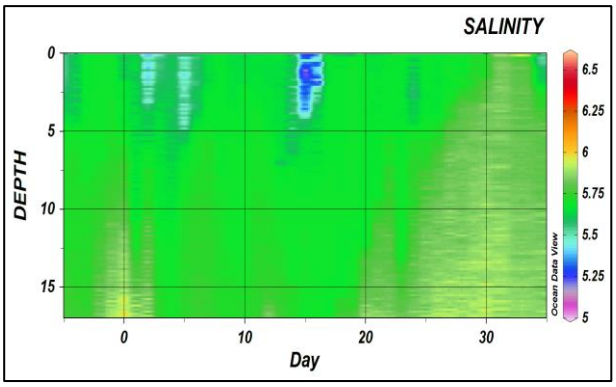

Figure 4. Measured changes to vertical distribution of salinity with time within the Baltic Sea, showing freshwater pulses in the surface and upwelling of higher salinity waters after T20. Data courtesy of Kai Schulz, GEOMAR.

3.3. Changes to pH and carbonate chemistry

Following the additions of CO_2 enriched water to the mesocosms, changes to the carbonate chemistry were evident from T1 (Figure 5 a and b). The highest pCO_2 was measured at 1644.6 µatm (pH of 7.32) in M8 on T3 after the final addition of CO_2 enriched water. Within the control mesocosms, pCO_2 gradually increased from T-3 to T35, from 242.9 - 417.0 µatm (pH of 7.98 to 7.81).

a) pCO_2

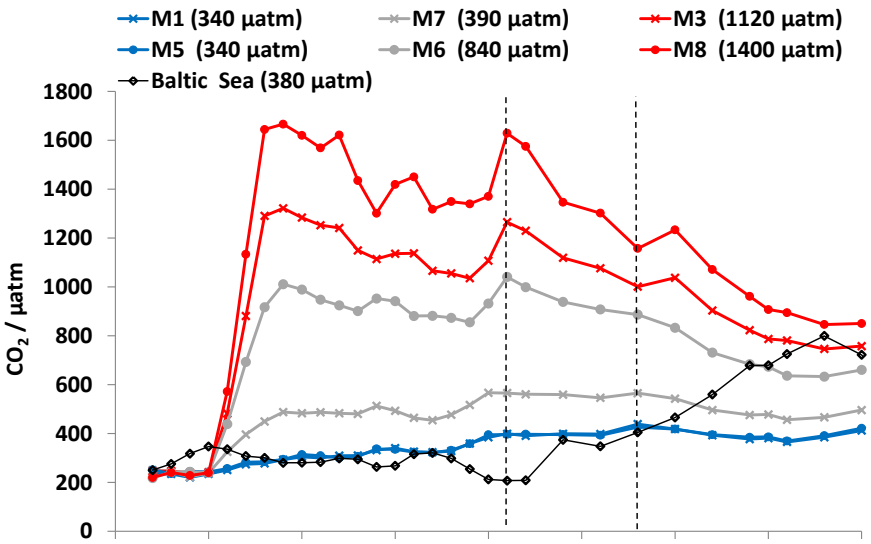

b) pH (total scale)

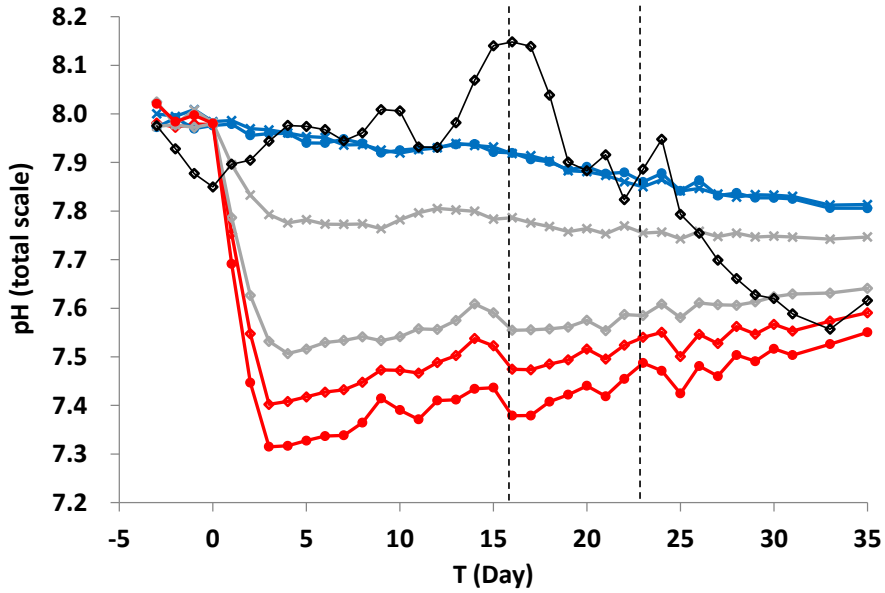

Figure 5. Daily measurements of a) pH (total scale) and b) pCO_2 (µatm) as calculated daily throughout the SOPRAN Tvärminne mesocosm experiment. Dashed lines indicate the three phases of the experiment. Data courtesy of Kai Schulz, GEOMAR.

Seawater pH from the Baltic Sea started at 7.98 (250 µatm pCO_2) and increased to 8.15 (207 µatm pCO_2) on T16 before decreasing after T18 with upwelling of low pH waters to a minimum of 7.56 on T33 (800 µatm; Figure 6a). The addition of further CO_2 enriched waters on T15 can be seen by an increase in CO_2 to 1629 µatm and decrease in pH to 7.38 in M8, and equivalent changes in the non-control mesocosms (Figure 6b, M8).

An overview of the measured mean pCO_2 and pH changes for the whole experiment and three separate phases is shown in Table 5 for the mesocosms and the Baltic Sea. All target pCO_2 were exceeded during the CO_2 enriched water additions, giving final starting pCO_2 as 1666 µatm in M8, 1321 µatm in M3, 1011 µatm in M6 and 487 µatm in M7. The control mesocosms M1 and M5 started at 234 µatm and 251 µatm in M1 and M5 respectively, with no addition of enriched water. CO_2 loss through sea-air exchange and carbon uptake resulted in all mesocosms showing mean pCO_2 below 900 µatm during Phase 3. Due to the second CO_2 additions to the mesocosms, the mean pCO_2 were highest in Phase 2.

a) Baltic Sea

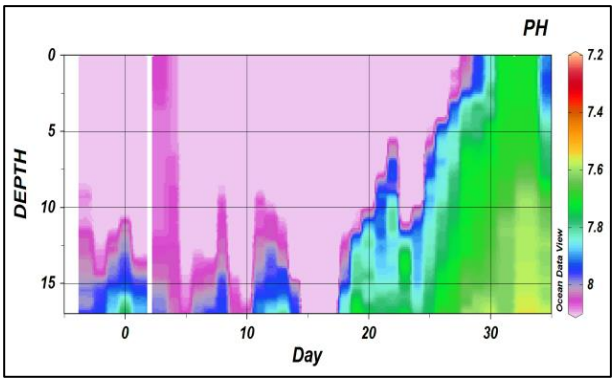

b) M8 (1400 µatm)

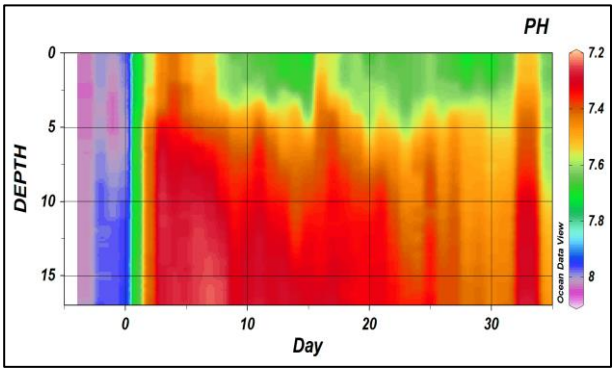

Figure 6. Measured changes to vertical distribution of pH with time within a) the Baltic Sea and b) M8 (1400 µatm). Data courtesy of Kai Schulz, GEOMAR.

Table 5. Summary of pCO_2 and pH (total scale) during the experiment and for each phase of the experiment.

Mesocosm	Target pCO_2 (µatm)	Whole Experiment (T-3 to T35)		Phase 1 (T-3 to T16)		Phase 2 (T16 – T23)		Phase 3 (T23 – T35)	
		Mean pCO_2 (µatm)	Mean pH (pH_T)	Mean pCO_2 (µatm)	Mean pH (pH_T)	Mean pCO_2 (µatm)	Mean pH (pH_T)	Mean pCO_2 (µatm)	Mean pH (pH_T)
M1	Control	335	7.91	301	7.95	405	7.89	396	7.84
M5	Control	339	7.91	306	7.95	401	7.89	399	7.84
M7	390	459	7.80	429	7.83	559	7.77	497	7.75
M6	840	765	7.63	756	7.65	954	7.57	717	7.61
M3	1120	937	7.56	939	7.58	1138	7.50	854	7.55
M8	1400	1146	7.49	1168	7.52	1402	7.42	990	7.49
Baltic Sea	380	377	7.89	285	7.97	308	7.97	629	7.70

3.4. Microbial community development and succession

3.4.1. Temporal development of Chlorophyll-*a* concentrations

The experiment was split into three phases based upon the temporal variation in Chl-*a* and the addition of further CO_2 enriched waters to the surface of the mesocosms (Figure 7). These Phases are defined as:

- Phase 1 T-3 to T16 (19 days): bloom/ production and prior to further CO_2 enrichment
- Phase 2 T16 to T23 (8 days): decreasing Chl-*a* concentrations
- Phase 3 T23 to T 35 (12 days): steady state.

All Chl-*a* data presented were taken from the 0-10 m depth integrated samples. Mixing of the mesocosms prior to T-3 did not trigger a notable increase in Chl-*a* concentrations in Phase 1. During this Phase, Chl-*a* varied around a mean mesocosm concentration of 1.98 (± 0.28) µg L^{-1}. No effect of CO_2 was identified for Chl-*a* during Phase 1 or at any stage of the experiment (F=0.330, p=0.89, DF=119).

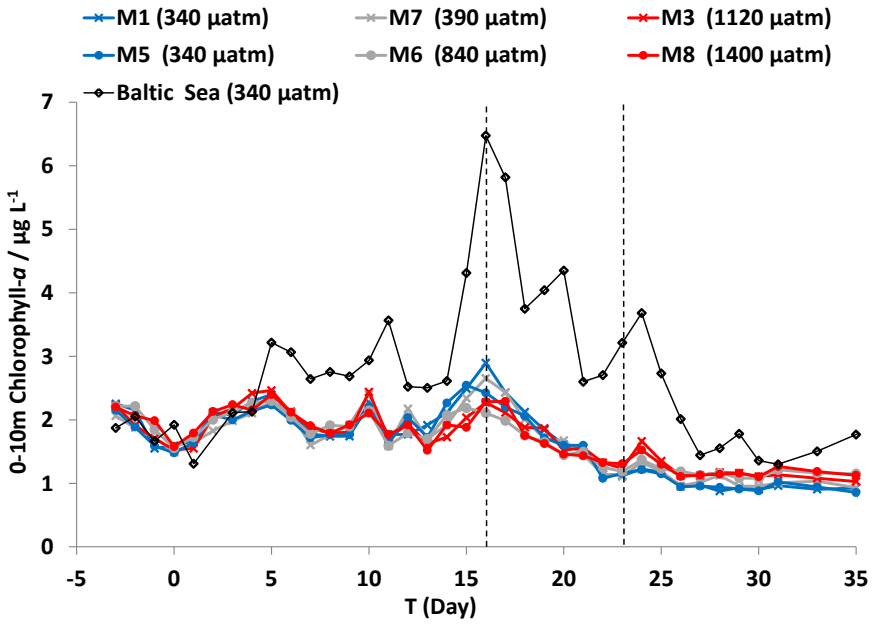

Figure 7. Concentrations of Chl-*a* (µg L^{-1}) measured in the top 10m of all mesocosms and the Baltic Sea. Dotted lines indicate the different phases of the experiment based upon this data. Data courtesy of L. Bach, GEOMAR.

Chl-*a* showed several small peaks in Phase 1 and the mesocosm daily mean varied between 1.48 and 2.54 µg L^{-1} before T16 after which Chl-*a* decreased to a mean of 1.21 µg L^{-1} on T23

(Phase 2). These low concentrations continued until the end of the experiment (steady-state, Phase 3), until the minimum of 1.10 µg L^{-1} on T31.

Baltic Sea Chl-*a* concentrations were similar to the mesocosm Chl-*a* concentrations until T4, after which they remained consistently higher, reaching a maximum of 6.48 µg L^{-1} on T16 (corresponding to the maximum mesocosm peak) before decreasing again. Over the period T15 – T20 Chl-*a* was present in the entire 17 m depth of the water column in the Baltic Sea, but in the mesocosms, the majority of production was in the surface 10m (Figure 8: example mesocosms M1 340 µatm and M8 1400 µatm). The highest Chl-*a* in the mesocosms occurred just above 5 m on T15 and T16, which corresponds to the maximum peak in Chl-*a* in the integrated samples.

a) M1 (340 µatm)

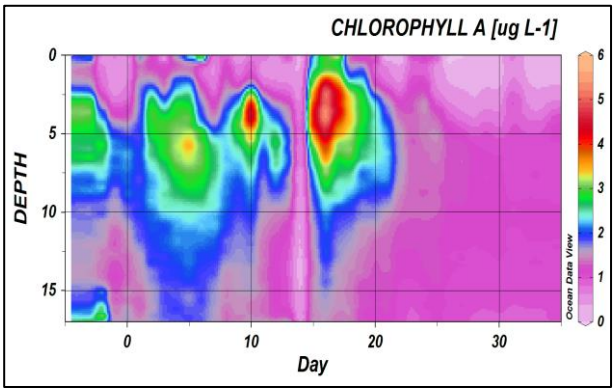

b) M8 (1400 µatm)

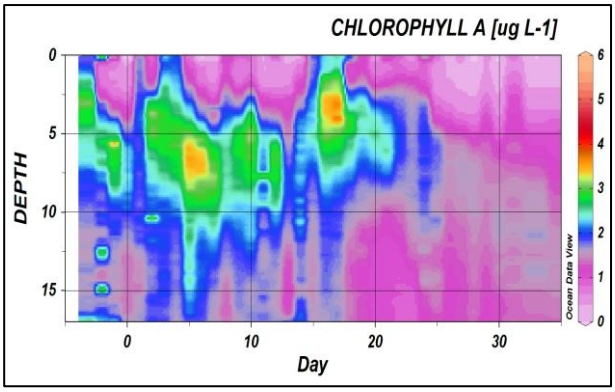

c) Baltic Sea

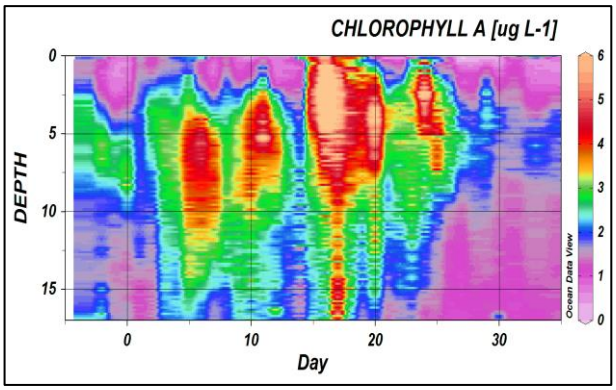

Figure 8. Time-integrated depth profiles of Chl-*a* fluorescence in a) M1 (340 µatm), b) M8 (1400 µatm) and c) the Baltic Sea (380 µatm), measured by CTD. Data courtesy of K. Schulz, GEOMAR.

3.4.2. Changes to inorganic nutrient concentrations

Concentrations of inorganic nitrogen (nitrate and nitrite) increased during the experiment in all mesocosms while inorganic phosphate remained relatively stable (See Figure 9 and Table 6). Concentrations of inorganic nitrate and phosphate measured in the mesocosms were in the nanomolar concentration range, rather than the micromolar range measured during SOPRAN Bergen. Elevated pCO_2 did not affect concentrations of inorganic N, P or NH_3 (Table 6).

Table 6. Mean mesocosm nutrient concentrations in the 0-10m range of the mesocosms and Baltic Sea during the three phases of the experiment, showing the standard deviation in brackets.

Nutrient	Mean concentration Phase 1 (nmol L^{-1})	Mean concentration Phase 2 (nmol L^{-1})	Mean concentration Phase 3 (nmol L^{-1})	Mean Baltic Sea concentration (nmol L^{-1})
Nitrate/ nitrite	22.5 (± 12.7)	35.7 (± 9.9)	50.7 (± 19.4)	32.8 (± 19.5)
Phosphate	121.2 (± 21.8)	127.5.6 (± 17.8)	143.5 (± 21.1)	152.3 (± 94.0)
Ammonium	145.5 (± 185.9)	89.7 (± 134.2)	61.1 (± 61.4)	86.8 (± 94.4)

a) Nitrogen (nitrate/ nitrite) **b) Phosphate**

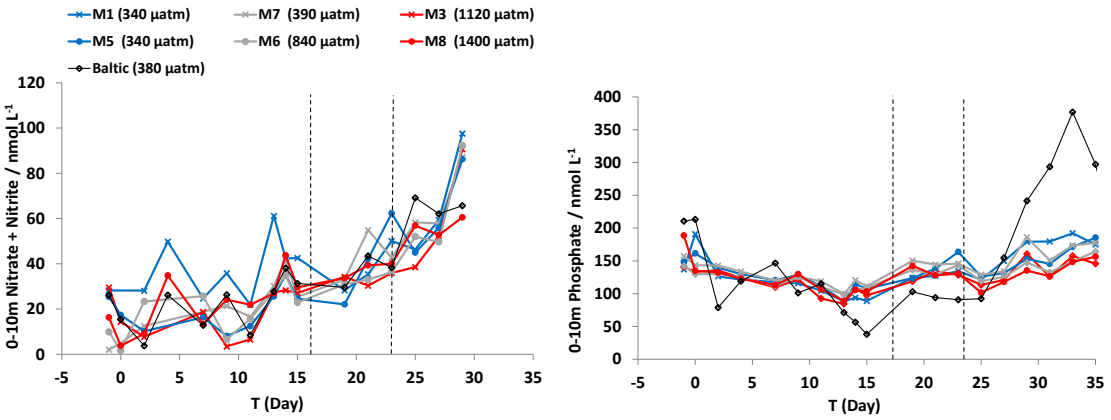

Figure 9. Depth integrated a) nitrogen (nitrite and nitrate µmol L^{-1}) and b) phosphate (µmol L^{-1}) concentrations measured in all mesocosms and the Baltic Sea. Dashed lines indicate the sectioning into three Phases of the experiment. Data courtesy of J. Ouriqua, National Oceanography Centre, UK.

3.4.1. Temporal development of phytoplankton groups as identified by photo-sensitive pigment analysis

Pigment analysis allowed determinations of the concentrations of different phytoplankton groups. Pigments are presented as concentration of equivalent Chl-*a* (µg L^{-1}). The most abundant taxa by equivalent Chl-*a* concentration were chlorophytes and cryptophytes (Figure 10), but identification to major species level within these groups was not performed. The cyanobacteria, as the target organisms for this experiment, contributed only 6.6 % of the total Chl-*a*.

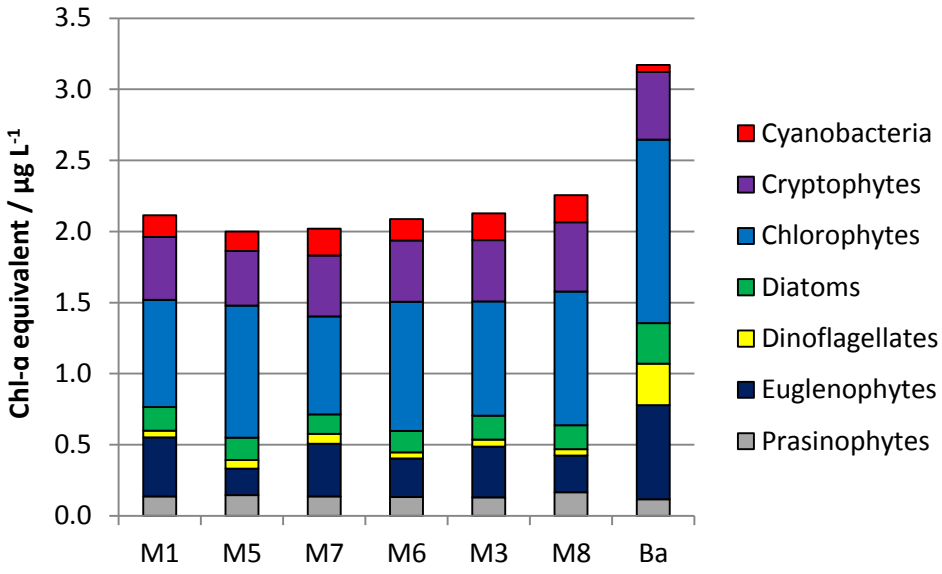

Figure 10. Total Chlorophyll-*a* (µg L^{-1}) showing the breakdown per taxa for each mesocosm and the Baltic Sea. Data courtesy of Yves Trense, GEOMAR.

3.4.2. Community development during Phase 1

Maximum total Chl-*a* concentrations (Figure 11a) were seen during Phase 1, with a mean of 2.32 (± 0.30) µg L^{-1} Chl-*a*, and no significant difference between CO_2 treatments (F=0.72, p=0.607, DF=119). Cyanobacteria and prasinophyte pigments peaked during Phase 1 (T5) (Figure 11b and c) whilst euglenophytes reached their maximum on T13 (Figure 11d). The only effect of CO_2 treatment was identified for the cyanobacteria (F=3.83, p<0.01, DF=64) with significantly higher pigment concentrations in the two highest pCO_2 mesocosms (M8, 1400 µatm and M3, 1120 µatm) compared to M1 (control 340 µatm). Mean cryptophyte equivalent Chl-*a* decreased throughout Phase 1, from 1.11 µg L^{-1} on T-3 to 0.28 µg L^{-1} on T15, but none of the other groupings show peaks in Phase 1.

Temporal phytoplankton growth in the Baltic Sea samples was higher in total Chl-*a* and in all individual groupings except the prasinophytes and cryptophytes.

3.4.2.1. Community development during Phase 2 and Phase 3

Cyanobacteria increased through Phase 2, and by Phase 3 the cyanobacteria equivalent Chl-*a* had reached a mean concentration in all mesocosms of 0.236 (± 0.10) µg L^{-1} compared to the Phase 1 mean of 0.127 (± 0.05) µg L^{-1}. Again in Phase 3 a difference was detected between the control (M5 340 µatm) and the two highest pCO_2 mesocosms (M8, 1400 µatm and M3, 1120 µatm; F=6.27, p<0.01, DF=35). All other groupings show decreases in equivalent Chl-*a* through Phases 2 and 3 and no effects of elevated pCO_2 were identified.

The equivalent Chl-*a* in the Baltic Sea decreased for all taxa during Phases 2 and 3. Cyanobacteria did not display the same increase in abundance as observed within the mesocosms (Figure 11b). Peaks in equivalent Chl-*a* were seen on T15-17 in most taxa, followed by a decrease, except in the cyanobacteria where equivalent Chl-*a* were below the mesocosm concentrations for the whole experiment.

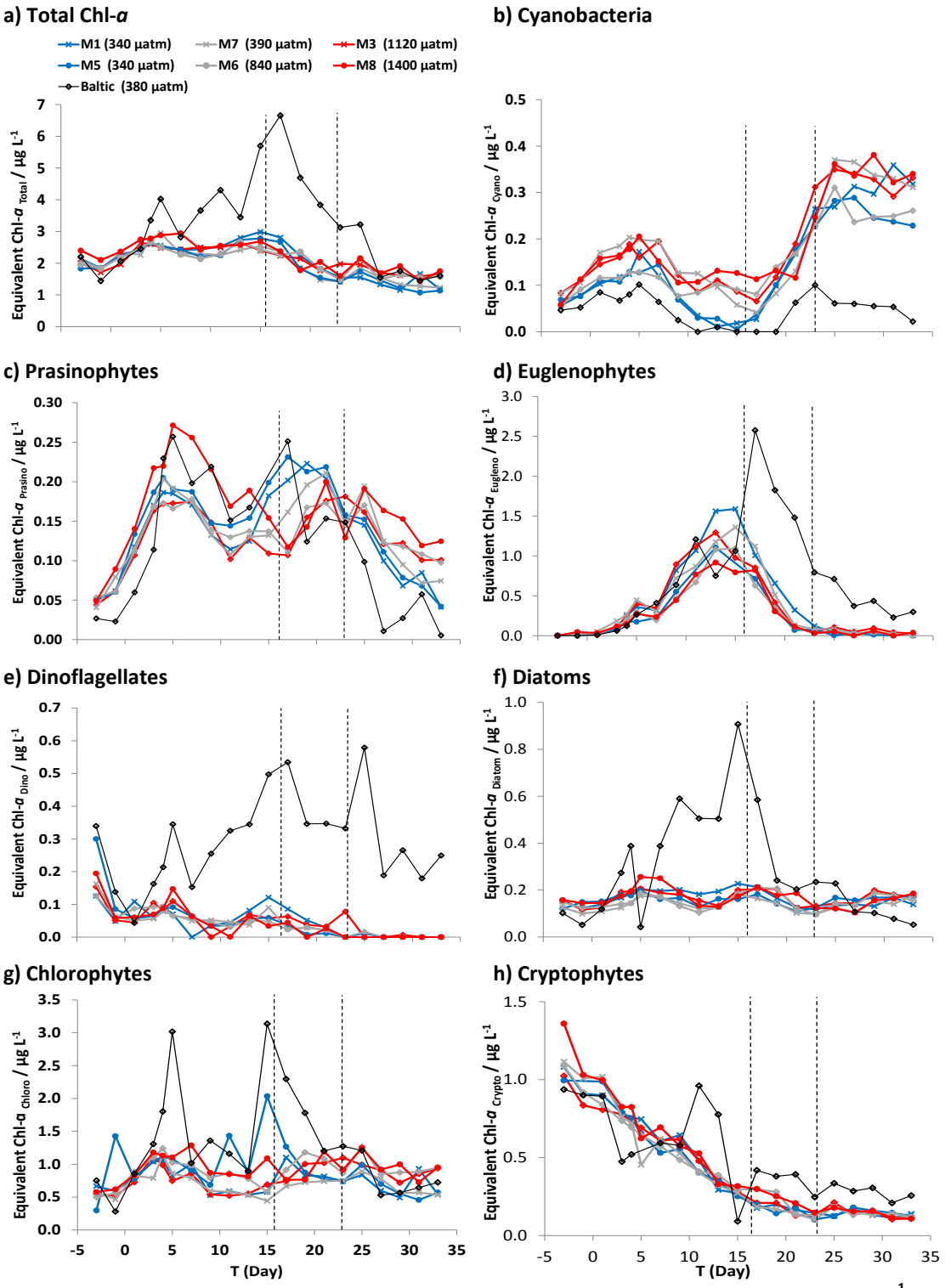

Figure 11. Temporal development of depth-averaged Chl-*a* equivalent concentrations (µg L^{-1}) of a) total equivalent Chl-*a*, within the 0-17m integrated samples, measured by HPLC. Individual Chl-*a* contributions by b) cyanobacteria c) prasinophytes d) euglenophytes e) dinoflagellates f) diatoms g) chlorophytes and h) cryptophytes were calculated using the CHEMTAX algorithm. Dashed lines indicate the sectioning into three Phases of the experiment. Data provided by Yves Trense of GEOMAR, Kiel, Germany.

3.4.3. Temporal development of small phytoplankton abundance (<10 µm)

Flow cytometry was used to identify six different groups of small phytoplankton (<10 µm) (Figure 12): single-celled cyanobacteria, picoeukaryotes and four different groupings of nanoeukaryotes.

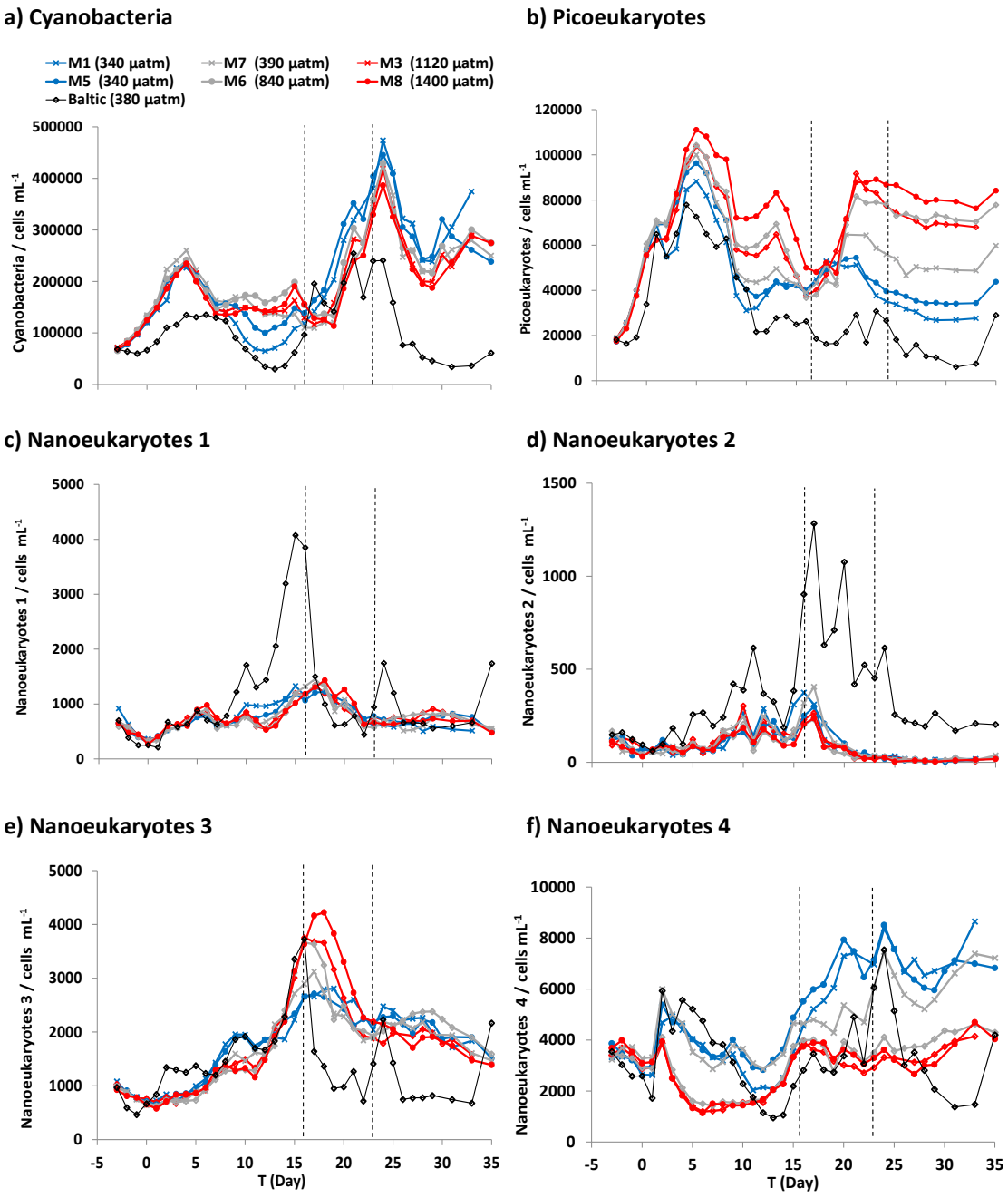

Figure 12. Cell enumeration by flow cytometry (cells mL^{-1}) for a) cyanobacteria, b) picoeukaryotes c) nanoeukaryotes 1 d) nanoeukaryotes 2, e) nanoeukaryotes 3 and f) nanoeukaryotes 4. Dashed lines indicate the sectioning into three Phases of the experiment. Data provided by Kate Crawfurd and Kirsten Kooijman of NIOZ.

3.4.4. Community development during Phase 1

Single-celled cyanobacteria (*Synechococcus* spp. and *Coelosphaerium* spp.) increased in abundance during Phase 1, and peaked on T4 in all mesocosms before decreasing to a minimum on T12. The lowest abundances on this day were observed in the control mesocosms (340 µatm). By the end of Phase 1, all mesocosms again showed similar cyanobacterial abundances. No response to CO_2 was identified, except during T10 and T15 when single-celled cyanobacterial abundance in the control mesocosms dropped, in accordance with the same pattern in the Baltic Sea.

Picoeukaryotes increased from T-3 and peaked on T5, and showed significantly higher abundance under high pCO_2 after T4 ($F=3.57$, $p<0.01$, $DF=71$). Four groups of nanoeukaryotes were identified by flow cytometry (Figure 12 c–f), and all four increased in abundance across the phase. Group 4 (Figure 12 f) showed significantly lower cell numbers in the three highest CO_2 treatments (M6, 840 µatm; M3, 1120 µatm and M8, 1400 µatm; $F=12.89$, $p<0.01$, $DF=112$).

3.4.4.1. Community development during Phase 2 and Phase 3

Cyanobacteria increased during Phase 2 in all mesocosms before peaking on T24 (Figure 12a). Maximum cyanobacterial abundance was 473689 cells mL^{-1} in M1 (340 µatm), but no effect of CO_2 treatment was identified between the control and treatment mesocosms ($F=1.43$, $p=0.220$, $DF=97$).

Picoeukaryotes increased again during Phase 2 (Figure 12b), and showed a strong positive effect of CO_2 treatment. Cell counts remained high through Phase 3, with a mean of 82568 cells mL^{-1} in M8 (1400 µatm) compared to 30865 cells mL^{-1} in M1 (340 µatm; $F=227.99$, $p<0.01$, $DF=58$).

Nanoeukaryote groups 1, 2 and 3 (Figure 12c, d and e) all showed decreasing abundances during Phases 2 and 3, and no differences were identified between CO_2 treatments. Group 4 (Figure 12f) showed a strong negative effect of increasing pCO_2 which was carried through from Phase 1: high pCO_2 treatments showed significantly lower cell abundances compared to the control (340 µatm) and lowest pCO_2 treatment in M7 (390 µatm; $F=94.3$, $p<0.01$, $DF=91$). Table 7 gives a summary of statistical analyses.

Table 7. Summary of the statistical analysis of phytoplankton taxonomy (HPLC pigment analysis) and cell abundance (flow cytometry) for Phase 1, and Phases 2 and 3 combined. Values shown are the F-values after one-way ANOVA on the datasets, and the effect of CO_2 is noted as either a positive or negative effect of increasing pCO_2 on growth at 99% significance. SD: significant difference.

	Phase 1 F-value	Effect of increased pCO_2	Phase 2 and 3 F-value	Effect of increased pCO_2
Phytoplankton Taxonomy (Equivalent Chlorophyll *a* µg L^{-1})				
Cyanobacteria	3.83	Positive	6.27	Positive
Prasinophytes	No SD		No SD	
Dinoflagellates	No SD		No SD	
Diatoms	No SD		No SD	
Chlorophytes	No SD		No SD	
Cryptophytes	No SD		No SD	
Euglenophytes	No SD		No SD	
Total Chlorophyll	No SD		No SD	
Small Phytoplankton (<10 µm) abundance (cells mL^{-1})				
Cyanobacteria	No SD		No SD	
Picoeukaryotes	3.57	Positive	227.99	Positive
Nanoeukaryotes 1	No SD		No SD	
Nanoeukaryotes 2	No SD		No SD	
Nanoeukaryotes 3	No SD		No SD	
Nanoeukaryotes 4	12.89	Negative	94.3	Negative

3.5. Microscopic enumeration of cyanobacteria

The data presented in this section was made available only shortly before this investigation was concluded. It has been included here to allow examination of the filamentous cyanobacterial abundance, but has not been statistically compared to trace gas data. One species of heterocystous colonial (*Aphanizomenon flos-aquae*) and one species of non-heterocystous colonial (*Pseudanabaena* spp.), cyanobacteria were identified in the mesocosms and both have been presented as the total length of colonial filament per litre of seawater sample.

A. Flos-aquae was undetectable in all mesocosms on T-3, and slowly increased in abundance during Phase 1 in all mesocosms (Figure 13a). The highest measured filament length was detected on T27 in M1 (340 µatm). Fluctuations in the measured filament length across the experiment were determined to be due to sampling error and filament break-up in the integrated water samplers. *Pseudanabaena* showed higher abundance during Phase 1 (Figure

13b), with highest abundance at 13966 mm filament L^{-1}, then decreased during Phase 2 to <200 mm filament L^{-1} in all mesocosms after T23.

a) *A. flos-aquae* **b) *Pseudanabaena* spp.**

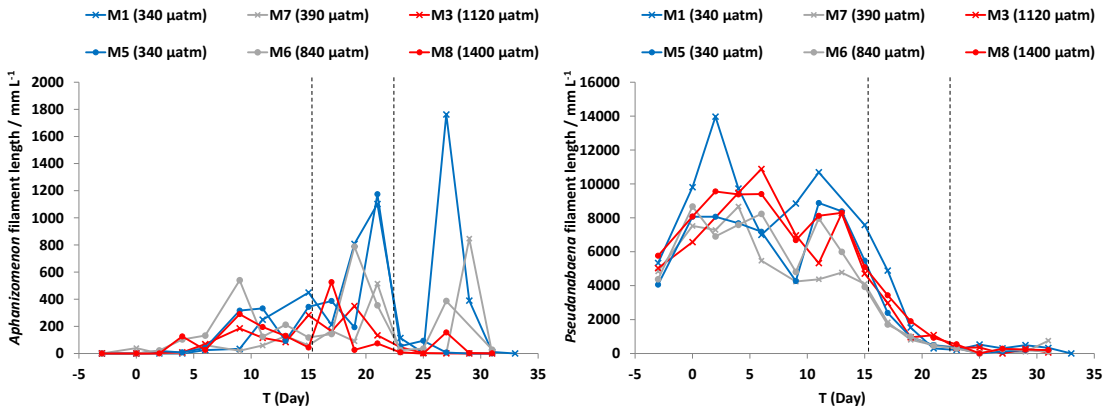

Figure 13. Abundance of heterocystous colonial cyanobacteria *Aphanizomenon flos-aquae* and *Pseudanabaena* spp. in the mesocosms during SOPRAN Tvärminne, measured as filament length in mm per litre. Dashed lines indicate the sectioning into three Phases of the experiment. Data courtesy of A. Stuhr, GEOMAR.

4. Trace gas concentrations

4.1. Dynamics of DMS and DMSP

4.1.1. Measured DMS and DMSP concentrations

DMS concentrations in the mesocosm fell within the range 2.66 – 6.79 nmol L^{-1}, and showed a clear effect of elevated pCO_2 after the start of Phase 2 (Figure 14). No DMSP was detected in any of the samples fixed in the SOPRAN Tvärminne experiment, so no results will be displayed here. This will be discussed further in Section 5.4.1.

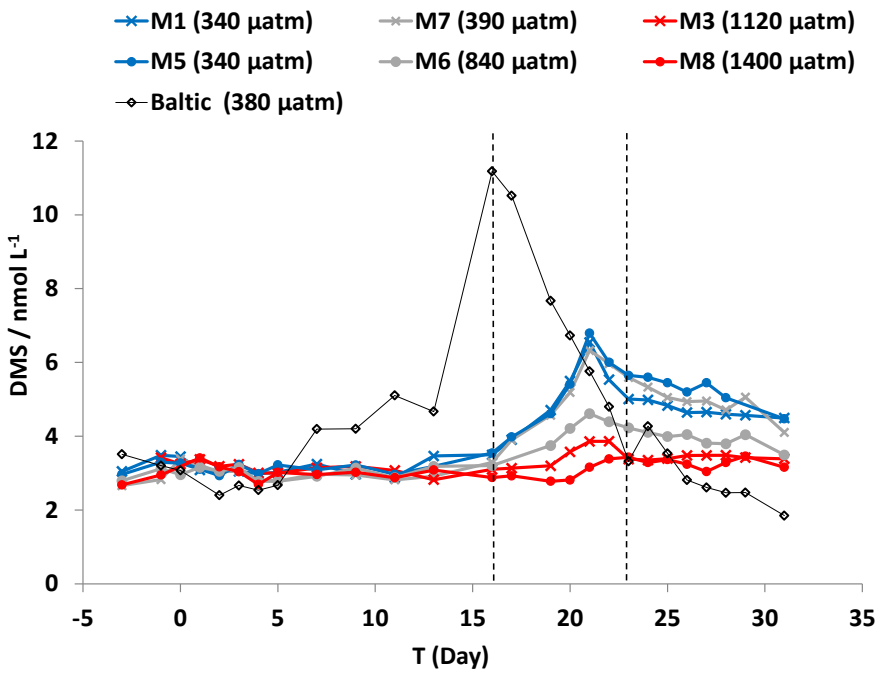

Figure 14. Temporal changes in DMS concentrations (nmol L^{-1}) from all mesocosms and the Baltic Sea during the SOPRAN Tvärminne mesocosm experiment. Dashed lines indicate the sectioning into three Phases of the experiment.

During Phase 1, DMS concentrations remained very similar in all mesocosms, with no significant CO_2 effect on concentrations within the mesocosms. After T16, the DMS concentrations in the control mesocosms started to increase, while those in the high pCO_2 mesocosms (1120 and 1400 µatm) stayed at the same concentration until T19, when a small increase was detected. DMS in the control (340 µatm) mesocosms and two mid-range pCO_2 mesocosms (390 and 840 µatm) peaked on T21 with a maximum of 6.79 nmol L^{-1} in M5. During Phases 2 and 3 (T16 to T31), there was significant difference between CO_2 treatments

(F=31.70, p<0.01, DF=87); DMS concentrations were inversely related to increasing pCO_2 during Phases 2 and 3 (Figure 15; R^2 = 0.96, p<0.01).

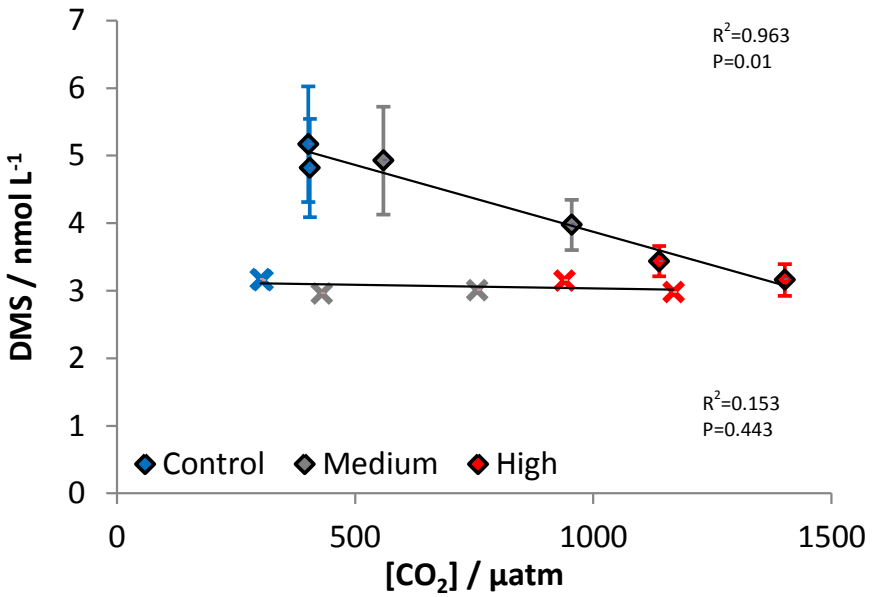

Figure 15. Mean DMS concentrations (nmol L^{-1}) plotted against pCO_2 (µatm) for Phase 1 (crosses; p=0.443) and Phases 2 and 3 combined (diamonds; p<0.01). Error bars show the standard deviation for each mesocosm.

DMS Concentrations in the Baltic Sea were higher than within the mesocosms for the period T6 – T20, with a clear DMS peak on T16 at 11.2 nmol L^{-1}, over 3 times higher than concentrations in the mesocosms. After this day concentrations decreased through Phases 2 and 3 to a minimum value of 1.85 nmol L^{-1} on T31.

4.1.2. DMS correlations with microbial community development

Spearman's Rank Correlation Analysis was used to identify relationships between DMS and biological parameters associated with the microbial community (Table 8). Results from the test range from strong negative correlation (-1), to no correlation (0) to strong positive correlation (1).

Table 8. Spearman's Rank correlation coefficients for DMS compared to Chl-*a*, the phytoplankton taxonomy (from HPLC pigment analysis) and small phytoplankton abundance (from flow cytometry). Coefficients are significant at 99% confidence limits, except those highlighted at only being significant at 95% (*). NC: no correlation between parameters.

	DMS		
	Whole Experiment	Phase 1	Phase 2 and 3
Chl-*a* (µg L^{-1})	-0.604	NC	-0.358
Phytoplankton Taxonomy (Equivalent Chlorophyll µg L^{-1})			
Total Equivalent Chlorophyll	-0.607	NC	-0.434
Cyanobacteria	0.424	NC	NC
Prasinophytes	NC	NC	NC
Euglenophytes	NC	NC	NC
Dinoflagellates	-0.618	NC	NC
Diatoms	-0.243*	NC	-0.475
Chlorophytes	NC	NC	-0.337*
Cryptophytes	-0.695	NC	-0.311*
Small Phytoplankton (<10 µm) abundance (cells mL^{-1})			
Cyanobacteria	0.575	NC	0.531
Picoeukaryotes	-0.256	NC	-0.380
Nanoeukaryotes 1	NC	NC	-0.373
Nanoeukaryotes 2	-0.512	NC	NC
Nanoeukaryotes 3	0.502	NC	NC
Nanoeukaryotes 4	0.603	NC	0.750

4.1.3. DMS and the relationship with Chl-*a*

The ratio of DMS to Chl-*a* (nmol ug^{-1}) was calculated daily for each mesocosm and the mean calculated for the low (340 µatm), medium (390 – 840 µatm) and high (1120 – 1400 µatm) CO_2 treatments (Figure 16). In Phase 1, a small peak was identified in all mesocosms, but indicated a change in Chl-*a* while DMS remained steady. After T16, the ratio began to increase in all mesocosms, with a clear effect of CO_2 treatment as DMS increased but Chl-*a* remained similar in all mesocosms.

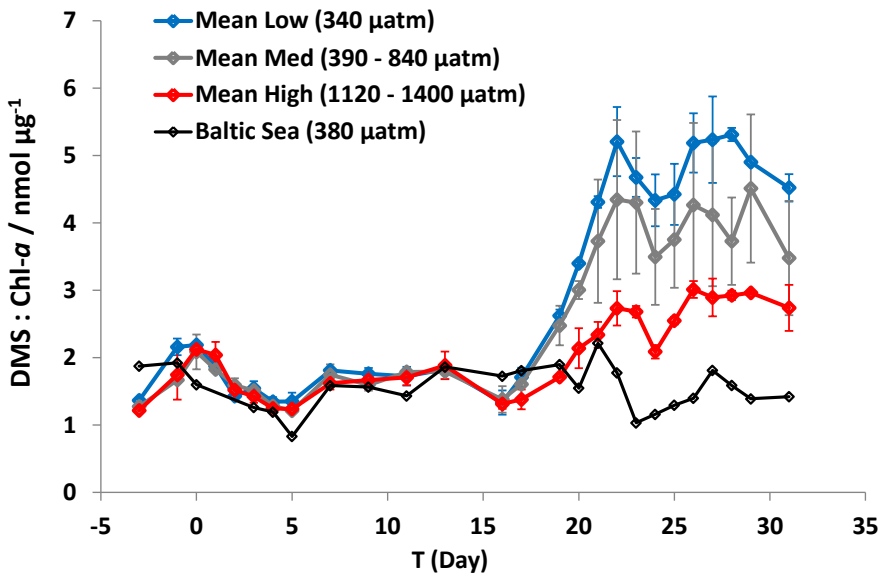

Figure 16. Temporal changes in the ratio between Chl-*a* and DMS for three different pCO_2 conditions: low pCO_2 (340 µatm), medium pCO_2 (390 – 840 µatm) and high pCO_2 (1120 – 1400 µatm). Error bars show standard deviation within the CO_2 ranges.

Across the duration of the whole experiment, DMS was strongly negatively correlated with Chl-*a* (ρ= -0.604, p<0.01; Table 8). Ratios in the Baltic Sea maintained a similar ratio in all Phases (mean 1.55 ± 0.33 nmol μg^{-1}) with a strong negative correlation (ρ= -0.842, p<0.01).

4.1.4. DMS relationships with cyanobacteria and community composition

During Phase 1, DMS showed no correlation with single-celled cyanobacteria abundance, but was highly correlated in Phase 2 and 3 (ρ=0.531, p<0.01). Correlations between DMS and the cyanobacterial equivalent Chl-*a* were correlated for the experiment as a whole (ρ=0.424, p<0.01) but not for the individual Phases (Table 8). Increasing pCO_2 did not have an effect on the ratio between DMS and single-celled cyanobacteria abundance, except for the period T9 – T16 where the ratio was higher under control pCO_2 levels (Figure 17 a). During this period, the cell count in M1 (340 µatm) was significantly lower than the other mesocosms (section 3.4.3, Figure 12). During the period T-3 to T9, the ratio decreased as the cyanobacterial cell abundance increased, while DMS remained at the same concentrations (Figure 17a). The DMS: cyanobacteria ratio fluctuated during Phases 2 and 3 with the changes in both cell abundance and DMS concentration, but no effect of pCO_2 was identified. These variations were not identified in the ratio between DMS and cyanobacteria equivalent Chl-*a* (Figure 17b), aside from the increase over the period T9-T16 of the experiment in M1 (340 µatm). The ratio in the high pCO_2 mesocosms remained stable throughout, suggesting no apparent relationship with

the cyanobacterial equivalent Chl-*a* concentration. This would include all filamentous cyanobacteria as well as the single-celled cyanobacteria identified by flow cytometry. No evaluation was made of the relationship between the filamentous cyanobacterial abundance and DMS concentration.

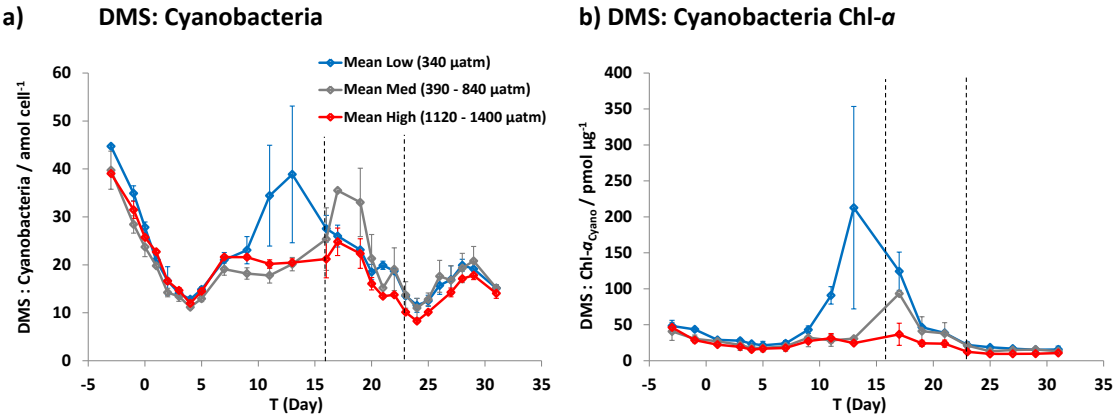

Figure 17. Temporal changes in the mean ratio between a) DMS and single-celled cyanobacteria (amol cell^{-1}) and b) DMS and cyanobacterial Chl-*a* (pmol µg^{-1}), for three different pCO_2 conditions: low (340 µatm), medium pCO_2 (390 - 840 µatm) and high pCO_2 (1120 – 1400 µatm). Error bars show standard deviation of the data within the three pCO_2 conditions and dashed lines indicate the sectioning into three Phases of the experiment. Single celled cyanobacteria abundance were obtained from flow cytometry data analysed by Kate Crawfurd (NIOZ) and cyanobacteria equivalent Chl-*a* data were obtained from the HPLC CHEMTAX algorithm by Yves Trense (Geomar).

DMS was not positively correlated with any other phytoplankton group identified by flow cytometry in Phase 1. The nanoeukaryotes 4 grouping were found to be strongly correlated with DMS in Phases 2 and 3 (ρ=0.750, p<0.01), and nanoeukaryotes 3 for the entire experiment but not for the individual phases (Table 8). In the Baltic Sea samples, strong correlations were identified between DMS and several groups: euglenophytes (ρ=0.888, p<0.01), dinoflagellates (ρ=0.608, p<0.05) and nanoeukaryotes 2 (ρ=0.880, p<0.01).

4.2. Dynamics of iodocarbon concentrations

4.2.1. Iodocarbon concentrations

The four iodocarbons (CH_3I, CH_2I_2, C_2H_5I, and CH_2ClI) generally showed the same trends (Figure 18). Only CH_2I_2 showed a small increase during Phase 2, but decreased again in Phase 3 in all mesocosms. Concentrations of all four iodocarbons were higher in the Baltic Sea than in the mesocosms.

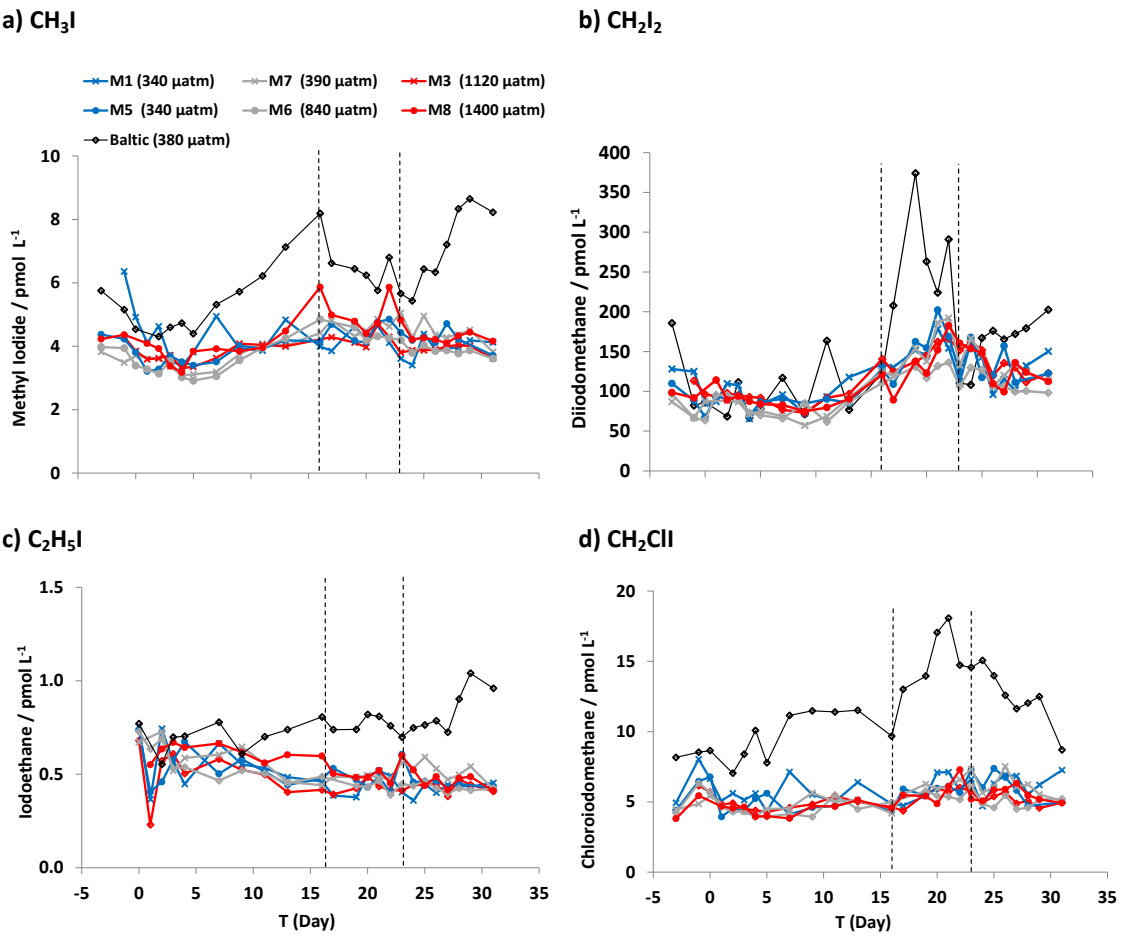

Figure 18. Temporal changes in concentrations of a) CH_3I, b) CH_2I_2, c) C_2H_5I and d) CH_2ClI concentrations (pmol L^{-1}) during the SOPRAN Tvärminne mesocosm experiment. Dashed lines indicate the sectioning into three Phases of the experiment.

Table 9. Summary of ANOVA performed on the iodocarbon data identifying significant differences between mesocosm iodocarbon concentrations. Data were analysed for the whole experiment and then by experiment Phase; as Phase 2 contained limited data points, Phases 2 and 3 were analysed together. * indicates the significance is not related to pCO_2 changes.

Compound	Statistical Details					
	Whole Experiment	Significant	Phase 1	Significant	Phases 2 and 3	Significant
CH_3I	F=3.07, p<0.05, DF=149	Yes*	F=3.21, p<0.05, DF=73	Yes*	F=5.78, p<0.01, DF=81	Yes*
CH_2I_2	F=1.68, p=0.143, DF=150	No	F=2.77, p<0.05, DF=74	Yes*	F=2.89, p<0.05, DF=98	Yes*
C_2H_5I	F=2.93, p=0.015, DF=149	No	F=1.47, p=0.217, DF=57	No	F=6.96, p<0.01, DF=81	Yes*
CH_2ClI	F=4.97, p<0.01, DF=150	Yes*	F=4.24, p<0.01, DF=74	Yes*	F=3.70, p<0.01, DF=81	Yes*

A summary of the statistical analysis performed on the four iodocarbons for the whole experiment and Phases 1 and 2/3 is given in Table 9. ANOVA identified differences between mesocosms, but none of these were a result of CO_2 treatment. Assessment of the linear change in iodocarbon concentrations with increasing pCO_2 (Figure 19) reinforced this finding.

CH_3I concentrations in all mesocosms in Phase 1 started at a mean of 3.88 pmol L^{-1} on T-1 and remained at a similar concentration until T31 (experiment mean 4.09 ± 0.55 pmol L^{-1}). CH_2I_2 started with a mean concentration of 108.1 (± 17.2) pmol L^{-1} in the mesocosms, and stayed stable throughout Phase 1 (Figure 18b) (Phase 1 overall mean 88.7 ± 15.7 nmol L^{-1}). Mean concentrations for Phases 2 and 3 combined was 140.0 ± 27.5 nmol L^{-1}. Concentrations increased during Phase 2, up to a peak on T21 in M1 and M5 (340 µatm) and T22 for M3 (1120 µatm), M6 (840 µatm), M7 (340 µatm) and M8 (1400 µatm). This peak on T21/22 corresponds with the peak in DMS on T21.

No linear change in CH_3I, C_2H_5I and CH_2I_2 was seen with increasing CO_2 treatment, but CH_2ClI showed a slight decrease (Figure 18). Concentrations of C_2H_5I were very close to the level of detection, and no effect of CO_2 was identified. CH_2ClI showed little variation during the experiment (mean 5.33 ± 0.91 pmol L^{-1}), and no obvious peaks in concentrations (Figure 18c).

Concentrations of CH_3I, C_2H_5I and CH_2ClI were significantly higher in the Baltic Sea than the mesocosms in all phases, and higher in Phase 2 for CH_2I_2 ($F=3.55$, $p<0.01$, $DF=47$).

Table 10. Range and mean (± SD) concentrations of iodocarbons within the mesocosms. DL: detection limit.

	CH_3I (pmol L^{-1})	CH_2I_2 (pmol L^{-1})	C_2H_5I (pmol L^{-1})	CH_2ClI (pmol L^{-1})	C_3H_7I (pmol L^{-1})
Mesocosm Range	2.91 – 6.36	57.25 – 217.98	0.23 – 0.76	3.81 – 8.03	Below DL
M1 (340 µatm)	4.21 (±0.63)	118.34 (±29.26)	0.49 (±0.11)	5.96 (±0.99)	Below DL
M5 (340 µatm)	4.06(±0.46)	115.85 (±35.11)	0.50 (±0.09)	5.45 (±0.99)	Below DL
M7 (390 µatm)	4.09 (±0.58)	112.29 (±37.96)	0.54 (±0.08)	5.45 (±0.95)	Below DL
M6 (840 µatm)	3.81(±0.49)	98.23 (±22.88)	0.49 (±0.09)	4.91 (±0.69)	Below DL
M3 (1120 µatm)	3.91 (±0.32)	119.22 (±28.01)	0.46 (±0.09)	5.13(±0.57)	Below DL
M8 (1400 µatm)	4.34 (±0.62)	113.43 (±29.38)	0.54 (±0.08)	5.08 (±0.82)	Below DL
Baltic Sea (380 µatm)	6.17 (±1.27)	154.89 (±77.30)	0.77 (±0.10)	11.67 (±2.94)	Below DL
Effect of CO_2	None	None	None	None	

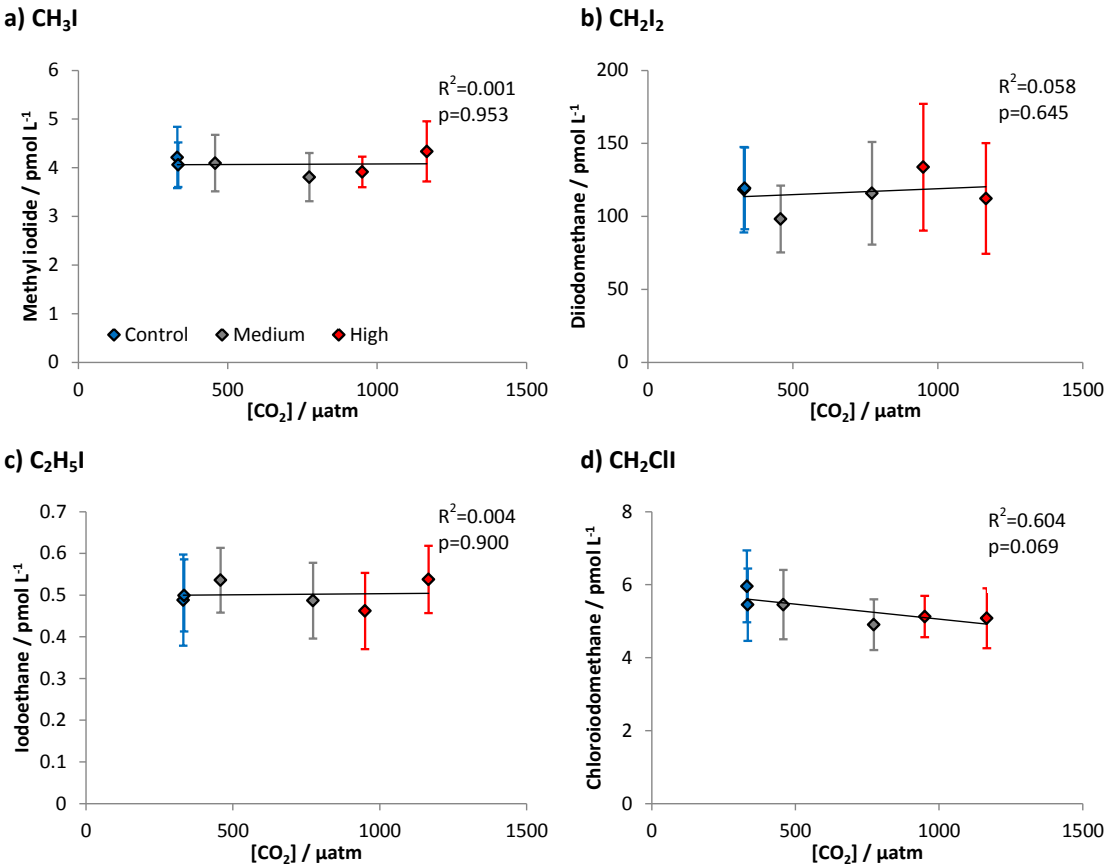

Figure 19. Changes in mean concentration (pmol L^{-1}) of a) CH_3I, b) CH_2I_2, c) C_2H_5I and d) CH_2ClI in each mesocosm plotted versus mean pCO_2. Error bars denote the standard deviation in each mesocosm, and the r^2 values for each line of best fit.

4.2.2. Iodocarbon relationships with microbial community development

Spearman's Rank Correlation analysis was carried out to identify relationships between concentrations of iodocarbons and biological parameters (Table 11).

Table 11. Spearman's Rank correlation coefficients for iodocarbon data compared to Chl-*a*, the HPLC pigment analysis and flow cytometry data. Coefficients are significant at 99% confidence limits, except those highlighted (*) which are significant at 95%. NC: non-correlated.

Compound	CH_3I	CH_2I_2	C_2H_5I	CH_2ClI
Chlorophyll-*a* (µg L^{-1})	-0.224	-0.406	0.405	-0.521
Phytoplankton Taxonomy (Equivalent Chlorophyll µg L^{-1})				
Total Equivalent Chlorophyll-*a*	-0.324	-0.601	0.418	-0.465
Cyanobacteria	NC	0.379	NC	0.230*
Prasinophytes	NC	NC	0.375	NC
Euglenophytes	NC	-0.351	0.287	NC
Dinoflagellates	-0.459	-0.499	0.276	-0.517
Diatoms	NC	NC	NC	-0.264*
Chlorophytes	NC	NC	NC	NC
Cryptophytes	-0.513	-0.672	0.454	-0.582
Small Phytoplankton (<10 µm) abundance (cells mL^{-1})				
Cyanobacteria	NC	0.520	-0.276	0.314
Picoeukaryotes	-0.293	NC	NC	-0.339
Nanoeukaryotes 1	0.367	0.346	-0.274	NC
Nanoeukaryotes 2	NC	-0.375	0.323	-0.297
Nanoeukaryotes 3	0.586	0.621	-0.441	0.335
Nanoeukaryotes 4	0.234	0.466	-0.208*	0.376

4.2.3. Iodocarbon correlations with Chlorophyll *a*

Chl-*a* was positively correlated with C_2H_5I (ρ=0.405, p<0.01) but was negatively correlated with CH_3I, CH_2I_2 and CH_2ClI (ρ=-0.224, -0.406 and -0.521 respectively, p<0.01). The same trend was noted for the total equivalent Chl-*a* (Table 11). All the iodocarbons showed very similar trends when calculated as production per unit Chl-*a* (Figure 20 for CH_3I); all showed increases through Phase 2 and levelled off during Phase 3. Phase 3 showed a significant effect of CO_2 on the production per unit Chl-*a* in all the iodocarbons: the results of the ANOVA assessing the CO_2 effect on iodocarbons: Chl-*a* ratio during Phase 3 is given in Table 12.

Table 12. F-values from the ANOVAs performed to identify the CO_2 effect on the iodocarbon: Chl-*a* ratio during Phase 3 of the experiment. All ANOVAs were significant at p<0.01. DF: degrees of freedom.

Compound	F-value	Degrees of Freedom
CH_3I	6.31	46
CH_2I_2	7.03	46
C_2H_5I	7.44	46
CH_2ClI	8.32	46

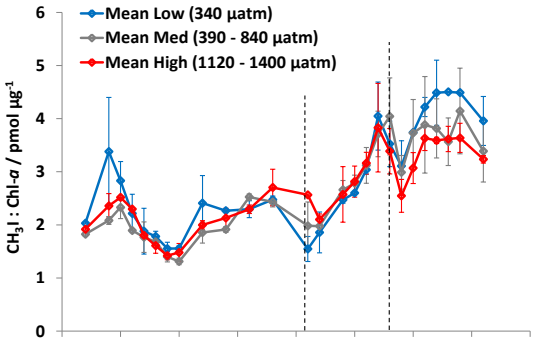

Figure 20. Temporal changes in the ratio between Chl-*a* and CH_3I for three different pCO_2 conditions: low (340 µatm), medium pCO_2 (390 – 840 µatm) and high pCO_2 (1120 – 1400 µatm). Error bars show standard deviation within the different pCO_2 conditions and dashed lines indicate the sectioning into three Phases of the experiment.

4.2.4. Iodocarbons and the relationships with community composition

Iodocarbons showed varying responses to both the community taxonomy as identified by HPLC and the cell abundances from flow cytometry (Table 11). CH_2I_2 and CH_2ClI showed positive correlations with both the cyanobacterial equivalent Chl-*a* (ρ=0.379, p<0.01 and ρ=0.230, p<0.05 respectively) and *Synechococcus* spp. (ρ=0.520, p<0.01 and ρ=0.314, p<0.01 respectively). Neither CH_3I nor C_2H_5I showed positive correlations with the cyanobacterial activity.

None of the iodocarbons were positively correlated with diatoms or chlorophytes; only C_2H_5I showed positive correlation with cryptophytes (ρ=0.454, p<0.01), dinoflagellates (ρ=0.276, p<0.01), euglenophytes (ρ=0.287, p<0.01) or prasinophytes (ρ=0.375, p<0.01). CH_3I, CH_2I_2 and CH_2ClI showed positive responses to nanoeukaryote groupings 3 and 4, but only weak correlations with the other cell abundances; in particular the picoeukaryotes were either not significantly (CH_2I_2 and C_2H_5I) or negatively correlated (CH_3I and CH_2ClI) to iodocarbon concentration.

4.3. Dynamics of bromocarbon concentrations

4.3.1. Measured bromocarbons

Concentrations of bromocarbons did not increase during the experiment, and particularly in the case of $CHBr_3$ and CH_2Br_2, concentrations decreased after T-3 until the end of the experiment on T31 (Figure 20 and Table 13). $CHBr_3$ concentrations stabilised and remained at a mean of 85.6 (± 8.3) pmol L^{-1} from T1 to T31.

a) $CHBr_3$

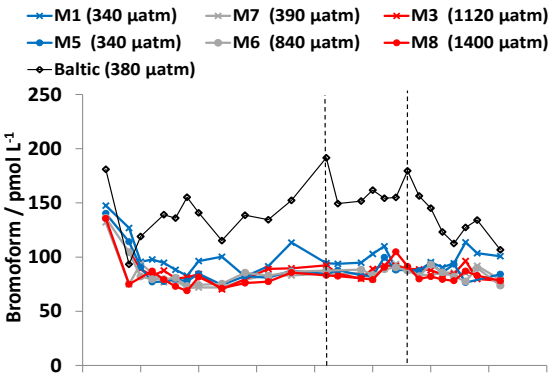

b) CH_2Br_2

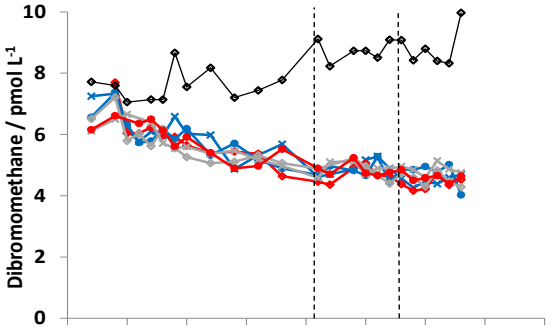

c) $CHBr_2Cl$

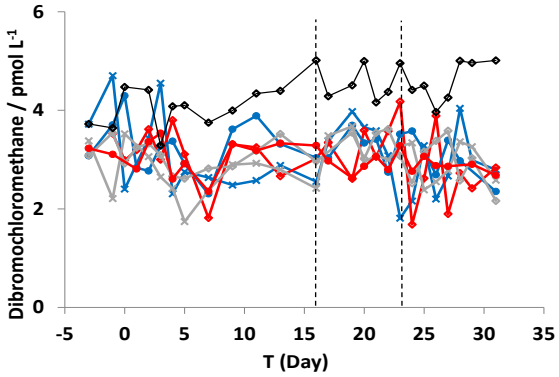

Figure 21. Temporal changes in concentrations of a) CH_3Br, b) CH_2Br_2 and c) $CHBr_2Cl$ (pmol L^{-1}) during the SOPRAN Tvärminne mesocosm experiment. Dashed lines indicate the sectioning into three Phases of the experiment.

Table 13. Range and mean (±SD) concentrations of bromocarbons within the mesocosms, showing the standard deviation in brackets. DL: detection limit.

	$CHBr_3$ (pmol L^{-1})	CH_2Br_2 (pmol L^{-1})	$CHBr_2Cl$ (pmol L^{-1})	CH_2BrI (pmol L^{-1})
Mesocosm Range	68.88 – 147.50	4.03 – 7.69	1.68 – 4.70	Below DL
M1 (340 µatm)	99.08 (± 14.13)	5.40 (± 0.88)	3.06 (± 0.75)	Below DL
M5 (340 µatm)	88.08 (± 13.76)	5.35 (± 0.77)	3.21 (± 0.47)	Below DL
M7 (390 µatm)	84.74 (± 11.72)	5.30 (± 0.61)	2.88 (± 0.48)	Below DL
M6 (840 µatm)	86.06 (± 12.54)	5.22 (± 0.74)	3.08 (± 0.38)	Below DL
M3 (1120 µatm)	86.33 (± 6.96)	5.17 (± 0.86)	3.03 (± 0.63)	Below DL
M8 (1400 µatm)	83.61 (± 13.07)	5.25 (± 0.71)	2.99 (± 0.29)	Below DL
Baltic (380 µatm)	142.15 (± 23.47)	8.21 (± 0.77)	4.34 (± 0.47)	Below DL
Effect of CO_2	None	None	None	-

No effect of CO_2 was identified on the concentrations of any bromocarbon (Table 14), and although differences were detected between mesocosms, this was not related to pCO_2. All bromocarbon concentrations were significantly higher in the Baltic Sea than the mesocosms.

Table 14. Summary of ANOVA statistical analyses on the bromocarbon data. As Phase 3 contained limited data points, Phases 2 and 3 were analysed together. * denotes differences not related to changes to pCO_2. DF: degrees of freedom.

Compound	Statistical Details					
	Whole experiment	Phase 1	Phase 2	Phase 3	Comparison with Baltic Sea	Effect of CO_2
$CHBr_3$	F=3.35, p<0.01*, DF=52	F=2.05, p=0.08, DF=74	F=2.46, p<0.05*, DF=34	F=3.35, p<0.05*, DF=52	F=28.11, p<0.01, DF=61	None
CH_2Br_2	F=0.32, p=0898, DF=139	F=0.31, p=0.904, DF=74	F=2.08, p=0.079, DF=70	F=3.23, p<0.05*, DF=35	F=208.81, p<0.01, DF=82	None
$CHBr_2Cl$	F=1.07, p=0.381, DF=148	F=1.53, p=0.192, DF=73	F=0.34, p=0.889, DF=80	F=0.27, p=0.926, DF=51	F=23.45, p<0.01, DF=173	None

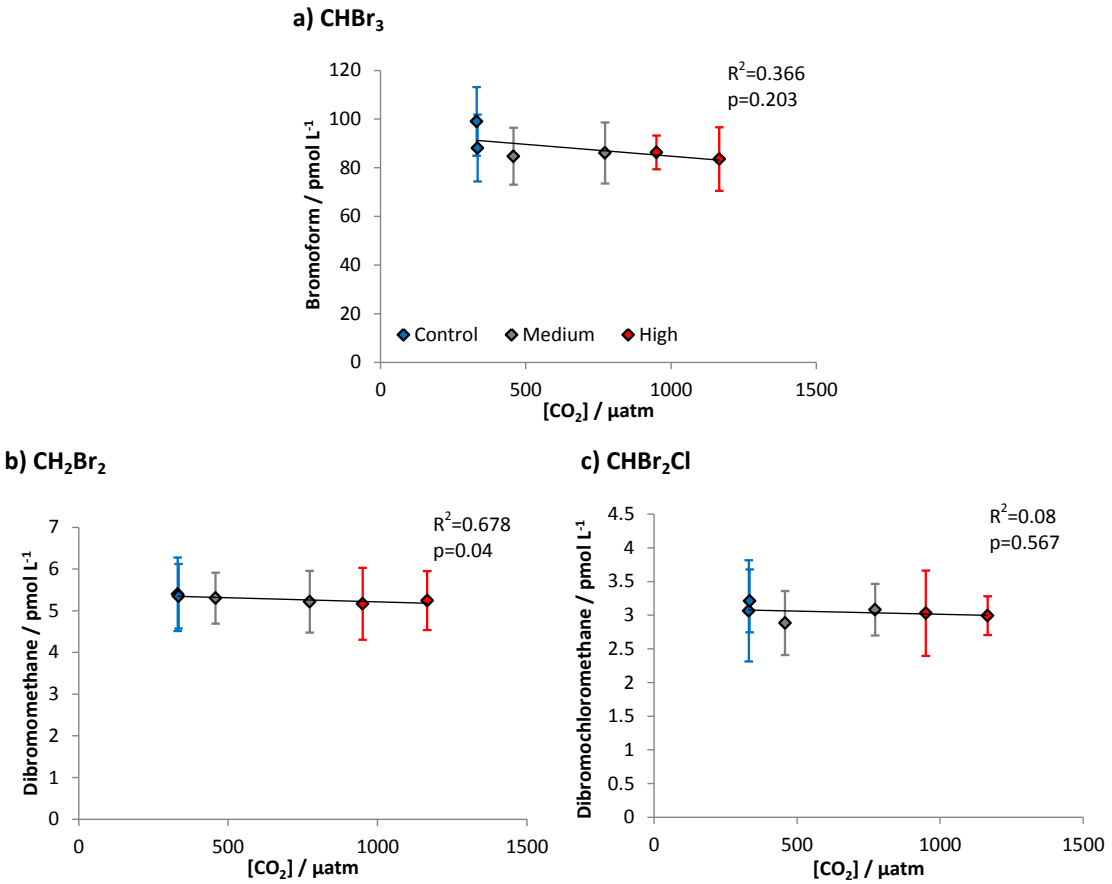

Figure 22. Changes in mean concentration of a) $CHBr_3$, b) CH_2Br_2, and c) $CHBr_2Cl$ with mean pCO_2. Error bars denote the standard deviation for each mesocosm, and the r^2 values for each line of best fit.

4.3.2. Bromocarbon correlation with microbial community development

Spearman's Rank Correlation Analysis was carried out to identify relationships between bromocarbons and the biological parameters (Table 15).

Table 15. Spearman's Rank correlation coefficients for the relationships between bromocarbon data and Chl-*a*, the HPLC pigment analysis and flow cytometry data. Coefficients are significant at 99% confidence limits, except those highlighted (*) at being significant at 95%. NC: non-correlated.

	$CHBr_3$	CH_2Br_2	$CHBr_2Cl$
Chlorophyll-*a* (µg L^{-1})	-0.209*	0.518	NC
Phytoplankton Taxonomy (Equivalent Chlorophyll µg L^{-1})			
Total Equivalent Chlorophyll-*a*	-0.373	0.337	NC
Cyanobacteria	NC	-0.379	-0.229*
Prasinophytes	-0.307	NC	NC
Euglenophytes	NC	NC	NC
Dinoflagellates	NC	0.652	NC
Diatoms	-0.235*	NC	NC
Chlorophytes	-0.330	NC	NC
Cryptophytes	-0.222*	0.864	NC
Small Phytoplankton (<10 µm) abundance (cells mL^{-1})			
Cyanobacteria	NC	-0.519	NC
Picoeukaryotes	-0.443	NC	NC
Nanoeukaryotes 1	NC	-0.477	NC
Nanoeukaryotes 2	NC	0.342	NC
Nanoeukaryotes 3	0.222	-0.752	NC
Nanoeukaryotes 4	0.223	-0.262	NC

4.3.3. Bromocarbons and the relationship with Chlorophyll *a*

CH_2Br_2 showed strong positive correlation with Chl-*a* (ρ=0.518, p<0.01), whereas $CHBr_3$ and $CHBr_2Cl$ were negatively correlated and non-correlated respectively (Table 15). This same trend was identified in the total equivalent Chl-*a* from the HPLC analysis.

Bromocarbon concentrations showed similar trends when calculated as production per unit of Chl-*a* (Figure 23 for $CHBr_3$) and also showed very similar trends to the iodocarbons (Figure 20). However, during Phase 3, only $CHBr_3$ displayed a significant decrease in production per µg Chl-*a* as pCO_2 increased (F=7.58, p<0.01, DF=46).

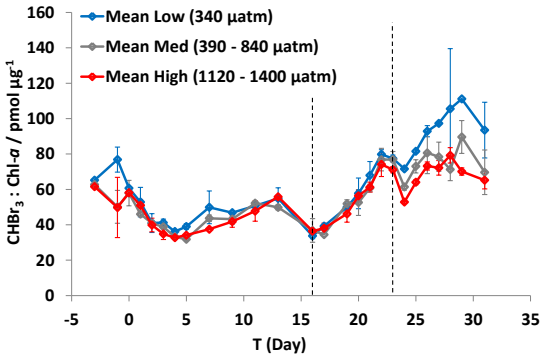

Figure 23. Temporal changes in the ratio between Chl-*a* and $CHBr_3$ for three different pCO_2 conditions: low (340 µatm), medium pCO_2 (390 – 840 µatm) and high pCO_2 (1120 – 1400 µatm). Error bars show standard deviation within the pCO_2 ranges and dashed lines indicate the sectioning into three Phases of the experiment.

4.3.4. Bromocarbons and the relationship with community composition

$CHBr_3$ was positively correlated with only nanoeukaryotes 4 (ρ=0.222, p<0.01) and was either negatively correlated or non-correlated with all other phytoplankton groupings or cell abundances, as well as Chl-*a*. CH_2Br_2 showed strong positive correlations with both dinoflagellates (ρ=0.652, p<0.01) and the cryptophytes (ρ=0.864, p<0.01), as well as nanoeukaryotes 3 (ρ=0.342, p<0.01). $CHBr_2Cl$ was non-correlated with all phytoplankton groups identified by HPLC and flow cytometry, apart from weak negative correlation with cyanobacteria (ρ=-0.229, p<0.05; see Table 15).

4.4. Mesocosm trace gas summary

All trace gas data underwent correlation analysis to identify inter-relationships (Table 16). DMS showed strong positive correlations with CH_2I_2 (ρ=0.717, p<0.01), CH_2ClI (ρ=0.590, p<0.01) and $CHBr_3$ (ρ=0.555, p<0.01), but no correlation with CH_2BrCl.

Table 16. Spearman's Rank correlation coefficients for all trace gas data. Coefficients are significant at 99% confidence limits, except those highlighted (*) as being significant at 95%. NC: non-correlated.

Compound	CH_3I	CH_2I_2	C_2H_5I	CH_3ClI	$CHBr_3$	CH_2Br_2	CH_2BrCl
DMS	0.461	0.717	-0.393	0.590	0.555	-0.437	NC
CH_3I							
CH_2I_2	0.566						
C_2H_5I	NC	-0.424					
CH_2ClI	0.568	0.451	NC				
$CHBr_3$	0.505	0.519	-0.248	0.603			
CH_2Br_2	-0.327	-0.580	0.675	NC	NC		
$CHBr_2Cl$	NC	NC	NC	NC	0.336	0.181*	

4.5. Trace gas concentrations in the Baltic Sea samples

The trace gas data from the Baltic Sea samples taken from outside the mesocosms underwent Spearman's correlation analysis to determine if there were relationships with any of the biological parameters measured from the same samples (Table 17). DMS and $CHBr_3$ showed strong correlations with Chl-*a*, and DMS was correlated with euglenophytes and dinoflagellates. CH_3I, CH_2I_2 and CH_2ClI showed strong correlations with the nanoeukaryotes 2 grouping. $CHBr_3$ and CH_2Br_2 showed no positive correlations with any of the phytoplankton groups or cell abundances.

Table 17. Spearmans Rank correlation coefficients for the Baltic Sea trace gas samples compared to Chl-*a*, the HPLC pigment analysis and flow cytometry data. Coefficients are significant at 99% confidence limits, except those highlighted (*) at being significant at 95%. NC denoted non-correlated parameters.

Compound	DMS	CH_3I	CH_2I_2	C_2H_5I	CH_3ClI	$CHBr_3$	CH_2Br_2	$CHBr_2Cl$
Chlorophyll-*a*	0.842	NC	NC	NC	NC	0.654*	NC	NC
Phytoplankton Taxonomy (Equivalent Chlorophyll µg L^{-1})								
Total Equivalent Chlorophyll-*a*	0.860	NC	NC	NC	NC	NC	NC	NC
Cyanobacteria	-0.746	-0.725	NC	NC	NC	NC	NC	NC
Prasinophytes	NC	NC	NC	NC	NC	NC	NC	NC
Euglenophytes	0.888	NC	0.629*	NC	0.678	NC	NC	0.622*
Dinoflagellates	0.608*	NC	NC	NC	0.769	NC	NC	0.671*
Diatoms	NC	NC	NC	NC	NC	NC	-0.615*	NC
Chlorophytes	NC	NC	NC	NC	NC	NC	NC	NC
Cryptophytes	NC	NC	NC	NC	-0.671*	NC	-0.734	NC
Small Phytoplankton (<10 µm) abundance (cells mL^{-1})								
Cyanobacteria	NC	NC	NC	NC	0.653	0.605	NC	NC
Picoeukaryotes	NC	-0.800	-0.731	NC	-0.489*	NC	-0.510*	NC
Nanoeukaryotes 1	NC	NC	NC	NC	NC	NC	NC	NC
Nanoeukaryotes 2	0.880	0.463*	0.527	NC	0.577	0.563	NC	NC
Nanoeukaryotes 3	NC	NC	NC	NC	NC	NC	NC	NC
Nanoeukaryotes 4	NC	NC	NC	NC	NC	NC	NC	NC

5. Discussion

5.1. Mesocosm behaviour and physical changes during SOPRAN Tvärminne

Temperature within the mesocosms fluctuated significantly in a 15°C range, compared to the range in SOPRAN Bergen of 6°C. Water temperature within the mesocosms was strongly influenced by the temperature in the waters outside, which can be seen when comparing the CTD-measured temperature with that of the Baltic Sea (Figure 3). Temperature stratification existed prior to mixing of the mesocosms, but salinity was constant with depth, and remained constant throughout the experiment with limited evidence of freshwater input from rainwater into the surface waters. This is likely because the salinity was below 6, compared to 31 during SOPRAN Bergen, so the relative difference between the mesocosms and rainwater was significantly lower.

On analysis of existing temperature records from Tvärminne station, the year 2012 was not identified as being significantly different in temperature to preceding years (Figure 24), however it was noted by staff at Tvärminne Zoological Station that the number of days of high sunlight were fewer than normal during June/ July.

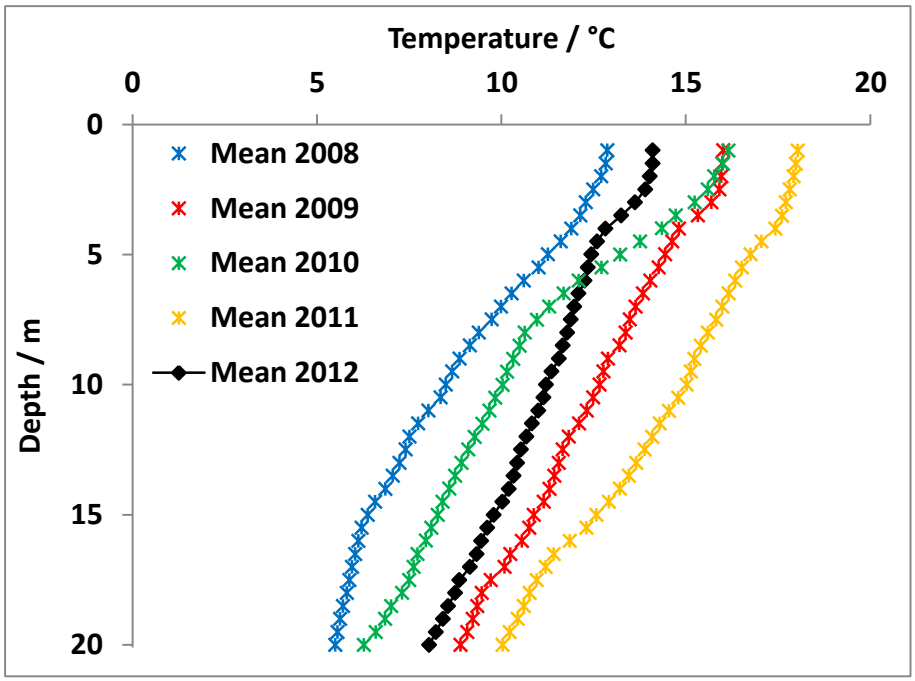

Figure 24. Mean temperatures profiles for the surface 20 m of Tvärminne Storfjärden for June/ July in the experiment year (2012) and the preceding 4 years.

Baltic Sea hydrography consists of two layers: fresher surface waters due to riverine runoff above 50 - 80 m with a permanent halocline established around this depth. During

summertime, a thermocline develops in the surface 20 m, below which the temperature can be measured below 10°C (Lehmann and Myrberg, 2008; Vahtera *et al.*, 2005). The waters below the thermocline remain at 2 - 4°C (Janssen *et al.*, 1999). Increasing surface temperature during Phase 1 was likely a result of solar warming. Summertime upwelling events are common and well described (Gidhagen, 1987; Lehmann and Myrberg, 2008), and are known to induce a significant temperature decrease in the surface waters (Baltic Sea Portal, 2014). Such an event was experienced during the experiment after T16, when temperatures decreased and salinity increased, eventually forming a mixed layer to the surface on T31.

The tidal movement at Tvärminne is minimal. Wind strength is important in the Baltic in determining the water level variation, particularly in the Gulf of Finland, due to the lack of tidal action. No severe wind events occurred during the experiment, with mean speed of 7.7 m s^{-1} and maximum speed measured below 20 m s^{-1}, but a change in wind direction was likely the cause for the upwelling event in Phases 2 and 3.

Observations of annual pH in waters off the Tvärminne coast in July ranged from 7.8 – 9.2, significantly higher than the regularly measured winter pH of <8.0 (Brutemark *et al.*, 2011). This increased pH was attributed to CO_2 uptake for photosynthesis (PHS) and higher water temperatures resulting in lower dissolved gas concentrations. Bottom waters within the Baltic are elevated in pCO_2 (Schneider *et al.*, 2002), and subsequently lower in pH. The upwelling event observed in the experiment carried lower pH waters to the surface, as seen in the pH depth profile from the Baltic Sea (Figure 6). This upwelled water measured at a pH lower than 7.6 on T31 below 10 m, and below 7.8 in the surface 0 - 10 m. These changes in pH and temperature as observed during the mesocosm experiment imply that the communities within the waters off Tvärminne are regularly exposed to rapid changes in pH and pCO_2. These regular measurements of pH below 8, with corresponding pCO_2 of up to 800 µatm (T33 in Baltic Sea) suggest that the Baltic Sea is a natural laboratory for ocean acidification experiments, with communities which have adapted to lowered pH and elevated pCO_2. The changes in trace gas concentrations in the Baltic Sea samples are discussed in Section 5.7.

The decrease in pH in the control mesocosms was pronounced after the start of Phase 2, during the time the temperature in the mesocosms decreased. Measured pCO_2 in the control mesocosms also increased during this time. The temperature change was likely the cause of the decrease in pH allowing a greater dissolution of CO_2 within the mesocosm waters.

5.2. Impact of high pCO_2 on community structure and composition

During summer, net planktonic primary production is based on nutrient availability (particularly inorganic nitrogen) and grazing (Kivi *et al.*, 1993). Inorganic nitrogen in the mesocosms increased during the experiment, showing evidence of Nitrate production, either by diazotrophic cyanobacteria due to the increase in *A. flos-aquae* abundance during Phases 2 and 3 (Figure 13), or by recycling of nutrients. Inorganic nitrate concentrations were highest during Phases 2 and 3, which was when Chl-*a* was lowest. During an upwelling event, Vahtera *et al.* (2005) found an initial increase in Chl-*a*, followed by a decrease in total phytoplankton biomass, similar to the observations in the Baltic Sea samples from this study. The mesocosm community populations were separated from the upwelled waters in terms of salinity, pH and nutrients, so these factors were not responsible for the decline in Chl-*a* observed through Phase 2 and into Phase 3. The only influencing factor from the upwelling was that of temperature, implying that lowered temperatures have a negative effect on the community growth in the mesocosms.

Microbial communities in the Baltic Sea are regularly exposed to lowered pH and elevated pCO_2 during upwelling events: the upwelling event experienced during SOPRAN Tvärminne increased $pCO_2$from 200 µatm up to 800 µatm over 16 days, and these events are a common occurrence over summer (Vahtera *et al.*, 2005). pCO_2 had no effect on total Chl-*a* concentrations in the mesocosms during any Phase, indicating that the community is adapted to elevated atmospheric pCO_2 through these regular upwelling events. Positive effects of CO_2 on the cell abundances were seen only in the picoeukaryotes and the Nanoeukaryotes 4, implying that atmospheric pCO_2 increase will not significantly affect the primary production during the summer phytoplankton bloom in the Baltic Sea. Higher pCO_2 in surface waters will allow for lower energy requirements in phytoplankton cells for carbon concentrating mechanisms (CCMs) to provide sufficient CO_2 for the operation of RubisCO (Chapter 1, Section 2.6). It is proposed that CCMs in Baltic Sea phytoplankton are already adapted to variations in CO_2 from upwelling events, and therefore the addition of further CO_2 does not encourage additional photosynthesis.

It is suggested that the Baltic Sea might make a potential site for *in-situ* experiments on the effects of ocean acidification without the requirement for mesocosms or other complex experimental setups. This will be discussed further in Chapter 6, comparing natural laboratories such as those suggested here to other experimental designs and setups, and discussing the advantages and disadvantages of each.

5.3. Growth of Cyanobacteria

Upwelling events are important in the development of cyanobacterial blooms due to the delivery of phosphate into surface waters (as noted in the Baltic Sea samples in Fig 10b), as well as the delivery of cyanobacterium inoculate into the surface waters (Vahtera *et al.*, 2005). Cyanobacterial growth within the Baltic Sea is an annual event in summer (Finni *et al.*, 2001), however informal observations in the summer of 2012 during the mesocosm experiment identified lower than normal cyanobacterial aggregations within the water column (Tvärminne Zoological Station). Satellite data is regularly used to track the development of cyanobacterial blooms in the Baltic (Figure 25) and the entrance to the Gulf of Finland is a common location for significant blooms. During 2012, however, the observed number of days with cyanobacterial growth was far lower than previous years.

Cyanobacterial blooms are triggered by particular environmental conditions: salinity within the range 3.8 to 11.5, temperatures approximately 16°C, wind speed <6m s^{-1} and >120 W m^{-2} radiation (Wasmund, 1997). Of these conditions, salinity was within this range, but temperatures were below 16°C (Figure 24) throughout the experiment even in surface waters, mean wind speed was 7.7 m s^{-1} and days of sunlight were limited (Tvärminne Zoological Station, Pers Comm). Combined, these conditions were sub-optimal for triggering a significant cyanobacterial bloom. Temperatures in 2011 were significantly higher, and the summer cyanobacterial bloom was substantial in the Northern Baltic Sea proper. Addition of phosphate from the 2012 upwelling event did not have a positive effect on cyanobacterial abundance, a situation which was also noted by (Nausch *et al.*, 2009).

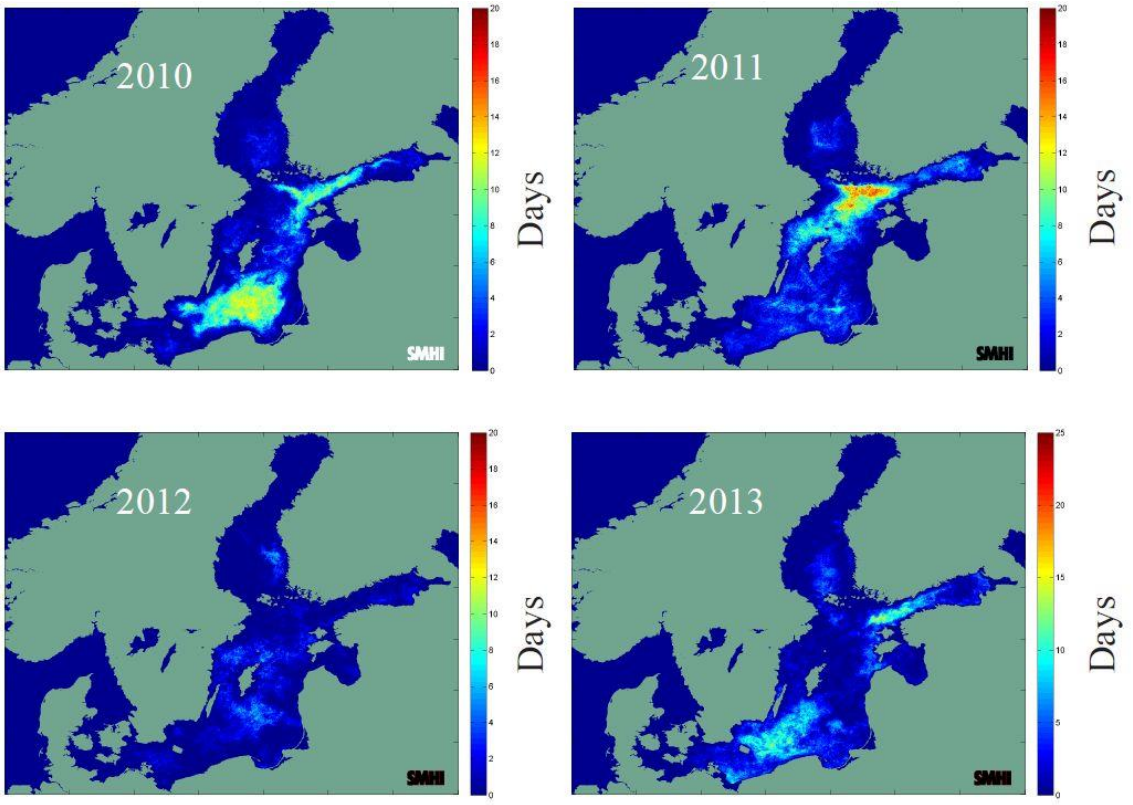

Figure 25. Summary of number of days with cyanobacterial blooms observed in each pixel during the period 2010-2013. From the Modis Satellite (Oberg, 2013)

Single celled cyanobacteria were likely the ubiquitous *Synechococcus* spp, and have been found to comprise as much as 80% of the cyanobacterial biomass and 50% of the total primary production during summertime in the Baltic Sea (Stal *et al.*, 2003). Although non-diazotrophic, these single-celled cyanobacteria have been found associated with the colonial blooms (Stal *et al.*, 2003) and showed significant growth in the mesocosms, especially during Phase 3. Also identified in the mesocosms were the picocolonial *Coelosphaerium* spp. and *Cyanodictyon* spp. (data not shown). These species have been identified as occurring in late autumn during cooler well-mixed periods (Laamanen, 1997), although as discussed the surface water temperatures during summer 2012 were lower than the average and may have encouraged the growth of these species earlier in the year.

Growth of two colonial cyanobacteria species in addition to those mentioned above were identified in different Phases of the experiment using light microscopy (this data was provided very late on in this investigation) but has been included to show the growth of these species. The heterocystous *A. flos-aquae* is a common component of the late summer cyanoprokaryotic assemblage (Laamanen, 1997), but growth is stimulated by higher surface water temperatures and high light intensity. The environmental conditions prevalent during the summer of 2012 may have allowed some growth of this species but prevented the formation of extensive

blooms. Increasing inorganic N concentrations in the mesocosms through Phases 2 and 3 are likely attributed to the fixation of N by this species, which can release surplus nitrogen into the surrounding waters (Ploug, 2008) and also into sediments in the Baltic Sea (Struck *et al.,* 2004). *A. flos aquae* showed higher abundance in the control and medium pCO_2 mesocosms, however it was acknowledged that the use of the integrated water samplers would have broken up the filaments and therefore affected the measurement of length within a sample, giving the strong fluctuations in filament length measured between sampling days and between mesocosms.

Growth of the non-heterocystous *Pseudanabaena* was during Phase 1, and abundance decreased significantly during Phase 2, where it was near undetectable in Phase 3. *Pseudoanabaena* abundance was relatively high when the mesocosms were closed, implying conditions for growth are different to those required by *A. flos-aquae*. This species has been previously identified in blooms in late June, prior to the late Autumn preference of *A. flos-aquae* (Laamanen, 1997), which corresponds to the order in which the two species developed in the mesocosms. *Pseudanabaena* are small picocyanobacteria, with filaments that break down easily into single cells (Stal et al., 2003), and they have shown significant contributions to the N-fixation within the Baltic Sea (Wasmund et al., 2001). On T17, analysis of sediment trap material following wall cleaning showed significant presence of cyanobacterial pigments (phycoerythrin and phycocyanin) in the supernatant (T. Boxhammer, GEOMAR, Pers. Comm.), suggesting the loss of the cells into the sediment trap after the bloom, and that the cells were growing on the mesocosm walls.

Analysis of zooplankton abundance within the mesocosms showed high numbers of heterotrophic cladocerans (*Bosmina* spp; data not shown). Grazing of these organisms on the filamentous cyanobacteria colonies was observed directly, and it was proposed that the cyanobacterial abundance in the mesocosms was kept low by grazing pressure. Grazing activity can remineralise cyanobacterially fixed N (Forsskahl et al., 1982), which was detected in the increasing concentrations of inorganic N as the experiment progressed. Grazer pressure is unlikely to be as intense in the Baltic Sea samples due to predation pressure not present in the mesocosms.

5.4. Production of DMS and DMSP

Concentrations of DMS measured in the mesocosms and Baltic Sea (1.8 – 11.2 nmol L^{-1}) fall within the range of concentrations reported in previous studies from this region. While concentrations over 100 nmol L^{-1} were detected by Orlikowska and Schulz-Bull (2009) during the spring phytoplankton bloom, Leck *et al.* (1990) measured concentrations of maximum 3.23

nmol L^{-1} during the summer bloom in July/ August. Measurements from the mesocosms fall well into the latter range. A DMS flux during a Baltic Sea bloom of up to 30 nmol m^{-2} d^{-1} was also reported by Orlikowska and Schulz-Bull (2009). This is an order of magnitude lower than fluxes of 0-10 µmol m^{-2} d^{-1} calculated by Scarratt *et al.* (2007) in the Northwest Atlantic and 4 µmol m^{-2} d^{-1} by Archer *et al.* (2002) in the North Sea.

Table 18. Comparison of DMS concentrations from the samples from SOPRAN Tvärminne and the literature. DL – detection limit.

Author	DMS (nmol L^{-1})	DMS flux July (nmol S m^{-2} d^{-1})
Leck *et al.* (1990)	DL – 3.23	-
Leck and Rodhe (1991)	0.35 – 2.82	1.77 – 2.42
Orlikowska and Schulz-Bull (2009)	0.3 - 120	30
SOPRAN Tvärminne Baltic Sea	1.85 – 11.18	-
SOPRAN Tvärminne Mesocosm	2.66 – 6.79	-

No DMSP was detected in samples fixed by the acidification method modified by Kiene and Slezak, (2006) and analysed by GC-FPD . Analysis of samples included those from T8 through to T25 from all mesocosms and the Baltic Sea. Two possible reasons are suggested here to explain this unexpected result: failure of the DMSP acidification fixing method (Section 5.4.1), or production of DMS via a pathway other than DMSP breakdown (Section 5.4.2).

An additional explanation for extremely low DMSP concentrations was an extremely rapid turnover rate through the demethylation pathway, diverting DMSP away from the production of DMS. Given the limited information on DMSP in the Baltic Sea, there is no data available on turnover rates, however in the North Sea, $DMSP_D$ turnover rates were calculated at 20-28 nmol L^{-1} d^{-1} (Zubkov *et al.*, 2001, 2002), 10 times the rate of DMS turnover, which indicated that most $DMSP_D$ loss was via the demethylation pathway. Calculated turnover times for DMS and DMSP were 12 and 10 hours respectively. Asher *et al.* (2011) calculated $DMSP_D$ turnover at 62 nmol L^{-1} d^{-1} in the Antarctic, and Kiene and Linn (2000) at 39 nmol L^{-1} d^{-1} in mesotrophic shelf seas of the Gulf of Mexico. These $DMSP_D$ turnover rates, if equivalent to the activity in the Baltic, would have been sufficient to support the concentrations of DMS detected (Kiene and Linn, 2000a), however, DMSP should still have been detected. In addition, turnover of $DMSP_D$ within surface waters does not account for the lack of DMSP detected from the particulate phase, unless no DMSP producers are present.

5.4.1. Issues with DMSP fixing method

The acidification method of DMSP fixation allows sterilisation of a seawater sample by the addition of 50% H_2SO_4, preventing enzyme-mediated DMSP breakdown to DMS. It also ensures the oxidation and thus removal of DMS from the sample, which would otherwise interfere with the DMSP signal. This method performed well during the SOPRAN Bergen mesocosm experiment (Chapter 3, Section 4.1), and also in previous studies requiring DMSP storage (Archer *et al.*, 2013; Hopkins and Archer, 2014; Kiene and Slezak, 2006). The acidification method avoids the use of crimp-sealed serum vials as commonly used by the alternative method of storage following hydrolysis of samples with NaOH. However, previous problems have been encountered using this method for the analysis of DMSP samples from colonial *Phaeocystis antarctica*, where 60 – 94 % loss of DMSP was reported from the acidified samples (del Valle *et al.* 2011). Tests revealed that this loss occurred immediately after acid addition, and was a result of intracellular DMSP cleavage by enzyme activity in the short period between acid addition and enzyme inhibition, and only occurred in the colonial form. Single-celled *Phaeocystis* cultures were unaffected, and DMSP concentrations remained stable after the initial loss.

Samples for DMSP analyses were fixed using the acidification method during SOPRAN Tvärminne and analysed within 6 weeks, but no DMSP was detected. Although colonial species were present within the mesocosms and could have undergone the same loss of DMSP as observed by del Valle *et al.* (2011), it is likely there were also DMSP producing single-celled species present within the mesocosms. $DMSP_P$ concentrations measured in the surface waters of the southern Baltic Sea in summer 2012 were 22.2 nmol L^{-1}, indicating the presence of DMSP-producing species (Zindler, GEOMAR, Pers. Comm.). In the study of del Valle *et al.* (2011), the loss of DMSP from acid addition resulted in significantly lower DMSP concentrations compared to immediate analysis by NaOH cleavage, but not a 100 % loss of DMSP, as the results of the present study suggest. Cyanobacteria, the principle colonial organisms within the Baltic Sea, contributed only 6.6 % to the total equivalent Chl-*a* concentration: if the problem with the samples was related to colonial organisms, DMSP would likely still have been detected from the single-celled components of the community composition, and yet was not. The implication is that DMSP was not present within the Baltic Sea samples.

The acidification method has not previously been tested in waters with salinity below 30, and thus it was proposed that the DMSP loss may have been related to the low salinity of the study site. A series of tests were carried out using water from the freshwater UEA Broad and Norfolk

Broads estuarine systems to test the acidification method compared to gas-tight NaOH addition. The results of these tests are presented in Appendix 1, but it was identified that salinity did not affect DMSP fixation. Although in the case of some samples taken in the UEA Broad, DMSP loss was observed; at no point were DMSP concentrations undetectable.

5.4.2. DMS production from non-DMSP source

DMS production in the oceans predominantly arises from the breakdown of DMSP into DMS and acrylate. The resulting DMS is either rapidly assimilated within the water column, or fluxes to the atmosphere through the sea surface micro-layer. However, there is evidence that a secondary pathway exists for DMS production, through the methylation of methanethiol (Drotar *et al.*, 1987; Visscher *et al.*, 2003). This production pathway is not well understood, but it may provide an alternative explanation for the high levels of DMS seen during this mesocosm experiment despite undetectable DMSP concentrations.

The methylation pathway for DMS production has previously been identified in anaerobic environments containing cyanobacteria, such as microbial mats (Visscher *et al.*, 2003) or salt marsh sediments (Kiene and Capone, 1988). Recent experiments on *Pseudomonas deceptionensis* from Deception Island in Antarctica has identified the same trait (J. Todd, Pers Comm) and have identified the methane thiol (MeSH) dependent DMS gene (Mdd). The pathway is likely a methyl-transferase: S-adenosyl L methionine-dependent thiol methyltransferase activities are widespread in bacteria and contribute to biogenic emissions of methylated sulphur gases including DMS (Drotar *et al.*, 1987).

The Mdd gene has been identified in several cold-water *Pseudomonas* spp and other bacterial clades, and in the filamentous cyanobacteria *Pseudanabaena*, which has been detected in the Baltic Sea (Kangro *et al.*, 2007; Nausch *et al.*, 2009). There is therefore a strong potential for DMS production from methanethiol by cyanobacterial species within the Baltic Sea, and given the absence of DMSP in the mesocosms, this pathway is a potential DMS source. The absence of DMSP from the Baltic Sea samples is unexpected, given that DMSP has previously been identified in freshwater as well as marine environments (see Appendix) it would be expected to be produced in the brackish Baltic Sea. However, DMSP is not ubiquitous across all phytoplankton groups and species, and significant DMSP producers may have been absent from the mesocosm seed populations upon closure of the mesocosms.

5.4.3. DMS concentrations in the mesocosms

DMS showed a clear effect of elevated pCO_2 during Phase 2 and 3: changes in community composition or physiology resulted in daily average DMS concentrations 33% lower at 1120 and 1400 µatm compared to the control (340 µatm). This percentage change compares to a 53 % decrease in DMS concentrations ($pCO_2$340 µatm vs 1400 µatm) in SOPRAN Bergen, and 35 % lower during the EPOCA Svalbard mesocosm experiment (Archer *et al.*, 2013) in surface water pCO_2 expected for 2100 compared to present day . In contrast to Vogt *et al.* (2008), elevated pCO_2 did not affect the temporal production of DMS. Further discussion of the changes in DMS concentrations under elevated pCO_2 will be discussed in Chapter 6.

Changes in DMS concentrations are likely a result of the complex interplay between DMS production and loss processes within the mesocosms, and the differential effect of CO_2 on each process. DMS is produced from the cleavage of DMSP by enzymes known as 'DMSP-lyase', of which a number of different enzymes are present in different groups of phytoplankton and bacteria (Chapter 1, Section 4.2; Todd *et al.*, 2007) and elevated pCO_2 could negatively affect one or more of these pathways to decrease the amount of DMS produced. Alternatively, elevated pCO_2 may divert the degradation of DMSP via the demethylation pathway without the production of DMS (Curson *et al.*, 2011). DMS can also be produced through the reduction of DMSO, which has been shown to occur in a wide range of microorganisms including prokaryotes and eukaryotes in both aerobic and anaerobic conditions (Jonkers *et al.*, 1996; Zinder and Brock, 1978). Mean surface DMSO concentrations of 25 nmol L^{-1} were measured in the southern Baltic Sea in the summer of 2012 (C. Zindler, Pers. Comm, unpublished data); if these concentrations were similar at Tvärminne, it would have required a significant proportion of DMSO to reduce to DMS to produce the DMS concentrations identified in the mesocosms and Baltic Sea samples.

DMS loss processes include consumption by marine bacteria as a carbon and sulphur source (Kiene *et al.*, 2000), and air-sea flux to the atmosphere, although this is a relatively minor sink for DMS (around 10%). DMS loss by photochemical breakdown (Brimblecombe and Shooter, 1986) was unlikely to cause the differences in concentrations identified between light exposure would have been very similar between mesocosms, combined with the 100% absorption of UV light by the mesocosm TPU film (Riebesell *et al.*, 2013).

5.4.4. DMS responses to microbial community development

During Phase 1, the lack of temporal variability in DMS concentrations in any of the mesocosms implied that the production processes were equal to loss processes. DMS

production and loss processes were unaffected by the addition of CO_2 during this phase, showing that either the DMS-producing community did not react immediately to the addition of CO_2, or that the production of DMS was not a response to cellular stress as a result of pCO_2 elevation (Chapter 1, Section 4.2.4; Sunda *et al.*, 2002). DMS was negatively correlated with Chl-*a* concentrations in the Baltic Sea, as previously identified in open waters (Simó and Pedrós-Alió, 1999; Toole *et al.*, 2003).

Supported by strong correlations with cyanobacteria in both the phytoplankton taxonomy (HPLC pigment analysis) and cell abundance (flow cytometry), it is suggested DMS was produced by cyanobacteria in the mesocosms. The findings of Leck *et al.* (1990) support this theory: they identified highest production during July/ August under nitrogen limiting conditions, both circumstances under which cyanobacterial growth is favoured in the Baltic Sea. Although no correlations were carried out between DMS concentrations and the abundance of the filamentous cyanobacteria, growth of *A. flos-aquae* was highest during Phases 2 and 3, when DMS concentrations were at their maximum. DMS production has previously been observed in both the single celled *Synechococcus* (Archer *et al.*, 2011; Wilson *et al.*, 1998) and in *A. flos-aquae* spp. (Leck *et al.*, 1990). No information is available for DMS or DMSP in relation to *Coelosphaerium* or *Pseudanabaena*, however other filamentous cyanobacteria *Nodularia* spp. (Vogt *et al.*, 1998) and *Anabaena* spp. (Caron and Kramer, 1994; Vogt *et al.*, 1998) have also been identified as corresponding to DMS production. DMS in mesocosms has previously been identified in the post-bloom phase (e.g. Avgoustidi *et al.,* 2012; Vogt *et al.*, 2008), and DMS showed significant increases in concentration as *Pseudanabaena* was decreasing, however the DMS concentrations remained high and slowly decreased during the whole of Phase 3 when *Pseudanabaena* abundance was very low. This suggests that DMS was not a result of *Pseudanabaena* bloom degradation.

Strong correlations between DMS and the nanoeukaryote groups 3 and 4 imply that production of DMS may not have been from a single source. It has been seen previously, including during the SOPRAN Bergen experiment, that DMS concentrations may not directly correlate with phytoplankton groups due to the competing pathways of microbial DMSP catabolism, DMS catabolism, sea-air gas exchange and abiotic loss processes (Kiene and Linn, 2000b).

5.5. Iodocarbons

Concentrations of all measured iodocarbons (CH_3I, CH_2I_2, C_2H_5I and CH_2ClI) were higher in the Baltic Sea samples than in the mesocosms for the majority of the experiment, but all

measurements fall well with the range of previous halocarbon concentrations recorded in the Southern Baltic Sea (Table 19). Maximum CH_3I concentrations in the mesocosms reached 6.36 pmol L^{-1} compared to the summer maximum of 15 pmol L^{-1} (Orlikowska and Schulz-Bull, 2009) and concentrations during a cyanobacterial bloom of 7.5 pmol L^{-1} (Karlsson *et al.* 2008). C_2H_5I concentrations ranged from just above D.L. to 0.8 pmol L^{-1}, comparable to the findings of Orlikowska and Schulz-Bull (2009) at 1.0 pmol L^{-1}. CH_2I_2 and CH_2ClI were also measured by Klick (1992) and Klick and Abrahamsson (1992) off a macroalgal bed in the Kattegat, where maximum concentrations were identified as 708 pmol L^{-1} and 74 pmol L^{-1} respectively, significantly higher than was identified in the mesocosms or the Baltic Sea during SOPRAN Tvärminne.

Table 19. Comparison of iodocarbon concentrations from the samples from SOPRAN Tvärminne and the literature. ND: not detected.

	CH_3I	CH_2I_2	C_2H_5I	CH_3ClI
Klick (1992)	-	ND – 242.5	-	ND – 56.8
Klick and Abrahamsson (1992)	-	15.3 – 708.7	-	11.4 – 73.8
Karlsson *et al.* (2008)	3.0 – 7.5	-	-	-
Orlikowska and Schulz-Bull (2009)	1 – 16	0 – 85	0.4 – 1.2	5 – 50
SOPRAN Tvärminne Baltic Sea	4.3 – 8.6	66.9 – 373.9	0.6 – 1.0	7.0 – 18.1
SOPRAN Tvärminne Mesocosm	2.9 – 6.4	57.3 – 202.2	0.2 – 0.8	3.8 – 8.0

As discussed previously, the input of the upwelled water into the Tvärminne region significantly altered the biogeochemical properties of the external waters compared to that in the mesocosms. As a result, it was inappropriate to directly compare the community structure and trace gas production from the Baltic samples and the mesocosms. Given the relative lack of information regarding trace gas concentrations in the Baltic Sea, the mesocosms will be discussed in terms of the trace gas changes under high pCO_2 and the Baltic samples as a record of the current trace gas production in Baltic waters during an upwelling event.

5.5.1. Iodocarbon concentrations in the mesocosms

None of the iodocarbons were affected by elevated pCO_2 within the mesocosms, but some differences were identified between individual mesocosms unrelated to pCO_2. The effects of CO_2 on the iodocarbons within the mesocosm will be discussed further in comparison with SOPRAN Bergen and other mesocosm experiments (Hopkins *et al.*, 2010, 2013; Wingenter *et al.*, 2007) in Chapter 6. As in SOPRAN Bergen, SOPRAN Tvärminne showed few correlations of

iodocarbons with Chl-*a* or specific groups, implying complex interactions with biotic and abiotic processes governing production and loss processes. Discussion of the production and loss processes for halocarbons was discussed previously in SOPRAN Bergen (Chapter 3, Section 5.5). Measurements of halocarbons by Karlsson *et al.* (2008) in the Baltic Sea showed production was mostly during daylight hours, with concentrations at night decreasing to 30% of the concentration measured in late afternoon. As the integrated water samples were collected before 11:00 am, concentrations are likely to be significantly lower than they would have been if collected later in the day. Based on this light-dependence, biogenic production is the most probable source of iodocarbons within the mesocosms.

5.5.2. Monoiodinated compounds (CH_3I and C_2H_5I)

Whilst CH_3I production has been associated with the single-celled cyanobacterium *Prochlorococcus* in the open ocean (Smythe-Wright *et al.*, 2006), *Synechococcus,* as identified in mesocosms has not been observed to produce this compound (Manley and De La Cuesta 1997). Although production of CH_3I within the mesocosms is unlikely to have originated from the *Synechococcus* single-celled cyanobacteria population, there is no information on the production of CH_3I from *Coelosphaerium*. *Pseudanabaena* has been confirmed to produce CH_3I in the Baltic Sea (Karlsson *et al.* 2008) however there was no increase in any of the iodocarbons, particularly CH_3I during Phase 1 around T3-T6 when *Pseudoanabaena* abundance was high. CH_3I showed no correlation with the cyanobacterial pigment analysis.

CH_3I showed relatively few positive relationships with measured biological parameters in the mesocosms, aside from the nanoeukaryote groupings, which were unidentified in terms of species. Laboratory cultures studied by Manley and De La Cuesta, (1997) identified CH_3I production by a number of diatom species, as well as the chrysophytes *Phaeocystis* spp., but not in chlorophytes or dinoflagellates. Hughes *et al.* (2006) also identified production from diatoms, and also the prasinophytes *Tetraselmis* spp., although CH_3I was not correlated to prasinophyte equivalent Chl-*a* in the mesocosms. In contrast, C_2H_5I was related to prasinophytes concentrations in the mesocosm, but in laboratory *Tetraselmis* culture no C_2H_5I production was detected (Hughes *et al.*, 2006).

Concentrations of monohalocarbons are reliant upon the availability of halide ions in seawater. Iodide production has been suggested to be inversely correlated with inorganic nitrate concentrations by Campos *et al.* (1999): in areas of low nitrate, iodide concentrations will be high due to nitrate reductase reducing iodate to iodide when nitrate is unavailable. If this relationship were operational in the Baltic Sea due to the low nitrogen conditions,

concentrations of CH_3I and C_2H_5I would be expected to be high, whereas concentrations were lower than SOPRAN Bergen when inorganic nitrate was added to the mesocosms. During SOPRAN Tvärminne, nitrate concentrations were below detection for the standard autoanalyser analysis method, prompting the requirement for the SCFA-LWCC (Section 2.4.2) to detect concentrations down to nmol L^{-1}. The CH_3I mean mesocosm concentration of 4.1 pmol L^{-1} was very close to open ocean concentrations: 6.2 pmol L^{-1} in the north Atlantic (Lovelock, 1975), 4.4 pmol L^{-1} in the Southern Atlantic (Chuck *et al.*, 2005), 2 - 6 pmol L^{-1} in the Pacific (Moore and Groszko, 1999) and up to 40 pmol L^{-1} in the Indian Ocean (Smythe-Wright *et al.*, 2005). There is therefore no evidence that nitrate concentrations affected the monoiodinated compound concentrations.

5.5.3. Polyhalogenated iodocarbons (CH_2ClI and CH_2I_2)

CH_2I_2 was the only iodocarbon that showed a clear peak in production on T22 which matched the DMS peak on the same day and correlated well with single-celled cyanobacterial cell abundance and with cyanobacterial pigment concentrations. These results suggest that the cyanobacterial community possessed halo-peroxidase enzymes and were responsible for the production of these compounds detected in the mesocosms. Bromoperoxidase activity, capable of producing polyiodinated and poly brominated compounds, has previously been detected in *Synechococcus* in the laboratory and in coastal waters off California (Johnson *et al.*, 2011), and therefore *Synechococcus* could have contributed to halocarbon production in the mesocosms. Both CH_2I_2 and CH_2ClI correlate with single-celled cyanobacterial abundance, and support this production mechanism (Table 16). Strong correlation of CH_2I_2 and CH_2ClI in the mesocosms once again supports the photoreaction of CH_2I_2 to CH_2ClI (Jones and Carpenter, 2005), and in addition, Orlikowska and Schulz-Bull (2009) identified the seasonal maxima of CH_2I_2 during late summer, and found a concurrent increase of CH_2ClI, again indicating a close relationship in the concentrations of these two compounds.

High grazing rates within the mesocosms from cladocerans may have contributed to the release of iodocarbons from algal cells, or released from the faecal pellets of the grazers. Production of CH_3I and C_2H_5I from marine aggregates has previously been reported by Hughes *et al.* (2008), likely through the alkylation of inorganic iodide (Urhahn and Ballschmiter, 1998) or the breakdown of organic matter by microbial activity to supply the precursors required for iodocarbon production (Smith *et al.*, 1992). Hughes *et al.* (2008) detected no CH_2I_2 or CH_2ClI produced from aggregates, but Carpenter *et al.* (2005) suggested the reaction of HOI with organic material in the Arctic sea—ice as a significant source of these compounds.

5.6. Bromocarbons

Concentrations of all three bromocarbons ($CHBr_3$, CH_2Br_2 and $CHBr_2Cl$) in both the mesocosm and the Baltic Sea samples were within the same range as previously measured concentrations in the Baltic Sea, despite none of the previous samples being measured as far north as Tvärminne. Maximum $CHBr_3$ concentrations in the mesocosms reached 147 pmol L^{-1} compared to the most recent studies by Orlikowska and Schulz-Bull (2009) in the southern Baltic Sea: a summer maximum of 41 pmol L^{-1}. In contrast, concentrations offshore of a large macroalgal bed in the Kattegat were 242 pmol L^{-1} (Klick, 1992). Both these studies identified seasonal $CHBr_3$ maxima during the summer months. Mesocosm concentrations of CH_2Br_2 and $CHBr_2Cl$ at 7.7 and 4.7 pmol L^{-1} respectively were again within the same range as Orlikowska and Schulz-Bull (2009), as well as Karlsson *et al.* (2008) from a cruise in the Southern Baltic (Table 20).

Table 20. Comparison of bromocarbon concentrations from the Baltic Sea samples from SOPRAN Tvärminne and the literature. Nd: Not Detected.

	$CHBr_3$	CH_2Br_2	CH_2Br_2Cl
Klick (1992)	39.5 – 790.4	ND – 86.2	ND – 28.8
Klick and Abrahamsson (1992)	13.8 – 584.9	-	-
Karlsson *et al.* (2008)	35 - 60	4.0 – 7.0	2.0 – 6.5
Orlikowska and Schulz-Bull (2009)	5.0 – 40	2.0 – 10	0.8 – 2.5
SOPRAN Tvärminne Baltic Sea	93 - 192	7.1 – 10	3.3 – 5.0
SOPRAN Tvärminne Mesocosm	68.9 – 147.5	4.0 – 7.7	1.7 – 3.1

5.6.1. Bromocarbons in the mesocosms

No CO_2 effect was observed on any measured bromocarbons. The results of this study will be compared to the SOPRAN Bergen experiment and other previous mesocosm experiments (Hopkins *et al.*, 2010, 2013) in Chapter 6.

The steady-state of $CHBr_3$ concentrations within the mesocosms suggested a production source, however $CHBr_3$ showed little correlation with any of the indicators of primary productivity. There were weak positive correlations with $CHBr_3$ and nanoeukaryote groups 2 and 3, but no correlation with the cyanobacteria or diatoms which have previously been identified as linked to $CHBr_3$ production. *Synechococcus* bromoperoxidase activity was suggested as a source of polyiodinated compounds, but none of the bromocarbons show correlations with single-celled cyanobacteria counted by flow cytometry, suggesting

production is not by this route. Moore *et al.*(1996) showed that CH_2I_2 and CH_2ClI were commonly produced by organisms that did not produce $CHBr_3$, and vice-versa. Karlsson *et al.* (2008) identified production of $CHBr_3$, CH_2Br_2 and CH_2Br_2Cl from large-size cyanobacteria such as *A. flos-aquae*, instead of the picocyanobacteria such as *Synechococcus* or *Pseudanabaena*. If *A. flos-aquae* were a major producer of these compounds, the concentrations would expect to increase through Phases 2 and 3 when *A. flos-aquae* abundance was highest, but this relationship is not identified, nor variation in concentrations due to the fluctuations in *A. flos-aquae* abundance. Loss processes of CH_2Br_2 such as sea-air exchange, microbial degradation and hydrolysis in surface waters are suggested to be higher than production in all mesocosms, and hence the slow decline in concentrations through the whole experiment.

Given the lack of variation in bromocarbon concentrations despite changes to populations of diatoms and cyanobacteria (both *Synechococcus* and filamentous forms), it is suggested that bromocarbon concentrations within the Baltic waters upon deployment of the mesocosms was key in determining the mesocosm concentrations of these compounds during the experiment. Correlations between the three bromocarbons and any of the indicators of biological activity were either low or, as in the case of $CHBr_2Cl$, non-existent. Elevated pCO_2 was found to have no effect on bromocarbon concentrations, implying that acidification was not affecting the production or loss processes.

Photolysis of $CHBr_3$ is a significant loss process, but due to the 100% UV absorbance of the TPU mesocosm film, would only be possible in the surface waters close to the mesocosm opening. As with the iodocarbons, Karlsson *et al.* (2008) found that the majority of bromocarbon production was during daylight, and therefore concentrations measured from morning samples may have been significantly lower than if they were taken later in the day.

If there was no production of $CHBr_3$ in the mesocosms, and the major loss was through air-sea exchange, it would be expected that $CHBr_3$ concentrations would decrease faster than CH_2Br_2 due to the higher concentration gradient of $CHBr_3$, despite the similar transfer efficiencies of the two compounds (Quack *et al.*, 2007). While $CHBr_3$ and CH_2Br_2 were likely linked to biological parameters, Schall *et al.* (1997) proposed that $CHBr_2Cl$ (and the similar compound bromodichloromethane $CHBrCl_2$, not measured) is produced in seawater by the nucleophilic substitution of bromide by chloride in the $CHBr_3$ molecule. This substitution could explain the greater variation between days seen for $CHBr_2Cl$ in the mesocosms.

5.6.2. Ratio of CH_2Br_2: $CHBr_3$

The ratio of CH_2Br_2 to $CHBr_3$ was unaffected by CO_2 and stayed within the range 0.04 to 0.08 (Figure 26). These ratios are lower than those identified for SOPRAN Bergen (0.05 – 0.2) and are due to a lower relative concentration of CH_2Br_2 to $CHBr_3$. Ratios are highest during the initial part of Phase 1 and then decrease as the experiment progresses up until T29. Using cluster analysis in the time-series study in the Southern Baltic Sea, Orlikowska and Schulz-Bull, (2009) identified $CHBr_3$ and CH_2Br_2 as originating from different species and different pathways of production. This was reinforced by Quack *et al.*(2007) in the Mauritanian upwelling.

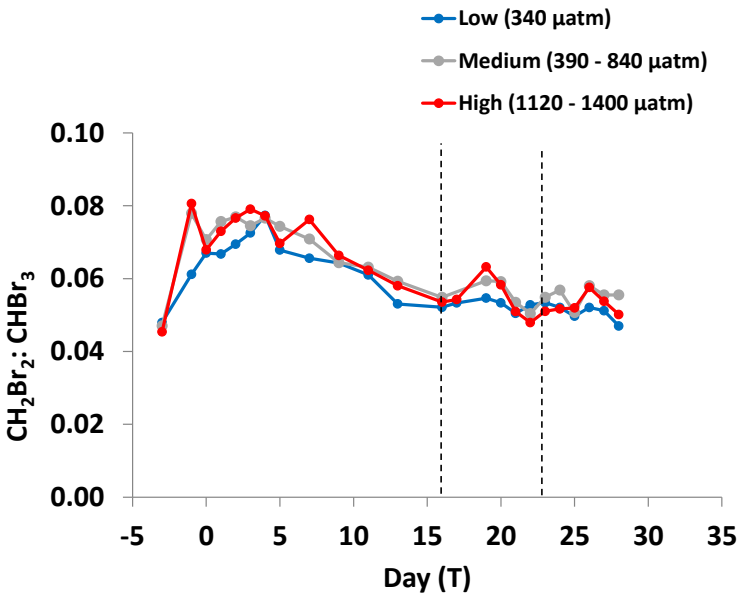

Figure 26. Ratio of CH_2Br_2 to $CHBr_3$ during SOPRAN Tvärminne in the three different pCO_2 treatments: low (control at 340 µatm), medium (390 – 840 µatm) and high (1120 – 1400 µatm).

Further evidence that CH_2Br_2 and $CHBr_3$ originated from different sources was derived from comparison with the iodocarbons and DMS data. $CHBr_3$ was reasonably correlated with DMS and all the iodocarbons except C_2H_5I. CH_2Br_2 showed no or negative correlation with all the other trace gases except C_2H_5I. A similar lack of correlation between brominated and iodinated compounds was identified by (Orlikowska and Schulz-Bull, 2009) within the Baltic Sea. CH_2Br_2 was correlated with cryptophytes and dinoflagellates.

5.7. Trace Gas production in the Baltic Sea

The upwelling event discussed in Section 5.1 was found to have influenced the concentrations of measured gases. This upwelling was likely to have significantly altered the community structure in the Baltic Sea samples compared to those of the mesocosms. The samples from

the Baltic Sea cannot be compared directly with the mesocosm samples, and the Baltic samples were excluded from the correlation analysis for the trace gas data to eliminate the possibility of them originating from a different source. As there are few measurements of trace gases in the Baltic Sea, and no measurements of DMS in this region of the Baltic Sea, this section discusses the data which will be available for inclusion in global trace gas databases.

5.7.1. DMS production in the Baltic Sea

DMS concentrations in the Baltic Sea samples showed concentrations twice as high as measured in the mesocosms and, in contrast to the mesocosms, showed very strong correlations with Chl-*a*, euglenophytes and dinoflagellates. Production peaked on T16 and then decreased, and is likely related to the upwelling event: warmer waters encouraged the development of high levels of primary production up until T16, after which the upwelling and dilution of the surface with cooler waters reduced Chl-*a* concentrations and subsequently DMS.

Reduction in DMS during Phases 2 and 3 in the Baltic Sea may have been linked to the change in pH associated with the upwelled water. As seen in the mesocosms, lower pH/ high pCO_2 is inversely related to DMS concentration: as the pH in the Baltic Sea decreased, DMS production may have been reduced accordingly. These upwelling events are common occurrence in the Baltic Sea, and it is likely that the microbial community is adapted for exposure to these conditions.

5.7.1. Iodocarbon production in the Baltic Sea

Mean experiment concentrations of iodocarbons within the samples from the Baltic Sea were higher than the mesocosm concentrations, in particular during Phases 2 and 3. Concentrations of CH_3I, C_2H_5I and CH_2ClI increased from mid-way through Phase 1, implying that the increased concentrations were unrelated to the upwelling event which started on T16 until the end of the experiment.

Klick and Abrahamsson (1992) studied iodocarbon concentrations in an algal belt in the Skagerrak, and while bromocarbon concentrations were significantly higher in the waters immediately adjacent to the algal belt, CH_2I_2 concentrations were equivalent to what was measured during SOPRAN Tvärminne in the Baltic Sea samples. Concentrations measured in the coastal waters offshore, however, gave concentrations up to 700 pmol L^{-1}, compared to 374 pmol L^{-1} measured in this study. The elevated concentrations of CH_2I_2 away from

macroalgal beds imply that production of this and CH_2ClI were from a microalgal source rather than macroalgal. The Baltic Sea correlations from this study confirm this with strong relationships between CH_3I, CH_2I_2 and CH_2ClI with nanoeukaryotes 2.

5.7.2. Bromocarbon production in the Baltic Sea

Mean experiment concentrations of the three bromocarbons within the Baltic Sea samples were higher than in the mesocosms. Prior to the addition of CO_2 enriched waters, concentrations were similar in the mesocosms and the Baltic Sea, subsequent to which the concentrations in the mesocosm decreased. Trends in all three Baltic Sea bromocarbons were similar: peaks were identified on T16 and T23 at the changeover between the three phases, implying a mutual source. Given the proximity of the mesocosms to the shoreline, and the seabed at 30 m, it is likely this production is macroalgal in origin, especially given the minimal phytoplankton production of bromocarbons within the mesocosms separate from macroalgal influence. Macroalgal production is the predominant source of bromocarbons in the coastal zones (Leedham Elvidge et al., 2014; Wever et al., 1991), and this is true in the Baltic Sea as in other coastal sites. Concentrations in coastal algal belts in the Baltic Sea measured $CHBr_3$ and CH_2Br_2 as high as 2000 pmol L^{-1} and 450 pmol L^{-1} respectively (Klick, 1992). A summary of the bromocarbon concentrations measured in the Baltic Sea are given in Table 20, although all previous measurements are taken in the Southern Baltic or Kattegat, where there is greater influence of Atlantic seawater inflow.

Finland has the highest area of boreal forest land in Europe, at 69 % of the total land area (FAO, 2014). Studies have suggested bromo and chloro-peroxidase activity in boreal forest soils have the ability to produce high concentrations of halocarbons such as $CHBr_3$, CH_3I and several chlorinated compounds, either direct release of these compounds into the atmosphere (Frank *et al.*, 1989; Frank and Frank, 1990; Keppler *et al.*, 2000; Laturnus *et al.*, 1995). Leaching of brominated compounds into groundwater is likely, and given the high influx of freshwater into the Baltic Sea, it is likely this groundwater will be a natural source of halocarbons into the Baltic Sea waters. No studies were found which identified halocarbon concentrations directly in the forest air, and it was therefore impossible to determine if the air concentrations over the Baltic Sea would affect the air-sea flux of halocarbons from the water.

5.8. Summary

Elevated pCO_2 and ocean acidification affected different parts of the Baltic Sea microbial community differently: while Chl-*a* concentrations were unaffected by elevated pCO_2, some

phytoplankton groups such as the picoeukaryotes showed better growth under high pCO_2, while others such as nanoeukaryote group 4 showed negative effects. It was difficult to determine the effect on heterocystous cyanobacteria due to the problems in enumerating these species, and therefore difficult to determine the effect on atmospheric nitrogen chemistry.

The trace gases measured in SOPRAN Tvärminne were within the same range as those of SOPRAN Bergen and previous studies within the Baltic Sea, and provide the first insight into the changes in Baltic Sea DMS and halocarbon concentrations in response to high pCO_2. DMS showed a strong clear inverse relationship with CO_2, with concentrations reduced by 33 % at 1400 µatm pCO_2 compared to the control. No DMSP data was available to determine the effects of elevated pCO_2 on DMSP production in the Baltic; this absence of detected DMSP has highlighted the potential of DMS production from the methylation of methanethiol, rather than the standard breakdown of DMSP. This is a pathway which requires further investigation by genetic techniques to identify and isolate the Mdd gene in the Baltic Sea and prove this pathway exists in a marine environment.

Neither the iodocarbons nor bromocarbons showed significant changes as pCO_2 increased, which was in contrast to SOPRAN Bergen where iodocarbon concentrations decreased under elevated pCO_2. Not only do the results presented here show the effects of increased pCO_2 on the microbial communities and trace gas production, but it also provides a baseline from which to compare the future trace gas concentrations from these waters.

BLANK

Chapter 6. Discussion

1. Increasing atmospheric pCO_2 and ocean acidification

As anthropogenic atmospheric pCO_2 has increased since the industrial revolution, the oceans have absorbed up to 50 % of excess CO_2 produced, and will continue to do so (Canadell *et al.*, 2007; Cubasch *et al.*, 2013). Atmospheric pCO_2 in excess of 400 µatm were recorded at Mauna Loa in Hawaii in 2014 (Scripps Institution of Oceanography at UC San Diego), a concentration higher than the past 800,000 years (Lüthi *et al.*, 2008), and likely as long as 20 M yr (Pearson and Palmer, 2000). Atmospheric concentrations are expected to rise to between 500 and 1400 µatm before the year 2100. The oceanic uptake of this excess CO_2 is expected to result in decrease in surface water pH of 0.7 units on the same timescale (Caldeira and Wickett, 2003), a process termed ocean acidification (Chapter 1, Section 2.2). Ocean acidification is a process expected to progress over a long timescale of hundreds of years, and the consequences and effects on biological organisms are largely unknown. As a result of this, it is also unknown how the changes will affect the production of marine biogenic trace gases which have important roles in atmospheric chemistry and regulating climate.

This investigation aimed to investigate the changes in DMS and halocarbon concentrations as ocean acidification and dissolved pCO_2 in seawater increase. The primary findings were that community DMS and DMSP concentrations were inversely related to increasing pCO_2, likely due to microbial interactions between the DMSP producers and consumers, as this effect was not identified in monoculture in the laboratory. Halocarbons exhibited a range of responses to elevated pCO_2, and require further investigation to project the concentrations in a future ocean.

2. Experimental options for studying ocean acidification

A number of experimental tools are available to study the microbial response to ocean acidification:

- Small scale laboratory cultures to investigate the short-term physiological response of individual species.
- Seawater incubations to investigate the short-term response of microbial communities adapted to different natural background pCO_2 (Richier *et al.*, 2014b).
- Mesocosm experiments (currently 2,400 – 77,000 L) to investigate the medium-term microbial community response, deployed in different geographical locations to take advantage of spatial variation in natural communities (Riebesell *et al.*, 2008).
- Ship-board sampling to identify spatial variation in oceanic pCO_2 at different geographical locations, and study the adaptation of natural microbial communities to those conditions (Richier *et al.*, 2014a)
- Time-series experiments on natural microbial communities or laboratory monocultures to evaluate the adaptation to environmental perturbations over the medium to long-term (Takahashi *et al.*, 2006).
- Natural CO_2 vent-sites to study the long-term perturbation of natural microbial communities to elevated pCO_2 (e.g. Johnson *et al.*, 2013).

These techniques need to be interpreted together to establish an overarching view of the likely changes to microbial communities under future pCO_2 scenarios. During this investigation, the medium-term response to elevated pCO_2 of a natural community-based *E. huxleyi* bloom was compared to a laboratory monoculture with limited bacterial interactions to study the changes in DMS and DMSP concentrations. The response identified allowed determination that it is likely the CO_2 influenced bacterial interactions with *E. huxleyi* and DMSP concentrations which determined the DMS response, rather than the direct effect of CO_2 on *E. huxleyi*.

2.1. Medium-term perturbation experiments

Small-scale laboratory experiments are relatively simple to design and operate. The larger the experiment, the greater the cost, operational requirements and manpower required for a successful campaign. The advantages of mesocosm experiments have been described in Chapter 3, Section 1, and represent the optimum experimental design currently available to study ocean acidification. The ability of mesocosms to replicate the interactions between different parts of the microbial community will improve as enclosures get larger through advances in technology. The KOSMOS mesocosms experiments represent the largest enclosures operated over the longest time period of any study of pCO_2 perturbation on surface water microbial communities. Larger mesocosms require greater operation cost and management, but require less perturbation through the addition of artificial nutrients or

prevention of interactions with the surrounding environment (e.g. rainfall, wind). An advantage of mesocosms is the community progression in close to natural environmental conditions; however the current design limits the action of physical parameters such as wind and wave action on the sea surface microlayer, which influences the sea-air exchange of the trace gases under investigation in this study (Liss and Slater, 1974; Nightingale *et al.*, 2000). Rainfall can enter the mesocosms, but this will be limited by a PVC cover which prevents unwanted nutrient additions from seabirds.

The larger size of mesocosms allows for extensive sampling over a 30 day period without removal of excessive water volume affecting community development. From a 77,000 L mesocosm during SOPRAN Bergen, an estimated 1000 L (1.3% of total) was removed over 30 days for all the sampling parameters. In comparison during the *E. huxleyi* batch experiments where approximately 70% of the total culture volume was removed for sampling over a period of 10 days. In a culture flask, removal of this volume of media will affect nutrient availability and increase light intensity, changing the parameters under which the experiment was set up. The semi-continuous cultures in this investigation used less than 40% of the total culture volume. Another way to circumvent this problem is through sacrificial sampling: the shipboard incubations performed by Richier *et al.* (2014b) set up incubations for 4 pCO_2 treatments up to 1000 µatm, and removed bottles in triplicate for sampling after 48 and 96 hours. This method requires confidence that the starting populations were identical, and all bottles experience the same environmental conditions to stimulate identical growth. For trace gas sampling, this method is ideal as not only are the bottles gas tight, but communities have not been disturbed prior to sampling (Hopkins and Archer, 2014) as occurs during daily mesocosm sampling. Sacrificial sampling is limited by the number of incubation bottles which can be replicated at the start of the experiment.

A drawback of the mesocosm experiments is the design of the enclosures themselves. Unlike laboratory experiments where fragile culture flasks remain in a controlled environment, mesocosm enclosures must be of sufficient strength to withstand 30-40 days of exposure to tidal forces and wave action, yet still allow transmission of sufficient PAR (Riebesell *et al.*, 2013; Schulz *et al.*, 2013). Community development during this time also causes biofouling of the mesocosm walls which blocks PAR (Watts and Bigg, 2001), and while regular wall cleaning will remove the periphyton, the action can elicit changes in bacteria abundance and nutrient loss through higher sedimentation rates (Chen and Kemp, 2004). This loss was identified during SOPRAN Tvärminne, when cyanobacterial photopigments were identified in sediment trap supernatant in the days following removal of filamentous species from the walls (T. Boxhammer, GEOMAR, Pers Comm).

2.2. Use of natural laboratories

Natural *in-situ* ocean acidification sites are areas where pCO_2 levels are high with corresponding lowered pH and carbonate saturation. These sites provide large spatial and temporal scales to allow the integration of ecosystem processes such as production, competition and predation (Barry *et al.*, 2010; Hall-Spencer *et al.*, 2008). Such *in-situ* sites include natural CO_2 vents (i.e.Ischia Island, Italy, Hall-Spencer *et al.*, 2008), submarine volcanoes (Lupton *et al.*, 2008) or coastal upwelling regions of CO_2 rich waters (Borges and Frankignoulle, 2002). During the latter, nutrients brought up from deeper waters encourages significant primary production which lowers the pCO_2 in the surface waters.

The main problem with *in-situ* observational experiments is that the site may be influenced by factors other than pCO_2 and seawater carbonate chemistry (i.e. temperature or methane at deep-sea vent sites; Barry *et al.*, 2010). Many of the studies on natural CO_2 sites have been focussed on benthic calcifying organisms or macroalgae (Cigliano *et al.*, 2010; Dias *et al.*, 2010; Hall-Spencer *et al.*, 2008; Porzio *et al.*, 2011) and not phytoplankton communities. In a natural phytoplankton assemblage, it is likely the upwelling event may affect some species more than others, but these species will be replenished through water movements from unaffected areas after the upwelling event has passed. Some of the changes observed in the mesocosm microbial communities under elevated pCO_2 may be a result of species being affected by high pCO_2 but not being replenished (i.e. dinoflagellate growth in both SOPRAN experiments).

Natural observational studies have exploited the gradients in pCO_2 and pH that exist along hydrothermal or CO_2 vent sites, or across spatial, temporal or depth-related changes in pH (Barry *et al.*, 2010). The island of Ischia in Italy is one such site, surrounded by a cold-vent area acidified by gas of up to 95 % CO_2, where pCO_2 increases in gradients to over 2000 µatm. Another site is at the D'Entrecastraux Islands Papua New Guinea, where coral communities are exposed to 99% CO_2 gas from cool volcanic seeps (Fabricius *et al.*, 2011). These sites are ideal for studying the effects of high CO_2 on sessile benthic community structure and calcareous organisms, and lends itself well to *in-situ* perturbation experiments (Hall-Spencer *et al.*, 2008). However Hopkins (2010) assessed Ischia as difficult for trace gas measurements due to the highly variable nature of seawater pH on spatial and temporal scales, as the rapid changes would have short-term impacts on pelagic communities compared to benthic communities. Additional sites such as deep sea hydrothermal vents (Lupton *et al.*, 2008) are clearly unsuitable for the in-situ study of surface water communities and their trace gas production due to their depth and the restricted potential for sea-air gas exchange.

The recent UK Ocean Acidification Research Programme NW European Shelf Cruise in 2011 undertook a number of shipboard bioassay experiments to study the effects of elevated pCO_2 on natural populations at 5 sites on the NW European Shelf (Hopkins and Archer, 2014; Poulton *et al.*, 2014; Richier *et al.*, 2014b). Although not strictly an *in-situ* observational experiment, the bioassays took advantage of the natural background variation in pH and pCO_2 to test the acclimation of the five different communities to elevated pCO_2, and allowed an assessment of regional differences. Bioassays and perturbation experiments using natural seawater can provide a different perspective than the longer-term isolated communities in a mesocosm experiment.

In Chapter 5 (SOPRAN Tvärminne) it was suggested that the Baltic Sea may represent a potential natural laboratory for studies on ocean acidification due to the regular upwelling of CO_2-rich seawater, although there was still temporal and spatial variability in pH and seawater pCO_2 as detected at Ischia. In the majority of upwelling systems along Eastern continental boundaries, CO_2 oversaturated, aragonite undersaturated waters are seasonally brought up onto the continental shelf (Feely *et al.*, 2008), and could provide suitable natural laboratories for CO_2 enrichment studies. High nutrient concentrations in these waters stimulate significant phytoplankton blooms (See Chavez and Messié, 2009), which lowers the surface water pCO_2. However, due to these high levels of primary production, it is uncertain whether the majority of these areas are net sources or sinks of CO_2 (Borges and Frankignoulle, 2002), although they are key sources of trace gases (Quack *et al.*, 2007a, 2007b; Zindler *et al.*, 2012). pCO_2 of up to 900 µatm have been measured in upwelling zones (Torres *et al.*, 1999), equivalent to the pCO_2 measured in the upwelled waters in the Baltic Sea during SOPRAN Tvärminne. In the upwelling off Tvärminne, Chl-*a* concentrations increased prior to the upwelling event when temperature was highest, and decreased as the cooler, CO_2-rich upwelled waters were brought to the surface. This is in contrast to the expected bloom during an upwelling event, however inorganic nitrogen concentrations during this period were no higher than in the SOPRAN experiments (below 100 nmol L^{-1}). It is suggested that the lack of additional nutrients in the upwelled water, combined with lowered pH below 7.6 on T33 was detrimental to phytoplankton growth (Chapter 5, Section 3.4). This suggests a short-term response to high pCO_2 which was not identified in the mesocosms, but was identified in short term incubation experiments (96hr) rapidly exposed to 1000 µatm pCO_2 (Richier *et al.*, 2014b).

Using Tvärminne as a natural high pCO_2 laboratory would be dependent upon the occurrence of an upwelling events; this, like the occurrence of cyanobacterial blooms, cannot be easily projected. However summertime upwelling in the Baltic Sea has been well-documented (Lehmann and Myrberg, 2008; Lehmann *et al.*, 2002) and is therefore likely to occur at

Tvärminne at least once annually. The Baltic Sea also has the advantage that in wintertime, the pH decreases across the surface waters during the breakdown of stratification (Brutemark *et al.*, 2011), and therefore has allowed the natural acclimation of phytoplankton communities to lowered pH over a timescale of years (greater than can be achieved in a perturbation experiment). Annual variation in pH is predictable between 7.9 and 8.6 (Omstedt *et al.*, 2010). CO_2 has a higher solubility in cooler winter waters, which is released from the water in spring back to the atmosphere as the water warms, as well as being utilised through biological activity.

2.3. Importance of experimental timescales

A major question during all CO_2 perturbation experiments is 'how long does it take the target species to acclimate to the conditions under which they are being tested'? As discussed in Section 2, small-scale perturbation experiments allow changes in physiological response of individual species to high pCO_2, whereas larger experiments such as the SOPRAN experiments study the response of multiple species and community interactions. However, in common to both these setups is the time over which the experiment is run: in this investigation, the SOPRAN experiments and the semi-continuous experiments lasted approximately 30 days. The shipboard CO_2 incubations evaluated the short-term response of the community and lasted 96 hours (Richier *et al.*, 2014b), whereas additional SOPRAN experiments have lasted 5 months (Riebesell, Pers Comm).

Most experiments use pCO_2 projected for the year 2100 according to the IPCC scenarios (Cubasch *et al.*, 2013). These scenarios allow for a gradual change in pCO_2 over the next 100 years, whereas during many perturbation experiments, the CO_2 adjustment is performed over a relatively short period of time (over 5 days during SOPRAN Bergen and SOPRAN Tvärminne and immediately in the laboratory cultures), followed by the assessment of the response to the pCO_2 on the target organism(s). Although Barcelos e Ramos *et al.* (2010) found that *E. huxleyi* cells acclimated to changed conditions within 24 hours, this response is on a single species, and has not been confirmed for every species in the mesocosm community assemblage. Any immediate response to the perturbation can be an authentic response or attributed to shock from which the organism may recover. The differing effect of CO_2 identified for Chl-α between the first and second blooms of SOPRAN Bergen could be attributed to initial shock with the later response more likely in 2100. The physical, chemical and biological parameters measured during SOPRAN Bergen in pCO_2 up to 3000 µatm may have shown different responses if the experiment had been carried out for several months to years with

slower addition of nutrients. This is impossible under the current mesocosm setup, without significant repeat additions of nutrients and CO_2.

A major question therefore is 'can we project and model the responses of different parameters in surface water microbial communities based on these short-term experiments?' Only a few longer term experiments have been performed: Lohbeck *et al.* (2012b) maintained *E. huxleyi* at high (1100 and 2200 µatm) pCO_2 for 500 generations, and Collins and Bell (2004) grew *Chlamydomonas reinhardtii* for 1000 generations at 1050 µatm pCO_2. Both experiments identified evolution of the cells to the new environmental conditions, which subsequently showed different growth rates to ambient cultures when returned to ambient conditions. The *E. huxleyi* experiments noted a partial restoration of calcification in the evolved cultures, although no measurements were made of DMSP production. The implications of these experiments are that evolution can allow species to adapt to changes in pCO_2, and the responses to elevated pCO_2 identified in phytoplankton during the relatively short-term mesocosm and laboratory experiments may not be identifiable given sufficient time. Adaptation may result in a reduction in genetic diversity, unless the microbes already possess the genetic flexibility for homeostasis of intracellular pH (Booth, 1985), or can acquire the abilities through lateral gene transfer (Joint *et al.*, 2011). *E. huxleyi* has shown high diversity of morphotype (Patil *et al.,* 2014), due to its global distribution, and Meier *et al.* (2014) postulated that high variability in ecological function was likely, allowing this species to evolve and survive environmental change. Further to this, Iglesias-Rodriguez *et al.* (2006) revealed high intraspecific genetic variability within *E. huxleyi*, and this might explain the differing responses of different *E. huxleyi* strains to elevated pCO_2 (a summary is given in Chapter 4, Section 1.1). During this investigation, CO_2 strongly affected *E. huxleyi* and subsequent DMSP production at all levels of elevated pCO_2 during SOPRAN Bergen, but in the CO_2 enrichment experiments at 890 µatm, *E. huxleyi* RCC1229 showed no significant difference in growth rate or DMS production, even after exposure to the high pCO_2 conditions for 28 days. Due to this diversity and the wide variation in response to different environmental variables, Fabry (2008) suggested that *E. huxleyi* is not a single globally distributed species.

2.4. Effects of multiple physical parameters on cell growth and volume

Elevated pCO_2 is not the only projected environmental change faced by marine organisms under the projected future IPCC scenarios. Other stressors include changes to temperature, light (through changes to turbidity) and nutrient concentrations (through changes to availability related to physical and chemical factors; Zondervan, 2007), and these factors often

act synergistically. Multifactorial experiments are expensive and time consuming, but as pCO_2 will not be increasing independently of temperature, these more complex studies are increasingly required to determine the effects of combined stressors, rather than individual effects. Mesocosm and open ocean experiments are needed for these studies, but altering temperature and light in a field situation is highly impractical: aside from the cost of designing and maintaining a temperature increase in the mesocosms over sustained period, any alterations could affect light penetration through the bag material (Lance, 2009). A mesocosm experiment in Korea was performed with a 2°C temperature increase alongside elevated pCO_2, but the mesocosms were only 2400L in total volume (Park et al., 2014).

During this investigation, the cells in the laboratory experiments were under no nutrient stress and at optimum light (Heinle, 2013), and a close to optimum temperature for this strain (Chapter 4, Section 2.2). Heinle (2013) determined growth rates of *E. huxleyi* RCC 1229 during batch experiments at various temperature and light levels in a thermal gradient bar, and identified the optimum temperature was 23.5°C, with the specific growth rate reaching 0.97 d^{-1}. Although no change in growth rates was identified during this investigation for a pCO_2 increase to 890 µatm, the combined effect of pCO_2 and elevated temperature on this strain could have increased the growth rate to >0.6 d^{-1} as measured in the semi-continuous and batch cultures (Chapter 4, Tables 7,8 and 9). Spielmeyer & Pohnert (2012) investigated the combined effects of pCO_2 and temperature on strains RCC1242 (non-calcifying) and RCC 1731 (calcifying) and found that the growth rate was lowest in the control (pH 8.28, 14.5 °C, ambient air) at 0.3 d^{-1}, increasing to 0.36 d^{-1} under elevated pCO_2 (790 µatm) and 0.67 d^{-1} under combined temperature and pCO_2 perturbation (20.5 °C and 790 µatm respectively). Combining light with these two parameters in the strain CCMP371 showed that increasing the light levels from 50 to 400 µmol photons mL^{-1} had a greater effect on the growth rate than either increases in pCO_2 or temperature (Feng *et al.*, 2008). In the study of *E. huxleyi* and *Gephyrocapsa oceanica* (Sett *et al.*, 2014) temperature was found to modify the sensitivity of metabolic processes to elevated pCO_2 effects, and responses to calcification and growth rate were different under combined conditions than pCO_2 alone. If temperature has a significant modulating effect on the pCO_2 response in more than a few species, any past mesocosm and lab experiments studying pCO_2 alone could be will require additional experiments showing the combined effect of elevated pCO_2 with temperature to correspond to the projected rise in atmospheric conditions by the end of the century. Despite the difficulties involved and cost implications, future laboratory and mesocosm investigations will need to incorporate multifactorial approaches in the design of new and existing experiments.

Kiene and Linn (2000) showed that temperature significantly affected the partitioning of sulphur during dissolved DMSP degradation, with higher temperatures resulting in greater uptake into the particulate phase. Studying the effect of elevated temperature on phytoplankton is therefore important in determining the future changes to DMS and DMSP concentrations. Initial studies on the combined effects of temperature and pCO_2 on concentrations of DMS and DMSP show varying responses: increased DMS and DMSP from *E. huxleyi* cultures (Arnold *et al.*, 2013) and in natural seawater incubations (Lee *et al.*, 2009, 2011) but decreased DMSP in two diatom cultures (Spielmeyer and Pohnert, 2012). In the only in situ mesocosm experiment studying 'greenhouse' conditions, increased temperature alone temperature resulted in decreased DMS and DMSP concentrations, with the combined effects eliciting an even stronger negative response with even lower concentrations, despite no change in Chl-α under any treatment (Park *et al.*, 2014). The response in DMSP is dependent upon the response of those species that are strong DMSP producers. The improved growth of picoeukaryotes at high pCO_2 was identified as an important DMSP source during EPOCA Svalbard (Archer *et al.*, 2011, 2013), and *E. huxleyi* was a likely source of DMSP during SOPRAN Bergen but had lower cell abundance at high pCO_2. It is clear that it would be worthwhile for the suggested multiple factor experiments to incorporate measurement of DMS and DMSP concentrations, as the added factor of temperature could overcome the negative impact of increased pCO_2 seen repeatedly on DMS and DMSP concentrations in future scenarios.

3. Changes to SOPRAN experiment target species under future pCO_2[1]

Algal photosynthesis is undertaken through the operation of ribulose biphosphate carboxylase oxygenase (RubisCO), but the saturation of RubisCO for CO_2 is less than half-saturated under current pCO_2 (Giordano *et al.*, 2005). In order to prevent carbon limitation, most macroalgae have developed mechanisms to concentrate CO_2 or HCO_3^- (CCMs) within the RubisCO cell machinery. CCMs differ in efficiency and regulation between species, and it is likely that species with inefficient CCMs will benefit from increased pCO_2 within seawater (Rost *et al.*, 2008). Species with highly efficient CCMs will also benefit from a down-regulation of the mechanisms and therefore a lower energy requirement. Many bloom-forming diatom species were able to compensate for low CO_2 supply using efficient CCMs (Trimborn *et al.*, 2008), but

[1] Data from the SOPRAN experiments in this section is used courtesy of Yves Trense (HPLC Pigment data), Aud Larsen (SOPRAN Bergen Flow Cytometry), Kate Crawfurd (SOPRAN Tvärminne Flow Cytometry) and Annegret Stuhr (SOPRAN Tvärminne light microscopy).

in high pCO_2 environments, this may be a disadvantage. For example, diatom equivalent Chl-*a* during SOPRAN Bergen was highest in the mid-range pCO_2 mesocosm (840 µatm) but was significantly lower in the highest pCO_2 mesocosm (3000 µatm; Chapter 3, Section 3.5), suggesting an optimum pCO_2 for the diatom assemblage. Studies have shown CO_2 to cause shifts in the dominance of diatom species (Tortell *et al.*, 2002), and in communities towards a diatom dominant community (Eggers *et al.*, 2014). *E. huxleyi* have been found to be strongly sensitive to CO_2 with low-affinity CCMs (Rost *et al.*, 2003). CCMs have been identified in chlorophytes (*Chlamydomonas* spp.) and cyanobacteria (Giordano *et al.*, 2005), both of which showed higher pigment concentrations under high pCO_2, with the chlorophytes being the only species which consistently showed higher growth under high pCO_2. The following sections cover the growth of the two target groups from this investigation: *E. huxleyi* from SOPRAN Bergen and the CO_2 enrichment experiments and cyanobacteria from SOPRAN Tvärminne.

3.1. *Emiliania huxleyi*

Coccolithophores have been a key focus of ocean acidification studies due to their ease of culturing, global distribution and ability to calcify. *E. huxleyi* is of particular interest to this study as it is a producer of DMSP, and has been associated with elevated surface water DMSP concentrations (e.g. Levasseur *et al.*, 1996; Malin *et al.*, 1993; Steinke *et al.*, 2002). It has also been a focus of all but one of the mesocosm experiments in Bergen, and was again targeted for SOPRAN Bergen (Chapter 3). Franklin *et al.* (2010) determined that *E. huxleyi* was a good representative member of the coccolithophores in terms of its cell DMSP quota, but was one of only two coccolithophores (along with *Gephyrocapsa oceanica*) found to contain DMSP-lyase and potentially able therefore to emit DMS directly into the sea. In terms of DMSP turnover it might not be a representative member of the group, but the majority of culture and open water experiments have focussed on *E. huxleyi*. Neither *E. huxleyi* or any other coccolithophores were found in the Baltic Sea during SOPRAN Tvärminne, as a combined result of low salinity and undersaturation of both aragonite and calcite in winter in the Baltic Sea (Tyrrell *et al.*, 2008).

Previous studies have identified differing responses into the growth of coccolithophores under high pCO_2, both in the lab and the field. The CO_2 enrichment experiments in this investigation with *E. huxleyi* strain RCC1229 showed higher cell concentrations in the high pCO_2 treatments during the semi-continuous cultures, which corresponded to the finding of Fiorini *et al.* (2011), Spielmeyer and Pohnert (2012) and Moheimani and Borowitzka (2011), as well as Paulino *et al.* (2008) during PeECE III. In other studies, *E. huxleyi* reached lower cell densities under high

pCO_2 (SOPRAN Bergen; PeECE II, Engel *et al.*, 2005; NERC Metagenomics experiment, Hopkins *et al.* 2010), or showed no significant difference (Arnold *et al.*, 2013; Bach *et al.*, 2013). *E. huxleyi* has been identified as operating a relatively low-affinity CCM compared to other groups such as diatoms (Rost *et al.*, 2003), and it has evolved to survive limiting CO_2 rather than excess (Bach *et al.*, 2013). Under elevated pCO_2 conditions, *E. huxleyi* would be advantaged by the higher dissolved pCO_2, and was found by Kottmeier *et al.* (2014) to increase the fraction of CO_2 uptake over HCO_3^- as CO_2 increased. Calcification has been suggested as a potential CCM in *E. huxleyi*, with protons from the calcification neutralised by hydroxyl ions from the carbonic anhydrase catalysed conversion of HCO_3^- to CO_2 for photosynthesis (Buitenhuis *et al.*, 1999; Paasche, 2001). This process was later refuted by Bach *et al.* (2013) and Leonardos *et al.*, (2009), as well as Moolna and Rickaby (2012) for *Gephyrocapsa oceanica* (a species similar to *E. huxleyi* in physiology), who also found no change in growth rate or calcification under elevated CO_2 in this second coccolithophore. If calcification is not needed as a CCM, there is a likelihood that as calcification has increasing energetic requirements as pCO_2 increases, is it likely the cell could convert to the diploid decalcified form (Chapter 1, Section 4.7) over the calcified form? As non-calcified cultures have been grown successfully in the laboratory, and many cultures have been seen to revert to the decalcified form under nutrient replete conditions (G. Malin, Pers. Comm), this would certainly be a survival strategy, but the question remains as to the purpose of the coccoliths if the cells can survive decalcified. As previously discussed, *E. huxleyi* shows high diversity of morphology and genetic variation (Iglesias-Rodriguez *et al.*, 2006; Meier *et al.*, 2014); increased pCO_2 may cause a decrease in calcification and loss of liths, or cells may originate from a less calcified morphotypes capable of survival without a coccosphere. Further study into the morphology and genetic variability of *E. huxleyi* is required to determine if there are genetically distinct sub-populations of de- or low-calcified morphotypes, and if increased pCO_2 will promote the distribution of these less-calcified sub-populations.

Few studies have looked at the response of diploid naked and calcified cells in the laboratory, and those that have were focussed on the haploid naked phase (e.g. Green *et al.*, 1996; Houdan *et al.*, 2005). Alongside establishing the potential for an increase in naked morphotypes under increased pCO_2, investigations of the DMSP production of calcified and naked coccolithophore cells would be very worthwhile, and would indicate if DMSP production is linked to calcification.

The reported effects of high pCO_2 on the calcification rates of coccolithophores are varied. Although calcification was not measured during SOPRAN Bergen, there was no change during PeECE III (Bellerby *et al.*, 2008) but decreased calcification during PeECE I (Delille *et al.*, 2005).

Laboratory experiments performed on single strains also showed differences (Chapter 4, Table 1). In the majority of the studies, calcification decreased, with exceptions of Iglesias-Rodriguez *et al.* (2008) and Shi *et al.* (2009). It would appear that there is no overall straightforward response of the species *E. huxleyi* to increasing pCO_2, as shown from the comparison of SOPRAN Bergen (Chapter 3) and the high pCO_2 enrichment experiments (Chapter 4), and the likelihood of high abundance of decalcified cells in the mesocosms, either as a response to elevated pCO_2, or as a significant proportion of the natural *E. huxleyi* population in the Norwegian Fjords during deployment of the mesocosms. Responses are likely due to a combination of temperature, salinity, nutrient availability and community response effects, as well as the genetic variability within the species. Based on the data available in the EPOCA database on ocean acidification, Muller and Nisbet (2014) project that *E. huxleyi* growth and calcification will show moderate decreases under the A2 climate change scenario (approximately 2000 µatm in 2100). A reduction in net calcification will have consequences for the export of calcium carbonate to deeper waters, and the associated removal of carbon from surface waters to deep ocean storage.

3.2. Cyanobacteria

Single-celled *Synechococcus* showed increased abundance under high pCO_2 in both SOPRAN experiments in this study (Chapter 3, Section 3.5; Chapter 5, Section 3.4), in a previous mesocosm experiment (Paulino *et al.*, 2008) and during a laboratory experiment (Fu *et al.*, 2007). Cyanobacteria have been identified as having efficient CCMs, with up to four modes of carbon uptake: two HCO_3^- transporters and two CO_2 uptake systems to transport inorganic carbon species into the cell (Badger and Price, 1992, 2003). RubisCO is present within a specialised microsome within the cell, containing specific carbonic anhydrase to maintain CO_2 in high concentrations. Analysis of cyanobacterial genomes revealed that some species (α-cyanobacteria) lack this carbonic anhydrase (Badger *et al.*, 2002).

Changes in nitrogen fixation and growth under elevated pCO_2 relative to ambient controls have been noted in both heterocystous and non-heterocystous nitrogen fixing cyanobacteria, although CO_2 had no significant effect on the abundance of *Aphanizomenon flos-aquae* or *Pseudanabaena* in SOPRAN Tvärminne (Chapter 5, Section 3.5, preliminary data). No data was available on nitrogen fixation, although inorganic nitrogen increased equally in all mesocosms (Chapter 5, Section 3.4.2). Nitrogen fixation is recognised as the major global source of reactive nitrogen to the water column (Falkowski, 1997), and has a key role in the net biologically mediated exchange of CO_2 between atmosphere and ocean. Decreased nitrogen

fixation under elevated pCO_2 of 700 µatm by the heterocystous cyanobacterium *Nodularia spumigena*, a key species in the Baltic Sea, was previously reported (Czerny *et al.*, 2009). Growth rates and nitrogen fixation both doubled in the ubiquitous non-heterocystous *Trichodesmium* spp.in pCO_2 up to 1500 µatm (Barcelos e Ramos *et al.*, 2007; Hutchins *et al.*, 2007; Levitan *et al.*, 2007), and it has been suggested that increased atmospheric pCO_2 and temperatures may expand oligotrophic areas, simultaneously increasing the geographical range of *Trichodesmium spp.* and increasing global nitrogen fixation rates (Boyd and Doney, 2002). Although the species from the Baltic Sea are of limited global importance, the difference in response in contrast to *Trichodesmium* spp. suggest that further evaluation to the responses of *Trichodesmium* spp. are required. It was suggested that the presence of heterocysts would increase sensitivity to CO_2, however the study by Czerny *et al.* (2009) is the only high pCO_2 experiment performed on any species of heterocystous cyanobacteria, although as *A. flos-aquae* did not show sensitivity to CO_2, the findings of Czerny *et al.* (2009) may be a species specific response for *Nodularia spumigena*.

4. Changes in trace gas concentrations under future pCO_2

4.1. DMS and DMSP

4.1.1. Mesocosm Experiment Comparison

A comparison was made between the trace gas data and the physical data collected during SOPRAN Bergen and SOPRAN Tvärminne (Table 1), for the control mesocosms with no CO_2 addition and the 1400 µatm mesocosm, the highest pCO_2 common to both experiments. In Table 2, DMS and DMSP concentrations from these two experiments were compared with previous mesocosm data from experiments in the Arctic (Archer *et al.*, 2013), Korea (Kim *et al.*, 2010; Park *et al.*, 2014) and Bergen, Norway (Avgoustidi *et al.*, 2012; Hopkins *et al.*, 2010; Vogt *et al.*, 2008b).

During SOPRAN Tvärminne, mean DMS concentrations of 4.1 nmol L^{-1} in the control and 3.1 nmol L^{-1}in the 1400 µatm pCO_2 treatment were three times higher than during SOPRAN Bergen (1.3 and 0.6 nmol L^{-1}) at the same pCO_2, although mean Chl-α in both experiments was similar at <3 µg L^{-1} in all mesocosms. CO_2 had a significant effect on DMS concentrations in both experiments (SOPRAN Bergen Chapter 3, Section 4.1; SOPRAN Tvärminne, Chapter 5, Section

4.1) with concentrations 52 % lower at SOPRAN Bergen between the control and 1400 µatm and 34 % lower in SOPRAN Tvärminne. The DMS responses are in strong agreement with data collected in previous mesocosm experiments under high pCO_2 conditions (Table 2), with the exception of the first Korean mesocosm study, where concentrations increased by 80 % to a maximum of 15 nmol L^{-1} (Kim *et al.*, 2010). SOPRAN Bergen was compared with previous mesocosm experiments in Chapter 3, and was found to have similar trends in DMS and DMSP concentrations, except, as previously observed by Vogt *et al.* (2008a), no changes to the temporal development of DMS concentrations were identified.

DMSP concentrations from SOPRAN Bergen were within the same range as EPOCA Svalbard (Archer *et al.*, 2013), where maximum DMSP was measured at 80 nmol L^{-1}. However, DMSP concentrations showed differing responses to high pCO_2. DMSP during SOPRAN Bergen showed a negative effect of elevated pCO_2, with a 32 % decrease compared to a 50 % increase in Svalbard. Response of DMSP concentrations to increased pCO_2 was likely a result of changes to DMSP production and bacterial consumption in different microbial communities.

.

Table 1. Comparison of trace gas and core parameter data from two mesocosm experiments from the control mesocosm and the 1400 µatm mesocosm. ND: not detected. [2]

Parameter	SOPRAN Bergen			SOPRAN Tvärminne		
	Mean 280 µatm pCO_2	Mean 1400 µatm pCO_2	% difference	Mean 340 µatm pCO_2	Mean 1400 µatm pCO_2	% difference
Trace Gases						
DMS (nmol L^{-1})	1.3	0.6	-52	4.1	3.1	-34
DMSP (nmol L^{-1})	46.2	34.9	-26			
CH_3I (pmol L^{-1})	17.5	13.6	-22	4.1	4.3	5
C_2H_5I (pmol L^{-1})	0.68	0.66	-3	0.49	0.54	9
CH_2I_2 (pmol L^{-1})	195.6	108.1	-45	117.81	113.43	-4
CH_2ClI (pmol L^{-1})	54.8	43.3	-21	5.7	5.1	-11
$CHBr_3$ (pmol L^{-1})	160.7	150.9	-6	93.7	83.6	-11
CH_2Br_2 (pmol L^{-1})	17.8	16.8	-6	5.4	5.2	-2
$CHBr_2Cl$ (pmol L^{-1})	6.6	6.0	-8	3.1	3.0	-5
Physical Parameters						
Volume (L)	77000			54000		
Depth (m)	25			17		
Salinity	31.9			5.7		
Temperature (°C)	9.2			11.5		

[2] TABLE CONTINUES OVERLEAF

Parameter	SOPRAN Bergen			SOPRAN Tvärminne		
	Mean 280 µatm pCO_2	Mean 1400 µatm pCO_2	% difference	Mean 340 µatm pCO_2	Mean 1400 µatm pCO_2	% difference
Equivalent Chl-α (µg L^{-1})						
Total Chl-α	2.7	2.9	-10	2.06	2.26	10
Cyanobacteria	0.018	0.036	98	0.14	0.19	34
Diatoms	1.06	1.15	8	0.16	0.17	5
Dinoflagellates	0.045	0.033	26	0.05	0.04	-9
Chlorophytes	0.45	0.54	19	0.84	0.94	12
Cryptophytes	0.52	0.78	50	0.42	0.49	15
Abundance (Cells mL^{-1})						
Picoeukaryotes	18445	35457	92	55665	72883	-31
Single-celled cyanobacteria	5823	13170	126	201504	180223	11
Calcified *E. huxleyi*	461	140	-70	ND		

Table 2. Comparison of DMS and DMSP concentrations from this study and previous high pCO_2 experiments which measured DMS and DMSP. ND: not detected

	Location	pCO_2 Range (µatm)	Range DMS (nmol L^{-1})	% change DMS	Range DMSP (nmol L^{-1})	% change DMSP	Author
SOPRAN Tvärminne, 2012	Tvärminne, Finland	340 – 1400	2.66 – 6.79	-34			This Study
SOPRAN Bergen, 2011	Raunesfjorden, Norway	280 – 3000	0.09 – 4.92	-60.3	14.3 – 88.2	-31.6	This Study
Korean Mesocosm Experiment 2, 2012	Jangmok, Korea	160 - 830	1.0 - 100	-82	10-350	-71	Park *et al.* (2014)
EPOCA Svalbard, 2010	Kongsfjorden, Svalbard	180 - 1420	ND - 14	-60	ND-80	+50	Archer *et al.* (2013)
NERC Microbial Metagenomics Experiment, 2006	Raunesfjorden, Norway	300-750	ND - 50	-57	30 - 500	-24	Hopkins *et al.* (2010)
Korean Mesocosm Experiment 1, 2008	Jangmok, Korea	400 - 900	1 - 12	+80			Kim *et al.* (2010)
PeECE III, 2005	Raunesfjorden, Norway	300 - 750	ND - 35	None	10 - 500	None	Vogt *et al.* (2008)
PeECE II, 2003	Raunesfjorden, Norway	300 - 750	3 - 30	-40	ND - 300	-40	Avgoustidi *et al.* (2012)
UKOA European Shelf Cruise, 2011	NW European Shelf	340 - 1000	0.5 - 12	225	5 - 80	-52	Hopkins and Archer (2014)

BLANK

DMS has shown linear inverse relationships with pCO_2 in a number of studies (This investigation; Archer *et al.*, 2013; Park *et al.*, 2014), in different global locations. This repeating pattern from communities with different species composition and dominance, suggests that global DMS concentrations will decrease as pCO_2 increases, although no studies have been carried out in the oligotrophic open ocean or at Eastern Boundary upwellings. In the large-scale KOSMOS experiments, a range of seawater pCO_2 based on the IPCC scenarios for 2100 allow investigation of linear relationships, with the disadvantage of limited replication. SOPRAN Bergen took the pCO_2 to 3000 µatm to extend the range of the linear trend and to attempt to identify 'tipping points' in some parameters, although none were identified for the trace gases. Park *et al.* (2014) identified a linear trend for decreasing DMS and DMSP concentrations with increasing pCO_2, during a mesocosm experiment with up to 840 µatm pCO_2 in Korea, similar to the relationship identified during SOPRAN Bergen.

The relationship of DMSP with increasing pCO_2 is not so clear: Archer *et al.* (2013) found DMSP increased with increasing pCO_2, as did Lee *et al.* (2009) in an incubation experiment on a natural community. During SOPRAN Bergen, however, DMSP concentrations were inversely related to increasing pCO_2, in line with the DMS response, and In a series of incubation experiments with European shelf sea waters, Hopkins & Archer (2014) found a consistent reduction in total DMSP under 1000 µatm pCO_2 but an increase in DMS in the same treatment, compared to ambient controls. This community response over 96 hours is likely dominated by decreased abundance of the picoeukaryote group, which can contribute between 40 and 57 % to the total DMSP pool (Archer *et al.*, 2011; Corn *et al.*, 1996; Richier *et al.*, 2014b). Picoeukaryotes in both SOPRAN experiments showed strong responses to pCO_2, with significantly higher abundance in the high pCO_2 mesocosms. Previous experiments (Brussaard *et al.*, 2013; Meakin and Wyman, 2011; Newbold *et al.*, 2012) have seen shifts in picoeukaryote community structure towards species with less efficient CCMs, and subsequent increases in picoeukaryote abundance. However, the increases in picophytoplankton during SOPRAN Bergen did not correspond to increased DMSP, which was non-correlated with picoeukaryotes abundance (Chapter 3, Section 4.1).

Park *et al.* (2014) attributed lower DMS under 830 µatm pCO_2 to the grazing activity of heterotrophic dinoflagellates: lower heterotrophic dinoflagellate abundance at higher pCO_2 resulted in reduced grazing activity, and lower subsequent release of DMSP from algal cells to the water column for breakdown to DMS. Heterotrophic dinoflagellate abundance decreased during SOPRAN Tvärminne (Annegret Stuhr, GEOMAR, Pers. Comm), and lower DMS

concentrations were detected at high pCO_2, however without a corresponding DMSP concentration it was difficult to determine if the response to DMS was directly related to grazing activity. During EPOCA Svalbard, heterotrophic dinoflagellate growth showed a positive response to high pCO_2 (Leu *et al.*, 2013; Schulz *et al.*, 2013), while DMS decreased. During the SOPRAN experiments, the abundance of mesozooplankton showed a limited response to elevated pCO_2 (Hildebrandt *et al.*, 2014; Silke Lischka, GEOMAR, Pers. Comm.), Grazing – mediated DMS production has been reported to be of greater importance than direct cell release of DMSP and viral infection combined (Dacey and Wakeham, 1986; Evans *et al.*, 2007). From the data collected in the mesocosm experiments, grazing is important in the release of DMSP into the dissolved phase, resulting in DMS production through interactions with the rest of the microbial community. As discussed in Chapter 3, the microbial interactions between DMS and DMSP are likely of greater importance, and grazing is only one factor influencing the concentrations of DMS.

During SOPRAN Bergen, the response of DMS to pCO_2 addition was apparent within days of the mesocosm pCO_2 enrichment, as seen from the measurements from the GEOMAR DMS dataset (Chapter 3, Figure 23a), whereas the response in SOPRAN Tvärminne was delayed for 16 days (Chapter 5, Figure 14), with no significant difference between pCO_2 treatments before then. The response during the NERC Metagenomics experiment was identified within 4 days (Hopkins *et al.* 2010) and in EPOCA Svalbard within 10 days (Archer *et al.* 2013). This variable response time was independent of nutrient addition and suggests that a reduction in DMS concentrations with increasing pCO_2 is not an immediate stress response. DMSP concentrations in SOPRAN Bergen did not respond to elevated pCO_2 until after T9, and in EPOCA Svalbard until T15. As discussed in Section 2.3, these experiments were all performed over short timescales and with rapid changes to seawater carbonate chemistry in relation to the time and rate of change expected before the year 2100. It is not known if the changes in DMS and DMSP were a result of acclimation of species to the changed conditions, or due to the abrupt nature of the environmental change, nor if the DMSP and DMS concentrations would remain lower if the experiments were run over much longer timescales. Laboratory experiments have shown that evolution of *E. huxleyi* over many generations can restore the functionality of microbial processes such as calcification and carbon fixation which are affected in the short-term (Lohbeck *et al.*, 2012a, 2012b). On the other hand, mesocosm experiments performed for hundreds of generations would not accurately reflect the evolution of a natural community as development is directly dependent on the starting seed populations. The observed response in a mesocosm is between the broad taxonomic groups instead of on a

species level, likened to that of a winners and losers scenario, rather than the rapid physiological response in a laboratory culture like the pCO_2 enrichment experiments, or the evolutionary response of the 500+ generation continuous cultures.

Bacterial increased during SOPRAN Bergen (Endres *et al.,* 2014) and bacterially-mediated processes show varying responses (Chapter 3, Section 5.3.4). The partitioning of $DMSP_D$ in seawater after catabolism by bacterially mediated processes is to one of three distinct pools: taken into the particulate phase as a C or S source (6-85 %), degraded into dissolved non-volatile degradation products (21-74 %) or volatile products (DMS and methanethiol 2-21 %; Kiene and Linn, 2000). Enhanced bacterial hydrolysis would increase $DMSP_D$ degradation via the demethylation pathway, using DMSP as a sulphur and carbon source (de Bont *et al.*, 1981; Curson *et al.*, 2011) and diverting DMSP into the particulate and non-volatile phase. This partitioning would result in lower percentages of $DMSP_D$ converted to DMS. DMS would also have been broken down by hydrolysis, and although turnover is slower than for DMSP (Kiene and Linn, 2000), with higher bacterial hydrolytic activity, turnover rates may increase at higher pCO_2. With changes to surface water carbon cycling and POC production (Engel *et al.*, 2013), increased usage of DMSP as a bacterial carbon source could divert a greater proportion of $DMSP_D$ away from DMS production pathways, and subsequently lower surface water DMS concentrations. However, the partitioning of $DMSP_D$ does not explain the reported decrease in $DMSP_P$ (Chapter 3, Section 4.1), which may affect the availability of $DMSP_D$ and therefore the overall bioavailability of sulphur for marine bacteria.

Endres *et al.* (2014) also found increases to the concentrations of transparent exopolymer particles (TEP) in the high pCO_2 mesocosms, which act as a substrate for bacterial growth and are therefore hotspots for microbial degradation (Verdugo *et al.*, 2004). Higher TEP concentrations were identified after the phytoplankton blooms, and have been associated with the formation and composition of the sea surface microlayer (SSM), through which gases must pass in order to flux to the atmosphere.

During SOPRAN Bergen, measurements were made of changes to the composition of the sea surface microlayer, with significant decreases in coverage of proteinaceous gels and increases in polysaccharidic gels at higher pCO_2 (Galgani, 2013). This changing composition may have affected the sea-air exchange of volatile compounds from the mesocosms, although to what degree is unknown. Gas transfer velocities will be primarily driven by temperature and evaporation (Liss, 1973) as the mesocosm enclosures limit the effects of wind on the exchange of gases rather (Czerny *et al.*, 2013). Future mesocosm experiments need to delve deeper into

the processes surrounding DMS production, and this could be performed through the use of stable isotopes within the mesocosms or parallel incubation experiments, as in Hopkins and Archer (2014).

4.1.2. Reduced DMS concentrations in surface waters

DMS is the main natural source of sulphur entering the atmosphere (Bates *et al.*, 1992), with an estimated 28 Tg sulphur transferring from the oceans annually as DMS (Lana *et al.*, 2011). In the atmosphere, DMS undergoes a series of oxidation reactions with $OH^{\bullet}$ to form sulphur dioxide, methanesulphonic acid (MSA), DMSO and dimethylsulphone (Andreae and Crutzen, 1997). According to the CLAW hypothesis, named for the authors who suggested it (Charlson *et al.*, 1987), these sulphate particles reflect light directly back into space and also act as cloud condensation nuclei (CCN), attracting water droplets. Changes in the number of CCN particles will influence cloud formation and cloud albedo, and subsequently affect the sunlight reaching the surface oceans and stimulating phytoplankton growth and subsequent DMS production (Chapter 1, Figure 9). This seemingly simple description assumes a direct relationship with phytoplankton growth and DMS production, yet DMS and Chl-α correlations are often poor (Anderson *et al.*, 2001; Lana *et al.*, 2011; Scarratt *et al.*, 2007). Furthermore, the CLAW hypothesis assumes a direct relationship between DMS and light, yet Derevianko *et al.* (2009) identified solar radiance as accounting for only 14 % of the variance in DMS production.

Using the results of this study incorporated into the CLAW hypothesis indicates a reduction in DMS flux to the atmosphere from an elevated pCO_2 ocean, and a subsequent reduction in CCN and therefore a greater proportion of sunlight reaching the surface oceans (Chapter 1. Figure 9). However, the results of this investigation also showed a relatively poor correlation of DMS and Chl-α, which indicates that increased primary productivity will not necessarily promote further DMS production as indicated by the CLAW hypothesis. It is clear from the discussion in this investigation that the processes that regulate DMS concentration in seawater are still yet to be fully understood, alongside the rate of transfer to the atmosphere, rates of CCN production and the effect of climate change on ocean productivity (Andreae and Crutzen, 1997).

There are limited observational and model data to accept or reject the CLAW hypothesis, although the development of the global DMS database is allowing development of more sophisticated Earth System models in the context of climate change (Halloran *et al.*, 2010). Quinn and Bates (2011) suggested that DMS does not control the production of cloud

condensation nuclei due to low sensitivity between change and response in several steps of the hypothesis, and thereby refuted the CLAW hypothesis. Nonetheless, the 20 years of observations have served in bringing forward recognition of the complexity of the ocean-atmosphere responses to changes in aerosol concentrations, and recognise that DMS emissions exert an important influence on the production of secondary aerosols in the MBL. Given the variables acting on DMS concentrations and sea-air flux, it is extremely difficult to model future atmospheric DMS concentrations. Sulphur emissions from DMS are a significant source of sulphur aerosols, and are still of greater importance than man-made sulphur emissions (Carslaw *et al.*, 2013; Rap *et al.*, 2013).

Model studies using DMS parameterisations in Earth system models project that with increasing pCO_2 there would be a small increase in DMS flux, but with large spatial heterogeneity (Bopp *et al.*, 2003, 2004). These studies did not incorporate the decreased concentration of surface water DMS concentrations under elevated pCO_2 as identified from mesocosm studies: lower DMS concentrations from a higher pCO_2 ocean would reduce the production of atmospheric CCN. The data from EPOCA Svalbard was used by Six *et al.* (2013) to estimate global level changes in DMS using Earth System model climate simulations, and determined that decreased oceanic DMS emissions will amplify global warming up to half a degree by 2100. However, the surface water DMS concentrations in the model were linked solely to the seawater pH, with no mechanistic understanding of DMS-DMSP interactions within the microbial community, or grazing activity or possible changes in DMS flux through an altered SSM. However, an international comparison of models that incorporated atmospheric DMS showed that to fit observational data, DMS needed to be decoupled from ecological processes and impacted more by environmental forcing such as irradiance and temperature (Le Clainche *et al.*, 2010).

4.1.3. How do concentrations from the Fjord and Baltic Sea compare with global DMS concentrations?

In the 1990s, DMS and DMSP measurements from natural waters were collated into a Global Surface Seawater DMS database (http://saga/pmel.noaa.gov/dms) along with associated Chl-α salinity and temperature data to develop the first climatology of DMS concentrations (Kettle *et al.*, 1999). The climatology was recently updated to include the more recent DMS measurements from the intervening 10 years, and it now comprises over 47,000 datapoints from across the globe (Lana *et al.*, 2011). Although concentrations of DMS in the mesocosms

cannot be included in the global database of DMS measurements, those from the Baltic Sea and Raunesfjord can be directly compared with surface water concentrations in the database, as well as with open water measurements from additional studies. The data available in the database for the northeast Atlantic and Baltic Sea are shown in Figure 1.

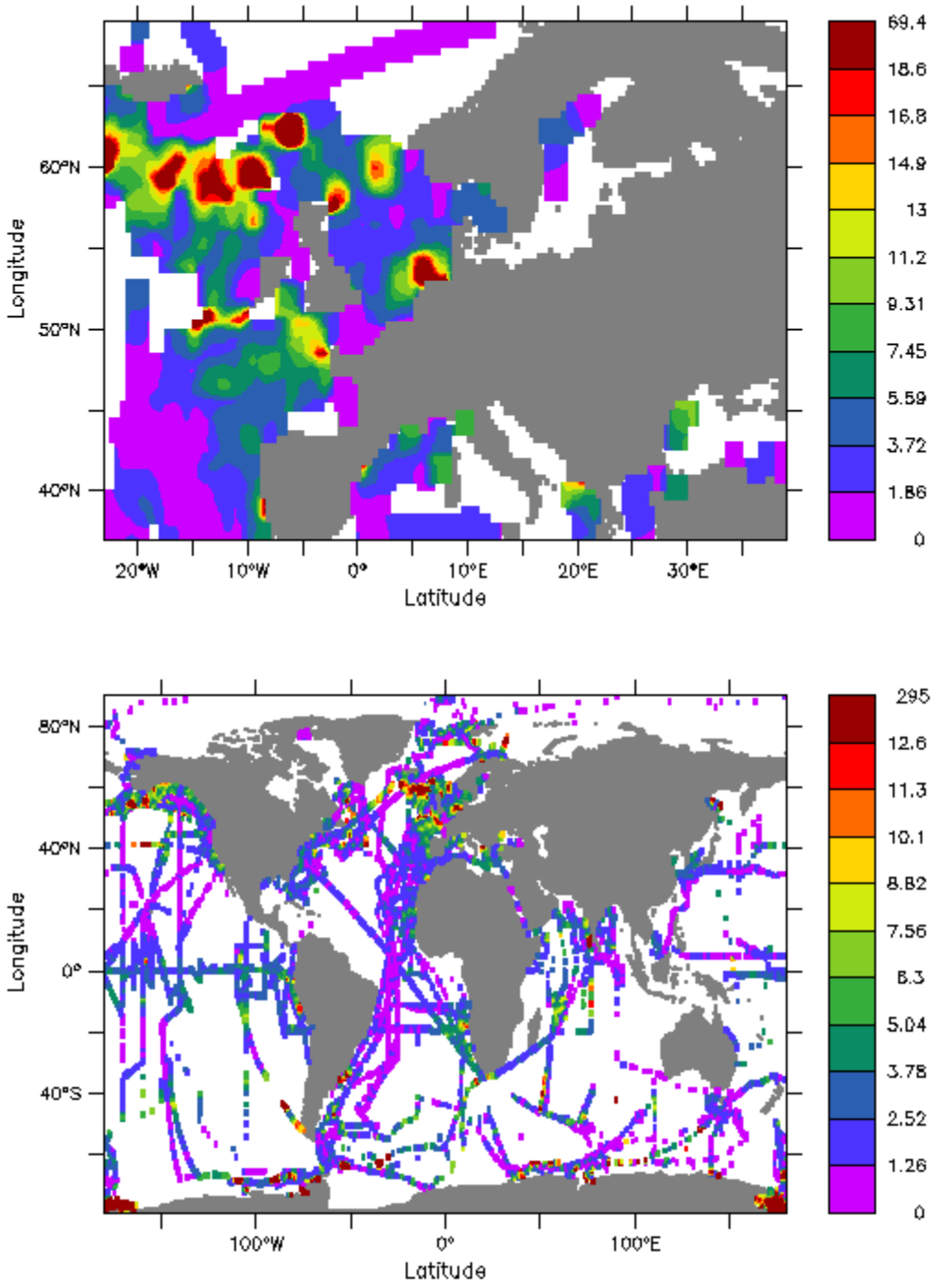

Figure 1. Surface water DMS concentrations from a) the northeast Atlantic and Baltic Sea, and b) the global ocean, downloaded from the Global Surface DMS Database September 2014.

Maximum measured DMS in Raunesfjord (Bergen) was 3.3 nmol L^{-1} and corresponds with the measured values incorporated into the global database for the regions around the coast of Norway (3.7 nmol L^{-1}; dark purple, Figure 1a). The DMS concentrations from Raunesfjord were higher than measured in the majority of the open oceans (<1.3 nmol L^{-1}; Figure 1b), but which are the same as measured in the mesocosms of SOPRAN Bergen. Measurements of DMS in the Baltic Sea at Tvärminne are not available in the global database, but those near the coast of Sweden were below 5.6 nmol L^{-1}, lower than the maximum measured integrated value of 11.2 nmol L^{-1} at Tvärminne. These values corresponded to DMS measured in areas of upwelling at eastern boundaries, specifically the West African coast and the Western coast of North America.

4.2. Halocarbons

4.2.1. Iodocarbons

The poor correlation of iodocarbons with Chl-*a* has previously been identified in a number of studies (Carpenter *et al.*, 2007; Hopkins *et al.*, 2010; Kurihara *et al.*, 2010; Schall *et al.*, 1997), implying production is not directly related to biomass.

SOPRAN Bergen and SOPRAN Tvärminne produced different trends in the iodocarbon concentrations. During SOPRAN Bergen, there was a linear decrease in iodocarbon concentrations as pCO_2 increased, in agreement with Hopkins *et al.* 2010 during the NERC Microbial Metagenomics experiments (Table 3). In contrast, CH_2ClI during the PeECE III experiment showed integrated concentrations higher by 131 % in high pCO_2 mesocosms up to 1150 µatm (Wingenter *et al.*, 2007). The trend of decreasing concentrations of various iodocarbons was not identified during SOPRAN Tvärminne, where there was no change in iodocarbon concentrations as pCO_2 increased to 1400 µatm, which was a similar finding to Hopkins *et al.* (2013) during EPOCA Svalbard. Concentrations of the measured iodocarbons are within the same ranges measured in the English channel by Archer *et al.* (2007) and the Atlantic Ocean (Chuck *et al.*, 2005). Iodocarbon concentrations compared between SOPRAN Bergen and SOPRAN Tvärminne were similar, except for CH_2ClI where SOPRAN Bergen was an order of magnitude higher. Changes in halocarbon concentrations between mesocosms were identified during SOPRAN Tvärminne, but these were not the result of changes to pCO_2. It is clear that there is no repeated trend of pCO_2 on iodocarbon concentrations, which, like the

response of DMS, needs to be quantified in different global surface waters before accurate projections can be made of future global production.

Production mechanisms for iodocarbons have been discussed in previous chapters. Production of monoiodinated compounds relies on the methylation of halides by methyl transferase enzymes (Manley, 2002), and this process may be affected by acidification in some species. Although the bromocarbons showed little effect of high pCO_2, any effect on methyl transferase enzymes will affect the concentrations of methyl bromide, and it is suggested this compound is measured in future mesocosm studies. A link has been suggested between DMS and Iodide (Andreae, 1990) surface water concentrations through the following reaction:

$$IO + DMS \longrightarrow DMSO + I \qquad 25$$

This reaction gives DMS significant role in the iodine cycle, and could provide I^- required for methylation to CH_3I and C_2H_5I, while affecting the surface water DMS concentration by up to 50 % (Chatfield and Crutzen, 1990). Through this mechanism, the decrease in DMS concentration due to acidification may be the cause of the decrease in iodocarbons identified in SOPRAN Bergen at higher pCO_2. A relationship has also been determined between DMS and BrO (von Glasow and Crutzen, 2004) through the equation:

$$BrO + DMS \longrightarrow DMSO + Br \qquad 26$$

however, no reduction in bromocarbons was identified at elevated pCO_2, implying that either the Br-DMS reaction was unaffected by the lowered pH, or the iodocarbon reductions were unrelated to this reaction process.

DOM concentrations may have a key role in the production of halocarbons, either through the photolysis of DOM producing methyl radicals (Moore and Zafiriou, 1994; Richter and Wallace, 2004), or through microbial activity on DOM producing the precursors required for halocarbon production (Hughes *et al.*, 2008). During SOPRAN Tvärminne and SOPRAN Bergen, bacterial degradation activity was higher at high pCO_2, which could have resulted in lower DOM concentrations in these mesocosms, and subsequent lower iodocarbon concentrations.

4.2.2. Bromocarbons

During both SOPRAN Bergen (Chapter 3) and SOPRAN Tvärminne (Chapter 5), pCO_2 had no effect on the concentrations of bromocarbons measured in the mesocosms. This was a finding noted by Hopkins *et al.* (2010) and Hopkins *et al.* (2013) during two previous mesocosm

experiments, and the only previous experiments measuring bromocarbon concentrations under elevated pCO_2. The range of bromocarbon concentrations was higher during SOPRAN Bergen than during SOPRAN Finland, but both experiments were within the same range as measurements in surface waters in other parts of the world (Table 4).

Production of polyhalogenated compounds in phytoplankton is as a by-product of bromoperoxidase (BrPO) enzyme activity, the major purpose of which is to react with harmful hydrogen peroxide within the cell (Manley, 2002; Theiler *et al.*, 1978). As evidence collected so far on bromocarbon concentrations has shown limited influence of elevated pCO_2, it is suggested that this process within the cell is more resilient to ocean acidification than the production of iodocarbons and monohalogenated compounds.

BLANK

Table 3. Range of iodocarbons from SOPRAN Bergen and SOPRAN Tvärminne compared to previous mesocosm experiments and surface seawater concentrations from studies in different parts of the world. DL: Detection limit.

Experiment	Location	pCO_2 Range (µatm)	CH_3I		C_2H_5I		CH_2I_2		CH_2ClI		
			Concentration range (pmol L^{-1})	% Change	Concentration range (pmol L^{-1})	% Change	Concentration range (pmol L^{-1})	% Change	Concentration range (pmol L^{-1})	% Change	
SOPRAN Tvärminne	Tvärminne Finland	340 – 1400	2.9 – 6.4	-0.3	0.2 – 0.8	4	57.3 – 202.2	1.3	3.8 – 8.0	-11	This Investigation
SOPRAN Bergen	Raunesfjorden Norway	280 – 3000	4.9 – 31.8	-37	0.1 – 2.2	-10	5.8 – 321.3	-48	9.0 – 122.5	-27	
EPOCA Svalbard	Kongsfjorden Svalbard	180 - 1420	0.04 – 10.3		0.1 – 3.3		0.01 – 2.5		0.3 – 1.6		Hopkins *et al.* (2013)
NERC Microbial Metagenomics Experiment	Raunesfjorden Norway	300-750	2-25	-41	DL – 2.0	-32	DL - 750	-33	DL – 700	-28	Hopkins *et al.* (2010)
PeECE III	Raunesfjorden Norway	300 - 750	-	-	-	-	-	-	2.5 - 37	+131	Wingenter *et al.* (2008)
ADOX, AMT 9, ANT XVIII/1 Cruises	Atlantic Ocean	N/A	0.5 – 18	-	-	-	-	-	0.5 – 15	-	Chuck *et al.* (2005)
Seasonal L4 study	English Channel UK	N/A	0.6 – 14.6	-	0.3 – 4.8	-	0.3 – 15.3	-	0.6 – 39.3	-	Archer *et al.* (2007)

BLANK

Table 4. Range of bromocarbons from SOPRAN Bergen and SOPRAN Tvärminne compared to previous mesocosm experiments and surface seawater concentrations from studies in different parts of the world. DL: detection limit.

			$CHBr_3$		CH_2Br_2		CH_2Br_2Cl		
	Location	pCO_2 Range (µatm)	Concentration range (pmol L^{-1})	% Change	Concentration range (pmol L^{-1})	% Change	Concentration range (pmol L^{-1})	% Change	
SOPRAN Tvärminne	Tvärminne Finland	340 – 1400	68.9 – 147.5	-9	4.0 – 7.7	-3	1.7 – 4.7	-4	This Investigation
SOPRAN Bergen	Raunesfjorden Norway	280 – 3000	64.2 – 306.0	-2	6.3 – 30.8	-4	3.9 – 13.5	-6	
EPOCA Svalbard	Kongsfjorden Svalbard	180 - 1420	35.3 – 151.3		6.3 – 33.3		1.6 – 4.7		Hopkins *et al.* (2013)
NERC Microbial Metagenomics Experiment	Raunesfjorden Norway	300 - 750	5 – 80	13	DL – 5.5	8	0.2 – 1.2	22	Hopkins *et al.* (2010)
RV Poseidon Cruise P320/1	Mauritanian Upwelling	N/A	5.2 - 32	-	3.1 – 7.1	-	-	-	Quack *et al.* (2007b)
ADOX, AMT 9, ANT XVIII/1 Cruises	Atlantic Ocean	N/A	0.5 – 30	-	-	-	0.2 - 12	-	Chuck *et al.* (2005)
GOMECC Cruise	Gulf of Mexico	N/A	4.4 – 366.8	-	1.9 – 37.3	-	0.1 – 3.9	-	Liu *et al.* (2011)

BLANK

4.2.3. What are the effects of changing halocarbon concentrations?

Halocarbons represent a key pool in the biogeochemical cycling of halogens in seawater, and facilitate the exchange of halogens to the atmosphere. Inorganic iodine is ubiquitous in seawater with concentrations of up to 500 nmol L^{-1}, with a vertical distribution showing surface depletion due to biological uptake (Wong, 1991). In surface waters, up to 80 % of iodine is present in the dissolved organic form in compounds such as the halocarbons (Wong and Cheng, 2001). A current climatology has provided air-sea flux estimates of up to 2.5 Gmol yr^{-1} for $CHBr_3$, 0.98 Gmol yr^{-1} for CH_2Br_2 and 1.45 Gmol yr^{-1} for CH_3I (Ziska *et al.*, 2013).

In the clean air of the marine atmosphere, halocarbons undergo photolysis to release the I-, Br- and Cl- radicals (Chameides and Davis, 1980), which in turn catalyse the ozone reactions:

$$X + O_3 \longrightarrow XO + O_2 \qquad 27$$

$$XO + XO \longrightarrow 2X + O_2 \qquad 28$$

Iodocarbons have relatively short atmospheric lifetimes (minutes to days) and undergo the majority of reactions in the troposphere. Due to their generally longer atmospheric lifetimes (days to weeks), bromocarbons are able to pass upwards into the stratosphere (Sturges *et al.*, 2000), along with CH_3I with its longer lifetime of 7 days (Montzka *et al.*, 2011; Solomon *et al.*, 1994). It is difficult to determine the effects of a change in halocarbon flux into the marine atmosphere, as ozone reactions recycle halide radicals, but the likely result is a decrease in tropospheric ozone destruction, and a reduction in the oxidative capacity of the atmosphere (Chameides and Walker, 1973; Crutzen, 1973). Halocarbon oxidation products in the marine boundary layer can also act as CCNs (O'Dowd *et al.*, 2002), and therefore influence climate-related processes similarly to DMS (Charlson *et al.*, 1987).

5. Future Research

A large proportion of research into ocean acidification has moved on from investigating the solo effect of lowered pH to the interactions with other salient factors such as changes to temperature, nutrients and light availability, all of which are likely to change in the future ocean compared to today. These investigations are extremely limited for trace gas measurements, particularly in the field, where adapting a mesocosm or large scale experiment for temperature change is cost-prohibitive. However it has been achieved in a small mesocosm (2400L) by Park *et al.* (2014), but the trends for DMS and DMSP were the same as presented in this investigation: measured concentrations were lower at high pCO_2 despite the increase in temperature. The assessment of changes to pCO_2 and other environmental parameters in open water or mesoscale experiments is certainly an area where further research could be applied, dependent upon the cost of setup and management. In association with these developments, it is likely that longer-term mesocosm experiments will be needed to study the community variation over timescales of months to years under future environmental scenarios. As mesocosm experiments progress, with improved technology available for ease of measurements, it is proposed that a mesocosm-specific database be developed to include all parameters measured during all experiments, to allow for rapid comparison of experiments to identify relevant trends, and allow the use of multiple datasets in modelling studies and meta-analysis. An example of where this would be useful is in the research by Six *et al.* (2013), where DMS data was only available from a single mesocosm experiment and used to determine changes to the global DMS flux. A single database would allow measurements from multiple mesocosm experiments performed at different locations around the globe to be used in such a modelling study, allowing for greater accuracy in the model projections.

This project has shown that there is a requirement for more closely determining the role of marine bacteria in the production and consumption of DMS and DMSP in surface waters, before taking into account the effect of future environmental change. Both DMS and $DMSP_D$ are consumed by marine bacteria as a sulphur and carbon source, and the proportion of the pools which are consumed directly affects the transfer of DMS through the sea-air interface to the atmosphere. However, very little is known about the DMS and DMSP consumption of different bacterial groups, nor the reasons behind the spatial variability in consumption and the weak relationship of DMS to $DMSP_D$ concentrations, as highlighted by Kiene and Linn (2000). .

6. Summary

The aim of this investigation was to study the changes in DMS, DMSP and a range of biologically produced halocarbon concentrations as oceanic surface water pCO_2 increase with a concurrent decrease in pH. This is a research question which is of critical importance, as these gases take part in a range of atmospheric reactions and cycles, and changes to surface ocean concentrations could affect their flux to the atmosphere, with implications for climate-related processes.

Studying changes to surface water microbial communities under elevated pCO_2 requires the use of large-scale experiments, either in open waters examining natural variations in pCO_2 and pH, or through the use of enclosures to artificially modify the pCO_2. Two of these experiments formed the backbone of this investigation: the SOPRAN mesocosm experiments used enclosures of >50m^3 and 17-25m depth to alter the surface water carbonate chemistry using the addition of CO_2 to study the effects on the microbial populations. The first experiment (SOPRAN Bergen 2011) was undertaken in the sheltered coastal waters of the North Sea in Bergen, Norway, and this investigation studied the effects of elevated pCO_2 on the growth and DMSP production of *E. huxleyi*. Further to this, the CO_2 enrichment experiments were designed to test if the changes identified during SOPRAN Bergen were due to physiological changes within the *E. huxleyi* cell, or a result of microbial community interactions in surface waters. In the second mesocosm experiment, the unique brackish waters of the Baltic Sea (SOPRAN Tvärminne 2012) were studied for trace gas production, to determine if filamentous cyanobacteria were a source of halocarbons and DMS. DMS decreased in a linear relationship with pCO_2 in both experiments, a finding which has been identified in every previous high pCO_2 mesocosm experiment. The changes in the other trace gases were less predictable: iodocarbons decreased during SOPRAN Bergen but showed no change during SOPRAN Tvärminne, and bromocarbons did not show noticeable changes in line with increasing pCO_2 in any investigation. *E. huxleyi* RCC1229 was also not a significant producer of and of the measured halocarbons.

Even after this investigation, the quantity of data available for the production of the trace gases under ocean acidification is small. More studies are required into the long-term physiological response of individual species over hundreds of generations under combined perturbations of temperature and pCO_2, as expected in a future climate, and these studies need to be realistically scaled into the community level to determine the changes in species

dominance, nutrient cycling, bacterial enzymatic activity and grazing, to then determine the results of these change on the trace gases studied here.

References

Aberle, N., Schulz, K. G., Stuhr, A., Malzahn, A. M., Ludwig, A. and Riebesell, U.: High tolerance of microzooplankton to ocean acidification in an Arctic coastal plankton community, Biogeosciences, 10(3), 1471–1481, doi:10.5194/bg-10-1471-2013, 2013.

Abrahamsson, K., Choo, K.-S., Pedersén, M., Johansson, G. and Snoeijs, P.: Effects of temperature on the production of hydrogen peroxide and volatile halocarbons by brackish-water algae, Phytochemistry, 64(3), 725–734, doi:10.1016/S0031-9422(03)00419-9, 2003.

Ackman, R. G., Tocher, C. S. and McLachlan, J.: Occurrence of Dimethyl-ß-propiothetin in marine phytoplankton, Can. J. Fish. Aquat. Sci., 23(3), 357–364, 1966.

Allgaier, M., Riebesell, U., Vogt, M., Thyrhaug, R. and Grossart, H.-P.: Coupling of heterotrophic bacteria to phytoplankton bloom development at different pCO_2 levels: a mesocosm study, Biogeosciences, 5(4), 1007–1022, doi:10.5194/bg-5-1007-2008, 2008.

Van Alstyne, K. L., Schupp, P. and Slattery, M.: The distribution of dimethylsulfoniopropionate in tropical Pacific coral reef invertebrates, Coral Reefs, 25(3), 321–327, doi:10.1007/s00338-006-0114-9, 2006.

Amachi, S.: Microbial contribution to global iodine cycling: volatilization, accumulation, reduction, oxidation, and sorption of iodine, Microbes Environ., 23(4), 269–276, doi:10.1264/jsme2.ME08548, 2008.

Amachi, S., Kamagata, Y., Kanagawa, T. and Muramatsu, Y.: Bacteria mediate methylation of iodine in marine and terrestrial environments, Appl. Environ. Microbiol., 67(6), 2718–2722, doi:10.1128/AEM.67.6.2718, 2001.

Andersen, R. A., Berges, J. A., Harrison, P. J. and Watanabe, M. M.: Algal culturing techniques, edited by R. Andersen, Imprint Academic Press., 2005.

Anderson, T. R., Spall, S. A., Yool, A., Cipollini, P., Challenor, P. G. and Fasham, M. J. R.: Global fields of sea surface dimethylsulfide predicted from chlorophyll, nutrients and light, J. Mar. Syst., 30, 1–20, doi:10.1016/S0924-7963(01)00028-8, 2001.

Andreae, M. O.: Ocean-atmosphere interactions in the global biogeochemical sulfur cycle, Mar. Chem., 30, 1–29, doi:10.1016/0304-4203(90)90059-L, 1990.

Andreae, M. O. and Crutzen, P. J.: Atmospheric aerosols: biogeochemical sources and role in atmospheric chemistry, Science., 276(5315), 1052–1058, doi:10.1126/science.276.5315.1052, 1997.

Anning, T., Nimer, N., Merrett, M. J. and Brownlee, C.: Costs and benefits of calcification in coccolithophorids, J. Mar. Syst., 9, 45–56, 1996.

Archer, S. D., Gilbert, F. J., Nightingale, P. D., Zubkov, M. V., Taylor, A. H., Smith, G. C. and Burkill, P. H.: Transformation of dimethylsulphoniopropionate to dimethyl sulphide during summer in the North Sea with an examination of key processes via a modelling approach, Deep Sea Res. Part II Top. Stud. Oceanogr., 49(15), 3067–3101, doi:10.1016/S0967-0645(02)00072-3, 2002.

Archer, S. D., Goldson, L. E., Liddicoat, M. I., Cummings, D. G. and Nightingale, P. D.: Marked seasonality in the concentrations and sea-to-air flux of volatile iodocarbon compounds in the western English Channel, J. Geophys. Res., 112(C8), doi:10.1029/2006JC003963, 2007.

Archer, S. D., Kimmance, S. A., Stephens, J. A., Hopkins, F. E., Bellerby, R. G. J., Schulz, K. G., Piontek, J. and Engel, A.: Contrasting responses of DMS and DMSP to ocean acidification in Arctic waters, Biogeosciences, 10(3), 1893–1908, doi:10.5194/bg-10-1893-2013, 2013.

Archer, S. D., Tarran, G., Stephens, J., Butcher, L. and Kimmance, S.: Combining cell sorting with gas chromatography to determine phytoplankton group-specific intracellular dimethylsulphoniopropionate, Aquat. Microb. Ecol., 62(2), 109–121, doi:10.3354/ame01464, 2011.

Arnold, H. E., Kerrison, P. and Steinke, M.: Interacting effects of ocean acidification and warming on growth and DMS-production in the haptophyte coccolithophore *Emiliania huxleyi*., Glob. Chang. Biol., 19(4), 1007–16, doi:10.1111/gcb.12105, 2013.

Asher, E., Dacey, J. W. H., Mills, M. M., Arrigo, K. R. and Tortell, P. D.: High concentrations and turnover rates of DMS, DMSP and DMSO in Antarctic sea ice, Geophys. Res. Lett., 38(23), doi:10.1029/2011GL049712, 2011.

Avgoustidi, V.: Dimethylsulphide production in a double CO_2 World, University of East Anglia., 2006.

Avgoustidi, V., Nightingale, P. D., Joint, I., Steinke, M., Turner, S. M., Hopkins, F. E. and Liss, P. S.: Decreased marine dimethyl sulfide production under elevated CO_2 levels in mesocosm and in vitro studies, Environ. Chem., 9(4), 399–404, doi:10.1071/EN11125, 2012.

Le B. Williams, P. and Egge, J.: The management and behaviour of the mesocosms, Estuar. Coast. Shelf Sci., 46, 3–14, doi:10.1006/ecss.1998.0330, 1998.

Bach, L. T., Bauke, C., Meier, K. J. S., Riebesell, U. and Schulz, K. G.: Influence of changing carbonate chemistry on morphology and weight of coccoliths formed by *Emiliania huxleyi*, Biogeosciences, 9(8), 3449–3463, doi:10.5194/bg-9-3449-2012, 2012.

Bach, L. T., Mackinder, L. C. M., Schulz, K. G., Wheeler, G., Schroeder, D. C., Brownlee, C. and Riebesell, U.: Dissecting the impact of CO_2 and pH on the mechanisms of photosynthesis and calcification in the coccolithophore *Emiliania huxleyi*., New Phytol., 199, 121–134, doi:10.1111/nph.12225, 2013.

Badger, M. R., Hanson, D. and Price, G. D.: Evolution and diversity of CO_2 concentrating mechanisms in cyanobacteria, Funct. Plant Biol., 29(3), 161–173, 2002.

Badger, M. R. and Price, G. D.: The CO_2 concentrating mechanism in cyanobacteria and microalgae, Physiol. Plant., 84(4), 606–615, doi:10.1111/j.1399-3054.1992.tb04711.x, 1992.

Badger, M. R. and Price, G. D.: CO_2 concentrating mechanisms in cyanobacteria: molecular components, their diversity and evolution, J. Exp. Bot., 54(383), 609–622, doi:10.1093/jxb/erg076, 2003.

Baker, A. R., Turner, S. M., Broadgate, W. J., Thompson, A., McFiggans, G. B., Vesperini, O., Nightingale, P. D., Liss, P. S. and Jickells, T. D.: Distribution and sea-air fluxes of biogenic trace gases in the eastern Atlantic Ocean, Global Biogeochem. Cycles, 14(3), 871–886, doi:10.1029/1999GB001219, 2000.

Balch, W. M., Holligan, P. M. and Kilpatrick, K. A.: Calcification, photosynthesis and growth of the bloom-forming coccolithophore, *Emiliania huxleyi*, Cont. Shelf Res., 12(12), 1353–1374, 1992.

Baltic Sea Portal: www.itameriportaali.fi, 2014.

Barcelos e Ramos, J., Biswas, H., Schulz, K. G., LaRoche, J. and Riebesell, U.: Effect of rising atmospheric carbon dioxide on the marine nitrogen fixer *Trichodesmium*, Global Biogeochem. Cycles, 21(2), GB2028, doi:10.1029/2006GB002898, 2007.

Barcelos e Ramos, J., Müller, M. N. and Riebesell, U.: Short-term response of the coccolithophore *Emiliania huxleyi* to an abrupt change in seawater carbon dioxide concentrations, Biogeosciences, 7(1), 177–186, doi:10.5194/bg-7-177-2010, 2010.

Barlow, R. G., Cummings, D. G. and Gibb, S. W.: Improved resolution of mono- and divinyl chlorophylls a and b and zeaxanthin and lutein in phytoplankton extracts using reverse phase C-8 HPLC, Mar. Ecol. Prog. Ser., 161, 303–307, 1997.

Barnola, J.-M., Raynaud, D., Lorius, C. and Barkov, N. I.: Historical CO_2 record from the Vostok ice core, in Trends: a Compendium of Data on Global Change, Carbon Dioxide Information Analysis Centre, Oak Ridge National Laboratory, U.S. Department of Energy, Oak Rodge, Tenn, U.S.A., 2003.

Barry, J. P., Hall-spencer, J. M. and Tyrrell, T.: In situ perturbation experiments: natural venting sites , spatial/ temporal gradients in ocean pH , manipulative in situ pCO_2 perturbations, in Guide to Best Practices for Ocean Acidification Research and Data Reporting, edited by U. Riebesell, V. J. Fabry, L. Hansson, and J.-P. Gattuso, pp. 123–136, Publications Office of the European Union, Luxembourg., 2010.

Bates, T. S., Lamb, B. K., Guenther, A., Dignon, J. and Stoiber, R. E.: Sulfur emissions to the atmosphere from natural sources, J. Atmos. Chem., 14, 315–337, 1992.

Beardall, J. and Raven, J. A.: The potential effects of global climate change on microalgal photosynthesis, growth and ecology, Phycologia, 43, 26–40, 2004.

Bell, T. G., Malin, G., Lee, G. A., Stefels, J., Archer, S. D., Steinke, M. and Matrai, P.: Global oceanic DMS data inter-comparability, Biogeochemistry, 110(1-3), 147–161, doi:10.1007/s10533-011-9662-3, 2012.

Bellerby, R. G. J., Schulz, K. G., Riebesell, U., Neill, C., Nondal, G., Heegaard, E., Johannessen, T. and Brown, K. R.: Marine ecosystem community carbon and nutrient uptake stoichiometry under varying ocean acidification during the PeECE III experiment, Biogeosciences, 5(6), 1517–1527, doi:10.5194/bg-5-1517-2008, 2008.

Bellerby, R. G. J., Silyakova, a., Nondal, G., Slagstad, D., Czerny, J., de Lange, T. and Ludwig, a.: Marine carbonate system evolution during the EPOCA Arctic pelagic ecosystem experiment in the context of simulated Arctic ocean acidification, Biogeosciences Discuss., 9(11), 15541–15565, doi:10.5194/bgd-9-15541-2012, 2012.

Benthien, A., Zondervan, I., Engel, A., Hefter, J., Terbruggen, A. and Riebesell, U.: Carbon isotopic fractionation during a mesocosm bloom experiment dominated by *Emiliania huxleyi:* Effects of CO_2 concentration and primary production, Geochim. Cosmochim. Acta, 71(6), 1528–1541, doi:10.1016/j.gca.2006.12.015, 2007.

Berge, T., Daugbjerg, N., Balling Andersen, B. and Hansen, P. J.: Effect of lowered pH on marine phytoplankton growth rates, Mar. Ecol. Prog. Ser., 416, 79–91, doi:10.3354/meps08780, 2010.

Berry, L., Taylor, A. R., Lucken, U., Ryan, K. P. and Brownlee, C.: Calcification and inorganic carbon acquisition in coccolithophores, Funct. Plant Biol., 29(3), 289–299, 2002.

De Bont, J. A. M., van Dijken, J. P. and Harder, W.: Dimethyl sulphoxide and dimethyl sulphide as a carbon, sulphur and energy source for growth of Hyphomicrobium S, J. Gen. Microbiol., 127, 315–323, 1981.

Booth, I.: Regulation of cytoplasmic pH in bacteria, Microbiol. Rev., 49(4), 359–378, 1985.

Bopp, L., Aumont, O., Belviso, S. and Monfray, P.: Potential impact of climate change on marine dimethyl sulfide emissions, Tellus B, 55(1), 11–22, doi:10.1034/j.1600-0889.2003.042.x, 2003.

Bopp, L., Boucher, O., Aumont, O., Belviso, S., Dufresne, J.-L., Pham, M. and Monfray, P.: Will marine dimethylsulfide emissions amplify or alleviate global warming ? A model study, Can. J. Fish. Aquat. Sci., 61, 826–835, doi:10.1139/F04-045, 2004.

Borges, A. V and Frankignoulle, M.: Distribution of surface carbon dioxide and air-sea exchange in the upwelling system off the Galician coast, Global Biogeochem. Cycles, 16(2), 1020, 2002.

Bouwer, E. J. and McCarty, P. L.: Transformations of 1-and 2-carbon halogenated aliphatic organic compounds under methanogenic conditions, Appl. Environ. Microbiol., 45(4), 1286 – 1294, 1983.

Boyd, P. W. and Doney, S. C.: Modelling regional responses by marine pelagic ecosystems to global climate change, Geophys. Res. Lett., 29(16), 1–4, 2002.

Brewer, P. G. and Barry, J. P.: The other CO_2 problem, Sci. Am. Earth 3.0, 18(4), 22–23, 2008.

Brimblecombe, P. and Shooter, D.: Photo-oxidation of dimethylsulphide in aqueous solution, Mar. Chem., 19(4), 343–353, doi:10.1016/0304-4203(86)90055-1, 1986.

Broecker, W. S.: Glacial to interglacial changes in ocean chemistry, Prog. Oceanogr., 11(2), 151–197, doi:10.1016/0079-6611(82)90007-6, 1982.

Broecker, W. S., Takahashi, T., Simpson, H. J. and Peng, T. H.: Fate of fossil fuel carbon dioxide and the global carbon budget, Science., 206(4417), 409–418, doi:10.1126/science.206.4417.409, 1979.

Brownell, D. K., Moore, R. M. and Cullen, J. J.: Production of methyl halides by *Prochlorococcus* and *Synechococcus*, Global Biogeochem. Cycles, 24(2), doi:10.1029/2009GB003671, 2010.

Brussaard, C. P. D., Noordeloos, A. A. M., Witte, H., Collenteur, M. C. J., Schulz, K., Ludwig, A. and Riebesell, U.: Arctic microbial community dynamics influenced by elevated CO_2 levels, Biogeosciences, 10(2), 719–731, doi:10.5194/bg-10-719-2013, 2013.

Brutemark, A., Engström-Öst, J. and Vehmaa, A.: Long-term monitoring data reveal pH dynamics, trends and variability in the western Gulf of Finland, Oceanol. Hydrobiol. Stud., 40(3), 91–94, doi:10.2478/s13545-011-0034-3, 2011.

Bucciarelli, E., Ridame, C., Sunda, W. G., Dimier-Hugueney, C., Cheize, M. and Belviso, S.: Increased intracellular concentrations of DMSP and DMSO in iron-limited oceanic phytoplankton *Thalassiosira oceanica* and *Trichodesmium erythraeum*, Limnol. Oceanogr., 58(5), 1667–1679, doi:10.4319/lo.2013.58.5.1667, 2013.

Buitenhuis, E. T., de Baar, H. J. W. and Veldhuis, M. J. W.: Photosynthesis and calcification by *Emiliania huxleyi* (Prymnesiophyceae) as a function of inorganic carbon species, J. Phycol., 35(5), 949–959, doi:10.1046/j.1529-8817.1999.3550949.x, 1999.

Burdett, H. L., Aloisio, E., Calosi, P., Findlay, H. S., Widdicombe, S., Hatton, A. D. and Kamenos, N. A.: The effect of chronic and acute low pH on the intracellular DMSP production and epithelial cell morphology of red coralline algae, Mar. Biol. Res., 8, 756–763, 2012.

Butler, A. and Carter-Franklin, J. N.: The role of vanadium bromoperoxidase in the biosynthesis of halogenated marine natural products, Nat. Prod. Rep., 21(1), 180–188, doi:10.1039/b302337k, 2004.

Caldeira, K. and Wickett, M.: Anthropogenic carbon and ocean pH, Nature, 425(September), 365, 2003.

Cameron-Smith, P., Elliott, S., Maltrud, M., Erickson, D. and Wingenter, O.: Changes in dimethyl sulfide oceanic distribution due to climate change, Geophys. Res. Lett., 38(7), L07704, doi:10.1029/2011GL047069, 2011

Campos, M. L. A. M., Sanders, R. and Jickells, T.: The dissolved iodate and iodide distribution in the South Atlantic from the Weddell Sea to Brazil, Mar. Chem., 65, 167–175, 1999.

Canadell, J. G., Le Quéré, C., Raupach, M. R., Field, C. B., Buitenhuis, E. T., Ciais, P., Conway, T. J., Gillett, N. P., Houghton, R. A. and Marland, G.: Contributions to accelerating atmospheric CO_2 growth from economic activity, carbon intensity, and efficiency of natural sinks., Proc. Natl. Acad. Sci. U. S. A., 104(47), 18866–18870, doi:10.1073/pnas.0702737104, 2007.

Caron, F. and Kramer, J. R.: Formation of volatile sulfides in freshwater environments, Sci. Total Environ., 153, 177–194, 1994.

Carpenter, L. J., Hopkins, J. R., Jones, C. E., Lewis, A. C., Parthipan, R., Wevill, D. J., Poissant, L., Pilote, M. and Constant, P.: Abiotic source of reactive organic halogens in the sub-arctic atmosphere?, Environ. Sci. Technol., 39(22), 8812–8816, 2005.

Carpenter, L. J. and Liss, P. S.: On temperate sources of bromoform and other reactive organic bromine gases, J. Geophys. Res., 105(D16), 20539, doi:10.1029/2000JD900242, 2000.

Carpenter, L. J., Wevill, D. J., Palmer, C. J. and Michels, J.: Depth profiles of volatile iodine and bromine-containing halocarbons in coastal Antarctic waters, Mar. Chem., 103, 227–236, doi:10.1016/j.marchem.2006.08.003, 2007.

Carpenter, L., Jones, C., Dunk, R. M., Hornsby, K. E. and Woeltjen, J.: Air-sea fluxes of biogenic bromine from the tropical and North Atlantic Ocean, Atmos. Chem. Phys., 9, 1805–1816, 2009.

Carslaw, K. S., Lee, L. A, Reddington, C. L., Pringle, K. J., Rap, A, Forster, P. M., Mann, G. W., Spracklen, D. V, Woodhouse, M. T., Regayre, L. a and Pierce, J. R.: Large contribution of natural aerosols to uncertainty in indirect forcing., Nature, 503(7474), 67–71, doi:10.1038/nature12674, 2013.

Carter, J. N., Beatty, K. E., Simpson, M. T. and Butler, A.: Reactivity of recombinant and mutant vanadium bromoperoxidase from the red alga Corallina officinalis., J. Inorg. Biochem., 91(1), 59–69, 2002.

Caruana, A. M. N., Steinke, M., Turner, S. M. and Malin, G.: Concentrations of dimethylsulphoniopropionate and activities of dimethylsulphide-producing enzymes in batch

cultures of nine dinoflagellate species, Biogeochemistry, 110, 87–107, doi:10.1007/s10533-012-9705-4, 2012.

Challenger, F.: Biological methylation, Adv. Enzymol. Relat. Areas Mol. Biol., 12, 429–491, 1951.

Chameides, W. L. and Davis, D. D.: Iodine: Its possible role in tropospheric photochemistry, J. Geophys. Res., 85(C12), 7383–7398, 1980.

Chameides, W. and Walker, J. C. C.: A photochemical theory of tropospheric ozone, J. Geophys. Res., 78(36), 8751 – 8760, 1973.

Chance, R., Baker, A. R., Küpper, F. C., Hughes, C., Kloareg, B. and Malin, G.: Release and transformations of inorganic iodine by marine macroalgae, Estuar. Coast. Shelf Sci., 82, 406–414, doi:10.1016/j.ecss.2009.02.004, 2009.

Charlson, R. J., Lovelock, J. E., Andreae, M. O. and Warren, S. G.: Oceanic phytoplankton, atmospheric sulphur, cloud albedo and climate, Nature, 326(6114), 655–661, 1987.

Chatfield, R. and Crutzen, P.: Are there interactions of iodine and sulfur species in marine air photochemistry?, J. Geophys. Res. Atmos., 95(89), 22319 – 22341, 1990.

Chavez, F. P. and Messié, M.: A comparison of Eastern Boundary Upwelling Ecosystems, Prog. Oceanogr., 83, 80–96, doi:10.1016/j.pocean.2009.07.032, 2009.

Chen, C.-C. and Kemp, W. M.: Periphyton communities in experimental marine ecosystems: scaling the effects of removal from container walls, Mar. Ecol. Prog. Ser., 271, 27–41, doi:10.3354/meps271027, 2004.

Chester, R. and Jickells, T.: Marine Geochemistry, in Marine Geochemistry, vol. 187, pp. 69–97, John Wiley & Sons, Ltd, Chichester, UK., 2009.

Chuck, A. L., Turner, S. M. and Liss, P. S.: Oceanic distributions and air-sea fluxes of biogenic halocarbons in the open ocean, J. Geophys. Res., 110(C10022), doi:10.1029/2004JC002741, 2005.

Ciais, P., Tans, P., White, J., Trolier, M., Francey, R. J., Berry, J. A., Randall, D. R., Sellers, P. J., Collatz, J. G. and Schimel, D. S.: Partitioning of ocean and land uptake of CO_2 as inferred by δ13C measurements from the NOAA Climate Monitoring and Diagnostics Laboratory Global Air Sampling, J. Geophys. Res., 100(D3), 5051–5070, 1995.

Cigliano, M., Gambi, M. C., Rodolfo-Metalpa, R., Patti, F. P. and Hall-Spencer, J. M.: Effects of ocean acidification on invertebrate settlement at volcanic CO_2 vents, Mar. Biol., 157(11), 2489–2502, doi:10.1007/s00227-010-1513-6, 2010.

Le Clainche, Y., Vézina, A., Levasseur, M., Cropp, R. A., Gunson, J. R., Vallina, S. M., Vogt, M., Lancelot, C., Allen, J. I., Archer, S. D., Bopp, L., Deal, C., Elliott, S., Jin, M., Malin, G., Schoemann, V., Simó, R., Six, K. D. and Stefels, J.: A first appraisal of prognostic ocean DMS models and prospects for their use in climate models, Global Biogeochem. Cycles, 24, doi:10.1029/2009GB003721, 2010.

Class, T. H. and Ballschmiter, K.: Chemistry of organic traces in air, J. Atmos. Chem., 6(1-2), 35–46, doi:10.1007/BF00048330, 1988.

Clayton, T. D. and Byrne, R. H.: Spectrophotometric seawater pH measurements: total hydrogen ion concentration scale calibration of m-cresol purple and at-sea results, Deep Sea Res. Part I Oceanogr. Res. Pap., 40(10), 2115–2129, 1993.

Collen, J. and Davison, I. R.: Reactive oxygen production and damage in intertidal Fucus Spp (Phaeophyceae), J. Phycol., 35, 54–61, 1999.

Collins, M., Knutti, R., Arblaster, J., Dufresne, J.-L., Fichefet, T., Frielingstein, P., Gao, X., Gutowski, W. J., Johns, T., Krinner, G., Shongwe, M., Tebaldi, C., Weaver, A. J. and Wehner, M.: Long-term climate change: projections, commitments and irreversibility, in Climate Change 2013: The Physical Science Basis. Contribution of Working Group 1 to the Fifth Assessment Report of the Intergovernmental Panel on Climate Change, edited by T.. Stocker, D. Qin, G.-K. Plattner, M. Tignor, S. K. Allen, J. Boschung, A. Nauels, Y. Xia, V. Bex, and P. M. Midgley, Cambridge University Press, Cambridge, UK., 2013.

Collins, S. and Bell, G.: Phenotypic consequences of 1,000 generations of selection at elevated CO_2 in a green alga., Nature, 431(7008), 566–9, doi:10.1038/nature02945, 2004.

Colomb, A., Yassaa, N., Williams, J., Peeken, I. and Lochte, K.: Screening volatile organic compounds (VOCs) emissions from five marine phytoplankton species by head space gas chromatography/mass spectrometry (HS-GC/MS)., J. Environ. Monit., 10(3), 325–330, doi:10.1039/b715312k, 2008.

Commission of the European Communities: Dimethylsulphide: Oceans, Atmosphere and Climate, edited by G. Restelli and G. Angeletti, Kluwer Academic Publishers, Dordrecht, The Netherlands., 1992.

Corn, M., Belviso, S., Partensky, F., Simon, N. and Christaki, U.: Origin and Importance of Picoplanktonic DMSP, in Biological and Environmental Chemistry of DMSP and Related Sulfonium Compounds SE - 17, edited by R. Kiene, P. Visscher, M. Keller, and G. Kirst, pp. 191–201, Springer US., 1996.

Covington, A. K., Bates, R. A. and Durst, R. A.: Definition of pH scales, standard reference values, measurement of pH and related terminology, Pure Appl. Chem., 57(3), 531–542, 1985.

Crutzen, B. P. J.: Photochemical reactions initiated by and influencing ozone in unpolluted tropospheric air, Tellus, 80302(1971), 47–57, 1973.

Cubasch, U., Wuebbles, D., Chen, D., Facchini, M. C., Frame, D., Mahowald, N. and Winther, J.-G.: Introduction, in Climate Change 2013: The Physical Science Basis. Contribution of Working Group 1 to the Fifth Assessment Report of the Intergovernmental Panel on Climate Change, edited by T.. Stocker, D. Qin, G.-K. Plattner, M. Tignor, S. K. Allen, J. Boschung, A. Nauels, Y. Xia, V. Bex, and P. M. Midgley, Cambridge University Press, Cambridge, UK., 2013.

Curran, M. A. J., Jones, G. B. and Burton, H.: Spatial distribution of dimethylsulfide and dimethylsulfoniopropionate in the Australasian sector of the Southern Ocean, J. Geophys. Res., 103(D13), 16677 – 16689, 1998.

Curson, A. R. J., Todd, J. D., Sullivan, M. J. and Johnston, A. W. B.: Catabolism of dimethylsulphoniopropionate: microorganisms, enzymes and genes, Nat. Rev. Microbiol., 9(12), 849–859, doi:10.1038/nrmicro2653, 2011.

Czerny, J., Barcelos e Ramos, J. and Riebesell, U.: Influence of elevated CO_2 concentrations on cell division and nitrogen fixation rates in the bloom-forming cyanobacterium *Nodularia spumigena*, Biogeosciences, 6, 1865–1875, 2009.

Czerny, J., Schulz, K. G., Boxhammer, T., Bellerby, R. G. J., Büdenbender, J., Engel, A., Krug, S. A., Ludwig, A., Nachtigall, K., Nondal, G., Niehoff, B., Silyakova, A. and Riebesell, U.: Implications of elevated CO_2 on pelagic carbon fluxes in an Arctic mesocosm study – an elemental mass balance approach, Biogeosciences, 10(5), 3109–3125, doi:10.5194/bg-10-3109-2013, 2013a.

Czerny, J., Schulz, K. G., Krug, S. A., Ludwig, A. and Riebesell, U.: Technical Note: The determination of enclosed water volume in large flexible-wall mesocosms "KOSMOS," Biogeosciences, 10, 1937–1941, doi:10.5194/bg-10-1937-2013, 2013b.

Czerny, J., Schulz, K. G., Ludwig, a. and Riebesell, U.: Technical Note: A simple method for air–sea gas exchange measurements in mesocosms and its application in carbon budgeting, Biogeosciences, 10(3), 1379–1390, doi:10.5194/bg-10-1379-2013, 2013c.

Dacey, J. W. and Wakeham, S. G.: Oceanic dimethylsulfide: production during zooplankton grazing on phytoplankton, Science., 233(4770), 1314–1316, doi:10.1126/science.233.4770.1314, 1986.

Davidovits, J.: Global warming impact on the cement and aggregates industries, World Resour. Rev., 6(2), 263–278, 1994.

Delille, B., Harlay, J., Zondervan, I., Jacquet, S., Chou, L., Wollast, R., Bellerby, R. G. J., Frankignoulle, M., Borges, A. V., Riebesell, U. and Gattuso, J.-P.: Response of primary production and calcification to changes of pCO_2 during experimental blooms of the coccolithophorid *Emiliania huxleyi*, Global Biogeochem. Cycles, 19(2), doi:10.1029/2004GB002318, 2005.

Derevianko, G. J., Deutsch, C. and Hall, A.: On the relationship between ocean DMS and solar radiation, Geophys. Res. Lett., 36, L17606, doi:10.1029/2009GL039412, 2009.

Dias, B. B., Hart, M. B., Smart, C. W. and Hall-Spencer, J. M.: Modern seawater acidification: the response of foraminifera to high-CO_2 conditions in the Mediterranean Sea, J. Geol. Soc. London., 167(5), 843–846, doi:10.1144/0016-76492010-050, 2010.

Dickson, A. G.: An exact definition of total alkalinity and a procedure for the estimation of alkalinity and total inorganic carbon from titration data, Deep Sea Res. Part A. Oceanogr. Res. Pap., 28A(6), 609–623, doi:10.1016/0198-0149(81)90121-7, 1981.

Dickson, A. G.: The measurement of sea water pH, Mar. Chem., 44, 131–142, doi:10.1016/0304-4203(93)90198-W, 1993.

Dickson, A. G.: The carbon dioxide system in seawater: equilibrium chemistry and measurements, in Guide to Best Practices for Ocean Acidification Research and Data Reporting, edited by H. L. & G. J.-P. (Eds.. Riebesell U., Fabry V. J., pp. 17–40, Publications Office of the European Union, Luxembourg., 2010.

Dickson, D. M., Jones, R. G. W. and Davenport, J.: Steady state osmotic adaptation in *Ulva lactuca*, Planta, 150, 158–165, 1980.

Doney, S. C., Fabry, V. J., Feely, R. A. and Kleypas, J. A.: Ocean acidification: the other CO_2 problem., Ann. Rev. Mar. Sci., 1, 169–192, doi:10.1146/annurev.marine.010908.163834, 2009.

Dong, L. F., Nimer, N. A., Okus, E. and Merrett, M. J.: Dissolved inorganic carbon utilization in relation to calcite production in *Emiliania huxleyi* (Lohmann) Kamptner, New Phytol., 123(4), 679–684, doi:10.1111/j.1469-8137.1993.tb03777.x, 1993.

Dore, J. E., Lukas, R., Sadler, D. W., Church, M. J. and Karl, D. M.: Physical and biogeochemical modulation of ocean acidification in the central North Pacific., Proc. Natl. Acad. Sci. U. S. A., 106(30), 12235–12240, doi:10.1073/pnas.0906044106, 2009.

Drotar, A., Burton, G. A., Tavernier, J. E. and Fall, R.: Widespread occurrence of bacterial thiol methyltransferases and the biogenic emission of methylated sulfur gases, Appl. Environ. Microbiol., 53(7), 1626–1631, 1987.

Eggers, S. L., Lewandowska, A. M., Barcelos e Ramos, J., Blanco-Ameijeiras, S., Gallo, F. and Matthiessen, B.: Community composition has greater impact on the functioning of marine phytoplankton communities than ocean acidification., Glob. Chang. Biol., 20(3), 713–723, doi:10.1111/gcb.12421, 2014.

Egleston, E. S., Sabine, C. L. and Morel, F. M. M.: Revelle revisited: Buffer factors that quantify the response of ocean chemistry to changes in DIC and alkalinity, Global Biogeochem. Cycles, 24(1), doi:10.1029/2008GB003407, 2010.

Elderfield, H.: Carbonate mysteries., Science., 296(5573), 1618–1621, doi:10.1126/science.1072079, 2002.

Elliott, S. and Rowland, F. S.: Methyl halide hydrolysis rates in natural waters, J. Atmos. Chem., 20, 229–236, 1995.

Endres, S., Galgani, L., Riebesell, U., Schulz, K.-G. and Engel, A.: Stimulated bacterial growth under elevated pCO_2: results from an off-shore mesocosm study., PLoS One, 9(6), e99228, doi:10.1371/journal.pone.0099228, 2014.

Engel, A.: Direct relationship between CO_2 uptake and transparent exopolymer particles production in natural phytoplankton, J. Plankton Res., 24(1), 49–53, doi:10.1093/plankt/24.1.49, 2002.

Engel, A., Borchard, C., Piontek, J., Schulz, K. G., Riebesell, U. and Bellerby, R. G. J.: CO_2 increases 14C primary production in an Arctic plankton community, Biogeosciences, 10(3), 1291–1308, doi:10.5194/bg-10-1291-2013, 2013.

Engel, A., Schulz, K. G., Riebesell, U., Bellerby, R. G. J., Delille, B. and Schartau, M.: Effects of CO_2 on particle size distribution and phytoplankton abundance during a mesocosm bloom experiment (PeECE II), Biogeosciences, 5(2), 509–521, doi:10.5194/bg-5-509-2008, 2008.

Engel, A., Zondervan, I., Aerts, K., Beaufort, L., Benthien, A., Chou, L., Delille, B., Gattuso, J.-P., Harlay, J., Heemann, C., Hoffmann, L., Jacquet, S., Nejstgaard, J. C., Pizay, M.-D., Rochelle-Newall, E., Schneider, U., Terbrueggen, A. and Riebesell, U.: Testing the direct effect of CO_2 concentration on a bloom of the coccolithophorid *Emiliania huxleyi* in mesocosm experiments, Limnol. Oceanogr., 50(2), 493–507, doi:10.4319/lo.2005.50.2.0493, 2005.

Evans, C., Kadner, S. V., Darroch, L. J., Wilson, W. H., Liss, P. S. and Malin, G.: The relative significance of viral lysis and microzooplankton grazing as pathways of dimethylsulfoniopropionate (DMSP) cleavage: An *Emiliania huxleyi* culture study, Limnol. Oceanogr., 52(3), 1036–1045, doi:10.4319/lo.2007.52.3.1036, 2007.

Fabricius, K. E., Langdon, C., Uthicke, S., Humphrey, C., Noonan, S., De'ath, G., Okazaki, R., Muehllehner, N., Glas, M. S. and Lough, J. M.: Losers and winners in coral reefs acclimatized to elevated carbon dioxide concentrations, Nat. Clim. Chang., 1, 165–169, doi:10.1038/nclimate1122, 2011.

Fabry, V. J.: Marine calcifiers in a high-CO_2 ocean., Science., 320(5879), 1020–1022, doi:10.1126/science.1157130, 2008.

Falkowski, P. G.: Evolution of the nitrogen cycle and its influence on the biological sequestration of CO_2 in the ocean, Nature, 387, 272 –275, 1997.

Falkowski, P. G., Kim, Y., Kolber, Z., Wilson, C., Wirick, C. and Cess, R.: Natural versus anthropogenic factors affecting low-level cloud albedo over the North Atlantic., Science., 256, 1311–1313, doi:10.1126/science.256.5061.1311, 1992.

FAO: Food and Agriculture Organisation of the United Nations: Statistics Division, 2014.

Feely, R. A., Alin, S. R., Newton, J., Sabine, C. L., Warner, M., Devol, A., Krembs, C. and Maloy, C.: The combined effects of ocean acidification, mixing, and respiration on pH and carbonate

saturation in an urbanized estuary, Estuar. Coast. Shelf Sci., 88(4), 442–449, doi:10.1016/j.ecss.2010.05.004, 2010.

Feely, R. A., Doney, S. C. and Cooley, S. R.: Ocean Acidification: present conditions and future changes in a high CO_2 world, Oceanography, 22(4), 36–47, 2009.

Feely, R. A., Sabine, C. L., Hernandez-Ayon, J. M., Ianson, D. and Hales, B.: Evidence for upwelling of corrosive "acidified" water onto the continental shelf, Science., 320(5882), 1490–1492, doi:10.1126/science.1155676, 2008.

Feng, Y., Hare, C. E., Leblanc, K., Rose, J. M., Zhang, Y., DiTullio, G. R., Lee, P. A., Wilhelm, S. W., Rowe, J. M., Sun, J., Nemcek, N., Gueguen, C., Passow, U., Benner, I., Brown, C. and Hutchins, D. A.: Effects of increased pCO_2 and temperature on the North Atlantic spring bloom. I. The phytoplankton community and biogeochemical response, Mar. Ecol. Prog. Ser., 388, 13–25, doi:10.3354/meps08133, 2009.

Feng, Y., Warner, M. E., Zhang, Y., Sun, J., Fu, F.-X., Rose, J. M. and Hutchins, D. A.: Interactive effects of increased pCO_2 , temperature and irradiance on the marine coccolithophore *Emiliania huxleyi* (Prymnesiophyceae), Eur. J. Phycol., 43(1), 87–98, doi:10.1080/09670260701664674, 2008.

Fenical, W.: Natural products chemistry in the marine environment, Science., 215(4535), 923–928, 1982.

Finni, T., Kononen, K., Olsonen, R. and Wallström, K.: The History of Cyanobacterial Blooms in the Baltic Sea, AMBIO A J. Hum. Environ., 30(4), 172–178, doi:10.1579/0044-7447-30.4.172, 2001.

Fiorini, S., Middelburg, J. J. and Gattuso, J.-P.: Testing the effects of elevated pCO_2 on coccolithophores (Prymnesiophyceae): comparison between haploid and diploid life stages, J. Phycol., 47(6), 1281–1291, doi:10.1111/j.1529-8817.2011.01080.x, 2011.

Fischer, E. and Jones, G.: Atmospheric dimethysulphide production from corals in the Great Barrier Reef and links to solar radiation, climate and coral bleaching, Biogeochemistry, 110(1-3), 31–46, doi:10.1007/s10533-012-9719-y, 2012.

Fischer, H. and Pusch, M.: Use of the [^{14}C] leucine incorporation technique to measure bacterial production in river sediments and the Epiphyton, Appl. Environ. Microbiol., 65(10), 4411 – 4418, 1999.

Forsskahl, M., Laakkonen, A. and Leppanen, J.-M.: Seasonal cycle of production and sedimentation of organic matter at the entrance to the Gulf of Finland, Netherlands J. Sea Res., 16, 290–299, 1982.

Frada, M. J., Bidle, K. D., Probert, I. and de Vargas, C.: In situ survey of life cycle phases of the coccolithophore *Emiliania huxleyi* (Haptophyta)., Environ. Microbiol., 14(6), 1558–69, doi:10.1111/j.1462-2920.2012.02745.x, 2012.

Frank, H., Frank, W. and Thiel, D.: C1- and C2 halocarbons in soil-air of forests, Atmos. Environ., 23(6), 1333–1335, 1989.

Frank, W. and Frank, H.: Concentrations of airborne C1- and C2-halocarbons in forest areas in west germany: results of three campaigns in 1986, 1987 and 1988, Atmos. Environ. Part A. Gen. Top., 24(7), 1735–1739, doi:10.1016/0960-1686(90)90506-I, 1990.

Franke, A. and Clemmesen, C.: Effect of ocean acidification on early life stages of Atlantic herring (*Clupea harengus* L.), Biogeosciences Discuss., 8(4), 7097–7126, doi:10.5194/bgd-8-7097-2011, 2011.

Franklin, D. J., Airs, R. L., Fernandes, M., Bell, T. G., Bongaerts, R. J., Berges, J. A. and Malin, G.: Identification of senescence and death in *Emiliania huxleyi* and *Thalassiosira pseudonana*: cell staining , chlorophyll alterations , and dimethylsulfoniopropionate (DMSP) metabolism, Limnol. Oceanogr., 57(1), 305–317, doi:10.4319/lo.2012.57.1.0305, 2012.

Franklin, D. J., Steinke, M., Young, J., Probert, I. and Malin, G.: Dimethylsulphoniopropionate (DMSP), DMSP-lyase activity (DLA) and dimethylsulphide (DMS) in 10 species of coccolithophore, Mar. Ecol. Prog. Ser., 410, 13–23, doi:10.3354/meps08596, 2010.

Fredrickson, K. A. and Strom, S. L.: The algal osmolyte DMSP as a microzooplankton grazing deterrent in laboratory and field studies, J. Plankton Res., 31(2), 135–152, doi:10.1093/plankt/fbn112, 2009.

Frische, M., Garofalo, K., Hansteen, T. H., Borchers, R. and Harnisch, J.: The origin of stable halogenated compounds in volcanic gases, Environ. Sci. Pollut. Res. Int., 13(6), 406–413, 2006.

Fu, F.-X., Warner, M. E., Zhang, Y., Feng, Y. and Hutchins, D. A.: Effects of increased temperature and CO_2 on photosynthesis, growth, and elemental ratios in marine *Synechococcus* and *Prochlorococcus* (Cyanobacteria), J. Phycol., 43, 485–496, doi:10.1111/j.1529-8817.2007.00355.x, 2007.

Gabric, A., Murray, N., Stone, L. and Kohl, M.: Modelling the production of dimethylsulfide during a phytoplankton bloom, J. Geophys. Res., 98, 22805–22816, 1993.

Galgani, L.: Biogenic composition of the sea-surface microlayer in response to a changing environment, Christian-Albrechts University, Kiel., 2013.

Galgani, L. and Engel, A.: Accumulation of gel particles in the Sea-Surface Microlayer during an experimental study with the diatom *Thalassiosira weissflogii*, Int. J. Geosci., 4, 129–145, 2013.

Gates, R. D., Baghdasarian, G. and Muscatine, L.: Temperature stress causes host cell detachment in symbiotic Cnidarians: implications for coral bleaching, Biol. Bull., 182(3), 324–332, doi:10.2307/1542252, 1992.

Gattuso, J., Frankignoulle, M., Bourne, I., Romaine, S. and Buddemeier, R. W.: Effect of calcium carbonate saturation of seawater on coral calcification, Glob. Planet. Change, 18(1-2), 37–46, doi:10.1016/S0921-8181(98)00035-6, 1998.

Gattuso, J.-P. and Buddemeier, R. W.: Calcification and CO_2, Nature, 407(September), 1–2, 2000.

Gattuso, J.-P., Gao, K., Lee, K., Rost, B. and Schulz, K. G.: Approaches and tools to manipulate the carbonate chemistry, in Guide to Best Practices for ocean acidification research and data reporting, edited by J.-P. Riebesell, U., Fabry, V. J., Hansson, L. Gattuso, pp. 41–52, Publications Office of the European Union, Luxembourg., 2010.

Gattuso, J.-P. and Lavigne, H.: Technical Note: Approaches and software tools to investigate the impact of ocean acidification, Biogeosciences, 6, 2121–2133, 2009.

Genthon, C., Barnola, J.-M., Raynaud, D., Lorius, C., Jouzel, J., Barkov, N. I., Korotkevich, Y. S. and Kotlyakov, V. M.: Vostok ice core-climatic response to CO_2 and orbital forcing changes over the last climatic cycle, Nature, 329, 414–418, 1987.

Ghosh, W. and Dam, B.: Biochemistry and molecular biology of lithotrophic sulfur oxidation by taxonomically and ecologically diverse bacteria and archaea, FEMS Microbiol. Rev., 33(6), 999–1043, doi:10.1111/j.1574-6976.2009.00187.x, 2009.

Gidhagen, L.: Coastal upwelling in the Baltic Sea—Satellite and in situ measurements of sea-surface temperatures indicating coastal upwelling, Estuar. Coast. Shelf Sci., 24, 449–462, 1987.

Giese, B., Laturnus, F., Adams, F. C. and Wiencke, C.: Release of volatile iodinated C1 −C4 hydrocarbons by marine macroalgae from various climate zones, Environ. Sci. Technol., 33(14), 2432–2439, doi:10.1021/es980731n, 1999.

Giordano, M., Beardall, J. and Raven, J. A.: CO_2 concentrating mechanisms in algae: mechanisms, environmental modulation, and evolution., Annu. Rev. Plant Biol., 56, 99–131, doi:10.1146/annurev.arplant.56.032604.144052, 2005.

Von Glasow, R. and Crutzen, P. J.: Model study of multiphase DMS oxidation with a focus on halogens, Atmos. Chem. Phys., 4(3), 589–608, doi:10.5194/acp-4-589-2004, 2004.

Gonzalez, J. M., Kiene, R. P. and Moran, M. A.: Transformation of sulfur compounds by an abundant lineage of marine bacteria in the a-subclass of the Class Proteobacteria, Appl. Environ. Microbiol., 65(9), 3810–3819, 1999.

Goodwin, K. D., North, W. J. and Lidstrom, M. E.: Production of bromoform and dibromomethane by giant kelp: factors affecting release and comparison to anthropogenic bromine sources, Limnol. Oceanogr., 42(8), 1725–1734, doi:10.4319/lo.1997.42.8.1725, 1997.

Goodwin, K., Schaefer, J. K. and Oremland, R. S.: Bacterial oxidation of dibromomethane and methyl bromide in natural waters and enrichment cultures, Appl. Environ. Microbiol., 64(12), 4629 –4636, 1998.

Gran, G.: Determination of the equivalence point in potentiometric titrations Part II, Analyst, 77, 661–671, 1952.

Green, J. C., Course, P. A. and Tarran, G. A.: The life-cycle of *Emiliania huxleyi*: a brief review and a study of relative ploidy levels analysed by flow cytometry, J. Mar. Syst., 9, 33–44, 1996.

Grennfelt, P.: Critical loads for nitrogen, Nordisk Ministerraad., 1992.

Gröne, T. and Kirst, G. O.: The effect of nitrogen deficiency, methionine and inhibitors of methionine metabolism on the DMSP contents of *Tetraselmis subcordiformis* (Stein), Mar. Biol., 112, 497–503, 1992.

Grossart, H. P., Allgaier, M., Passow, U. and Riebesell, U.: Testing the effect of CO_2 concentration on dynamics of marine heterotrophic bacterioplankton, Limnol. Oceanogr., 51(1), 1–11, 2006.

Gutowska, M., Pörtner, H. and Melzner, F.: Growth and calcification in the cephalopod *Sepia officinalis* under elevated seawater pCO_2, Mar. Ecol. Prog. Ser., 373(2007), 303–309, doi:10.3354/meps07782, 2008.

Gypens, N. and Borges, A. V.: Increase in dimethylsulfide (DMS) emissions due to eutrophication of coastal waters offsets their reduction due to ocean acidification, Front. Mar. Sci., 1, 1–6, doi:10.3389/fmars.2014.00004, 2014.

Halloran, P. R., Bell, T. G. and Totterdell, I. J.: Can we trust empirical marine DMS parameterisations within projections of future climate?, Biogeosciences, 7, 1645–1656, doi:10.5194/bg-7-1645-2010, 2010.

Hall-Spencer, J. M., Rodolfo-Metalpa, R., Martin, S., Ransome, E., Fine, M., Turner, S. M., Rowley, S. J., Tedesco, D. and Buia, M.-C.: Volcanic carbon dioxide vents show ecosystem effects of ocean acidification, Nature, 454(7200), 96–99, doi:10.1038/nature07051, 2008.

Hansson, I.: A new set of pH-scales and standard buffers for sea water, Deep Sea Res., 20(January), 479–491, 1973.

Hartmann, D. L., Klein Tank, A. M. G., Rusticucci, M., Alexander, L. V., Bronnimann, S., Charabi, Y., Dentener, F. J., Dlugokencky, E. J., Easterling, D. R., Kaplan, A., Soden, B. J., Thorne, P. W., Wild, M. and Zhai, P. M.: Observations: Atmosphere and Surface, in Climate Change 2013: The Physical Science Basis. Contribution of Working Group 1 to the Fifth Assessment Report of the Intergovernmental Panel on Climate Change, edited by T. F. Stocker, D. Qin, G.-K. Plattner, M. Tignor, S. K. Allen, J. Boschung, A. Nauels, Y. Xia, V. Bex, and P. M. Midgley, Cambridge University Press, Cambridge, Cambridge, UK., 2013.

Harvey, B. P., Gwynn-Jones, D. and Moore, P. J.: Meta-analysis reveals complex marine biological responses to the interactive effects of ocean acidification and warming., Ecol. Evol., 3(4), 1016–1030, doi:10.1002/ece3.516, 2013.

Hein, M. and Sand-Jensen, K.: CO_2 increases oceanic primary production, Nature, 388(6642), 526–527, 1997.

Heinle, M.: The effects of light, temperature and nutrients on coccolithophores and implications for biogeochemical models, University of East Anglia., 2013.

HELCOM: Eutrophication status of the Baltic Sea 2007 - 2011 - a concise thematic assessment., 2014.

Helsinki Convention: Convention on the protection of the marine environment of the Baltic Sea Area 1974., 1993.

Hense, I. and Quack, B.: Modelling the vertical distribution of bromoform in the upper water column of the tropical Atlantic Ocean, Biogeosciences, 6(4), 535–544, doi:10.5194/bg-6-535-2009, 2009.

Hewitt, C. N. and Davison, B.: Field measurements of dimethyl sulphide and its oxidation products in the atmosphere, Philos. Trans. R. Soc. B Biol. Sci., 352(1350), 183–189, doi:10.1098/rstb.1997.0013, 1997.

Hildebrandt, N., Sartoris, F. J., Czerny, J., Budenbender, J., Boxhammer, T., Schulz, K. G. and Niehoff, B.: Ocean acidification effects on a boreal mesozooplankton community - a mesocosm study, , In Press, 2014.

Hill, R. W., White, B. A., Cottrell, M. T. and Dacey, J. W.: Virus-mediated total release of dimethylsulfoniopropionate from marine phytoplankton : a potential climate process, Aquat. Microb. Ecol., 14, 1–6, 1998.

Hill, V. L. and Manley, S. L.: Release of reactive bromine and iodine from diatoms and its possible role in halogen transfer in polar and tropical oceans, Limnol. Oceanogr., 54(3), 812–822, doi:10.4319/lo.2009.54.3.0812, 2009.

Hinga, K. R.: Effects of pH on coastal marine phytoplankton, Mar. Ecol. Prog. Ser., 238, 281–300, 2002.

Hofmann, G. E., Barry, J. P., Edmunds, P. J., Gates, R. D., Hutchins, D. A., Klinger, T. and Sewell, M. A.: The effect of ocean acidification on calcifying organisms in marine ecosystems: an organism-to-ecosystem perspective, Annu. Rev. Ecol. Evol. Syst., 41(1), 127–147, doi:10.1146/annurev.ecolsys.110308.120227, 2010.

Holligan, P. M., Fernandez, E., Aiken, J., Balch, W. M., Boyd, P., Burkill, P. H., Finch, M., Groom, S. B., Malin, G., Muller, K., Purdie, D. A., Trees, C. C., Robinson, C., Turner, S. M. and van der Wal, P.: A biogeochemical study of the coccolithophore *Emiliania huxleyi* in the North Atlantic, Global Biogeochem. Cycles, 7(4), 879–900, 1993.

Hopkins, F. E.: Ocean Acidification and Marine Biogenic Trace Gas Production, University of East Anglia., 2010.

Hopkins, F. E. and Archer, S. D.: Consistent increase in dimethyl sulphide (DMS) in response to high CO_2 in five shipboard bioassays from contrasting NW European waters, Biogeosciences, 11(2), 4925 – 4940, doi:10.5194/bgd-11-2267-2014, 2014.

Hopkins, F. E., Kimmance, S. A., Stephens, J. A., Bellerby, R. G. J., Brussaard, C. P. D., Czerny, J., Schulz, K. G. and Archer, S. D.: Response of halocarbons to ocean acidification in the Arctic, Biogeosciences, 10(4), 2331–2345, doi:10.5194/bg-10-2331-2013, 2013.

Hopkins, F. E., Turner, S. M., Nightingale, P. D., Steinke, M., Bakker, D. and Liss, P. S.: Ocean acidification and marine trace gas emissions., Proc. Natl. Acad. Sci. U. S. A., 107(2), 760–765, doi:10.1073/pnas.0907163107, 2010.

Houdan, A., Probert, I., Lenning, K. Van and Lefebvre, S.: Comparison of photosynthetic responses in diploid and haploid life-cycle phases of *Emiliania huxleyi* (Prymnesiophyceae), Mar. Ecol. Prog. Ser., 292, 139–146, 2005.

Houghton, J. T., Ding, Y., Griggs, D. J., Noguer, M., Van der Linden, P. J., Dai, X., Maskell, K. and Johnson, C. A.: Climate change 2001: The scientific basis. Contribution of Working Group I to the Third Assessment Report of the Intergovernmental Panel on Climate Change, Cambridge University Press., 2001.

Howard, E. C., Henriksen, J. R., Buchan, A., Reisch, C. R., Bürgmann, H., Welsh, R., Ye, W., González, J. M., Mace, K., Joye, S. B., Kiene, R. P., Whitman, W. B. and Moran, M. A.: Bacterial taxa that limit sulphur flux from the ocean, Science., 314, 649–652, doi:10.1126/science.1130657, 2006.

Howard, E. C., Sun, S., Reisch, C. R., del Valle, D. A., Bürgmann, H., Kiene, R. P. and Moran, M. A.: Changes in dimethylsulfoniopropionate demethylase gene assemblages in response to an induced phytoplankton bloom., Appl. Environ. Microbiol., 77(2), 524–531, doi:10.1128/AEM.01457-10, 2011.

Hughes, C.: Biogenic Iodocarbon Production in the Sea, University of East Anglia., 2004.

Hughes, C., Chuck, A. L., Rossetti, H., Mann, P. J., Turner, S. M., Clarke, A., Chance, R. and Liss, P. S.: Seasonal cycle of seawater bromoform and dibromomethane concentrations in a coastal bay on the western Antarctic Peninsula, Global Biogeochem. Cycles, 23, doi:10.1029/2008GB003268, 2009.

Hughes, C., Franklin, D. J. and Malin, G.: Iodomethane production by two important marine cyanobacteria: *Prochlorococcus marinus* (CCMP 2389) and *Synechococcus* sp. (CCMP 2370), Mar. Chem., 125(1-4), 19–25, doi:10.1016/j.marchem.2011.01.007, 2011.

Hughes, C., Malin, G., Nightingale, P. D. and Liss, P. S.: The effect of light stress on the release of volatile iodocarbons by three species of marine microalgae, Limnol. …, 51(6), 2849–2854, 2006.

Hughes, C., Malin, G., Turley, C. M., Keely, B. J., Nightingale, P. D. and Liss, P. S.: The production of volatile iodocarbons by biogenic marine aggregates, Limnol. Oceanogr., 53(2), 867–872, 2008.

Hughes, L.: Biological consequences of global warming: is the signal already apparent?, Trends Ecol. Evol., 15(2), 56–61, 2000.

Hutchins, D. A., Fu, F.-X., Zhang, Y., Warner, M. E., Feng, Y., Portune, K., Bernhardt, P. W. and Mulholland, M. R.: CO_2 control of *Trichodesmium* N_2 fixation, photosynthesis, growth rates, and elemental ratios: Implications for past, present, and future ocean biogeochemistry, Limnol. Oceanogr., 52(4), 1293–1304, doi:10.4319/lo.2007.52.4.1293, 2007.

Iglesias-Rodriguez, M. D., Halloran, P. R., Rickaby, R. E. M., Hall, I. R., Colmenero-Hidalgo, E., Gittins, J. R., Green, D. R. H., Tyrrell, T., Gibbs, S. J., von Dassow, P., Rehm, E., Armbrust, E. V. and Boessenkool, K. P.: Phytoplankton calcification in a high-CO_2 world, Science., 320(5874), 336–340, doi:10.1126/science.1154122, 2008.

Iglesias-Rodriguez, M. D., Schofield, O. M., Batley, J., Medlin, L. K. and Hayes, P. K.: Intraspecific genetic diversity in the marine coccolithophore *Emiliania huxleyi* (Prymnesiophyceae): the use of microsatellite analysis in marine phytoplankton population studies, J. Phycol., 42, 526–536, doi:10.1111/j.1529-8817.2006.00231.x, 2006.

Imbrie, J., Boyle, E. A., Clemens, S. C., Duffy, A., Howard, W. R., Kukla, G., Kutzbach, J., Martinson, D. G., McIntyre, A., Mix, A. C., Molfino, B., Morley, J. J., Peterson, L. C., Pisias, N. G., Prell, W.. L., Raymo, M. E., Shackleton, N. J. and Toggweiler, J. R.: On the structure and origin of major glaciation cycles: 1. linear responses to Milankovitch Forcing, Paleocenography, 7(6), 701–738, 1992.

IPCC: Climate Change 1995: The Science of Climate Change, edited by J. T. Houghton, L. G. Meira Filho, B. A. Callander, N. Harris, A. Kattenburg, and K. Maskell, cam, Cambridge, UK., 1995.

IPCC: Climate Change 2001: The Scientific Basis, edited by J. T. Houghton, Y. DING, D. J. Griggs, M. Noguer, P. J. van der Linden, X. Dai, K. Maskell, and C. A. Johnson, Cambridge University Press, Cambridge, UK., 2001.

Jacobsen, A., Egge, J. K. and Heimdal, B. R.: Effects of increased concentration of nitrate and phosphate during a springbloom experiment in mesocosm, J. Exp. Mar. Bio. Ecol., 187(2), 239–251, doi:10.1016/0022-0981(94)00183-E, 1995.

Jacquet, S., Heldal, M., Iglesias-Rodriguez, M. D., Larsen, A., Wilson, W. and Bratbak, G.: Flow cytometric analysis of an *Emiliana huxleyi* bloom terminated by viral infection, Aquat. Microb. Ecol., 27, 111–124, 2002.

Janssen, F., Schrum, C. and Backhaus, J.: A climatological data set of temperature and salinity for the Baltic Sea and the North Sea, Dtsch. Hydrogr. Zeitschrift, Supplement, 1999.

Joassin, P., Delille, B., Soetaert, K., Harlay, J., Borges, A. V., Chou, L., Riebesell, U., Suykens, K. and Grégoire, M.: Carbon and nitrogen flows during a bloom of the coccolithophore *Emiliania huxleyi:* Modelling a mesocosm experiment, J. Mar. Syst., 85(3-4), 71–85, doi:10.1016/j.jmarsys.2010.11.007, 2010.

Johnson, K. M., King, A. E. and Sieburth, J. M.: Coulometric TCO_2 analyses for marine studies: an introduction, Mar. Chem., 16, 61–82, 1985.

Johnson, T. L., Palenik, B. and Brahamsha, B.: Characterization of a functional vanadium-dependent bromoperoxidase in the marine cyanobacterium *Synechococcus* Sp. Cc93111, J. Phycol., 47(4), 792–801, doi:10.1111/j.1529-8817.2011.01007.x, 2011.

Johnson, V. R., Brownlee, C., Rickaby, R. E. M., Graziano, M., Milazzo, M. and Hall-Spencer, J. M.: Responses of marine benthic microalgae to elevated CO_2, Mar. Biol., 160, 1813–1824, doi:10.1007/s00227-011-1840-2, 2013.

Johnston, A., Todd, J. D., Sun, L., Nikolaidou-Katsaridou, M., Curson, A. and Rogers, R.: Molecular diversity of bacterial production of the climate-changing gas, dimethyl sulphide, a molecule that impinges on local and global symbioses, J. Exp. Bot., 59(5), 1059–1067, doi:10.1093/jxb/erm264, 2008.

Joint, I., Doney, S. C. and Karl, D. M.: Will ocean acidification affect marine microbes?, ISME J., 5(1), 1–7, doi:10.1038/ismej.2010.79, 2011.

Jones, C. E. and Carpenter, L. J.: Solar photolysis of CH_2I_2, CH_2ICl, and CH_2IBr in water, saltwater, and seawater, Environ. Sci. Technol. Technol., 39(16), 6130–6137, 2005.

Jones, C. E., Hornsby, K. E., Dunk, R. M., Leigh, R. J. and Carpenter, L. J.: Coastal measurements of short-lived reactive iodocarbons and bromocarbons at Roscoff, Brittany during the RHaMBLe campaign, Atmos. Chem. Phys., 9(4), 8757–8769, doi:10.5194/acpd-9-17125-2009, 2009.

Jonkers, H. M., van Der Maarel, M. J. E. C., van Gemerden, H. and Hansen, T. A.: Dimethylsulfoxide reduction by marine sulfate-reducing bacteria, FEMS Microbiol. Lett., 136(3), 283–287, doi:10.1111/j.1574-6968.1996.tb08062.x, 1996.

Kangro, K., Olli, K., Tamminen, T. and Lignell, R.: Species-specific responses of a cyanobacteria-dominated phytoplankton community to artificial nutrient limitation in the Baltic Sea, Mar. Ecol. Prog. Ser., 336, 15–27, 2007.

Karlsson, A., Auer, N., Schulz-Bull, D. and Abrahamsson, K.: Cyanobacterial blooms in the Baltic — A source of halocarbons, Mar. Chem., 110, 129–139, doi:10.1016/j.marchem.2008.04.010, 2008.

Keeling, C. D., Bacastow, R. B., Bainbridge, A. E., Ekdahl, C. A., Guenther, P. R., Waterman, L. S. and Chin, J. F. S.: Atmospheric carbon dioxide variations at Mauna Loa Observatory, Hawaii, Tellus, 28(6), 538–551, doi:10.1111/j.2153-3490.1976.tb00701.x, 1976.

Keller, M. D.: Dimethyl sulfide production and marine phytoplankton: the importance of species composition and cell size, Biol. Oceanogr., 6, 3755–382, doi:10.1080/01965581.1988.10749540, 1989.

Keppler, F., Eiden, R., Niedan, V., Pracht, J. and Schöler, H. F.: Halocarbons produced by natural oxidation processes during degradation of organic matter, Nature, 403(6767), 298–301, doi:10.1038/35002055, 2000.

Kersen, P., Kotta, J., Bučas, M., Kolesova, N. and Deķere, Z.: Epiphytes and associated fauna on the brown alga *Fucus vesiculosus* in the Baltic and the North Seas in relation to different abiotic and biotic variables, Mar. Ecol., 32(Supplement 1), 87–95, doi:10.1111/j.1439-0485.2010.00418.x, 2011.

Kettle, A. J., Andreae, M. O., Amouroux, D., Andreae, T. W., Bates, T. S., Berresheim, H., Bingemer, H., Boniforti, R., Curran, M. A. J., DiTullio, G. R., Helas, G., Jones, G. B., Keller, M. D.,

Kiene, R. P., Leck, C., Levasseur, M., Malin, G., Maspero, M., Matrai, P., Mctaggart, A. R., Mihalopoulos, N., Nguyen, B. C., Novo, A., Putaud, J. P., Rapsomanikis, S., Roberts, G., Schebeske, G., Sharma, S., Simo, R., Staubes, R., Turner, S. and Uher, G.: A global database of sea surface dimethylsulfide (DMS) measurements and a procedure to predict sea surface DMS as a function of latitude, longitude, and month, Global Biogeochem. Cycles, 13(2), 399–444, 1999.

Kiene, R. P. and Bates, T. S.: Biological removal of dimethyl sulphide from sea water, Nature, 345, 702–705, 1990.

Kiene, R. P. and Capone, D. G.: Microbial transformations of methylated sulfur compounds in anoxic salt marsh sediments, Microb. Ecol., 15, 275–291, 1988.

Kiene, R. P. and Linn, L. J.: Distribution and turnover of dissolved DMSP and its relationship with bacterial production and dimethylsulfide in the Gulf of Mexico, Limnol. Oceanogr., 45(4), 849–861, 2000a.

Kiene, R. P. and Linn, L. J.: The fate of dissolved dimethylsulfoniopropionate (DMSP) in seawater: tracer studies using ^{35}S-DMSP, Geochim. Cosmochim. Acta, 64(16), 2797–2810, 2000b.

Kiene, R. P., Linn, L. J. and Bruton, J. A.: New and important roles for DMSP in marine microbial communities, J. Sea Res., 43(3-4), 209–224, doi:10.1016/S1385-1101(00)00023-X, 2000.

Kiene, R. P., Linn, L. J., González, J., Moran, M. A. and Bruton, J. A.: Dimethylsulfoniopropionate and methanethiol are important precursors of methionine and protein-sulfur in marine bacterioplankton, Appl. Environ. Microbiol., 65(10), 4549–4558, 1999.

Kiene, R. P. and Slezak, D.: Low dissolved DMSP concentrations in seawater revealed by small-volume gravity filtration and dialysis sampling, Limnol. Oceanogr. Methods, 4, 80–95, 2006.

Kim, J.-M., Lee, K., Yang, E. J., Shin, K., Noh, J. H., Park, K.-T., Hyun, B., Jeong, H.-J., Kim, J.-H., Kim, K. Y., Kim, M., Kim, H.-C., Jang, P.-G. and Jang, M.-C.: Enhanced production of oceanic dimethylsulfide resulting from CO_2-induced grazing activity in a high CO_2 world., Environ. Sci. Technol., 44(21), 8140–8143, doi:10.1021/es102028k, 2010.

Kirchman, D., K'nees, E. and Hodson, R.: Leucine incorporation and its potential as a measure of protein synthesis by bacteria in natural aquatic systems, Appl. Environ. Microbiol., 49(3), 599–607, 1985.

Kirst, G. O., Thiel, C., Wolff, H., Nothnagel, J., Wanzek, M. and Ulmke, R.: Dimethylsulfoniopropionate (DMSP) in icealgae and its possible biological role, Mar. Chem., 35, 381–388, doi:10.1016/S0304-4203(09)90030-5, 1991.

Kivi, K., Kaitala, S., Kuosa, H., Kuparinen, J., Leskinen, E., Lignell, R., Marcussen, B. and Tamminen, T.: Nutrient limitation and grazing control of the Baltic plankton community during annual succession, Limnol. Oceanogr., 38(5), 893–905, 1993.

Klaveness, D.: Coccolithus huxleyi (Lohm.) Kamptn II. The flagellate cell, aberrant cell types, vegetative propagation and life cycles, Br. Phycol. J., 7(3), 309–318, doi:10.1080/00071617200650321, 1972.

Klick, S.: Seasonal variations of biogenic and anthropogenic halocarbons in seawater from a coastal site, Limnol. Oceanogr., 37(7), 1579–1585, 1992.

Klick, S. and Abrahamsson, K.: Biogenic volatile iodated hydrocarbons in the ocean, J. Geophys. Res., 97(C8), 12683–12687, 1992.

De Kluijver, A., Soetaert, K., Czerny, J., Schulz, K. G., Boxhammer, T., Riebesell, U. and Middelburg, J. J.: A 13C labelling study on carbon fluxes in Arctic plankton communities under elevated CO_2 levels, Biogeosciences, 10(3), 1425–1440, doi:10.5194/bg-10-1425-2013, 2013.

Kononen, K.: Phytoplankton summer assemblages in relation to environmental factors at the entrance to the Gulf of Finland during 1972-1985, Kieler Meeresforsch. Sonderh, 6, 281–294, 1988.

Kononen, K., Kuparinen, J., Makela, K., Laanemets, J., Pavelson, J. and Nommann, S.: Initiation of cyanobacterial blooms in a frontal region at the entrance to the Gulf of Finland, Baltic Sea, Limnol. Oceanogr., 41(1), 98–112, 1996.

Kottmeier, D. M., Rokitta, S. D., Tortell, P. D. and Rost, B.: Strong shift from HCO_3^- to CO_2 uptake in *Emiliania huxleyi* with acidification: new approach unravels acclimation versus short-term pH effects., Photosynth. Res., 121, 265–75, doi:10.1007/s11120-014-9984-9, 2014.

Kroeker, K. J., Kordas, R. L., Crim, R., Hendriks, I. E., Ramajo, L., Singh, G. S., Duarte, C. M. and Gattuso, J.-P.: Impacts of ocean acidification on marine organisms: quantifying sensitivities and interaction with warming., Glob. Chang. Biol., 19(6), 1884–96, doi:10.1111/gcb.12179, 2013.

Kroeker, K. J., Kordas, R. L., Crim, R. N. and Singh, G. G.: Meta-analysis reveals negative yet variable effects of ocean acidification on marine organisms, Ecol. Lett., 13(11), 1419–1434, doi:10.1111/j.1461-0248.2010.01518.x, 2010.

Kurihara, M., Iseda, M., Ioriya, T., Horimoto, N., Kanda, J., Ishimaru, T., Yamaguchi, Y. and Hashimoto, S.: Brominated methane compounds and isoprene in surface seawater of Sagami Bay: Concentrations, fluxes, and relationships with phytoplankton assemblages, Mar. Chem., 134-135, 71–79, doi:10.1016/j.marchem.2012.04.001, 2012.

Kurihara, M. K., Kimura, M., Iwamoto, Y., Narita, Y., Ooki, A., Eum, Y.-J., Tsuda, A., Suzuki, K., Tani, Y., Yokouchi, Y., Uematsu, M. and Hashimoto, S.: Distributions of short-lived iodocarbons and biogenic trace gases in the open ocean and atmosphere in the western North Pacific, Mar. Chem., 118, 156–170, doi:10.1016/j.marchem.2009.12.001, 2010.

Kwint, R. L. J. and Kramer, K. J. M.: Dimethylsulphide production by plankton communities, Mar. Ecol. Prog. Ser., 121, 227–237, 1995.

Laamanen, M. J.: Environmental factors affecting the occurrence of different morphological forms of cyanoprokaryotes in the northern Baltic Sea, J. Plankton Res., 19(10), 1385–1403, doi:10.1093/plankt/19.10.1385, 1997.

Lana, A., Bell, T. G., Simó, R., Vallina, S. M., Ballabrera-Poy, J., Kettle, A. J., Dachs, J., Bopp, L., Saltzman, E. S., Stefels, J., Johnson, J. E. and Liss, P. S.: An updated climatology of surface dimethlysulfide concentrations and emission fluxes in the global ocean, Global Biogeochem. Cycles, 25(1), doi:10.1029/2010GB003850, 2011.

Lana, A., Simó, R., Vallina, S. M. and Dachs, J.: Re-examination of global emerging patterns of ocean DMS concentration, Biogeochemistry, 110, 173–182, doi:10.1007/s10533-011-9677-9, 2012.

Lance, V. P.: Carbon productivity responses to increased dissolved inorganic carbon concentrations in surface ocean: exploring the feasibility of an in situ mesocscale carbon addition experiment, in LDEO in situ CO_2 workshop, 23 -24 Mrach 2009, New York., 2009.

Langer, G., Nehrke, G., Probert, I., Ly, J. and Ziveri, P.: Strain-specific responses of *Emiliania huxleyi* to changing seawater carbonate chemistry, Biogeosciences, 6, 2637–2646, doi:10.5194/bg-6-2637-2009, 2009.

Larsen, J. B., Larsen, A., Thyrhaug, R., Bratbak, G. and Sandaa, R.-A.: Response of marine viral populations to a nutrient induced phytoplankton bloom at different pCO_2 levels, Biogeosciences, 5, 523–533, 2008.

Larsson, U., Hajdu, S., Walve, J. and Elmgren, R.: Baltic Sea nitrogen fixation estimated from the Summer increase in upper mixed layer total nitrogen, Limnol. Oceanogr., 46(4), 811–820, 2001.

Laturnus, F., Giese, B., Wiencke, C. and Adams, F. C.: Low-molecular-weight organoiodine and organobromine compounds released by polar macroalgae--the influence of abiotic factors, Fresenius. J. Anal. Chem., 368, 297–302, 2000.

Laturnus, F., Mehrtens, G. and Gron, C.: Haloperoxidase-like activity in spruce forest soil - a source of volatile halogenated organic compounds?, Chemosphere, 31(7), 3709–3719, 1995.

Leck, C., Larsson, U., Bågander, L. E., Johansson, S. and Hajdu, S.: Dimethyl sulfide in the Baltic Sea: annual variability in relation to biological activity, J. Geophys. Res., 95(C3), 3353–3363, doi:10.1029/JC095iC03p03353, 1990.

Leck, C. and Rodhe, H.: Emissions of marine biogenic sulfur to the atmosphere of northern Europe, J. Atmos. Chem., 12, 63–86, 1991.

Lee, P. A., Mora, S. J. De, Gosselin, M., Levasseur, M., Bouillon, R.-C., Nozais, C. and Michel, C.: Particulate dimethylsulphoxide in Arctic sea ice algal communities: the cryoprotectant hypothesis revisited, J. Phycol., 37, 488–499, 2001.

Lee, P. A., Riseman, S. F., Hare, C. E., Hutchins, D. A., Leblanc, K. and DiTullio, G. R.: Potential impact of increased temperature and CO_2 on particulate dimethylsulfoniopropionate in the Southeastern Bering Sea, Adv. Oceanogr. Limnol., 2(1), 33–47, doi:10.1080/19475721.2011.574433, 2011.

Lee, P. A., Rudisill Jr, J. R., Neeley, A. R., Maucher, J. M., Hutchins, D. A., Feng, Y., Hare, C. E., Leblanc, K., Rose, J. M., Wilhelm, S. W., Rowe, J. M. and DiTullio, G. R.: Effects of increased pCO_2 and temperature on the North Atlantic spring bloom. III. Dimethylsulfoniopropionate, Mar. Ecol. Prog. Ser., 388, 41–49, doi:10.3354/meps08135, 2009.

Leedham, E.: Emission of biogenic halocarbons in temperate and tropical coastal zones, University of East Anglia., 2013.

Leedham, E. C., Hughes, C., Keng, F. S. L., Phang, S.-M., Malin, G. and Sturges, W. T.: Emission of atmospherically significant halocarbons by naturally occurring and farmed tropical macroalgae, Biogeosciences, 10(6), 3615–3633, doi:10.5194/bg-10-3615-2013, 2013.

Leedham Elvidge, E. C., Phang, S.-M., Sturges, W. T. and Malin, G.: The effect of desiccation on the emission of volatile bromocarbons from two common temperate macroalgae, Biogeosciences Discuss., 11(7), 10673–10701, doi:10.5194/bgd-11-10673-2014, 2014.

Lehmann, A. and Myrberg, K.: Upwelling in the Baltic Sea — A review, J. Mar. Syst., 74, S3–S12, doi:10.1016/j.jmarsys.2008.02.010, 2008.

Lehmann, B. A., Krauss, W. and Hinrichsen, H.: Effects of remote and local atmospheric forcing on circulation and upwelling in the Baltic Sea, Tellus A, 54A, 299–316, 2002.

Leonardos, N. and Geider, R. J.: Elevated atmospheric carbon dioxide increases organic carbon fixation by *Emiliania huxleyi* (Haptophyta), under nutrient-limited high-light conditions, J. Phycol., 41(6), 1196–1203, doi:10.1111/j.1529-8817.2005.00152.x, 2005.

Leonardos, N., Read, B., Thake, B. and Young, J. R.: No mechanistic dependence of photosynthesis on calcification in the coccolithophorid *Emiliania huxleyi* (Haptophyta), J. Phycol., 45(5), 1046–1051, doi:10.1111/j.1529-8817.2009.00726.x, 2009.

Lessard, E. J., Merico, A. and Tyrrell, T.: Nitrate: phosphate ratios and *Emiliania huxleyi* blooms, Limnol. Oceanogr., 50(3), 1020–1024, 2005.

Lesser, M. P.: Oxidative stress causes coral bleaching during exposure to elevated temperatures, Coral Reefs, 16(3), 187–192, doi:10.1007/s003380050073, 1997.

Lesser, M. P.: Oxidative stress in marine environments: biochemistry and physiological ecology, Annu. Rev. Physiol., 68(3), 253–278, doi:10.1146/annurev.physiol.68.040104.110001, 2006.

Lesser, M. P. and Farrell, J. H.: Exposure to solar radiation increases damage to both host tissues and algal symbionts of corals during thermal stress, Coral Reefs, 23(3), 367–377, doi:10.1007/s00338-004-0392-z, 2004.

Leu, E., Daase, M., Schulz, K. G., Stuhr, a. and Riebesell, U.: Effect of ocean acidification on the fatty acid composition of a natural plankton community, Biogeosciences, 10(2), 1143–1153, doi:10.5194/bg-10-1143-2013, 2013.

Levasseur, M.: Impact of Arctic meltdown on microbial cycling of sulphur, Nat. Geosci., 6(September), 691–700, doi:10.1038/NGEO1910, 2013.

Levasseur, M., Gosselin, M. and Michaud, S.: A new source of dimethylsulfide (DMS) for the arctic atmosphere: ice diatoms, Mar. Biol., 121, 381–387, doi:10.1007/BF00346748, 1994.

Levasseur, M., Michaud, S., Egge, J., Cantin, G., Nejstgaard, J. C., Sanders, R., Fernandez, E., Solberg, P. T., Heimdal, B. and Gosselin, M.: Production of DMSP and DMS during a mesocosm study of an *Emiliania huxleyi* bloom: influence of bacteria and *Calanus finmarchicus* grazing, Mar. Biol., 126(4), 609–618, doi:10.1007/BF00351328, 1996.

Levitan, O., Rosenberg, G., Setlik, I., Setlikova, E., Grigel, J., Klepetar, J., Prasil, O. and Berman-Frank, I.: Elevated CO_2 enhances nitrogen fixation and growth in the marine cyanobacterium *Trichodesmium*, Glob. Chang. Biol., 13(2), 531–538, doi:10.1111/j.1365-2486.2006.01314.x, 2007.

Lewis, E. and Wallace, D.: Program developed for CO_2 system calculations, 1988.

Li, Y. H., Takahashi, T. and Broecker, W. S.: Degree of saturation of $CaCO_3$ in the oceans, J. Geophys. Res., 74(23), 5507 –5525, 1969.

Lin, M., Horowitz, L. W., Oltmans, S. J., Fiore, A. M. and Fan, S.: Tropospheric ozone trends at Mauna Loa Observatory tied to decadal climate variability, Nat. Geosci., 7(January), 136 – 143, doi:10.1038/NGEO2066, 2014.

Liss, P. S.: Processes of gas exchange across an air-water interface, Deep Sea Res., 20, 221–238, 1973.

Liss, P. S., Hatton, A. D., Malin, G., Nightingale, P. D. and Turner, S. M.: Marine sulphur emissions, Philos. Trans. R. Soc. B Biol. Sci., 352, 159–169, doi:10.1098/rstb.1997.0011, 1997.

Liss, P. S. and Slater, P. G.: Flux of gases across the air-sea interface, Nature, 247, 181–184, 1974.

Liu, Y., Yvon-Lewis, S. A., Hu, L., Salisbury, J. E. and O'Hern, J. E.: $CHBr_3$, CH_2Br_2 , and $CHClBr_2$ in U.S. coastal waters during the Gulf of Mexico and East Coast Carbon cruise, J. Geophys. Res., 116, C10004, doi:10.1029/2010JC006729, 2011.

Liu, Y., Yvon-Lewis, S. A., Thornton, D. C. O., Butler, J. H., Bianchi, T. S., Campbell, L., Hu, L. and Smith, R. W.: Spatial and temporal distributions of bromoform and dibromomethane in the

Atlantic Ocean and their relationship with photosynthetic biomass, J. Geophys. Res. Ocean., 118(8), 3950–3965, doi:10.1002/jgrc.20299, 2013.

Lochte, K., Ducklow, H., Fasham, M. J. R. and Stienen, C.: Plankton succession and carbon cycling at 47N 20W during the JGOFS North Atlantic Bloom Experiment, Deep Sea Res. Part II Top. Stud. Oceanogr., 40(1), 91–114, 1993.

Lohbeck, K. T., Riebesell, U., Collins, S. and Reusch, T. B. H.: Functional genetic divergence in high CO_2 adapted *Emiliania huxleyi* populations., Evolution (N. Y)., 67(7), 1892–1900, doi:10.1111/j.1558-5646.2012.01812.x, 2012a.

Lohbeck, K. T., Riebesell, U. and Reusch, T. B. H.: Adaptive evolution of a key phytoplankton species to ocean acidification, Nat. Geosci., 5, 346–351, doi:10.1038/ngeo1441, 2012b.

Lohmann, H.: Die Coccolithophoridae, eine Monographie der Coccolithen bildenden Flagellaten, zugleich ein Beitrag zur Kenntnis des Mittelmeerauftriebs, Arch. für Protistenkd., 1, 89–165, 1902.

Lovelock, J. E.: Natural halocarbons in the air and in the sea, Nature, 256, 193 – 194, 1975.

Lovelock, J. E., Maggs, R. J. and Rasmussen, R. A.: Atmospheric dimethyl sulphide and the natural sulphur cycle, Nature, 237, 452–453, 1972.

Lovelock, J. E. and Margulis, L.: Atmospheric homeostasis by and for the biosphere: the Gaia hypothesis, Tellus, 26, 2–10, doi:10.1111/j.2153-3490.1974.tb01946.x, 1974.

Lupton, J., Lilley, M., Butterfield, D., Evans, L., Embley, R., Massoth, G., Christenson, B., Nakamura, K. and Schmidt, M.: Venting of a separate CO_2-rich gas phase from submarine arc volcanoes: examples from the Mariana and Tonga-Kermadec arcs, J. Geophys. Res., 113, B08S12, doi:10.1029/2007JB005467, 2008.

Lüthi, D., Le Floch, M., Bereiter, B., Blunier, T., Barnola, J.-M., Siegenthaler, U., Raynaud, D., Jouzel, J., Fischer, H., Kawamura, K. and Stocker, T. F.: High-resolution carbon dioxide concentration record 650,000-800,000 years before present, Nature, 453(7193), 379–382, doi:10.1038/nature06949, 2008.

Mackey, M. D., Mackey, D. J., Higgins, H. W. and Wright, S. W.: CHEMTAX a program for estimating class abundances from chemical markers: application to HPLC measurements of phytoplankton, Mar. Ecol. Prog. Ser., 144, 265–283, 1996.

Malin, G., Turner, S., Liss, P., Holligan, P. and Harbour, D. S.: Dimethylsulphide and dimethylsulphoniopropionate in the Northeast Atlantic during the summer coccolithophore bloom, Deep Sea Res. Part I Oceanogr. Res. Pap., 40(7), 1487 – 1508, doi:10.1016/0967-0637(93)90125-M, 1993.

Malin, G., Turner, S. M. and Liss, P. S.: Sulphur: the plankton/ climate connection, , 28, 590–597, 1992.

Malin, G., Wilson, W. H., Bratbak, G., Liss, P. S. and Mann, N. H.: Elevated production of dimethylsulfide resulting from viral infection of cultures of *Phaeocystis pouchetii*, Limnol. Oceanogr., 43(6), 1389–1393, 1998.

Manley, S. L.: Phytogenesis of halomethanes: A product of selection or a metabolic accident?, Biogeochemistry, 60, 163–180, 2002.

Manley, S. L. and De La Cuesta, J. L.: Methyl iodide production from marine phytoplankton cultures, Limnol. Oceanogr., 42(1), 142–147, doi:10.4319/lo.1997.42.1.0142, 1997.

Markes International Technical Support: TDTS 20: Confirming sorbent tube retention volumes and checking for analyte breakthrough., 2014a.

Markes International Technical Support: Technical Support Application Note 005 Advice on sorbent selection, tube conditioning , tube storage and air sampling., 2014b.

Martinez-Martinez, J., Norland, S., Thingstad, T. F., Schroeder, D. C., Bratbak, G., Wilson, W. H. and Larsen, A.: Variability in microbial population dynamics between similarly perturbed mesocosms, J. Plankton Res., 28(8), 783–791, doi:10.1093/plankt/fbl010, 2006.

Martinez-Martinez, J., Schroeder, D. C. and Wilson, W. H.: Dynamics and genotypic composition of *Emiliania huxleyi* and their co-occurring viruses during a coccolithophore bloom in the North Sea., FEMS Microbiol. Ecol., 81(2), 315–323, doi:10.1111/j.1574-6941.2012.01349.x, 2012.

Martino, M., Liss, P. S. and Plane, J. M. C.: The photolysis of dihalomethanes in surface seawater., Environ. Sci. Technol., 39(18), 7097–7101, 2005.

Martino, M., Liss, P. S. and Plane, J. M. C.: Wavelength-dependence of the photolysis of diiodomethane in seawater, Geophys. Res. Lett., 33(6), L06606, doi:10.1029/2005GL025424, 2006.

Mattson, E., Karlsson, A., Smith, W. O. and Abrahamsson, K.: The relationship between biophysical variables and halocarbon distributions in the waters of the Amundsen and Ross Seas, Antarctica, Mar. Chem., 140-141, 1–9, doi:10.1016/j.marchem.2012.07.002, 2012.

Meakin, N. G. and Wyman, M.: Rapid shifts in picoeukaryote community structure in response to ocean acidification, ISME J., 5(9), 1397–1405, doi:10.1038/ismej.2011.18, 2011.

Meier, K. J. S., Beaufort, L., Heussner, S. and Ziveri, P.: The role of ocean acidification in *Emiliania huxleyi* coccolith thinning in the Mediterranean Sea, Biogeosciences, 11, 2857–2869, doi:10.5194/bg-11-2857-2014, 2014.

Miles, C. J., Bell, T. G. and Suntharalingam, P.: Investigating the inter-relationships between water attenuated irradiance, primary production and DMS(P), Biogeochemistry, 110(1-3), 201–213, doi:10.1007/s10533-011-9697-5, 2012.

Milliman, J. D. and Droxler, A. W.: Neritic and pelagic carbonate sedimentation in the marine environment: ignorance is not bliss, Geol. Rundschau, 85(3), 496–504, doi:10.1007/BF02369004, 1996.

Moheimani, N. R. and Borowitzka, M.: Increased CO_2 and the effect of pH on growth and calcification of *Pleurochrysis carterae* and *Emiliania huxleyi* (Haptophyta) in semicontinuous cultures., Appl. Microbiol. Biotechnol., 90(4), 1399–1407, doi:10.1007/s00253-011-3174-x, 2011.

Montzka, S. A., Reimann, S., Engel, A., Kruger, K., O'Doherty, S., Sturges, W. and *et al.:* Ozone depleting substances (ODSs) and related chemicals, in Scientific Assessment of Ozone Depletion: 2010, p. 516., 2011.

Moolna, A. and Rickaby, R. E. M.: Interaction of the coccolithophore *Gephyrocapsa oceanica* with its carbon environment: response to a recreated high-CO_2 geological past, Geobiology, 10(1), 72–81, doi:10.1111/j.1472-4669.2011.00308.x, 2012.

Moore, R. M.: Methyl halide production and loss rates in sea water from field incubation experiments, Mar. Chem., 101(3-4), 213–219, doi:10.1016/j.marchem.2006.03.003, 2006.

Moore, R. M. and Groszko, W.: Methyl iodide distribution in the ocean and fluxes to the atmosphere, J. Geophys. Res., 104(C5), 11163 – 11171, 1999.

Moore, R. M. and Tokarczyk, R.: Volatile biogenic halocarbons in the northwest Atlantic, Global Biogeochem. Cycles, 7(1), 195–210, 1993.

Moore, R. M., Webb, M., Tokarczyk, R. and Wever, R.: Bromoperoxidase and iodoperoxidase enzymes and production of halogenated methanes in marine diatom cultures, J. Geophys. Res., 101(C9), 20899, doi:10.1029/96JC01248, 1996.

Moore, R. M. and Zafiriou, O. C.: Photochemical production of methyl iodide in seawater, J. Geophys. Res., 99(D8), 16415–16420, doi:10.1029/94JD00786, 1994.

Muller, E. B. and Nisbet, R. M.: Dynamic energy budget modelling reveals the potential of future growth and calcification for the coccolithophore *Emiliania huxleyi* in an acidified ocean, Glob. Chang. Biol., 20, 2031–2038, doi:10.1111/gcb.12547, 2014.

Müller, M. N., Schulz, K. G. and Riebesell, U.: Effects of long-term high CO_2 exposure on two species of coccolithophores, Biogeosciences, 7(3), 1109–1116, doi:10.5194/bg-7-1109-2010, 2010.

Nanninga, H. J. and Tyrrell, T.: Importance of light for the formation of algal blooms by *Emiliania huxleyi*, Mar. Ecol. Prog. Ser. Oldend., 136(1), 195–203, 1996.

National Measurement Institute of Australia: Proficiency Study 12-23: DMS in seawater., 2013.

Nausch, M., Nausch, G., Lass, H. U., Mohrholz, V., Nagel, K., Siegel, H. and Wasmund, N.: Phosphorus input by upwelling in the eastern Gotland Basin (Baltic Sea) in summer and its effects on filamentous cyanobacteria, Estuar. Coast. Shelf Sci., 83(4), 434–442, doi:10.1016/j.ecss.2009.04.031, 2009.

Newbold, L. K., Oliver, A. E., Booth, T., Tiwari, B., DeSantis, T., Maguire, M., Andersen, G., van der Gast, C. J. and Whiteley, A. S.: The response of marine picoplankton to ocean acidification, Environ. Microbiol., 14(9), 2293–2307, doi:10.1111/j.1462-2920.2012.02762.x, 2012.

Nguyen, B. C., Belviso, S., Mihalopoulos, N., Gostan, J. and Nival, P.: Dimethyl sulfide production during natural phytoplanktonic blooms, Mar. Chem., 24, 133–141, doi:10.1016/0304-4203(88)90044-8, 1988.

Ni, X. and Hager, L. P.: Expression of *Batis maritima* methyl chloride transferase in *Escherichia coli*., Proc. Natl. Acad. Sci. U. S. A., 96(7), 3611–3615, 1999.

Niehoff, B., Schmithüsen, T., Knüppel, N., Daase, M., Czerny, J. and Boxhammer, T.: Mesozooplankton community development at elevated CO_2 concentrations: results from a mesocosm experiment in an Arctic fjord, Biogeosciences, 10(3), 1391–1406, doi:10.5194/bg-10-1391-2013, 2013.

Nielsen, M.: Photosynthetic characteristics of the coccolithophorid *Emiliania huxleyi* (prymnesiophyceae) exposed to elevated concentrations of dissolved inorganic carbon, J. Phycol., 31, 715–719, 1995.

Niemisto, L., Rinne, I. and Melvasalo, T.: Blue-green algae and their nitrogen fixation in the Baltic Sea in 1980, 1982 and 1984, Meri, 17, 1–59, 1989.

Nieuwenhuijsen, M. J., Toledano, M. B., Eaton, N. E., Fawell, J. and Elliott, P.: Chlorination disinfection byproducts in water and their association with adverse reproductive outcomes: a review., Occup. Environ. Med., 57(2), 73–85, 2000.

Nightingale, P. D., Malin, G., Law, C. S., Watson, A. J., Liss, P. S., Liddicoat, M. I., Boutin, J. and Upstill-Goddard, R. C.: In situ evaluation of air-sea gas exchange parameterizations using novel conservative and volatile tracers, Global Biogeochem. Cycles, 14(1), 373–387, 2000.

Nightingale, P. D., Malin, G. and Liss, P. S.: Production of chloroform and other low-molecular-weight halocarbons by some species of macroalgae, Limnol. Oceanogr., 40(4), 680–689, 1995.

Nimer, N. A. and Merrett, M. J.: Calcification and utilization of inorganic carbon by the coccolithophorid *Emiliania huxleyi* Lohmann, New Phytol., 121(2), 173–177, 1992.

Nimer, N. A. and Merrett, M. J.: Calcification rate in *Emiliania huxleyi* Lohmann in response to light, nitrate and availability of inorganic carbon, New Phytol., 123, 673–677, 1993.

O'Dowd, C. D., Jimenez, J. L., Bahreini, R., Flagan, R. C., Seinfeld, J. H., Hameri, K., Pirjola, L., Kulmala, M., Jennings, S. G. and Hoffmann, T.: Marine aerosol formation from biogenic iodine emissions, Nature, 417(6889), 632–636, doi:10.1038/nature00773.1.2.3.4.5.6.7.8.9.10., 2002.

Oberg, J.: Cyanobacterial blooms in the Baltic Sea in 2013, HELCOM Balt. Sea Environ. Fact Sheet, 2013.

Ohsawa, N., Ogata, Y., Okada, N. and Itoh, N.: Physiological function of bromoperoxidase in the red marine alga, *Corallina pilulifera*: production of bromoform as an allelochemical and the simultaneous elimination of hydrogen peroxide., Phytochemistry, 58(5), 683–692, 2001.

Oliver, A. E., Newbold, L. K., Whiteley, A. S. and van der Gast, C. J.: Marine bacterial communities are resistant to elevated carbon dioxide levels, Environ. Microbiol. Rep., n/a–n/a, doi:10.1111/1758-2229.12159, 2014.

Omstedt, A., Edman, M., Anderson, L. G. and Laudon, H.: Factors influencing the acid-base (pH) balance in the Baltic Sea: a sensitivity analysis, Tellus B, 62(4), 280–295, doi:10.1111/j.1600-0889.2010.00463.x, 2010.

Orlikowska, A. and Schulz-Bull, D. E.: Seasonal variations of volatile organic compounds in the coastal Baltic Sea, Environ. Chem., 6, 495–507, doi:10.1071/EN09107, 2009.

Orr, J. C., Fabry, V. J., Aumont, O., Bopp, L., Doney, S. C., Feely, R. A., Gnanadesikan, A., Gruber, N., Ishida, A., Joos, F., Key, R. M., Lindsay, K., Maier-Reimer, E., Matear, R., Monfray, P., Mouchet, A., Najjar, R. G., Plattner, G.-K., Rodgers, K.. B., Sabine, C. L., Sarmiento, J. L., Schlitzer, R., Slater, R. D., Totterdell, I. J., Weirig, M.-F., Yamanaka, Y. and Yool, A.: Anthropogenic ocean acidification over the twenty-first century and its impact on calcifying organisms., Nature, 437(7059), 681–6, doi:10.1038/nature04095, 2005.

Osingal, R., Rik, L. J., Lewis, E., Kraay, G. W., Lont, J. D., Lindeboom, H. J. and Van, F. C.: Production and fate of dimethylsulfide and dimethylsulfoniopropionate in pelagic mesocosms : the role of sedimentation, Mar. Ecol. Prog. Ser., 131, 275–286, 1996.

Paasche, E.: Coccolith Formation, Nature, 193, 1094–1095, 1962.

Paasche, E.: A review of the coccolithophorid *Emiliania huxleyi* (Prymnesiophyceae), with particular reference to growth, coccolith formation, and calcification-photosynthesis interactions, Phycologia, 40(6), 503–529, 2001.

Pakulski, J. D. and Kiene, R. P.: Foliar release of dimethylsulfonioproprionate from *Spartina alterniflora*, Mar. Ecol. Prog. Ser., 81, 277–287, 1992.

Park, K.-T., Lee, K., Shin, K., Yang, E. J., Hyun, B., Kim, J.-M., Noh, J. H., Kim, M., Kong, B., Choi, D. H., Choi, S.-J., Jang, P.-G. and Jeong, H. J.: Direct linkage between dimethyl sulfide production and microzooplankton grazing, resulting from prey composition change under high partial pressure of carbon dioxide conditions., Environ. Sci. Technol., 48(9), 4750–4756, doi:10.1021/es403351h, 2014.

Parker, L. M., Ross, P. M. and O'Connor, W. A.: Comparing the effect of elevated pCO_2 and temperature on the fertilization and early development of two species of oysters, Mar. Biol., 157(11), 2435–2452, doi:10.1007/s00227-010-1508-3, 2010. 348

Parsons, T. R.: The use of controlled experimental ecosystems: a review, J. Oceanogr. Soc. Japan, 37, 294–298, 1981.

Patey, M. D., Rijkenberg, M. J. A., Statham, P. J., Stinchcombe, M. C., Achterberg, E. P. and Mowlem, M.: Determination of nitrate and phosphate in seawater at nanomolar concentrations, Trends Anal. Chem., 27(2), 169–182, doi:10.1016/j.trac.2007.12.006, 2008.

Patil, S. M., Mohan, R., Shetye, S., Gazi, S. and Jafar, S.: Morphological variability of *Emiliania huxleyi* in the Indian sector of the Southern Ocean during the austral summer of 2010, Mar. Micropaleontol., 107, 44–58, doi:10.1016/j.marmicro.2014.01.005, 2014.

Paulino, A. I., Egge, J. K. and Larsen, A.: Effects of increased atmospheric CO_2 on small and intermediate sized osmotrophs during a nutrient induced phytoplankton bloom, Biogeosciences, 5(3), 739–748, doi:10.5194/bg-5-739-2008, 2008.

Pearson, P. N. and Palmer, M. R.: Atmospheric carbon dioxide concentrations over the past 60 million years., Nature, 406, 695–699, doi:10.1038/35021000, 2000.

Pedersen, M., Collen, J., Abrahamsson, K. and Ekdahl, A.: Production of halocarbons from seaweeds: an oxidative stress reaction?, Sci. Mar., 60(Supplement 1), 257–263, 1996.

Petit, J. R., Jouzel, J., Raynaud, D., Barkov, N. I., Barnola, J.-M., Basile, I., Benders, M., Chappellaz, J., Davis, M., Delaygue, G., Delmotte, M., Kotlyakov, V. M., Legrand, M., Lipenkov, V. Y., Lorius, C., Pepin, L., Ritz, C., Saltzman, E. and Stievenard, M.: Climate and atmospheric history of the past 420,000 years from the Vostok ice core, Antarctica, Nature, 399, 429 – 436, 1999.

Pinhassi, J., Simó, R., González, J. M., Vila, M., Alonso-Saez, L., Kiene, R. P., Moran, M. A. and Pedrs-Alio, C.: Dimethylsulfoniopropionate turnover is linked to the composition and dynamics of the bacterioplankton assemblage during a microcosm phytoplankton bloom, Appl. Environ. Microbiol., 71(12), 7650 – 7660, doi:10.1128/AEM.71.12.7650, 2005.

Piontek, J., Borchard, C., Sperling, M., Schulz, K. G., Riebesell, U. and Engel, A.: Response of bacterioplankton activity in an Arctic fjord system to elevated pCO_2: results from a mesocosm perturbation study, Biogeosciences, 10, 297–314, doi:10.5194/bg-10-297-2013, 2013.

Plinski, M. and Codd, G. A.: Coastal and inland cyanobacterial blooms (blue-green algae) - hazards to human and animal health, Oceanologia, 40(4), 399–403, 1998.

Ploug, H.: Cyanobacterial surface blooms formed by Aphanizomenon sp. and Nodularia spumigena in the Baltic Sea: Small-scale fluxes, pH, and oxygen microenvironments, Limnol. Oceanogr., 53(3), 914–921, doi:10.4319/lo.2008.53.3.0914, 2008.

Porzio, L., Buia, M.-C. and Hall-Spencer, J. M.: Effects of ocean acidification on macroalgal communities, J. Exp. Mar. Bio. Ecol., 400(1-2), 278–287, doi:10.1016/j.jembe.2011.02.011, 2011.

Poulton, A. J., Stinchcombe, M. C., Achterberg, E. P., Bakker, D. C. E., Dumousseaud, C., Lawson, H. E., Lee, G. A., Richier, S., Suggett, D. J. and Young, J. R.: Coccolithophores on the north-west European shelf: calcification rates and environmental controls, Biogeosciences, 11, 3919–3940, doi:10.5194/bg-11-3919-2014, 2014.

Quack, B., Atlas, E., Petrick, G. and Wallace, D. W. R.: Bromoform and dibromomethane above the Mauritanian upwelling: atmospheric distributions and oceanic emissions, J. Geophys. Res., 112, D09312, doi:10.1029/2006JD007614, 2007a.

Quack, B., Peeken, I., Petrick, G. and Nachtigall, K.: Oceanic distribution and sources of bromoform and dibromomethane in the Mauritanian upwelling, J. Geophys. Res., 112, C10006, doi:10.1029/2006JC003803, 2007b.

Quack, B. and Wallace, D. W. R.: Air-sea flux of bromoform: controls, rates, and implications, Global Biogeochem. Cycles, 17(1), 1023, doi:10.1029/2002GB001890, 2003.

Quinn, P. K. and Bates, T. S.: The case against climate regulation via oceanic phytoplankton sulphur emissions., Nature, 480(7375), 51–56, doi:10.1038/nature10580, 2011.

Raateoja, M., Kuosa, H. and Hällfors, S.: Fate of excess phosphorus in the Baltic Sea: A real driving force for cyanobacterial blooms?, J. Sea Res., 65(2), 315–321, doi:10.1016/j.seares.2011.01.004, 2011.

Raitsos, D. E., Lavender, S. J., Pradhan, Y., Tyrrell, T., Reid, P. C. and Edwards, M.: Coccolithophore bloom size variation in response to the regional environment of the subarctic North Atlantic, Limnol. Oceanogr., 51(5), 2122–2130, doi:10.4319/lo.2006.51.5.2122, 2006.

Rap, A., Scott, C. E., Spracklen, D. V., Bellouin, N., Forster, P. M., Carslaw, K. S., Schmidt, A. and Mann, G.: Natural aerosol direct and indirect radiative effects, Geophys. Res. Lett., 40(12), 3297–3301, doi:10.1002/grl.50441, 2013.

Raven, J. A.: Putting the C in phycology, Eur. J. Phycol., 32, 319–333, 1997.

Read, K. A., Mahajan, A. S., Carpenter, L. J., Evans, M. J., Faria, B. V. E., Heard, D. E., Hopkins, J. R., Lee, J. D., Moller, S. J., Lewis, A. C., Mendes, L., McQuaid, J. B., Oetjen, H., Saiz-Lopez, A., Pilling, M. J. and Plane, J. M. C.: Extensive halogen-mediated ozone destruction over the tropical Atlantic Ocean., Nature, 453(7199), 1232–1235, doi:10.1038/nature07035, 2008.

Reisch, C. R., Moran, M. A. and Whitman, W. B.: Dimethylsulfoniopropionate-dependent demethylase (DmdA) from *Pelagibacter ubique* and *Silicibacter pomeroyi*., J. Bacteriol., 190(24), 8018–8024, doi:10.1128/JB.00770-08, 2008.

Reisch, C. R., Stoudemayer, M. J., Varaljay, V. A., Amster, I. J., Moran, M. A. and Whitman, W. B.: Novel pathway for assimilation of dimethylsulphoniopropionate widespread in marine bacteria., Nature, 473(7346), 208–211, doi:10.1038/nature10078, 2011.

Revelle, R. and Suess, H. E.: Carbon dioxide exchange between atmosphere and ocean and the question of an increase of atmospheric CO_2 during the past decades, Tellus, 9, 18–27, 1957.

Riahi, K., Grübler, A. and Nakicenovic, N.: Scenarios of long-term socio-economic and environmental development under climate stabilization, Technol. Forecast. Soc. Change, 74(7), 887–935, doi:10.1016/j.techfore.2006.05.026, 2007.

Richier, S., Achterberg, E. P., Archer, S., Bretherton, L., Brown, I., Clark, D., Dumousseaud, C., Holland, R. J., Hopkins, F. E. and MacGilchrist, G. A.: Ocean acidification impacts on sea surface biology and biogeochemistry in Northwest European Shelf Seas: a highreplicated shipboard approach, Br. Oceanogr. Data Centre–Natural Environ. Res. Counc. UK, doi, 10, 2014a.

Richier, S., Achterberg, E. P., Dumousseaud, C., Poulton, a. J., Suggett, D. J., Tyrrell, T., Zubkov, M. V. and Moore, C. M.: Phytoplankton responses and associated carbon cycling during shipboard carbonate chemistry manipulation experiments conducted around Northwest European shelf seas, Biogeosciences, 11, 4733–4752, doi:10.5194/bg-11-4733-2014, 2014b.

Richter, U. and Wallace, D. W. R.: Production of methyl iodide in the tropical Atlantic Ocean, Geophys. Res. Lett., 31(23), L23S03, doi:10.1029/2004GL020779, 2004.

Riebesell, U.: Effects of CO_2 enrichment on marine phytoplankton, J. Oceanogr., 60(4), 719–729, doi:10.1007/s10872-004-5764-z, 2004.

Riebesell, U., Bellerby, R. G. J., Engel, A., Fabry, V. J., Hutchins, D. A., Reusch, T. B. H., Schulz, K. G. and Morel, F. M. M.: Comment on“ phytoplankton calcification in a high-CO_2 world,” Science., 322, 4–5, 2008a.

Riebesell, U., Bellerby, R. G. J., Grossart, H.-P. and Thingstad, F.: Mesocosm CO_2 perturbation studies: from organism to community level, Biogeosciences, 2, 1157–1164, 2008b.

Riebesell, U., Czerny, J., von Bröckel, K., Boxhammer, T., Büdenbender, J., Deckelnick, M., Fischer, M., Hoffmann, D., Krug, S. A., Lentz, U., Ludwig, A., Muche, R. and Schulz, K. G.: Technical Note: A mobile sea-going mesocosm system – new opportunities for ocean change research, Biogeosciences, 10(3), 1835–1847, doi:10.5194/bg-10-1835-2013, 2013a.

Riebesell, U., Gattuso, J.-P., Thingstad, T. F. and Middelburg, J. J.: Arctic ocean acidification: pelagic ecosystem and biogeochemical responses during a mesocosm study, Biogeosciences, 10, 5619–5626, doi:10.1594/PANGAEA.769833, 2013b.

Riebesell, U., Schulz, K. G., Bellerby, R. G. J., Botros, M., Fritsche, P., Meyerhöfer, M., Neill, C., Nondal, G., Oschlies, A., Wohlers, J. and Zöllner, E.: Enhanced biological carbon consumption in a high CO_2 ocean., Nature, 450, 545–548, doi:10.1038/nature06267, 2007.

Riebesell, U., Wolf-Gladrow, D. and Smetacek, V.: Carbon dioxide limitation of marine phytoplankton growth rates, Nature, 361, 249 –251, 1993.

Riebesell, U., Zondervan, I., Rost, B., Tortell, P. D., Zeebe, R. E. and Morel, F. M. M.: Reduced calcification of marine plankton in response to increased atmospheric CO_2, Nature, 407(6802), 364–367, doi:10.1038/35030078, 2000.

Rodolfo-Metalpa, R., Houlbrèque, F., Tambutté, É., Boisson, F., Baggini, C., Patti, F. P., Jeffree, R., Fine, M., Foggo, a., Gattuso, J.-P. and Hall-Spencer, J. M.: Coral and mollusc resistance to ocean acidification adversely affected by warming, Nat. Clim. Chang., 1(6), 308–312, doi:10.1038/nclimate1200, 2011.

Ross, P. M., Parker, L., O'Connor, W. A. and Bailey, E. A.: The impact of ocean acidification on reproduction, early development and settlement of marine organisms, Water, 3(4), 1005–1030, doi:10.3390/w3041005, 2011.

Rost, B., Riebesell, U., Burkhardt, S. and Sultemeyer, D.: Carbon acquisition of bloom-forming marine phytoplankton, Limnol. Oceanogr., 48(1), 55–67, 2003.

Rost, B., Zondervan, I. and Wolf-Gladrow, D.: Sensitivity of phytoplankton to future changes in ocean carbonate chemistry: current knowledge, contradictions and research directions, Mar. Ecol. Prog. Ser., 373, 227–237, doi:10.3354/meps07776, 2008.

Roy, R.: Short-term variability in halocarbons in relation to phytoplankton pigments in coastal waters of the central eastern Arabian Sea, Estuar. Coast. Shelf Sci., 88(3), 311–321, doi:10.1016/j.ecss.2010.04.011, 2010.

Roy, R., Pratihary, A., Narvenkar, G., Mochemadkar, S., Gauns, M. and Naqvi, S. W. A.: The relationship between volatile halocarbons and phytoplankton pigments during a *Trichodesmium* bloom in the coastal eastern Arabian Sea, Estuar. Coast. Shelf Sci., 95(1), 110–118, doi:10.1016/j.ecss.2011.08.025, 2011.

Ruiz-gonza, C., Lefort, T., Gasol, J. M., Cardelu, C., Romera-castillo, C. and Simo, R.: Spectral irradiance dependence of sunlight effects on plankton dimethylsulfide production, , 58(2), 489–504, doi:10.4319/lo.2013.58.2.0489, 2013.

Sabine, C. L., Feely, R. A., Gruber, N., Key, R. M., Lee, K., Bullister, J. L., Wanninkhof, R., Wong, C. S., Wallace, D. W. R., Tilbrook, B., Millero, F. J., Peng, T.-H., Kozyr, A., Ono, T. and Rios, A. F.: The oceanic sink for anthropogenic CO_2, Science., 305(5682), 367–371, doi:10.1126/science.1097403, 2004.

Saenko, G. N., Kravtsova, Y. Y., Ivanenko, V. V and Sheludko, S. I.: Concentration of iodine and bromine by plants in the Seas of Japan and Okhotsk, Mar. Biol., 47, 243–250, 1978.

Sandén, P. and Rahm, L.: Nutrient trends in the Baltic Sea, Environmetrics, 4(1), 75–103, doi:10.1002/env.3170040106, 1993.

Sarazin, G., Michard, G. and Prevot, F.: A rapid and accurate spectroscopic method for alkalinity measurements in sea water samples, Water Res., 33(1), 290–294, 1999.

Savoca, M. S. and Nevitt, G. a: Evidence that dimethyl sulfide facilitates a tritrophic mutualism between marine primary producers and top predators., Proc. Natl. Acad. Sci. U. S. A., 111(11), 4157–61, doi:10.1073/pnas.1317120111, 2014.

Scarratt, M. G., Levasseur, M., Michaud, S. and Roy, S.: DMSP and DMS in the Northwest Atlantic: Late-summer distributions, production rates and sea-air fluxes, Aquat. Sci., 69(3), 292–304, doi:10.1007/s00027-007-0886-1, 2007.

Scarratt, M. G. and Moore, R. M.: Production of methyl bromide and methyl chloride in laboratory cultures of marine phytoplankton II, Mar. Chem., 59(3-4), 311–320, doi:10.1016/S0304-4203(97)00092-3, 1998.

Schäfer, H., Myronova, N. and Boden, R.: Microbial degradation of dimethylsulphide and related C1-sulphur compounds: organisms and pathways controlling fluxes of sulphur in the biosphere, J. Exp. Bot., 61(2), 315–334, doi:10.1093/jxb/erp355, 2010.

Schall, C., Heumann, K. G. and Kirst, G. O.: Biogenic volatile organoiodine and organobromine hydrocarbons in the Atlantic Ocean from 42°N to 72°S, Fresenius. J. Anal. Chem., 359(3), 298–305, doi:10.1007/s002160050577, 1997.

Schneider, B., Nausch, G., Kubsch, H. and Petersohn, I.: Accumulation of total CO_2 during stagnation in the Baltic Sea deep water and its relationship to nutrient and oxygen concentrations, Mar. Chem., 77, 277–291, 2002.

Schulz, K. G., Bellerby, R. G. J., Brussaard, C. P. D., Büdenbender, J., Czerny, J., Engel, A., Fischer, M., Koch-Klavsen, S., Krug, S. A., Lischka, S., Ludwig, A., Meyerhöfer, M., Nondal, G., Silyakova, A., Stuhr, A. and Riebesell, U.: Temporal biomass dynamics of an Arctic plankton bloom in response to increasing levels of atmospheric carbon dioxide, Biogeosciences, 10(1), 161–180, doi:10.5194/bg-10-161-2013, 2013.

Schulz, K. G. and Riebesell, U.: Diurnal changes in seawater carbonate chemistry speciation at increasing atmospheric carbon dioxide, Mar. Biol., 160, 1889–1899, doi:10.1007/s00227-012-1965-y, 2013.

Schulz, K. G., Riebesell, U., Bellerby, R. G. J., Biswas, H., Meyerhöfer, M., Müller, M. N., Egge, J. K., Nejstgaard, J. C., Neill, C., Wohlers, J. and Zöllner, E.: Build-up and decline of organic matter during PeECE III, Biogeosciences, 5(3), 707–718, doi:10.5194/bg-5-707-2008, 2008.

Sciandra, A., Harlay, J., Lefèvre, D., Lemée, R., Rimmelin, P., Denis, M. and Gattuso, J.-P.: Response of coccolithophorid *Emiliania huxleyi* to elevated partial pressure of CO_2 under nitrogen limitation, Mar. Ecol. Prog. Ser., 261, 111–122, doi:10.3354/meps261111, 2003.

Sett, S., Bach, L. T., Schulz, K. G., Koch-Klavsen, S., Lebrato, M. and Riebesell, U.: Temperature modulates coccolithophorid sensitivity of growth, photosynthesis and calcification to increasing seawater pCO_2, PLoS One, 9(2), e88308, doi:10.1371/journal.pone.0088308, 2014.

Shaw, G. E.: Bio-controlled thermostasis involving the sulfur cycle, Clim. Change, 5(3), 297–303, 1983.

Sheppard Brennand, H., Soars, N., Dworjanyn, S. A., Davis, A. R. and Byrne, M.: Impact of ocean warming and ocean acidification on larval development and calcification in the sea urchin *Tripneustes gratilla*., PLoS One, 5(6), e11372, doi:10.1371/journal.pone.0011372, 2010.

Shi, D., Xu, Y. and Morel, F. M. M.: Effects of the pH/pCO_2 control method on medium chemistry and phytoplankton growth, Biogeosciences, 6(7), 1199–1207, doi:10.5194/bg-6-1199-2009, 2009.

Shi, Q., Petrick, G., Quack, B., Marandino, C. and Wallace, D.: Seasonal variability of methyl iodide in the Kiel Fjord, J. Geophys. Res. Ocean., 119, 1609–1620, doi:10.1002/2013JC009328.Received, 2014.

Sieracki, M. E., Verity, P. G. and Stoecker, D. K.: Plankton community response to sequential silicate and nitrate depletion during the 1989 North Atlantic spring bloom, Deep Sea Res. Part II Top. Stud. Oceanogr., 40(1), 213–225, 1993.

Sievert, S. M., Kiene, R. P. and Schulz-Vogt, H. N.: The Sulfur Cycle, Oceanography, 20(2), 117–123, 2007.

Sigman, D. M. and Boyle, E. A.: Glacial/ interglacial variations in atmospheric carbon dioxide, Nature, 407, 859–869, 2000.

Sigman, D. M., Hain, M. P. and Haug, G. H.: The polar ocean and glacial cycles in atmospheric CO_2 concentration, Nature, 466(7302), 47–55, doi:10.1038/nature09149, 2010.

Silyakova, A., Bellerby, R. G. J., Schulz, K. G., Czerny, J., Tanaka, T., Nondal, G., Riebesell, U., Engel, A., De Lange, T. and Ludvig, A.: Pelagic community production and carbon-nutrient stoichiometry under variable ocean acidification in an Arctic fjord, Biogeosciences, 10(7), 4847–4859, doi:10.5194/bg-10-4847-2013, 2013.

Simó, R.: From cells to globe : approaching the dynamics of DMS(P) in the ocean at multiple scales, Can. J. Fish. Aquat. Sci., 61, 673–684, doi:10.1139/F04-030, 2004.

Simó, R. and Pedrós-Alió, C.: Role of vertical mixing in controlling the oceanic production of dimethyl sulphide, Nature, 402, 396–398, 1999.

Sivonen, K., Kononen, K., Carmichael, W. W., Dahlem, A. M., Rinehart, K. L., Kirivanta, J. and Niemela, S. I.: Occurrence of the hepatotoxic cyanobacterium *Nodularia spumigena* in the Baltic Sea and structure of the toxin., Appl. Environ. Microbiol., 55(8), 1990 – 1995, 1989.

Sivonen, K., Niemela, S. I., Niemi, R. M., Lepisto, L., Luoma, T. H. and Rasanen, L. A.: Toxic cyanobacteria (blue-green algae in Finnish fresh and coastal waters, Hydrobiologia, 190, 267–275, 1990.

Six, K. D., Kloster, S., Ilyina, T., Archer, S. D., Zhang, K. and Maier-Reimer, E.: Global warming amplified by reduced sulphur fluxes as a result of ocean acidification, Nat. Clim. Chang., 3(8), 1–4, doi:10.1038/nclimate1981, 2013.

Slovacek, R. E. and Hannann, P. J.: In vivo fluorescence determinations of phytoplankotn chlorophyll a, Limnol. Oceanogr., 22(5), 919–925, 1977.

Smith, D. C., Simon, M., Alldredge, A. L. and Azam, F.: Intense hydrolytic enzyme activity on marine aggregates and implications for rapid particle dissolution, Nature, 359, 139 – 142, 1992.

Smith, S. V.: Coral reef area and the contributions of reefs to processes and resources of the world's oceans, Nature, 273, 225–226, 1978.

Smyth, T. J., Tyrrell, T. and Tarrant, B.: Time series of coccolithophore activity in the Barents Sea, from twenty years of satellite imagery, Geophys. Res. Lett., 31(11), L11302, doi:10.1029/2004GL019735, 2004.

Smythe-Wright, D., Boswell, S. M., Breithaupt, P., Davidson, R. D., Dimmer, C. H. and Eiras Diaz, L. B.: Methyl iodide production in the ocean: Implications for climate change, Global Biogeochem. Cycles, 20(3), doi:10.1029/2005GB002642, 2006.

Smythe-Wright, D., Boswell, S. M., Lucas, C. H., New, A. L. and Varney, M. S.: Halocarbon and dimethyl sulphide studies around the Mascarene Plateau., Philos. Trans. A. Math. Phys. Eng. Sci., 363, 169–85, doi:10.1098/rsta.2004.1485, 2005.

Solomon, S., Garcia, R. R. and Ravishankara, A. R.: On the role of iodine in ozone depletion, J. Geophys. Res., 99(D10), 20491–20499, doi:10.1029/94JD02028, 1994.

Souza, M. De and Yoch, D.: Comparative physiology of dimethyl sulfide production by dimethylsulfoniopropionate lyase in *Pseudomonas doudoroffii* and *Alcaligenes* sp. Strain M3A., Appl. Environ. Microbiol., 61, 3986 – 3991, 1995.

Spielmeyer, A. and Pohnert, G.: Influence of temperature and elevated carbon dioxide on the production of dimethylsulfoniopropionate and glycine betaine by marine phytoplankton., Mar. Environ. Res., 73, 62–69, doi:10.1016/j.marenvres.2011.11.002, 2012.

Spiese, C. E., Kieber, D. J., Nomura, C. T. and Kiene, R. P.: Reduction of dimethylsulfoxide to dimethylsulfide by marine phytoplankton, Limnol. Oceanogr., 54(2), 560–570, doi:10.4319/lo.2009.54.2.0560, 2009.

Stal, L. J., Albertano, P., Bergman, B., von Bröckel, K., Gallon, J. R., Hayes, P. K., Sivonen, K. and Walsby, A. E.: BASIC: Baltic Sea cyanobacteria. An investigation of the structure and dynamics of water blooms of cyanobacteria in the Baltic Sea—responses to a changing environment, Cont. Shelf Res., 23(17-19), 1695–1714, doi:10.1016/j.csr.2003.06.001, 2003.

Stefels, J.: Physiological aspects of the production and conversion of DMSP in marine algae and higher plants, J. Sea Res., 43, 183–197, 2000.

Stefels, J. and van Boekel, W. H. M.: Production of DMS from dissolved DMSP in axenic cultures of the marine phytoplankton species *Phaeocystis* spp., Mar. Ecol. Prog. Ser., 97, 11–18, 1993.

Stefels, J., Steinke, M., Turner, S., Malin, G. and Belviso, S.: Environmental constraints on the production and removal of the climatically active gas dimethylsulphide (DMS) and implications for ecosystem modelling, Biogeochemistry, 83, 245–275, doi:10.1007/s10533-007-9091-5, 2007.

Steinke, M., Evans, C., Lee, G. A. and Malin, G.: Substrate kinetics of DMSP-lyases in axenic cultures and mesocosm populations of Emiliania huxleyi, Aquat. Sci., 69, 352–359, doi:10.1007/s00027-007-0893-2, 2007.

Steinke, M., Malin, G., Archer, S. D., Burkill, P. H. and Liss, P. S.: DMS production in a coccolithophorid bloom: evidence for the importance of dinoflagellate DMSP lyases, Aquat. Microb. Ecol., 26, 259–270, doi:10.3354/ame026259, 2002.

Strom, S., Wolfe, G., Holmes, J., Stecher, H., Shimeneck, C., Lambert, S. and Moreno, E.: Chemical defense in the microplankton I: Feeding and growth rates of heterotrophic protists on the DMS-producing phytoplankter *Emiliania huxleyi*, Limnol. Oceanogr., 48(1), 217–229, doi:10.4319/lo.2003.48.1.0217, 2003.

Struck, U., Pollehne, F., Bauerfeind, E. and v. Bodungen, B.: Sources of nitrogen for the vertical particle flux in the Gotland Sea (Baltic Proper)—results from sediment trap studies, J. Mar. Syst., 45(1-2), 91–101, doi:10.1016/j.jmarsys.2003.11.012, 2004.

Sturges, W. T., Oram, D. E., Carpenter, L. J., Penkett, S. A. and Engel, A.: Bromoform as a source of stratospheric bromine, Geophys. Res. Lett., 27(14), 2081–2084, doi:10.1029/2000GL011444, 2000.

Suffrian, K., Simonelli, P., Nejstgaard, J. C., Putzeys, S., Carotenuto, Y. and Antia, A. N.: Microzooplankton grazing and phytoplankton growth in marine mesocosms with increased CO_2 levels, Biogeosciences, 5(4), 1145–1156, doi:10.5194/bg-5-1145-2008, 2008.

Suikkanen, S., Laamanen, M. and Huttunen, M.: Long-term changes in summer phytoplankton communities of the open northern Baltic Sea, Estuar. Coast. Shelf Sci., 71(3-4), 580–592, doi:10.1016/j.ecss.2006.09.004, 2007.

Suikkanen, S., Pulina, S., Engström-Öst, J., Lehtiniemi, M., Lehtinen, S. and Brutemark, A.: Climate change and eutrophication induced shifts in northern summer plankton communities, PLoS One, 8(6), e66475, doi:10.1371/journal.pone.0066475, 2013.

Sunda, W., Kieber, D. J., Kiene, R. P. and Huntsman, S.: An antioxidant function for DMSP and DMS in marine algae, Nature, 418(6895), 317–320, doi:10.1038/nature00851, 2002.

Suwa, R., Nakamura, M., Morita, M., Shimada, K., Iguchi, A., Sakai, K. and Suzuki, A.: Effects of acidified seawater on early life stages of scleractinian corals (Genus Acropora), Fish. Sci., 76, 93–99, 2010.

Taalba, A., Xie, H., Scarratt, M. G., Bélanger, S. and Levasseur, M.: Photooxidation of dimethylsulfide (DMS) in the Canadian Arctic, Biogeosciences Discuss., 10(2), 2093–2126, doi:10.5194/bgd-10-2093-2013, 2013.

Takahashi, T., Sutherland, S. C., Feely, R. A. and Wanninkhof, R.: Decadal change of the surface water pCO 2 in the North Pacific: A synthesis of 35 years of observations, J. Geophys. Res., 111, C07S05, doi:10.1029/2005JC003074, 2006.

Tang, X., Madronich, S., Wallington, T. and Calamari, D.: Changes in tropospheric composition and air quality., J. Photochem. Photobiol. B., 46(1-3), 83–95, 1998.

Theiler, R., Cook, J. C., Hager, L. P. and Siuda, J. F.: Halohydrocarbon synthesis by bromoperoxidase, Science., 202(December), 1094 – 1096, 1978.

Todd, J. D., Curson, A. R. J., Nikolaidou-Katsaraidou, N., Brearley, C. A., Watmough, N. J., Chan, Y., Page, P. C. B., Sun, L. and Johnston, A. W. B.: Molecular dissection of bacterial acrylate

catabolism--unexpected links with dimethylsulfoniopropionate catabolism and dimethyl sulfide production., Environ. Microbiol., 12(2), 327–343, doi:10.1111/j.1462-2920.2009.02071.x, 2010.

Todd, J. D., Rogers, R., Li, Y. G., Wexler, M., Bond, P. L., Sun, L., Curson, A. R. J., Malin, G., Steinke, M. and Johnston, A. W. B.: Structural and regulatory genes required to make the gas dimethyl sulfide in bacteria, Science., 315(2007), 666–669, doi:10.1126/science.1135370, 2007.

Toole, D. A., Kieber, D. J., Kiene, R. P., Siegel, D. A. and Nelson, N. B.: Photolysis and the dimethylsulfide (DMS) summer paradox in the Sargasso Sea, Limnol. Oceanogr., 48(3), 1088–1100, 2003.

Torres, R., Turner, D. R., Silva, N. and Rutllant, J.: High short-term variability of CO_2 fluxes during an upwelling event off the Chilean coast at 30 S, Deep Sea Res., 46, 1161–1179, 1999.

Tortell, P., DiTullio, G., Sigman, D. and Morel, F.: CO_2 effects on taxonomic composition and nutrient utilization in an Equatorial Pacific phytoplankton assemblage, Mar. Ecol. Prog. Ser., 236, 37–43, doi:10.3354/meps236037, 2002.

Trimborn, S., Lundholm, N., Thoms, S., Richter, K.-U., Krock, B., Hansen, P. J. and Rost, B.: Inorganic carbon acquisition in potentially toxic and non-toxic diatoms: the effect of pH-induced changes in seawater carbonate chemistry, Physiol. Plant., 133, 92–105, doi:10.1111/j.1399-3054.2007.01038.x, 2008.

Tunzi, M. G., Chu, M. Y. and Bain, R. C.: In vivo fluorescence, extracted fluorescence and chlorophyll concentrations in algal mass measurements, Water Res., 8(9), 623–635, 1974.

Turley, C. M. and Findlay, H. S.: Ocean acidification as an indicator for climate change, in Climate Change: observed impacts on Planet Earth, edited by T. M. Letcher, pp. 367–390, Elsevier., 2009.

Turner, S. M. and Liss, P. S.: Measurements of various sulphur gases in a coastal marine environment, J. Atmos. Chem., 2, 223–232, 1985.

Turner, S. M., Malin, G., Bågander, L. E. and Leck, C.: Interlaboratory calibration and sample analysis of dimethyl sulphide in water, Mar. Chem., 29, 47–62, doi:10.1016/0304-4203(90)90005-W, 1990.

Turner, S. M., Malin, G., Liss, P. S., Harbour, D. S. and Holligan, P. M.: The seasonal variation of dimethyl sulfide and dimethylsulfoniopropionate concentrations in nearshore waters, Limnol. Oceanogr., 33(3), 364–375, 1988.

Tyrrell, T. and Merico, A.: *Emiliania huxleyi*: bloom observations and the conditions that induce them, in Coccolithophores SE - 4, edited by H. Thierstein and J. Young, pp. 75–97, Springer Berlin Heidelberg., 2004.

Tyrrell, T., Schneider, B., Charalampopoulou, A. and Riebesell, U.: Coccolithophores and calcite saturation state in the Baltic and Black Seas, Biogeosciences, 5, 485–494, 2008.

Tyrrell, T. and Taylor, A.: A modelling study of *Emiliania huxleyi* in the NE Atlantic, J. Mar. Syst., 9, 83–112, 1996.

Urhahn, T. and Ballschmiter, K.: Chemistry of the biosynthesis of halogenated methanes: C1-organohalogens as pre-industrial chemical stressors in the environment?, Chemosphere, 37(6), 1017–1032, doi:10.1016/S0045-6535(98)00100-3, 1998.

Vahtera, E., Laanemets, J., Pavelson, J., Huttunen, M. and Kononen, K.: Effect of upwelling on the pelagic environment and bloom-forming cyanobacteria in the western Gulf of Finland, Baltic Sea, J. Mar. Syst., 58(1-2), 67–82, doi:10.1016/j.jmarsys.2005.07.001, 2005.

Vairavamurthy, A., Andreae, M. O. and Iverson, R. L.: Biosynthesis of dimethylsulfide and dimethylpropiothetin by *Hymenomonas carterae* in relation to sulfur source and salinity variations, Limnol. Oceanogr., 30, 59–70, 1985.

Del Valle, D. A., Slezak, D., Smith, C. M., Rellinger, A. N., Kieber, D. J. and Kiene, R. P.: Effect of acidification on preservation of DMSP in seawater and phytoplankton cultures: Evidence for rapid loss and cleavage of DMSP in samples containing Phaeocystis sp., Mar. Chem., 124, 57–67, doi:10.1016/j.marchem.2010.12.002, 2011.

Verdugo, P., Alldredge, A., Azam, F., Kirchman, D. L., Passow, U. and Santschi, P. H.: The oceanic gel phase: a bridge in the DOM–POM continuum, Mar. Chem., 92(1-4), 67–85, doi:10.1016/j.marchem.2004.06.017, 2004.

Veron, J. E. N., Hoegh-Guldberg, O., Lenton, T. M., Lough, J. M., Obura, D. O., Pearce-Kelly, P., Sheppard, C. R. C., Spalding, M., Stafford-Smith, M. G. and Rogers, A. D.: The coral reef crisis: the critical importance of <350 ppm CO_2, Mar. Pollut. Bull., 58(10), 1428–1436, doi:10.1016/j.marpolbul.2009.09.009, 2009.

Vila-Costa, M., Simó, R., Harada, H., Gasol, J. M., Slezak, D. and Kiene, R. P.: Dimethylsulfoniopropionate uptake by marine phytoplankton, Science, 314(5799), 652–4, doi:10.1126/science.1131043, 2006.

Visscher, P. T., Baumgartner, L. K., Buckley, D. H., Rogers, D. R., Hogan, M. E., Raleigh, C. D., Turk, K. A. and Des Marais, D. J.: Dimethyl sulphide and methanethiol formation in microbial mats: potential pathways for biogenic signatures, Environ. Microbiol., 5(4), 296–308, 2003.

Visscher, P. T. and Taylor, B. F.: A new mechanism for the aerobic catabolism of dimethyl sulfide., Appl. Environ. Microbiol., 59(11), 3784–3789, 1993.

Vogt, C., Rabenstein, A., Rethmeier, J. and Fischer, U.: Alkali-labile precursors of dimethyl sulfide in marine benthic cyanobacteria, Arch. Microbiol., 169(3), 263–266, 1998.

Vogt, M., Steinke, M., Turner, S. M., Paulino, A., Meyerhöfer, M., Riebesell, U., LeQuéré, C. and Liss, P. S.: Dynamics of dimethylsulphoniopropionate and dimethylsulphide under different CO_2 concentrations during a mesocosm experiment, Biogeosciences, 5(2), 407–419, doi:10.5194/bg-5-407-2008, 2008a.

Vogt, M., Turner, S. M., Yassaa, N., Steinke, M., Williams, J. and Liss, P. S.: Laboratory inter-comparison of dissolved dimethyl sulphide (DMS) measurements using purge-and-trap and solid-phase microextraction techniques during a mesocosm experiment, Mar. Chem., 108, 32–39, doi:10.1016/j.marchem.2007.10.001, 2008b.

Walsby, A. E., Hayes, P. K. and Boje, R.: The gas vesicles, buoyancy and vertical distribution of cyanobacteria in the Baltic Sea, Eur. J. Phycol., 30(2), 87–94, doi:10.1080/09670269500650851, 1995.

Walsby, A. E., Hayes, P. K., Boje, R. and Stal, L. J.: The selective advantage of buoyancy provided by gas vesicles for planktonic cyanobacteria in the Baltic Sea, New Phytol., 136, 407–417, 1997.

Wang, L., Moore, R. M. and Cullen, J. J.: Methyl iodide in the NW Atlantic: spatial and seasonal variation, J. Geophys. Res., 114(C07007), doi:10.1029/2007JC004626, 2009.

Wasmund, N.: Occurrence of cyanobacterial blooms in the Baltic Sea in relation to environmental conditions, Iny. Rev. ges. Hydrobiol., 82(2), 169–184, 1997.

Wasmund, N., Voss, M. and Lochte, K.: Evidence of nitrogen fixation by non-heterocystous cyanobacteria in the Baltic Sea and re-calculation of a budget of nitrogen fixation, Mar. Ecol. Prog. Ser., 214(1988), 1–14, 2001.

Watts, M. C. and Bigg, G. R.: Modelling and the monitoring of mesocosm experiments: two case studies, J. Plankton Res., 23(10), 1081–1093, 2001.

Watts, S. F.: The mass budgets of carbonyl sulphide, dimethyl sulphide, carbon disulphide and hydrogen sulphide, Atmos. Environ., 34, 761–779, 2000.

Weinberg, I.: Emission and dynamics of halocarbons from seagrass meadows traced by stable carbon isotopes, University of Hamburg., 2013.

Welschmeyer, N. A.: Fluorometric analysis of chlorophyll a in the presence of chlorophyll b and pheopigments, Limnol. Oceanogr., 39(8), 1985–1992, 1994.

Wever, R., Tromp, M. G. M., Krenn, B. E., Marjani, A. and Van Tol, M.: Brominating activity of the seaweed *Ascophyllum nodosum*: impact on the biosphere, Environ. Sci. Technol., 25(3), 446–449, doi:10.1021/es00015a010, 1991.

Wilson, W., Turner, S. and Mann, N. H.: Population dynamics of phytoplankton and viruses in a phosphate-limited mesocosm and their effect on DMSP and DMS production, Estuar. Coast. Shelf Sci., 46(Supplement A), 49–59, doi:10.1006/ecss.1998.0333, 1998.

Wingenter, O. W., Haase, K. B., Zeigler, M., Blake, D. R., Rowland, F. S., Sive, B. C., Paulino, A., Thyrhaug, R., Larsen, A., Schulz, K. G., Meyerhöfer, M. and Riebesell, U.: Unexpected consequences of increasing CO_2 and ocean acidity on marine production of DMS and CH_2ClI: Potential climate impacts, Geophys. Res. Lett., 34(5), doi:10.1029/2006GL028139, 2007.

Wolfe, G. V and Kiene, R. P.: Radioisotope and chemical inhibitor measurements of dimethyl sulfide consumption rates and kinetics in estuarine waters, Mar. Ecol. Prog. Ser., 99, 261–269, 1993.

Wolfe, G. V., Sherr, E. and Sherr, B. F.: Release and consumption of DMSP from *Emiliania huxleyi* during grazing by Oxyrrhis marina, Mar. Ecol. Prog. Ser., 111, 111–119, 1994.

Wolfe, G. V. and Steinke, M.: Grazing-activated production of dimethyl sulfide (DMS) by two clones of *Emiliania huxleyi*, Limnol. Oceanogr., 41(6), 1151–1160, 1996.

Wolfe, G. V., Steinke, M. and Kirst, G. O.: Grazing-activated chemical defence in a unicellular marine alga, Nature, 387, 894–897, 1997.

Wolf-Gladrow, D. A., Riebesell, U., Burkhardt, S. and Bijma, J.: Direct effects of CO_2 concentration on growth and isotopic composition of marine plankton, Tellus, 51(2), 461–476, 1999.

Wong, G. T. F.: The marine geochemistry of iodine, Rev. Aquat. Sci., 4(1), 45–73, 1991.

Wong, G. T. F. and Cheng, X.-H.: Dissolved organic iodine in marine waters: role in the estuarine geochemistry of iodine, J. Environ. Monit., 3(2), 257–263, doi:10.1039/b007229j, 2001.

Wong, G. T. F., Piumsomboon, A. U. and Dunstan, W. M.: The transformation of iodate to iodide in marine phytoplankton cultures, Mar. Ecol. Prog. Ser., 237, 27–39, doi:10.3354/meps237027, 2002.

Wood, H. L., Spicer, J. I. and Widdicombe, S.: Ocean acidification may increase calcification rates, but at a cost, Proc. R. Soc. B, 275(1644), 1767–73, doi:10.1098/rspb.2008.0343, 2008.

Wright, K. L. B., Pichegru, L. and Ryan, P. G.: Penguins are attracted to dimethyl sulphide at sea, J. Exp. Biol., 214(Pt 15), 2509–2511, doi:10.1242/jeb.058230, 2011.

Wu, Y., Gao, K. and Riebesell, U.: CO_2-induced seawater acidification affects physiological performance of the marine diatom *Phaeodactylum tricornutum*, Biogeosciences, 7(9), 2915–2923, doi:10.5194/bg-7-2915-2010, 2010.

Wuori, T.: The effects of elevated pCO_2 in the physiology of *Emiliania huxleyi*, Western Washington University., 2012.

Wuosmaa, A. M. and Hager, L. P.: Methyl chloride transferase: a carbocation route for biosynthesis of halometabolites., Science, 249(4965), 160–162, 1990.

Wyman, M., Davies, J. T., Weston, K., Crawford, D. W. and Purdie, D. A.: Ribulose-1,5-biphosphate carboxylase/oxygenase (RubisCO) gene expression and photosynthetic activity in nutrient-enriched mesocosm experiments, Estuar. Coast. Shelf Sci., 46(Supplement A), 23–33, 1998.

Yang, G., Li, C. and Sun, J.: Influence of salinity and nitrogen content on production of dimethylsulfoniopropionate (DMSP) and dimethylsulfide (DMS) by *Skeletonema costatum,* Chinese J. Oceanol. Limnol., 29(2), 378–386, doi:10.1007/s00343-011-0087-6, 2011.

Yokouchi, Y., Mukai, H., Yamamoto, H., Otsuki, A., Saitoh, C. and Nojiri, Y.: Distribution of methyl iodide, ethyl iodide, bromoform, and dibromomethane over the ocean (east and southeast Asian seas and the western Pacific), J. Geophys. Res., 102(D7), 8805–8809, doi:10.1029/96JD03384, 1997.

Young, J. R.: Functions of Coccoliths, in Coccolithophores, edited by A. Winter and W. G. Siesser, pp. 63–82, Cambridge University Press, Cambridge., 1994.

Yung, Y., Pinto, J., Watson, R. T. and Sander, S. P.: Atmospheric bromine and ozone perturbations in the lower stratosphere, J. Atmos. Sci., 37, 339 – 353, 1980.

Zeebe, R. E. and Wolf-Gladrow, D.: CO_2 in seawater: equilibrium, kinetics, isotopes, Elsevier, Amsterdam., 2001.

Zika, R. G., Gidel, L. T. and Davis, D.: A comparison of photolysis and substitution decomposition rates of methyl iodide in the ocean, Geophys. Res. Lett., 11(4), 353–356, 1984.

Zimmer-Faust, R. K., de Souza, M. P. and Yoch, D. C.: Bacterial chemotaxis and its potential role in marine dimethylsulfide production and biogeochemical sulfur cycling, Limnol. Oceanogr., 41(6), 1330–1334, 1996.

Zinder, S. H. and Brock, T. D.: Dimethyl sulphoxide reduction by micro-organisms, J. Gen. Microbiol., 105(2), 335–342, 1978.

Zindler, C., Peeken, I., Marandino, C. A. and Bange, H. W.: Environmental control on the variability of DMS and DMSP in the Mauritanian upwelling region, Biogeosciences, 9, 1041–1051, doi:10.5194/bg-9-1041-2012, 2012.

Ziska, F., Quack, B., Abrahamsson, K., Archer, S. D., Atlas, E., Bell, T. G., Butler, J. H., Carpenter, L. J., Jones, C. E., Harris, N. R. P., Hepach, H., Heumann, K. G., Hughes, C., Kuss, J., Krüger, K., Liss, P., Moore, R. M., Orlikowska, A., Raimund, S., Reeves, C. E., Reifenhäuser, W., Robinson, a. D., Schall, C., Tanhua, T., Tegtmeier, S., Turner, S., Wang, L., Wallace, D., Williams, J., Yamamoto, H., Yvon-Lewis, S. and Yokouchi, Y.: Global sea-to-air flux climatology for bromoform, dibromomethane and methyl iodide, Atmos. Chem. Phys., 13(17), 8915–8934, doi:10.5194/acp-13-8915-2013, 2013.

Zondervan, I.: The effects of light, macronutrients, trace metals and CO_2 on the production of calcium carbonate and organic carbon in coccolithophores—A review, Deep Sea Res. Part II Top. Stud. Oceanogr., 54(5-7), 521–537, doi:10.1016/j.dsr2.2006.12.004, 2007.

Zondervan, I., Rost, B. and Riebesell, U.: Effect of CO_2 concentration on the PIC/POC ratio in the coccolithophore *Emiliania huxleyi* grown under light-limiting conditions and different daylengths, J. Exp. Mar. Bio. Ecol., 272, 55–70, doi:10.1016/S0022-0981(02)00037-0, 2002.

Zubkov, M., Linn, L. J., Amann, R. and Kiene, R. P.: Temporal patterns of biological dimethylsulfide (DMS) consumption during laboratory-induced phytoplankton bloom cycles, Mar. Ecol. Prog. Ser., 271, 77–86, doi:10.3354/meps271077, 2004.

Zubkov, M. V, Fuchs, B. M., Archer, S. D., Kiene, R. P., Amann, R. and Burkill, P. H.: Linking the composition of bacterioplankton to rapid turnover of dissolved dimethylsulphoniopropionate in an algal bloom in the North Sea., Environ. Microbiol., 3(5), 304–11, 2001.

Zubkov, M. V, Fuchs, B. M., Archer, S. D., Kiene, R. P., Amann, R. and Burkill, P. H.: Rapid turnover of dissolved DMS and DMSP by defined bacterioplankton communities in the stratified euphotic zone of the North Sea, Deep Sea Res. Part I Oceanogr. Res. Pap., 49, 3017–3038, 2002.

Appendix 1. Assessment of the viability of the DMSP acidification sample fixation method at varying salinities

1. DMSP in UEA Broad (Salinity 1)

1.1. Methods

Samples were collected from the UEA Broad in summer 2012 and summer 2013. During the first sampling, six 20 mL vials were filled with 19ml of UEA Broad water, three of which had 100 µL of 50% sulphuric acid (H_2SO_4) added, and the other three 1 mL of 1M NaOH as a control. All vials were crimp sealed for gas tightness, and stored for 24 hours in the dark prior to analysis. Samples were analysed for DMS content immediately to DMS-correct the NaOH samples. The second sampling used five replicates for each treatment, prepared in an identical manner, with an additional three samples analysed immediately for DMSP concentration. Samples were analysed using purge- and-cryotrap GC-FPD.

1.2. Results

The results of the samples from 2012 are shown in Figure 1 and those from 2013 shown in Figure 2, both figures showing the concentrations measured in individual samples and the mean. A t-test ($T=-6.51$, $p<0.01$) showed the acidification method had significantly lower DMSP content than the NaOH samples. In contrast, the samples taken in 2013 showed no significant difference between the acidified samples and the NaOH samples.

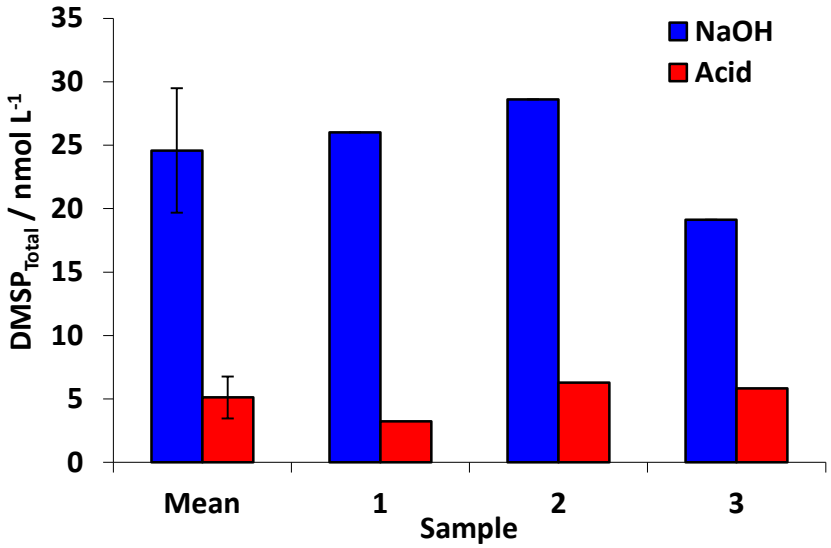

Figure 1. DMSP concentrations measured from UEA Broad water samples in 2012 fixed using NaOH (blue) and the acidification method (NaOH). Error bars on the mean samples denote the standard deviation of the three samples.

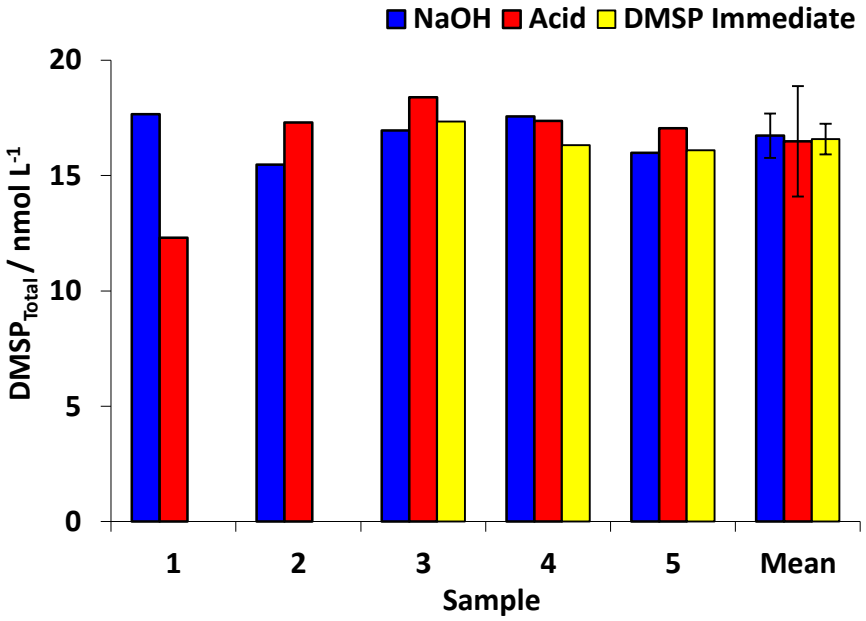

Figure 2. DMSP concentrations measured from UEA Broad water samples taken in August 2013 using NaOH (blue), the acidification method (NaOH) and DMSP measured immediately (yellow). Error bars on the mean samples denote the standard deviation of the three samples.

2. Norfolk Broads (Salinity <1 – 31)

2.1. Methods

The Norfolk Broads are an area of wetland containing the estuaries of the Rivers Bure and Yare, and gave an easily accessible location with a salinity gradient ranging from seawater to freshwater. DMSP was previously identified in both seawater and freshwater environments in the Broads. Figure 3 provides details of the sampling locations around the Broads; access to the waterside was difficult along the River Yare. High tide occurred at 14.59 BST at Great Yarmouth, with tide times +2 hours for Reedham Ferry and the Embrujo restaurant. Samples were taken according to the salinity readings and were not dependent upon the state of the tide. Samples were collected and stored in 250 mL amber glass bottles in a gas-tight manner and sealed with ground glass stoppers to prevent air bubbles. Samples were returned to UEA in a coolbox for preparation and analysis. Salinity and temperature were measured *in-situ*.

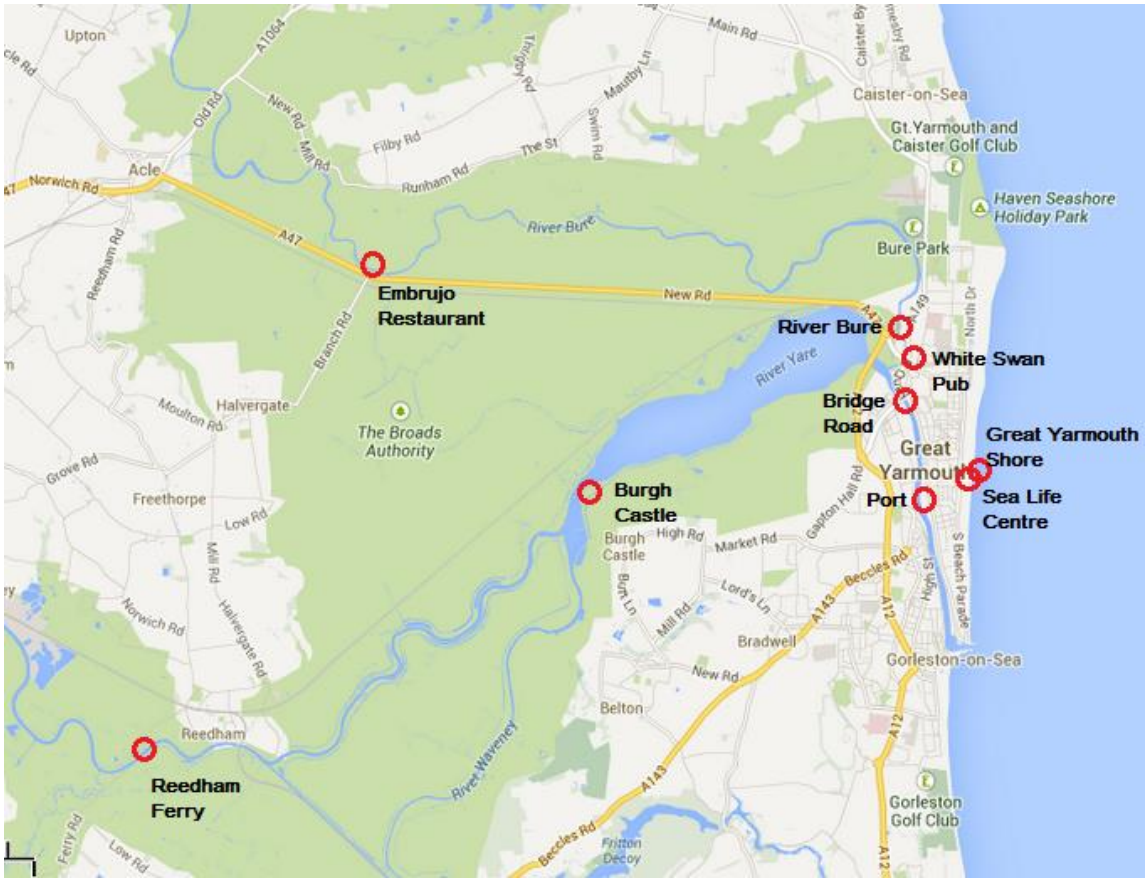

Figure 3. Map of the Norfolk Broads and Great Yarmouth. Red circles indicate the DMSP sampling locations.

Immediately on return to the laboratory, a 2mL sub-sample was taken from each location sample in turn and analysed for DMS content using the purge-and-cryotrap GC-FPD. Four 20mL vials were prepared for each treatment: NaOH or acidification, and each was filled with 19 mL of sample using a pipette. The samples were treated either with 100 µL H_2SO_4 or 1 mL NaOH and crimp-sealed for gas tightness. The samples were stored overnight and analysed after 24 hours using purge-and-cryotrap GC-FPD.

2.2. Results

The salinities measured from 31.9 in the seawater off the Great Yarmouth shoreline, to 0.3 at Reedham Ferry. The Salinities are shown in Table 1. Sampling locations were chosen for their salinity, although it was difficult to obtain access to the estuaries to get a full range of salinities. As the investigation was to study the differences in the two storage methods for DMSP samples under different salinities, it was deemed unnecessary to perform all the sampling at a particular tide height.

Table 1. Salinities and in-situ temperatures from all the sites sampled in Great Yarmouth and the Norfolk Broads.

Sampling Location	Coordinates	Salinity	In situ temperature (°C)
Great Yarmouth Sealife Centre		31.4	20.3
Great Yarmouth Shoreline (Brittania Pier)	N 52° 36.103 E 001° 44.208	31.9	19.7
Great Yarmouth Port	N 52° 35.334 E 001° 43.791	26.1	19.6
Great Yarmouth Bridge Road	N 52° 36.386 E 001° 43.348	22.5	19.3
Burgh Castle	N 52° 35.376 E 001° 39.014	15.2	22.3
White Swan Pub	N 52° 36.453 E 001° 43.272	14.7	20.5
River Bure	N 52° 37.200 E 001° 43.316	12.5	20.6
Embrujo Restaurant	N 52° 37.470 E 001° 36.106	0.9	20.7
Reedham Ferry	N 52° 33.514 E 001° 33.062	0.3	21.2

Mean concentrations of DMSP measured by the two storage methods are shown in Figure 4, along with the standard deviation between the five replicate samples. No significant difference was identified between the NaOH and acidified samples from any location. Figure 5 shows the same DMSP results plotted against salinity, and show that both the sample fixation methods work equally well for DMSP samples at lower salinities.

Samples from the Sealife Centre Water inlet showed DMSP below detection limits of the GC-FPD for all the samples taken, both NaOH and acidified, likely due to the water passing through a sand filter beforehand. DMSP samples from Reedham Ferry were very close to the detection limits of the GC-FPD, and were below detection for the acidified samples at the Spanish restaurant.

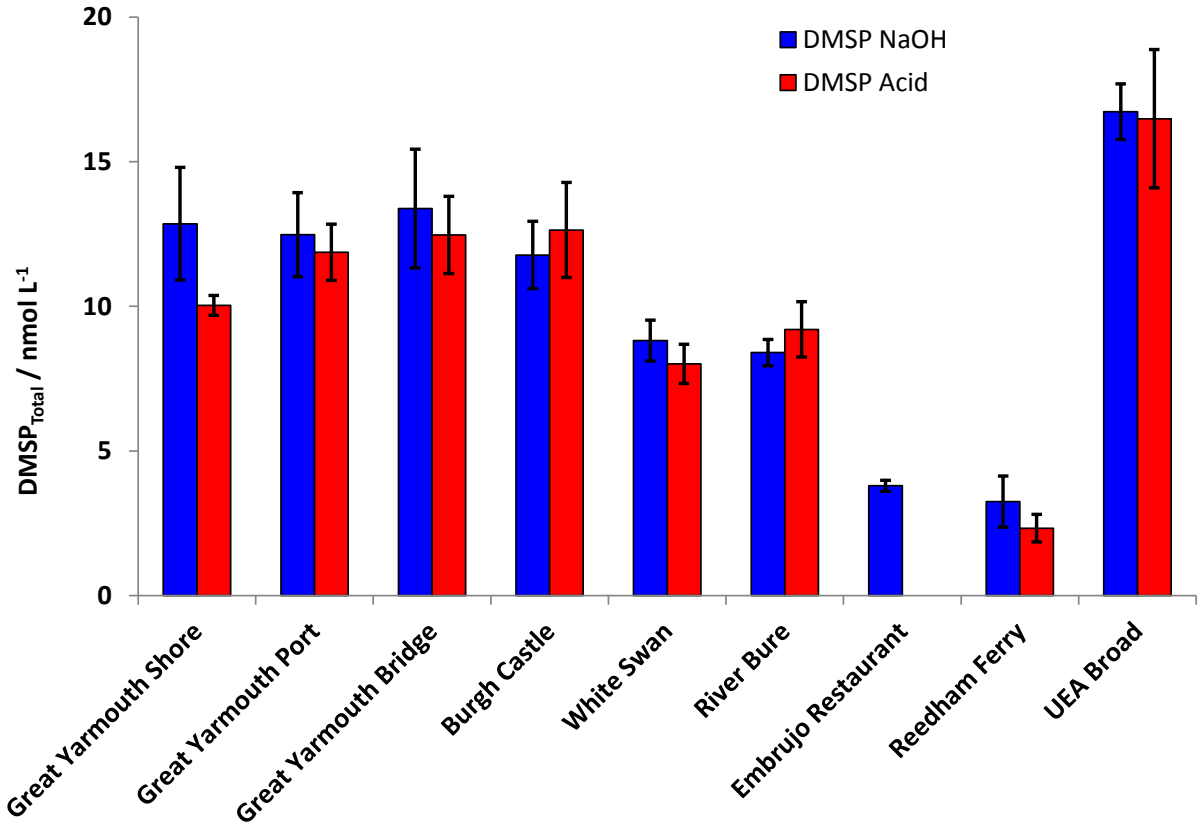

Figure 4. DMSP concentrations measured at locations throughout the Norfolk Broads. Red bars show the concentrations measured in the acidified samples, and blue bars show the NaOH samples, and error bars denote the standard deviation of four samples.

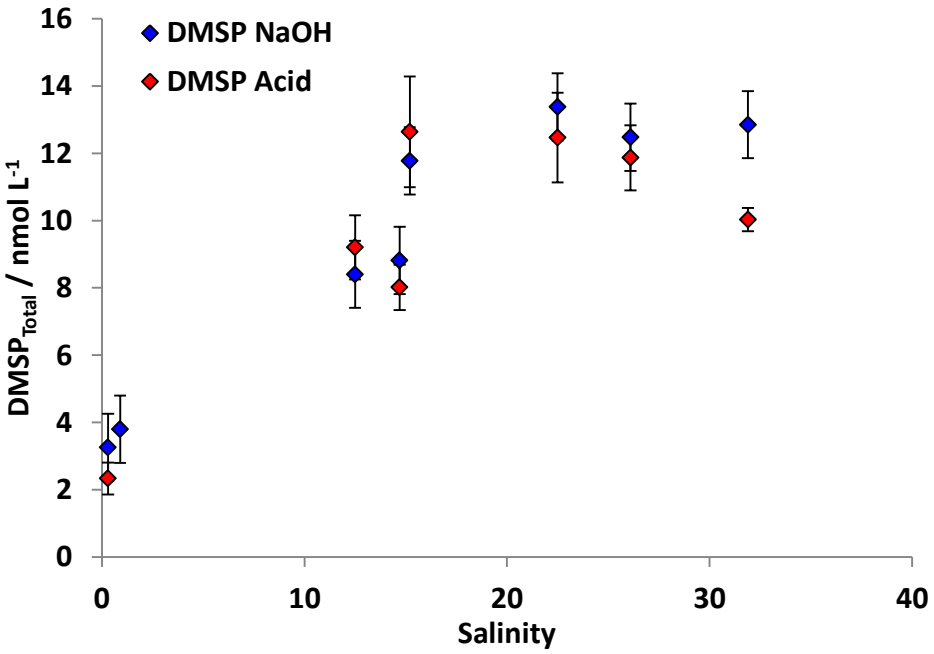

Figure 5. DMSP concentrations plotted against salinity for NaOH addition (blue) and acid addition (red).